LOAN DOCUMENT

PHOTOGRAPH THIS SHEET

AD-A229 199

DTIC ACCESSION NUMBER

LEVEL

DTIC FILE COPY

INVENTORY

AFOSR-90 1054

DOCUMENT IDENTIFICATION

Sept 1990

DISTRIBUTION STATEMENT

H
A
N
D
L
E

W
I
T
H

C
A
R
E

ACCESSION FOR

NTIS	GRA&I
DTIC	TRAC
UNANNOUNCED	
JUSTIFICATION	

BY

DISTRIBUTION/

AVAILABILITY CODES

DISTRIBUTION	AVAILABILITY AND/OR SPECIAL

A-1

DISTRIBUTION STAMP

DTIG
COPY
INSPECTED
6

**DTIC
S ELECTE
E NOV 19 1990
D**

DATE ACCESSIONED

DATE RETURNED

DATE RECEIVED IN DTIC

REGISTERED OR CERTIFIED NUMBER

PHOTOGRAPH THIS SHEET AND RETURN TO DTIC-FDAC

DTIC FORM 70A
JUN 90

DOCUMENT PROCESSING SHEET

PREVIOUS EDITIONS MAY BE USED UNTIL
STOCK IS EXHAUSTED.

LOAN DOCUMENT

VOLUME 171

Polymer Based
Molecular Composites

EDITORS
Dale W. Schaefer
James E. Mark

REPORT DOCUMENTATION PAGE

Public reporting burden for this collection of information is estimated to average 1 hour per response, including the time for reviewing instructions, searching existing data sources, gathering and maintaining the data needed, and completing and reviewing the collection of information. Send comments regarding this burden estimate or any other aspect of this collection of information, including suggestions for reducing this burden, to Washington Headquarters Services, Directorate for Information Operations and Reports, 1215 Jefferson Davis Highway, Suite 1204, Arlington, VA 22202-4302, and to the Office of Management and Budget, Paperwork Reduction Project (0704-0188), Washington, DC 20503.

1. AGENCY USE ONLY (Leave blank)	2. REPORT DATE September 1990	3. REPORT TYPE AND DATES COVERED Final 26 Nov 89 – 25 Nov 90

4. TITLE AND SUBTITLE
Polymer Based Molecular Composites

5. FUNDING NUMBERS
61102F   2303   A3

6. AUTHOR(S)
Dale W. Schaefer, and James E. Mark

7. PERFORMING ORGANIZATION NAME(S) AND ADDRESS(ES)
Materials Research Society
9800 McKnight Road, Suite 327
Pittsburgh, PA   15237-6005

8. PERFORMING ORGANIZATION REPORT NUMBER

AFOSR-TR· 90   1054

9. SPONSORING/MONITORING AGENCY NAME(S) AND ADDRESS(ES)
AFOSR/NC
Building 410
Bolling AFB, DC   20332-6448

10. SPONSORING/MONITORING AGENCY REPORT NUMBER
AFOSR-90-0089

11. SUPPLEMENTARY NOTES

12a. DISTRIBUTION/AVAILABILITY STATEMENT

Approved for public relaese; distribution is unlimited

12b. DISTRIBUTION CODE

13. ABSTRACT (Maximum 200 words)

A symposium entitled "Polymer Based Molecular Composites" was organized as part of the Materials Research Society Fall Meeting Held November 27-30, 1989 in Boston, Massachusetts. A total of 57 papers were presented during the symposium. The papers were arranged in the following eight categories: (1) Inorganics/Emulsions; (2) Emulsions/Blocks; (3) Rigid-Flexible Systems; (4) Blends/IPN's; (5) Ionomers/Structure; (6) Synthesis/Electrooptical Properties; (7) Interfaces/Mechanical Properties; (8) Miscellaneous/ Conventional Composites. Two papers were recognized by the symposium organizers with awards as outstanding contributed papers. Two other papers in the symposium were recognized by the Materials Research Society with Graduate Student Awards to their presenters. All papers appear in their entirety in the Materials Research Society Symposium Proceedings, Volume 171, edited by Dale W. Schaefer and James E. Mark, and published by the Materials Research Society, Pittsburgh, PA.

14. SUBJECT TERMS

15. NUMBER OF PAGES
431

16. PRICE CODE

17. SECURITY CLASSIFICATION OF REPORT	18. SECURITY CLASSIFICATION OF THIS PAGE	19. SECURITY CLASSIFICATION OF ABSTRACT	20. LIMITATION OF ABSTRACT

**BEST
AVAILABLE COPY**

90 11 15 120

Polymer Based Molecular Composites

Symposium held November 27-30, 1989, Boston,
Massachusetts, U.S.A.

EDITORS:

Dale W. Schaefer

Sandia National Laboratories, Albuquerque, New Mexico, U.S.A.

James E. Mark

University or Cincinnati, Cincinnati, Ohio U.S.A.

CODEN: MRSPDH

Contents

*Invited Paper

*Invited Paper

*Invited Paper

*Invited Paper

*Invited Paper

Preface

The development of polymeric materials over the last 30 years is directly traceable to the chemist's ability to manipulate structure and tailor the properties of organic materials for specific applications. The phenomenal success of polymer chemistry, of course, rests on a half century of small-molecule chemical research. In the current technological environment, demands for organic materials often involve competing requirements which cannot be met by single-component polymers. Although multicomponent systems are often proposed to meet these competing demands, the complex interrelation between chemical and physical factors makes it difficult to synthesize these materials much less optimize their properties. It has become clear, therefore, that a research base is needed in multiphase polymeric materials similar to that which underlies single-phase organics. This symposium was organized to encourage the development of such a research base.

When we first proposed this symposium, we were anticipating a one or two day starter symposium. In fact we received over 80 papers from all over the world indicating the tremendous interest in molecular composites. In addition, the meeting supported another closely-related symposium titled "Multifunctional Materials," which was equally large.

The symposium was deliberately organized to include not only "traditional molecular composites (miscible blends of rod and coil molecules,)" but also to include a variety of other alloy systems from blends to copolymers' to microphase-separated systems. To some extent this broad definition recognizes the fact that true molecularly miscible rod/coil systems are exceedingly rare. The idea of materials development by intimately mixing polymers with fundamentally different properties, however, remains viable if phase separation can be restricted to microscopic scales.

We were delighted that two graduate student award winners presented their papers in Symposium O. Karen Winey, University of Massachusetts, received the award for her paper titled "The Ordered Bicontinuous Double Diamond Structure in Blends of Diblock Copolymer and Homopolymer," and Dan Q. Wu, State University of New York at Stony Brook, received the award for his paper titled "Small Angle X-Ray Scattering on Poly(Ethylene-Methacrylic Acid) Lead and Lead Sulfide Ionomers." In addition, Dr. Wu chaired the session on Synthesis/Electro-Optical Properties.

Two additional contributions were recognized by the symposium organizers as outstanding contributed papers. These papers were given a $500 grant to cover travel expenses at the meeting. The two outstanding papers were O-2.8, "Dynamic IR Studies of Microdomain Interphases of Isotope-Labeled Block Copolymers," by I. Noda, S.D. Smith,

A.E. Dowrey, J.T. Grothaus, and C. Marcott from the Procter & Gamble Company, and O-6.4, "Synthesis and Characterization of Segmented Copolymers of a Methylated Polyamide and a Thermotropic Liquid Crystalline Polyester," by Gregory T. Pawlikowski, R.A. Weiss, and S.J. Huang of the University of Connecticut.

December 1989

Dale W. Schaefer
James E. Mark

GRADUATE STUDENT AWARD WINNERS

Fall 1989

Symposium O

Karen Winey

Dan Q. Wu

Acknowledgments

MATERIALS RESEARCH SOCIETY SYMPOSIUM PROCEEDINGS

MATERIALS RESEARCH SOCIETY SYMPOSIUM PROCEEDINGS

MATERIALS RESEARCH SOCIETY MONOGRAPH

Earlier Materials Research Society Symposium Proceedings listed in the back.

PART I

Inorganics/Emulsions

INORGANIC-ORGANIC COMPOSITES BY SOL-GEL TECHNIQUES

Helmut SCHMIDT
Fraunhofer-Institut für Silicatforschung, Neunerplatz 2, D-8700
Würzburg, Federal Republic of Germany

ABSTRACT

The sol-gel process opens the possibility of combining in-
organic and organic units to new hybrid polymers. Organic units
can be used for structural modification of the inorganic back-
bone, for creating new functions within an inorganic network
and for building up organic polymeric chains. The materials show
interesting perspectives with respect to structural (surface
hardness, strength) and functional properties (e. g. diffusion,
photocuring, incorporation of dyes, optical properties). A re-
view over structural and functional properties of sol-gel de-
rived inorganic-organic polymers (ORMOCERs = organically modi-
fied ceramics) is given.

INTRODUCTION

The sol-gel process is a synthesis route to inorganic non-
metallic materials. Reactive monomers, oligomers or colloids
can be used as starting materials. They have to be "activated"
in order to undergo a polycondensation step and to form poly-
meric networks. This can be achieved by various means but, in
general, by creating reactive ≡MeOH groups, which are able to
form ≡Me-O-Me≡ bonds during the condensation step. A convenient
route is the use of alkoxides as precursors which react with
water to hydroxides, condensing spontaneously to polymeric spe-
cies (1). Similar reactions are well-known from inorganic salts,
forming hydroxides and precipitates (2) by pH change.

$$
\begin{aligned}
&\quad\quad H_2O \\
&\equiv MeOR \;\; \text{----}\rightarrow \;\; \equiv MeOH \text{ (irreversible step)} \\
&\equiv MeOH \;+\; ROMe\equiv \;\rightarrow\; \equiv MeOMe\equiv + HOR \quad\quad\quad (1) \\
&\quad\quad\quad\;+\; HOMe\equiv \;\rightarrow\; \equiv MeOMe\equiv + H_2O \\
&\quad\quad\quad\quad\quad\quad\quad\quad\quad\quad\quad\quad R = alkyl
\end{aligned}
$$

$$
\begin{aligned}
&\quad\quad H_2O \\
&\equiv MeX \;\; \text{----}\rightarrow \;\; \equiv MeOH \text{ (reversible step, pH!)} \\
&\equiv MeOH \;+\; XMe\equiv \;\rightarrow\; \equiv MeOMe\equiv \;+\; HX \quad\quad\quad (2) \\
&\quad\quad\quad\;+\; HOMe\equiv \;\rightarrow\; \equiv MeOMe\equiv \;+\; H_2O \\
&\quad\quad\quad\quad\quad\quad\quad\quad\quad X = anion\ (Cl^-, NO_3^-, ..)
\end{aligned}
$$
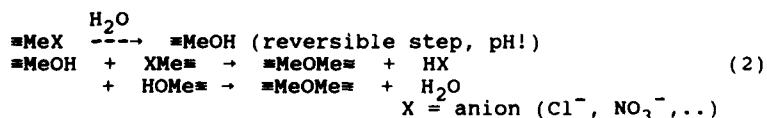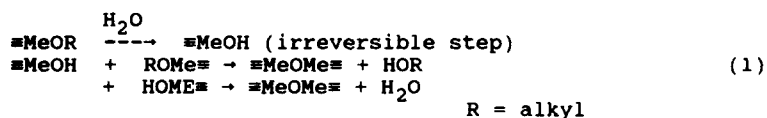
Another route is the destabilization of colloidal sols by
pH change either in organic solvents or in water. All these
reactions lead to gels, containing solvent or air after drying.
Due to the (in general) high specific surface areas of these
gels, they contain adsorbed molecules from the processing steps
(water or organics) or, in the case of the alkoxide route, un-
hydrolysed alkoxy groups. Organics are oxidized or pyrolyzed
during heat treatments of gels, converting them into glasses or
ceramics. Heat treatments are necessary to enhance diffusion

4

processes (for crystallization) or to decrease viscosity (for
glass formation) in gels. The viscosity of inorganic gels is
high due to the three dimensional crosslinking of the inorganic
building units (e. g. SiO_4^{4-} tetrahedron) leading to the typical
brittleness of ceramics.

Decreasing network connectivity by introducing organic
groupings can cause a remarkable decrease of viscosity of sy-
stems with pure inorganic backbones and leads to dense materials
at temperatures between 50 and 150 °C, as shown in [1-2]. An
analogue effect can be observed in inorganic glasses where the
introduction of inorganic network modifiers leads to lower vis-
cosities compared to fused silica. The combination of organic
groupings with ceramics can take place via various routes, e. g.
mechanical mixing, infiltration and chemical synthesis as indi-
cated in figure 1. Mechanical processes are the most common and
most economical processes, but the chemical routes offer new and
interesting perspectives. Linking organic units to inorganic
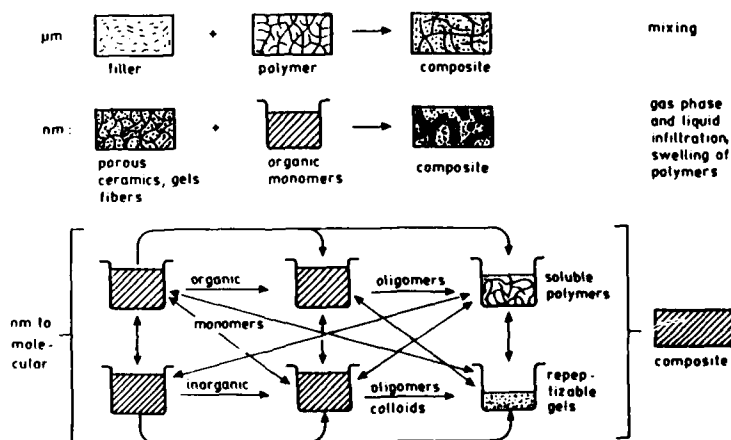
Figure 1. Routes to inorganic organic composites.

ones provides the possibility of controlling the size scale of
inorganic and organic domains in the final product but also to
keep them on the liquid-liquid mixing level (molecular or oli-
gomer). Therefore, crosslinking and phase separation mechanisms
have to be controlled. The simplest way to prevent separation of
inorganic from organic units is to have them attached together
by chemical bonds, for example in precursors like substituted
alkoxy silanes, with appropriate functional groupings, alkoxides
with complex formers or salts of organic acids (figure 2).

≡Me–C≡	Me = Si, Sn, Ge ...	σ bond
≡Me–O–C≡	Me = Si, ...	σ bond
≡Me⁺⁻OCO–C≡	Me = Al, Zr, Ti, ...	ionic bond
≡Me ←L–C–	Me = Al, Zr, Ti, Cu, Pt ...	coordination bond

Figure 2. Chemical links between
organic and inorganic units.

Then, the inorganic crosslinking reaction can take place by
hydrolysis and condensation of the alkoxy group via a typical
sol-gel reaction (equation 3). The properties of the reaction

$$RMe(OR)_3 \rightarrow RMe(OH)_3 \rightarrow \quad \overset{R}{-Me}-O-\overset{R}{Me}-O-\overset{R}{Me}-O- \quad (3)$$
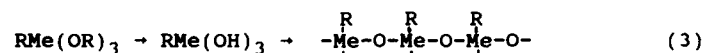
product depend strongly on the type and the number of R per in-
organic unit. In silicones, RSi≡ and $R_2Si=$ units are used [3].

The ≡Si–C≡ bond can be used as a general link between the
inorganic and the organic side. For R corresponding to a non-
reactive organic group, a pure organic network modification
results. This principle is used for spin-on glasses [4] which
can be densified at temperatures as low as 200 - 300 °C, com-
pared to 800 - 900 °C of sol-gel silica and applied in thick-
nesses of more than 20 μm. This type of material represents the
group of organically network modified glasses and ceramics.

For R corresponding to a functional organic group, chemical
functions can be introduced into these networks, leading to spe-
cial properties like adsorptive properties [5], reactive sur-
faces to special molecules [6] or sensors [7]. This group repre-
sents the type of organofunctional modified glasses or ceramics.
Functional groups which are able to be polymerized lead to the
additional organic chains within the inorganic network and to
hybrid polymers (inorganic-organic polymers), equation (4). This
principle can be varied by incorporation of organic monomers as
indicated in equation (5).

The construction principles shown above are all character-
ized by a chemical bond between the inorganic network and the
organic group. A lack of this bond leads to two independent or
interpenetrating networks. In opposition to the "chemically
linked" case, the possibility of separation of the "organic"
from the "inorganic" phase exists, leading to a composit type
of material, as indicated in figure 1. Examples, therefore, are
given by Mark and Wilkes [8-9] and [10]. These inorganic-organic
phase separated materials show a drastic change in mechanical
properties compared to the original organic polymer (e. g. in-
crease of tensile strength and modulus of elasticity).

$CH_2=CH-Si-CH_3$ $CH_2=CH-Si-CH_3$

(4)

$CH_2=CH-Si-CH_2-CH_2-CH_2-Si-CH_3$

alkene   R—

methacrylate   —COOC$_3$H$_6$Si

R—

polymerisation

SiC$_3$H$_6$OOC—

—R

—R

R—

R—

—COOC$_3$H$_6$Si

R—

SiC$_3$H$_6$OOC—

—R

—R

polyethylen chain

(5)

— = • CH=C(Me)—

R = e.g. COOMe

COOCH$_2$CHCH$_2$-O—
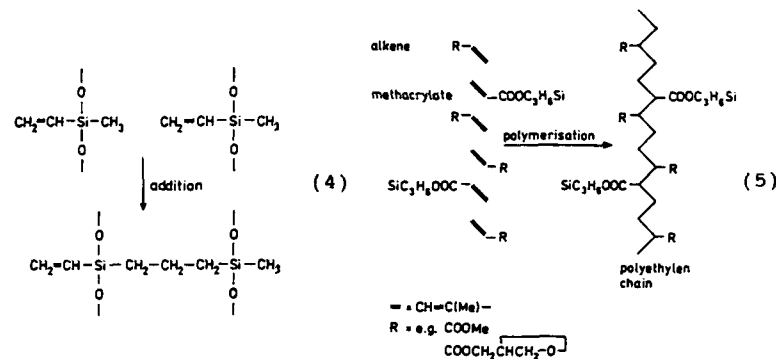
ASPECTS OF PROPERTIES

General aspects

As indicated above, the introduction of organic groupings into an inorganic network leads to structural variations. On the average a decrease of the network connectivity number decreases Tg and increases the thermal expansion coefficient (TCE) α. Figure 3 shows Tg and α as a function of different "organic-inorganic" bonds ≡Me-R (x) per total number of inorganic groupings. There is a clear tendency showing that for these properties x is the dominating parameter.
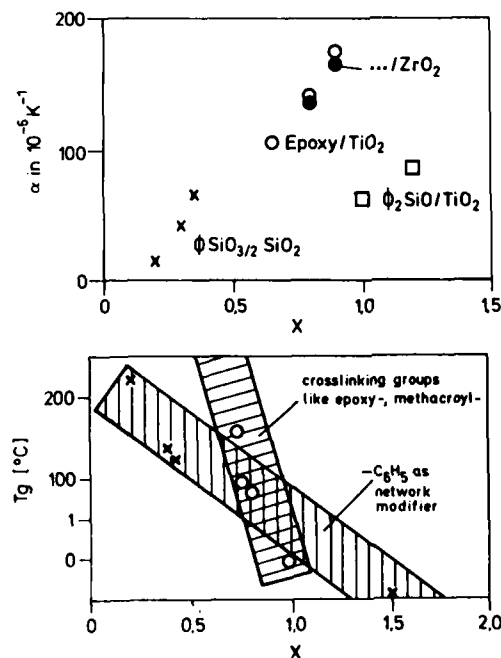
Figure 3. α and Tg depending on x.

$$x = \frac{≡Me-X}{≡Me-O-}$$

The influence of the type of the organic group does not seem to play the most important role, but a tendency to a steeper slope of the Tg function with increasing concentration of cross-linking organic units (figure 3) is observed; for x = < 0.7 no Tg values could be measured below decomposition, probably due to the increasing immobilization of the organic group within the inorganic network.

The densities (compared to the pure inorganic materials) decrease drastically as a result of the organic modification. As pointed out in [11], the computed densities (between 2 and 3 g/cm^3) differ from the measured ones remarkably which are between 1.35 and 1.65 g/cm^3. This indicates the existence of a free volume similar to organic polymers [12]. In [13] neutron scattering experiments show that the glass transition can be correlated with the chain movement, supporting the hypothesis of a free volume based low density. The investigations were carried out with amino modified SiO$_2$ condensates.

Homogeneity is an important property if optical applications are of interest. In a single component system without intergranular interfaces optical transparency should be obtained easily. Organic polymers, however, tend to form crystalline phases thus disturbing optical transparency. This can also be induced by ageing, thermal or mechanical stresses and leads to the question of structural stability. Basically, a three-dimensional inorganic network should be stable and no structural rearrangement should be possible after sufficient curing. For the preparation of sol-gel derived multicomponent systems one has to take into consideration phase separation effects based on different rates of reactions of the precursors, e. g. Ti and Si alkoxides. Adaption of rates is limited and cannot successfully be used to enable a simple addition of water to a mixture of Ti(OEt)$_4$ and (CH$_3$O)$_3$Si-CH$_2$-CH$_2$-O-CH$_2$-CH-CH$_2$-O (Si-epoxy): If water is added, TiO$_2$ precipitates. Controlled release systems for water in order to avoid high concentration, accompanied by heavy stirring leads to a partial hydrolysis of the fast reacting components and to a condensation via the alkoxide substitution (6).

$$Ti(OEt)_4 \xrightarrow{\text{x's } H_2O} Ti(OH)_4 \rightarrow TiO_2 \cdot H_2O$$

$$Ti(OEt)_4 \xrightarrow[\text{of water}]{\text{slow release}} (RO)_3TiOH \tag{6}$$

$$\text{■MeOR} + HOTi(OR)_3 \rightarrow \text{■MeOTi(OR)}_3$$
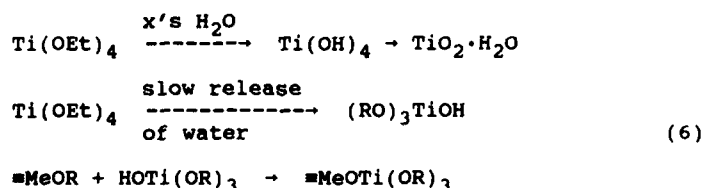
This is in accordance with Livage's electronegativity driven reaction scheme [14]. In a composition (molar ratio) of about 30 Ti(OEt)$_4$, 65 Si-epoxy and 5 Si(OEt)$_4$, the addition of only 1/16 of the total amount of water is necessary to be added by a controlled release process (CCC according to [15] or H$_2$O doped silica) to prevent precipitation after addition of the full amount. The reaction scheme is shown in figure 4. The hydrolysis rates increase in the order Si(OEt)$_4$ < Si-epoxy < Ti(OEt)$_4$. The preparation leads to a homogeneous liquid with a general structure proposed in figure 4 which can be used for coatings [16].

The material does not show any phase separation down to 1 nm (resolution of the TEM).

R' Si(OR)$_3$ + Ti(OR)$_4$ + H$_2$O $\xrightarrow{-OHR}$ R' Si(OR)$_3$ + HO Ti(OR)$_3$

R' Si(OR)$_3$ + HO Ti(OR)$_3$ $\xrightarrow{-OHR}$ R' Si(OR)$_2$

$\overset{|}{O}$-Ti(OR)$_3$

kinetics (IR): K$_H$ Ti(OR)$_4$ $\gg$ K$_H$ R' Si(OR)$_3$ > K$_H$ Si(OR)$_4$
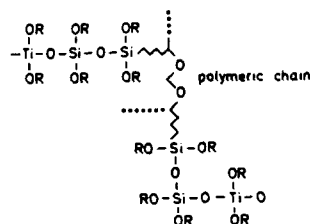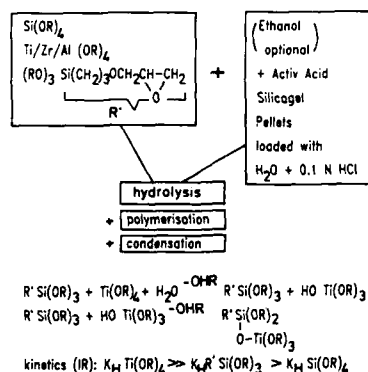
Figure 4. Reaction scheme for the preparation of Ti containing hard coatings.

Similar techniques can be used for combinations with other alkoxides like Al(OR)$_3$, Zr(OR)$_4$ or Sn(OR)$_4$. This demonstrates that homogeneous multicomponent materials can be prepared by an appropriate chemical processing.

Structural properties and aspects

One of the most interesting properties of these groups of compositions is the abrasion resistance if used as coatings [16]. Haze measurements after taber abrader tests show values close to those of float glass surfaces. The moduli of elasticity are between 1 and 7 GPa, that means remarkably lower than those of glass and ceramics. However, the low moduli are an important prerequirement for coating organic polymer surfaces. First, the lower modulus can help to overcome stresses resulting from TCE differences between substrate and coating (high CTE of the coating materials according to figure 3 is helpful, too). Second, for practical use, coating thicknesses for abrasion resistance have to be in the range of ≥ 5 μm, a thickness which can be achieved for densified inorganic sol-gel coatings only by a multiple coating process and which leads to cracks caused by stresses due to the CTE mismatch dependent on the preparation technique. As a consequence, there are no pure inorganic thick protective coatings on soft plastics available. The comparison of the behavior of ORMOCER coatings on ceramic coatings is schematically illustrated in figure 5.

The modulus is very sensitive to the concentration of inorganic units and to the type of inorganic network formers and increases in the order Zr < Ti < Al. The abrasion resistance corresponds to this order. Based on these findings, various scratch resistant systems have been developed, as described in [16-17], for example for CR 39, polycarbonates, PC, PMMA, but also for metals, like brass.

inorganic, brittle coating   E = 50 GPa

organically modified flexible coating   E = 5 GPa

polymer substrate

polymer substrate

crack formation by indentation

polymer substrate

polymer substrate

crack formation by CTE mismatch based stresses
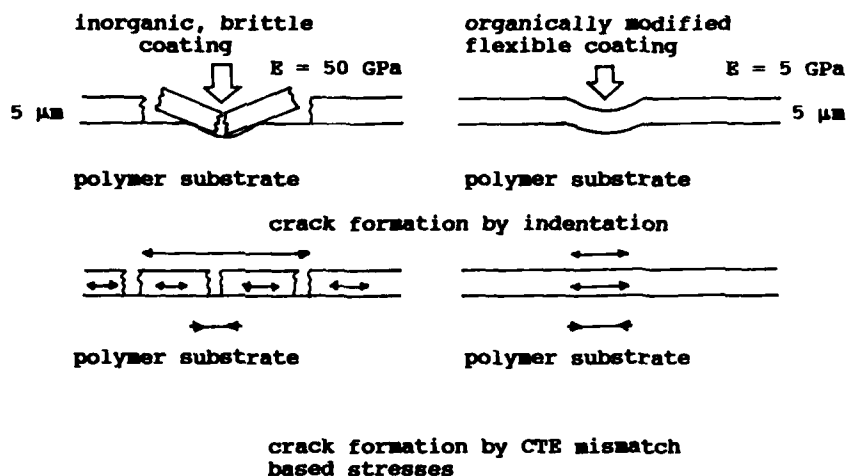
Figure 5. General behaviour of low and high moduli coatings on plastics.

Other mechanical properties like bending strength depend, as expected, very much on the degree of organic crosslinking. In table I, the results of 3-point bending experiments are given.

Table I. 3-point bending experiments on various polymers.

Type	Curing	σ_B(MPa)
A SiO_2/Si-epoxy/ TiO_2	thermal (130 °C)	3
B SiO_2/Si-epoxy Si methacryl/TiO_2*	thermal (130 °C) + photo	4 - 5
C SiO_2/Si-epoxy/Si-methacryl/TiO_2 MMA*	thermal (130 °C) + photo	8 - 9
D SiO_2/$(C_6H_5)_2SiO$/ $CH_3(CH_2=CH)SiO$**	thermal (200 °C) + photo + thermal (130 °C)	30
E ZrO_2 (methacrylic acid (MA) Si-methacryl***	photo + thermal (100 - 150 °C)	80 - 90

* according to [18]   ** according to [2]
*** complexation of $Zr[o\text{-}prop]_4$ with methacrylic acid (1:1) and subsequent hydrolysis and condensation by photocuring with Irgacure 184 (Ciba Geigy) [19]

In composition A the epoxy is reacted to a glycol group that means no organic crosslinking takes place. The materials are brittle, they are cured in polypropylene moulds, the surface quality of which is defining the number and size of surface flaws (influence of flaws on strength has not been investigated). The number of organic crosslinking units increases from A to E, but all materials are brittle with negligible plastic deformation. According to this data, a clear connection between strength and organic crosslinking exists. The first results obtained from methacrylic acid condensates show bending strength values, already suitable for structural applications, even if the systems are not optimized so far.

Another example for property changes is the building up of inorganic networks within already formed organic polymers, for example ethylvinyl acetate copolymer (EVA) according to [10] where the extremely low EVA modulus increases to about 5 GPa by addition of 50 wt.% $Ti(OEt)_4$ to the polymer solution in toluene. Depending on the route of addition of water, phase separated (figure 6a; H_2O is added rapidly via atmosphere) or non-phase separated polymers (figure 6b, H_2O is added via a controlled chemical condensation process [16]; phase separation not visible within the resolution of the instrument $\approx$ 2 nm).
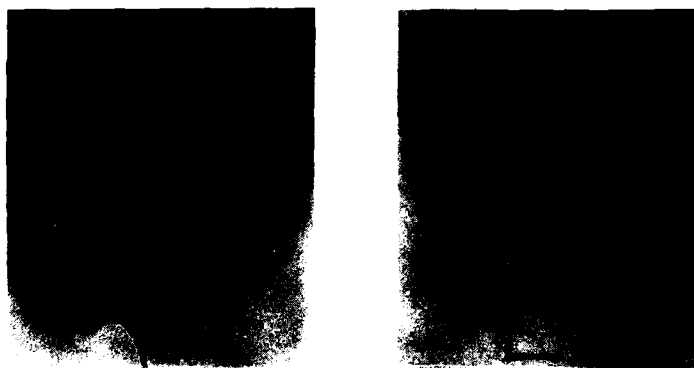
Figure 6a and 6b. TEM of a TiO_2/EVA copolymer. 6a: phase separation about 100 nm; 6b: no phase separation or separation $\leq$ 2 nm; bar: 100 nm.

Functional properties

Despite the fact that the investigation of structural properties of ORMOCERs (except abrasion resistance) is at its beginning, the question arises whether they can be combined with functional properties. Developments of special functional properties have already been published elsewhere. Table II gives a survey over various developments.

As one can see from these examples, the introduction of func-
tions into ORMOCERs can lead to interesting properties and
potentials for applications.

Table II. Development of functional ORMOCERs
and corresponding organofunctional groups.

Property	Application	Chemical Function	Reference
hydropho-bicity	contact lenses	epoxy to glycol	[18]
reactive surfaces	carrier for enzymes radioimmunoassay	$\sim NH_2$, $\sim COOH$	[20]
adsorption of CO_2	heat pump	$-CH_3$, $\sim NH_2$	[5]
SO_2 adsorption	SO_2 gas sensor	$\sim NR_2$	[7, 21]
mild abrasion	acne ointment	$(CH_3)_2SiO/SiO_2$	[23]
adhesion to glass sur-faces	protective coat-ings on medieval glasses; sealing agent	$(C_6H_5)_2Si\langle^{O-}_{OH}$ $\equiv SiOR$	[24-25]
NIR absorp-tion	solar protection	V^{4+}	[26]
H^+ conducti-vity	solid state electrolytes	$\sim NH_3^+X^-$	[27-28]
low ϵ, high resistance	dielectric materials	SiO_2, hydro-carbons	[29]
low hydrocar-bon diffusion	gas tanks	$\equiv Si-O-$ $-Al\langle^{O-}$	[29]
micro pat-terns by pho-tolithography	SMT technologies, laser writing, resists	$\equiv Si$-methacryl $\equiv Si$-vinyl $\equiv Si$-epoxy	[30]
fluorescent coatings	solar collectors	fluorescent organic dyes	[31]
thermo-plasticity	hot melts	$(C_6H_5)_2SiO$	[32]
refractive index	optical coatings	Ti, Zr, aryl	[33]

CONCLUSIONS

The combination of functional with structural properties in most
cases can be achieved and functions can be transferred to hard
coatings. Of special interest is the question, how far these
materials are able to play an important role for key technolo-
gies. Their ability of being patterned is important for micro-
electronics or microsystems, especially in combination with
other properties like sensor properties, low or high dielectric
constants, low H_2O diffusion or temperature stability. There-
fore, the knowledge of structure to property relations has to be
improved. The high homogeneity shows an interesting potential
for optical applications, especially in combination with other
functions like dye incorporation. The properties of nanocompo-
sites based on ORMOCERs are hardly investigated up to now des-
pite the possibility to tailor such composites by controlled
phase separation.

REFERENCES

[1] H. Schmidt, H. Scholze, G. Tünker: J. Non-Cryst. Solids 80
     (1986) 557.

[2] H. Schmidt, G. Philipp, H. Patzelt, H. Scholze: Collected
     Papers, XIV. Intl. Congress on Glass, Vol. II, 1986, 429.

[3] W. Noll: Chemie und Technologie der Silicone. 2. Aufl.,
     Weinheim. Verlag Chemie 1968.

[4] B. G. Bagley, W. E. Quinn, P. Barboux, S. A. Khan, J. M.
     Tarascon: In: Proceedings Fifth International Workshop on
     Glasses and Ceramics from Gels. August 1989, Rio/Brazil.
     J. Non-Cryst. Solids (in print).

[5] H. Schmidt, J. Strutz, H. G. Gerritsen, H. Mühlmann: DP
     35 18 738, 24.05.85.

[6] H. Schmidt, O. von Stetten, G. Kellermann, H. Patzelt, W.
     Naegele: IAEA-SM-259/67, Wien 1982, 111.

[7] F. Hutter, K. H. Haas, H. Schmidt: In: Proceedings of the
     Second International Meeting on Chemical Sensors. Eds.:
     J.-L. Aucouturier et al., Bordeaux, July 1986, 443.

[8] J. E. Mark: In: Ultrastructure Processing of Advanced Cera-
     mics. Eds.: J. D. Mackenzie, D. R. Ulrich. John Wiley &
     Sons, New York, 1988, 623.

[9] G. L. Wilkes, B. Orler, H. H. Huang, Polym. Prepr. 26 (1985)
     300.

[10] H. Schmidt: ACS Symposium Series No. 360 (1988) 333.

[11] H. Schmidt: J. Non-Cryst. Solids 112 (1989) 419.

[12] H. Scholze, P. Strehlow: Wiss. Ztschr. Friedrich-Schiller-
     Univ. Jena, Naturwiss. R. 36 (1987) 753.

[13] Y. Charbouillot: Ph.D. thesis. Institut National Polytechnique, Grenoble, 1987.

[14] J. Livage, M. Henry: In: Ultrastructure Processing of Advanced Ceramics. Eds.: J. D. Mackenzie, D. R. Ulrich. John Wiley & Sons, New York, 1988, 183.

[15] H. Schmidt, B. Seiferling: Mat. Res. Soc. Symp. Proc. 73 (1986) 739.

[16] H. Schmidt, B. Seiferling, G. Philipp, K. Deichmann: In: Ultrastructure Processing of Advanced Ceramics; Eds.: J. D. Mackenzie, D. R. Ulrich. John Wiley & Sons, New York 1988, 651.

[17] H. Schmidt, H. Wolter: In: Proceedings Fifth International Workshop on Glasses and Ceramics from Gels, August 1989, Rio/Brasilien. J. Non-Cryst. Solids (in print).

[18] G. Philipp, H. Schmidt: J. Non-Cryst. Solids 63 (1984) 283.

[19] E. Arpac, R. Naß, H. Schmidt: to be published separately.

[20] A. Kaiser, H. Schmidt, H. Hasenfratz-Schreier, K. D. Kulbe: Chem.-Ing.-Tech. 56 (1984) 653.

[21] K. H. Haas, F. Hutter, H. Schmidt: In: Proceedings of the International Conference on Materials with Exceptional Properties, EXPERMAT 87. Bordeaux, 1987.

[22] H. Schmidt, A. Kaiser, H. Patzelt, H. Scholze: J. Phys. 43 (1982), Coll. C9, Suppl. 12, 275.

[23] G. Tünker, H. Patzelt, H. Schmidt, H. Scholze: Glastech. Ber. 59 (1986) 272.

[24] F. Hutter, H. Schmidt, H. Scholze: J. Non-Cryst. Solids 82 (1986) 373.

[25] D. Ravaine, A. Seminel, Y. Charbouillot, M. Vincens: J. Non-Cryst. Solids 82 (1986) 210.

[26] F. Rousseau, M. Popall, H. Schmidt, C. Poinsignon, M. Armand: In: Proceedings Second International Symposium on Polymer Electrolytes. Juni 1989, Siena/Italien. Elsevier Applied Science Publishers Ltd., UK (in print).

[27] H. Schmidt, M. Popall, J. Schulz: In: Proceedings of the Second International Symposium on New Glass, Tokyo, November 1989 (in print).

[28] K.-H. Haas, H. Schmidt, H. Roggendorf: In: Proceedings of the Topical Meeting on Glasses for Optoelectronics, Tokyo, December 1989 (in print).

[29] B. Lintner, N. Arfsten, H. Dislich, H. Schmidt, G. Philipp, B. Seiferling: J. Non-Cryst. Solids 100 (1988) 378.

THE SYNTHESIS, STRUCTURE AND PROPERTY BEHAVIOR OF INORGANIC-ORGANIC HYBRID NETWORK MATERIALS PREPARED BY THE SOL GEL PROCESS

G.L. WILKES, A.B. BRENNAN, HAO-HSIN HUANG, DAVID RODRIGUES AND BING WANG
Dept. of Chemical Engineering. Polymer Materials & Interfaces Laboratory,
Virginia Polytechnic Institute & State University, Blacksburg, VA 24061

ABSTRACT

The synthesis, structure/property behavior of inorganic-organic hybrid network materials prepared by the sol gel process have been chronologically reviewed with emphasis on those systems prepared in the authors laboratory. Specific features of reactions as well as the nature of reactants are included. The morphological features of these "ceramer" systems formed have many features in common even though the reactants may be quite different. The mechanical properties of the final materials in conjunction with SAXS have proven beneficial in establishing the basics of their morphological texture. Finally, it is demonstrated how microwave radiation in some cases, can serve as an efficient way in processing the ceramer systems.

INTRODUCTION

In 1985 work was initiated within our laboratories with the objective being to develop novel organic-inorganic hybrid network materials by reacting metal alkoxides with functionalized polymeric/oligomeric species by the sol gel process [1]. This paper addresses this topic with emphasis on work from our laboratory but also will touch upon related work of others. Since the authors will principally address their research, omissions to the other workers has not been by design but is due to space limitations.

The classic sol gel reaction generally involves both the hydrolysis and condensation of metal alkoxides. Generally, these two reactions occur simultaneously once the hydrolysis step has been initiated. The reaction rates of each are highly dependent upon such variables as the temperature, pressure, local pH, nature of the metal alkoxide and the environment in which the reaction takes place (e.g. concentration of water, alcohols and other solvent media components utilized). Of course, the condensation step generally lead to loss of a water molecule while each hydrolysis step leads to the production of an alcohol component - both of these features contribute to the high shrinkage that occurs during the sol-gel process. However, there is still much more information needed to understand the classical sol gel reactions. Our goal, however, has not been to focus on these features as much as to <u>utilize</u> the sol gel reactions of metal alkoxides as a means of developing new materials by the <u>incorporation of appropriately functionalized organic oligomeric/polymeric components</u>. Restated, the goal has been to incorporate both inorganic and organic based materials into a single network system that may possess properties that are either unique and/or somewhat intermediate between those of the pure organic and pure inorganic networks. They might also allow control of a wide range of refractive index values and at the same time the material may still retain flexibility. Such flexibility would be in contrast to the more brittle nature common to the alkoxide networks. These hybrids might allow new "window" materials to be developed for specific regions of the electromagnetic spectrum. Furthermore, their mechanical and dielectric behavior may suggest their potential for coatings, encapsulants, etc. for commercial applications. Indeed, within this paper, controlling the optical property of refractive index will be

illustrated as a means of showing the novelty of our hybrid network materials.

The majority of our efforts in this field has emphasized the oligomeric/polymeric species as the dominant component within the final network material. Hence, the materials tend to be flexible. We have termed such materials "ceramers" to imply some combination of ceramic like behavior with that of polymeric behavior. However, it is recognized the firing of such materials would lead to the destruction of the organic component and thus destroy the original network. Yet, high temperature treatment of these materials could potentially lead to novel materials in terms of controlled porosity. These materials might be suitable for chromatographic supports, catalyst supports, etc. However, our goal has been not to utilize high temperature treatments of the final system but rather to investigate the initial hybrid network.

Other researchers, in particular Schmidt, have reported studies on related materials. Schmidt and coworkers have developed hybrid systems which they termed "ormosils" for organically modified silicates [2]. Their studies have emphasized the use of tetraethylorthosilicate (TEOS) and related silicon based alkoxides. The ormosils, in general, arc based on the incorporation of much lower molecular weight, functionalized organics for purposes of modifying the more alkoxide dominated systems. This is in contrast with the work that will be reviewed principally in this paper. Mark, et al. have also developed hybrid inorganic/organic systems, but their approach in general has been the base catalyzed formation of small particulate "in situ" inorganic fillers within a polydimethylsiloxane network dominated matrix [3].

Some Structural Features of the Ceramer Systems

The initial ceramers that we prepared utilized silanol terminated polydimethylsiloxane (PDMS) oligomers which were of functionality two. They were incorporated into a silicate network by condensation of their terminal groups with the silicic acid species from hydrolyzed TEOS. These reactions were acid catalyzed to promote more chainlike inorganic structures as reported by Schaefer, et al. [4]. The effect of acid level, acid type, water content and oligomer molecular weight were investigated for their effect on the morphology and general structure property behavior. As reported elsewhere [1,5,6], the final materials in multi-mil film form (i.e. typically 5 to 20 mils thick) showed flexibility and optical transparency. However, brittleness occurred if only a small amount of the PDMS component was utilized. While these materials did demonstrate our ability to prepare hybrid networks, they did not display high tensile strength or elongation which was attributed to some loose or dangling chain ends. Dangling chain ends, which may result from lack of incorporation of the silanol endcapped PDMS, would promote network defects. These network defects and the generally poorer mechanical properties of PDMS would contribute to lower tensile strength. In order to promote better mechanical properties in terms of strain to break and tensile strength, we utilized hydroxyl terminated poly(tetramethylene oxide) (PTMO), another flexible, functionalized oligomer. The PTMO was further functionalized by reacting the terminal hydroxyl group with isocyanatopropyltriethoxysilane which leads to a reactive oligomer of functionality six. The molecular weight of these oligomers was varied from 650 to 2900 g/mol and reacted with TEOS to produce transparent flexible materials. The moduli (stiffness) of these materials was found to be dependent on the oligomer molecular weight as well as the composition ratio of alkoxide to PTMO. The high transparency, along with recognition of the large difference in refractive index between the two components clearly illustrated that no major macro phase separation

occurred. However, on a very localized scale, i.e., ca. 10 nm, a variation in composition was developed as noted by small angle x-ray scattering (SAXS) [7,8,9,10]. The general morphological model that was developed based on this work is schematically given in Fig. 1. The reader should recognize that a variation in the level of phase mixing can occur
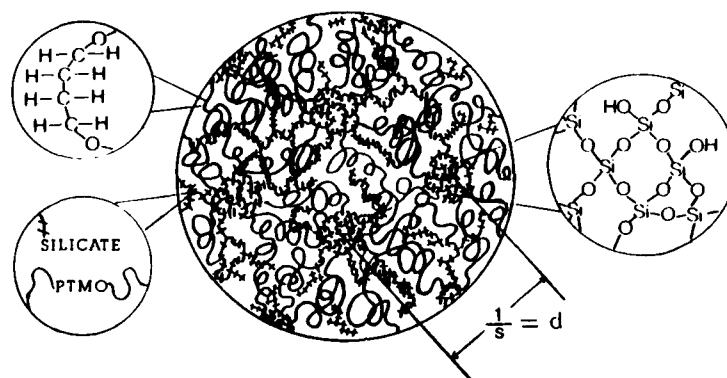
Fig. 1. Schematic showing general morphology of a ceramer on a molecular level - see text for details.

depending on the relative compatibility of the reacting components as well as the specifics of the reaction conditions. The basis for the model in Fig. 1 extends from the observation that the SAXS behavior typically illustrated a single shoulder or peak with an estimated correlation distance of ca. 10 nm. However, this distance has varied somewhat depending upon oligomer molecular weight, composition ratios, etc. [7,8,9,11,12,13,14,18]. Furthermore, the high angular tail of the scattering curve also generally suggested that some level of mixing of the inorganic occurs within the oligomeric phase thereby broadening the scattering profile. This same conclusion regarding partial phase mixing was also based on the many dynamic mechanical spectra (DMS) that have been gathered on the PTMO/TEOS hybrids as well as other ceramers that will be discussed.

In these earlier studies, we noted that the level of reaction may be influenced by diffusion control following vitrification which limits mechanical properties. However, if the gels that had been cast under ambient conditions were heated to a higher temperature, the extent of reaction was increased. In some cases, this post gelation treatment put elongation to break through a maximum while tensile strength tended to be enhanced [19,20]. Depending upon the general glass transition behavior of the functionalized oligomeric species, the importance of diffusion control reactivity was also more or less enhanced as would be anticipated. This suggested that higher temperature glass transition oligomers would need to be processed into ceramer networks above their respective glass transition values accordingly. A good example of this latter situation has been demonstrated by our studies of triethoxysilane capped poly(ether ketone)

(PEK) oligomers of ca. 3500 grams per mole [18]. These species were compatible within a reacting mixture of TEOS up to reasonably high levels, but gelation and vitrification occurred at low extents of reaction due to the higher glass transition behavior of the PEK component (Tg ca. 180°C). Thus, the final network solids needed to be post-cured above 200°C to make strong transparent films.

Following the studies just described, our efforts began to focus on the incorporation of other metal alkoxides in conjunction with TEOS. Titanium (IV) tetraisopropoxide (Ti(OPr)) was a principal alkoxide since this species promotes a higher refractive index network. However, due to the much higher hydrolysis and condensation rates of the Ti(OPr) one cannot add water directly to the reaction system. Thus, a new reaction scheme was established by modifying Schmidt's procedure denoted as controlled chemical condensation [21]. Our modification of this procedure has been discussed elsewhere [8,20]. It was successful in promoting transparent multi-mil films of the two mixed metal alkoxides with a variety of functionalized PTMO or triethoxysilane capped poly(dimethylsiloxane) oligomers. In all cases, an acidic environment was utilized for purposes of minimizing any particulate growth of the inorganic component. It was also noted that any time the titanium reactant was used, the modulus of a given system was higher following network formation. This suggested that this reactant served to catalyze the reaction to a higher level of conversion. Thus the final product developed a higher network density and higher modulus accordingly as denoted by DMS [8,20]. Further proof of this speculation came from the fact that post curing caused less change in properties again indicating that a higher extent of reaction had occurred.

The morphological features of these mixed alkoxide systems also seemed to be rather similar to those discussed earlier. Their SAXS behavior suggested that the general schematic model given previously in Fig. 1 was still valid as a simplified description of these systems. However, the inorganic regions would now likely contain both alkoxide moieties.

Recent Ceramer Systems and Their Structure-Property Features

Turning to some of our more recent studies (hence more details will be provided) we have been successful in directly incorporating aluminum alkoxides or titanium alkoxide with functionalized oligomers but without any TEOS. Our first success in this endeavor was to utilize a bidentate chelating agent - that of ethyl acetoacetate (EACAC). EACAC promoted a stable sol when reacted with the alkoxides of aluminum secondary butoxide or Ti(OPr). This sol could be reacted later with additional alkoxide and functionalized oligomer leading to transparent multi-mil films of these EACAC modified ceramers. One disadvantage found was noted specifically for the alumina based materials. They illustrated that on the order of 15 weight percent could be extracted from the final network. The extractable by-products were speculated to be based on a cyclic species from the self condensation of the EACAC component [23]. Yet, the Ti(OPr)/EACAC based ceramers showed only a very small percentage (1-2 wt. %) of extractables.

SAXS analysis of the latter ceramer systems again illustrated that a single correlation distance existed on the order of 10 nm. Therefore, the morphological features were somewhat similar to what was illustrated earlier in Fig. 1. DMS data and stress strain response provided general support of this same model. [Later within this paper, another newer route for preparing the more highly reacted metal alkoxides into ceramer systems but without the chelating agent will be discussed.

On a somewhat different subject, we have recently demonstrated that a polymeric catalyst can be effectively utilized to promote reactivity in

the ceramer systems. This approach is in contrast to the general classic sol gel reactions that utilize low molecular weight acidic or basic catalysts such as hydrochloric acid (HCl) or an organic amine respectively [24]. In fact, our newer approach should also function for the classic sol gel reactions where no additional oligomer is added. Basically, our goal was to illustrate that the use of a higher molecular weight polymeric catalyst, (e.g., polystyrene sulfonic acid (PSS)) would not greatly change the final materials compared to those prepared by a lower molecular weight catalyst as HCl. Also, with the polymeric species present, the viscosity would be enhanced more quickly which therefore would influence the rheological behavior of this system - a feature of importance in coating or spinning operations. Indeed, shown in Fig. 2 are the DMS obtained on a TEOS-PTMO system where the initial weight fraction of the TEOS component and the 2000 g/mol molecular weight functionalized PTMO were each 50 weight percent [11,15]. One hundred percent of the stoichiometric amount of water required for the hydrolysis of the alkoxide groups was utilized. A constant equivalence of acid of both the PSS as well as the HCl was
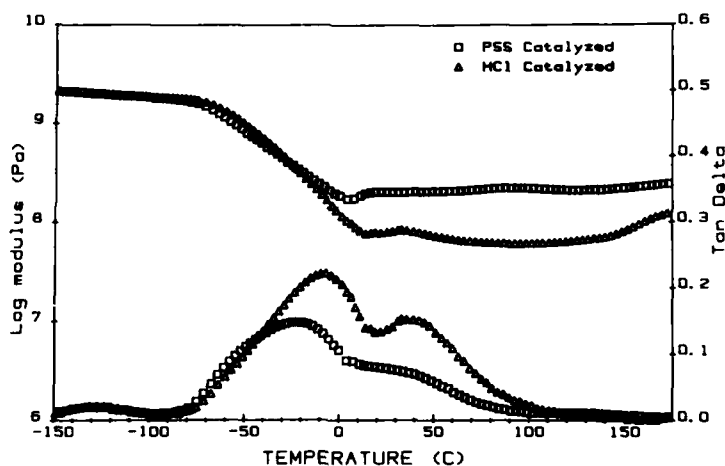
Fig. 2.   Storage modulus and tan δ behavior (at a frequency of 11 Hz) illustrating a higher extent of reaction in TEOS/PTMO ceramers catalyzed with PSS vs. HCl.

maintained at 0.0143 eq. The PSS polymer was of 70,000 g/mol molecular weight and was fully functionalized into the acid form as was determined by end point titration. The resulting DMS of the ceramers in Fig. 2 indicated that there is some difference between the two catalyzed materials. Above Tg, the modulus of the PSS system is higher relative to the HCl catalyzed system. Certainly this suggests a higher level of network formation. In addition, the tan δ response is of a bimodal nature for both materials with nearly equivalent breadth of the combined dispersions. As discussed elsewhere [15], the higher modulus in conjunction with the somewhat lower tan δ response for the PSS catalyzed system has been attributed to the "tightening" of the network promoted

from the condensation of the TEOS that is partially mixed within the PTMO phase. This restricts the PTMO mobility and decreases the tan δ response accordingly. However, since the thermal breadth of the dispersion for both samples is nearly the same, i.e., -75°C to +100°C, the general features of the morphological character were speculated to be the same although the extent of curing is different. Further proof for this extended from Fig. 3 where the relative SAXS intensity obtained is provided and plotted against the scattering variable s where s is defined as $(2/\lambda)\sin\theta$ with λ being the wavelength utilized (1.54Å) and θ
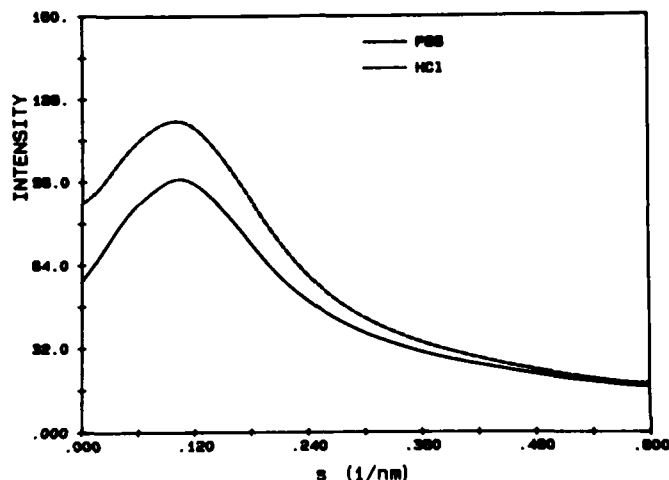
Fig. 3.   SAXS profiles demonstrating a higher scattering contrast factor for a TEOS/PTMO ceramer catalyzed with PSS versus HCl.

representing one half of the radial scattering angle. One clearly notes from Fig. 3 that both the PSS and HCl catalyzed materials display a scattering peak with the estimated correlation distance between regions of comparable electron density to be about 10 nm. (This latter result and those prior to it are based on smeared SAXS scans. Desmearing procedures however, lead to rather comparable results and therefore the general correlation distance mentioned before is still approximately correct.) One notes from these SAXS scans that the PSS material shows a higher intensity at smaller s relative to that of the HCl catalyzed system yet the high angular tail regions of each are nearly the same. Indeed, this was expected since the PSS material was believed to have a higher extent of reaction (recall Fig. 3). This in turn would also lead to a greater level of condensation of the metal alkoxide which would raise its electron density relative to PTMO. Thus, the scattered intensity would increase accordingly [15]. The overall results therefore suggested that the same morphological features exist and were similar for the two materials but that the level of network density was higher in the PSS catalyzed system. Certainly it must be recognized that the greater modulus in the PSS catalyzed material was not a consequence of the polymeric nature of the catalyst but more likely due to the difference in the reactivity features promoted by the polymeric sulfonic acid moiety in contrast to HCl. Further work is being undertaken utilizing para toluene

sulfonic acid at an equivalent acid content to investigate this point. These results will be reported in the near future.

As indicated earlier, one of our goals has been to develop higher refractive index materials by the incorporation of the high refractive index metal alkoxide Ti(OPr) but to do so without the use of a chelating agent. To achieve this goal, a reaction scheme was developed to partially react Ti(OPr) into a stable sol that could later be reacted with functionalized PTMO components. A successful procedure for doing this is shown in Scheme 1 [22]. This recipe incorporates a 2000 g/mol functionalized PTMO using the reaction conditions of ambient temperature

PREPARATION OF HYBRID WITH Ti(OPr)$_4$

5gm Ti(OPr)$_4$

SLOW ADDITION OF

$\begin{cases} \text{0.1 ml 10N HCl} \\ \text{0.6 ml WATER} \\ \text{20 ml IPA} \end{cases}$

$\begin{cases} \text{5gm PTMO(2K)} \\ + \quad \text{10ml THF} \end{cases}$

MIX FOR 5 TO 10 MIN.
CAST INTO MOLD, COVER

GEL 1 DAY, AMBIENT

DRY 2 to 3 DAYS

ANALYZE
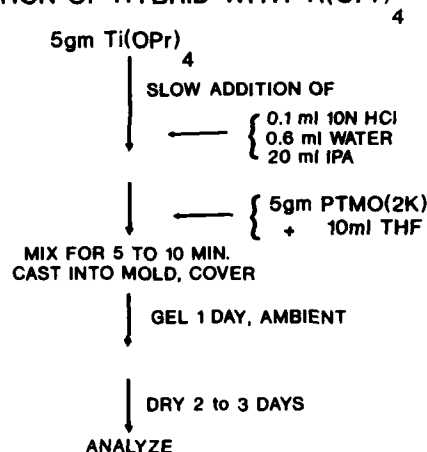
Scheme 1.   Methodology for preparation of Ti(OPr)/PTMO ceramers.

in a THF/HCl water isopropanol (IPA) media. The result of casting these materials into multi-mil films usually led to optically transparent materials. Sometimes a slight yellow color developed which is believed to be caused by the difference in oxidation states for titanium. However, the high transparency clearly indicated good dispersion of the two components. The DMS data for two such compositions are shown in Fig. 4 where the weight percentages of the Ti(OPr) are 49 and 58 percent respectively. One notes that upon raising the temperature of these materials to over 150°C, there was little sign of post curing. Again this suggested Ti(OPr) promoted a higher extent of reaction. Also noted from these data was that the Tg dispersion of the PTMO was somewhat different from the bimodal character displayed by the TEOS ceramers. In particular, while the γ transition (-125°C) was common to all materials resulting from the rotational features of the methylene groups in the PTMO chain [24], Tg of the PTMO component was clearly more narrowed than before. This transition was now initiated at approximately -80°C and passed through a minimum just above 0°C with a smaller dispersion above at higher temperatures. Also, the general temperature range over which the modulus decays to a lower level was narrower for these materials. Both of these facts together suggested less phase mixing between the two components such that the PTMO oligomer now displayed more of a Tg as would be expected of its own pure phase [19]. This is not to say that no mixing occurred for indeed if the

22
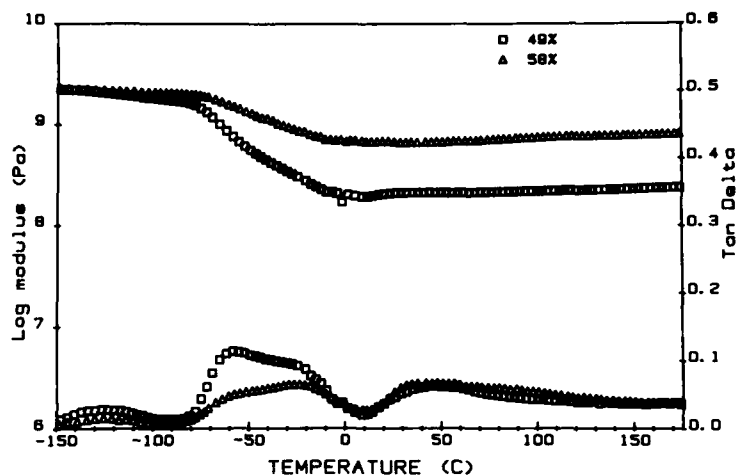
Fig. 4. Storage modulus and tan δ behavior (at a frequency of 11 Hz) for two selected Ti(OPr)/PTMO ceramers at 49 and 58 wt.% fraction of Ti(OPr).

PTMO were totally unrestricted and in pure form, one would anticipate the tan δ response to go to a minimum somewhere around -30°C at the frequency which the DMS spectrum were determined (11 Hz). Corresponding SAXS profiles of these same materials along with two additional ones are shown in Fig. 5. A single maximum was measured again whose intensity was in proportion to the amount of the Ti(OPr) species. Also, the correlation distance was the order of 10 nm. It was somewhat larger than the ceramers discussed earlier that utilized identical functionalized PTMO. We have speculated that this slight increase was due to less mixing of the titanium based species with the PTMO thereby building slightly larger inorganic domains and hence slightly increasing the correlation distance. Furthermore, analysis of the high tail region of the SAXS curves given in Fig. 5 showed there was a sharper interface in contrast to the previous samples. Again this gave support to less phase mixing as was suggested from the DMS results.

The general stress-strain response of these systems as determined at ambient at an initial elongation rate of 2 mm/min is given in Table 1. This table provides the modulus, stress at break as well as the elongation at break for ceramers of four different Ti(OPr)/PTMO contents where again the PTMO oligomer was of 2000 g/mol. As expected, the modulus and tensile strength, at ambient, increased as the content of the inorganic species was increased. The corresponding decrease in the elongation at break was due to the lower content of the elastomeric PTMO oligomer. While the data will not be shown here, we have also successfully incorporated zirconium tetraisopropoxide in a similar manner to that of the titanium alkoxide. DMS and stress strain results in conjunction with the SAXS behavior suggested that these latter systems were also quite comparable to those just discussed. Thus, there was a higher level of phase separation in these systems in contrast to the earlier TEOS/PTMO or TEOS/Ti(OPr)/PTMO comixed ceramers.
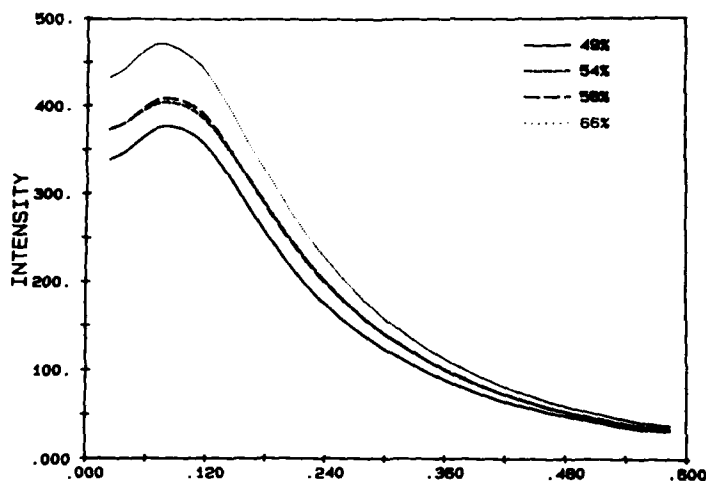
Fig. 5. SAXS profiles indicating an increasing scattering intensity with increasing weight fraction of Ti((OPr) (as shown in the figure) in selected Ti(OPr)/PTMO ceramers.

Table 1) Elastic modulus, stress at break and elongation at break for increasing weight percent (Ti(OPr) loadings in the Ti-PTMO ceramers.

Wt. Percent $[Ti(OPr)_4]$	Elastic Modulus (MPa)	Stress at Break (MPa)	Elongation at at Break (%)
X = 49%	101	19	58
X = 54%	185	20	51
X = 58%	244	23	25
X = 66%	411	34	10

As indicated above, we have been successful in directly incorporating the titanium alkoxide with functionalized PTMO into transparent monolithic systems. The materials not only displayed reasonable mechanical behavior as presented above but also provided control of optical properties as illustrated in Fig. 6. Here, the refractive index (sodium line) has been plotted against the weight percent of what is denoted as TiO_2 of the titania-PTMO material - see curve A. In this figure, the weight percent of TiO_2 was calculated using the assumption that the titanium alkoxide undergoes complete hydrolysis and condensation and therefore leads to TiO_2. This assumption is not likely perfect but appears to be reasonable. The extrapolated value of the refractive index at 100% TiO_2 achieves a value just below 1.8 as would be anticipated for the more amorphous form of TiO_2 [26]. A linear rise in the refractive index occurred as the titania content increased. In fact, the initial value of about 1.45 for pure PTMO can be raised substantially to 1.65 at about 60 weight percent of the calculated TiO_2 component. This is a significant increase of refractive index in a flexible polymer based system which shows a very strong dependence of refractive index on this particular alkoxide. No such large rise in refractive index occurred with the zirconium based alkoxide due to its lower refractive index properties (data not shown

24
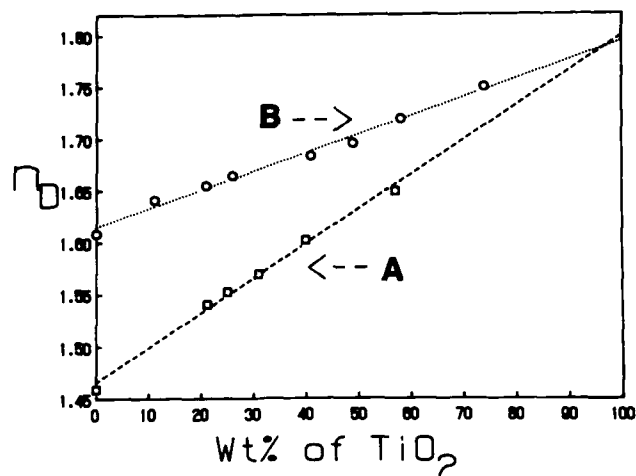
Fig. 6. Linear response of the refractive index as a function of
calculated wt. % TiO₂ for selected ceramers. A) Ti(OPr)/PTMO and
B) Ti(OPr)/PSF.

here). Clearly these results are very positive in terms of controlling
this optical property. However, it would be of interest to start with a
higher refractive index oligomer for purposes of achieving even higher
refractive index materials that might serve as optical coatings, etc. In
an attempt to achieve this goal, functionalized polyethersulfone oligomers
were prepared in a similar manner to the other triethoxysilane capped
systems. In this case, amine capped oligomers of the poly(ethersulfone)
(PSF) were reacted with isocyanatopropyltriethoxy silane. Thus a urea
linkage was formed in contrast to the urethane linkages promoted by the
end capping reactions of the hydroxyl terminated PTMO discussed earlier.
We then developed a reaction scheme between the Ti(OPr) sol and that of
the end capped PSF species using a procedure similar to Scheme 1 except
for a post curing step at 200°C. This latter step was necessary in order
to extend the reaction to a higher network density that could not be
achieved at room temperature due to limitation by vitrification caused by
the high Tg oligomeric backbone (Tg ca. 200°C). Transparent amber colored
films were prepared using this procedure that maintained good flexibility
up to reasonably high levels of titanium. At higher levels, the materials
became more brittle as expected.

An indication of the general DMS obtained on one of these materials
is shown in Fig. 7. This material which contained 25 weight percent of
the Ti(OPr) component showed the typical glassy modulus expected up to the
range of 200°C where the Tg for the PSF component was initiated. The fact
that this dispersion was quite narrow and in the temperature region
expected for a pure PSF phase, clearly indicated that good phase occurred.
Indeed this was expected due to the fact that the titanium component was
utilized. However, enhanced phase separation likely occurred because the
oligomeric molecular weight was of the order of over 7000 g/mol greater
incompatibility with the alkoxide might well be anticipated. The SAXS
data obtained for this same material as well as materials of higher
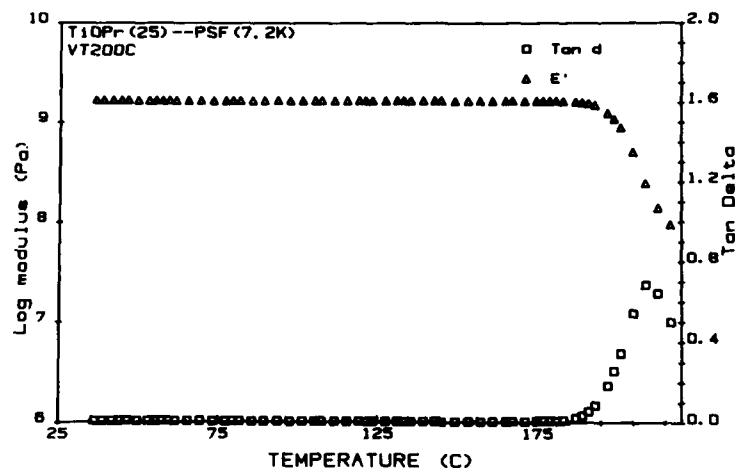
Fig. 7. Storage modulus and tan δ behavior (at a frequency of 11 Hz) for a selected Ti(OPr)/PTMO ceramer.

titanium content (data not shown here) clearly illustrated a sharper decay in scattering intensity with angle. The tail region was flatter which indicated that the phase separation was sharper. Of particular interest is to recall Fig. 6 where the refractive index for this Ti(OPr)/PSF series of materials is shown in curve B but now the line initiates at the refractive index value of the pure PSF component which is about 1.6. Indeed, PSF is one of the higher refractive index polymers known and hence one of the reasons that we selected it as the basis for developing this ceramer material. It is also of interest to note that the extrapolated value to 100% TiO_2 was in agreement with that obtained from the PTMO based systems. This suggested that the form of the TiO_2 domains were of an equivalent nature.

In the last stage of this paper some time is spent pointing out a potential way to process these systems more effectively than by the usual ambient temperature casting procedure utilized in the classic sol gel approach. As part of a much larger project in our laboratory, the use of microwaves as a means of processing polymers has been under investigation. For this reason we included our ceramer materials as one potential system in this study. The details of the instrumentation for the microwave cavity and its control in terms of power input, control, etc. are presented elsewhere [27]. Briefly, the basic instrument was a tunable, cylindrical cavity equipped with a temperature monitoring fiber optics probe in direct contact with the sample. The microwave frequency of 2.45 GHz was used. This allowed one to rapidly heat the material if its dipole character responds to this microwave frequency. Basically the power absorbed scales with the second power of the applied voltage, the first power of the frequency as well as the dissipation factor of the dielectric constant [29]. While these laws are well known, the ability of the microwave to potentially promote a higher rate of reaction due to specific interactions with the dipoles of the appropriate functionalized reacting groups may potentially lead to different reaction kinetics than would be

promoted at an equivalent bulk temperature of the system. Indeed, differences in reaction kinetics (but at the same temperature) have been demonstrated in other network forming systems e.g., epoxies, as recently reported [27]. We therefore anticipated that this same approach might be effective in promoting the sol gel reaction and the development of the ceramers in a much shorter time scale. One is limited initially in going to high reaction temperatures due to the higher volatility of the alkoxide and the solvent(s) in which the reaction is carried out. However, we found that depending on the alkoxide and choice of reacting media, it was possible to rapidly achieve gelation and almost final properties of the ceramer systems in a matter of minutes [13]. This was in contrast to the usual several days over which gelation occurs at ambient temperatures. As an example, we have studied one microwave processed system where the temperature of the reactants was ramped to 70°C in 400 seconds and then held at that temperature for 12 min. This material, prepared in that 20 minute time period, was analyzed shortly thereafter. Its general stress-strain properties (modulus, stress at break, and elongation at break) were compared with the same material that had been cast at room temperature for six days. Also a third material, prepared by processing in a simple conventional oven at 70°C for two hours, was included for comparison. Table 2 shows a major difference in the results of these

Table 2) Stress strain analysis for a TEOS-PTMO system cured in a microwave cavity (M.W.), in a conventional oven (O.C.) and at room temperature (R.T.) [12].

	Elastic Modulus (MPA)	Stress at Break (MPa)	Elongation at Break (%)
Fresh			
M.W. 70°C (20 min)	250	40	21
RT cure (6 days)	153	29	29
O.C. 70°C (2 hrs)	4	1	50
Aged (1 Month)			
M.W. 70°C	380	38	21
R.T. cure	380	40	21
O.C. 70°C	150	7	7

three experiments. In particular it is noted that the sample that had undergone the microwave treatment at 70°C (M.W. 70C) achieved a modulus nearly equivalent to a glassy polymer with a significant stress at break. The corresponding oven cured sample (O.C. 70°C) that was heat treated for two hours was a very soft material with a low stress at break and a much higher elongation at break due to poor network formation. The conventional room temperature cured material that was also not completely cured even at six days showed a slightly lower modulus and stress at break than that of the microwave prepared material. The properties of a corresponding one month aged sample of each is shown in the lower part of the table to illustrate that some additional level of curing did take place even at room temperature following the microwave treatment. One can see that the microwave treated material achieved a slightly higher modulus and the room temperature cured material also achieved this same level (given the extra time period). However, the oven cured 70°C sample never

achieved the same properties. In essence, then it was shown that microwave processing is effective in shortening the time period to reach the solid state characteristics. Although, an additional post cure at a higher temperature may be required for these systems to achieve their ultimate properties. Investigations of this nature are being actively pursued in our laboratory at this time.

Addressing the SAXS behavior of these three materials, it is of interest to inspect the results given in Fig. 8. Here one notes
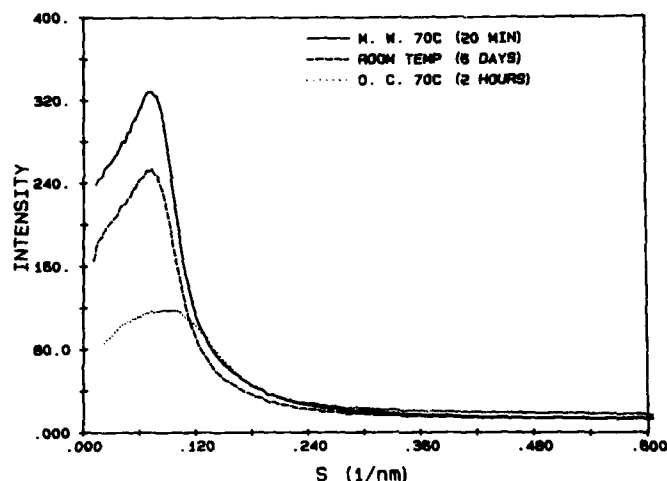
Fig. 8. SAXS profiles for selected TEOS/PTMO system prepared by different processing conditions - see text for details [13].

particularly sharp scattering peaks with a decrease to a flat tail region over the same angular range utilized in the earlier plots. There were some particular points that have been noted, the first being that the level of intensity was highest for the microwave treated sample with the room temperature material being second and the lowest level of peak intensity being for the oven cured materials. This was exactly as expected based on the level or extent of reaction being the least in the oven cured and the highest for the microwave treated systems. In the latter the electron density contrast would be higher as the extent of reaction increased. Secondly, the flat tail region that extended from using DMF as the liquid reacting media lead to a much higher level of phase separation. The cause for this higher level of phase separation in a TEOS/PTMO ceramer is unknown but we have further verified it by DMS in conjunction with SAXS and TEM analysis. Further work is proceeding on the influence of different reaction media and how it influences the microwave versus conventional casting procedures. In addition, we have prepared many of the other ceramers more rapidly by microwave processing. There were some differences between these systems and how they respond to microwaves which will be the subjects of separate publications [29].

CONCLUSIONS

This paper has attempted to review the chronological development of the ceramer materials as prepared under the direction of one of the authors (GLW). Details regarding the earlier studies were presented in brief form since numerous other publications provide many of the details. More emphasis has been given to those studies that have led to the incorporation of the more reactive metal alkoxides based on aluminum, titanium and in more limited cases zirconium. Higher refractive index flexible ceramers were made by incorporating titanium alkoxide into high refractive index functionalized oligomers such as poly(ether sulfone) or poly(ether ketone). Finally, it has been demonstrated that the use of microwave processing of the sol gel ceramer hybrids can effectively decrease the time to achieve final properties. However, it has been shown that the choice of reaction media, as well as alkoxide and oligomer, will influence the relative differences between microwave and conventional processing.

Acknowledgement

References

1. G. L. Wilkes, B. Orler and H. Huang, *Polymer Prepr.* 26(2), 300 (1985).
2. H. Schmidt, *Mate. Res. Soc. Symp. Proc.* 32, 327 (1984).
3. J. E. Mark, C. Y. Jiang and M. Y. Tang, *Macromol.*, 17, 2613 (1984).
4. D. W. Schaefer and K. D. Keefer, *Mate. Res. Soc. Symp. Proc.* 32, 1 (1984).
5. H. Huang, B. Orler and G. L. Wilkes, *Polym. Bull.* 14, 557 (1985).
6. H. Huang, B. Orler and G. L. Wilkes, *Macromolecules* 20(6), 1322 (1987).
7. H. Huang and G. L. Wilkes, *Polym. Prep.* 28(2), 244, (1987).
8. H. Huang, R. H. Glaser and G. L. Wilkes, *ACS Symposium on "Inorganic and Organometallic Polymers"*, 360, 354 (1987).
9. H. Huang and G. L. Wilkes, *Polym. Bull.* 18, 455-462 (1987).
10. H. Huang, R. H. Glaser, A. B. Brennan, D. E. Rodrigues and G. L. Wilkes, *Symposium on Ultrastructure Processing of Materials* Tucson, 1989 in press.
11. H. Huang and G. L. Wilkes, *Polym. Prep.* 30(2), 105-106 (1989).
12. B. Wang, H. H. Huang, A. B. Brennan and G. L. Wilkes, *Polym. Prepr.* 30(2), 146-147 (1989).
13. B. Wang, H. H. Huang, A. B. Brennan and G. L. Wilkes, *Polym. Prepr.* 30(2), 227-228 (1989).
14. B. Wang, A. B. Brennan, H. Huang and G. L. Wilkes, *J. Appl. Polym. Sci.* submitted.
15. A. B. Brennan and G. L. Wilkes, In preparation.
16. M. Spinu, A. B. Brennan, G. L. Wilkes and J. E McGrath, *Mat. Res. Symp. Polym. Based Mol. Comps.* (1989).
17. R. H. Glaser, G. L. Wilkes and C. E. Bronnimann, *J. Non-Cryst. Solids* submitted.
18. John Lee W. Noell, G. L. Wilkes, D. K. Mohanty, J. E. McGrath, *J. Appl. Polym. Sci.* submitted
19. H. Huang, Ph.D. Dissertation, Virginia Polytechnic Institute & State University, 1987.

20. R. H. Glaser, Ph.D. Dissertation, Virginia Polytechnic Institute & State University, 1988.
21. H. Schmidt, H. Scholze, A. Kaiser, *J. Non-Cryst. Solids* 63, 1 (1984).
22. B. Wang, A. B. Brennan, H. Huang, D. Rodrigues and G. L. Wilkes, manuscript in preparation.
23. B. Wang and G. L. Wilkes, manuscript in preparation.
24. K. D. Keefer, *Mate. Res. Soc. Symp. Proc.* 32, 15 (1984).
25. N. G. McCrum, B. E. Reed and G Williams, *Anelastic and Dielectric Effects in Polymer Solids, John Wiley & Sons*, London (1967).
26. *Handbook of Physics and Chemistry*, CRC Press, 68, B140 (1987).
27. D. A. Lewis, T. C. Ward, J. D. Summers and J. E. McGrath, *Polym. Prepr.* 29(1), 174 (1988).
28. A. C. Metaxas and R. J. Meredith, *Industrial Microwave Heating*, Peter Peregrinus Ltd., London (1988).
29. D. Rodrigues and G. L. Wilkes, manuscript in preparation.

THE CATALYTIC SYNTHESIS OF INORGANIC POLYMERS FOR HIGH TEMPERATURE APPLICATIONS AND AS CERAMIC PRECURSORS

Jeffrey A. Rahn, Richard M. Laine* and Zhi-Fan Zhang
Contribution from the Department of Materials Science and Engineering
and the Polymeric Materials Program of the Washington Technology
Center, University of Washington, Seattle, WA 98195

ABSRACT:

Polysilsesquioxanes,-$[RSi(O)_{1.5}]_x$-, exhibit many properties that are
potentially quite useful for industrial applications. These properties
include high temperature stability ($\approx$ 600°C in O_2); good adhesion and,
liquid crystal-like behavior for some derivatives. Moreover, $[MeSi(O)_{1.5}]_x$,
polymethylsilsesquioxane has been used successfully as a precursor for
the fabrication of carbon fiber/"black glass" (SiO_2/SiC/C) composites and
"black glass" fibers.

Current methods of preparation depend on hydrolysis of $RSiCl_3$ or
$RSi(OR)_3$. Unfortunately, this approach leads to several products that are
difficult to purify because polysilsesquioxanes exhibit a great propensity
for forming gels. We describe here a simple catalytic approach to the
synthesis of polymethylsilsesquioxane copolymers of the type
-$[MeRSiO]_3[MeSi(O)_{1.5}]_7$- where R = H, OMe, OEt, OnPr and OnBu. The R = H
copolymer is produced by catalytic redistribution of -$[MeHSiO]_x$-
oligomers using dimethyltitanocene, Cp_2TiMe_2 as the catalyst precursor.

Following catalytic redistribution, the resulting copolymer,
-$[MeHSiO]_3[MeSi(O)_{1.5}]_7$-, is reacted *in situ* with alcohols to produce
-$[Me(R'O)SiO]_3[MeSi(O)_{1.5}]_7$- (where R' = Me, Et, nPr and nBu) which serve
as masked forms of the polymethylsilsesquioxane. These new copolymers
have been characterized by ^{1}H, ^{13}C and ^{29}Si NMR TGA and DTA. The NMR
studies allow us to assign structures for the copolymer.

These new copolymers exhibit improved tractability. Their high
temperature properties are all quite similar; although, the MeO-, EtO- and
especially the nPrO- derivatives give much higher ceramic yields than
expected.

INTRODUCTION

Polysilsesquioxane polymers,[1] $-[RSi(O)_{1.5}]_x-$, represent a very poorly exploited area of polysiloxane chemistry despite the fact that they exhibit a variety of potentially useful properties including: high temperature stability in air;[2] good adhesion to a wide variety of substrates[3] and, in some instances, liquid crystal-like behavior.[1] Moreover, $-[MeSi(O)_{1.5}]_x-$, polymethylsilsesquioxane has been used as a preceramic polymer for fabrication of silicon carbide powders,[4] "black glass" (70% SiO_2/20% SiC/10% C) composite matrices for carbon fibers[5] and for the fabrication of black glass fibers.[6]

The primary problems associated with using polysilsesquioxanes for engineering applications are: (1) the lack of good, high yield synthetic routes and, (2) the highly crosslinked nature of the polymers which limits their tractability and ease of purification. Literature syntheses generally rely on the hydrolysis of $RSiCl_3$ or $RSi(OR')_3$:[1]

$$RSiCl_3 [RSi(OR')_3] + H_2O \xrightarrow{\text{catalyst}} HCl (R'OH) + [RSi(O)_{1.5}]_x +$$

$$-[RSi(O)_{1.5}]_x[RSi(OH)O]_y- + -[RSi(O)_{1.5}]_x- \qquad (1)$$
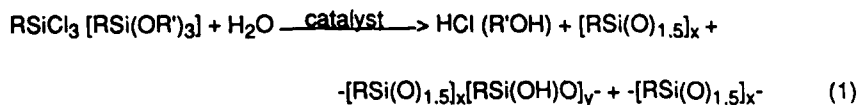
These reactions usually lead to the coincident formation of polyhedral oligosilsesquioxanes, $[RSi(O)_{1.5}]_x$, where $x = 8, 10, 12$; polysilsesquioxanes with partially condensed monomer units, $-[RSi(O)_{1.5}]_x[RSi(OH)O]_y-$, and polyhedral polysilsesquioxane itself. Because polysilsesquioxanes exhibit a strong propensity to form intractable gels with organic solvents, there are significant problems with purification which result in low yields. Thus, this synthetic route is unattractive for the rapid, large-scale preparations.

Harrod and coworkers have recently developed a novel titanium catalyzed redistribution reaction, as illustrated in reaction (2),[7] that can

$$3MeHSi(OEt)_2 \xrightarrow{\text{0.05 mole \% Cp}_2\text{TiMe}_2/20°C} MeSiH_3 + 2MeSi(OEt)_3 \qquad (2)$$
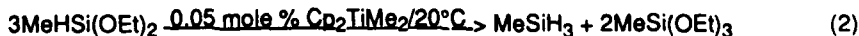
also be used to prepare methylsilsesquioxane copolymers, reaction (3):[2,8]

$$-[MeHSiO]_x- \xrightarrow{\text{0.05 mole \% Cp}_2\text{TiMe}_2/20°C}$$

$$0.33xMeSiH_3 + -[MeHSiO]_{0.3}[MeSi(O)_{1.5}]_{0.7}- \qquad (3)$$
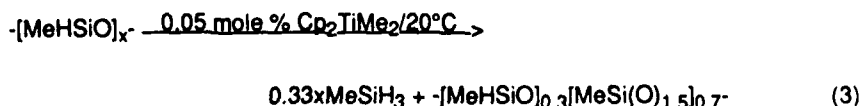
The copolymer $-[MeHSiO]_{0.3}[MeSi(O)_{1.5}]_{0.7}-$ forms as a gel if neat oligomethylhydridosiloxane, $Me_3SiO-[MeHSiO]_x-H$ ($M_n \sim 2K$ D), is exposed to the catalyst. Fortunately, gelation can be avoided if polymerization is conducted in toluene with a greater than 5:1 toluene to $-[MeHSiO]_x-$ volume ratio. The resulting polymer can be used to prepare coatings, fibers and monolithic shapes.[8] At lower volume ratios, gels form quite readily.

Although the 5:1 volume ratio solutions can be used for some applications, the gel-like material that results on solvent removal limits the copolymer's utility for some applications, e.g. as a matrix material for composites. As such, we sought to modify the copolymer's physical characteristics by taking advantage of the reactive Si-H bonds. Reactions at these bonds should permit one to vary the side chains on the copolymer backbone and thereby control some of its physical properties.

The long term objectives of the work described here are to prepare tractable silsesquioxane copolymers that exhibit improved high temperature performance and that are also useful for the fabrication of polymer and ceramic, membranes and fibers. This report concerns preliminary studies on the modification of the $-[MeHSiO]_x[MeSi(O)_{1.5}]_y-$ copolymer by alcoholysis of Si-H bonds.

RESULTS AND DISCUSSION

The copolymer produced in reaction (3) either neat or in toluene gives the same results when characterized by magic angle spinning (MAS), multinuclear NMR, solution NMR, diffuse reflectance infrared fourier transform spectroscopy (DRIFTS), chemical analysis, TGA or DTA. These extensive studies are described elsewhere.[2,7] For illustration purposes, the TGA of $-[MeHSiO]_{0.3}[MeSi(O)_{1.5}]_{0.7}-$ is shown below (Figure 1). This Figure also contains the elemental analyses (at selected temperatures) as the polymer is heated in nitrogen at 5°C/min to 900°C.

At 400°C, the elemental analysis corresponds to pure $-[MeSi(O)_{1.5}]_x-$ without any of the starting monomer. This is confirmed by the MAS ^{29}Si NMR which shows a single peak at -65.7 δ relative to TMS.[2] Consequently, the 20% weight loss at temperatures below 400°C corresponds to the depolymerization and volatilization of almost all of the $-[MeHSiO]_x-$ units.

OR	$^{29}Si(\delta)$	$^{13}C(\delta)$	$^{1}H(\delta)$ (integration)
Starting oligomer	-34.6	1.75 $OSi(CH_3)_3$ 1.04 $SiCH_3$	4.69 (3.43) MeHSiO 0.18 (1.02) $OSi(CH_3)_3$ 0.10 (9.68) $HSiCH_3$
H (72 h)	-33.5, -34.4, -35.9 -57.2, -65.5	1.58 $OSi(CH_3)_3$ 0.66 $HSiCH_3$ -3.27 $OSiCH_3$	4.68 (8) SiH 0.18 (x) $OSi(CH_3)_3$ 0.13 (80-x,y) $HSiCH_3$ 0.10 (y) $OSiCH_3$
OCH_3		49.70 OCH_3 1.54 $OSi(CH_3)_3$ -3.29 br $OSiCH_3$ -5.10 br $MeOSiCH_3$	4.70 (1.7) SiH 3.48 (17) OCH_3 0.13 (49-x) $OSiCH_3$ 0.10 (x) $MeOSiCH_3$
OCH_2CH_3		57.99 OCH_2 18.16 CH_2CH_3 0.70 br $ROSiCH_3$ -3.25 br $OSiCH_3$	3.76 (7) OCH_2 1.20 (10) CH_2CH_3 0.12 $SiCH_3$
$O(CH_2)_2CH_3$	-36.7, -57.9, -66.3	64.02 OCH_2 25.55 OCH_2CH_2 10.27 CH_2CH_3 1.85 $OSi(CH_3)_3$ -3.12 $OSiCH_3$ -4.52 $ROSiCH_3$	4.70 (3) $HSiCH_3$ 3.65 (6.4) OCH_2 1.55 (6) OCH_2CH_2 0.87 (8) CH_2CH_3 0.12 (33-x) $OSiCH_3$ 0.10 (x) $OSiCH_3$
$O(CH_2)_3CH_3$	-36.5 w, -57.94, -64.33, -66.45	62.10 OCH_2 34.50 OCH_2CH_2 18.94 CH_2CH_3 13.82 CH_2CH_3 -3.0 → -3.5 $OSiCH_3$	3.68 (9.6) OCH_2 1.50 (9) OCH_2CH_2 1.34 (8) CH_2CH_3 0.89 (11) CH_2CH_3 0.12 (30) $SiCH_3$

Table 1. NMR Spectra for -[-Me(OR)SiO]$_x$[MeSi(O)$_{1.5}$]$_y$-. Spectra taken in $CDCl_3$ using TMS as an internal standard.
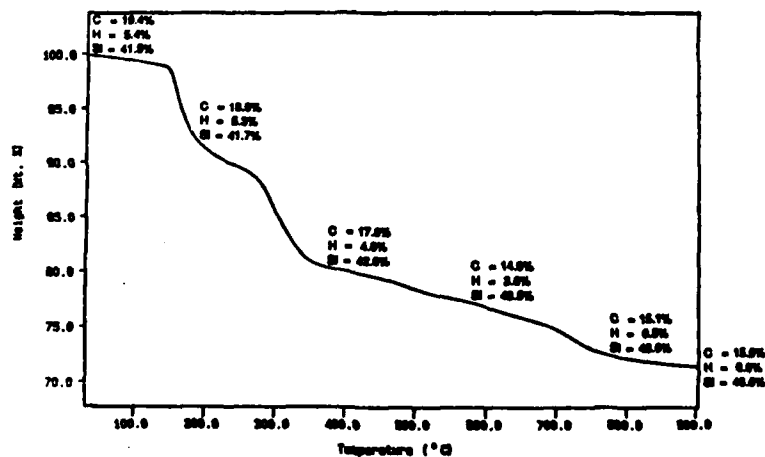
Figure 1. Thermogravimetric Analysis of -[MeHSiO]$_{1.5}$[MeSi(O)$_{1.5}$]$_7$- as a Function of Temperature. The TGA heating schedule was 5°C/min in N_2. Bulk samples for the analyses were heated in a similar manner.

Copolymer Preparation and Characterization

Efforts to modify the -$[MeHSiO]_x[MeSi(O)_{1.5}]_y$- copolymer began with attempts to promote alcoholysis of the Si-H groups, reaction (4),[9,10] *in situ*, following completion (72 h) of reaction (3).

-$[MeHSiO]_{0.3}[MeSi(O)_{1.5}]_{0.7}$- + ROH $\xrightarrow{\text{0.5 mole \% Cp}_2\text{TiMe}_2/20°C}$

$$H_2 + \text{-}[Me(RO)SiO]_{0.3}[MeSi(O)_{1.5}]_{0.7}\text{-} \quad (4)$$

The motivation for the alcoholysis experiments was to create a polysilsesquioxane wherein some of the T groups, $[MeSi(O)_{1.5}]$, are masked as the alkoxy derivative, $[MeSi(O)OR]$. In this way, the yield of T groups in the polymer would increase significantly. Moreover, if R is a long chain alkyl group it would also be possible to introduce more flexibility and perhaps reduce or eliminate the elastomeric or gel character.

To our surprise, the addition of alcohols rapidly extinguishs the royal blue Ti(III) color of the original active catalyst system that forms in reaction (3) leaving a yellow solution. If the alcohol is MeOH, then rapid, almost violent H_2 evolution ensues coincident with the color change. The reaction can be somewhat exothermic depending on the initial catalyst concentration.

Removal of the solvent and characterization by NMR indicates that almost all of the Si-H bonds react with alcohol converting the remaining silicons to T groups. NMR characterization, Table 1, confirms the 30:70 composition of the initial copolymer in that the integrated ratios of the alkoxy groups to T groups in the product copolymer are nearly the same.

To date, we have made the derivatives R = Me, Et, Pr, nBu and bis-1,4-(2-hydroxyethoxy)benzene (hydroquinone). These alcohols exhibit reactivities with the copolymer strictly in accord with the size of the alkyl group. The MeOH reaction is quite vigorous and is over in minutes to hours while the nBuOH reaction requires two to three days. The hydroquinone reaction results in extensive crosslinking that makes further characterization impossible. The other copolymers are moderately (MeO-) to completely (nBuO-) tractable following solvent removal; however, it is expedient to redissolve the polymer in the corresponding alcohol as these polymers still show a tendency to gel with time (days to weeks).

The alkoxy copolymers have been characterized by ^1H, ^{13}C and in part

by ^{29}Si as recorded in Table 1. The ^{13}C shifts of the alkoxy carbon bound directly to the oxygen are quite similar (except for MeO). Consequently, characterization by ^{29}Si was not deemed essential in all instances. The proton and carbon spectra are all standard values for alcohols or alkoxy substituents. However, the ^{29}Si results are interesting because they provide some understanding of the polymer backbone structure if we use published ^{29}Si peak assignments for standard siloxane monomer units.[11]

The ^{29}Si and ^{13}C spectra for $Me_3SiO[MeHSiO]_xH$, ($M_n \approx 2K$ D), the starting oligomer, are very simple. The MeHSiO ^{29}Si peak appears at -34.6 δ. The product, $-[MeHSiO]_{0.3}[MeSi(O)_{1.5}]_{0.7}$, obtained from Ti catalyzed redistribution, shows several ^{29}Si peaks in the same vicinity, -33 to -36 δ. It also shows two peaks at -57.2 and -65.5 δ. These results, when coupled with the reproducible 30:70, [MeHSiO] : [MeSi(O)$_{1.5}$] ratio, suggest a polymer structure consisting of open cubes of T groups bridged by one or two -MeHSiO- groups as depicted below. By visual inspection, the peak at
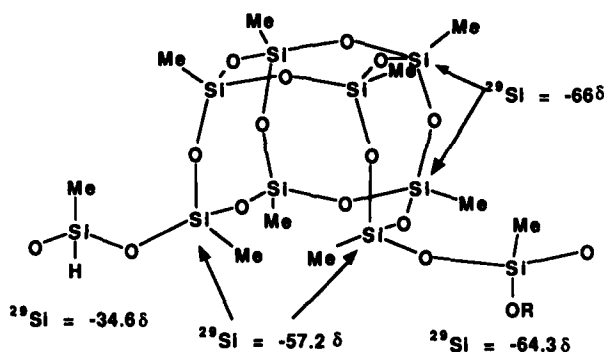
-57.2 δ is much smaller than the peak at -65.5 δ. Consequently, we assign this peak to the open silicons in the cube and the -65.5 δ peak to the remaining T group silicons in the cube. In the nBuO- derivative, the -34.6 δ peak is replaced by the appearence of a peak at ca. -64 δ. This peak appears to overlap with the T groups in the cube in the nPrO derivative. We assign this peak to the alkoxy substituted silicons.

High Temperature Studies

TGA studies indicate that the high temperature stability of the alkoxy derivatives is very similar to that of the starting copolymer. The 900°C ceramic yields for the set of copolymers are 76% (MeHSiO), 75%

[Me(MeO)SiO], 74% [Me(EtO)SiO], 78% [Me(nPrO)SiO] and 62% for the [Me(nBuO)SiO] derivative. As in Figure 1, most of the weight loss occurs below 400-450°C. If weight loss in the alkoxy derivatives occurs by a mechanism similar to that found for the hydrido copolymer, then weight loss must occur by depolymerization and volatilization of Me(RO)SiO groups. One would expect increasing weight losses with increases in the size of the R' group. Clearly this is not the case with the R' = Me, Et or nPr derivatives. In these cases, the ceramic yields are comparable to that of the original copolymer. Even in the nBuO- derivative, the mass of the group increases from 60 D (MeHSiO) to 132 D [Me(OnBu)SiO]. If complete loss of 60 D leads to a ceramic yield of 75% then complete loss of 132 D should lead to a ceramic yield of <50%. These results inidcate that the ceramic products from pyrolysis of these materials retain the carbons in the alkoxy groups.

This is in contrast to studies by Fox et al.[4] on the pyrolysis of the polyalkylsilsesquioxanes, $-[RSi(O)_{1.5}]_x-$, where increasing the size of R from Me to Et to Pr resulted in drops in the 900°C ceramic yields from 86% (Me) to 47% (Et) to 44% (nPr). In all instances, except for the Me derivative, our ceramic yields are much higher.

It is likely that these differences arise because the bond dissociation energy for Si-C bonds is approximately 85-90 kcal/mole whereas O-C bond dissociation energies are typically around 100 kcal/mole.[12] Thus, the decomposition mechanisms for the two types of polymers are quite different. The important point to be made is that proportionately, the EtO- and nPrO- derivatives incorporate more carbon in the ceramic product than the EtSi and nPrSi derivatives, which should result in a higher proportion of SiC in the final composite ceramic/black glass.

ACKNOWLEDGEMENTS

REFERENCES

1. a. M. G. Voronkov, V. I. Lavrent'yev, Top. Curr. Chem. 102, 199 (1982). b. C. L. Frye, J. M. Klosowski, J. Am. Chem. Soc., 93, 4599 (1971).

2. R. M. Laine, J.A. Rahn, K. A. Youngdahl, F. Babonneau, J. F. Harrod submitted to Chem. Mat.

3. See for example: a. J. R. January; U. S. Patent No. 4,472,510. b. S. Uchimara, Eur. Pat. Appl. EP 312,280--CA 111:156040j. c. H. Adachi, E. Adachi, O. Hayashi, K. Okabashi, Jpn. Kok. Tokk. Koho JP 01 92,224.

4. a. D. A. White, S. M. Oleff, R. D. Boyer, P. A. Budringer, J. R. Fox, Adv. Cer. Mat., 2, 45 (1987). b. D. A. White, S. M. Oleff, J. R. Fox, ibid p. 53.

5. a. R. Baney in Ultrastructure Processing of Ceramics, Glasses, and Composites, edited by L. L. Hench and D. R. Ulrich, (Wiley-Interscience, 1984) pp 245-255. b. H. Zhang and C. Pantano in "Proceedings of the Fourth Internat. Confer. on Ultrastruct. of Ceramics, Glasses and Composites, edited by D. Uhlmann and D. R. Ulrich 1989, in press.

6. K. Kamiya, O. Makoto, T. Yoko, J. Noncryst. Sol.; 83, 208 (1986).

7. a. J. F. Harrod, S. Xin, C. Aitken, Y. Mu, and E. Samuel, International Conference on Silicon Chemistry, June,1986; St. Louis, Mo. b. J. F. Harrod, S. Xin, C. Aitken, Y. Mu, E. Samuel, submitted to Can. J. Chem. c. For a review on transition metal catalyzed synthesis of inorganic polymers see: , R. M. Laine in Aspects of Homogeneous Catalysis, edited by R. Ugo (Kluwer pub., Dorchecht, 1989) vol 7, in press.

8. K. A. Youngdahl, M. L. Hoppe, R. M. Laine, J. A. Rahn, and J. F. Harrod, "Proceedings of the 4th Internat. Confer. on Ultrastruct. of Ceramics, Glasses and Composites, edited by D. Uhlmann and D. R. Ulrich (Wiley-Interscience, 1989) in press.

9. R. M. Laine, Z.-F. Zhang and J. A. Rahn unpublished results. Detailed experimental results will be reported elsewhere.

10. X-L. Luo and R. H. Crabtree, J. Am. Chem. Soc. 111, 2527 (1989).

11. a. H. Marsmann and J. P. Kintzinger in Oxygen 17 and Silicon 29 NMR, (Springer-Verlag, 1981) New York pp 74-239. b. E. A. Williams in The Chemistry of Organic Silicon Compounds, edited by S. Patai and Z. Rappoport (John-Wiley and Sons, 1989) pp 512-554.

12. a. Handbook of Chemistry and Physics, CRC Co. (Chemical Rubber Co. 64th Ed.) p F-193. b. R. Walsh in The Chemistry of Organic Silicon Compounds, edited by S. Patai and Z. Rappoport (John-Wiley and Sons, 1989) pp 371-392 and references therein.

CONDUCTING MOLECULAR MULTILAYERS:
INTERCALATION OF CONJUGATED POLYMERS IN LAYERED MEDIA

V. MEHROTRA AND E.P. GIANNELIS
Department of Materials Science and Engineering, Cornell University,
Ithaca, NY 14853.

ABSTRACT

Polyaniline has been synthesized in the galleries of fluorohectorite, a two-dimensional mica-type layered silicate. Intercalation of aniline in the intracrystalline region of Cu-exchanged fluorohectorite results in oxidative polymerization to polyaniline (emeraldine base form) as demonstrated by electronic, infrared and Raman spectroscopy and x-ray diffraction data. The intercalated insulating form of polyaniline becomes conducting on exposure to HCl. In-plane electrical conductivity data measured in the temperature range 274 to 573 K show a complex thermally activated behavior with room temperature conductivity 0.05 $Ohm^{-1}cm^{-1}$. The polyaniline/layered silicate hybrids represent a new class of nanocomposites consisting of synthetic conductors with molecular dimensions contained in a quasi two-dimensional environment of a crystalline host.

INTRODUCTION

Research on electrically conducting polymers has recently focused on the synthesis and characterization of environmentally robust materials with high degree of processability and high conductivity [1]. An intriguing new challenge in the area of conducting polymers is to isolate or confine them in a well defined environment. Such systems would not only provide fundamental information on the electronic structure and the conduction mechanism but they could also represent a new class of hybrid composites with nanometer dimensions. The properties of these new materials can be tailored by inserting suitable guest molecules into the well defined galleries of the host lattice.

Previous work in this area includes intercalation of polypyrrole and polythiophene in layered FeOCl [2], intercalation of aniline in V_2O_5 [3], and encapsulation of chains of aniline, pyrrole and thiophene in zeolites [4,5].

Formation of conjugated polymers in the galleries of mica-type silicates was first observed almost twenty years ago by Pinnavaia and Mortland by a unique charge-transfer reaction [6]. Certain aromatic molecules can be incorporated into the galleries of layered silicates whose exchangeable cations have been replaced by transition metal ions like Cu, Ru, etc., and form charge-transfer complexes. For example in the case of benzene, intercalation leads to the formation of poly-p-phenylene under exhaustively dry conditions.

Previous studies focused mainly on spectroscopic studies offering no information on their electronic properties or conduction mechanism [7,8]. In addition, intercalation of aniline in layered silicates has not been studied. Polyaniline (PANI) is a novel conducting polymer, that in contrast to other conducting polymers its electronic properties can be switched from insulating to conducting by electrochemical oxidation and/or chemical protonation.

We report here the first successful synthesis of in situ intercalation/polymerization of aniline in layered mica-type silicates. The resulting materials constitute a pseudo two-dimensional composite with nanometer architecture.

EXPERIMENTAL

Materials

Synthetic fluorohectorite was kindly provided by Corning Inc. Typical particles have a platelike morphology with an average layer diameter of 5 microns. The cation exchange capacity for fluorohectorite is 190 meq/100 g. The copper-exchange form was prepared by treating the host with 1 M solution of $Cu(NO_3)_2$, centrifuging and discarding the supernatant liquid. Excess $Cu(NO_3)_2$ was removed by washing with deionized water.

Thin films of fluorohectorite (0.5 - 25 microns) were prepared by evaporation of a suspension on a polyethylene plate (for self-supporting films) or on a glass substrate. Aniline was intercalated in a P_2O_5 containing desiccator from the vapor phase until the reaction was completed within 3-4 days. An alternative route employed dipping the fluorohectorite film into aniline for a few days. The conducting form of polyaniline was formed by exposing the PANI/fluorohectorite films to HCl vapors for 2 to 3 hours followed by mild heating at 45^oC to remove excess HCl.

Instrumentation and Methods

X-ray diffraction patterns of oriented film samples were obtained on a Scintag x-ray diffractometer using Ni-filtered CuKα radiation. Infrared spectra of self-supporting films were recorded on a Perkin Elmer 1330 spectrometer. Electronic absorption spectra were obtained with a Perkin Elmer Lambda 4A spectrophotometer. Raman experiments were performed with a SPEX 1877 triplemate spectrometer, using a Coherent Nova 90-5 Ar^+ laser with a maximum power of 2 W in the 457.9 nm line. Four-point "bulk" conductivity measurements were performed at room temperature using a Prometrix Versaprobe VP10 System. In-plane conductivity of oriented films was measured by a Hewlett-Packard 4145B semiconductor parameter analyzer. Samples for conductivity measurements were prepared by depositing a film onto HF cleaned glass slides. Silver electrodes were deposited on both edges of the film. The current-voltage characteristics of the sample were measured at each temperature in a shielded test enclosure. Transient currents were allowed to dissipate before each measurement. The applied voltages ranged from -10 to +10 Volts in steps of 0.5 V at each temperature. Electrical properties were studied in the 1^oC to 300^oC range.

RESULTS AND DISCUSSION

Fluorohectorite is a synthetic mica-type silicate (MTS) with a layered lattice structure in which two-dimensional multiple cross-linked planes of atoms are separated by layers of hydrated cations. Figure 1 schematically illustrates the layered structure where two tetrahedral silicate sheets are fused to a central octahedral sheet of magnesium hydroxide [9]. The stacking of these layers to form crystals leads to the formation of interlayers or "galleries" where the layers are held together by van der Waals forces. In fluorohectorite and other charged silicates the galleries are occupied by hydrated cations in order to balance the charge deficiency

$[M(H_2O)_x]^{n+}$
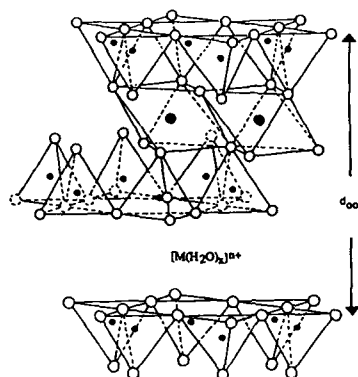
Figure 1. Idealized structure of a mica-type silicate.

that has been generated by the isomorphous substitution in the tetrahedral or octahedral sheets. The strong intraplanar and weak interplanar binding forces that arise from the two-dimensional structure allow the introduction (intercalation) of guest species into the galleries of the host lattice.

Simple intercalative and/or ion exchange procedures permit a variety of neutral molecules or cations of virtually any size to be accommodated in the galleries of MTSs. Principal themes that have emerged from various spectroscopic techniques is that the properties of the gallery species are generally preserved upon intercalation.

Intercalation of aniline in Cu-exchanged fluorohectorite from the gaseous phase is relatively slow; however, when the film is dipped into neat aniline a rapid color change occurs and the reaction is complete within 24 hours. In contrast, no polymerization occurs when Li^+ ions are present in the galleries. Chemical oxidation of aniline yields the emeraldine base form of polyaniline that consists of equal number of the amine $[-(C_6H_4NH)-]$ and quinoidal $[-(C_6H_4NH)-]$ repeating units. In contrast, when polymerization is carried out in acidic media, the protonated poly(semiquinone), a radical cation structure is formed. This conducting form of polyaniline is believed to consist of equal numbers of reduced $[-(C_6H_4NH)-]$ and oxidized, protonated quinone $[-(C_6H_4NH^+)-]$ repeat units [10].

Gallery Cu^{2+} ions, intː Juced by an intercalative ion exchange process, serve as the oxidation centers for the oxidative polymerization of aniline in the intracrystalline environment of the host structure. The reaction, by analogy to other conjugated polymers in layered silicates, can be represented by the following equation, where the horizontal lines identify the layered structure.

$$\underline{Cu^{2+}} \quad + \quad nC_6H_5NH_2 \quad \longrightarrow \quad \underline{Cu^{2+}(PANI)}$$

X-ray diffraction patterns of oriented films show that in situ intercalation/polymerization of aniline results in a highly ordered composite with a quasi two dimensional structure (Figure 2). Several (001) harmonics are observed corresponding to a primary repeat unit (d spacing) of 14.9 Å. The difference of 5.3 Å from the corresponding 9.6 Å for the silicate framework is in agreement with intercalation of single chains of polyaniline.

The electronic absorption spectrum of the as prepared material shows an absorption band at 510 nm (2.4 eV) and 330 (3.7 eV) which have been attributed to the quinone diimine structure $[-N=(C_6H_4)=N-]$ of the emeraldine base (Figure 3). The host exhibits a characteristic absorption at 4.5 eV. However, when the sample is exposed to HCl vapors the band at 510 nm gradually disappears and a new broad band appears centered at 760 nm (1.6 eV) that extends into the near ir. The absorption at 3.4 eV and the broad feature extending into ir have been associated with radical cations supporting polarons as charge carriers.

Further evidence for the presence of intercalated polyaniline comes from ir and Raman spectroscopy. Ir spectra of oriented films show typical vibrations of polyaniline at 1595, 1490, 1305 and 1245 cm^{-1}. The bands at 1595 and 1245 cm^{-1} are associated with the reduced repeat units [-(C_6H_4NH)-] while the 1490 and 1305 cm^{-1} are attributed to the quinone diimine and protonated oxidized repeat units respectively. The 1305 cm^{-1} band is also characteristic of an electron-phonon interaction. Raman spectroscopy with 457.9 nm excitation shows absorptions at 1630, 1370, 1325 and 1205 cm^{-1} in agreement with the above assignments.

The role of Cu^{2+} in initiating the polymerization of analogous aromatic systems in the silicate galleries has been established in the past by electron paramagnetic resonance and x-ray photoelectron spectroscopy [6-8]. Similar experiments for the polyaniline intercalate are underway in our laboratory and the results will be communicated in the near future.

The as prepared polyaniline intercalate shows excellent thermal stability up to 700°C. After an initial weight loss of approximately 3% presumably due to residual monomer trapped during the reaction and/or adsorbed atmospheric moisture there is no further weight loss up to 700°C.

Electrical conductivity measurements were performed in the four-probe and in-plane geometry using oriented film samples. The room temperature conductivity of HCl exposed samples is 0.05 Ohm^{-1}cm^{-1} an increase by five orders of magnitude with respect to Cu-exchanged host. Figure 4 shows the variable temperature in-plane conductivity of samples exposed to HCl. The current-voltage characteristics were ohmic throughout the temperature range. Experimental points in the figure are connected as a guide to the eye. As the sample is heated from room temperature the conductivity increases with increasing temperatures as expected for semiconducting behavior or in different variable range hopping models. The conductivity increases reversibly from room temperature to about 60 °C, above which the conductivity starts to decrease slowly. After heating to temperatures higher than 300 °C and rapidly cooling to room temperature the sample exhibits a conductivity substantially lower from that at room temperature but the behavior is now metallic; i.e. an increase in temperature leads to a decrease in conductivity. The variable temperature conductivity data agree very well with the behavior observed for bulk polyaniline [11]. Preliminary conductivity measurements perpendicular to the silicate layers affirm the highly anisotropic nature of the material.
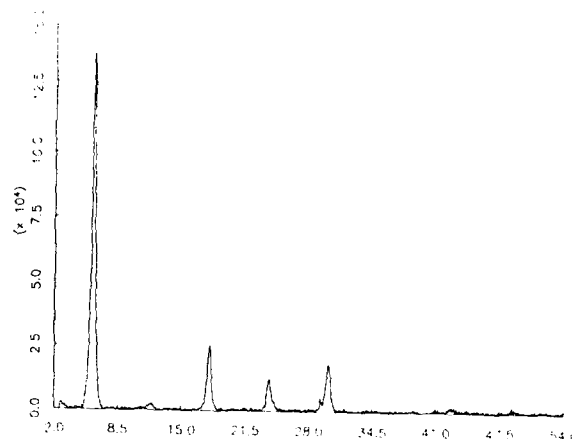
Figure 2. X-ray diffraction pattern for PANI-MTS multilayer
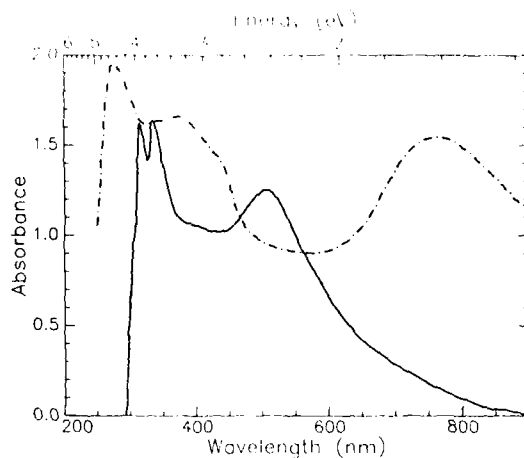
Figure 3. Electronic absorption spectra of: (a) as prepared PANI intercalated MTS (solid line); (b) after exposure to HCl vapors (broken line).

The polyaniline/layered silicate hybrids represent a new class of conducting nanocomposites. These materials consist of conducting polymer chains and insulating host layers alternately stacked to form a multilayered structure with molecular dimensions and atomically sharp interfaces. We have extended this approach of intercalative polymerization to other polymer/host systems. The structural, spectroscopic and transport properties of these systems will be reported in the future.
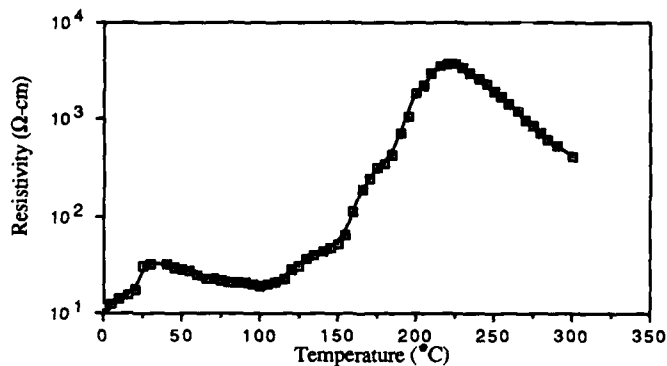
Figure 4. Resistivity of PANI intercalated MTS exposed to HCl as a function of temperature.

REFERENCES

1. T.A. Skotheim Ed., Handbook of Conducting Polymers, Vol. 1, (Marcel Dekker, New York, 1986).

2. M.G. Kanatzidis, H.O. Marcy, W.J. McCarthy, C.R. Kannewurf and T.J. Marks, Solid State Ionics, 32/33, 594 (1989).

3. M.G. Kanatzidis, C.-G. Wu, H.O. Marcy and C.R. Kannewurf, J. Am. Chem. Soc., 111, 4139 (1989).

4. P. Enzel and T. Bein, J. Phys. Chem., 93, 6270 (1989)

5. P. Enzel and T. Bein, J. Chem. Soc., Chem. Commun., 1326 (1989)

6. M.M. Mortland and T.J. Pinnavaia, Nature, 229, 75 (1971)

7. J.P. Rupert, J. Phys. Chem., 77, 784 (1973).

8. Y. Soma, M. Soma and I. Harada, J. Phys. Chem., 88, 3034 (1984).

9. T.J. Pinnavaia, Science, 220, 365 (1983).

10. J.C. Chiang and A.G. MacDiarmid, Synth. Met., 13, 193 (1986).

11. K. Uvdal, M.A. Hasan, J.O. Nilsson, W.R. Salaneck, I. Lundstrom, A.G. MacDiarmid, A. Ray and A. Angelopoulos, in Electronic Properties of Conjugated Polymers, edited by H. Kuzmany, M. Mehring and S. Roth (Springer-Verlag, Berlin, 1987).

NYLON 6-CLAY HYBRID

AKANE OKADA, MASAYA KAWASUMI, ARIMITSU USUKI,
YOSHITSUGU KOJIMA, TOSHIO KURAUCHI AND OSAMI KAMIGAITO
Toyota Central Research and Development Laboratories, Inc.,
Nagakute, Aichi, 480-11, Japan

ABSTRACT

ε-Caprolactam was polymerized in the interlayer
spacing of montmorillonite, a clay mineral, yielding
a nylon 6-clay hybrid (NCH) [1].
X-ray and TEM measurements revealed that each template of
the silicate, which is 10 Å thick, was dispersed in the
nylon 6 matrix and that the repeat unit increased from 12 Å
in unintercalated material to 214 Å in the intercalated
material.
Thus NCH, is a "polymer based molecular composite" or
"nanometer composite". NCH, when injection-molded, shows
excellent properties as compared to nylon 6 in terms of
tensile strength, tensile modulus and heat resistance.
Heat distortion temperature increased from 65 ℃ for nylon 6
to 152 ℃ for NCH, containing 4 wt% (1.6 vol%) of clay
mineral.

INTRODUCTION

Nylon 6 (polycaploractam) has good mechanical
properties and is a commonly used engineering polymer. It
has been successfully reinforced by glass fiber or other
inorganic materials [2]. In these reinforced composites, the
polymer and additives are not homogeneously dispersed at the
microscopic level. If the dispersion could be achieved at
the microscopic level, the mechanical properties would be
expected to be further improved and/or new unexpected
features might appear. Clay mineral is a potential candidate
for the additive since it is composed of layered silicates,
10 Å thick, and undergoes intercalation with organic
molecules. A conceptive picture is illustrated in Figure 1.

EXPERIMENTAL

Materials

Montmorillonite "Kunipia F" was supplied by Kunimine
Ind. Co., with a cation exchange capacity of 119 mili
equivalents/100 g. Montmorillonite is a fine sheet-like
particle with a dimension of about 0.1 μm in length, 0.1 μm
width and 10 Å in thickness. Other inorganic and organic
materials were commercially available.
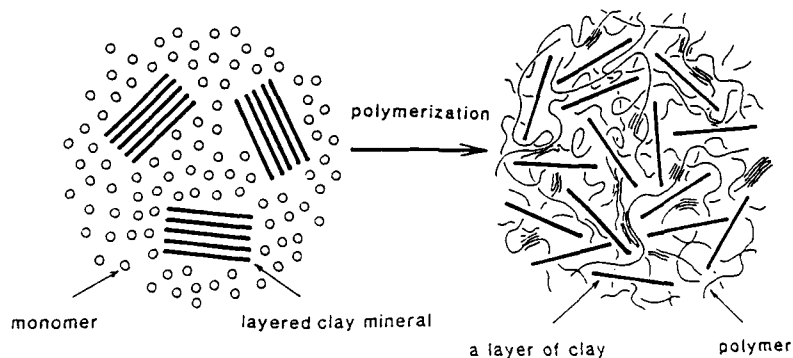
Fig.1   A conceptive picture of polymerization
in the presence of clay

Preparation of 12-montmorillonite

In an electric mixer, 25 g of montmorillonite and
1.75 l of water were mixed.   The mixture was stirred at 5000
rpm for 5 min., and then an aqueous suspension of clay was
obtained.   12.8 g of 12-aminolauric acid and 6.0 ml of
hydrochloric acid was then added to the suspension and the
mixture was further stirred at 5000 rpm for 5 min. The
product was filtered, washed with 1 l of water, freeze-dried
and dried in vacuo at 100 ℃, which finally yielded
intercalated montmorillonite with 12-aminolauric acid
(termed as 12-montmorillonite).

Preparation of hybrid

A typical run is described. The reaction vessel was
composed of a 500 ml-three necked separable flask with
mechanical stirrer.   In the vessel, 113 g of ɛ-caprolactam
and 5.97 g of 12-montmorillonite was placed. The mixture
was heated at 100 ℃ in an oil bath with stirring for 30
min. The temperature was then elevated to 250 ℃ and
maintained for 48 hr.   After cooling, the product was
mechanically crushed.   The finely divided particles were
washed with 2 l of water at 80 ℃ for 1 hr. Drying at 80 ℃
overnight yielded a nylon 6-clay hybrid (termed as NCH).
Nylon 6-clay composites (termed as NCC) were
prepared by blending commercial nylon-6 and montmollironite
in an extruder for comparison with NCH.   These materials
were injection-molded for measurement.

Characterization

X-ray measurement was done with a Rigaku RU-3L X-ray Diffractometer using Co Kα radiation.

Transmission electron micrographs were obtained with a Jeol-200CX TEM using an acceleration voltage of 200 kV.

Viscoelastic measurement was done using Iwamoto Seisakusho VES-F Viscoelastometer.

Tensile strength and other mechanical properties were measured following ASTM.

RESULTS AND DISCUSSION

Polymerization

When ε-caprolactam (mp 70 ℃) and 12-montmorillonite were heated at 100 ℃ under stirring, the mixture yielded a viscous dispersion. Interlayer distance in the suspension was 40 λ as compared to 17 λ for 12-montmorillonite. This indicates that the monomer was intercalated into the silicates. Polymerization was performed at 250 ℃. Interlayer distance, D, could be directly obtained in XRD diagrams. Figure 2 compares the transmission electron micrographs of sections of molded NCH. The dark lines are intersections of sheet silicate of 10 λ thickness and spacings between the dark lines are interlayer distances.

Table 1 shows the interlayer distance, D, obtained by XRD and TEM. The D values agree very well. D was found to be inversely proportional to the montmorillonite content. A maximum D of 214 λ was observed.

The thickness of a layer of silicate is about 10 λ. This is of the order of molecular-size and therefore can be thought to be an "inorganic macromolecule" so that in NCH, the polymer and montmorillonite are mixed at a molecular level forming a "polymer based molecular composite". On the other hand, D in the NCC was 12 λ and therefore it is not a "nanometer composite".

Properties

The dynamic elastic moduli (E') were obtained at 10 Hz between -150 ℃ and 250 ℃. The moduli of NCH-5 exceeded those of NCC-5 and nylon 6 in all the region of temperature. The modulus of NCH-5 was more than twice that of other specimens around 120 ℃.

Mechanical properties of NCH-5 are shown in Table 2 together with nylon 6 and NCC-5. The tensile strength and tensile modulus of NCH were superior to others. Impact strength of NCH was comparable to nylon 6.

(a)NCH-15   1000A

(b)NCH-30   1000A

Fig. 2 TEM of sections of NCHs

Table 1   Interlayer distances of NCHs

Specimen	Montmorillonite (wt%)	Distance (X-ray, A)	Distance (TEM, A)
NCH-5	4.2	>150	214
NCH-10	9.0	121	115
NCH-15	14.5	64	62
NCH-30	25.0	51	50
NCC-5	5.0	12	

Table 2   Properties of NCH-5 (1)

Specimen Montmorillonite (wt%)	Tensile strength (MPa)	Tensile modulus (GPa)	Charpy impact strength (KJ/m²)
NCH-5 (4.2)	107	2.1	6.1
NCC-5 (5.0)	61	1.0	5.9
nylon 6 (0)	69	1.1	6.2

Table 2 (continued)   Properties of NCH-5 (2)

Specimen Montmorillonite (wt%)	HDT at 18.5kg/cm² (°C)	Rate of water absorption 23°C,1 day (%)	Coefficient of thermal expansion flow direction	Coefficient of thermal expansion perpendicular direction (cm/cm°C)
NCH-5 (4.2)	152	0.51	6.3×10^{-5}	13.1×10^{-5}
NCC-5 (5.0)	89	0.90	10.3	13.4
nylon 6 (0)	65	0.87	11.7	11.8

The most prominent effect was observed in heat distortion temperature (HDT). HDT of NCH-5 containing only 4 wt% of montmorillonite was 152 ℃, which was 87 ℃ higher than that of nylon 6. This effect in NCH is a drastic improvement in the quality of nylon 6.

Resistance to water was also improved. The rate of water absorption in NCH was lowered by 40 % as compared to nylon 6 and NCC.

The molded specimen was found to be anisotropic. The coefficient of thermal expansion of NCH-5 in the flow direction was lower than half of that in the perpendicular direction. Nylon 6 was isotropic and NCC was intermediate. Sheets of silicate were parallel to the flow direction of the mold. The polymer chains also oriented in the same direction. It seems that anisotropy of thermal expansion resulted from the orientations of silicate and polymer chains.

Excellent properties in NCH can be considerd to have origin in an enormous surface area and ionic bonds between the organic polymer and inorganic silicate sheet.

CONCLUSION

ι-Caprolactam was polymerized in the interlayer spacing of montmorillonite, a clay mineral, yielding a nylon 6-clay hybrid (NCH).
XRD and TEM studies have revealed that this NCH is a real "polymer based molecular composite" or "nanometer composite".

NCH can be injection-molded and shows excellent properties as compared to nylon 6 in terms of tensile strength, tensile modulus and heat resistance.

NCH is now open to practical use.
We believe that this method has opened a new field and is a novel processing technique exploiting the intercalation properties of layered compounds.

REFERENCE

1. Presented in part at the 194th National Meetings of American Chemical Society, New Orleans, La., August 1987, Polymer Preprint 28, 447 (1987).
2. M. I. Kohan Ed., "Nylon Plastics", Interscience, New York 1973.

REINFORCEMENT OF ELASTOMERS BY THE *IN-SITU* GENERATION OF FILLER PARTICLES

JAMES E. MARK* AND DALE W. SCHAEFER**
*University of Cincinnati, Dept. of Chemistry, Cincinnati, OH 45221
**Sandia National Laboratories, Albuquerque, NM 87185

ABSTRACT

The goal of primary interest in these investigations was the development of novel methods for filling elastomeric networks. The techniques developed employ the *in-situ* generation of reinforcing fillers such as silica or a glassy polymer such as polystyrene either after, during, or before network formation. The reaction involves decomposition of organometallic compounds, using a variety of catalysts and precipitation conditions, or free-radical polymerization of a suitable monomer. The effectiveness of the technique is gauged by stress-strain measurements carried out on these elastomeric composites to yield values of the maximum extensibility, ultimate strength, and energy of rupture. Also of interest are calorimetric studies of the networks, to determine their crystallizability. Information on the filler particles themselves is obtained from density determinations, electron microscopy, and scattering measurements.

INTRODUCTION

There are a number of disadvantages to reinforcing an elastomer by the usual technique [1,2] of blending a finely divided filler (such as carbon black or silica) into a polymer before cross linking it [3]. A number of alternative techniques are therefore also under development. Examples of such techniques are presented here, with a strong emphasis on results beyond those described in three recent reviews which are at least partly on the same subject [4-6]. They include hydrolysis of organometallic compounds within a polymeric matrix to give ceramic particles such as silica and titania. The semi-inorganic polymer, poly(dimethylsiloxane) (PDMS) has been most studied in this regard. The case where the ceramic predominates and becomes the continuous phase is also mentioned. An alternative approach where monomers such as styrene or methyl methacrylate are polymerized *in-situ* to give glassy polymers is also described, as are some related systems in which there are magnetic particles or zeolites.

Of primary interest here is the reinforcement provided by these fillers. It is easy to switch the focus, however, so that the elastomer is viewed as only a matrix in which the ceramic materials are being generated. In this "matrix isolation" approach [7], X-ray and neutron scattering techniques, for example, can be used to obtain information that transcends these particular systems. It should be useful in a variety of areas, including the new sol-gel technique for preparing ceramics of carefully controlled ultrastructure [8-11].

IN-SITU PRECIPITATIONS

Typical Hydrolysis Reactions

The most important reaction in this area is the acid or base catalyzed hydrolysis of tetraethoxysilane (TEOS) as described by the chemical equation [4-6],

$$Si(OC_2H_5)_4 + 2H_2O \rightarrow SiO_2 + 4C_2H_5OH \qquad (1)$$
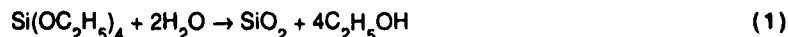
Analogous reactions [8-11] can be carried out, however, on titanates [12-14], aluminates [15], zirconates [16]. In the sol-gel technique, the process first gives a (swollen) gel, which is then dried, fired, and densified into a final, monolithic piece of silica [8-11]. There have now been a number of additional studies using essentially the same reactions, but in a very different context [4-6]. Specifically, the hydrolysis reactions are carried out within a polymeric matrix, with the

ceramic frequently generated in the form of very small, well-dispersed particles. When the matrix is an elastomer, these particles provide the same highly desirable reinforcing effects obtained by the usual blending of a filler (such as carbon black) into polymers (such as natural rubber) prior to their being cross-linked or cured into tough elastomers of commercial importance [1,2].

These reactions can be carried out in three ways [4-6]. In the first, the polymer is cross linked and then swelled with the organometallic, which is then hydrolyzed *in-situ*. In the second, hydroxyl-terminated chains are blended with enough TEOS to both end link them and provide silica by the hydrolysis reaction. Thus, curing and filling take place simultaneously, in a one-step process. In the final technique, TEOS is blended into polymer having end groups (e.g. vinyls) that are unreactive under hydrolysis conditions. The silica is then formed in the usual manner [Eqn (1)], and the product dried. The resulting slurry of polymer and silica is stable and can be cross linked later using any of the standard cross linking techniques, such as vinyl-silane coupling [5,17,18].

The kinetics of this reaction are being studied [19] using air-pressure deformation measurements [20] on the gels, in a manner similar to that used to characterize thermoreversible polyethylene gels [21].

Comparisons Among Various Silica-Based Fillers

There are a variety of ways to generate silica-type fillers useful for reinforcing PDMS networks. The extent to which such fillers provide reinforcement was characterized in a recent study [22]. The materials and techniques employed were (i) incorporating a commercial silica which had been treated with hexamethyldisilazane as a coupling agent, (ii) PDMS with silica which had been precipitated from an aqueous dispersion, (iii) precipitating silica directly into PDMS during its curing, (iv) precipitating silica directly into a swollen PDMS network after it was cured, (v) incorporating silica prepared from tetraethoxysilane (TEOS) and containing some PDMS, and (vi) incorporating silica prepared from partially hydrolyzed TEOS and also containing some PDMS. The resulting filled elastomers showed the largest values of the ultimate strength in the case of (iv) and (vi), and the largest value of the rupture energy for (iv).

Other Polymers

Most of the studies to date have involved PDMS, primarily because of its great miscibility with TEOS. Similar studies [23] on the related polymer, poly(methylphenyl-siloxane), however, are of considerable importance. In this case the stereochemically irregular structure of the polymer prevents strain-induced crystallization [5,24]. Good *in-situ* generated reinforcement was also achieved in this polymer, suggesting that such crystallization is not necessary for reinforcement [23].

The same techniques have also been shown to give good reinforcement in polyisobutylene elastomers [25], and in poly(ethyl acrylate) [26]. In the latter case, it appears that the precipitation can be carried out during an emulsion polymerization [26].

Other Ceramic-Type Fillers

Silica particles in PDMS elastomers can be a problem at high temperature, since the silanol groups on their surfaces can cause degradation of the polymer [13,27]. For this, and other reasons, a variety of other fillers have been precipitated into this polymer. Included are titania (TiO_2) [12-14], alumina (Al_2O_3) [15], and zirconia (ZrO_2) [16].

These non-silica fillers also provide good reinforcement. One interesting difference, however, is the observation that the stress-strain isotherms in these cases frequently have much better reversibility [14]. Reversibility is presumably due to different interactions between the surface groups present on these particles and the PDMS elastomeric matrix.

Aging Effects

Permitting precipitated silica particles to remain in contact with their aqueous catalyst solution can permit them to "age" or "digest" [28,29]. Electron microscopy results suggest that some reorganization is occurring, with the particles becoming better defined, more uniform in size, and possibly even less aggregated. There seem to be interesting parallels with "Ostwald ripening" in the area of colloid science [30].

Density Measurements

Comparisons between the values of wt % filler obtained from density measurements and the values obtained directly from weight increases can give very useful information on the filler particles. For example, the fact that the former estimate is smaller than the latter in the case of silica-filled PDMS elastomers [31] indicates that there are probably either voids or unreacted organic groups in the filler particles.

Calorimetry

Differential scanning calorimetry measurements at low temperatures were carried out on PDMS elastomers containing *in-situ* precipitated silica [32]. The presence of the silica was found to reduce both the extent of crystallization and the rate of crystallization when the elastomers were in the unstretched state in contrast to similar studies of PDMS in the stretched state, where the filler may facilitate the crystallization process [33].

Electron Microscopy

Both transmission [4-6,28] and scanning [34] electron microscopy have been used to characterize these novel composite materials. The information obtained in this way includes (i) the nature of the precipitated phase (particulate or non-particulate), (ii) the average particle size, if particulate, (iii) the distribution of particle sizes, (iv) the degree to which the particles are well defined, and (v) the degree of agglomeration of the particles.

One interesting result of this type is the conclusion that basic catalysts generally yield particles that are well defined, whereas acidic catalysts yield particles that are rather "fuzzy" [4,28]. This conclusion is in agreement with results obtained earlier in sol-gel ceramics investigations [35].

Scattering Studies

A number of X-ray and neutron scattering studies have been carried out on these filled elastomers [4,5,36,37]. Although the results are generally consistent with those obtained by electron microscopy, there are some intriguing differences. Of particular interest is the observation that some fillers which appear to be particulate in electron microscopy, appear to consist of a continuously interpenetrating phase by scattering measurements [36,37]. Additional comparisons could certainly be very illuminating in this regard.

POLYMER-MODIFIED CERAMICS

The technique of hydrolyzing an organometallic substance such as an alkyl silicate can be generalized to make the silica generated the continuous phase, with domains of PDMS dispersed in it. Of course, relatively high concentrations of the silicate are necessary. By varying its amount, composite materials can be obtained ranging from relatively soft elastomers, to tough hybrid materials, to brittle ceramics [38-40]. Important properties to be correlated with composition would include impact resistance, ultimate strength, maximum extensibility, and viscoelastic effects.

IN-SITU POLYMERIZATIONS

Isotropic Systems

It is also possible to obtain reinforcement by polymerizing a monomer such as styrene to yield hard glassy domains within the elastomer [41]. In PDMS, low concentrations of styrene give low molecular weight polymer that acts more like a plasticizer than a reinforcing filler. The initial plasticization effect is revealed by the stress-strain results which show an initial decrease in the energy of rupture. This conclusion is supported by the absence of evidence for polystyrene (PS) particles at lower styrene concentrations. Polyisobutylene has also been reinforced in this manner [42]. In both cases, the particles are roughly spherical and the system isotropic.

The glassy particles thus generated are relatively easy to extract from the elastomeric matrix, which means that there is little effective bonding between the two phases. It is possible, however, to get excellent bonding onto the filler particles. One way is to include some $R'Si(OC_2H_5)_3$, where R' is an unsaturated group. The R' groups on the surfaces of the particles then participate in the polymerization, thereby bonding the elastomer chains to the reinforcing particles [43]. Alternatively, the $R'Si(OC_2H_5)_3$ can be used as one of the end-linking agents, placing unsaturated groups at the cross links [44]. Their participation in the polymerization would now tie the PS domains to the elastomer's network structure.

The PS domains have the disadvantage of having a relatively low glass transition temperature T_g (~100°C) [45] and being totally amorphous. Above T_g they would therefore soften and presumably lose their reinforcing capability. For this reason, similar studies have been carried out using poly(diphenylsiloxane) as the reinforcing phase. For an elastomer, this material has a relatively high T_g of 49°C [46], is crystalline, and has an extraordinarily high melting point of 550°C [46].

Anisotropic Systems

It is possible to convert the essentially spherical PS domains described above to rod-like ellipsoidal particles [34]. First, the PS-elastomer composite is raised to a temperature well above the T_g of PS. It is then stretched uniaxially, and cooled while in the stretched state. The particles are deformed into prolate ellipsoids, and retain this slope when cooled. When the deforming force is removed, the elastomer is observed to retract, but only part of the way back to its original dimensions. The particles themselves were characterized using scanning and transmission electron microscopy, and found to have axial ratios of approximately 2, and to have their axes preferentially oriented in the direction of the high-temperature stretching. The reinforcement they provided were characterized using stress-strain measurements in elongation at room temperature. In these anisotropic materials, the moduli in the direction parallel to the *original stretching direction was found to be significantly higher than that of the untreated* (isotropic) PS-PDMS elastomer, whereas in the perpendicular direction it was significantly lower.

It should also be possible to generate oblate ellipsoids by stretching such a PS-PDMS elastomer biaxially, for example, by inflation of a sheet of the material. Such experiments are in progress [34].

SOME RELATED SYSTEMS

Magnetic Particles

Some filler particles can be manipulated with a magnetic field [47,48]. For example, magnetic ferrite particles dispersed in PDMS can be aligned in a magnetic field during the cross-linking process. In this way anisotropic mechanical properties can be obtained, even from essentially spherical particles. The reinforcement is found to be significantly larger in the direction parallel to the magnetic lines of force.

This technique could be combined with the *in-situ* approach by generating metal or metal oxide magnetic particles in a magnetic field [49,50] for example by the thermolysis or photolysis of a metal carbonyl.

Zeolites

One of the problems with fillers used to reinforce elastomers, however introduced, is their amorphous nature [1,2]. This lack of a well-defined structure makes them poor choices for determining how the structure of a filler affects the reinforcement it provides [51].

The zeolites are a related group of silicate-based materials which (i) are crystalline, (ii) have conveniently-sized holes or cavities, and (iii) have had their structures extensively documented [51,52]. Two zeolites have been investigated as fillers and found to give good reinforcement of PDMS elastomers [51]. The one that had cavities 3 Å in diameter was not nearly as effective as the one having 13 Å diameter cavities. In the latter case, the cavities may have been large enough for them to be invaded by the PDMS chains, which could explain the enhanced reinforcement.

It would be particularly exciting if such sieve-like materials of known structures could be prepared *in-situ*.

ACKNOWLEDGEMENTS

REFERENCES

1. B. B. Boonstra, Polymer, **20**, 691 (1979).
2. Z. Rigbi, Adv. Polym. Sci., **36**, 21 (1980).
3. J. E. Mark and S.-J. Pan, Makromol. Chem., Rapid Commun., 3, 681 (1982).
4. J. E. Mark, in Ultrastructure Processing of Advanced Ceramics, ed. by J. D. MacKenzie and D. R. Ulrich, Wiley, New York, 1988. Reprinted in CHEMTECH, **19**, 230 (1989).
5. J. E. Mark and B. Erman, Rubberlike Elasticity. A Molecular Primer, Wiley-Interscience, New York (1988).
6. J. E. Mark, in Frontiers of Macromolecular Science, ed. by T. Saegusa, T. Higashimura, and A. Abe, Blackwell, Oxford, 1989.
7. S. Craddock and A. Hinchliffe, Matrix Isolation, Cambridge University Press, New York, 1975.
8. L. L. Hench and D. R. Ulrich, Eds., Ultrastructure Processing of Ceramics. Glasses. and Composites, John Wiley & Sons, New York, 1984.
9. L. L. Hench and D. R. Ulrich, Eds., Science of Ceramic Chemical Processing, John Wiley & Sons, New York, 1986.
10. Ultrastructure Processing of Advanced Ceramics, ed. by J. D. MacKenzie and D. R. Ulrich, Wiley, New York, 1988.
11. D. R. Ulrich, CHEMTECH, **18**, 242 (1988).
12. G. S. Sur and J. E. Mark, Eur. Polym. J., **21**, 1051 (1985).
13. S.-B. Wang and J. E. Mark, Polym. Bulletin, **17**, 271 (1987).
14. S. J. Clarson and J. E. Mark, Polym. Commun., **30**, 275 (1989).
15. J. E. Mark and S.-B. Wang, Polym. Bulletin, **20**, 443 (1988).
16. S.-B. Wang and J. E. Mark, ms. in preparation.
17. M. A. Llorente and J. E. Mark, Macromolecules, **13**, 681 (1980).
18. K. O. Meyers, M. L. Bye, and E. W. Merrill, Macromolecules, **13**, 1045 (1980).

19. J. Li and J. E. Mark, unpublished results.
20. P. R. Saunders and A. G. Ward, in Proceedings of Second International Congress of Rheology, Butterworths, London, 1953.
21. Z. Li, J. E. Mark, E. K. M. Chan, and L. Mandelkern, Macromolecules, 22, 000 (1989).
22. C.-C. Sun and J. E. Mark, Polymer, 30, 104 (1989).
23. S. J. Clarson and J. E. Mark, Polym. Commun., 28, 249 (1987).
24. J. E. Mark, Polym. Eng. Sci., 19, 409 (1979).
25. C.-C. Sun and J. E. Mark, J. Polym. Sci., Polym. Phys. Ed., 25, 1561 (1987).
26. W. Qu and J. E. Mark, unpublished results.
27. D. K. Thomas, Polymer, 7, 99 (1966).
28. J. E. Mark, Y.-P. Ning, M.-Y. Tang, and W. C. Roth, Polymer, 26, 2069 (1985).
29. P. Xu, S. Wang, and J. E. Mark, ms. in preparation.
30. W. Ostwald, Z. Physik. Chem., 34, 495 (1900).
31. J. E. Mark, C.-Y. Jiang, and M.-Y. Tang, Macromolecules, 17, 2613 (1984).
32. S. J. Clarson, J. E. Mark, and K. Dodgson, Polym. Commun., 29, 208 (1988).
33. V. Y. Levin, G. L. Slonimskii, K. A. Andrianov, A. A. Zhdanov, Y. K. Godovskii, V. S. Papkov, and Y. A. Lyubavskaya, Polym. Sci. USSR, 15, 256 (1973).
34. S. Wang and J. E. Mark, ms. in preparation.
35. D. W. Schaefer and K. D. Keefer, Phys. Rev. Lett., 53, 1383 (1984).
36. D. W. Schaefer, L. Jian, C.-C. Sun, D. McCarthy, C.-Y. Jiang, Y.-P. Ning, J. E. Mark, and S. Spooner, submitted to "Proceedings of Fourth International Conference on Ultrastructure Processing of Ceramics, Glasses, and Composites", ed. by D. R. Ulrich and D. R. Uhlman, Wiley, New York, 1989.
37. D. W. Schaefer, J. E. Mark, L. Jian, C.-C. Sun, D. McCarthy, C.-Y. Jiang, and Y.-P. Ning, in Polymer-Based Molecular Composites, ed. by D. W. Schaefer and J. E. Mark, (Mat. Res. Soc. Symp. Proc, 171, Pittsburgh PA, 1989).
38. H. K. Schmidt, in Inorganic and Organometallic Polymers, ed. by M. Zeldin, K. J. Wynne, and H. R. Allcock, Am. Chem. Soc., Washington, DC, 1988, and relevant references cited therein.
39. H.-H. Huang, G. L. Wilkes, and J. G. Carlson, Polymer, 30, 2001 (1989), and relevant references cited therein.
40. J. E. Mark and C.-C. Sun, Polym. Bulletin, 18, 259 (1987).
41. F.-S. Fu and J. E. Mark, J. Polym. Sci., Polym. Phys. Ed., 26, 2229 (1988).
42. F.-S. Fu and J. E. Mark, J. Appl. Polym. Sci., 37, 2757 (1989).
43. G. S. Sur and J. E. Mark, Polym. Bulletin, 20, 131 (1988).
44. G. S. Sur and J. E. Mark, Eur. Polym. J., 24, 913 (1988).
45. Polymer Handbook, 3rd Ed., ed. by J. Brandrup and E. H. Immergut, Wiley-Interscience, New York, 1989.
46. J. Ibemesi, N. Gvozdic, M. Keumin, M. J. Lynch, and D. J. Meier, Polym. Preprints, 26(2), 18 (1985).
47. Z. Rigbi and J. E. Mark, J. Polym. Sci., Polym. Phys. Ed., 23, 1267 (1985).
48. G. B. Sohoni and J. E. Mark, J. Appl. Polym. Sci., 34, 2853 (1987).
49. S. Liu and J. E. Mark, Polym. Bulletin, 18, 33 (1987).
50. G. S. Sur and J. E. Mark, Polym. Bulletin, 18, 369 (1987).
51. A. M. S. Al-ghamdi and J. E. Mark, Polym. Bulletin, 20, 537 (1988).
52. Perspectives in Molecular Sieve Science, ed. by W. H. Flank and T. E. Whyte, Jr., Am. Chem. Soc., Washington, DC, 1988.

STRUCTURE OF MICROPHASE-SEPARATED SILICA/SILOXANE MOLECULAR COMPOSITES

DALE W. SCHAEFER*, JAMES E. MARK*◆, DAVID McCARTHY‡, LI JIAN‡, C. -C. SUN‡ AND BELA FARAGO†

*Sandia National Laboratories, Albuquerque, NM 87185, USA

‡Department of Chemistry and the Polymer Research Center, The University of Cincinnati, Cincinnati, OH 45221, USA

†Insititut Laue-Langevin, 38042 Grenoble, France

ABSTRACT

The structure of several classes of silica/siloxane molecular composites is investigated using small-angle x-ray and neutron scattering. These filled elastomers can be prepared through different synthethic protocols leading to a range of fillers including particulates with both rough and smooth surfaces, particulates with dispersed interfaces, and polymeric networks. We also find examples of bicontinuous filler phases that we attribute to phase separation via spinodal decomposition. *In-situ* kinetic studies of particulate fillers show that the precipitate does not develop by conventional nucleation-and-growth. We see no evidence of growth by ripening whereby large particles grow by consumption of small particles. Rather, there appears to be a limiting size set by the elastomer network itself. Phase separation develops by continuous nucleation of particles and subsequent growth to the limiting size. We also briefly report studies of polymer-toughened glasses. In this case, we find no obvious correlation between organic content and structure.

INTRODUCTION

Historically, the development of specialty polymers has proceeded largely through the manipulation of polymer chain architecture. Glassy vs rubbery behavior, for example, can be adjusted with backbone stiffness. Strain-induced crystallization can be enhanced via stereoregularity. Flame retardancy is augmented by incorporation of chlorinated moieties. Silicon-based systems provide enhanced high-temperature stability. In all these cases, the enhancement of a targeted property usually implies the sacrifice of another. If backbone stiffness is increased to raise the glass transition temperature, for example, toughness is bound to suffer.

Multicomponent systems that are homogeneous on length scales exceeding $1\mu m$ offer new promise to meet the competing requirements of high-performance polymers. The hope is that by appropriate manipulation of phase structure, it will be possible to simultaneously enhance multiple properties. Unfortunately, successful techniques for achieving these so-called molecular composites (MCs) are limited. In the absence of systematic relationships between synthetic protocol, structure and properties, it is difficult to optimize these materials. Even for conventional composites prepared by mixing, for example, the properties (ramification, stiffness, interfacial properties etc.) of the ideal filler are not well established.

Two factors have limited the understanding of the microstructure of complex phase-separated materials: the absence of unambiguous methods for characterizing structure, and the lack of reasonable models to predict structure based on chemical and physical parameters. Substantial progress, however, has been made in both these areas due to advances in instrumentation, advances in the interpretation of scattering from disordered systems, and advances in development of simple models describing complex disorderly growth processes. Here we attempt to build on these advances to enhance our understanding of silica/siloxane MC's.

We focus on the structure of microphase-separated silica-filled siloxane elastomers[1]. We study materials ranging from the unfilled siloxane rubber to polymer-toughened silicate glasses. Based on insights from kinetic growth models and known results for solution polymerization of silicon alkoxides[2], we formulate synthetic recipes designed to generate fillers of varying degrees of ramification. We infer relevant aspects of the filler structure from small-angle x-ray (SAXS) and small-angle neutron scattering (SANS). We establish that filler structure does indeed depend on synthetic protocol. Elsewhere we discuss the relationship between structure and mechanical properties[3].

Because of the importance of "structure" to our study, we first review the nature of small-angle scattering of neutrons (SANS) and x-rays (SAXS) from multiphase materials. To understand the relationship between structure, scattering and synthetic technique it is useful to consider the distinction between equilibrium, and kinetic factors that influence morphology, and therefore scattering behavior.

STRUCTURE AND SMALL-ANGLE SCATTERING

Even a brief review of the history of crystalline materials reveals that Bragg's discovery of sharp x-ray diffraction lines played a crucial role in the understanding of the structure and properties of crystalline solids. No less important were the advances in the interpretation the broad x-ray diffraction features from disordered systems such as liquids and glasses. In both cases the knowledge extracted from diffraction pertains to atomic and molecular length scales.

Molecular composites are typically disordered with "structure" occuring on length scales that are large compared to atomic dimensions. Often this large-scale morphology is of dominant importance in determining material properties. Diffraction (actually diffuse scattering) from these materials is found at small angles (<1°) and is often rather featureless. Interpretation of these featureless profiles is the key to structure/property relationships in microphase-separated materials.

Recently, fractal geometry[4, 5] has emerged as the pertinent description for countless random physical phenomena and disordered natural forms ranging from branched polymers to geographic coastlines. Fractal geometry not only delivers a quantitative measure of disorder but also provides insight into the origin of that disorder in terms of growth models[6]. In addition, the featureless scattering curves (often power-law in form) described above fall to simple interpretation using fractal geometry.

Disordered fractal forms are often observed in systems that develop far from equilibrium via kinetic growth processes. Order, by contrast, is the signature of equilibrium and results because the system has the opportunity to test many configurations and find the lowest energy state, albeit in accordance with Boltzmann's law. An example of an equilibrium structure is a crystal grown from solution where depositing atoms or molecules can move on the surface to find an optimum solidification front. Kinetic growth, on the other hand, occurs when bonds, once formed, do not dissociate so the system develops far from equilibrium. By near-equilibrium growth we envision an intermediate process where thermodynamic factors, like surface tension, influence growth as the system approaches the lowest-energy equilibrium state.

Figure 1 compares typical scattering patterns expected for equilibrium, near-equilibrium and kinetic systems. The scattered intensity I(Q) is parameterized by the momentum transfer or scattering wave vector Q, which, for elastic scattering, is simply proportional to $\sin(\emptyset/2)$ with $\emptyset$ being the scattering angle measured from the transmitted beam,

$$I(Q) = \int g(r) \exp(iQr) \, d^3r.$$

Here g(r) is the autocorrelation function of scattering centers (e.g., electrons in the case of x rays). Qualitatively I(Q) measures the strength of the spatial Fourier component with wave vector Q in the spectrum of density or concentration fluctuations. Thus, the sharp lines in Fig. 1-A correspond to discrete Fourier components (Bragg reflections) and
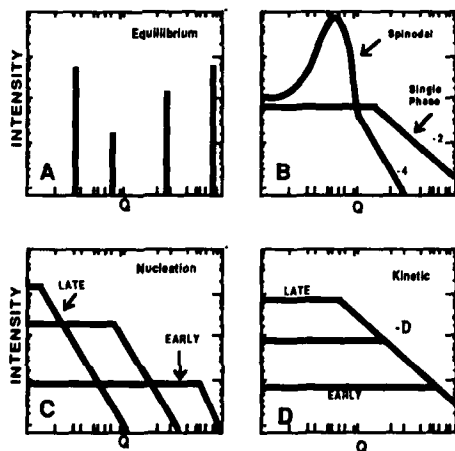
FIG. 1. Scattering profiles for ordered equilibrium systems compared to those expected from three growth processes.

represent the pattern seen for ordered, equilibrium systems. *If the growth process is accelerated, say by a quench, then new broad features are found in the scattering profiles particularly at small angles corresponding to large distances (actually exceedingly large compared to atomic scales) equivalent to Bragg spacings of 100 Å or more.* Figure 1-B, for example, shows the development of a peak in the scattering profile for growth following a spinodal quench. Fig. 1-C is the corresponding profile for nucleation-and-growth, *a process characteristic of quenches into the metastable regime.* Here the limiting slope is -4, the signature of smooth sharp interfaces and the scattering profile develops in a characteristic manner as indicated in the figure. For these near-equilibrium growth processes, thermodynamic concepts like surface tension are valid and provide an essential understanding of the observed structures and their time development[7, 8, 9].

FIG. 2. Scattering profiles for thick samples polymerized under acidic and basic conditions by the two-step procedure.

A qualitatively distinct scattering profile is observed in kinetic systems that evolve far from equilibrium. In this case featureless power-law scattering is observed (Fig. 1-D), indicating a power-law continuum of Fourier components[2, 5, 6]. From the slope S of log-log plots of I vs Q, *one can distinguish smooth surfaces (S = -4) from fractally rough surfaces (S = -3 to -4) from a branched or linear polymer (S = -1 to -3). Slopes less (i.e. steeper) than -4 indicate a gradient in the concentration of the two phases at the interface. Detailed analysis of the shape of* the scattering curve for these systems yields the interfacial profile[10, 11].

REINFORCED ELASTOMERS

Based on the above ideas, we studied the structure of a series of silica-filled siloxane elastomers[1]. Typically the elastomer was prepared from hydroxy-terminated polydimethylsiloxane (PDMS) of number-average molecular weight 18.0×10^3 end-linked with TEOS (tetraethylorthosilicate), using stannous-2-ethylhexanoate as a catalyst. The weight ratios of PDMS:TEOS:CATALYST were 100:0.58:0.3 These networks were extracted using tetrahydrofuran and dried.

The above networks were then filled by first swelling in pure TEOS and subsequently placing swollen strips into acidic and basic water solutions prepared from acetic acid and ammonia at pH = 2.5 and 11. We call this a two-step procedure. Room temperature reactions were carried out for 6 to 12 hours. The amount of filler was calculated from the weight gain.

Fig. 2 shows the scattering profiles for acid and base-catalyzed filler precipitated in 3 mm thick PDMS elastomers. In Fig. 2 as in Figs 4 and 5, a Q-independent background has been subtracted from the data. The limiting slopes of -4 (acid) and -4.5 (base) in Fig. 2 imply compact particulate fillers with sharp and diffuse interfaces respectively. In some cases, we observe slopes of exactly -4.0 for basic systems at low filler content, although the rule is that the slopes are steeper indicating a gradient in the two phases at the interface. The base-catalyzed data were fit to a model[11] that assumes a sigmoidal interfacial gradient between SiO_2 and PDMS yielding an interfacial layer of 10Å. For the acid-catalyzed system, the interface is sharp (limiting slope = -4). For both systems, the surface area (SA) was calculated from the invariant and the magnitude of the scattering in the limiting high Q regime[12]. Assuming independent particulate fillers, these surface areas give particle radii R_p listed in Table 1. These radii match reasonably with those obtained from Guinier analysis(log I vs Q^2) in the regime near $0.02Å^{-1}$. For comparison we also include the average chord R_c for lines passing through a random two-phase system[13]. The similarity of these lengths supports the assumption of independent particles.
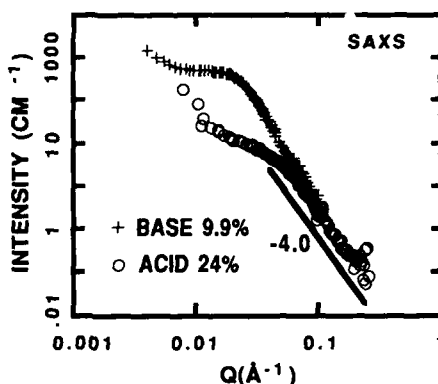
TABLE I: SURFACE AREAS AND LENGTH SCALES (Å)

R_c is the average chord calculated from the surface area (SA), R_p is the particle radius, calculated from SA, R_g is the Guinier radius, and R_h is the hard sphere radius from R_g.

CATALYSIS	% SILICA	SA (m²/gm)	R_c	R_p	R_g	R_h
BASE	10	14	118	89	87	112
ACID	24	39	71	53	57	74
ACID	17	----	----	----	56	----

The upturn in the data below 0.01Å⁻¹ signals the presence of long-range structure. In general slopes near -4 are observed in this regime, consistent sharp interfaces with no evidence of a limiting length-scale below 1000Å. To further elucidate the relationship between this large-scale structure and the 100Å particulates, we studied the kinetics of the glassy phase development by *in-situ* SANS during precipitation.

Fig. 3 shows the time development of the glassy phase for an ammonia vapor-catalyzed precipitation. As can be seen in data taken 5 minutes after catalyst introduction, large scale structure is present in the swollen networks before there is any evidence of particulates. The particulate form factor develops later and is superimposed on the large-scale structure. This large-scale structure is presumably due to incompatibility between TEOS polymerization product and PDMS which leads to microscopic phase separation very early in the polymerization.
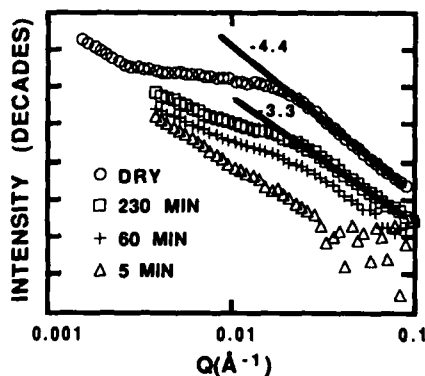
Fig. 3. *In-situ* neutron scattering data for ammonia vapor catalyzed precipitation. Dry sample was studied 3 months after the kinetic runs.

It is interesting to note that the developing particulates in Fig. 3 show slopes of -3.3 consistent with a fractally rough interface[14]. Rough particulates have previously been observed by Keefer and Schaefer for base-catalyzed solution-polymerized TEOS[15]. When the sample is dried, a limiting slope of -4.4 is found consistent with a graded interface. It should be noted that the data for dried samples in the regime $0.005 \text{ Å}^{-1} \le Q \le 0.1 \text{Å}^{-1}$ were acquired by SAXS whereas all the rest of the data were by SANS. With one exception (Fig. 7), nevertheless, we have never observed limiting slopes between -3 and -4 for any dry samples using either SAXS or SANS.

Note that the time progression in Fig. 3 does not follow the nucleation-and-growth pattern in Fig. 1-C. In normal surface-tension-driven growth, large particles grow at the expense of small. For *in-situ* precipitation, however, growth is limited to about 100Å. Later growth occurs by nucleation of new particles leading to the time-development seen in Fig. 3. Similar behavior is reported by Gilliom, Schaefer and Mark[16] for MC's produced by catalytic hydrogenation in bulk polybutadiene.

Because of the possibility of effects due to leaching of the TEOS from the sample during polymerization, we also studied thin (.3mm) samples in addition to the 3mm samples described above which have a visible skin. For base-catalyzed systems, we found particulate fillers in all cases, whereas for acid-catalyzed systems we occasionally found polymer-like fillers, particularly at low loading and in thin samples. Fig. 4, for example, shows the SAXS data for an acid-catalyzed system with 17% filler. The limiting slope of -2.8 is consistent with a branched polymeric filler, probably an interpenetrating network. In solution, alkoxides are known to produce polymer-like clusters in acid solution due to a growth mechanism called reaction-limited cluster aggregation[2]. By contrast, polymerization in basic systems is believed to proceed by reaction-limited monomer-cluster growth which leads to compact particles. Of course, one of the motivations for our work was to exploit these different classes of growth to control the morphology of filler phases. Clearly, however, the essential controlling factors for filled systems are not yet totally clear.
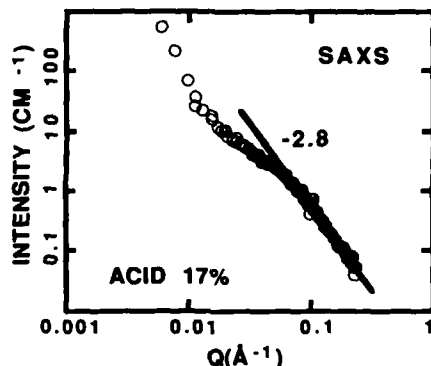
Fig. 4. SAXS scattering profile for a thin sample polymerized under acidic conditions. Limiting slope of -2.8 indicated a non-particulate filler morphology.
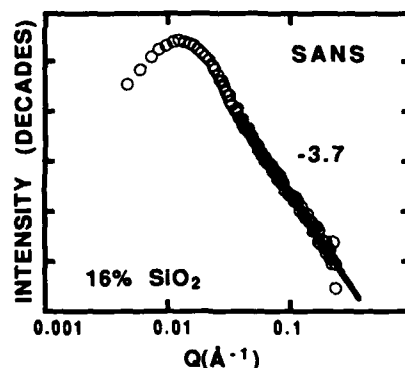
Fig. 5. Scattering profile for silica filled PDMS showing a peak characteristic of spinodal decomposition.

In a few samples, we observed[3] a peak in the scattering profiles (Fig. 5) consistent with those reported by Wilkes et al[17] for "ceramers." We interpret the peak to be the remnant of phase separation by spinodal decomposition. Since phase incompatibility usually increases during polymerization[18], we believe that crosslinking of the glassy phase induces phase separation in the fluid precursor. The resulting spinodal morphology is then locked in place by "gelation" of the glassy phase. The shape of the curve in Fig. 5 is very close to that found in simulations of spinodal decomposition reported by Chakrabarti et al[7].

It is interesting to note that the material in Fig. 5 is quite brittle showing a maximum extensibility of only 1.2. We believe that the brittle nature of the material as well as the peak in the scattering profile indicate that the glassy phase is continuous. The spinodal process is known to produce bicontinuous morphologies[9, 19].

POLYMER-TOUGHENED GLASSES

We also studied glassy sol-gel silicates toughened by the incorporation of PDMS. The samples studied here are those previously reported by Mark and Sun[20]. These materials were characterized via the D-hardness method. Mark and Sun found that the D-hardness decreased smoothly with increasing organic content as shown in Fig. 6. The materials with high organic/Si ratio have mechanical properties similar to the reinforced elastomers discussed above whereas those with D ≈ 50 are leathery.

The SAXS profiles of the toughened glasses in Fig. 7 reflect a variety of structures. For low silica-content glasses (D = 2 and 18), there is evidence of the formation of a spinodal-like peak, but the limiting slope does not approach -4 indicating that the short-scale structure should be viewed as an interpenetrating network, rather than as a distinctly separate
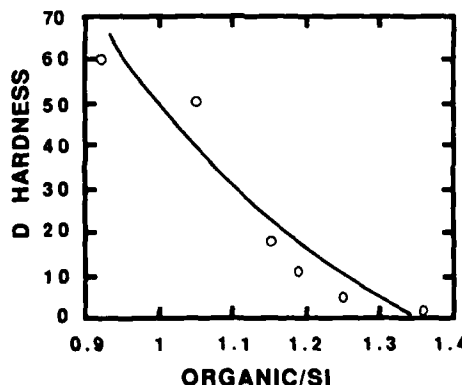
Fig. 6. Hardness as a function of organic content for polymer toughened silica glasses.

phase. At higher glass content, however, phase separation is distinct (slope ≈ -4) at the 100Å level. The SAXS profile for the material with the highest glass content (D = 60) is flat in the region near 0.1Å⁻¹ This plateau implies composition or density fluctuations on very short scales (<20Å) beyond the limits of SAXS.

All of the toughened samples show evidence of structure on scales exceeding 500Å. The limiting slopes of about -4 at small Q in Fig. 7 are consistent with large-scale phase separation similar to that discussed in connection with reinforced elastomers. To establish the structure of the large-scale domains, we studied the two extreme materials in Fig. 7 using the high resolution D-11 SANS camera at the Institut Laue-Langevin in Grenoble, France. The data, presented in Fig. 8, demonstrate that the large-scale domains are similar for the two materials. Both data sets are consistent with uniform domains with a Guinier radius

Fig. 7. SAXS data for the series of polymer-toughened glasses shown in Fig. 6.

of 1500Å. The flat background at large Q in Fig. 8 is due to incoherent scattering so data in this regime cannot be directly compared with the SAXS data in Fig. 7.

We conclude that hardness for toughened glasses is determined largely by organic content. No obvious correlations exist between the hardness and observed scattering patterns. Large-scale structure is independent of filler whereas distinct changes in intermediate structure (100Å) are found as a function of organic content.

CONCLUSION

The morphological tendencies observed in silica-filled siloxanes are clearly dependent on synthetic protocol. Although particulate fillers are the rule, we can generate both polymeric fillers and particulates with varied interfacial properties ranging from fractally rough surfaces to compositionally graded interfaces. In general, the degree of filler ramification follows that previously observed in the solution polymerization of alkoxides. Although correlations exist between structure and mechanical properties for filled elastomers[3], no clear pattern is obvious for the rubber toughened glasses.

Fig. 8. High-resolution SANS data for two polymer-toughened glasses. The Guinier radius is independent of hardness.

ACKNOWLEDGEMENT

REFERENCES

♦Permanent address: Department of Chemistry and the Polymer Research Center, The University of Cincinnati, Cincinnati, OH 45221, USA.

1. J. E. Mark and D. W. Schaefer in Polymer-Based Molecular Composites, edited by D. W. Schaefer and J. E. Mark (Mat. Res. Soc. Symp. Proc. 171, Pittsburgh, PA 1990).
2. D. W. Schaefer, Science 243, 1023 (1989).
3. D. W. Schaefer, J. E. Mark, L. Jian, C.-C. Sun, D. McCarthy, C.-Y. Jiang, Y.-P. Ning and S. Spooner, in Ultrastructure Processing of Ceramics, Glasses and Composites, edited by D. R. Uhlman, D. R.Ulrich and S. H. Risbut (J. Wiley, N. Y., 1990).
4. B. B. Mandelbrot, The Fractal Geometry of Nature (Freeman, San Francisco, 1982).
5. J. E. Martin and A. J. Hurd, J. Appl. Cryst. 20, 61 (1987).
6. D. W. Schaefer, Bull. Mat. Res. Soc. 13 (2), 22 (1988).
7. A. Chakrabarti, A. Toral, J. D. Gunton and M. Muthukumar, Phys. Rev. Lett. 63, 2071 (1989).
8. W. Haller and P. B. Macedo, Physics Chem. Glasses 9, 153 (1968).
9. J. W. Cahn, J. Chem. Phys. 42, 93 (1965).
10. W. Ruland, J. Appl. Cryst. 4, 70 (1971).
11. J. T. Koberstein, B. Morra and R. S. Stein, J. Appl. Cryst. 13, 34 (1980).
12. A. J. Hurd, D. W. Schaefer and A. M. Glines, J. Appl. Cryst. 21, 864 (1988).
13. A. Guinier and G. Fournet, Small-Angle Scattering of X-Rays (Available from University Microfilms International, Ann Arbor, MI, 1955).
14. H. D. Bale and P. W. Schmidt, Phys. Rev. Lett. 53, 596 (1984).
15. K. D. Keefer and D. W. Schaefer, Phys. Rev. Lett. 56, 2376 (1986).
16. L. R. Gilliom, D. W. Schaefer and J. E. Mark in Polymer-Based Molecular Composites, edited by D. W. Schaefer and J. E. Mark (Mat. Res. Symp. Proc. 171, Pittsburgh, PA 1990).
17. G. L. Wilkes, A. B. Brennan, H. Huang, D. Rodrigues and B. Wang in Polymer Based Molecular Composites, edited by D. W. Schaefer and J. E. Mark (Mat. Res. Soc. Symp. Proc. 171, Pittsburg, PA 1990).
18. P. G. deGennes, Scaling Concepts in Polymer Physics (Cornell University Press, Ithaca, NY, 1979).
19. N. F. Berk, Phys. Rev. Lett. 22, 2718 (1987).
20. J. E. Mark and C.-C. Sun, Polym. Bull. 18, 259 (1987).

NMR IMAGING OF SILICA-SILICONE COMPOSITES

LEONCIO GARRIDO*, JEROME L. ACKERMAN* AND JAMES E. MARK**
* NMR Center, Massachusetts General Hospital, 149 13th St., Charlestown, MA 02129.
** Department of Chemistry and the Polymer Research Center, University of Cincinnati, Cincinnati, OH 45221.

ABSTRACT

Polydimethylsiloxane (PDMS) model networks reinforced by in situ precipitated SiO_2, and polymer-modified silica glasses were obtained following the usual sol-gel methods. The conditions were chosen to increase the probability of observing inhomogeneities: (i) bulky samples, and (ii) limited reaction times. These composites were characterized by measuring bulk spin-lattice (T_1) and spin-spin (T_2) relaxation times and using ^1H NMR two-dimensional Fourier transform (2DFT) spin echo imaging techniques. The T_1 and T_2 maps show clear and significant variations of NMR signal intensity throughout the sample due to nonuniform hydrolysis of the tetraethylorthosilicate (TEOS) in the specimens.

INTRODUCTION

The search for materials with optimal properties for specific applications, including new pathways for their synthesis and processing, is a continuing process. Over the past 20 years, sol-gel processes have been extensively studied as alternatives to the existing preparation methods for composites [1,2]. The ability to manipulate the composite microstructure by the sol-gel reaction results in materials with improved and sometimes unexpected physical and chemical properties. The understanding of a material's behavior requires knowledge of how the properties of interest depend upon its chemical composition and molecular structure. Nuclear magnetic resonance (NMR) spectroscopy is very sensitive to both the chemical composition and the structure of a substance. These material properties are reflected in the chemical shift spectrum as well as in the NMR relaxation parameters. NMR imaging techniques [3-11], by producing visual pictures of the spatial variation of selected NMR properties, offer the possibility of selectively mapping the distribution of particular chemical species in a region of interest. Moreover, NMR imaging can also provide spatial information about changes in NMR properties that can be correlated with alterations in molecular structure and dynamics.

The aim of this work is to develop NMR imaging techniques for the characterization of sol-gel prepared organic-inorganic composites by mapping the organic phase distribution and the degree of alkoxide hydrolysis. We have obtained ^1H NMR images of intentionally heterogeneous polydimethylsiloxane (PDMS) model networks reinforced by in situ precipitated silica (SiO_2) and polymer-modified silica glasses. In these images the variations in NMR signal intensity between different regions in the sample (image contrast) are a function of proton density, spin-lattice (T_1) and spin-spin (T_2) relaxation times. Such maps of NMR parameters provide a measure of the molecular mobility, which can in turn be related to the spatial variation of the relationship between the organic and inorganic phases throughout the specimen.

EXPERIMENTAL

Preparation of reinforced PDMS model networks.

PDMS model networks were prepared by end-linking reaction of dihydroxyl-terminated PDMS chains having a number average molecular weight, M_n, of 4,200 g mol^{-1} with tetraethylorthosilicate (TEOS) in the usual manner [12]. The networks obtained, cyclindrical pieces 20 mm in diameter and 9 mm in height, were swollen at equilibrium in TEOS (which correspond to a volume fraction of polymer of 0.70). Each swollen sample was then immersed in aqueous solution of CF_3COOH at 5 percent w/w for 15 to 120 min. The acidic catalyst was chosen because of its high efficiency to hydrolyze TEOS [13]. The samples were dried under vacuum to constant weight. The increase in dry weight gave the amount of SiO_2 precipitated within the sample in the elapsed time (see Table I). The large sample size and the short hydrolysis time assure inhomogeneous specimens.

Preparation of polymer-modified silica glasses.

The polymer-modified silica glasses studied in this work were prepared as described elsewhere [14]. Briefly, the functionality of divinyl-terminated PDMS was greatly increased by a substitution reaction to give PDMS with triethosilyl chain ends [15]. Samples having M_n of 720 and 17,600 g mol^{-1}, and mixtures thereof, were added to TEOS or related silane. The functionalized PDMS/silane mixtures were hydrolyzed in aqueous solutions of acetic acid following the usual sol-gel procedures.

Instrumentation and techniques.

All NMR measurements were performed in a Bruker MSL 400 spectrometer/imager equipped with an Oxford 9.4 T (proton frequency at 400.13 MHz) 8.9 cm vertical bore superconducting magnet. The RF coils used are saddle type with diameters ranging from 10 to 30 mm and their longitudinal axis parallel to the static magnetic field. The pulsed gradient amplitudes in the imaging experiments varied between 4 and 40 G cm^{-1}.

Bulk T_1 and T_2 measurements were carried out using inversion recovery and spin echo sequences, respectively. The results are shown in Table I. The inversion time in the IR sequence was varied between 0 and 10 s. The echo time (TE, time between the 90° RF pulse and the center of the echo) in the spin echo sequence ranged from 0.2 to 300 ms. The repetition time, TR, was 10 s in both cases, more than five times T_1.

^{1}H NMR images of the reinforced networks and modified glasses were obtained using two-dimensional Fourier transform (2DFT) spin echo techniques with TEs on the order of 3 to 20 ms. The selective excitation of a slice throughout the sample 500 μm thick was achieved with a 1 ms wide sinc-function amplitude modulated RF pulse. The pulse sequence TR was typically 3s. The total imaging time varied between 25.6 and 76.8 min. The digital resolution was 128X by 128Y pixels ranging from 65 to 200 μm in both axes.

Table I: Amount of silica, T_1 and T_2 values of reinforced PDMS model networks

Sample ref.	Hydrolysis time (min)	SiO_2 (% w/w)	T_1 (s)	T_{2s}[a] (ms)	f_s[b]	T_{2l}[c] (ms)
1	120	4.7	1.26	0.86	0.968	106.3
2	90	–	1.19	0.86	0.965	68.6
3	60	4.6	1.21	0.81	0.970	74.4
4	45	4.2	1.23	0.82	0.966	51.6
5	30	2.4	—	0.84	0.967	113.7
6	15	1.9	1.24	0.79	0.962	220.7

[a] Spin-spin relaxation time of the major component.

[b] Fraction of major component contributing to the NMR signal ($f_s + f_l = 1$).

[c] Spin-spin relaxation time of the minor component.

RESULTS AND DISCUSSION

The T_1 data was analyzed assuming the presence of only one component (a monoexponential function). The agreement found between the theoretical curves and the experimental results was very good. As shown in Table I, T_1 does not depend significantly on the time allowed for the hydrolysis of TEOS (increasing amount of SiO_2). The NMR spin-lattice relaxation mechanism is apparently not affected by the presence of silica and the T_1 values obtained are similar to those of unfilled PDMS model networks with molecular weight between crosslinks, M_c, between 3,700 and 18,000 g mol^{-1} [16].

The analysis of the T_2 data is more complex. An apparent two component model gives the best fit to the experimental results. The values thus obtained are shown in Table I. This may be interpreted as the result of two contributions to the NMR signal, one from a major fraction of material attributed to the PDMS chains forming the network and the other, most likely, from the ethyl groups in partially hydrolyzed TEOS. The T_2 values of the major component agree very well with the results obtained for unfilled PDMS model networks [16]. The T_2 of the minor component (3 to 4 percent) varies with the hydrolysis time of TEOS. It is known that TEOS tent to form polymeric chains when the hydrolysis reaction is catalyzed by acids [17]. Therefore, it is possible to have TEOS polymer with ethoxyl and hydroxyl side groups in various proportions. Their relative contribution to the NMR signal is uncertain at this point and further ongoing experiments might clarify it.

The complexity of the process is clearly manifested by the ^{1}H NMR imaging experiments. Figure 1 shows two images, along its longitudinal axis, of a PDMS model network (sample # 6 in Table I) obtained with a two dimensional spin echo sequence having TE of 3.3 (A) and 22.7 (B) ms. The rest of the experimental conditions were the same for both images. The heterogeneity of the sample is readily apparent. The dark rim around the sample in Figure 1 A may indicate the reduced mobility of the network chains in this region compared to that in the sample core, probably because of a high concentration of SiO_2. The availability of water and catalyst in the sample periphery might be the reason for the observed difference. At long TE the PDMS chains do not contribute to the echo [16] and only material with high molecular mobility, i.e. oligomers
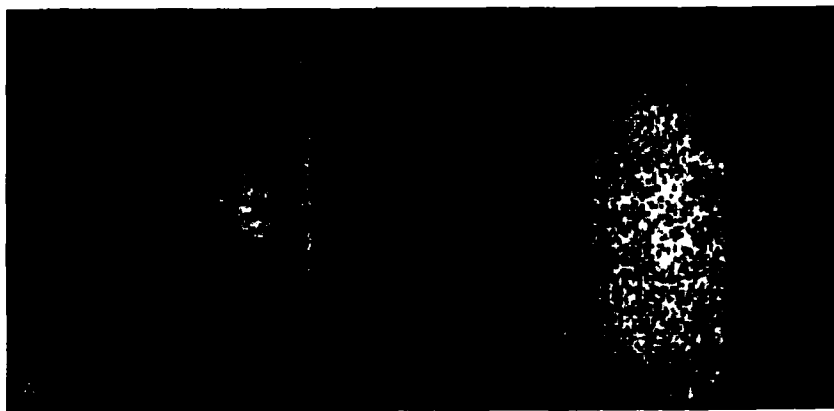
Figure 1. ^{1}H NMR images of the sample # 6 obtained with a two dimensional spin echo sequence having a TE of 3.3 (A) and 22.7 (B) ms. TR was 3 s in both cases. Selective excitation was used to define a 500 μm slice thickness in the sample axial plane. The resolution is 128X by 128Y pixels of 180 and 200 μm, respectively. The time required to acquire the data for each image was 25.6 min. The dark rim at the edge of the sample may indicate a reduced molecular mobility of the network chains due to the presence of SiO_2.

from partial TEOS hydrolysis, is visible to the NMR experiment. A significant change in the NMR images with short TE is not observed with increasing hydrolysis time. However, T_2-weighted images (long TE) show some variations in signal intensity. Figure 2 shows two images (A and B) of sample # 4 obtained with the same conditions as Figures 1 A and B, respectively. As mentioned above, CF_3COOH is a very efficient catalyst in promoting the TEOS hydrolysis. Therefore, changes at the edges of the sample will occur relatively fast while at the center those changes are controlled by the
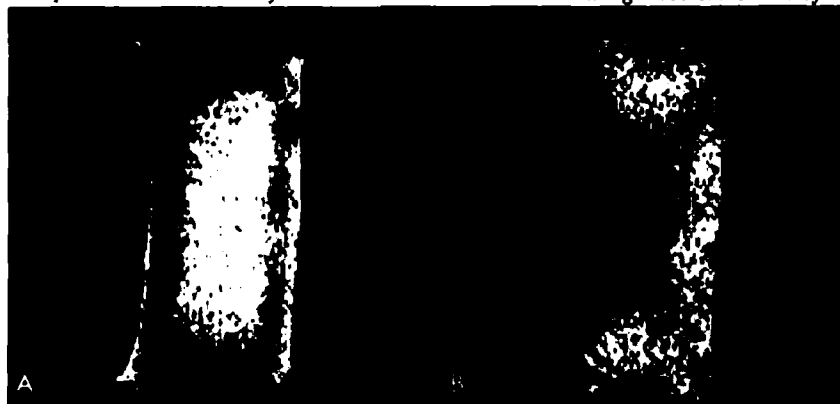
Figure 2. Axial ^{1}H NMR images of sample # 3. Both images, Figures A and B, were taken with the same experimental conditions as for Figures 1 A and B, respectively. A significant variation of NMR signal intensity in Figure 2 B (T_2-weighted image) is observed when compared to that of Figure 1 B.

Figure 3. On the left (A) is shown the ^{1}H NMR image of a modified silica glass which corresponds approximately to the cross-sectional photograph displayed on the right (B). A pulse sequence similar to that described in the previous figures was used. TE was changed to 3.0 ms. The resolution is 128X by 128Y pixels of 110 μm in both axes. The total imaging time was 76.8 min.

diffusion rates of the water and catalyst in the swollen rubber.

As a part of the characterization of silica-silicone composites by NMR imaging, we are currently investigating polymer-modified silica glasses. Figure 3 B shows a photograph of the sample section of a modified glass which corresponds approximately to the NMR image shown in Figure 3 A. There is a correlation between the visual appearence and the NMR experiment. Heterogeneities are visible in the latter but, as in the case of reinforced PDMS rubbers, more detailed understanding requires further studies.

CONCLUSIONS

Our results demonstrate that proton magnetic resonance imaging is capable of revealing inhomogeneities in *in situ* precipitated SiO_2-filled PDMS networks and in polymer-modified silica glasses, at least when relatively short reaction times and thick sections are employed. The contrast between different regions is highlighted with T_2-weighted imaging pulse sequences, suggesting that the underlying variations seen in the images may be closely related to variations in the mobility of the network segments. In the case of the filled networks there is a clear, if nonmonotonic, progression of spin-spin relaxation time values of the long T_2 component with hydrolysis time; T_1 values are constant. We suggest a variation in ethyl group concentration in partially hydrolyzed TEOS as a possible source of this long T_2 signal.

Additional investigations into the molecular nature of the spatial inhomogeneities seen in the composite networks and glasses are required for a more complete understanding of these materials. Destructive analysis such as electron microscopy or local measurements of specific gravity could be used to validate these NMR results, as well as aid in further elucidation of the origin of the T_2 variations. We are currently pursuing these and other avenues. However, it is clear that NMR imaging will be extremely use-

ful as a nondestructive tool for monitoring the uniformity of these and other synthetic materials and for learning about the details of spatially varying chemistry.

ACKNOWLEDGEMENTS

REFERENCES

1. Ultrastructure Processing of Advanced Ceramics, edited by J. D. Mackenzie and D. R. Ulrich (John Wiley & Sons Inc., New York, 1988).

2. Better Ceramics Through Chemistry III, edited by C. J. Brinker, D. E. Clark and D. R. Ulrich (Mater. Res. Soc. Proc., 121, Pittsburg, PA 1988).

3. P. Mansfield and P. K. Grannell, Phys. Rev. B 12, 3618 (1975).

4. A. N. Garroway, J. Baum, M. G. Munowitz and A. Pines, J. Magn. Reson. 60, 337 (1984).

5. N. M. Szeverenyi and G. Maciel, J. Magn. Reson. 60, 460 (1984).

6. F. De Luca and B. Maraviglia, J. Magn. Reson. 67, 169 (1986).

7. C. G. Chingas, J. B. Miller and A. N. Garroway, J. Magn. Reson. 66, 530 (1986).

8. W. A. Ellingson, J. L. Ackerman, J. D. Weyand, R. A. DiMilia and L. Garrido, Ceram. Eng. Sci. Proc. 8, 503 (1987).

9. L. Garrido, J. L. Ackerman, W. A. Ellingson and J. D. Weyand, Ceram. Eng. Sci. Proc. 9, 1465 (1988).

10. D. G. Cory, J. C. de Boer and W. S. Veeman, Macromolecules 22, 1618 (1989).

11. J. B. Miller and A. N. Garroway, J. Magn. Reson. 82, 529 (1989).

12. J. E. Mark and J. L. Sullivan, J. Chem. Phys. 66, 1006 (1977).

13. C.-Y. Jiang and J. E. Mark, Makromol. Chem. 185, 2609 (1984).

14. J. E. Mark and C.-C. Sun, Polym. Bull. 18, 259 (1987).

15. G. S. Sur and J. E. Mark, Eur. Polym. J. 21, 1051 (1985).

16. L. Garrido, unpublished results.

17. K. D. Keefer, in Better Ceramics Through Chemistry, edited by C. J. Brinker, D. E. Clark and D. R. Ulrich (Mater. Res. Soc. Proc., 32, Elsevier, New York, 1984), p. 15-24.

SYNTHETIC POLYMERS IN WATER-IN-OIL MICROEMULSIONS

FRANCOISE CANDAU
Institut Charles Sadron (CRM-EAHP),CNRS-ULP 6, rue Boussingault 67083 Strasbourg Cedex, France

ABSTRACT

High molecular weight water-soluble polymers are usually supplied in the form of water-in-oil emulsions which have advantages of low viscosity and easy storage and dissolution. Most uses in water treatment, flocculation, paper manufacture or mining fields require polymer latexes formed of finely dipersed particles. Polymerization in reverse micelles or microemulsions appears to be an attractive technique because it can lead, under appropriate formulations, to high molecular weight polymers entrapped within small-sized stable particles. The main characteristics and properties of the latexes and polymers formed by this process are described.

INTRODUCTION

Polymerization of water-soluble monomers in hydrocarbon fluids has attracted a renewed interest over the past decade, owing to the suitability of the process for producing high molecular weight polymers at high reaction rates. In this process, a water-soluble monomer (usually in aqueous solution) is emulsified in a continuous oil medium using a water-in-oil emulsifier. Polymerization can be initiated with either oil -or -water-soluble initiators. The product is a dispersion of fine particles of an aqueous high polymer solution which can be easily inverted into water so that the water-swollen polymer particles dissolve rapidly, contrary to solid-powder which forms gels or aggregates when added to water. These high viscosity polymer solutions find applications in water-treatment, flocculation of colloidal suspensions, tertiary oil recovery as pushing fluids, fines retention in paper manufacturing etc [1]. Inverse emulsion polymerization has been far less investigated than conventional (i.e. aqueous) emulsion polymerization. Apart from a large number of patents, there have been few fundamental studies. The pioneering work is due to Vanderhoff et al [2] who studied in 1962 the polymerization of sodium-p-vinyl benzene sulphonate in xylene. More recently, polymerization processes in different inverse colloidal systems, i.e. suspension [3], microsuspension [4,5], dispersion [6], and emulsion [7-12] have been described in the literature.

In general, the problems of latex stability are more severe than for aqueous latexes, due to the absence of electrostatic forces between particles, and to the large difference in density between the organic continuous medium and the polymer core. This led us in the past years to investigate the possibilities offered by a polymerization reaction proceeding in a thermodynamically stable microemulsion rather than in an emulsion. Microemulsions are water-oil colloidal dispersions stabilized by an appropriate mixture of surface-active agents. While inverse emulsions are unstable, turbid and consist basically of two populations with a broad particle size distribution (fig.1), microemulsions are thermodynamically stable and can adopt a large variety of labile structural organizations. The small size of the domains explains their optical transparency [13]. In the oil-rich regions, they are formed of water-swollen spherical droplets of uniform and small size (d $\approx$ 6 nm) dispersed in the oil medium (fig.2a). When the amount of the aqueous phase tends to be of the same order of magnitude as that of the organic phase, the description generally given is that of a bicontinuous structure formed of randomly interconnected oily and aqueous domains [14,15], with the surfactant molecules located at the interface (fig.2b). It should be noted that the formation of a microemulsion requires a
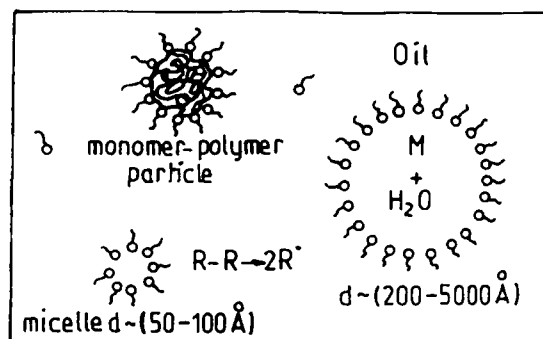
Figure 1 : Schematic representation of an inverse emulsion
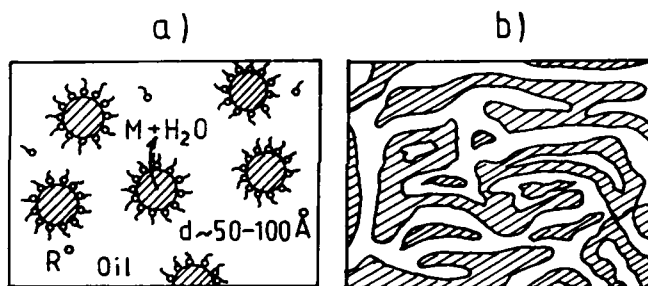
Figure 2 : Schematic representation of a microemulsion
a) inverse globular structure
b) bicontinuous structure

minimum amount of surfactant of around 10%, imposed by the surface coverage of the small domains while somewhat smaller amounts are sufficient for an emulsion.

The microemulsion polymerization of various water-soluble monomers, mostly used in industrial applications, has been investigated. In this paper, we report the main characteristics and properties of the latexes and polymers formed by this process.

STRUCTURE OF OIL/(WATER+MONOMER)/SURFACTANT MICROEMULSIONS

The choice of the system to be polymerized is of critical importance, since it controls the properties of the resultant latexes. Water-soluble monomers such as acrylamide (AM), were polymerized either inside water-swollen micelles (d ~ 6.10^{-3} µm) stabilized with an ionic surfactant, aerosol OT, (sodium 1,4-bis (2 ethylhexyl)sulfosuccinate) [16] or in nonionic microemulsions [17-19]. The latter systems have proven to be the most effective, as they can incorporate up to 25% monomer still remaining stable.

The addition of monomer to the microemulsion produces a considerable extension of the microemulsion domain in the phase diagram. This was interpreted as a cosurfactant effect of the monomer which preferentially

locates at the w/o interface [16,18,19]. The presence of monomer molecules between the surfactant molecules increases both the flexibility and the fluidity of the interface, resulting in a change of its curvature. Eventually, when the radius of curvature becomes very large the globular configuration converts into a bicontinuous structure. The latter structure is favoured by addition of monomers producing a salting-out of the nonionic ethoxylated surfactants. This is the case of sodium acrylate (NaA) [18] or methacryloyloxyethyltrimethylammonium chloride (MADQUAT) [20].

In the case of AOT systems, there is no clear evidence of a globular → bi_continuous transition. However, under certain conditions, addition of acrylamide induces sharp rises in conductivity, indicative of the formation of transient conducting water channels from particle to particle which were attributed to a percolation process [21].

A typical polymerization recipe is the following : cyclohexane : 37.5% ; MADQUAT : 25% ; water : 25% ; nonionic surfactants (Arlacel 83 + Tween 80 ; HLB = 12.9) : 12.5%.

POLYMERS PREPARED IN MICROEMULSIONS

The control of molecular weight of the final polymer is of paramount importance since most applications require ultra-high molecular masses. The polymer molecular weight has been determined from viscometry experiments in aqueous solutions, using the Mark-Houwink relationship [16,22], or from static light scattering [23]. Various parameters control the molecular weight. The production of high molecular weights (10^6-10^7) is achieved by polymerization at lower temperature and at high (monomer)/surfactant levels (fig.3) [22,23].

The properties of poly(acrylamide-co-acrylates) prepared in nonionic microemulsions have been studied by means of several techniques [24,25]. The free radical copolymerization of acrylamide with ionogenic monomers is strongly influenced by the microenvironment. A ^{13}C NMR study performed on poly(acrylamide-co-acrylates) prepared in microemulsions confirmed the influence of the reaction medium. The average copolymer composition was found to be independent of the degree of conversion, also the sequence monomer distribution analyzed from triad proportions, conforms to Bernouillan statistics. The reactivity ratios of both monomers are therefore close to unity, contrary to the literature values reported for copolymers prepared in solution ($r_A = 0.3$, $r_M = 1$) [26]. As the local monomer concentration is much higher in a microemulsion ($= 5$ M) than in a solution ($= 1$ M), this could produce an increased screening of the carboxylate groups by sodium ions. The observed increase in the reactivity parameter of sodium acrylate in the microemulsion ($r_A = 1$) is consistent with this expectation.

The copolymers exhibit high intrinsic viscosities in aqueous solutions (up to 3700 cm^3/g) with maximum around 40 mol% acrylate content due to a superimposition of electrostatic effects and of intramolecular bonds.

STRUCTURAL PROPERTIES OF LATEXES

The inverse latexes formed after polymerization are clear, fluid and highly stable with no apparent settling. A common feature, found in all experiments, is that the final system always consists of an uniform dispersion of spherical latex particles, regardless of the structure of the starting system (globular or bicontinuous). This can be accounted for by the internal dynamics of microemulsions which are constantly rearranging on the time-scale of microseconds. The size of the latex particles has been determined by quasi-elastic light scattering (QELS) and electron microscopy (EM) experiments. Both techniques require an examination with dilute samples, which, in turn, implies that the structure and the particle size are not affected by the dilution process. One thousandfold dilution and the drying process used in EM for the water-swollen polymer particles dispersed in oil can introduce artefacts. A
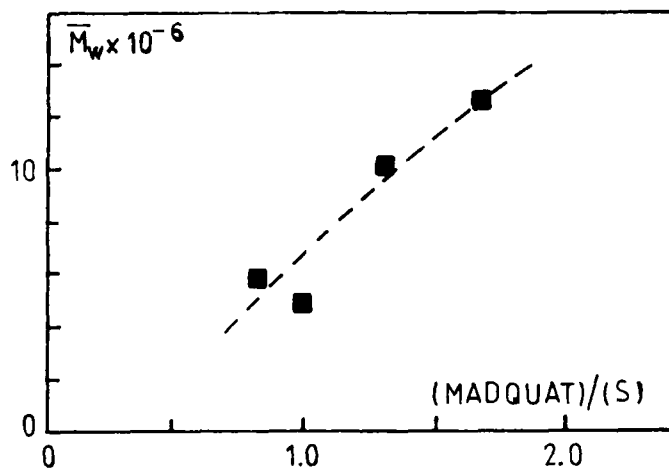
Figure 3 : Variation of the molecular weight of polyMADQUAT with the MADQUAT over surfactant ratio (wt/wt) in the initial microemulsion (from ref.23).
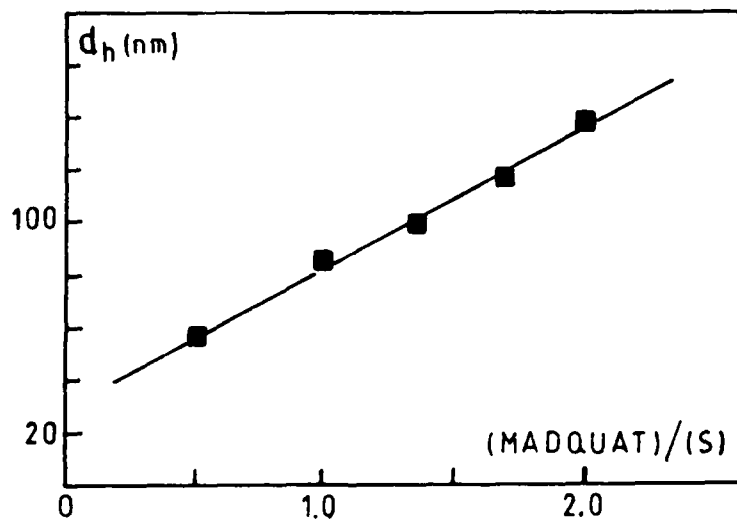
Figure 4 : Variation of the hydrodynamic diameter of the latex particle with the MADQUAT over surfactant ratio (wt/wt) in the initial microemulsion (from ref.23).

flattening of the particles has indeed been observed in some cases [21].

In the case of AOT micellar systems, one observes a notable increase of the particle size during the polymerization so that each final latex particle is the result of the fusion of around a hundred initial micelles [16]. The particle size ranges typically between 30 nm and 120 nm depending upon the experimental conditions; it augments upon increasing monomer content or decreasing surfactant concentration (fig.4) [22,23].

From the value of the average diameter of the dry polymer particle and that of the polymer molecular weight, one can estimate the number of macromolecules, N_p, contained in a particle. Calculations give extremely low values of N_p, around 1 or 2, in contrast with what is usually found in emulsion polymerization, where thousands of chains are commonly observed. This result was supported by a thorough mechanistic study performed on AOT systems [21,27,28] where a continuous particle nucleation was shown to occur all throughout the reaction and not only at the very early stages as is the case in emulsion polymerization. The high molecular weight polymeric chain must be strongly collapsed since it is entrapped within a water-swollen particle of small size (d < 100 nm). For comparison, the radius of gyration of a 5.10^6 molecular weight polyMADQUAT is around 160 nm. The water in the particle core acts here more as a plasticiser than as a solvent for the polymer.

These inverse microlatexes provide interesting models for rheological studies [29]. They differ from the more conventional aqueous or nonaqueous colloidal dispersions by a lower particle size and by a large swelling of the particles (e.g. 50% water, 50% polymer). In addition, the process permits to attain large volume fractions of the disperse phase (up to 60%) and thus to accurately characterize the latex rheological behavior.

Figure 5 shows an example of the variation of the relative viscosity with the shear stress for a typical latex. Qualitatively, one has the usual behavior observed for colloidal dispersions, that is a Newtonian behavior at low volume fractions and a shear-thinning effect for the largest volume fractions investigated.

However, the shear-thinning effect occurs at volume fractions much higher than those observed for conventional latexes (50-53% as against 25%). A possible explanation is deformability of the microspheres due to the low interfacial tension and to the high water content of the dispersed phase. The full lines in Figure 5 represent the best fit of the well-known Williamson equation [30] $[\eta_r = \eta_{r\infty} + (\eta_{r0} - \eta_{r\infty})/(1 + \sigma/\sigma_m)$ where η_{r0} and $\eta_{r\infty}$ are the low shear and high shear limiting relative viscosities and σ_m the shear stress for which $\eta_r = (\eta_{r0} + \eta_{r\infty})/2)]$ to the experimental data.

We have determined the intrinsic viscosity $[\eta]$ and the close-packing volume fraction φ_m of a series of copolymer latexes containing various contents of sodium acrylate, by using the Krieger-Dougherty equation [31]

$$\eta_r = (1 - \varphi/\varphi_m)^{-[\eta]\varphi_m}$$

A value of ≈ 2.5 is found for $[\eta]$ in good agreement with was is obtained for hard spheres suspensions. The data shows that φ_m decreases when increasing the percentage of electrically charged sodium acrylate in the comonomer feed. For instance, φ_m is around 59% for a sodium acrylate concentration of 12%. This value is significantly lower than that of 64% predicted for a random packing of hard spheres. On the other hand, other experiments performed on neutral polyacrylamide latexes have given values of φ_m around 64%. The divergence of viscosity which occurs at smaller characteristic volume fractions for poly(acrylamide-co-acrylates) latexes is probably due to the effect of electrical charges in the system, which prevent particles from approaching too closely to each other. Rheological studies on other ionogenic monomers are in progress to check this hypothesis.

σ (dynes/cm²)
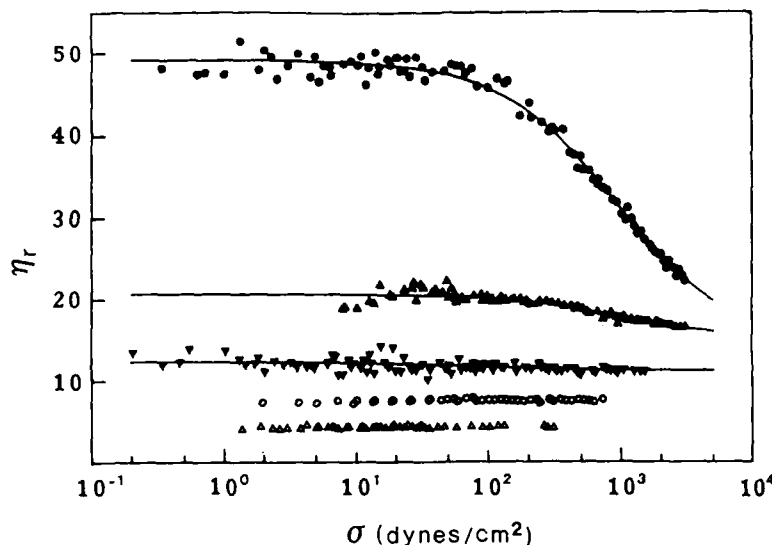
Figure 5 : Variation of the relative viscosity with shear stress for a poly(acrylamide-co-sodium acrylate) latex containing 9.10% sodium acrylate (wt/wt) and with a particle size of 62 nm [29].
Δ : φ - 0.35 ; O : φ - 0.44 ; ▼ : φ - 0.48 ; ▲ : φ - 0.52 ; ● : φ - 0.55.

APPLICATIONS OF MICROLATEXES AND POLYMERS

Polymerization in inverse microemulsions overcomes some of the problems classically encountered in emulsions and provides a novel technique for the production of high molecular weight water-soluble polymers. The main advantages are the low viscosity and high stability of the microlatex formed. The small particle size prevents flocculation since gravity forces are reduced. The large number of micelles contained in microemulsions compared to that in emulsions contributes to the formation of high degrees of polymerization (DP α N). Also, the microlatex is self-inverting so that no additional surfactant is needed to promote its inversion. With respect to the economical aspect, the main drawback of the process is the rather expensive formulation (high surfactant concentration). This is partially balanced by the very high rate of polymerization due to the great number of micelles, loci of the polymerization. Total conversions are usually achieved in a few minutes compared with hours in the usual process.

Most of the applications described for water-soluble polymers prepared in water-oil emulsions can in principle be extended to the inverse microemulsion polymerization process and several patents have recently been issued [32-35]. For example, inverse microlatexes can be used after dilution to water to form thickened solutions for improving the production of oil fields. They have advantages with respect to conventional latexes, as a result of their lower particle size, their lower degree of polydispersity and their great stability. They result in a better scavenging of the oil formation and thus in a more efficient oil recovery.

Most uses in the paper manufacture, water treatment and mining fields are based on the ability of water-soluble polymers such as polyacrylamides to flocculate solids in aqueous suspensions [1]. Small mineral or pigment particles settle very slowly and are difficult to eliminate or recover. Addition of charged polyacrylamides permits them to agglomerate. The ultra-high molecular weight polymers produced in the microemulsion process can be very effective in connecting together the small particles through bridging or charge neutralization. Moreover, classical polyacrylamide emulsions are subjected to rapid changes in temperature (in winter time) which cause them to coagulate rather than remain finely dispersed particles. This reduces drastically their usefulness as flocculants. Inverse microlatexes exhibit excellent freeze-thaw properties and contain finely divided polymer particles (≃ one polymer chain in a low size particle) which should insure a higher activity.

Other applications include surface coatings, adhesives, photographic emulsions, lubricating and cleaning drains, retention aid in paper making and food processing. Finally, the low viscosity and good stability of microlatexes can be useful for assembling glass fibers.

REFERENCES

1. W.M. Thomas and D.W. Wang, in Encyclopedia of Polymer Science and Engineering, edited by H. Mark, N. Bikales, C.G. Overberger and G. Menges, 2nd ed, New York, 1985, p.169.
2. J.W. Vanderhoff, H.L. Tarkowski, J.B. Shaffer, E.B. Bradford and R.M. Wiley, Adv. Chem. Ser. 34, 32 (1962).
3. M.V. Dimonie, G.M. Boghina, N.N. Marinescu, M.M. Marinescu, C.I. Cincu and C.G. Oprescu, Eur. Polym. J. 18, 639 (1982).
4. D. Hunkeler, A.E. Hamielec and W. Baade, Polymer 30, 127 (1989).
5. W. Baade, D. Hunkeler and A.E. Hamielec, Am. Chem. Soc. Div. PMSE Preprints, 57, 850 (1987).
6. W. Baade and K.H. Reichert, Eur. Polym. J. 20, 505 (1984).
7. V.F. Kurenkov, T.M. Osipova, E.V., Kuznetsov and V.A. Myagchenkov, Vysokomol. Soedin. Ser. B20, 647 (1978).
8. C. Graillat, C. Pichot, A. Guyot and M.S. El-Aasser, J. Polym. Sci. Polym. Chem. Ed. 24, 427 (1986).
9. V. Glukhikh, C. Graillat and C. Pichot, J. Polym. Sci. Polym. Chem. Ed. 25, 1127 (1987).
10. J.W. Vanderhoff, F.V. Distefano, M.S. El-Aasser, R. O'Leary, O.M. Shaffer and D.L. Visioli, J. Disp. Sci. Tech. 5, (3&4) 323 (1984).
11. D.L. Visioli, PhD thesis, Lehigh University, 1984.
12. M.T. McKechnie, Proceedings of the Conference on Emulsion Polymers, London, Paper 3/1 (1982).
13. See for example : A.M. Bellocq, J. Biais, P. Bothorel, B. Clin, G. Fourche, P. Lalanne, B. Lemaire, B. Lemanceau and D. Roux, Adv. Colloid Interface Sci. 20, 167 (1984).
14. L.E. Scriven, Nature (London), 263, 123 (1976).
15. S. Friberg, I. Lapczynska and G. Gillberg, J. Colloid Interface Sci. 56, 19 (1976).
16. F. Candau, Y.S. Leong, G. Pouyet and S.J. Candau, J. Colloid Interface Sci. 101, 167 (1984).
17. C. Holtzscherer and F. Candau, Colloids Surf. 29, 411 (1988).
18. F. Candau, Z. Zekhnini and J.P. Durand, J. Colloid Interface Sci. 114, 398 (1986).
19. C. Holtzscherer and F. Candau, J. Colloid Interface Sci. 125, No.1, 97 (1988).
20. P. Buchert and F. Candau, J. Colloid Interface Sci. (in press).
21. M.T. Carver, E. Hirsch, J.C. Wittmann, R.M. Fitch and F. Candau, J. Phys. Chem. 93, 4867 (1989).

78

22. C. Holtzscherer, J.P. Durand and F. Candau, Colloid Polym. Sci. 265, 1067 (1987).
23. P. Buchert, PhD thesis, Louis Pasteur University, Strasbourg, 1988.
24. F. Candau, Z. Zekhnini and F. Heatley, Macromolecules 19, 1895 (1986).
25. F. Candau, Z. Zekhnini, F. Heatley and E. Franta, Colloid Polym. Sci. 264, 676 (1986).
26. S. Ponratnam and S.L. Kapur, Makromol. Chem. 178, 1029 (1977).
27. M.T. Carver, U. Dreyer, R. Knoesel, F. Candau and R.M. Fitch, J. Polym. Sci. Polym. Chem. 27, 2167 (1989).
28. M.T. Carver, F. Candau and R.M. Fitch, J. Polym. Sci. Polym. Chem. 27, 2179 (1989).
29. D. Collin, F. Kern and F. Candau, presented at the 3rd European Colloid and Interface Society Conference, Basel (Switzerland), 1989 (to be published).
30. R.V. Williamson, J. Rheol. 1, 283 (1930).
31. I.M. Krieger and T.J. Dougherty, Trans. Soc. Rheol. III 137 (1959).
32. F. Candau, Y.S. Leong, N. Kohler and F. Dawans, French Patent (to CNRS-IFP) No. 2 524 895 (1984).
33. J.P. Durand, D. Nicolas, N. Kohler, F. Dawans and F. Candau, French Patent (to IFP) No 2 565 623 and 2 565 592 (1987).
34. J.P. Durand, D. Nicolas and F. Candau, French Patent (to IFP) No 2 567 525 (1987).
35. F. Candau and P. Buchert, French Patent (to Soc. Chim. Charb.) No 87 08925 (1987).

POLYMER-DERIVED Si_3N_4/BN COMPOSITES

Wayde R. Schmidt[1], William J. Hurley, Jr[1]., Vijay Sukumar[1], Robert H. Doremus[1], and Leonard V. Interrante[2], Departments of [1]Materials Engineering and [2]Chemistry, Rensselaer Polytechnic Institute, Troy, NY   12180-3590.

ABSTRACT

Partially crystalline silicon nitride, with a specific surface area greater than 200 m^2/g, is obtained by the pyrolysis of an organometallic, polymeric precursor under NH_3 to 1000 °C. Additional heating to 1400 °C under N_2 produces alpha-Si_3N_4. The addition of up to 15% h-BN was found to affect the coarsening characteristics of amorphous silicon nitride by promoting surface area reduction and suppressing crystallinity.   By combining Si_3N_4 and BN molecular and polymeric precursors prior to ceramic conversion, or incorporating Si, N, and B into a single preceramic polymer, the relative proportion and crystallinity of the ceramic phases can be controlled in the resulting Si_3N_4/BN composites.

INTRODUCTION

Silicon nitride has a unique combination of properties which makes it an important material for high temperature and electronic applications.   In addition to its resistance to thermal shock, creep, corrosion, and oxidation, dense Si_3N_4 has high electrical resistivity, a low coefficient of thermal expansion, low density, and good high temperature strength.   These attributes are exemplified by the use of Si_3N_4 as crucibles, turbine blades, nozzles, tiles, bearings, cutting tools, and electronic components.

Boron nitride is another useful material for high temperature and electronic applications due to its high melting point, low density, low coefficient of thermal expansion, and resistance to oxidation up to 1000 °C.   BN is also transparent over a large spectral range and is often used as a boron diffusion source, a surface passivator, or a solid lubricant.

A composite consisting of homogeneously dispersed BN in a Si_3N_4 matrix may exhibit beneficial properties of both components.   To date however, limited research has been reported on such a material.   Past work with Si_3N_4/BN composites has concentrated on their preparation by CVD and CVI techniques [1-5].   Fukunaga, et. al. [1] prepared electrically conductive films of amorphous Si_3N_4/BN composites.   They concluded that the 10 A voids within the amorphous Si_3N_4/BN composite were occupied by turbostratic BN since Si_3N_4 and BN do not constitute a solid solution even in the amorphous state.   They also claimed a decreased free volume in the Si_3N_4/BN composite and an increased crystallization temperature of the amorphous Si_3N_4 matrix in the composite.   Annealing at ca. 1600 °C led to precipitation of h-BN in the amorphous Si_3N_4.   Hirai and coworkers [2,3] produced opaque and transparent amorphous Si_3N_4/BN composite films with up to 36% BN by weight using CVD.   Mazdiyasni and Ruh [6] found improved electrical and thermal shock behavior of powder-based, hot-pressed Si_3N_4/BN composites over Si_3N_4 alone.   The dispersion of the low modulus BN in the high strength, high modulus Si_3N_4 matrix significantly improved the thermal stress resistance, lowered the dielectric constant by ca. 20%, and   did not drastically affect the mechanical integrity of the composite.

Fabrication of uniform Si_3N_4/BN material by more conventional ceramic powder fabrication methods is virtually impossible due to the large differences in the melting points of Si (1415 °C) and B (2177 °C) and the differences in N diffusivities in both materials.   The use of organometallic precursors to ceramic composites may provide several advantages, including 1) improved compositional

homogeneity due to atomic and molecular mixing of the elemental components, 2) lower processing temperature, 3) higher purity ceramic products with controllable microstructures, and 4) processing flexibility to prepare thin films, powders, binders, fibers, and monoliths.

Past researchers have employed polysilazanes as organometallic precursors to Si_3N_4. Unfortunately, the resulting ceramics typically consisted of mixed alpha- and beta-Si_3N_4 phases, with considerable contamination by SiC, SiO_2, and C phases[7,8]. Polymeric precursors to boron nitride are generally based on substituted borazines [9-11], but were also obtained from decaborane- [12] and pentaborane-based systems [13], or from substituted borane Lewis Base adducts [14].

Our approach to fabricating Si_3N_4/BN composites from organometallics is to mix a polymeric precursor to Si_3N_4 with a polymeric or molecular precursor to BN prior to ceramic conversion and in addition, to prepare a single polymer which contains Si, N, and B. The effects of incorporated BN on crystallinity, phase type and distribution, and surface area of the solid phases were examined.

EXPERIMENTAL METHODS

Glovebox and Schlenk techniques were employed whenever possible. Dried solvents, starting materials, and glassware were used throughout. Precursor and ceramic materials were characterized by a combination of FTIR, XRD, and BET.

A vinylic polysilane (VPS) with the approximate composition $[(Me_3Si)_w(CH_2=CHSiMe)_x(HSiMe)_y(SiMe_2)_z]$, where Me represents a methyl group, was used as the precursor for Si_3N_4. We have recently described the conversion of this polymer to "amorphous" Si_3N_4 at 1000 °C in NH_3, and the subsequent crystallization of the ceramic to high purity alpha-Si_3N_4 with heating above 1400 °C in N_2 [15].

The polymeric BN precursor was a poly(borazinylamine) (PBZA), which was prepared according to the method described by Narula et. al. [11]. Briefly, 2 g (10.9 mmol) of trichloroborazine was added to 50 ml of dry diethyl ether. The solution was stirred and cooled to -65 °C. Hexamethyldisilazane, (HMDS) 2.63 g (16.32 mmol), was added at once and the mixture was slowly warmed to room temperature. The reaction was carried out under N_2. Volatiles were removed under vacuum, leaving a white, fluffy powder. The powder was transferred into a N_2-filled glovebox whereby 25 ml of dry hexane was added to create a suspension. NH_3 was bubbled through the suspension for 12 hours, after which volatiles and remaining solvent were removed under vacuum. The resulting material was a white powder.

VPS was mixed with the PBZA in 1:1 and 10:1 wt ratios. In both instances, the powder was evenly dispersed in the VPS by preparing and mixing a slurry with dry hexane, followed by removal of the solvent under vacuum. The resulting white, gluey pastes were placed in a molybdenum pyrolysis boat and heated in anhydrous, prepurified NH_3 to 1000 °C according to the schedule described for preparing the Si_3N_4 [15]. The resulting white solids were subsequently heated up to 1600 °C under N_2 for 4 hours.

In separate experiments, $(CH_3CH_2)_3B:NH_3$, an adduct prepared by condensing NH_3 over a pentane solution of $(CH_3CH_2)_3B$ at -50 °C followed by removal of excess NH_3 and solvent by vacuum, was mixed with VPS in a 1:3 wt ratio and heated as above.

A polymeric precursor which contains Si, N, and B was synthesized to provide a homogeneous mixture of the elements on the atomic scale. The

preparation and characterization of this polymer will be reported in a future publication. This poly(borosilazane) (PBS) was pyrolyzed in NH_3 by heating from 25 °C to 1000 °C in 10 hours and holding at 1000 °C for an additional 10 hours. The resulting solid was subsequently annealed under N_2 up to 1600 °C for 4 hours.

EXPERIMENTAL RESULTS

The effect on heating on the physical appearance of the various samples is summarized in Table I.

Table I. Si_3N_4/BN Composite Appearance as Determined by Temperature

Sample	1000 °C/NH_3	1600 °C/N_2
VPS	tan solid	white solid
1:1 VPS:PBZA	white solid	white solid
10:1 VPS:PBZA	tan solid	white solid
3:1 VPS:$(CH_3CH_2)_3$B-NH_3	black-tan solid	white solid
PBS	orange-tan solid	white solid

Infrared Analysis

Typical FTIR spectra for the various composites are shown in Figures 1-2. For the 1:1 and 10:1 VPS:PBZA samples, the presence of B-N stretches at 1390 cm^{-1} and 801 cm^{-1} [16], and the Si-N stretch between 1100 cm^{-1} and 800 cm^{-1} [16], confirm the formation of composite materials (Figure 1). The Si-N stretches are significantly more intense in the 10:1 samples than in the 1:1 samples, with simultaneous reduction in the B-N stretches. As the temperature is increased from 1000 °C to 1600 °C, fine structure in the spectra becomes more pronounced as crystallization occurs, and the intensities of residual bands at 3430 cm^{-1} (N-H) and 2900 cm^{-1} (C-H) decrease.

Mixtures of 3:1 VPS:$(CH_3CH_2)_3$B-NH_3 do not form detectable silicon nitride/boron nitride composites upon pyrolysis. The FTIR of the 1000 °C sample shows only a broad Si-N stretch centered near 900 cm^{-1}, which is typical of amorphous Si_3N_4 (Figure 2). No peaks representing B-N bonding are observed near 1400 cm^{-1} or 900 cm^{-1}, although these bands may be hidden beneath the large Si-N band. With heating to 1600 °C, the FTIR shows only the increased crystallinity of the amorphous Si_3N_4, and confirms the absence of BN.

The PBS sample shows an extremely broad band ranging from 1600 cm^{-1} to 500 cm^{-1} (Figure 2) after heating to 1000 °C. Residual N-H and C-H bands are also apparent. With heating to 1600 °C, however, the skewed band near 1400 cm^{-1}, indicative of BN and the large structured band from 1100 cm^{-1} to 800 cm^{-1}, attributed to the Si-N stretch, confirm the presence of both ceramics.

X-Ray Diffraction

Powder diffraction patterns for the various composites are shown in Figures 3-4. The 1:1 VPS:PBZA 1000 °C powder shows two broad peaks near 25 and 43 degrees (Figure 3), which are due to the presence of turbostratic BN [17]. Upon heating at 1600 °C, these peaks sharpen, due to increased crystallinity of the BN, and several smaller peaks are now obvious, due to crystalline alpha-Si_3N_4.

The 10:1 composite provides very different patterns (Figure 3). At 1000 °C, the sample primarily consists of amorphous Si_3N_4, noted by the very broad peaks centered near 33 and 70 degrees [15]. By 1600 °C, the alpha-Si_3N_4 has extensively crystallized, but the presence of turbostratic or crystalline BN is not obvious.

1000 °C

A

1600 °C

1000 °C

B

1600 °C

4000   3000   2000 1600 1200 800   400

WAVENUMBER (CM^{-1})
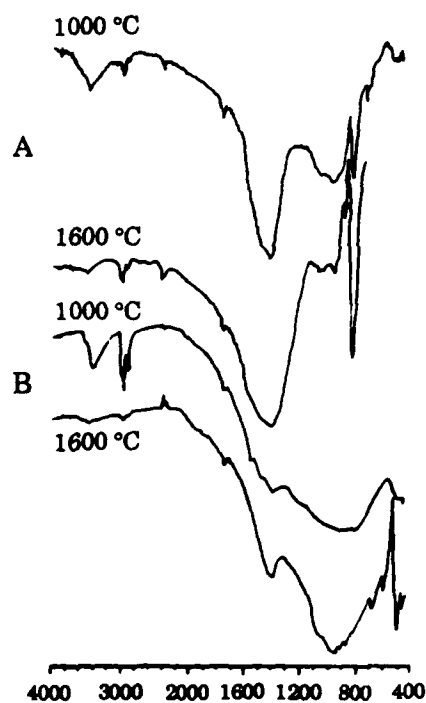
Figure 1. FTIR spectra of Si$_3$N$_4$/BN composites
A) 1:1 VPS:PBZA, B) 10:1 VPS:PBZA

A 1000 °C

1600 °C

1000 °C

B

1600 °C

4000   3000   2000 1600 1200   800   400

WAVENUMBER (CM^{-1})

Figure 2. FTIR spectra of Si$_3$N$_4$/BN composites
A) 3:1 VPS:Et$_3$B-NH$_3$, B) PBS

1600 °C

1750 °C

A

1000 °C

1600 °C

1600 °C

1000 °C

B

1000 °C

15   25   35   45   55   66   75

2θ

Figure 4. XRD patterns of PBS

15   25   35   45   55   65   75

2θ
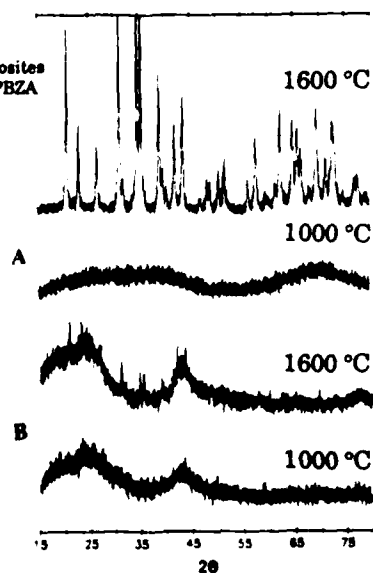
Figure 3. XRD patterns of various Si$_3$N$_4$/BN composites
A)10:1 VPS:PBZA, B)1:1 VPS:PBZA

The patterns obtained for pyrolyzed VPS:$(CH_3CH_2)_3B$-NH_3 show only the crystallization of the Si_3N_4, suggesting that the borane adduct does not serve as a BN source in this context.

PBS also exhibits a unique series of diffractograms (Figure 4). At 1000 °C and 1600 °C, the very broad peaks indicate that the product is amorphous [15]. Heating to 1750 °C for 2 hours, however, produces a mixed composition of both alpha- and beta-Si_3N_4. The amount of crystalline BN is below the detection limit of XRD, however, BN is present since the B-N stretch is detected by FTIR.

Surface Area Measurements

Preliminary surface area measurements are listed in Table II. Initial results indicate that BN generated in-situ from polymeric precursors reduces the surface area of the ceramic product, as observed for added h-BN powder [18,19]. This trend is clearly seen at 1000 °C, where the surface area decreases from 247 m^2/g to 50.2 m^2/g as the initial concentration of BN precursor is increased. The borane adduct, $(CH_3CH_2)_3B$-NH_3, is a poor BN precursor as shown by the relatively unchanged surface areas relative to VPS alone.

Table II. Specific Surface Area (m^2/g) Dependence on Temperature

Precursor	1000 °C	1600 °C
VPS	247	12.3
10:1 VPS:PBZA	226	19.7
1:1 VPS:PBZA	50.2	7.5
3:1 VPS:$(CH_3CH_2)_3B$-NH_3	260	11.6
VPS+10% h-BN	220	2.2

DISCUSSION

Previous efforts in our laboratory have shown that for temperatures ranging from 1000 °C to 1600 °C, the addition of up to 15 wt % of commercial BN powder to precursor-derived Si_3N_4 reduces both the surface area and crystallinity of the solid compared to precursor-derived Si_3N_4 alone [18,19]. Added BN does not help sintering of Si_3N_4 since it suppresses crystallization and mass transport, which are the first steps toward complete densification. The effect is possibly due to the lowering of oxygen activity in the presence of boron.

By combining polymeric precursors to both Si_3N_4 and BN prior to pyrolysis, composites can be fabricated. The relative proportion of the ceramic phases can be controlled by varying the weight ratio of the starting polymers, as seen with the 1:1 and 10:1 VPS:PBZA composites. The adduct $(CH_3CH_2)_3B$-NH_3 was not a useful precursor to BN, probably because the adduct decomposes prior to reaction with the VPS. A polymer which contains Si, N, and B provided a single component, homogeneous, molecularly mixed precursor to Si_3N_4/BN composites.

FTIR analyses indicate a mixture of both Si-N and B-N bonding environments following pyrolysis of the VPS:PBZA and PBS precursors. XRD suggests that phase separation of the Si_3N_4 and BN occurs; this is particularly evident for the 1600 °C 1:1 VPS:PBZA sample. The crystallinity of the Si_3N_4 in the 1600 °C 10:1 composite was somewhat lower than that obtained from the precursor-derived Si_3N_4 alone, while that of the 1:1 composite was significantly less. These results indicate that molecularly mixed BN from a polymeric precursor also suppresses crystallinity of amorphous Si_3N_4, as seen for added h-BN powder [18, 19].

The PBS polymeric precursor resulted in both alpha- and beta-Si_3N_4 at 1750 °C, yet showed little crystallinity after 1600 °C treatment. This observation

suggests that the BN has increased the crystallization temperature of the Si_3N_4. It is possible that the presence of both phases is due to a better distribution of the B-N species within the polymer or the formation of a high temperature liquid.

The reduction in surface area of Si_3N_4/BN composites relative to Si_3N_4 alone may be explained by the formation of B_2O_3 or borosilicate glass through reaction with surface oxygen and B, added either in precursor form or as h-BN. These reactions lead to a reduction of free volume in the Si_3N_4 and thus a reduction in surface area.

Composites derived from polymeric precursors are expected to show increased strength and toughness over the component ceramic phases while retaining characteristic refractoriness and resistance to abrasion and corrosion. This preparation method also shows potential for producing glass/ceramics or amorphous material for high temperature applications in composites.

ACKNOWLEDGEMENT

REFERENCES

1. T. Fukunaga, T. Goto, M. Misawa, T. Hirai, and K. Suzuki, *J. Non-Cryst. Solids*, 95/96 (1987) 1119.
2. T. Hirai in Emergent Process Methods for High-Technology Ceramics, Materials Science Research Vol. 17, eds. R. F. Davis, H. Palmour, and R. L. Porter, Plenum Press (1984) 329.
3. T. Hirai, T. Goto, and T. Sakai in Emergent Process Methods for High-Technology Ceramics, Materials Science Research Vol. 17, eds. R. F. Davis, H. Palmour, and R. L. Porter, Plenum Press (1984) 347.
4. T. Goto and T. Hirai, *J. Mater. Sci. Letters*, 7 (1988) 548.
5. K. Sugiyama and Y. Ohsawa, *J. Mater. Sci. Letters*, 7 (1988) 1221.
6. K. S. Mazdiyasni and R. Ruh, *J. Am. Ceram. Soc.*, 64[7] (1981) 415.
7. R. M. Laine, Y. Blum, R. Hamlin, and A. Chow in Ultrastructure Processing of Advanced Ceramics, eds. J. D. Mackenzie and D. R. Ulrich, J. Wiley & Sons (1988) 761.
8. D. Seyferth, G. H. Wiseman, and C. Prud'homme, *J. Am. Ceram. Soc.*, 66 (1983) C-13.
9. K. J. L. Paciorek and R. H. Kratzer, *Ceram. Eng. Sci. Proc.*, 9[7-8] (1988) 993.
10. K. J. L. Paciorek, D. H. Harris, and R. H. Kratzer, *J. Polym. Sci. Polym. Chem.*, 24 (1986) 173.
11. C. K. Narula, R. Schaeffer, and R. T. Paine, *J. Am. Chem. Soc.*, 109 (1987) 5556.
12. D. Seyferth and W. S. Rees, Jr., *Mat. Res. Soc. Symp. Proc.*, Vol. 121, Materials Research Society (1988).
13. M. Mirabelli and L. Sneddon, *Inorg. Chem.*, 27 (1988) 3271.
14. J. Beck, C. Albani, A. McGhie, J. Rothman, and L. Sneddon, *Chemistry of Materials*, 1 (1989) 433.
15. W. R. Schmidt, V. Sukumar, W. J. Hurley, Jr., R. Garcia, R. H. Doremus, L. V. Interrante, and G. M. Renlund, submitted to *J. Am. Ceram. Soc.*, Oct. 1989.
16. R. A. Nyquist and R. O. Kagel, Infrared Spectra of Inorganic Compounds, Academic Press (1971) 114.
17. J. Thomas, Jr., N. E. Weston, and T. E. O'Connor, *J. Am. Chem. Soc.*, 84[24] (1963) 4619.
18. V. Sukumar, Master's Thesis, Rensselaer Polytechnic Institute, December, 1989.
19. V. Sukumar, W. R. Schmidt, R. H. Doremus, and L. V. Interrante, submitted to *Mat. Letters.*, Dec. 1989.

Emulsions/Blocks

STABILIZED NANOPARTICLES OBTAINED FROM SYNTHETIC
POLYMERIZABLE MICELLES AND VESICLES.

CONSTANTINOS M. PALEOS
NRC "Demokritos", Aghia Paraskevi, 15310 Attiki, Greece.

ABSTRACT

The structural characteristics and the formation of monomeric and stabilized polymeric micelles and vesicles are reviewed. Characterization of these nanoparticles involved stability studies, molecular weight determination, permeability and fluorescence investigations, as well as electron microscopy and DSC studies.

INTRODUCTION

Spherical micelles of 3-6 nm in diameter [1] are in a dynamic equilibrium with their monomers and can be stabilized either by the solubilization within them of appropriate monomers and subsequent polymerization, or by the polymerization of micelle-forming monomer surfactants [2]. Synthetic vesicles on the other hand with diameters from 30 to 300nm possess greater kinetic stability than micelles [1]. In addition, the dependence of the structrure and size of vesicles on the mode of their formation [3,4] allows greater structural flexibility than micelles. However further stabilization [5,6] of these particles is required and this was achieved by addition polymerization or polycondensation.

In the present study we will discuss the stuctural requirements for the formation of micelle and vesicle forming polymerizable surfactants and the diversified methods for the formation of the their polymerized counterparts. The stability of nanoparticles was the main property to be investigated. Furthermore their molecular weights were determined and the structure of micelles was investigated by fluorescence spectroscopy whereas vesicles were further characterized by permeability studies, electron microscopy, DSC and currently by video enhanced optical microscopy. Current and prospected applications of both monomeric and polymerized particles include their use as energy conversion systems [7,8], drug-carriers [5,9] in medicine, and as media for biomimetic reactions [10].

1. POLYMERIZED MICELLES - FORMATION AND CHARACTERIZATION

1.1. Synthesis of micelle-forming polymerizable surfactants.

Surfactants bearing one long alkyl-chain coupled with a hydrophilic head associate in water above a critical concentration (CMC) forming micelles. Introduction of a polymerizable group does not in general
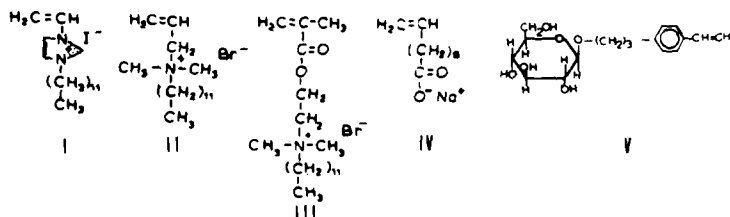
drastically modify the basic molecular structure and the resulting monomers also aggregate forming micelles. The functionalization of surfactant structure by polymerizable groups can be performed either near the head or at the lipophilic group, as in monomers I-V.

1.2. General considerations of micellar polymerization

Studies on micellar polymerization have been limited to addition polymerization under conventional polymerization conditions. Certainly polycondensation cannot be ignored for the formation of polymerized aggregates. These latter nanoparticles, in addition to their other properties will be biodegradable.

The study here will be restricted to the polymerization of monomers which are themselves surfactants. Several parameters may in principle affect micellar polymerization and structure of nanoparticles [11] such as:

a) The concentration which controls the size and shape of monomeric micelles may very well affect polymerized counterparts. The type of aggregates as a function of surfactant concentration is shown pictorially below.
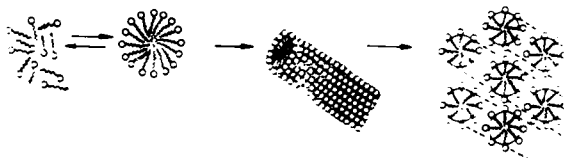
b) The location and the nature of the polymerizable group at the head or lipophilic moiety of the surfactant may in principle affect polymerization and also the architecture and conformation of polymerized micellar particles. Thus two types of polymerized micelles can be envisaged, named H (for head) and T (tail) respectively. In type H spherical or ellipsoidal polymerized micelles is very difficult to visualize because their formation is prevented by formidable packing constraints. In this case disk-like intermicellar aggregates or bilayer structures will be visualized.

O Polar head
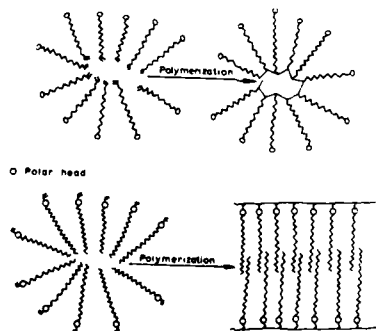
Above considerations on polymerized micelles are however valid if the polymerization occurs intramicellarly under topochemical conditions. Dynamics of micellization [12] fall into two categories: a) The millisecond domain in which whole micelles dissolve and reform and b) the microsecond domain when a single surfactant exchanges between the micelle and the solution. In order for the polymerized particles to have more or less the shape and size of the monomeric aggregates the polymerization must be fast enough that is there is no chance for monomeric micelles to be altered.

1.3. Polymerized micelles obtained through micellar polymerization.

In reviewing polymerized aggregates originating from micelle-forming monomeric surfactants a more or less chronological order is followed. Studies performed sofar are rather fragmentary and above mentioned general aspects have only been partially taken into account in micelle formation.

a. Heterocyclic polyquaternary ammonium salts.

The first examples in micellar polymerization involved certain methyl substituted vinylpyridinium salts[13-16], the structures of which are not typical of micelle-forming surfactants and which aggregate at abnormally high concentrations. The investigations concerning these salts focused primarily on the polymerization mechanism rather than on the effect of organization-aggregation on polymerization and the structure of polymerized particles. Thus we should not further discuss these polymers.

The polymerization of micelle-forming 3-n-dodecyl-1-vinylimidazolium iodide (I) [17] was performed comparatively in isotropic and micellar media [18]. Although polymerization kinetics were not performed and the particles obtained were not characterized it seems that micellization, at least as judged from the isolated polymeric products, does not affect polymerization [18]. Thus polymers obtained by the two modes of polymerization cannot be differentiated as far as viscosity, microstructure and solubility of the polymers are concerned. However, CMC obtained by electrical conductivity for this salt is zero because of its polysoap structure.

b. Poly(sodium 10-undecenoate)

Sodium 10-undecenoate (IV) has been studied rather extensively. Since it bears the double bond at the end of the aliphatic chain it can form T-type polymerized micelles. Polymerization was accomplished by γ-rays [19,20] or UV light [21] and the degree of polymerization was found equal to the aggregation number of the monomeric micelles i.e. equal to 10. Thus polymerization occured intramicellarly each polymer chain forming a micelle. When polymerization was conducted below CMC the rate was practically zero. The type of organization of polymerized particles was somehow illustrated when this monomer was polymerized in the liquid crystalline state [22]. In this case, structure changes from hexagonal closely packed cylinders to a lamella structure. The degree of polymerization was 270.

The same monomer forms intermolecular micelles composed of more than one intramolecular micelles with a CMC = 10^{-2} M. The aggregational behavior of monomeric and polymerized micelles has been studied by electrical conductivity and confirmed by dye solubilization [18]. The intrinsic viscosities of monomeric and polymerized micelles had shown that they both have equal hydrated sizes while a larger hydrated size was found for the intermolecular micelle [18].

By fluorescence probing [23] with pyrene and employing the I_3/I_1 micropolarity index the internal structure of monomeric and polymerized micelles were compared. Thus polymerized micelles show a more compact structure as compared to monomeric counterparts. As a consequence pyrene does not penetrate inside polymerized micelles as deeply as in the monomeric micelles which is attributed to the proximity of the aliphatic chains due to their attachment on the backbone at the core of the polymerized micelles.

The dependence of polymerization and polymerized micelles on the structure of monomeric micelles was also exemplified in the polymerization of the same monomer with UV light [21].

c.Aliphatic polyquaternary salts

Allyldimethyldodecyl ammonium bromide (II) [24] was polymerized comparatively under micellar and isotropic conditions with γ-rays. Isotropically obtained polymer was partially destructed from the radiolysis products of water. It seems that micellization protects the aliphatic chains from the same agents. For this monomer the aggregation number of monomeric micelles was found equal to the degree of polymerization of polymerized micelles i.e 33. This may be interpreted by the fact polymerization is fast enough that polymerized micelles are formed before the surfactants of monomeric micelles can exchange with the monomers in solution. As it was found by fluorescence probing polymerized micelles are more compact than the monomeric ones.

Other examples of micelle-forming monomers are the long alkyl chain derivatives of dimethylaminoethyl methacrylate (III) quaternary ammonium salts [25,26]. For these monomers the rate of polymerization in aqueous media increases as the alkyl chain length becomes longer. This behavior had been interpreted as indicating that polymerization is taking place in the micellar state. The same head methacrylate derivatives were polymerized by S. Hamid and D. Sherrington [25] and determined their average molecular weights which range from about 10,000 to 11,000. It appears that polymerization is facilitated in micellar media as compared to isotropic and topochemical polymerization has been achieved. However since polymeric solutions become increasingly opaque due to the presence of polymerized species of higher molecular weights as polymerization proceeds, a skepticism was expressed whether really polymerized micelles were formed through topochemical polymerization. According to their analysis on micellar dynamics, topochemical polymerization was rather excluded and the experimentally determined low molecular weight was fortuitous or attributed to the facility of monomer transfer reaction. For these methacrylate derivatives however micellization dynamics and polymerization rate data were not available and therefore the parameters employed [25] were taken from the literature for alkyl sulfates and various other monomers.

The structure of polymerized micelles may be affected by the position of the polymerizable group, at the head or at the tail [28] as shown for monomers VI and VII. The micellar parameters obtained by fluorescence measurements for monomeric and polymerized micelles are summarized in Table I.

VI   VII
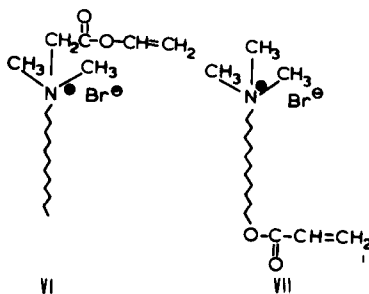
According to these results pyrene senses the same micropolarity in both monomeric VI and polymerized VI micelles while senses higher polarity in polymerized micelles VII than VI. Thus in polymerized micelles originating from the tail monomer it is easy for water to penetrate into the interior thus enhancing its polarity. Concernig aggregation number of polymerized micelle VI it is seen that it is almost half of of its monomeric counterpart which very probably arizes from the structural constraints when the backbone is formed at the interface. On the contrary it is twice as large for the polymerized micelle of monomer VII. In this case the location of the main

chain at the core of the polymerized micelle does not create significant packing problems.

Table I. Polarity Index (I_3/I_1) and aggregation number N_m of monomeric and polymerized micelles of monomers VI and VII.

Surfactant		I_3/I_1	N_m
Monomeric	VI	0.83	62
Monomeric	VII	–	–
Polymerized	VI	0.83	24
Polymerized	VII	0.72	42

d. Polymerized micelles from non-ionic surfactants

The monomer 1-O-3-(4-vinylphenyl)propyl-β-D-glycopyranose (V) [29] a stiff polymerizable surfactant polymerized with free radical initiators above and below the CMC. 2,2 azoisobutyronitrile(AIBN), dipotassium peroxodisulfate ($K_2S_2O_8$) and 2-(phenylazothio)naphthalene (ATE) were employed as initiators but only polymerization by ATE led to polymerization with preservation of aggregation number. The polymerization with the other catalysts resulted primarily in the formation of bigger aggregates. When ATE catalyst was used it was speculated that the phenyl radicals might initiate the polymerization and that the naphtyl thio radicals might terminate growing chains before diffusion effects become noticeable. Thus it was possible to have topochemical polymerization conditions by changing the employed catalyst.

2. POLYMERIZED VESICLES – SYNTHETIC APPROACHES

2.1. Formation of polymerized vesicles from monomeric vesicles by conventional addition polymerization.

The usual structural feature of vesicle-forming surfactants is the presence of two long alkyl chains in conjuction with a polar head group. These structures when functionalized by the introduction polymerized groups form vesicle-forming monomers [30,31] whose polymerization leads to the formation of polymerized vesicles. The monomers VIII-XVII are indicative of the diversity of molecular structures that form vesicles.

Utilization of vesicles for drug encapsulation has led to extensive research on the formation of single and multi-compartment vesicles. For this purpose the methods of sonication, reverse phase, evaporation, solvent injection, extruction have been developed [3,4]. Depending on the method and conditions, multilamellar and unilamellar vesicles have been prepared. Methods for the formation of vesicles have been critically reviewed by Szoka-Papahadjopoulos [3] and Hope et al. Quite recently a method has been developed [32] based on the swelling of phospholipid films deposited on special supports in excess water. The method is simple and it is performed under mild experimental conditions.

Polymerization is accomplished by conventional methods. Irradiation polymerized groups in the exterior and interior of the vesicles. On the contrary, polymerization may be limited to external double bonds when the initiator ,added to sonicated vesicles, cannot permeate to the interior.

Depending on the position of the polymerizable group, polymerized vesicles can either be linked at the polar head, at the middle, or at the end of the lipophilic chains as shown below. The location of the backbone in polymerized vesicles certainly affects their properties. Head group

92
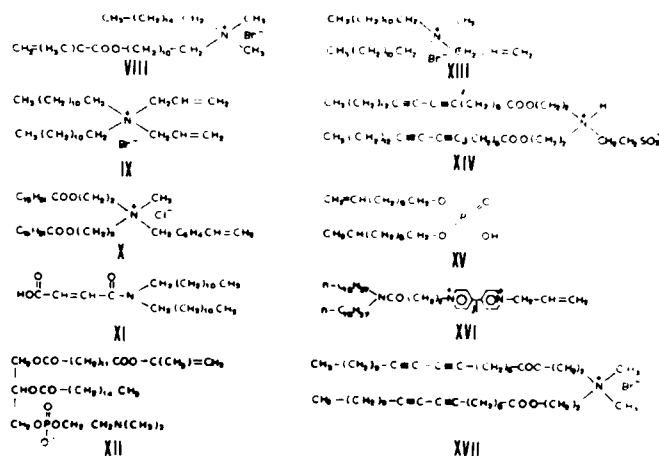
mobility is preserved when the monomers are linked at the end of the long aliphatic chains, whereas head group mobility is lost when the main chain is located near the head group. In diacetylene monomers, polymerization leads to extremely rigid structures which do not exhibit phase transitions.
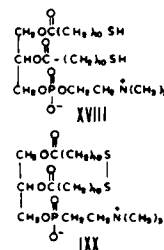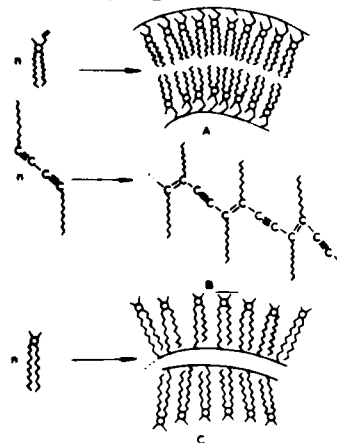
2.2. Formation of polymerized vesicles from nonconventional monomeric vesicles by redox reactions.

The synthesis of monomers, XVIII and IXX, forming this type of vesicles is accomplished by a functionalization of typical vesicle-forming molecules either with the disulfide group or with two thiol groups. Monomer XVIII forms bilayer structures which are polymerized [33] or rather "switched on" by oxidation. The resulting polymer is reversibly depolymerized,"switched off," by reduction. It has also been found that the macrocyclic analogue IXX is polymerized [34] in the vesicular phase by ring opening polymerization initiated with catalytic amount of dithiothreitol(DTT). These vesicles are promising candidates for mechanistic and practical applications due to their biodegredability

2.3 Formation of polymerized vesicles from amphiphilic amino acids.

Functionalization of amino acids with long alkyl chains may, in principle, lead to the formation of vesicle forming molecules whose condensation results in the formation of polypeptides which can also form vesicles. It has been found that the formation of stable polypeptide vesicles is governed by proper balance of hydrophilic and hydrophobic moieties in the monomers. Such monomers [35] fulfilling above condition are the XX and XXI. The presence of the carboxylic group enhances the hydrophilicity of the resulting polypeptide after polycondensation. The vesicles are stable but susceptible to biodegradation. Polycondensation occurs in the vesicular phase, in the presence of a water soluble carbodiimide. It must be noted, however, that in general vesicle formation is not a prerequisite for the polycondensation.
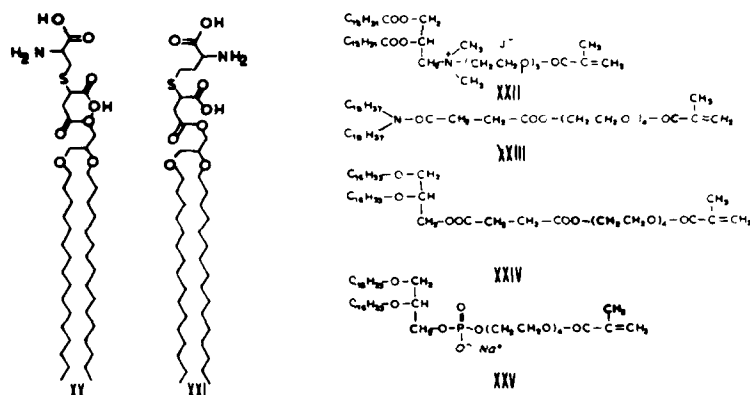
2.4. Formation of vesicles from ionene polymers.

In this case a long-chain dibromide interacts with a ditertiary amine of the same chain length, forming ionene polymers [36] leading to vesicles after sonication. Ionene polymers composed of alkyl chain of different lengths do not form membrane structures. Further work is required for the synthesis and structure elucidation of this type of vesicle forming polymers.
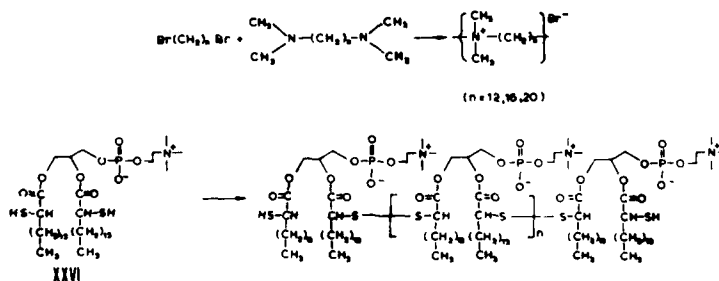
2.5. Formation of polymerized vesicles from preformed polymers.

A crucial problem of polymerized vesicles is whether their formation

requires formation of monomeric vesicles which subsequently polymerize. This problem had been answered recently. Thus polymers prepared isotropically from monomers [37] XXII-XXV, formed polymerized vesicles under usual conditions. A characteristic of these monomers is the introduction of a hydrophilic spacer between the polymerizable group and the amphiphilic moiety. In this way an efficient decoupling of the motion of the polymer backbone and the amphiphilic groups is achieved. The fluidity of the polymerized vesicles, due to these spacers, is preserved and this results in membrane structures simulating biological membranes. However, it has been reported recently that spacers are not essential for preserving "monomer-like" packing behavior of polymeric surfactants. Monomer [38] XXVI was polymerized through oxidation of the thiol groups. Sonication of the polymer dispersion afforded vesicles having diameters 200-1000 A.

3. KINETICS IN THE VESICULAR PHASE.

Understanding of the potential of polymerized vesicles necessitates a detailed elucidation of the kinetics and mechanism of their formation as they affect vesicle structure. Such studies had been performed for styrene bearing quaternary ammonium surfactants [39-41] XXVII-XXIX. Continuous UV irradiation of monomer XXVII, or irradiation by laser pulses, decreases styrene absorbance in a first order process. Calculated rate constants were independent of the vesicle concentration but increased linearly with increasing intensity of the laser pulses. Rates were considerably slower in isotropic ethanolic solution compared to vesicular medium, and in contrast to vesicle polymerization the rate depended on monomer concentration. This finding ,and the fact that the sizes of vesicles remained practically unchanged on polymerization, suggest that polymerization occurs intravesicularly on the surface with an apparent reduced dimensionality which can be analysed on a per vesicle rather than per volume basis.
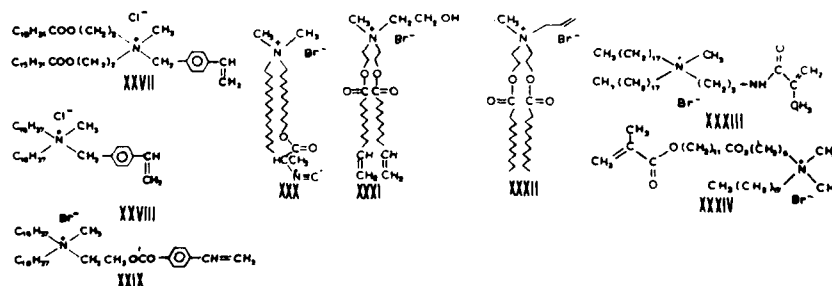
4. CHARACTERIZATION OF POLYMERIZED VESICLES.

4.1. Stability Studies

Polymerized vesicles in general retain the structure of their monomeric counterparts. For instance, the hydrodynamic radius R_h of the vesicles formed from monomer XXVII is 2500 A and changes to 2750 A upon polymerization [28]. Electron microscopy also provides excellent evidence for the retention of vesicular structure of the momeric vesicles upon polymerization.

Evaluation of polymerized vesicle stabilities is performed by the addition to their dispersions of surfactants such as sodium dodecyl sulfate [42] or of increasing quantities of ethanol [43]. In the latter case, UV absorbance of solutions was found constant for polymerized vesicles upon addition of 0-25% (V/V) ethanol. Monomeric counterparts showed a dramatic

decrease in turbidity. Thus, polymerized vesicles originating from monomers VIII [43] IVX [44, 45] XV [46] of Table I, as well as XXX [47] XXXI [48] XXXII [46] showed enhanced stability as compared to their monomeric ones.

An interesting case in which excellent stabilization was obtained involves the polymerization of di(undecenyl)phosphate [46]. Polymerized vesicles resulting from this monomer were stable for years (own unpublished results) without precipitating. Their stabilization was attributed to crosslinking of the adjacent layers of the vesicles, (below on the left) involving 50% polymerization of the vinyl groups.

The stabilization achieved through polymerization of monomeric vesicles is not always a staightforward process nor is it always predictable. For instance, it has been found for allyl and diallyl vesicle-forming quaternary ammonium salts [44,45] that only the polymerized vesicles derived from the diallyl derivative (below on the right), incorporating a pyrrolidine moiety in the backbone, and prepared by a mechanism involving alternate intramolecular and intermolecular growth steps exhibited good stability. Polymerized vesicles obtained from the allyl derivative are unstable and dissipate shortly after γ-irradiation. Although this behavior is not easily rationalized, it seems that the insertion of pyrrolidine moiety in the backbone of diallyl polymerized vesicles is probably responsible for the stabilization of the vesicles.
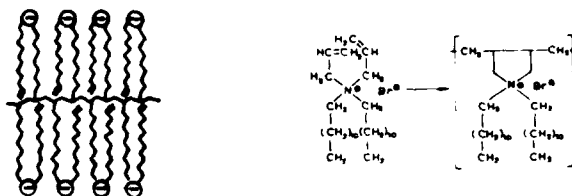
Stabilization of synthetic vesicles was also treated in a manner analogous to that which nature uses in stabilizing biomembranes, i.e. by coating their surface with polypeptides or polysaccharides. Polymers were attached to vesicles surface by ionic interactions, hydrophobic anchor groups, or polymerization of charged, water-soluble monomers. These ionic monomers were attached to charged lipid molecules either via salt formation or as counterions [5, 48]. In the latter case methacrylate was the counterion of vesicle-forming molecule dioctadecyldimethylammonium methacrylate [48]. Upon polymerization of the methacrylate counterions, the vesicles were encased within two concentric poly(methacrylate) monolayers. Salt formation at the vesicle surfaces is demonstrated [51] by the use of 4-vinylpyridine (4VP) which polymerizes in organic solvents or water with the addition of protic acids. In the present case, dicetyl phosphate is used as vesicle-forming acid. Salt formation is achieved by the addition of 4VP which is followed by spontaneous polymerization. A polyaddition poly(1,4 pyridiniumdimethylene salt) is obtained covering the surface of the vesicles. Retention of the liposome structure after coating with the polymer was confirmed by electron microscopy. In this connection it should be mentioned that cetyltrimethylammonium bromide (CTAB), a well-known micelle-forming surfactant, is forming bilayer membrane structures when the bromide is replaced by a polyacrylate counterion. In this way, the nature of the counterion controls [52] micellar or bilayer phase formation from a single-chain surfactant.

4.2. Permeability Studies

Controlled permeability is a significant property of both monomeric and polymerized vesicles. Vesicle permeability can be determined with any water-soluble marker using methods based on fluorescence, enzymatic, redox

detection, electron paramagnetic resonance spectroscopy, and radiochemical tecqniques. [3H] glucose is a preferred compound because it does not interact with cationic surfactants and can be used at low ionic strength. This is required since vesicles formed from cationic surfactants tend to aggregate at salt concentrations exceeding 20mM. Thus the permeability of poly(XXXIII) and poly(XXXIV) vesicles is about half of those derived from their respective monomers, XXXIII and XXXIV.

Copolymerization with a cross-linking agent further reduces the leakage rate. In contrast, formation of peptide vesicles through the condensation of long-chain amino acids [35] XX and XXI showed increased permeability. Thus, permeability of vesicles from the homocysteine derivative is 0.2 to 0.4 of that of cysteine vesicles. The difference in permeability behavior is likely due to the higher lactam content, and hence, lower amounts of oligopeptides in vesicles from XX than in vesicles from XXI.

4.3. Molecular Weight Determination.

Concerning molecular weights of polymerized vesicles it has been found that many vesicles consist of several polymer fragments and not, of only two polymer chains resulting from the polymerization of each layer of an one-compartment vesicle. The structure of polymerized vesicles may be related to or modeled as intermolecular micelles consisting of individual polymeric chains (each being an intramolecular micelle) aggregated into bigger assemblies. The fragments vary signigicantly depending on the specific structure of vesicle-forming monomers and conditions of the experiments. Thus, while for monomer XXVII [39] chain length is 20, the two methacryloyl monomers [53], (XXXIII) and (XXXIV) which were polymerized catalytically, exhibited chain lengths consisting of about 500 units. For the polymerized vesicles derived from XXXIII the calculated number of monomers per vesicle was 10^4-3.10^5 and therefore there must be 600 chains per vesicle while for those from XXXIV, with a number of monomer units per vesicle equal to 10^4-8.10^4, there must be only 20-60 polymeric chains. In addition, preliminary experiments showed that the molecular weight of poly(XXXIII) varies inversely with the time subjected to sonication before polymerization. These results suggest that lower molecular weight polymers are formed in smaller vesicles.

4.4 Miscellaneous Characterization Studies.

The thermal behavior of polymerized vesicles as investigated by Differential Scanning Calorimetry depends on the type and position [54] of the polymerizable group of their monomeric counterparts and the phase transitions that are observed correspond to changes from the gel to liquid crystalline phases [30]. Thus the phase transition of polymerized vesicles is retained when the backbone is located in their hydrophilic surface while is lacking when a rigid, fully conjugated main-chain is formed by the polymerization of monomers bearing diacetylenic moiety at the middle of the hydrocarbon chains. It seems that the crucial parameter for the exhibition of phase transition by polymerized vesicles is a decoupling of motion of the backbone from that of the amphiphilic side-chain. In addition, when a spacer is introduced between the polymerizable group and the amphiphilic moiety the phase transition appears at higher temperatures, and is narrower as compared to that of monomeric vesicles [37]. This behavior is in contrast with that of polymerized vesicles without spacers [54,55] in which transitions are broadened and shifted to lower temperatures.

Recently introduced video microscopy [56] and specifically video-enhanced differential interference contrast microscopy [57,58] for the study of molecular assemblies can effectively been used for the study of polymerized aggregates. Specifically this technique allows an immediate and

rapid characterization of organized assemblies and other colloidal suspensions free from artifacts by direct visualization on a television screen. Particles with sizes down to 50nm, their dynamics, stability and slow flocculation can be directly pictured, recorded, analysed in real time.

CONCLUDING REMARKS

Elucidation of micellar polymerization and characterization of polymerized micelles has rather delayed, primarily due to the lack of systematic studies. At the moment, what is needed, is the right choice of a series of micelle forming monomers, each with minor structural differentiation from the other, and the investigation of the effect of these modifications on polymerized micelles. In polymerized vesicles, on the other hand, intensive and systematic work resulted in the clarification of vesicular polymerization and of the problems associated with the structure of these particles. The diversity of methods that have been developed for their formation coupled with varying degrees of stability and permeability render these aggregates appropriate for a wide variety of applications.

REFERENCES

1. J. H. Fendler, J. Phys. Chem., 89, 2730 (1985).
2. V. V. Egorov and V. P. Zubov, Russ. Chem. Reviews, 56, 1153 (1987).
3. F. Szoka, and D. Papahadjopoulos, Ann. Rev. Biophys. Bioeng., 9, 467 (1980)
4. M. J. Hope, M. B. Bally, L. D. Mayer, A. S. Janoff, Cullis., J. Chem. and Phys. of Lipids, 40, 89 (1986).
5. H. Ringsdorf, B.Schlarb, J. Venzmer, Angew. Chem. Int. Ed. Engl., 27, 114 (1988)
6. C. M. Paleos, Chem. Soc. Rev., 45 (1985).
7. M. Gratzel, Ber. Bunsenges. Phys. Chem., 84, 981 (1980).
8. J. F. Rabek, Prog. Polym. Sci., 13, 83 (1988).
9. D. A. Tirell, L. G. Donamura, A. B. Turek, Eds., Macromolecules as Drugs and as Carriers for Biologically Active Materials, Annals of the New York Academy of Sciences, Vol. 446, 1985.
10. J. H. Fendler, Membrane Mimetic Chemistry, Wiley-Interscience, New York, 1982.
11. C. M. Paleos and A. Malliaris, J. Macrom. Sci., Rev. Macrom. Chem. Phys. C28 (3&4), 403, (1988).
12. J. Lang, T. Tondre R. Zana, R. Bauer, H. Hoffmann, and W. Ulbright, J. Phys. Chem.,79, 276, (1975).
13. V. A. Kabanov, Pure Appl. Chem., 15, 391 (1987).
14. J. C. Salamone, M. V. Mahmud, A. C. Watterson, and A. P. Olson, J. Polym. Sci., Polym. Chem. Ed., 20, 11⁵³, (1982).
15. V. Martin, W. Sutter, and H. Ringsdorf, Makrom. Chem., 177, 89 (1976).
16. C. M. Paleos and Dais, J. Polym. Sci., Polym. Chem. Ed., 16, 1945 (1978).
17. J. C. Salamone, S. C. Israel, P. Taylor, and B. Snider, J. Polym. Sci., Polym. Symp., 45, 85 (1974).
18. C. M. Paleos, S. Voliotis, G. Margomenou-Leonidopoulou and P. Dais, J. Polym. Sci. Chem. Ed., 18, 3484, (1980).
19. E. D. Sprague, D. C. Duecker, and C. E. Larrabee, J. Colloid Interface Sci., 92, 416 (1983).
20. C. M. Paleos, C. I. Stassinopoulou, and A. Malliaris, J. Phys. Chem., 87, 251 (1983).
21. K. Arai, Y. Maseki, Y. Ogiwara, Makrom. Chem., Rapid Commun., 8, 563, (1987).
22. R. Thundathil, J. O. Stoffer and S. E. Friberg, J. Polym. Sci., Polym. Chem. Edit.,18, 2629, (1980).

23. J. K. Thomas, Acc. Chem. Res., 10, 133 (1977).
24. C. M. Paleos, P. Dais, and A. Malliaris, J. Polym. Sci., Polym. Chem. Ed., 22, 3383 (1984).
25. K. Nagai, Y. Ohishi, H. Inaba, and S. Kudo, Ibid., 23, 1221 (1985).
26. K. Nagai and Y. Ohishi, Ibid., 25, 1 (1987).
27. S. Hamid and D. Sherrington, J. Chem. Soc., Chem Commun., 936 (1986).
28. C. M. Paleos, G. Margomenou- Leonidopoulou and A. Malliaris, Mol. Cryst. Liq. Cryst., 161, 385, (1988).
29. K. Nagai, H. G. Elias, Makromol. Chem., 188, 1095, (1987).
30. J. H. Fendler, P. Tundo, Acc. Chem. Res., 17, 17, (1984).
31. C. M. Paleos, J. Macrom. Sci., Rev. Macrom. Chem. Phys., In Press.
32. D. Lasic, J. Colloid and Interface Science, 124, 428 (1988).
33. S. L. Regen, K. Yamaguchi, N. K. P. Samuel, M. Singh, M., J. Am. Chem. Soc., 1983, 105, 6354-6355.
34. S. L. Regen, N. K. P. Samuel, J. M. Khurana, J. Am. Chem. Soc., 107, 5804 (1985).
35. R. Neumann, H. Ringsdorf, E. V. Patton, D. F O'Brien, Biochim. Biophys. Acta, 898, 338 (1987).
36. T. Kunitake, N. Nakashima, K. Takarabe, M. Nagai, A. Tsuge, H. Yanagi, J. Am. Chem. Soc., 103, 5945 (1981).
37. R. Elbert, A. Laschewsky, H. Ringsdorf, J. Am. Ch   Soc., 107, 4134 (1985)
38. B. A. Weber, N. Dodrer, S. L. Regen, J. Am. Chem. Soc., 109, 4419 (1987).
39. W. Reed, L. Guterman, P. Tundo, J. H. Fendler, J. Am. Chem. Soc., 106, 1897 (1984).
40. J. Serrano, S. Murino, S. Millan, R. Reynoso, L. Fucugauchi, . W. Reed, F. Nome, P. Tundo, J. H. Fendler, Macromolecules, 18, 1999 (1985).
41. F. Nome, W. Reed, M. Politi, P. Tundo, J. H. Fendler, J. Am. Chem. Soc., 106, 8086 (1984).
42. A. Sadownik, J. Stefely, S. L. Regen, J. Am. Chem, Soc., 108, 7789 (1986).
43. S. L. Regen, B. Czech M. Singh, . J. Am. Chem. Soc., 102, 6638 (1980).
44. D. Babilis, P. Dais, L. H. Margaritis, C. M. Paleos, J. Polym. Sci. Chem. Edit., 23, 1089 (1985).
45. D. Babilis, C. M. Paleos, P. Dais, J. Polym. Sci., Chem. Edit., 26, 2141 (1988).
46. C. M. Paleos C. Christias, G. P. Evangelatos, P. Dais, J. Polym. Sci. Chem. Ed. 20, 2565 (1982).
47. M. F. Poks, H. G. J. Visser, J. W. Zwikker, A. J. Verkley, R. J. M. Nolte, J. Am. Chem. Soc. 105, 4507 (1983).
48. P. Tundo, D. J. Kippenberger, P. L. Klahn, N. E. Prieto, T. C. Jao, J. H. Fendler, J. Am. Chem. Soc. 104, 456 (1982).
49. H. Ringsdorf, B. Schlarb, Makromol. Chem., 188, 299 (1988).
50. H. Fukuda, T. Diem, J. Stefely, F. J. Kezdy, S. L. Regen, J. Am. Chem. Soc., 108, 2321, (1986).
51. K. V. Aliev, H. Ringsdorf, B. Scharb, K. H. Leister, Makromol. Chem., Rapid Commun., 5, 345 (1984).
52. M. Wakita, K. A. Edwards, S. L. Regen, D. Turner, S. M. Gruner, , J. Am. Chem. Soc., 110, 5221 (1988).
53. K. Dorn, E. V. Patton, R. T. Klingbiel, D. F. O' Brien, H. Ringsdorf, Macromol. Chem., Rapid Commun., 4, 513 (1983).
54. R. Buschl, T. Folda, H. Ringsdorf, Makromol. Chem. Suppl., 6, 245 (1984).
55. T. Kunitake, M. Nakashima, K. Takarabe, M. Nagai, A. Tsuge, H. Yamani, J. Am. Chem. Soc., 103, 5945 (1981).
56. S. Inoue, Video Microscopy, Plenum Press, New York and London, 1986.
57. D. F. Evans, J. Brady, B. Kachar, and B. W. Ninham, J. Solution Chemistry, 14, 141, 1985.
58. D. D. Miller, J. R. Bellare, D. F. Evans, Y. Talmon, and B. W. Ninham, J. Phys. Chem., 91, 674, 1987.

THE PHYSICAL PROPERTIES OF MICROCELLULAR COMPOSITE FOAMS

Alice M. Nyitray and Joel M. Williams, Los Alamos National Laboratory, Los Alamos, NM
David Onn and Adam Witek, Applied Thermal Physics Laboratory, University of Delaware, Newark, DE

ABSTRACT

Recently we reported on a method of preparing microcellular composite foams. In this procedure an open-celled polystyrene foam is prepared by the polymerization of a high-internal-phase water-in-oil emulsion containing styrene, divinylbenzene, surfactant, free-radical initiator and water. After drying, the cells of the polystyrene foam are then filled with other materials such as aerogel or resoles. The physical properties of these materials e.g., surface area, density, thermal conductivity, and compressive strength will be presented.

INTRODUCTION

Physics experiments require very special materials. For inertial confinement fusion (ICF) experiments, foams have been suggested as ideal material to hold uniformly a mixture of liquid deuterium and tritium in a fusion target.[1] To do this, the foam must be a material of low atomic number with very small cells (< 0.1 μm), low density (< 40 mg/cm^3) but handleable. Other experiments require open-celled foams with specific densities that can range from 7 mg/cm^3 (5 X the density of air) to nearly full density, and range in length from a millimeter to meters. One type of foam that we use extensively is a polystyrene emulsion foam[2] prepared by a technique introduced by Unilever.[3] The foam is prepared by mixing styrene, divinylbenzene, sorbitan monooleate and free radical initiator with water to form a water-in-oil emulsion that can be polymerized by heating at 60°C. The solid mass is then oven-dried to remove the water. In this way, foams with densities from 0.012g/cm^3 to 0.20 g/cm^3 and cell diameter of 3-100 μm can be prepared depending on the concentration of monomers, surfactant, initiator and salt used to prepared them. (Fig. 1)

10 μm

0.025 g/cm^3 0.133 g/cm^3
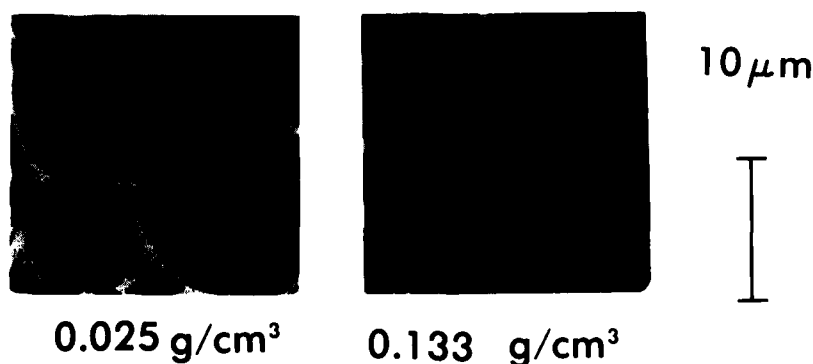
Figure 1. The size of the cell "windows" decreases with increasing foam density.

Composite foams were developed to reduce the cell size of the foam matrix by backfilling the cells of the polystyrene foam with materials such as aerogel, or resole.[4] The preparation of the composite foams have been reported on elsewhere.[5] The polystyrene foam can be filled completely (Fig. 2,3), or the cell walls can be coated depending upon the concentration of filler. This method has been extended to other filler materials such as backfilling with styrene and divinylbenzene to prepare foams of higher density.[6] In the remainder of this paper we will examine some of the physical properties of the composite materials.
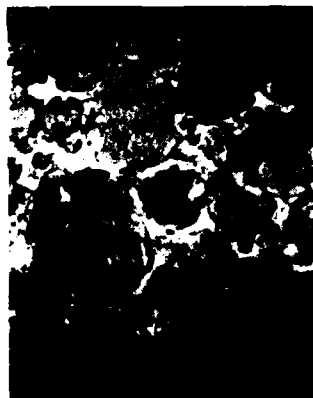
Fig.2

Fig. 3

Figure 2. Composite foams prepared by backfilling polystyrene emulsion foam with (10%) Si aerogel.
Figure 3. Composite foams prepared by backfilling polystyrene emulsion foam with (6%) Resorcinol-Formaldehyde (RF).

RESULTS AND DISCUSSION

Specific surface area measurements were made on a Monosorb (Quantachrome Corporation) single point surface analyzer using 30 mole percent nitrogen in helium. The single point method was used to obtain specific surface areas; therefore, the data (Table 1) should be considered as relative values only.

Compression analyses were determined on 0.75 cm right cylinders using a Materials Testing System (MTS) with a 500 lb. load and a platen speed of 0.005 inch/minute. Results are reported in Table II. The composite foams were found to have physical characteristics similar to those of the polystyrene foam. Compression testing data show the filler increased the density, but in the case of the Si aerogel filler, added nothing to the modulus. Conversely, the resole matrix increased the modulus. Although intrinsically weak, the resole appeared to stiffen the walls of the polystyrene foam. This effect is very dramatic in the carbonized forms of these materials which appear to be one of the best materials for ICF targets.[7,8]

Table 1. Specific surface area measurements on foam composites

Sample I.D.	Foam Type	Density (g/cm^3)	Specific Surface Area (m^2/g)	SEM Observations
C-1	PS	0.105	3	empty cells
141-3	PS+(2%)RF	0.116	35	coating on cell walls
141-2	PS+(4%)RF	0.118	27	coating on cell walls
141-1	PS+(6%)RF	0.116	28	filled cells
146-3	PS+(2%)PF	0.121	30	coating on cell walls
146-2	PS+(3%)PF	0.126	14	filled cells
146-1	PS+(7%)PF	0.158	20	filled cells
14-5	PS+(5%)Si aerogel	0.119	127	partially filled cells
14-3	PS+(7.5%) Si aerogel	0.139	138	coating on cell walls
Control	PS	0.100	5	empty cells
118G	PS+(4%)RF	0.149	105	filled cells
92-1	PS+(10%) Si aerogel	0.111	391	filled cells
92-2	PS+(7.5%) Si aerogel	0.090	538	filled cells
92-3	PS+(5%)Si aerogel	0.089	309	partially filled cells
C-2	PS	0.021	9	empty cells
28A	PS+(2%)RF	0.048	252	filled cells
67-1B	PS+(1%)RF (carbonized)	0.032	800	filled cells

Table II. Compression strength on foam composite

Foam Type	Density (g/cm^3)	Yield Strength (psi)	Compression at Yield (psi)	E-mod. (psi)
PS	0.105	174	4.7	5800
PS+(10%)Si aerogel	0.139	183	6.4	5800
PS+(7.5%)Si aerogel	0.126	181	6.4	5900
PS+(5%)Si aerogel	0.106	181	6.4	5900
PS+(2%)RF	0.111	248	6.2	7600
PS+(4%)RF	0.122	294	6.8	9500
PS+(6%)RF	0.131	367	6.4	10600

Since aerogels are known to be good insulating materials,[9] we have attempted to make thermal conductivity measurements on the composite foams. Thermal diffusivity (@) of the composite samples was measured using a laser-flash thermal diffusivity system at the Applied Thermal Physics Laboratory (ATPL), University of Delaware. This system and its associated analytical software is described elsewhere.[10] The samples in the form of discs 1 cm in diameter by 1.5 mm or 2.5 mm thick were pre-coated on both sides with copper, followed by a thin graphite surface to ensure uniform lateral heat dispersion on both surfaces.

Following energy deposition by the infra-red laser pulse on the front face of the sample, the temperature rise of the second face of the sample was monitored. The temperature showed a time dependence distinctly different from a homogeneous isotropic material. The theoretical thermal diffusivity values were calculated from the fractional temperature rise at each 0.1 fraction of the trace rise-time (t_v: V=0.1 to 0.9) between the pulse and the peak temperature rise of the second face. Only the relative values of thermal diffusivity ($t_{1/2}$) are reported in Table III.

We noted that for values of V between 0.1 and 0.5 the calculated values of @ decreased steadily with time. Thus the values for V-0.1 are approximately three times the values reported in Table III. These initial high diffusivity measurements may be due to residual effects of rapid radiant heat transfer through the composite materials since there is no component in the composite which should give such a high initial diffusivity. For values of V from 0.5 to 0.9 the average calculated value @ was typically within 10% of the value at V=0.5. This suggests that thermal transport in this time range is more typical of a homogeneous, isotropic material and is due to a combination of skeletal conductivity and thermal transport through the entrapped air.

Pending further transient analysis, we can gain a qualitative understanding of the changes in heat transport mechanism in these composite foams by comparing the $t_{1/2}$ values of @ listed in Table III. We assume that the contribution to thermal transport by radiation are small, while contriubtions from skeletal diffusivity and entrapped air diffusiyity are comparable to each other. Using the blank foam value of 0.0018 cm^2/s as a reference, we note that only for sample 146-1 is there a reduction of @ below the blank foam value. We assume that in this material the phloroglucinol-formaldehyde (PF) foam completely filled the polystyrene foam thus reducing the cell-size for the entrapped air. The resulting reduction in gas molecule mean-free-path reduced the entrapped air diffusivity while the skeletal diffusivity was not altered. At the other extreme we note that sample 14-5 has the highest @ value despite the low density. This suggest that the silica filler (which as a thermal conductivity about ten times that of the polystyrene) has enhancing the skeletal conductivity without inhibiting the air diffusivity. The other two PF aerogels and the three RF aerogels give values equal to, or slightly above, those of the blank foam. We propose that this relatively small enhancement could be due to partial filling of the foam cells possibly providing thermally conductive bridges across the cells. This effect may be partially compensated by a reduced gas mfp due to some reduction in cell size. Similar comments apply to the other Si airglass sample 14-3 though in this case wall-coating giving enhanced skeletal diffusivity is more likely than for the organic fillers. Further analysis and modeling of the transient thermal response of the composite foams is in progress.

CONCLUSIONS

Although the materials needed for laser fusion targets or other physics experiments are highly specialized, we envision that composite foam technology can be extended to other foam combinations and that novel filters, insulation, catalytic devices and chromatographic materials could be made from these materials. At this time we are continuing to study a way to optimize these materials.

Table III. Measurement and Analysis of Thermal Diffusivity

Sample I.D.	Foam Type	Density (g/cm³)	Thermal Diffusivty (cm²/sec)	Comments
C-1	PS	0.1044	0.0018	Blank foam: provides reference level for interpretations below.
14-3	PS+(7.5%)Si aerogel	0.1386	0.0022	Partial filling, partial coating. θ enhanced by wall-coating but not as much as 14-5.
14-5	PS+(5%)Si aerogel	0.1190	0.0025	Well-coated walls enhance skeletal diffusivity; air diffusivity unaffected.
146-1	PS+(7%)PF	0.1554	0.0014	Best and most complete filling. The reduced cell-size reduces mfp and thus redues θ below the blank foam value.
146-2	PS+(3%)PF	0.1262	0.0019	Values very close to blank foam suggest that filling not effective in reducing mfp but little enhancement due to wall coating since filler has lower diffusivity than 14-3,5.
141-1	PS+(6%)RF	0.116	0.0022	Enhanced value above blank foam suggests that some enhancement of skeletal diffusivity has taken place despite the low bulk diffusivity of the filler.
141-2	PS+(4%)RF	0.1175	0.0020	Similar to 146-2.
141-3	PS+(2%)RF	0.1159	0.0019	Similar to 146-2.

REFERENCES

1.   Sacks, R.A. and Darling, D.H., Nuclear Fusion, 27, 44 (1987).

2.   Williams, J.M., Langmuir, 4, 44 (1988).

3.   Unilever Research Laboratory, European Patent 60138, (Sept. 3, 1982).
4.   Pekala, R.W. and Kong, F.M., UCRL-99846 (1988).

5.   Nyitray, A.M. and Willliams, J.M., J. Cellular Plastics, 25, 217 (1989).

6.   Williams, J.M. and Wilkerson, M.H., accepted for publication in Polymer (1989).

7.   Kong, F.M., Polymer Preprints, 30, 258 (1989).

8.   Nyitray, A.M., J. Vac. Sci. Technol., submitted for publication, 1989.

9.   Fricke, J., in Aerogels, (Springer-Verlag 1985), p. 94.

10. Allitt, M., Whittaker, A., and Onn, D., to be published in Thermal Conductivity (21), Plenum Press, NY.

SYNTHESIS AND PROPERTIES OF COPOLYMERS OF
DIPHENYLSILOXANE WITH OTHER ORGANOSILOXANES

J. Ibemesi[a], N. Gvozdic[b], M. Kuemin[c], Y. Tarshiani[d] and D. J. Meier[*]
Michigan Molecular Institute, 1910 W. St. Andrews Rd., Midland, MI 48640

ABSTRACT
    We describe the synthesis, characterization and properties of various
types of siloxane polymers containing diphenylsiloxane (P) as a component.
The polymer types include di-and tri-block copolymers with dimethylsiloxane
(M) as the second component, and random and statistical copolymers with
dimethylsiloxane or methylphenylsiloxane (P/M) as the second component. Such
copolymers combine siloxane units whose polymers have very different
properties. The polydiphenylsiloxane chain is rigid and inflexible, and the
polymer is a highly crystalline solid with a liquid crystalline or condis
crystalline state and a very high melting (clearing) temperature. In
contrast, the polydimethylsiloxane or polymethylphenylsiloxane chains are
very flexible and the polymers have very low glass transition temperatures.
    Polymers of controlled molecular composition, size and architecture
were prepared by anionic polymerization of the "cyclic trimers", using
lithium-based initiators.
    The physical properties of the copolymers vary dramatically with
composition and architecture. Two types of "random" copolymers can be
prepared. In one type, siloxane units of a given type are randomly placed in
the chain in groups of three, i.e., the minimum sequence length of a given
siloxane type is three siloxane units. In the other type of random
copolymer, individual siloxane units are randomly distributed so that the
minimum sequence length is a single siloxane unit. The properties of the two
types are quite different, showing that subtle changes in sequence
distribution can have major effects on physical properties. At molar ratios
near 1/1 and with molecular weights of ~10^5 , the first type of "random"
copolymer is an elastic solid with appreciable mechanical properties,
whereas the latter type is a sticky gum.
    Diblock copolymer (P-M) with dimethylsiloxane as the major component
are paste-like, whereas the triblock (P-M-P) and star-block copolymers of
the same composition are tough elastomers. The block copolymers are
molecular composites, in which the polydiphenylsiloxane component separates
into crystalline microphases with very uniform fibrillar or lamellar
morphologies, and with widths or thicknesses comparable to the length of the
polydiphenylsiloxane block, i.e, typically of the order of 100 Å.

INTRODUCTION
    A program has been underway at MMI for several years to investigate
the synthesis and properties of homopolymer and copolymers of diphenyl-
siloxane with other organosiloxanes. A wide variety of homopolymers and
copolymers have been prepared by ring-opening polypmerization of the "cyclic
trimers" e.g., hexaphenylcyclotrisiloxane and hexamethylcyclotrisiloxane,
using lithium-based anionic polymerization techniques, as first described by
Bostic[1]. Polymers of controlled size and molecular architecture can be
prepared by these techniques since, when properly used, lithium-based

initiators do not "scramble" or randomize the sequence distributions of resulting copolymers. Polydiphenylsiloxane is of interest since the polymer is highly crystalline, with a liquid crystalline (or condis) transition near 250°C and a clearing temperature above 500°C. The polydiphenylsiloxane chain is quite rigid in contrast to the highly-flexible polydimethylsiloxane or polymethylphenylsiloxane chains.

A variety of block copolymers of the di-block (P-M), triblock (P-M-P) and star-block, (P-M)$_n$-x types have been made, where "P" and "M" represent polydiphenylsiloxane and polydimethylsiloxane blocks, respectively, and "x" represents the common junction of n-arms of a star-block molecule. With appropriate block compositions, the tri- and star-block copolymers are highly elastic, with strength properties among the highest ever reported for a siloxane elastomer[2].

Random and statistical copolymers are of interest since they demonstrate in a striking way the influence that subtle differences in molecular architecture can have on physical properties. The term "statistical copolymer" is used here to designate polymers prepared by the lithium-initiated copolymerization of the cyclic trimers. The resulting copolymers are "random", but the randomness is for groups of three siloxane units of a given type, i.e., the siloxane moities appear in the chain in minimum sequence lengths of three. With the polymerization conditions used, lithium-based initiators do not scramble the units of each cyclic trimer molecule. In contrast, truly random copolymers can be prepared using other types of initiators and monomer types, e.g., KOH with the cyclic tetramers[5]. With such initiators, the siloxane moities are completely scrambled and hence appear in the chain in minimum sequence lengths of one. Although the difference between minimum lengths of one unit vs. three units would appear to be minor, the differences in the physical properties of the two types of "random" copolymers are very large, as will be shown.

EXPERIMENTAL

As mentioned, the various siloxane polymers are prepared using lithium-based anionic polymerization techniques to initiate the polymerization of the cyclic trimers (obtained from Hüls Petrarch Systems Inc., Bristol, PA). The sensitivity of anionic polymerizations to adventitious impurities such oxygen, moisture, polar substances, etc. requires careful precautions to purify monomers and solvents and to exclude air during the polymerizations. Hexaphenylcyclotrisiloxane (HPTS) was purified by repeated recrystallization from toluene, hexamethylcyclotrisiloxane (HMTS) by vacuum sublimation at room temperature, and triphenyltrimethylcyclotrisiloxane (TPTMTS) by distillation. Trivinyltrimethylcyclotrisiloxane (TVTMTS) was used as received. Diphenylether (DPE) and tetrahydrofuran (THF) used as solvents in the polymerization were purified by distillation over n-butyllithium (DPE) or LiAlH$_4$ (THF). The polymerizations were conducted under a positive-pressure of purified nitrogen.

Diblock P-M copolymers

The diphenylsiloxane-dimethylsiloxane diblock copolymers are prepared by polymerizing the diphenylsiloxane block first and then followed by

polymerization of the dimethylsiloxane block. This sequence, as shown in
Figure 1, allows the dimethylsiloxane block to be terminated with reactive
end-groups, e.g., vinyl groups, for post-polymerization coupling reactions
to produce star-block copolymers.

FIGURE 1
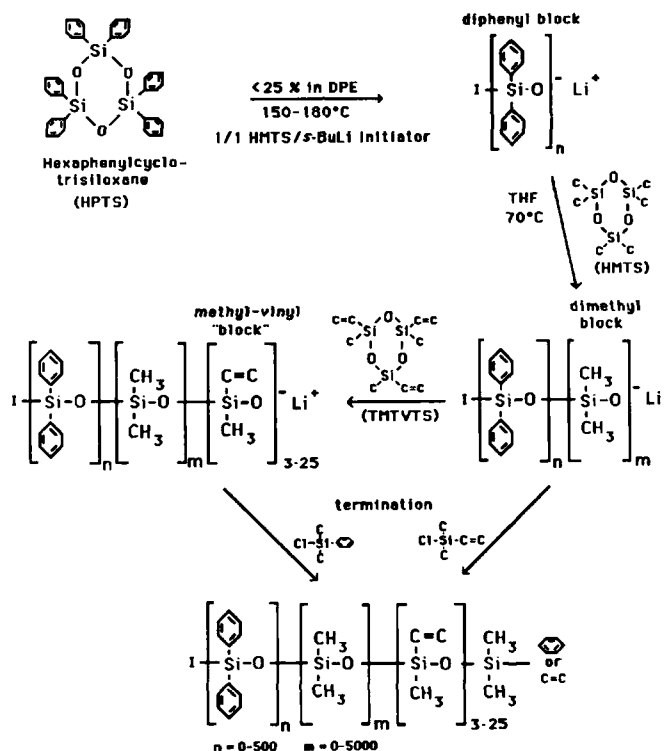
SYNTHESIS OF VINYL-TERMINATED DIBLOCK P-M COPOLYMERS

Polymerization of the diphenysiloxane block is done at 150 - 180°C in DPE
solution at concentrations below 25% to avoid phase separation during the
polymerization. Lithium dimethylbutylsilanolate, which is formed by
reacting s-butyl lithium and HMTS in a 1/1 molar ratio (Li/Si), is used as
the initiator[2]. The silanolate reaction product is required for initiation
of the polymerization of HPTS, since, in contrast to HMTS, s-butyl lithium
will not initiate the polymerization of HPTS. A small concentration (e.g.,
0.2-0.4 molar) of a polar additive such as tetrahydrofuran (THF) is

required as a polymerization "promoter" for polymerization of the diphenylsiloxane block. The polymerization of the diphenylsiloxane block is complete in approximately two hours, after which the solution is cooled to 70°C and a solution of HMTS in THF (20 w/v %) is added. Polymerization of the polydimethylsiloxane block also requires approximately two hours for completion. The reaction is terminated by the addition of vinyldimethylchlorosilane to provide a single terminal vinyl group, or, alternatively, trivinyltrimethylcyclotrisiloxane can be added and polymerized to give a short terminal methylvinylsiloxane "block" with additional terminal vinyl groups. Typically only a few (3-20) methyl-vinylsiloxane units are added to each polymer chain The polymers are recovered and impurities and unreacted monomers are eliminated by repeated washing with acetone and methanol.

Triblock P-M-P Copolymers

The triblock polymers P-M-P are prepared in the manner first described by Bostic[1]. The polymerization sequence is shown in Figure 2.

FIGURE 2
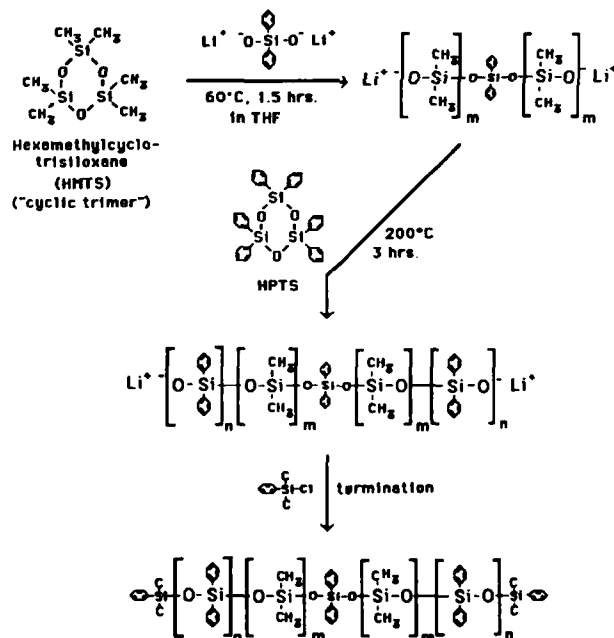
SYNTHESIS OF P-M-P TRIBLOCK COPOLYMERS

A difunctional lithium silanolate initiator is used to polymerize the center dimethylsiloxane block first, then followed by polymerization of the end diphenylsiloxane blocks.

Statistical copolymers

Poly(diphenylsiloxane-stat-dimethylsiloxane) (P-s-M) and poly(diphenyl-stat-phenylmethylsiloxane) (P-s-P/M) are prepared by copolymerization of the cyclic trimers at 150-180°C, using 1/1 HMTS/s-BuLi as initiator and THF or dimethylsulfoxide (DMSO) as promoters. The P-s-M copolymers are prepared in DPE solution, while the P-s-P/M copolymers are prepared in DPE solution or in bulk. The yield of polymer is typically 75-90%. The reactivity of diphenyl cyclic trimer is slightly greater than that of the dimethyl or methylphenyl analogues, as shown in Table 1 which displays the feed and copolymer composition (determined by ^{29}Si NMR and FTIR) of several poly(diphenylsiloxane-stat-dimethylsiloxane) copolymers.

It should be noted that the polymerization of the cyclic trimers to form block and statistical polymers of controlled architecture and molecular weights is the result of the polymerization being under kinetic control. Under equilibrium conditions, the polymer is in equilibrium with cyclic species and the polymer can be the minor component[3]. Veith and Cohen[4] have

Table I

STATISTICAL COPOLYMERS OF DIPHENYLSILOXANE AND DIMETHYLSILOXANE

Sample	Promoter	Polymerization		Diphenylsiloxane, mole %	
		Temperature (°C)	Time (min)	Feed	Copolymer
1	THF	175	240	27	30
2	THF	180	240	57	60
3	THF	170	180	72	76
4	THF	170	180	80	86
5	THF	175	240	88	93
6	DMSO	145	45	20	33
7	DMSO	150	15	30	36
8	DMSO	155	30	40	46

Samples 1-5: 25-30% concentration in DPE, 0.2 molar THF promoter
Samples 6-8: 75% concentration in DPE, 0.2 molar DSMO promoter

examined the kinetics of ring-opening siloxane polymerizations. Although the initiation of polymerization of the cyclic trimers with lithium-based initiators minimizes the tendency towards equilibration, such reactions can occur at higher temperatures when higher concentrations of promoters are present. An example of the effect of higher concentrations of a promoter on the polymerization of HPTS is shown in Figure 3. With a limited concentration of the THF promotor present, the yield of polydiphenylsiloxane approached 80% and remained constant with additional reaction time. In

contrast, with an excess amount of THF present, the yield of polymer also reached approximately 80%, but then rapidly declined as the system began equilibrating, with conversion of the polymer to the cyclic tetramer as the predominant product.

FIGURE 3

	Composition	
	"limited THF"	"excess THF"
HPTS	15 g	12.5 g
DPE	45 ml	50 ml
THF	2 ml	10 ml
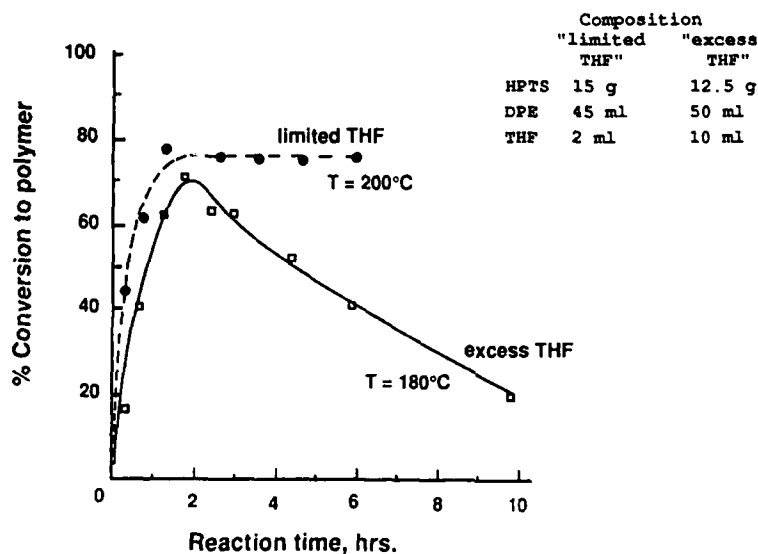
KINETIC VS. EQUILIBRIUM POLYMERIZATION OF HEXAPHENYLCYCLOTRISILOXANE

Random Copolymer

A random copolymers of diphenylsiloxane and phenylmethylsiloxane was prepared by the ring-opening polymerization of the cyclic tetramers, octaphenylcyclotetrasiloxane and tetraphenyltetramethycyclotetrasiloxane. The polymerizations was conducted in a concentrated (85%) DPE solution at 120°C, using KOH as initiator. Since this polymerization is a equilibrium polymerization, only a 35% yield of polymer (MW = 22,000) was obtained after purification by repeated precipitation from toluene solution with MeOH and heating in vacuum at high temperatures to remove the remaining cyclics by sublimation.

CHARACTERIZATION

NMR and sequence distribution

^{29}Si NMR data have been used to characterize the sequence distribution of the random and statistical copolymers of 1/1 diphenylsiloxane and phenylmethylsiloxane, and these data are shown in Figure 4, with assignments of the various peaks as given by Babu, Christopher and Newmark[5] and by Ziemelis, Lee and Saam[3]. These data show clearly that there are major differences in the sequence distributions of the two polymer types. In

particular, the P̱ḎP and ḎP̱D triads, in which a central siloxane unit is
flanked on both sides by the opposite siloxane type, are present in the
random copolymer, but not in the statistical copolymer. These triads can be
formed only if the elements of the cyclic monomers are scrambled. Their
absence in the statistical copolymers then shows that the repeat unit in the
statistical copoymers has a minimum length of three siloxane units,
corresponding to the three units of the cyclic trimer.
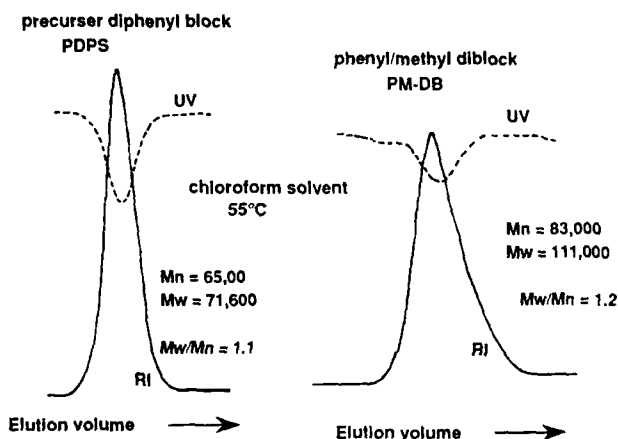
FIGURE 4

diphenyl - phenyl/methyl siloxane
statistical copolymer

D = PhMeSIO
P = Ph$_2$SIO

a = P D D   c = P P P
b = D D D   d = D P P

diphenyl-phenyl/methyl siloxane
random copolymer

D = PhMeSIO
P = Ph$_2$SIO

a = P D P   d = P P P
b = P D P   e = P P D
c = D D D   f = D P D
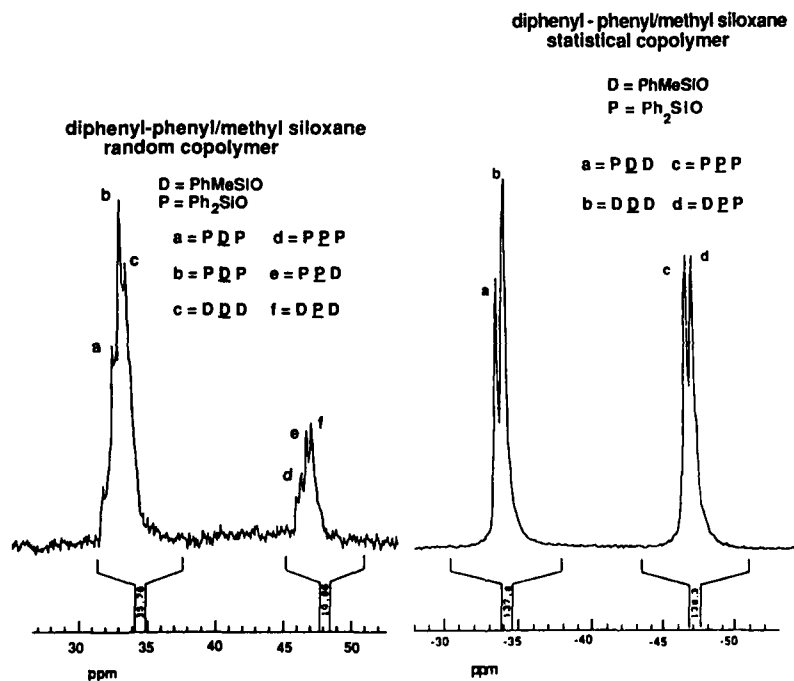
^{29}SI NMR OF RANDOM AND STATISTICAL COPOLYMERS OF
DIPHENYLSILOXANE AND METHYLPHENYLSILOXANE

Molecular weights

As a result of the high crystallinty and high melting point of
polydiphenylsiloxane, polymers and block copolymers of it are soluble in
very few solvents and then only at high temperatures. This makes the
molecular characterization of such polymers quite difficult. However, we
found that it was possible to prepare solutions for analysis at moderate
temperatures by pouring a dilute solution of the polymers in DPE (at 160°C)
into chloroform at 50°C. Although the solutions are unstable and the polymer

will eventually crystallize and precipitate, the polymer will remain in solution for approximately an hour, which is sufficient time for the molecular weight and its distribution to be determined by gel permeation chromatography (GPC). We find, in general, that the GPC molecular weights (based on polystyrene standards) agree well with those expected from stoichiometry, and that the molecular weight distribution can be quite narrow, e.g., $M_w/M_n \sim 1.1$-1.2. Figure 5 shows GPC traces obtained during the polymerization of a P-M diblock copolymer

FIGURE 5

precurser diphenyl block
PDPS

phenyl/methyl diblock
PM-DB

UV

UV

chloroform solvent
55°C

Mn = 83,000
Mw = 111,000

Mn = 65,00
Mw = 71,600

Mw/Mn = 1.2

Mw/Mn = 1.1

RI

RI

Elution volume ⟶

Elution volume ⟶

GPC OF POLYDIPHENYLSILOXANE AND
POLY(DIPHENYLSILOXANE-B-DIMETHYLSILOXANE) POLYMERS

Thermal properties

Thermal analysis of the block copolymers shows, as expected, the characteristic transitions of the homopolymers, i.e., T_g at $-125°C$ and T_m at $-40°C$ for the dimethylsiloxane block, and transitions near $260°C$ and $500°C$ for the diphenylsiloxane block. We believe the $260°C$ transition is a crystal/liquid crystal transition and the $500°C$ transition is the transition to the isotropic liquid ("clearing temperature"). Liquid crystal formation has also been reported for other polyorganosiloxanes[6,7]. The glass transition of polydiphenylsiloxane is not directly observable because of its very high degree of crystallinity. Literature data[3,5] for the glass transition behavior of random copolymers of diphenylsiloxane and dimethyl-siloxane (prepared by ring-opening polymerization of the cyclic tetramers) are not particularly informative either in establishing Tg for polydiphenyl-siloxane, since depending on the extrapolation used, e.g., Tg or 1/Tg vs weight or mole %, the data can be extrapolated to give Tg of polydiphenyl-siloxane between 13°C and 60°C. The variation between various sets of data perhaps can be understood in terms of sequence distribution when it is noted

that the statistical copolymers of this investigation have Tg's approx-
imately 20°C above those of their random counterparts.

PHYSICAL PROPERTIES

Triblock copolymers P-M-P

Tri-block copolymers of the P-M-P type (with polydimethylsiloxaneas
the major component) are thermoplastic elastomers which can be molded (with
difficulty) at very high temperatures (>300°C). It proved to be more
practical to prepare samples for testing by casting films from DPE solution,
even though it was difficult to prevent flaws in the films from bubbles from
the high-temperature evaporation of the DPE solvent. Such films showed
tensile strength properties as high as 8 MPa and ultimate elongations above
600%. In addition, appreciable mechanical properties were retained at
temperatures as high as 150°C (at the highest temperature tested). However,
in order to avoid the difficult processing of the P-M-P triblock copolymers,
we examined the end-to-end coupling of P-M-v diblock copolymers[2] to form
tri- and star-block copolymers in situ. The diblock copolymers are soft
pastes which are easily processed, e.g., by compression molding or
extrusion, after which the reactive terminal vinyl groups on the
polydimethylsiloxane block allow the diblock copolymer to be coupled to give
the desired tri- and star-block copolymers.

Coupled diblock copolymers P-M-v

The effect of the number of terminal vinyl groups and of molecular
weight on the tensile properties of coupled P-M-v diblock copolymers is
shown in Table II.

Table II
TENSILE PROPERTIES OF COUPLED P-M-v COPOLYMERS

Sample	Vinyl units	HPTS mol %	MW x 10^{-3}	Tensile strength MPa	Elongation %
DB3	1	20	102	0.4	195
DB4	10	20	70	2.7	90
DB5	16	27	72	5.0	70
DB6	16	27	150	9.8	195

The vinyl-specific peroxide 2,5 dimethyl-2,5 di(t-butylperoxy)hexane was
used for coupling through the terminal vinyl groups (3 phr, 15 min. at
170°C). The data in Table II show that the strength properties increase with
increasing numbers of terminal vinyl groups, most likely as the result of
increased coupling efficiency. The tensile strength of Sample DB6 approaches
the highest levels attainable with conventional silica-reinforced silicone
elastomers, in spite of the fact that these star-block copolymers are not
filled (in the conventional sense).

114

Since a silica filler is necessary in conventional silicone elastomers to achieve appreciable strength properties, it was of interest to see if the addition of a silica filler to our block copolymer systems would lead to a further enhancement of properties. Various amounts of a hydrophobic silica (Cab-O-Sil N70-TS) were added by mill mixing to a P-M-v block copolymer (70K-110K-2.5K). After coupling (3.5 phr of 2,5 dimethyl-2,5 di(t-butylperoxy)-hexane, 15 min. at 170°C), it was found that the mechanical properties were improved, and the improvement maximized with the addition of about 20 phr of silica. At this concentration the tensile strength increased from 4 MPa to 8.5 MPa and the ultimate elongation increased from 400% to 650%. The 100% modulus remained more-or-less constant until the silica concentration was above 20 phr. Additional experiments are required to determine if similar improvements will occur when the polymer itself has inherent strength properties comparable to the values achieved here with added filler.

SUMMARY

Table III summarizes our results on the effect of molecular architecture on the character of siloxane homopolymers and copolymers.

Table III
SILOXANE POLYMERS

P = DIPHENYLSILOXANE	M = DIMETHYLSILOXANE
MW = 100,000	
POLYMER	CHARACTER
P homopolymer	rigid, crystalline solid
M homopolymer	viscous liquid
P-M random copolymer (30-70)	sticky gum
P-M statistical copolymer (30-70)	flexible elastic solid
P-M diblock copolymer (30-70)	paste-like
P-M-P triblock copolymer (15-70-15)	"snappy" tough elastomer
(P-M-)$_n$ starblock copolymer (15-35-)$_n$	"snappy" tough elastomer

PRESENT ADDRESSES
a. University of Nigeria, Nsukka, Nigeria
b. Dow Corning Corporation, Midland, MI 48686
c, Dow Chemical Europe, Horgen, Switzerland
d. Silar Optical, St. Petersburg, FL 33709
* To whom inquiries should be addressed

REFERENCES

1. E. E. Bostic, ACS Polymer Preprints, 10, 877 (1965).

2. J. Ibemesi, N. Gvozdic, M. Kuemin, M. J. Lynch and D. J. Meier, ACS Polymer Preprints 26, 18 (1985).

3. M. Ziemelis, M. Lee and J. C. Saam, ACS Polymer Preprints, 31, No.1, in press.

4. C. A. Veith and R. E. Cohen, J. Poly. Sci: Part A: Polymer Chemistry, 27, 1241 (1989).

5. B. N. Babu, S. S. Christopher and R. A. Newmark, Macromolecules 20, 2654 1987).

6. C. L. Beatty, J. M. Pochan, M. F. Froix and D. D. Hinman, Macromolecules 8, 547 (1975).

7. Yu. K. Godovskii, N. N. Makarova and N. N. Kuz'min, Polymer Science U.S.S.R., 30, 341 (1988).

DYNAMIC IR STUDIES OF MICRODOMAIN INTERPHASES
OF ISOTOPE-LABELED BLOCK COPOLYMERS

I. NODA, S. D. SMITH, A. E. DOWREY, J. T. GROTHAUS, and C. MARCOTT
The Procter & Gamble Company, Miami Valley Laboratories, P.O. Box 398707,
Cincinnati, OH 45239-8707

ABSTRACT

By probing the localized segmental motion of isotope-labeled block copolymers, the physical nature of the interphase region between microphase-separated domains of block polymers was examined. Dynamic infrared linear dichroism (DIRLD) spectroscopy, which measures the reorientations of submolecular structures induced by a small-amplitude oscillatory strain, was combined with specific isotope-labeling using deuterium-substituted monomers. The latter technique enabled us to differentiate the dynamic responses of well-defined parts of block segments, e.g., near the segment junction, chain end, or middle of the block. The degree of segmental interactions near the interphase region of styrene-isoprene diblock copolymers were studied as a function of the segment location and temperature. The reorientational motion of the polystyrene segment, especially near the block junction, was monitored around the glass transition temperature of the polyisoprene matrix. From this result, the degree of segmental mixing in the interphase region which leads to local plasticization of the polystyrene segment was determined.

INTRODUCTION

Block copolymers owe their unique properties to the molecular architecture consisting of different polymer segments joined together by a covalent bond. The repulsive interactions between dissimilar block segments often results in microphase separation where the size of the phase domain is restricted to a scale comparable to the block segment length. It has been postulated for some time that the boundary between the adjacent microphase domains is not a sharp two-dimensional layer but rather a region of finite thickness characterized by a substantial intermixing of different block segments. The existence of the microdomain interphase [1] due to the diffuse concentration gradient across the boundary has been predicted by statistical thermodynamic theories based on the mean-field approach [2,3]. The results of several experimental works (e.g., the systematic deviation of SAXS intensity profiles from the behavior of sharp-boundary systems described by Porod's law [4,5] and the modeling of rheological behavior measured by dynamic mechanical analysis [6]) support the view of a segmentally mixed interphase. Different models, such as a coarse interface with a sharp boundary [7], may also account for some of the observed results.

Spectroscopic techniques which can provide direct information at a molecular scale are especially suited for probing the presence of segmental mixing at the interphase. Recent NMR studies [8] of isotope-labeled block copolymers with relatively low molecular weights, for example, reveal the existence of substantial segmental interactions at the domain boundary. We used a recently developed analytical technique called dynamic infrared linear dichroism (DIRLD) spectroscopy in conjunction with the selective deuterium labelling of well-defined portions of the block segment to investigate the submolecular environment of microphase separated block copolymers.

BACKGROUND

DIRLD spectroscopy [9,10] is a rheo-optical polymer characterization technique based on the combination of dynamic mechanical analysis and IR dichroism spectroscopy. In this technique, a polymer sample is deformed with a small-amplitude oscillatory strain, and strain-induced IR dichroism (i.e., difference in absorbances between the directions parallel and perpendicular to the applied strain) is monitored with polarized light as a function of time, temperature, and IR wavenumber (Fig. 1). Dynamic dichroism induced by the applied strain is directly related to the local reorientational motions of polymer molecules. Thus, DIRLD spectroscopy can be used as a powerful tool to probe the detailed local dynamics of polymer chains.
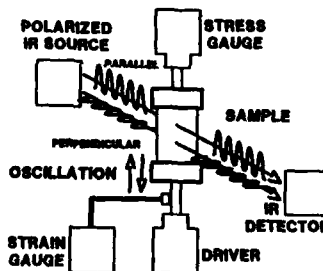

Fig. 1. Schematic representation of a DIRLD spectrometer.

For a small-amplitude sinusoidal strain, $\tilde{\varepsilon}(t) = \hat{\varepsilon} \sin \omega t$, the dynamic variation of dichroic difference $\Delta \tilde{A}(\nu, t)$ is given by

$$\Delta \tilde{A}(\nu, t) = \Delta A'(\nu) \sin \omega t + \Delta A''(\nu) \cos \omega t \tag{1}$$

where the wavenumber dependent terms, $\Delta A'(\nu)$ and $\Delta A''(\nu)$, are referred to as the **in-phase** and **quadrature** spectrum of dynamic dichroism. These spectra represent, respectively, the components of dynamic dichroism proportional to the extent and rate of applied strain. From a pair of such DIRLD spectra, strain-induced reorientations of various functional groups contributing to individual molecular vibrations can be determined. Figure 2 shows a typical set of DIRLD spectra. A positive peak indicates the dipole-transition moment associated with the band is reorienting parallel to the strain direction, while negative peaks indicate perpendicular reorientations.
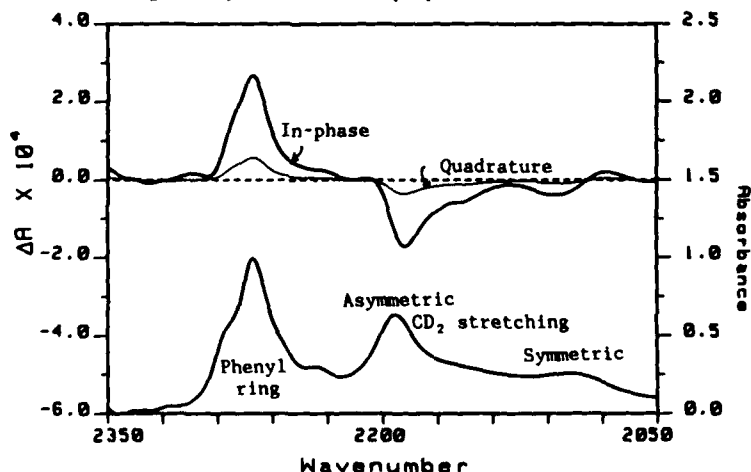

Fig. 2. DIRLD spectra of deuterium-substituted atactic polystyrene obtained under a 23-Hz oscillatory strain at room temperature.

EXPERIMENTAL SECTION

Polymer synthesis: A series of styrene and isoprene block and homo-
polymers were synthesized by anionic polymerization. Cyclohexane (Burdick
and Jackson HPLC Grade) was degassed and passed through columns containing
activated alumina and molecular sieves. Dibutyl magnesium and s-butyl lithi-
um were used as received from Lithium Corp. of America. Styrene (Aldrich)
was purified by titration with dibutyl magnesium then passed through an acti-
vated alumina column under an inert atmosphere to remove magnesium salts.
Deuterated styrene-d8-(98%) (Cambridge Isotopes Labs) was purified similarly
to styrene. Isoprene was provided by the Goodyear Tire & Rubber Company.

The reactions were carried out in Chemco reactors as described in
Ref. 11. A reactor at 60°C was charged with the appropriate amount of sty-
rene and cyclohexane. This was titrated slowly with s-butyl lithium till
the first yellow persistent color was obtained. The calculated charge of
butyl lithium was then added to obtain the desired molecular weight. The
second purified monomer was added after one hour to ensure complete conver-
sion. By these steps block copolymers were synthesized consisting of sty-
rene, deutero styrene, and isoprene blocks. The copolymers were terminated
with degassed isopropanol and stabilized with Irganox 1010. The molecular
weights and molecular-weight distributions of polymers were analyzed by GPC
(Ultra Styragel columns ranging from 10^3 to 10^6 Å porosities in THF). Com-
positions were determined using a combination of ^{1}H and ^{13}C NMR (GE QE300).
Films of these copolymers were prepared by dissolving an appropriate amount
of copolymer in toluene and allowing this solution to slowly evaporate from
a Teflon mold. After being allowed to air dry for 48 hours, the films were
vacuum-dried at room temperature for 12 hours then annealed under vacuum for
8 hours at 125°C. The sample-film thickness was selected so that the IR
transmittance for the phenyl band at 2280 cm^{-1} was approximately 10%.

DIRLD Analysis: Dynamic dichroism data were obtained with the time-
resolved IR spectrometer described in Ref. 10. The IR dichroism measurement
was carried out by mechanically perturbing the sample films at specified tem-
peratures with an oscillatory tensile strain (ca. 0.1% amplitude and 23-Hz
frequency) and recording the time-dependent fluctuations of directional IR
absorbances induced by the perturbation at a spectral resolution of 8 cm^{-1}.
The effect of small variations in sample thickness and deformation amplitude
were corrected by normalizing the results to a condition of 0.1% strain amp-
litude and 10% IR transmittance for the phenyl ring band at 2280 cm^{-1}.
All spectra were plotted on the same scale as Fig. 2 except for the room
temperature traces on Figs. 4 and 6 which were expanded by 20X.

RESULTS

The in-phase and quadrature DIRLD spectra and normal IR absorbance
spectrum of perdeuterated atactic polystyrene (PS) obtained under an oscil-
latory deformation have already been shown in Fig. 2. Peaks located at 2100
and 2180 cm^{-1} are assigned, respectively, to the symmetric and asymmetric
CD$_2$-stretching modes of the PS mainchain backbone. The peak near 2280 cm^{-1}
is attributed to the CD-stretching vibrations of phenyl ring side groups.
The dipole-transition moments for the CD$_2$ modes are oriented perpendicular
to the backbone of the polymer chain; they are also oriented orthogonal to
each other. The sign of the two DIRLD peaks for the CD$_2$-stretching vibra-
tions are both negative, indicating that the electric dipole-transition
moments associated with the peaks are both reorienting in the direction per-
pendicular to the sample-stretch direction. Thus, the molecular chain of PS
is reorienting parallel to the direction of the applied tensile strain.

Another dynamic dichroism peak, associated with the reorientation of phenyl groups attached to the main chain, is observed near 2280 cm^{-1}. The positive sign of this peak indicates that the reorientation of dipole-transition moments of phenyl ring CD-stretching vibrations of perdeuterated PS occur predominantly in the direction parallel to the applied strain. The complete identification of side group reorientation direction, however, is not straightforward, since the peak consists of several overlapping bands corresponding to different types of CD-stretching vibrations of phenyl rings.

Significant changes are observed for DIRLD spectra when the temperature is raised above the glass-to-rubber transition (Tg) of PS. Figure 3 shows a comparison of DIRLD spectra for perdeuterated PS in the glassy (a) and rubbery (b) state. In going from the glassy to the rubbery state, the magnitude of dynamic dichroism is decreased for all peaks, and the sign of the peak associated with the reorientation of phenyl rings near 2280 cm^{-1} is inverted. The dipole-transition moments of phenyl groups in rubbery PS are predominantly reorienting in the direction perpendicular to the applied strain. Such shifts of the local orientational motions of functional groups are believed to be a consequence of a change in the submolecular environment, e.g., the local free volume accessible to the reorienting groups. Thus, the characteristic inversion of the dynamic dichroism peak for the phenyl groups above and below Tg may be used as a molecular level indicator of the glass transition phenomenon.
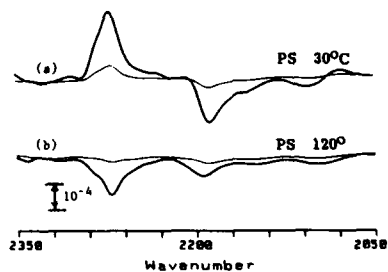

Fig. 3. DIRLD spectra of perdeuterated PS below and above Tg.

Figure 4 shows the CD-stretching region of DIRLD spectra at -70°C and 30°C for a 1:3 homopolymer blend of perdeuterated PS and hydrogenous polyisoprene (PI) and for a microphase-separated diblock copolymer made of a perdeuterated PS segment and hydrogenous PI segment. The molecular weights of the blend components are about 100,000 each, while those of PS and PI blocks are 50,000 and 150,000 respectively. For both systems, macro- or microphase-separated domains of PS components are dispersed in a continuous PI matrix. Because of the selective deuterium substitution, the DIRLD spectra in this wavenumber region show only the dynamic reorientation of PS components.
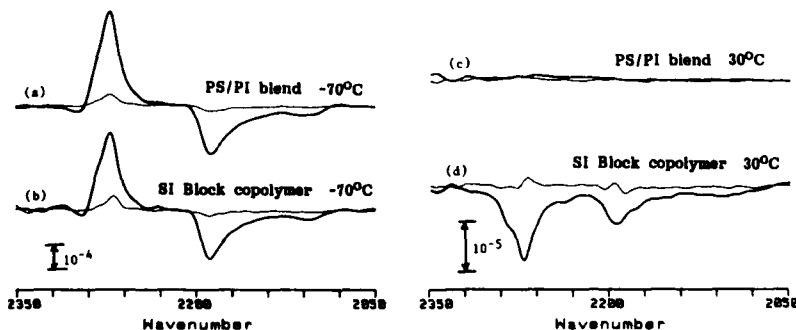

Fig. 4. DIRLD spectra at -70°C and 30°C for a homopolymer blend and diblock copolymer.

At -70°C, the basic feature of DIRLD spectra for both blend and block copolymer is very similar to that of the spectra for pure PS at room temperature (Fig. 2). DIRLD spectra for these heterogeneous systems all exhibit characteristic glassy responses with positive peaks for phenyl groups. Such results are expected since PS and PI phases at -70°C are both in the glassy state. Consequently, the applied strain is evenly distributed within the system as in pure glassy PS. At room temperature, on the other hand, deformation should occur predominantly in a rubbery PI phase. As long as the dispersed PS phase remains rigid, no significant orientational motions of segments in glassy PS domains should be expected. Interestingly, while the DIRLD spectra of the PS/PI blend at room temperature (Fig. 4c) have no significant peaks to indicate the existence of PS segmental motion, spectra of the SI block copolymer (Fig. 4d) clearly show peaks associated with dynamic reorientation of the PS segments. The sign of the dynamic dichroism peak for the phenyl ring in Fig. 4d is negative, which is a characteristic of the response of rubbery PS. For pure PS, such a response can be observed only at temperatures well above 100°C. This result shows that, even at room temperature, a portion of the PS segment apparently is in a plasticized state where the chain can move around in a manner similar to those at temperatures above Tg.

The response of the PS segment of the SI block copolymer at room temperature could be explained by the possible existence of a diffuse interphase region between microdomains where substantial mixing of PS and PI segments is believed to take place. Such mixing can plasticize PS segments, causing them to behave like rubber. To test this hypothesis, two types of selectively segment-labeled block copolymers consisting of PS and PI blocks (block MW of 50,000 and 150,000) were studied. The PS block is further divided into two distinct subsegments: deuterium-substituted and hydrogenous portions. A deuterium-labeled subsegment (MW of 10,000) is placed either at the tail end of the PS block (Fig. 5a) or near the junction with the PI block (Fig. 5b). While the part of the PS segment at the tail end of the copolymer may concentrate at the interior of the microdomain (Fig. 5c), the part near the block junction is expected to be located close to the domain boundary region (Fig. 5d). Thus, if plasticization of the PS segment occurs in the diffuse interphase region between microdomains, the molecular mobility of the segment near the junction is expected to be much higher than the tail end.
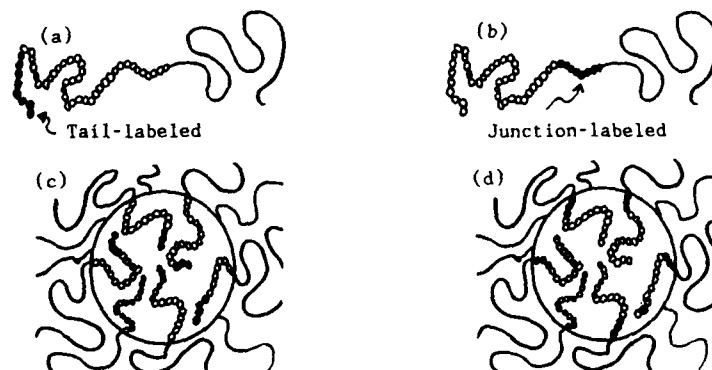
Tail-labeled (a)   Junction-labeled

Fig. 5. Tail-labeled (a) and junction-labeled (b) SI diblock copolymers and their spatial distributions in the microphase-separated domains. The deuterium-labeled portion of each PS block is indicated by (●●●●●).

The DIRLD spectra of the selectively segment-labeled SI diblock co-
polymers at -70°C (Figs. 6a and b) show typical glassy response of PS. For
the junction-labeled block (Fig. 6d), a rubber-like reorientation response
similar to that of the fully labeled block (Fig. 4d) is observed at room tem-
perature. Thus, PS segments near the junction appear to be plasticized,
most likely by intermixing with PI segments. DIRLD signals for the tail-
labeled block (Fig. 6c), on the other hand, virtually disappear at room tem-
perature. The core of the PS microdomain, where the tail ends of the block
segments are concentrated, remains in the rigid glassy state. Unlike the
rubbery PI matrix or plasticized interphase, significant segmental reorienta-
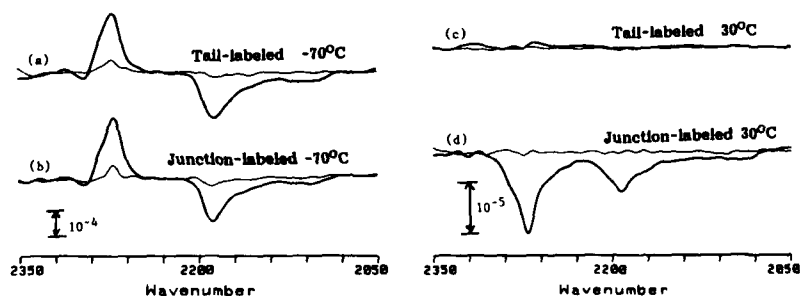tions do not take place in this part.

Fig. 6. DIRLD spectra at -70°C and 30°C for
selectively segment-labeled SI diblock copolymers.

CONCLUSIONS

DIRLD analysis of PS above and below the Tg reveals the existence of
distinct reorientational molecular motions characteristic of rubbery and
glassy states. Diblock copolymers consisting of PS and PI blocks show cer-
tain rubber-like DIRLD response of PS segments at a temperature well below
the Tg of normal PS homopolymer. By using selectively segment-labeled block
copolymers, it was found that the rubber-like behavior of the PS block at
room temperature takes place predominantly in the segment near the PS-PI
junction. Meanwhile, the tail end of the PS block remains glassy. This
result is consistent with the model that the PS segment near the block
junction is located in a diffuse, segmentally mixed interphase region where
the PS segment is plasticized by PI, thus leading to rubber-like behavior.

REFERENCES

1. D.F. Learry and M.C. Williams, J. Polym. Sci., Polym. Phys. Ed. 12, 265
   (1974).
2. D. Meier, J. Polym. Sci., Part C 26, 81 (1969).
3. E. Helfand and Z.R. Wasserman, Macromolecules 9, 879 (1976).
4. W. Ruland, J. Appl. Crystallogr. 13, 34 (1971).
5. T. Hashimoto, M. Fujimura, and H. Kawai, Macromolecules 13, 1660 (1980).
6. G. Kraus and K.W. Rollman, J. Polym. Sci., Polym. Phys. Ed. 14, 1133
   (1976).
7. W. Ruland, Macromolecules 20, 87 (1987).
8. W. Gronski and G. Stöppelmann, Polym. Prepr. 29 (1), 46 (1988).
9. I. Noda, A.E. Dowrey, and C. Marcott, in Fourier Transform Infrared
   Characterization of Polymers, edited by H. Ishida (Plenum, New York,
   1987), pp. 33-59.
10. I. Noda, A.E. Dowrey, and C. Marcott, Appl. Spectrosc. 42, 203 (1988).
11. J.M. Hoover and J.E. McGrath, Polym. Prepr. 27 (2), 150 (1986).

PART III

Rigid-Flexible Systems

LIGHT SCATTERING STUDIES OF THE STATE OF DISPERSION IN MOLECULAR COMPOSITES

Benjamin S. Hsiao[*], Richard S. Stein and Silvie Cohen Addad[+], Polymer Research Institute, University of Massachusetts, Amherst, MA 01003.
Russell Gaudiana and Norman Weeks, Polaroid Corporation, Cambridge, MA 02139.

*Present address: Fibers Department, E. I. du Pont de Nemours Co. Inc., Wilmington, DE 19880-0302.
+Present address: College de France, Paris, France.

ABSTRACT

Polymer solutions comprising stiff-chain polyester and flexible polysulfone were examined via light scattering techniques. Results were analyzed using the Stein-Wilson extension of the Debye-Bueche theory, in which the correlation lengths due to orientation fluctuations and mean-squared fluctuations of the molecular anisotropy were obtained. For a molecular dispersion, the correlation length is small and a function of concentration; as the anisotropy is attributed to the rod molecules. Aggregation of rods is associated with an increase in the magnitude and size of the density fluctuations, and a change in anisotropy fluctuations is dependent on the degree of orientation correlation of the rods in the aggregate. Blends prepared by solution casting were studied by a small-angle light scattering method. Results thus far demonstrate that aggregates are present in most of the rod/coil composites prepared.

INTRODUCTION

Molecular composites comprising stiff-chain molecules and flexible matrices offer potential advantages over the conventional composites in terms of processing, optical and certain mechanical properties. However, attempts to prepare molecular composites with a true molecular dispersion have often been unsuccessful. This may be explained by the theories of Onsager [1] and Flory [2], which stated that rod molecules are not soluble in random coil polymers.

Preparation of molecular composites usually employs solutions of rods and coils, where aggregation of rods may often be present prior to or during the making of the composite. In this case, the light scattering technique can be used to characterize the state of dispersion of the rod molecules in these solutions. Light scattering studies of dilute solutions of isotropic molecules and of anisotropic molecules [3-5] are well developed; however studies of concentrated solutions comprising rod and coil molecules are rare. It is conceivable that one can use the Stein-Wilson theory [6] extended from the Debye-Bueche approach [7] to determine the correlation functions for both density and orientation fluctuations in these solutions.

In a binary solution of rod molecules, intensity measured from polarized light scattering (Vv) is attributed to the density plus orientation fluctuations of the rods, whereas intensity of the depolarized light scattering (Hv) is only due to orientation fluctuations. For a solution comprising rod and coil molecules, intensity of Hv scattering is mostly from the orientation fluctuations of rods, but not appreciably from the isotropic coils, whereas intensity of Vv scattering is from the combination of density and orientation fluctuations of both rods and coils. Therefore, the measurements of Hv scattering reflect the state of molecular dispersion of the rods.

In many systems, the orientation correlation function f(r) can be represented by the empirical exponential equation [8]

$$f(r) = \exp(-r/a) \tag{1}$$

where "r" is the scattering distance and "a" is a correlation length. In the case of randomly correlated assemblies of rods, intensities measured from Hv and Vv scattering can be expressed as

$$I_{HV}(q)=K<\eta^2>(a_o^3/(1+q^2a_o^2)^2) \tag{2}$$

$$I_{VV}(q)=K[15<\delta^2>(a_r^3/(1+q^2a_r^2)^2)+(4/3)<\eta^2>(a_o^3/(1+q^2a_o^2)^2)] \tag{3}$$

where K is a constant, depending on the number of rod molecules, the scattered volume and the wavelength of the light; $<\delta^2>$ and $<\eta^2>$ are mean-squared fluctuations of two average refractive indices and its anisotropy, respectively; a_o and a_r are correlation lengths from the orientation and density fluctuations, respectively; and q is the magnitude of the scattering vector. It is noted that a plot of $I_{HV}(q)^{-1/2}$ vs. q^2 should be linear with a (slope/intercept) equal to a_o, and a plot of $(I_{VV}(q)-(4/3)I_{HV}(q))^{-1/2}$ vs. q^2 should determine a_r. This approach is referred to as the Debye-Bueche plot.

In this work, it is our intention to characterize the orientation correlation of rod molecules in rod/coil solutions by using the depolarized light scattering technique. A change in orientation correlation lengths will reveal information about the state of dispersion of rods in these solutions. Additional work also includes the small-angle light scattering study of polymer films prepared from solutions with various rod/coil ratios. The purpose of this study is to correlate the phase behavior of solid blends with that of the concentrated solutions.

EXPERIMENTAL

Materials and Sample Preparation

The stiff-chain polymer is a wholly aromatic polyester containing substituent groups on the aromatic rings. This material is synthesized by Polaroid Corp., Cambridge MA [9], and has a chemical structure as shown:
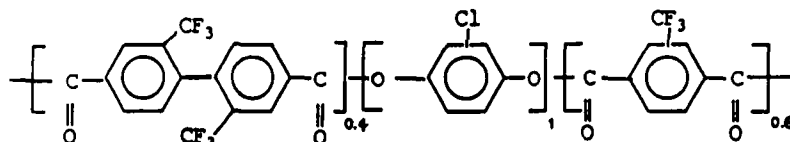
The substituting groups have improved the solubility in many solvents, including tetrahydrofuran (THF) which was used in this work. This polyester is completely amorphous with a glass transition temperature of 110°C, but exhibits thermotropic behavior. No lyotropic behavior has been observed, even as the solution concentration exceeds 50% (w/v), the maximum solubility in THF. Its weight-average molecular weight Mw is 21800, determined by light scattering measurements on dilute solutions. The flexible polymer is a polysulfone (from Aldrich Chemical), which has a Mw of 30,000 and is also soluble in THF. The glass transition temperature of the polysulfone is about 180°C. Solutions of various concentrations were prepared, ranging from 0.1% to 30% (w/v), with different rod/coil ratios. Dry polymer films, a few microns thick, were obtained by spin-coating of these solutions. These films were annealed above the glass transition temperatures of both polymers to equilibrate their phase behavior.

Instrumentation

A laser light scattering goniometer (Brookhaven Instrument Corp., Ronkonkoma, NY), was used to collect the scattering data in polymer solutions. This

instrument consists of a 15mW He-Ne laser, polarizer/analyzer and an automated photomultiplier/goniometer, that is capable of measuring both polarized and depolarized light scattering. Toluene, whose Rayleigh ratio and depolarization ratio are known [10], was used as a calibrient. Absolute scattered intensity was calculated after suitable corrections were made, which included the corrections for scattering volume, reflection, refraction, absorption, multiple scattering and dark current subtraction [11]. Multiple scattering was proven insignificant at the range of the chosen concentrations. The small-angle light scattering device consisting of a two-dimensional optical multichannel analyzer (OMA3, by EG&G PARC, Princeton, NJ), a 2mW He-Ne laser, and assemblies of optical components, was utilized to characterize the polymer films. The detail of this device has been described before [12].

RESULTS AND DISCUSSION

The non-coplanar biphenyl unit coupled with the random configuration of repeat unit dipoles in the chosen polyester has significantly increased the solubility in THF. Though the solutions show evidence of the molecules being stiff (Mark-Howink exponent is 1.1), no lyotropic behavior has been observed, even when solution concentration approaches 50% (w/v). This may be attributed to the intermolecular interactions which oppose the aggregation of anisotropic molecules and/or the unusually large molecular diameter which may reduce the molecular aspect ratio below the level requiring for the formation of an order phase. It is thought that this system may offer a unique opportunity, that molecules are stiff enough to give reinforcement in a blend, but permit solubility in a flexible coil matrix to form true molecular dispersion.

A phase diagram of the solutions containing stiff-chain polyester and flexible polysulfone, determined by a laser cloud-point measurement, is shown in Figure 1. It is noted that above the phase line, a miscible single-phase region is present, where below this boundary, the immiscible multiple-phase systems occur. The phase separation in high concentrations is expected, since the entropy of mixing is unfavorable for mixtures of rods and coils. It is conceivable that although strong repulsive interactions are present among the stiff molecules, the unfavorable entropy of mixing prevents the molecular dispersion of these molecules at high concentrations.
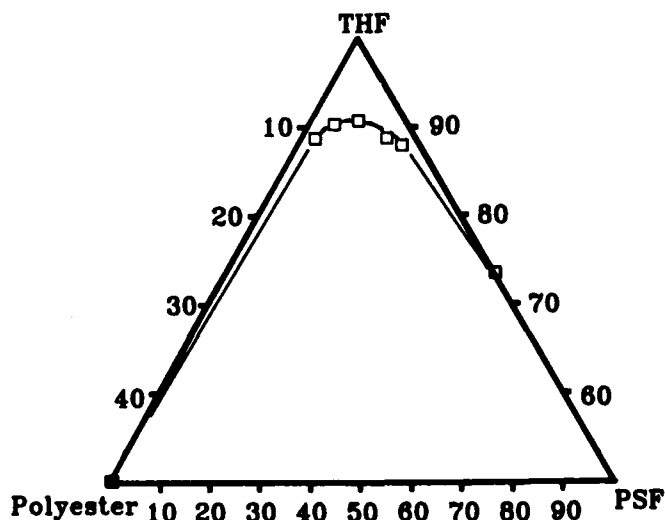

Figure 1. Phase diagram of solutions of stiff-chain polyester and flexible polysulfone.
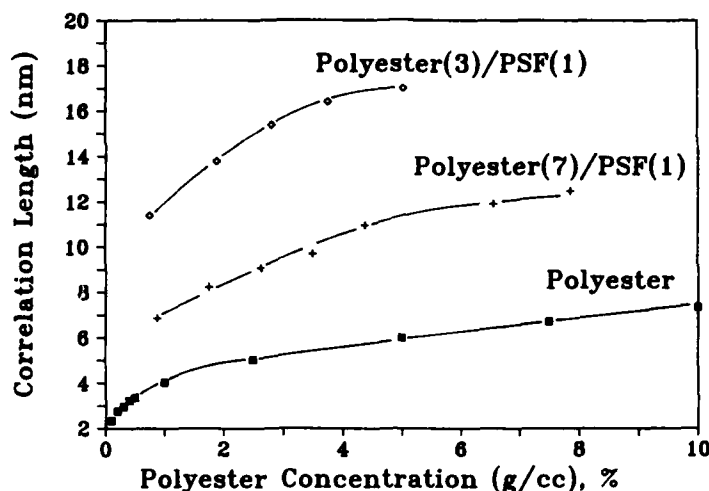
Figure 2. Plot of the orientation correlation length vs. polyester concentration at various rod/coil ratios.

Results from the Debye-Bueche plot of depolarized intensity (Hv) for the rod/coil solutions in the single-phase region are illustrated in Figure 2, where the orientation correlation lengths are plotted against the polyester concentration at various rod/coil ratios. These characteristic lengths represent the correlation of the orientation fluctuations of the rod molecules, which reflect the state of anisotropic molecular dispersion. An increase in the orientation correlation length indicates that the molecular dispersion becomes unfavorable and the rods tend to aggregate. This is seen in Figure 2, where the correlation length increases with polyester concentration and also increases with the coil composition. The addition of coil molecules obviously enhances the segregation of rods and coils; the entropy of mixing is so unfavorable that it has hindered the molecular dispersion.

Similar results are found from the small-angle light scattering (SALS) study of polymer films. Figure 3 shows photographs of the Hv scattering patterns at six different rod/coil compositions. In this figure, the pure polyester exhibits a 0/90 cross pattern, which has been reported before [13], whereas an increase in the coil content changes this pattern to a 45° cloverleaf shape. The azimuthal dependence of the Hv pattern, which may be due to the interactions between the anisotropic and isotropic domains, indicates non-random orientation correlations which also suggests aggregation. It was verified via Vv scattering, optical microscopy and DSC analysis that phase separation occurred at the high coil content. Intensity obtained from Vv scattering was always stronger than that from Hv (about 2 times), an indication of phase separation, since aggregation of rods is associated with an increase in the magnitude and size of the density fluctuations. Such an observation was consistent with the optical microscopic observation of isolated anisotropic domains. Results from DSC showed two glass transition temperatures, again indicating two separate phases. However a slight glass temperature shift suggested that a partial miscibility might be present.

A particularly interesting case is the blend made of 7/1 rod/coil ratio. As seen in Figure 3, the Hv scattering pattern of this blend remains a 0/90 cross shape, similar to

that of the polyester, which suggests that its orientation correlation resembles pure polyester. In the polymer films, Hv scattering is angularly dependent, therefore the previous equations derived for the random assemblies of rods are no longer applicable.
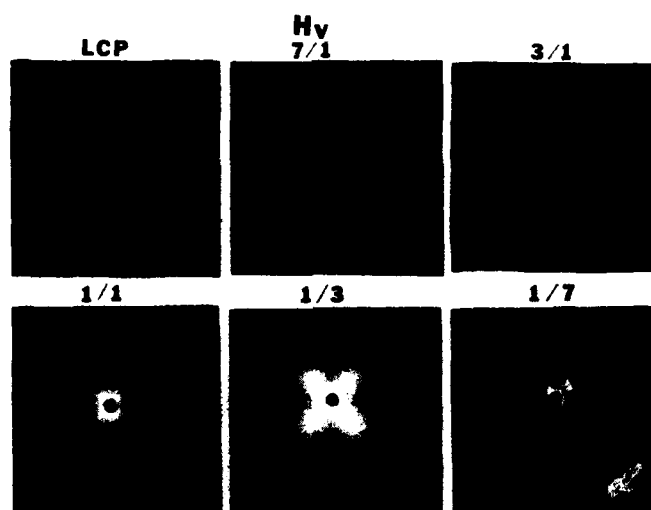

Figure 3. Photographs of Hv scattering of polymer films prepared from various rod/coil ratio solutions.
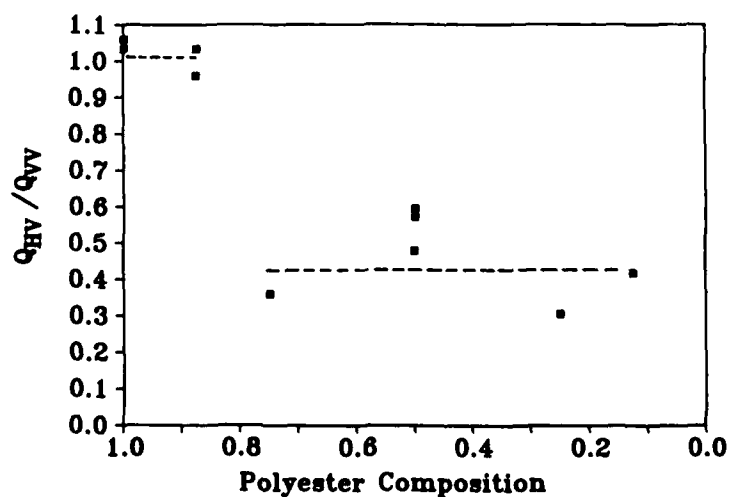

Figure 4. Depolarization ratio of total integrated intensity vs. polyester composition.

130

However, the state of molecular dispersion in these films can be estimated by the use of total integrated intensity Q [14]. This is seen in Figure 4, where the depolarization ratio (Q_{HV}/Q_{VV}) of total integrated intensity vs. the polyester concentration is illustrated. It is noted that the depolarization ratio of the polyester and that of a blend of a 7/1 rod/coil ratio are both about unity. This observation indicates that the magnitude of orientation fluctuations dominate the scattered intensity and that of density fluctuations is small, which implies phase separation may not occur in this blend. Therefore, a blend of 7/1 rod/coil ratio may form a composite having a molecular dispersion at the level of wavelength of the light.

CONCLUSION

In summary, solutions comprising stiff-chain polyester and flexible polysulfone were characterized by light scattering techniques. The orientation correlation lengths in these solutions were determined by the Stein-Wilson theory for depolarized light scattering. It was found that orientation correlation lengths increased with concentration as well as with addition of coil molecules. An increase in these lengths indicates the molecular dispersion of rods is depressed and the molecular aggregation is more favorable. The modification of the rod molecules with strong polarized substituting groups has improved solubility in non-interactive solvents, indicating that solubility in flexible polymer matrices may also be enhanced, though the effect of unfavorable entropy of mixing is significantly greater. A polymer blend made of a 7/1 rod/coil ratio solution showed a possible molecular dispersion, at least at the level of wavelength of the light, was determined by a small-angle light scattering method.

ACKNOWLEDGMENT

REFERENCES

1. L. Onsager, Ann. N.Y. Acad. Sci., 51, 627 (1949).
2. P. J. Flory, Macromolecules, 11, 1119 (1978).
3. C. P. Wang, H. Ohnuma and G. Berry, J. Polym. Sci. Polym. Symp., 65, 173 (1978).
4. Q. Ying, B. Chu, R. Qian, J. Bao, J. Zhang and C. Xu, Polymer, 26, 1401 (1985).
5. Q. Ying and B. Chu, Macromolecules, 20, 871 (1987).
6. R. S. Stein and P. R. Wilson, J. Appl. Phys., 33(6), 1914 (1962).
7. P. Debye and A. Bueche, J. Appl. Phys., 20, 518 (1940).
8. R. S. Stein and S. N. Stidham, J. Appl. Phys., 35(1), 42 (1964).
9. R. Sinta, R. A. Gaudiana, R. Minns and H. G. Rogers, Macromolecules, 20, 2374 (1987).
10. W. Kaye and J. B. McDaniel, Appl. Optics, 13(8), 1934 (1974).
11. Brookhaven Instrum. Corp., Instruction Manual For Laser Light Scattering Goniometer, 1985.
12. R. J. Taber, R. S. Stein and M. B. Long, J. Polym. Sci. Polym. Phys., 20, 2041 (1982).
13. S. Rojstaczer and R. S. Stein, Mol. Cryst. Liq. Cryst., 157, 293 (1988).
14. J. Koberstein, T. P. Russell and R. S. Stein, J. Polym. Sci. Polym. Phys., 17, 1719 (1979).

RECENT ADVANCES IN MORPHOLOGY AND MECHANICAL PROPERTIES OF RIGID-ROD MOLECULAR COMPOSITES

STEPHEN J. KRAUSE* AND WEN-FANG HWANG**
*Dept. of Chemical, Bio, and Materials Engineering, Arizona State University, Tempe, AZ 85287
**Dow Chemical Co., Central Research Laboratories - Advanced Polymeric Systems, Midland MI 48674

ABSTRACT

Rigid-rod molecular composites are a new class of high performance structural polymers which have high specific strength and modulus and also high thermal and environmental resistance. The concept of using a rigid-rod, extended chain polymer to reinforce a ductile polymer matrix at the molecular level has been demonstrated with morphological and mechanical property studies for aromatic heterocyclic systems, but new materials systems and processing techniques will be required to produce thermoplastic or thermoset molecular composites. Improved characterization and modeling will also be required. In this regard, new results on modeling of mechanical properties of molecular composites are presented and compared with experimental results. The Halpin-Tsai equations from "shear-lag" theory of short fiber composites predict properties reasonably well when using the theoretical modulus of rigid-rod molecules in aromatic heterocyclic systems, but newer matrix systems will require consideration of matrix stiffness, desired rod aspect ratio, and rod orientation distribution. Application of traditional and newer morphological characterization techniques are discussed. The newer techniques include: Raman light scattering, high resolution and low voltage SEM, parallel EELS in TEM, synchrotron radiation in X-ray scattering, and ultrasound for integrity studies. The properties of molecular composites and macroscopic composites are compared and it is found that excellent potential exists for use of molecular composites in structural applications including engineering plastics, composite matrix resins, and as direct substitutes for fiber reinforced composites.

INTRODUCTION

Since the concept of a self-reinforcing molecular composite of rigid-rod and flexible coil polymer components was first proposed by Helminiak et al. [1, 2], and first successfully applied by Hwang et al. [3], a variety of candidate systems have been studied. The advantages of rigid-rod molecular composites over macroscopic fiber reinforced composites are based upon the elimination of discrete fiber/matrix interfaces and upon the intrinsically superior properties of the aromatic heterocyclic chemistry of the rod molecules. These advantages include: higher specific mechanical properties; higher environmental and thermal resistance; and the potential for a wider choice of processing options. Possible applications for molecular composites include: engineering plastics; high performance fibers; composite matrix resins; and direct substitutes for fiber reinforced composites.

The choice of the reinforcing molecule for a molecular composite is critical, in order to maintain both high aspect ratio (ratio of length to diameter) for efficient reinforcement and to have a molecule with inherently high strength and stiffness. The rigid-rod aromatic-heterocyclics are a class of molecules which fulfill these criteria. Table 1 list various high performance fibers. The rigid-rod molecule fibers, poly(p-phenylene benzobisthiazole) (PPBT) (Fig. 1) and poly(p-phenylene benzobisoxazole) (PBO) (Fig. 1), have uniaxial tensile strength and stiffness, which significantly exceed the properties of other commercial fibers used for composites. The limiting factor of application of organic fibers to composites, including PPBT, PBO, poly(p-phenylene terepthalate) (PPTA) - Kevlar 149, and gel-spun polyethylene (PE) - Spectra 1000, is the low compressive strength, which is two orders of magnitude less than graphite T300 or E-glass fibers. However, for reinforcement at a molecular level, PPTA and PBO are superior since PE cannot maintain an extended chain conformation in solution and PPTA, with a relatively high persistence length, has intrinsic stiffness and strength that are much less than the rigid-rod molecules.

After synthesis of the appropriate molecule, the critical factor in processing a molecular composite from the solution to the solid state is that the rigid-rod reinforcing component be well dispersed and not phase separate from the matrix component during any stage of solution processing, including blending, extrusion, and coagulation, and during solid state consolidation. Phase separation of the components of a molecular composites can significantly affect mechanical and thermal properties. A high aspect ratio (the ratio of length to diameter) of the reinforcing phase must be maintained for efficient reinforcement. Phase separation will also limit thermal stability to that of the minimum of the individual homopolymer components. The mechanical properties of a molecular composite are chiefly controlled by the composition, orientation, and dispersion of the reinforcing rod molecules and can be predicted by using appropriate models with a knowledge of the intrinsic properties of the homopolymer components and their morphological arrangement in the material. Thus, a thorough description of morphology is necessary for assessing, understanding, and predicting ultimate properties of rigid-rod molecular composites.

In this paper the study of molecular composite candidates with a variety of characterization techniques, including optical microscopy (OM), electron microscopy (EM), and x-ray scattering will be discussed and new techniques will be highlighted. Results will be discussed with regard to models for traditional composite theory of mechanical properties, such as "shear lag" theory for short fiber composites, in order to compare experimentally observed and theoretically predicted properties. Molecular composite properties will then be considered for macroscopic systems to assess the potential for molecular composites in engineering applications.
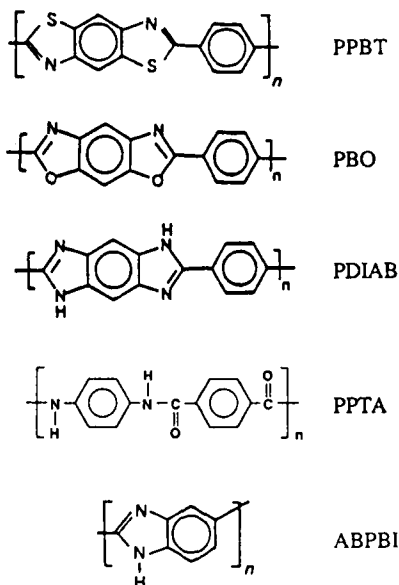
Figure 1. Chemical structures of PPBT, PBO, PDIAB, PPTA, and ABPBI.

TABLE 1

Mechanical Properties of High Performance Fibers

Material	Modulus		Strength		Ductility	Density
	Predicted GPa, (Msi)	Measured GPa, (Msi)	Tensile GPa, (ksi)	Compressive GPa, (ksi)	%elong.	(g/cc)
PPBT	615 (88)	328 (47)	4.2 (600)	0.027 (39)	1.6	1.58
PBO	635 (90)	363 (52)	5.8 (830)	0.021 (30)	1.6	1.58
30PPBT/70ABPBI	184 (26)	120 (17)	1.3 (190)	- -	1.4	1.58
Graphite T300	1100 (157)	237 (34)	3.3 (470)	2.9 (417)	1.0	1.76
PPTA - Kevlar 149	220 (32)	186 (27)	3.5 (500)	0.033 (48)	1.2	1.47
E - glass	- -	76 (11)	2.0 (286)	2.0 (286)	2.5	2.6
PE - Spectra 1000	300 (43)	174 (25)	3.0 (435)	0.017 (24)	-	0.97

MODELING OF MECHANICAL PROPERTIES OF MOLECULAR COMPOSITE

The ability of the Air Force Materials Laboratory (AFML), Polymer Branch to synthesize aromatic heterocyclic molecules that were chemically similar, but configurationally different, led to the creation of both the inherent rigid-rod and the semi-flexible coil molecular architectures used in the first molecular composites [4]. The molecular composite concept was first tested by blending rigid-rod polyparaphenylene benzimidazole (PDIAB) and semi-flexible coil poly 2,5(6)benzimidazole (ABPBI) (Fig. 1) in a dilute solution of methanesulfonic acid (MSA) and casting thin films in a glass container placed in a vacuum evaporator [5]. The properties of this material are listed in Table 2, along with those of other molecular composite systems. Although the properties of the PDIAB/ABPBI films were somewhat enhanced over that of cast homopolymer ABPBI, especially when stretched 55%, they did not approach what could be expected from the intrinsic properties of the rigid-rod PDIAB, which would probably be in the range of those for PPBT, as shown in Table 1. It was found from optical microscopy (OM) and scanning electron microscopy (SEM) that the bright yellow opaque films showed that large scale phase separation (1-5 μm) had occurred during the casting process, resulting in a loss of potential for reinforcement at the molecular level. This problem was addressed by developing an understanding of the phase behavior of rigid-rod solutions and then applying this knowledge to the technology for processing for rigid-rod systems from the solution to the solid state.

This work contained the earliest application of the "rule of mixtures" to molecular composites (5). The "rule of mixtures" is a special case of the Halpin-Tsai equations, which is a simplification of "shear-lag" theory, which models the modulus of short fiber reinforced composites [6]. The "rule of mixtures" predicts that the modulus of a material with a uniaxially oriented reinforcing phase and is given by a parallel element model, which states that the overall modulus is the sum of the volume fraction times the modulus of each component. In order for the "rule of mixtures" to be applied, the Halpin-Tsai equations show that the reinforcing phase must have a high aspect ratio (typically >100) to approach 100% efficiency, as given for the modulus of a continuous fiber reinforced composite. Donaldson [7] has applied short fiber composite theory (ie. shear-lag theory) to molecular composites to predict the effect of the factors of rod length, concentration, dispersion, and orientation variables on properties.

The phase behavior of rigid-rod homopolymer and blend systems was first elucidated by Hwang et al. [3] by applying Flory's [8] theory of phase equilibria of rigid-rod polymers. This theory predicts that, when the total concentration (C) of a rigid-rod polymer system in a solvent is above a critical concentration (Ccr), liquid crystalline domains will phase separate from a homogeneous solution. Hwang et al. [3] calculated the ternary phase diagram for a blend of rigid-rod poly(p-phenylene benzobisthiazole) (PPBT) and semi-flexible coil poly-2,5(6) benzimidazole (ABPBI) as components in a dilute solution of MSA and used OM hot stage techniques to verify the predictions. It was then necessary develop processing techniques for retaining the dispersion as the rod and coil components in solution are processed into the solid state.

Molecular composite fibers were produced with the dry-jet/wet-spin technology used in processing of poly-p-phenylene terepthalate fibers. Processing homogeneous of dilute solutions of PPBT / ABPBI "froze-in" the dispersion of rod molecules in the matrix polymer to form molecular composite films and fibers (3). This process of rapid immersion of the polymer acid solution into water was referred to as "quenching" or "coagulation". After subsequent neutralization, drying, and heat treatment the 30 PPBT / 70 ABPBI films and fibers were optically transparent and had excellent mechanical properties, as shown in Table 2. Any phase separation which occurred was clearly below the resolution limit in OM, since the film was clear, but it was also found to be below the resolution limit of the SEM of 20 nm. WAXS showed that any crystalline phase separation could be calculated to be <5nm). Thus, morphology results demonstrated that the concept of a rigid-rod molecular composite had been achieved.

Application of the "rule of mixtures" to a 30 PPBT / 70 ABPBI spun fiber, based upon the experimentally measured modulus of PPBT fiber, also indicated that a molecular composite had been achieved (3). The problem in extending the "shear-lag" or Halpin-Tsai theory from the macroscopic to the molecular level is the choice of the value of the modulus of the reinforcing phase. The theoretically predicted value of the modulus of PPBT is 615 GPa, which is almost double the value of the highest measured modulus of a macroscopic PPBT fiber [24]. It seems that, for molecular composites, the basis for modulus predictions should be the theoretical modulus of the rod molecules, rather than the experimental fiber modulus, since factors such as local misorientation, disorder, and defects will degrade the macroscopic fiber modulus, but should not affect the modulus of rod molecules acting to reinforce a material at the molecular level. If the theoretical modulus of PPBT is used with the "rule of mixtures" then the modulus of the 30 PPBT / 70 ABPBI spun fiber is about 60% of the value predicted theoretically (9). This still approaches the value for an ideal molecular composite, although some reduction from the ideal could have resulted from PPBT rod molecules which may not have been entirely well enough oriented or dispersed. Improved processing could improve the value.

TABLE 2

Mechanical Properties of Rigid-Rod Molecular Composite Candidate Systems

Material	Epredicted GPa, (Msi)	Emeasured GPa, (Msi)	Tensile Str. GPa, (ksi)	%elong.
30 PD1AB / 70 ABPBI				
* Cast ABPBI	- -	1.0 (0.15)	0.080 (12)	-
* Cast film (C>Ccr)	- -	3.1 (0.46)	0.092 (13)	15
* Cast film (C>Ccr) + 55% Draw	- -	9.7 (1.4)	0.24 (35)	3
30 PPBT / 70 ABPBI Blend				
* PPBT fiber	615 (88)	328 (47)	3.3 (470)	1.6
* ABPBI fiber	- -	36 (5.4)	1.1 (160)	5.2
* Spun fiber (C<Ccr)	184 (26)	120 (17)	1.3 (190)	1.4
* Spun fiber (C>Ccr)	- -	11 (1.6)	0.31 (45)	13
* Extruded film (C<Ccr)	87 (12)	88 (13)	0.92 (130)	2.4
* Cast film (C>Ccr)	- -	1.1 (0.16)	0.035 (5)	5.6
30 PPBT / 70 ABPBT Blend				
* ABPBT fiber	- -	36 (5.4)	1.1 (160)	5.2
* Spun fiber (C<Ccr)	184 (26)	120 (17)	0.9 (130)	1.4
30 PPBT / 70 ABPBI Copolymer				
* Spun fiber (C<Ccr)	184 (26)	100 (15)	1.7 (250)	2.4
* Cast film (C>Ccr)	- -	2.4 (0.35)	2.2 (32)	43
30 PPBT / 70 PPQ				
* Spun fiber (C<Ccr)	184 (26)	18 (2.7)	0.35 (50)	2.4
PPBT / Nylon				
* Nylon 6	- -	0.9	0.051 (7)	5.3
* 25 / 75 Spun fiber (C<Ccr)	154 (22)	36 (5)	0.35 (50)	7.0
* 30 / 70 Spun fiber (C<Ccr)	185 (26)	31 (5)	0.35 (50)	2.4
* 50 / 50 Spun fiber (C<Ccr)	308 (43)	80 (12)	0.88 (116)	1.4
* 60 / 40 Spun fiber (C<Ccr)	370 (52)	80 (12)	0.90 (130)	1.4
30 PPBT / 70 PPOT-50				
* Spun fiber (C<Ccr)	184 (26)	140 (21)	- -	2.4
* Extruded film	87 (12)	103 (14)	1.1 (100)	1.5
5 PPTA / 95 Nylon				
* Spun fiber (C<Ccr)	11 (.012)	1.7 (0.26)	0.058 (250)	2.4

Molecular composite films of 30 PPBT / 70 ABPBI had a morphology which showed that the rod molecules were well dispersed in very small crystallites randomly oriented parallel to the surface of the film suggesting that the film was a planar isotropic molecular composite. Mechanical property modeling used an extension of "shear lag" theory for planar isotropic orientation results in a value for in-plane modulus which is 3/8 of the value for uniaxial orientation (9). In Table 2 the properties of the 30 PPBT / 70 ABPBI film give a modulus of 88 GPa and tensile strength of 0.92 GPa. The modulus exceeds the theoretically predicted value by 30%, which indicates that the film is a molecular composite, and also that improved modeling may be required to predict properties on a molecular level. The film had a modulus closer to the theoretical than the fiber, probably because random rod orientation in the film improved the their dispersion compared to the uniaxially oriented fiber.

Until recently, it has not been possible to determine the efficiency of the reinforcing phase in a molecular composite. Day et al. [10] have developed a technique using Raman spectroscopy of fibers in a stressed

macroscopic composite, from which it is possible to directly measure strain distribution along the length of the fibers. They were then able to compare the results to those predicted by "shear lag" theory and found a good correlation over a wide range of strains. Young [11] has extended the technique to molecules in a stressed 30 PPBT / 70 ABPBI molecular composite film and were able to directly measure strain in rod molecules along the macroscopic stress direction. This makes possible a comparison of macroscopic for a direct assessment of reinforcement efficiency of the rod phase.

The discussion of mechanical property modeling of molecular composites with the Halpin-Tsai equations has only dealt with the concept of requiring a high aspect ratio, eg. 100, for efficient reinforcement. However, the required value of the aspect ratio for efficient reinforcement, according to "shear lag" theory for short fiber composites, is strongly dependent on the ratio of the modulus of the fiber (Ef) to that of the matrix (Em) (7). The term "reinforcement efficiency" refers to the ratio of the stress carried by chopped fibers in a short fiber composite to the stress which could be carried by unbroken fibers in a continuous fiber composite. For example, for 90% efficiency when Ef/Em = 5 the aspect ratio must be only about 30 compared to the case where, with Ef/Em = 100, requires an aspect ratio of 400. This demonstrates that the problem of phase separation, which reduces the aspect ratio, becomes more critical when a softer polymer is chosen for the matrix material in candidate systems.

OTHER MOLECULAR COMPOSITE CANDIDATE SYSTEMS

Although the PPBT/ABPBI system formed a molecular composite, it did not have a glass transition temperature below the degradation temperature and could not be consolidated by traditional thermal processing techniques. Because of the versatility in fabrication and use of a thermoplastic polymers, new blends and copolymers have been synthesized and processed with the potential for achieving thermoplastic and thermoset rigid-rod molecular composites. A variety of polymer systems have been examined as rigid-rod molecular composite candidates. The properties of some of these systems are listed in Table 2. This section will provide brief descriptions of some aromatic heterocyclic systems and also some of the thermoplastic and thermoset systems.

The earliest systems studied were all aromatic heterocyclic polymers consisting of components of rigid-rod and semi-flexible coil molecules. As previously mentioned, the PDIAB / ABPBI blend was examined as a molecular composite and, although properties of the matrix were increased somewhat (Table 2), they did not approach the high values, expected of a molecular composite, due to phase separation [5]. The first successful system, as previously discussed, was 30 PPBT / 70 ABPBI, first processed and characterized by Hwang et al. [3] and later studied by Krause et al. [9]. Another system was the blend of PPBT and poly-2,5(6) benzthiazole (ABPBT) which achieved excellent property enhancement (Table 2) [12]. Another system, a coil / rod / coil triblock copolymer of ABPBI / PPBT / ABPBI, as synthesized by Tsai et al. [13], was processed into a molecular composite with correspondingly excellent properties (Table 2) [14]. This system demonstrated that excellent properties could be obtained over a range of rod lengths, indicating that the minimum aspect ratio had been achieved with the shortest rod components. Because these systems do not have a glass transition temperature below the degradation temperature and cannot be consolidated by thermal processing techniques they are intractable and can only be used in the form in which they have been processed. The need for improved processability could be answered with thermoplastic matrix systems.

The first efforts to develop a thermoplastic molecular composite system at the AFML were reported by Hwang et al. [15] for a nylon / PPBT blend which was also examined later by other researchers [16-18]. Table 2 shows that the properties of the neat matrix resin are enhanced, by a factor of 30 to 80, but are still only about a quarter as much as the PPBT / ABPBI systems. These lower-than-expected values are due to a number of factors including the need for a higher aspect ratio because of the higher value of Ef/Em, reduced chemical compatibility which would enhance phase separation (19), and some probable misorientation. PPBT / PPQ is another thermoplastic blend examined by the AFML was, but, here also, only limited property enhancement was achieved due to phase separation. Another system studied was a blend composed of PPBT / polyetheretherketone (PEEK), and it was found that the molecular weight of the PEEK was so low that it readily phase separated during processing. Overseas, another block copolymer of PPBT / PPO was synthesized and processed into a material which had achieved properties predicted for a molecular composite [15], but still was not thermally processable, so the search for an appropriate system continues.

Other concepts to achieve a molecular composite system have also been examined. A thermoset blend composed of PPBT and benzocyclobutane has also been examined, but large scale phase separation occurred during processing, resulting in correspondingly poor mechanical properties. Another system under study is the "in-situ" rod molecular composite, in which a rod molecule is formed by a ring-closing reaction after solution processing.

It might be noted here that numerous researchers are exploring the possibility of a producing a molecular composite with stiff and semi-flexible chain molecules as the reinforcing phase. In this sense, the term "molecular composite" really refers to a fine dispersion of molecules which may, or may not, be in an extended chain conformation. Although property enhancement of the matrix may occur, it will not be to the same extent as the rigid-rod molecules, which have intrinsically higher properties and an inherent extended chain conformation. Takayanagi [21] studied several stiff chain / flexible-coil polymer blends and observed that the finest dispersion was 15-30 nm diameter microfibrils of poly(p-phenylene terephthalamide) (PPTA) in a matrix of nylon 6 or nylon 66. He also studied a block copolymer of an aramid and nylon 6 (Table 2) and suggested that a finer dispersion was achieved but dimensions were not quantified.

PROCESSING OF MOLECULAR COMPOSITES

After synthesis, processing of the molecular composite candidate materials is the most important factor in achieving a fine dispersion of rod molecules or segments in the matrix material. Phase separation has many disadvantages for material performance, including the reduced aspect ratio of the reinforcing phase, reduced interaction and entanglement of the matrix polymer with the reinforcing phase, an increasing amount of unreinforced matrix, and development of discrete interfaces. To date, the primary technique for processing molecular composites has been dry-jet / wet-spinning of particles, fibers, or films of a dilute homogeneous acid solution into a coagulating water bath. Ideally, subsequent thermal consolidation would then be used for fabricating thermoplastic molecular composites to the desired component geometry. To achieve the desired mechanical and thermal properties of a molecular composite, large scale phase separation must not occur at any stage of processing, including solution blending, extrusion, coagulation, and solid state consolidation.

MORPHOLOGICAL CHARACTERIZATION OF MOLECULAR COMPOSITES

A thorough description of morphology is necessary for assessing, understanding, and predicting the ultimate properties of rigid-rod molecular composites. A variety of characterization techniques, including optical and electron microscopy and x-ray scattering, must be used to determine the composition, orientation, and dispersion of the reinforcing rod molecules in a molecular composite. With this information, and a knowledge of the intrinsic properties of the homopolymer components, it is possible to model mechanical properties, both to evaluate the efficiency of reinforcement of the rod molecules and also to predict the ultimate properties possible for a rigid rod molecular composite. In this section capabilities of major morphological characterization tools will be briefly reviewed and the potential for application of new characterization techniques will be discussed.

Light-optical characterization techniques, which use the visible wavelengths of light, provide information down to a scale of about 0.5 μm. The techniques include optical microscopy, light scattering, and Raman spectroscopy which have proven to be valuable tools for assessing morphology, phase behavior, and structure-property correlations. Transmission, reflection, and binocular OM has been used to assess the morphology of fibers, films, and fracture surfaces of consolidated material. Large scale phase separation (>0.5μm) is easily detected, and enhanced by color differences, in transmission OM. Ductility, or conversely, brittleness, of fracture surfaces and adhesion in consolidated molecular composites can be evaluated with reflection and binocular OM. Hot stage OM to detect phase separation as a function of temperature and composition for PPBT / ABPBI blend and copolymer systems to determine their ternary phase diagrams (3). More recently a hot stage light scattering apparatus was used to determine the kinetics of solid state phase separation of a PPBT/nylon system (19).

Electron-optical characterization techniques of transmission electron microscopy (TEM) and SEM, which use electrons accelerated from 1 to 200keV or more, have resolution which vary from about 0.2 nm to 2 μm, depending upon the operational mode. In SEM each mode is capable of analyzing a sample point-by-point as the beam scans over the surface. Fracture surfaces of films and fibers can be examined for phase separation, ductility, and orientation in molecular composite candidate systems with secondary electron imaging (SEI) (typical resolution = 5 nm) backscattered electron imaging (BEI) (resolution = 20 nm), which reveals atomic number differences. The SEM is the simplest and most versatile tool for studying morphology down to 10 nm (9,14). Recent advances in SEM equipment technology have introduced a field emission gun (FEG) SEM which is capable of operating with excellent resolution at both higher and lower voltage, (0.7 nm at 30 keV and 4 nm at 1 keV) (23). Overall resolution limits in the FEG SEM are significantly improved over those of the traditional tungsten hairpin gun SEM. They are about 1 nm in SEI, 5 nm in BEI, and 50 nm in EDS (18). The FEG SEM has excellent potential for analysis of molecular composite candidates because of the capability for direct observation of uncoated surfaces at low voltages and because of the improved resolution limits in all operating modes (24).

TEM is capable of achieving the highest resolution (0.2 nm) of any morphological characterization technique, but electron beam damage can cause significant alteration of the original structure of the sample, so skill and patience are required to obtain useful results. Additionally, TEM sample preparation techniques are difficult and may themselves induce artifacts into the original sample structure. Thus, caution must exercised in interpreting TEM results. TEM dark field (DF) imaging, using diffraction contrast, is usually used to image the size, shape, and orientation of phase separation of a crystalline component of a molecular composite candidate (9,14). Selected area electron diffraction (SAED) may be used to determine the orientation and crystal structure of crystalline regions in a sample. Phase separation of size, shape, and orientation of amorphous regions of a molecular composite candidate can be studied with TEM bright field (BF) imaging, using mass-thickness contrast (18). An important recent development in analytical electron microscopy is simultaneous parallel acquisition of electron energy loss spectra (EELS) which has the potential for acquiring entire spectra before significant beam damage (25).

WAXS provides a rapid and very useful means for assessing important morphological features, such as lattice parameters, crystallite size, and orientation, in molecular composites. One of the most valuable capabilities of WAXS is its ability to assess orientation, which has a significant effect on material properties. In rigid-rod molecular composite systems crystallite orientation of the rod-rich and the matrix-rich can be qualitatively assessed by the degree of arcing of equatorial reflections which are usually perpendicular to the machine processing direction. A more improved method of evaluating orientation is with the orientation function, which assigns a weighted numerical value to orientation (9). A recent development in this field is the use to high intensity synchrotron radiation, which will make possible real-time studies of dynamic phenomena such as phase separation kinetics.

Other morphological characterization techniques have been applied to molecular composites to a lesser extent, mainly to determine the level of phase separation. Ultrasound has been used to examine phase separation of a blend on a scale of 0.1 to 5 μm and should prove useful in examining the integrity of consolidated molecular composite systems. There are other promising techniques which need to be explored and developed, such as scanning tunneling microscopy, for improved characterization of morphological features, such as phase separated material, in rigid-rod molecular composite candidate systems.

ENGINEERING APPLICATIONS OF MOLECULAR COMPOSITES

The driving force for development of molecular composites is their excellent potential for use in structural applications. Although success has not been achieved in synthesizing and processing a "consolidatable" thermoplastic molecular composite, it would be interesting and useful to see what would be the potential for such a system. Table 3 lists, for a 30 PPBT / 70 ABPBI system, for fiber, film and bulk geometries for measured and theoretically predicted properties. "Shear-lag" theory was used to calculate theoretical properties. It will be assumed briefly, for the sake of argument, that this system can be thermally consolidated and compare the properties, for the appropriate geometry, for applications of: engineering plastics; high performance fibers; composite matrix resins; and direct substitutes for fiber reinforced composites.

Many engineering resins have similar mechanical properties including PEEK, polyamideimide (Torlon), polyetherimide (Torlon), polyimide (Avimid), polysulfone (Udel), and polyester (Xydar). The moduli are about 3.5 GPa (0.5 Msi) and tensile strengths about 0.11 GPa (15ksi). The maximum operating temperatures of the engineering resins vary from about 150 to 300°C. The bulk 30 PPBT / 70 ABPBI exceeds mechanical properties of other engineering resins by a factor of 5 to 10. Since it is expected that the Tg of a thermoplastic molecular composite would probably range from 300 to 400°C the thermal stability would probably exceed that of engineering resins by 100°C or more. There would be excellent potential for molecular composites for complex shapes in parts for underhood applications in the auto industry, where thermal properties are critical, and in the aerospace industry, where high specific properties are critical.

For high performance fibers Table 1 lists the properties of some of the commonly used materials. The fiber 30 PPBT / 70 ABPBI does not compete particularly well with the highest performance fibers, T300, Kevlar, and PBO. However, compared to E-glass the, 30 PPBT / 70 ABPBI has double the specific modulus and about the same specific strength. Thus, it appears that applications of molecular composites as high performance fibers are limited, unless properties can be increased with increased loading of the rigid-rod molecules.

Matrix resin applications for bulk 30 PPBT / 70 ABPBI can be considered for both continuous and chopped fiber macroscopic composites, with predicted properties in Table 3. It can be seen that substituting the 30 PPBT / 70 ABPBI for epoxy in a unidirectional composite would result in only small increases in properties since overall properties are chiefly controlled by the fiber component. However, in substituting the 30 PPBT / 70 ABPBI for epoxy in a planar isotropic composite would give a modest increase in modulus, but could result in up to a 3 fold

increase in tensile strength because lateral strength is strongly dependent on the matrix resin. Additionally, a major limiting factor of matrix resins is thermal stability and it may be possible to produce molecular composites with thermal stability of 100oC or so more than traditional resins.

TABLE 3

Mechanical Properties of Rigid-Rod Molecular Composites and Macroscopic Composites

Material	Modulus		Tensile Strength		%el.	Density
	Predicted GPa, (Msi)	Measured GPa, (Msi)	Predicted GPa, (ksi)	Measured GPa, (ksi)		
Molecular Composite						
30 PPBT / 70 ABPBI blend						
* Spun fiber (C<Ccr)	184 (26)	120 (17)	1.8 (260)	1.3 (190)	1.4	1.58
* Spun film (C<Ccr)	87 (12)	88 (13)	0.87 (120)	0.92 (130)	2.4	1.58
* Ideal 3-D bulk material	69 (10)	- -	0.69 (100)	- -	-	1.58
Continuous Fiber Macro-Composite						
60 graphite / 40 epoxy						
* Unidirectional	- -	132 (19)	- -	1.3 (185)	1.0	1.90
* "Planar" Isotropic (0/45/0/90)	- -	70 (10)	- -	0.17 (24)	1.0	1.90
60 graph. / 40 (30PPBT/70ABPBI)						
* Unidirectional	160 (23)	- -	1.6 (225)	- -	-	1.78
* "Planar" Isotropic (0/45/0/90)	98 (14)	- -	0.47 (64)	- -	-	1.78
Chopped Fiber Macro-Composite						
40 fiber / 60 matrix						
* Glass / Epoxy	- -	30 (4.2)	- -	0.25 (35)	-	1.90
* Glass / 30PPBT/70ABPBI	92 (12)	- -	0.41 (60)	- -	-	1.72
* Graphite / Epoxy	- -	51 (7.2)	- -	0.21 (30)	-	1.50
* Graphite / Nylon	- -	24 (3.4)	- -	0.25 (36)	-	1.33
* Graphite / PEEK	- -	23 (3.2)	- -	0.28 (39)	-	1.46
* Graphite / 30PPBT/70ABPBI	99 (14)	- -	0.36 (52)	- -	-	1.72

Substituting the 30 PPBT / 70 ABPBI bulk for epoxy in a (40 fiber / 60 matrix) chopped fiber composite would yield significant increases in modulu· by a factor of 2 to 5 in comparison with other thermoplastic and thermoset resins. Modest increases in strength of roughly 50% or so might be possible. Once again, a major advantage could be gained with the thermal stability of molecular composites.

The potential for direct substitution of 30 PPBT / 70 ABPBI material for continuous and chopped fiber composites can be considered. Substituting a 30 PPBT / 70 ABPBI fiber for a 60 graphite / 40 epoxy unidirectional composite would give similar specific properties, even though the level of loading of the molecular composite is 1/2 of that of the macroscopic composite. The 30 PPBT / 70 ABPBI film has similar specific modulus compared to that of the 60 graphite / 40 epoxy planar isotropic composite, but its specific strength is more than doubled. In comparing ideal bulk 30 PPBT / 70 ABPBI to chopped fiber composites it is seen that specific strength is 1.5 to 3 times greater and specific modulus is up to 4 times greater, even though loading is 30% in the molecular composite compared to 40% in the chopped fiber. The potential for improvements in thermal stability is good, as previously discussed. Although the potential for direct substitution of molecular composites for macroscopic composites seems excellent, a comparison of other important properties, especially compressive strength, compressive modulus, and toughness cannot be made until a thermoplastic or thermoset molecular composite system is devised.

SUMMARY AND CONCLUSIONS

The molecular composite concept has been demonstrated with morphological and mechanical property studies for aromatic heterocyclic systems, but new materials systems and processing techniques will be required to produce thermoplastic or thermoset molecular composites. Improved characterization and modeling of these systems will be required. In this regard, recent work in modeling of mechanical properties of molecular composites

has been reviewed here. The Halpin-Tsai equations from "shear-lag" theory of short fiber composites predict properties reasonably well when using the theoretical modulus of rigid-rod molecules in all aromatic heterocyclic systems. However, modeling of newer matrix systems with the "shear-lag" theory will require additional consideration of matrix stiffness, desired rod aspect ratio, and rod orientation distribution. Traditional morphological characterization techniques were discussed and new techniques were considered including: Raman light scattering for in-situ morphology property-morphology correlation, high resolution and low voltage SEM, parallel EELS for chemical analysis in TEM, synchrotron radiation in X-ray scattering for dynamic studies, and ultrasound for integrity studies in consolidated material. Excellent potential exists for use of molecular composites in structural applications including engineering plastics, composite matrix resins, and as substitutes for fiber reinforced composites. Some limitations may exist when compressive and toughness properties are evaluated, but these factors cannot be considered until a thermoplastic or thermoset molecular composite is devised.

ACKNOWLEDGEMENTS

REFERENCES

1. T.E. Helminiak, F.E. Arnold, and C.L. Benner, Am. Chem. Soc. Poly. Preprints, 16, 659 (1975).
2. T. E. Helminiak, C.L. Benner, F. Arnold, G. Husman, U.S. Pat. Appl. 902,525 (1978).
3. W-F. Hwang, D.Wiff, C.Benner, T.Helminiak, J. Macromol. Sci. Phys., B22, 231 (1983).
4. J. Wolfe, "Polybenzthiazole and Polybenzoxazole Review" in Encyclopedia of Polymer Science and Engineering, 2nd Edition, J. Wiley & Sons, New York, 1988.
5. G. Husman, T.E. Helminiak, W.W. Adams, D. Wiff, and C.L. Benner, Am. Chem. Soc. Symp. Ser., 132, 203 (1980).
6. R.M. Christensen, Mechanics of Composite Materials, Wiley, New York, 1979.
7. S. Donaldson, private communication.
8. P.J. Flory, Proc. Roy. Soc. London, A234, 73 (1956).
9. S.J. Krause, T. Haddock, G.E. Price, P.G. Lenhert, J.F. O'Brien, T.E. Helminiak, and W.W. Adams, J. Polymer Sci. - Polym. Physics Edition, 24, 1991 (1986).
10. R.J. Day, I.M. Robinson, M. Zakikhani, and R.J. Young, Polymer, 28, 1833 (1988).
11. R.J. Young, private communication.
12. W-F. Hwang, D.Wiff, C.Verschoore, G. Price, T.Helminiak, and W.W. Adams, Poly. Eng. and Sci., 23, 784 (1983).
13. T.T. Tsai, F.E. Arnold, and W.F. Hwang, Am. Chem. Soc. Poly. Preprints, 26, 144 (1985).
14. S.J. Krause, T.B. Haddock, P.G. Lenhert, W-F. Hwang, G. Price, T.E. Helminiak, J.F. O'Brien, and W.W. Adams, Polymer, 29, 1353 (1988).
15. W.F. Hwang, D.R. Wiff, T.E. Helminiak, and W.W. Adams, ACS Preprints, Org. Coat. and Plast. Chem., 48, 922 (1983).
16. S.M. Wickliffe, M.F. Malone, and R.J. Farris, J. Appl. Polym. Sci., 34, 931 (1987).
17. O. Nehme, C. Gabriel, R.J. Farris, E.L. Thomas, and M. Malone, J. Appl. Polym. Sci., 35, 1955 (1988).
18. S.J. Krause and W.W. Adams, Elect. Mic. Soc. Am. Proc., 46, 748 (1988)
19. H.C. Chauh, T. Kyu, and T.E. Helminiak, Am. Chem. Soc. Poly Eng. Sci. Proc., 59, 1106 (1988)
20. T. Nishihara, H. Mera, and K. Matsuda, Am. Chem. Soc. Poly. Eng. Sci. Proc., 55, 821 (1986).
21. H.C. Chauh, L.S. Tan, and F.E. Arnold, Poly. Eng. and Sci., 29, 107 (1989).
22. M. Takayanagi, T. Ogata, M. Morikawa, T. Kai, J. Macro. Sci. Phys., B17, 519 (1980).
23. S.J. Krause, W.W. Adams, S. Kumar, T. Reilly, and T. Suzuki Elect. Mic. Soc. Am. Proc., 45, 466 (1987).
24. S.J. Krause, W.W. Adams, and D.C. Joy, Elect. Mic. Soc. Am. Proc., 47, 336 (1989).
25. O.L. Krivanek, Elect. Mic. Soc. Am. Proc., 46, 660 (1988).

RHEOLOGY OF BLENDS OF A RODLIKE POLYMER (PBO) AND ITS FLEXIBLE CHAIN ANALOG

V. J. SULLIVAN AND G. C. BERRY
Carnegie Mellon University, Dept. of Chemistry, 4400 Fifth Avenue, Pittsburgh, PA 15213

ABSTRACT

Rheological properties of isotropic solutions of rodlike poly(p-phenylene benzbisoxazole), PBO, flexible chain poly(2,5-benzoxazole), ABPBO, and their miscible blends in solution are described. Measurements include steady state properties (the viscosity and recoverable compliance as functions of shear rate), transient properties (the recoverable compliance), and dynamic mechanical properties (the loss and storage compliances as functions of frequency). The relaxation spectrum of the blends is broader than that for the rodlike chain, and tends to occur at longer times, reflecting a viscosity enhancement that occurs with the blends. The measured zero shear viscosities for rod and blend solutions are compared with predictions based on the model of Doi and Edwards.

INTRODUCTION

Rodlike polymers containing heterocyclic aromatic groups in the main chain have shown promise as reinforcing agents in rod-flexible chain composites [1]. Above a critical composition for formation of a nematic phase, rod-coil-solvent mixtures typically exhibit a broad biphasic regime, in which the flexible chain is predicted to be essentially excluded from the nematic phase [2]. In order to maintain an intimate dispersion of the rodlike chain in the flexible chain matrix, fibers and films are processed from the isotropic phase. It is therefore important to understand the dynamics of isotropic mixtures of rods and flexible chains.

The model of Doi and Edwards for isotropic solutions of caged rods treats the rod constraint release mechanism, for movement of a rod into a new cage, as the translation of a rod along its length by a distance proportional to its contour length [3]. This treatment gives a result for the rotational diffusion of a caged rod which leads to an expression for the zero shear viscosity η_0 given by

$$\eta_0/\eta_s = KM[\eta] \, (cL/M_L)^3 \, f$$

$$f = [1 - B(c/c*)]^{-2}$$

(1)

where η_s is the solvent viscosity, c, M, L and $[\eta]$ are the rod concentration, molecular weight, length and intrinsic viscosity, respectively, $M_L = M/L$ and K and B are parameters determined by fitting the equation to experimental data. Here, f is a crowding factor accounting for the severe restriction of the rod rotation which occurs at concentrations approaching (but less than) the critical rod concentration c_R* for the formation of an ordered phase [4]. In practice, B is found to be close to unity [4]. In the following, eq. 1 will be used to predict the viscosities of both rod and blend solutions.

EXPERIMENTAL

Dry polymers were received from the Dow Chemical company. Static and dynamic light scattering and intrinsic viscosity measurements give a weight average chain length $L_w = 170$ nm for PBO, and $L_w = 320$ nm for ABPBO. Rheological experiments included steady state viscosity and recovery, transient creep and recovery and dynamic mechanical measurements. Steady state viscosity and creep and recovery measurements were carried out using either a wire suspension rheometer [5] or a gas bearing rheometer [6]. Dynamic mechanical measurements were performed using the latter.

The linear transient shear creep compliance $J(t) = \gamma(t)/\sigma$ is given by [7]

$$J(t) = R(t) + t/\eta_o \qquad (2)$$

where $\gamma(t)$ is the strain at time t after imposition of a constant stress σ, η_o is the linear steady state shear viscosity and $R(t)$, the recoverable compliance. The latter may be determined as $\gamma_r(t)/\sigma$, where $\gamma_r(t)$ is the recovered strain at time t after cessation of an imposed stress σ for a time long compared to the longest relaxation time of the sample. At long times $R(t)$ equals the linear steady state recoverable compliance R_o; $R(t)$ is often represented as a discrete spectrum of retardation times λ_i and weight factors R_i [7]:

$$R_o - R(t) = \sum_{i=1}^{N} R_i \exp\{-t/\lambda_i\} \qquad (3)$$

The dynamic storage and loss compliances, $J'(\omega)$ and $J''(\omega)$, respectively, were determined by measurement of the in-phase and out-of-phase components of the sinusoidal strain $\gamma(t)$ resulting from imposition of a sinusoidal stress. The complex viscosity $\eta_d(\omega) = [\omega J_d(\omega)]^{-1}$ and the dynamic viscosity $\eta'(\omega) = J''(\omega)/[\omega J_d(\omega)^2]$, where $J_d(\omega) = [J'(\omega)^2 + J''(\omega)^2]^{1/2}$, will be discussed below.

RESULTS

The viscosities of isotropic PBO/MSA solutions are described by eq. 1 with the $K = 8.6 \times 10^{-5}$ and $B = 0.96$. These are in accord with values obtained with other rod solutions [4]. The viscosities of solutions of PBO and ABPBO are plotted against cL_w in Fig. 1. The enhancement of η_o on addition of flexible chain to rod solutions is also shown in Fig. 1, where the viscosities for blend systems are plotted against total polymer concentration times the rod length. In Fig. 1 and in the following, the rod concentration in a rod or blend system is denoted c_R.

Data on $J'(\omega)$ and $J''(\omega)$ for two blend compositions are shown in Fig. 2, along with data on $J(t)$ and $R(t)$ for these systems. As has been reported elsewhere [4,8,9], rheological functions for solutions of rod, flexible chain and blend systems can be reduced using the parameter $\tau_c = \eta_o R_o$. For example, $R(t)$ is plotted as $R(t)/R_o$ versus t/τ_c in Fig. 2 for different rod concentrations. For both rod and blend systems, the steady state viscosities η_κ, at shear rate κ, is about equal to $\eta'(\omega)$ for $\kappa = \omega$, as expressed by the Cox-Merz relation [7]; $\eta_d(\omega)$ tended to be larger than η_κ for the larger ω. In addition, over the range in the time scale for which both dynamic and transient data are available, the Markovitz-Riande relation [7]
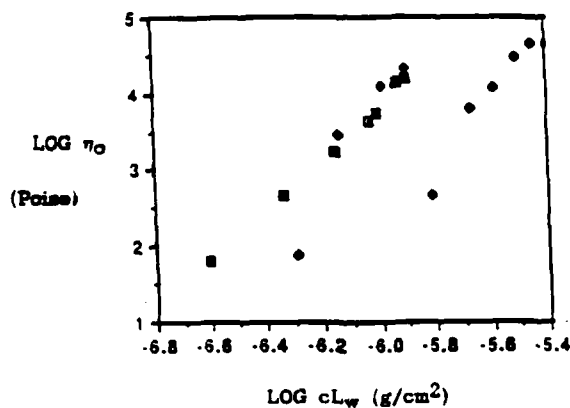
FIGURE 1: Zero shear viscosities of rod (■) and flexible chain (●) solutions as a function of cL (see equation 1). For comparison with rod viscosities, blend viscosities are plotted versus the product of total polymer concentration and rod length. The symbol ● denotes blends in which various amounts of flexible chain were added to rod solutions at $c_R = 0.028$ g/ml; ■ denotes blends with $c_R = 0.043$ g/ml.
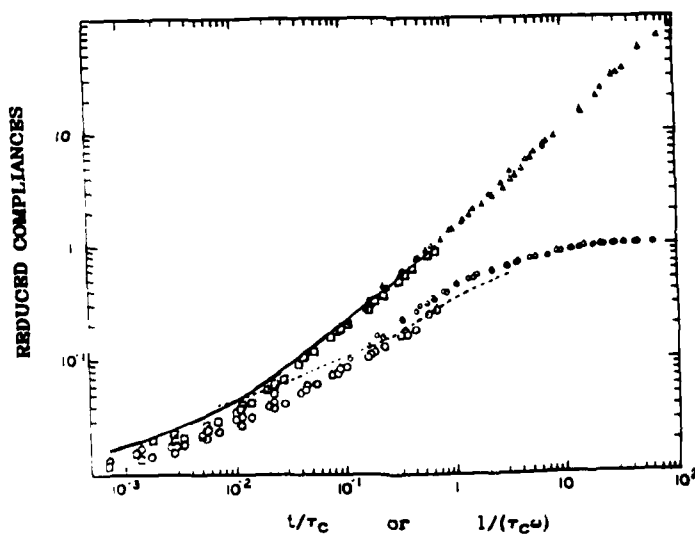
FIGURE 2: Dynamic and transient rheological functions for two blend compositions: $c_R = 0.043$ g/ml, $c_F = 0.031$ g/ml (with pips) and $c_R = 0.043$ g/ml, $c_F = 0.015$ g/ml (without pips). Symbols denote the following functions: $J'(\omega)/R_0$ ○ , $J''(\omega)/R_0$ □ , $R(t)/R_0$ ● , $J(t)/R_0$ · · . The solid line gives $J_d(\omega)/R_0$ for the blends; the dotted lines is $J'(\omega)/R_0$ for a rod solution at $c_R = 0.043$ g/ml.

$$J(t) \approx J_d(\omega) \qquad \text{at } \omega^{-1} = t \qquad\qquad (4)$$

is a reasonable approximation for these systems. The addition of the flexible chain to rod solutions broadens the relaxation spectrum, as can be seen by the change in the shapes of rheological functions in the short time regime (see Fig. 2).

DISCUSSION

The nonlinear viscoelastic behavior exhibited by the materials examined in the present study is described by a factorized form of the BKZ constitutive equation [10]:

$$\sigma(t) = \int_{-\infty}^{t} K^*[(t - s); \gamma(t) - \gamma(s)] \, [\gamma(t) - \gamma(s)] \, ds \qquad (5)$$

where $\gamma(t,s) = \gamma(t) - \gamma(s)$. A form for K^* which has proved successful for both isotropic rodlike and flexible chain polymer solutions is [4,8]

$$K^*((t - s); \gamma(t,s)) = -f(\gamma(t,s)) \, \frac{\partial G(t - s)}{\partial(t - s)}$$

where

$$f(\gamma(t,s)) = \exp\left[-m \, \frac{|\gamma(t,s)| - \gamma'}{\gamma''} \right] \qquad (6)$$

$$m = 0 \quad \text{for } |\gamma(t,s)| < \gamma'$$
$$m = 1 \quad \text{for } |\gamma(t,s)| \geq \gamma'$$

Here, $G(t)$ is the linear shear relaxation modulus. The latter may usually be represented as a discrete relaxation spectra. An experimental procedure to determine γ' and γ'' is described in reference 8. This model, previously successfully applied to the blend system PBT/nylon/MSA [9], provides good fits to the nonlinear behavior of the PBO/ABPBO/MSA blend and the PBO/MSA systems. The narrow range of relaxation times available for the ABPBO/MSA system prohibited adequate representation of its nonlinear behavior.

A phase diagram for the room temperature phase behavior of the PBO/ABPBO/MSA system is shown in Fig. 3. As can be seen in Fig. 3, the addition of flexible chain causes a drop in the critical rod concentration required for the onset of the ordered phase. For a given rod system, eq. 1 indicates that the critical rod concentration c_R^* affects the zero shear viscosity through the crowding factor f. For blends in which the relaxation mechanism of longest time scale is rod rotation, i.e. $\tau_F < \tau_{R\perp}$, where τ_F is the time scale for flexible chain disengagment and $\tau_{R\perp}$ is the time scale for rod rotational diffusion, we may consider the rod rotational diffusion to be the sole determinant of $\eta_{0,s}$, the blend zero shear viscosity. In this case, $\eta_{0,s}$ is given by eq. 1, with c_R^* replaced by $\hat{c}_R$, the critical rod concentration for formation of an ordered phase in the blend. The ratio of $\eta_{0,s}$ and η_0 for a given rod concentration is then given by

$$\frac{\eta_{0,s}}{\eta_0} = \left[\frac{1 - B(c_R/c_R^*)}{1 - B'(c_R/\hat{c}_R)} \right]^2 \qquad (7)$$
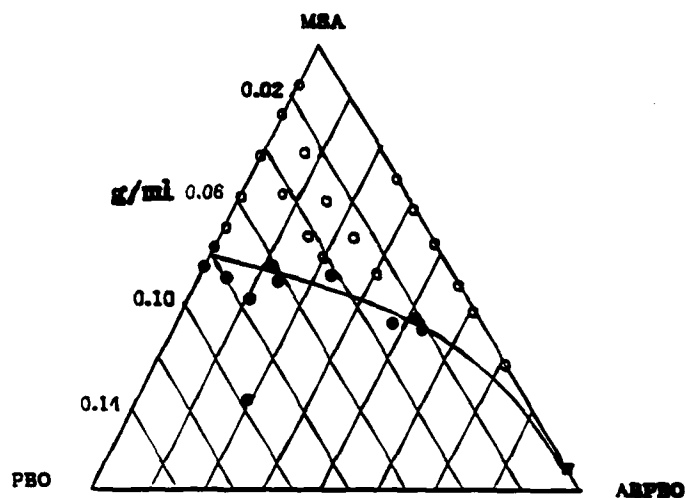
FIGURE 3: Phase diagram, at T = 25 °C, for PBO/ABPBO/MSA: Open circles denote the isotropic phase; filled circles denote the ordered phase; the coexistence line shown represents the prediction of the Flory model [2].
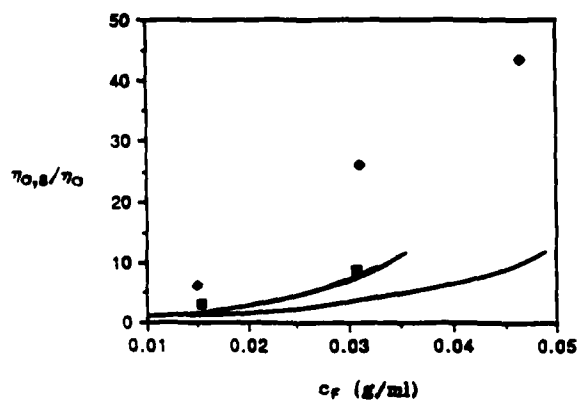
FIGURE 4: Ratios of blend to rod viscosities as a function of flexible chain concentration c_F. Points denote experimentally determined values, with symbols denoting blend compositions as in FIGURE 1. Lines denote viscosity ratios calculated by equation 7, as described in text. Upper line; blends with $c_R = 0.043$ g/ml. Lower line; blends with $c_R = 0.028$ g/ml.

For the blends $\hat{c}_R$ will be estimated from the phase diagram shown in Fig. 3. A line from the solvent (MSA) apex through a given point represents all compositions with rod to flexible chain ratios equal to that of the blend represented by that point; $\hat{c}_R$ is estimated as the rod concentration for the point at which this line intersects the isotropic-nematic coexistence line. With $\hat{c}_R$ values obtained in this way from Fig. 3, and assuming $B' = B$, eq. 7 can be used to calculate $\eta_{O,s}/\eta_O$. Calculated $\eta_{O,s}/\eta_O$ values, along with experimentally determined values, are presented in Fig. 4.

For the two blends at the higher rod concentration ($c_R = 0.043$ g/ml), the calculated viscosity ratios are close to the measured values. For blends with $c_R = 0.028$ g/ml, the calculated viscosity ratios are substantially lower than the measured values. Thus the above calculation underestimates the extent of viscosity enhancement that occurs upon adding flexible chain to rods at this concentration. This discrepancy may result from neglect of the possibility of a contribution to the blend viscosity involving the disengagement time of the flexible chain. This possibility must be considered for the present system, since the pure component viscosities are comparable (see Fig. 1). Indeed the broadening of the relaxation spectrum upon addition of flexible chain (Fig. 2) suggests significant contributions from relaxation mechanisms involving the flexible chain. In this case, the relation $\tau_F < \tau_{R\perp}$ cited above as a neccessary condition for the use of eq. 7, would no longer be valid, and should be replaced by $\tau_F \approx \tau_{R\perp}$. Models which predict the viscosity of rod-coil blends in the latter regime are not yet available.

REFERENCES

1) S. J. Krause, T. Haddock, G. E. Price, P. G. Lenhert, J. F. O'Brien, T. E. Helminiak and W. W. Adams, Polym. Sci.: Part B: Polym. Phys., 24, 1991 (1986)

2) P. J. Flory, Macromol., 11, 1138 (1979)

3) M. Doi and S. F. Edwards, The Theory of Polymer Dynamics (Clarendon Press, Oxford, 1986)

4) S. Venkatramen, G. C. Berry and Y. Einaga, J. Polym. Sci.: Polym. Phys. Ed., 23 , 1275 (1985)

5) G. C. Berry and C.-P. Wong, J. Polym. Sci.: Polym. Phys. Ed., 13, 1761 (1975)

6) G. C. Berry, J. O. Park, D. W. Meitz, M. H. Birnboim and D. J. Plazek, J. Polym. Sci.: Part B: Polym. Phys., 27, 273 (1989)

7) G. C. Berry and D. J. Plazek, in Glass: Science and Technology, Vol. 3, Ed. by D. R. Uhlmann and N. J. Kreidl (Academic Press, New York, 1986), Chapter 6

8) K. Nakamura, C.-P. Wong and G. C. Berry, J. Polym. Sci. Polym. Phys., 22, 1119 (1984)

9) C. S. Kim, Ph.D. Thesis, Carnegie Mellon University, Pittsburgh, PA (1988)

10) B. Bernstein, E. A. Kearsley and L. J. Zapas, Trans. Soc. Rheol., 1, 391 (1963)

PBZT MICROCOMPOSITES WITH ADVANCED THERMOPLASTIC MATRICES

W. MICHAEL SANFORD AND GERARD M. PRILUTSKI
E. I. du Pont de Nemours and Co., Inc., Experimental Station, P.O. Box 80302,
Wilmington, Delaware   19880-0302

Thermoplastic microcomposites offer the potential for better economics and improvements in composite processing, and possibly performance, over conventional "string-and-glue" composites. The early development of molecular composite technology focused on polyamide matrix polymers; however, for many aerospace applications higher use temperatures and greater solvent resistance than that of conventional polyamide matrices will be required. This paper describes work performed under contract to the U.S. Air Force to develop PBZT (poly p-phenylene benzobisthiazole)/thermoplastic molecular composites with high performance matrix resins into a viable technology.

A scaleable process has been defined based on a novel technology developed by Du Pont. Advantages of this process include better economics, superior processing performance, and improved MC fiber tensile properties versus prior art. Using this process we have obtained rule-of-mixtures properties in our microcomposite fibers with matrix polymers offering use temperatures from 330 to 600°F. Consolidation of PBZT/PEKK fibrous preforms into uniaxial panels up to 10" x 15" has been demonstrated and material property evaluation and data base development are in progress. Uniaxial property levels achieved to date for all systems compare favorably with conventional "string-and-glue" PBZT/epoxy composites although as with other organic fiber reinforcements, compressive and shear performance may be limiting factors in MC applications.

INTRODUCTION

Conceptually, molecular composites are dispersions on a molecular scale of rigid rod polymer molecules in a matrix of flexible coil polymers, formed by the coagulation of a dilute isotropic solution containing these components [1-3]. In the original concept, phase segregation of the rod and coil polymers into separate phases was to be avoided, because the rigid rod molecules tended to aggregate to form domains with low aspect ratios ("footballs") which led to ineffective reinforcement and hence low mechanical properties [2]. To avoid phase segregation, very low concentrations (below the critical concentration of 3.5%) were generally used. We have found, however, that under certain conditions, and using higher, more practical, solution concentrations, the rigid rod polymer aggregates to form a fibrillar microscopic rather than molecular dispersion (rod domains of 1,000-10,000 vs. <30 angstroms), with high aspect ratio rigid rod domains. These "microcomposites", (MC's), exhibit higher tensile properties in fiber preforms than molecular composites [4]. These thermoplastic microcomposites offer the potential for better economics (no resin impregnation step) and performance over conventional "string-and-glue" composites.

MATRIX SELECTION CRITERIA

There are several important requirements for the matrix resins to be used in PBZT-based molecular or microcomposites. Particularly, the matrix must be soluble and stable in the strong acid solvents (e.g., methanesulfonic, polyphosphoric) required for processing rigid rod polymers. Additionally, the polymer must be sufficiently thermally and thermo-oxidatively stable to permit heat treatment at elevated temperatures. Lastly, the matrix must be capable of forming a stiff, strong molecular composite preform which can be

consolidated by heat and pressure. Additionally, for the "new thermoplastic" matrix resin, we sought to identify polymers which offered advantages over the polyamides used in earlier studies of molecular composites, primarily higher Tg and improved solvent resistance. Goal levels for the use temperature of the matrix were set at 250, 350, 450 and 600°F (121, 177, 232 and 315°C). On the basis of processibility and potential use temperature, three polymers were selected for in-depth study in this program, PEKK, and the polyimides used in Du Pont's Avimid* K and N reinforced resin composite structures (referred to as "K-polymer" and "N-polymer" respectively). The work described in this paper focuses on these three matrix systems.

MICROCOMPOSITE PREPARATION

Microcomposite preforms (e.g., fiber, film) are prepared via a process similar to that described for forming molecular composite preforms [2,3]. First, a solution consisting of both rigid rod and flexible coil polymers in an appropriate solvent is prepared and intimately mixed to effect dispersion. After deaeration, the solution is then extruded to produce the desired preform, which in this work has primarily been in the form of continuous fibers. The preforms are produced via air gap spinning, with orientation imparted to the rigid rod component (PBZT) through shear in the capillary and spin draw in the air gap. After spinning and solvent extraction, the fibrous microcomposite preforms are heat treated under tension to increase orientation, thereby enhancing tensile strength and modulus.

The microcomposite fibrous preforms are converted into three dimensional structures via a two-step process. First, the preform is wrapped around a flat plate and pressed to form a coherent sheet with the fiber axes aligned unidirectionally, analogous to a conventional composite prepreg. Secondly, the sheet is cut into plies of the desired size which can be stacked to form a laminate which is then consolidated via application of heat and pressure.

PBZT/PEKK MC's

PEKK (poly(etherketoneketone)) is a semi-crystalline thermoplastic resin offering intermediate use-temperature performance comparable to 3501-6 epoxy or PEEK (poly(etheretherketone)) resins. It has a glass transition temperature of 156°C and offers excellent resistance to organic solvents [5,6]. Based on these properties as well as its excellent solubility and stability in the strong acid solvents required to process PBZT, PEKK was selected as a matrix for microcomposites evaluation.

Acid solutions of PBZT/PEKK (60/40 v/v rod/coil ratio) were air-gap spun on a capillary rheometer over a range of conditions with excellent continuity (no filament breaks) to form 10 filament fibrous microcomposite precursor yarns (nominal denier 45). High spin stretch was achieved, which resulted in a high degree of orientation of the rigid rod molecules in the as-spun fibers, as evidenced by average orientation angles for the PBZT of 12-17 degrees measured by X-ray diffraction. The apparent crystal size was typically in the range 20-25 angstroms. As-spun tensile strengths were in the range of 100-200 ksi, with elongations to break in the range 1-2.5% and moduli of 9-14 Msi. Tension heat treatment of the as-spun yarns increased the degree of orientation, resulting in average orientation angles of 5-7 degrees and apparent crystal sizes of 50-56 angstroms. Typical tensile properties of the heat treated PBZT/PEKK microcomposite fibrous preforms were 200-310 ksi strength, 19-25 Msi modulus and 0.5-1.2% elongation to break, (single filament breaks), with heat treated property levels varying with the as-spun fiber properties and the temperature and tension used in heat treatment. If these properties are normalized to account for the fraction of PBZT

----

* Du Pont Registered Trademark.

(60% by volume), a strength and modulus of 500 ksi/38 Msi are obtained for
the PBZT reinforcement. These property levels are typical of neat PBZT fi-
bers [7], indicating that "rule-of-mixtures" properties have been obtained
in the microcomposite fibrous preforms.

PBZT/PEKK fibrous preforms were molded into 6" x 1/2" unibars by the
two-step process described above. These bars had theoretical densities and
good C-scans (loss <2 dB at 5 MHz) indicating good consolidation. The mech-
anical properties of PBZT/PEKK (60/40 v/v) unibars are summarized in Table I.
The specific mechanical properties are compared to several other composite
materials in Figures 1-2. The tensile properties and flex and compressive
moduli are comparable to those obtained for conventional composites reinforced
with PBZT or a mid-range carbon fiber such as T300. In Figure 2, the specific
tensile strength reported for the PBZT/PEKK MC bar is somewhat lower than for
the PBZT/epoxy conventional composite; however if full translation of the MC
yarn strength to the bar can be achieved, the tensile strength of the PBZT/
PEKK should be approximately that of the PBZT/epoxy. The lower density of
the microcomposite versus carbon reinforced composites leads to an advantage
in specific tensile properties. Preliminary tensile tests of 9" microcompos-
ite specimens have yielded somewhat higher moduli, up to 24 Msi. Based on
these high moduli, the microcomposites would be suitable for stiffness-critical
applications.

TABLE I: **Mechanical Properties of PBZT/PEKK (60/40) Unibars**

	Tensile	Flex	Compressive	Short-Beam Shear
Strength (ksi)	175	80	32	4.8
Modulus (Msi)	19	20	20	---

The flex and compressive strengths compare poorly with carbon fiber
reinforced materials. The properties are typical of organic fiber reinforced
composites and reflect the poor compressive strength of PBZT. This deficiency
in compressive and flexural strength will limit the utility of rigid rod MC's
for primary structural applications. Note that no significant advantage is
found for microcomposites versus conventional composites in mechanical prop-
erties, including compressive strength, based on our results to date.
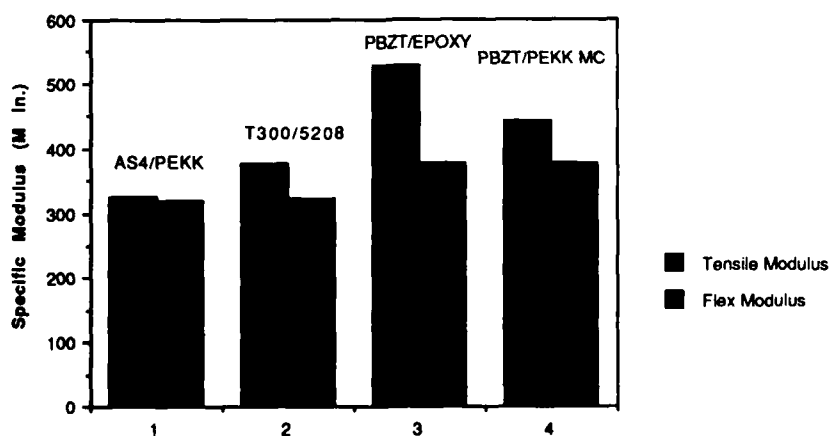
FIGURE 1: Specific moduli of PBZT/PEKK MC compared to conventional composites
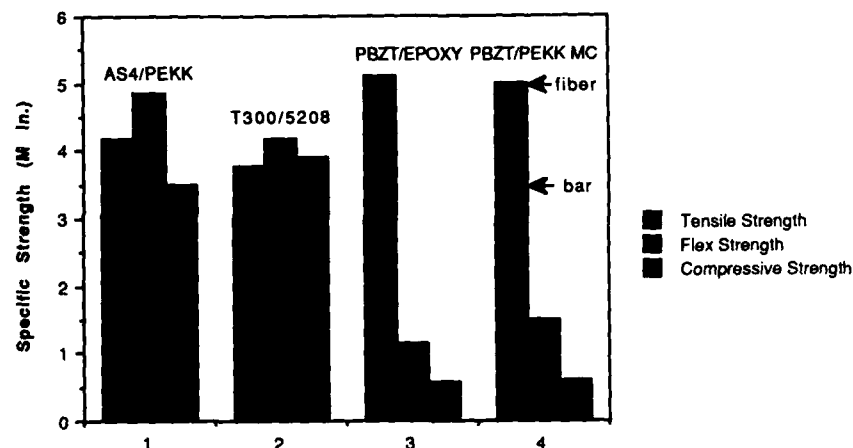
FIGURE 2: Specific strengths of PBZT/PEKK MC compared to conventional composites

    In addition to molding 6" x 1/2" unibars, several 6" x 3" panels were
also consolidated. These panels had theoretical densities and good C-scan
quality, similar to that of the smaller unibars. Tensile and flexural test
coupons cut from these panels had mechanical properties typical of the indi-
vidually molded unibars. Panels up to 10" x 15" x 0.100" in size with theo-
retical densities and acceptable C-scans have been produced and shipped to
Boeing Advanced Systems Co. for evaluation.

PBZT/PI MC's

    K-polymer is the matrix resin used in Du Pont's composites of Avimid® K.
This amorphous polyimide has a glass transition temperature of 250°C, good
thermo-oxidative stability and excellent resistance to organic solvents. N-
polymer is the polyimide matrix resin used in Du Pont's composites of Avimid®
N. This non-crystalline polymer has a glass transition temperature of 340-
370°C, excellent thermo-oxidative stability and good resistance to organic
solvents. Because of their high Tg's and stability, both K and N polymers
are of interest in high temperature applications.
    Acid solutions of K polymer and PBZT were mixed and spun similarly to
the PBZT/PEKK microcomposite solutions to form 10-filament yarns of the fi-
brous microcomposite precursor. The PBZT/K yarn, however, did not sustain as
much spin stretch as the PBZT/PEKK. The effect of this lower attenuation was
evident in the as-spun orientation angles of 25 to 32 degrees for PBZT/K as
compared to the 12-17 degree orientation angles obtained for as-spun PBZT/
PEKK. Tensile properties of the as-spun PBZT/K yarns were in the range 100-
163 ksi strength, 2.5-7% elongation to break, 4-8 Msi modulus. Tension heat
treatment of the PBZT/K yarns decreased the orientation angle to 8-12 degrees.
The tensile properties of heat treated PBZT/K microcomposite preform yarns were
increased to 250 ksi/25 Msi strength and modulus, which represent approximately
"rule-of-mixtures" properties and are comparable to carbon fiber reinforced
composite tensile properties.
    Heat treated PBZT/K yarns were consolidated into 6" x 1/2" unibars by
the same process used for PBZT/PEKK. The as-molded bars had good C-scans
(6 dB loss at 5 MHz) and near theoretical densities. Tensile strength and
moduli of the bars averaged 70 ksi and 15 Msi, respectively. The low strength
is believed to be the result of tab failure rather than true tensile breaks.

Flex strength and modulus of the PBZT/K bars averaged 58 ksi and 15 Msi, which are comparable to the values reported for PBZT/epoxy conventional composites [8]. Similarly to the PBZT/PEKK values, the low flexural strength of the PBZT/K microcomposite is attributed to the low compressive strength of the PBZT reinforcement. The average short beam shear strength measured for the PBZT/K unibars was only 2.5 ksi, approximately half that of the PBZT/PEKK microcomposite and a PBZT/epoxy conventional composite. This indicates that even though the PBZT/K microcomposite consolidated well, there is relatively poor adhesion within the laminate.

An acid solution of PBZT/N (60/40 v/v) was spun in a similar manner to the PBZT/K. High spin stretch and moderate orientation (25 degrees) were obtained in the as-spun fibrous preform which had tensile properties of 200 ksi strength and 9.4 Msi modulus. Tension heat treatment decreased the average orientation angle to 6.5 degrees with a corresponding increase in tensile strength and modulus to 280-400 ksi and 23.8-29.5 Msi, respectively, depending on the heat treatment conditions. An initial attempt at consolidating the PBZT/N yarns was only marginally successful; however, this experiment was performed at relatively low pressures and further experimentation is expected to lead to improved adhesion. Based on the temperature capabilities of PBZT/N polymer microcomposites and the excellent tensile properties obtained, this material appears quite promising if good consolidation can be obtained.

SUMMARY

PBZT-based microcomposites with advanced thermoplastic matrices have been investigated. A scaleable spinning process has been developed to produce high yields of PBZT/PEKK microcomposite preform yarns having "rule-of-mixtures" tensile properties. PBZT/PEKK microcomposite unibars have moduli comparable to T300 or AS-4 carbon fiber reinforced composites and may be suitable for stiffness-critical applications. Microcomposite fibrous preforms of PBZT/K have been produced with high tensile properties and compression molded to form well-consolidated unibars. PBZT/N microcomposite fibrous preforms have outstanding tensile properties and may be suitable for applications at temperatures >650°F, although consolidation of these preforms has yet to be demonstrated. Further effort will be aimed at developing these polyimide matrix microcomposites. Preliminary data indicates that microcomposites offer no distinct differences in static mechanical properties vs. conventional composites with the same constituents. Structural applications for rigid rod microcomposites are likely to be limited by the poor compressive strengths, which are typical of organic polymer reinforced composites.

ACKNOWLEDGMENTS

REFERENCES

1. Thaddeus E. Helminiak et al., U.S. Patent No. 4,207,407 (1980).

2. W.-F. Hwang, D.R. Wiff, C.L. Benner, T.E. Helminiak, J. Macromol. Sci. Phys., B22 (2) 231-257 (1983).

3. W.-F. Hwang, D.R. Wiff, C. Verschoore, G.E. Price, T.E. Helminiak, W.W. Adams, Polym. Eng. Sci., 23 (14) 784-788 (1983).

4. W.C. Uy, G.M. Prilutski, W.M. Sanford, WRDC-TR-89-4040 (1989).

PBZT/POLYAMIDE THERMOPLASTIC MICRO-COMPOSITES -
AN OUTGROWTH OF MOLECULAR COMPOSITES DEVELOPMENT

WILLIAM C. UY AND E. R. PERUSICH
E. I. du Pont de Nemours & Co., Inc., Experimental Station, P. O. Box 80302,
Wilmington, DE 19880-0302

ABSTRACT

Molecular composites are dispersions of rigid-rod polymer molecules in a matrix of flexible coil polymers, formed by the coagulation of a solution containing these components. Where there is aggregation of the rigid-rod molecules, such composites are called micro-composites (MC's). These composites offer the potential for better economics and improvements in composite processing, and possibly performance, over conventional "string and glue" composites. This paper describes work performed under contract to the U. S. Air Force to develop PBZT/thermoplastic molecular composites into a viable technology.

A commercially viable MC spinning and heat-treatment process has been defined based on a novel mixed solvent/quaternary solution technology developed by Du Pont. Advantages of this process include better economics, superior processing performance, and improved MC fiber tensile properties versus prior art. PBZT/polyamide MC fibers with strength/modulus of 332 ksi/29 Msi have been produced using this process. Adhesion equivalent to that obtained in conventional composites has been demonstrated. Uni-axial properties achieved to date compare favorably with conventional "string and glue" PBZT/epoxy composites although compressive and shear strengths may be limiting factors in MC applications.

INTRODUCTION

This work was carried out at the Advanced Structural Materials Technology Center of the Fibers Department of E. I. du Pont de Nemours & Co., Inc.

This presentation is on the development of general process technology for PBZ-based molecular composites and, in particular, of PBZT-based products in thermoplastic polyamide matrix system.

Du Pont involvement with PBZ* technology, the Air Force Materials Laboratory and SRI International dates back to 1981, when research focused on the neat PBZT polymer in developing spinning and heat-treatment processes for this true rigid-rod polymer from its unusually viscous as-polymerized polyphosphoric acid solution [1]. In the following year the process was refined and scaled-up [2]. In 1985 and 1987, we expanded the experimental production of PBZT fiber for the Air Force and converted a total of 160 lbs. of the polymer to heat-treated fiber in continuous 290-filament yarn. As-spun PBZT fiber has a purplish brown color while optimally heat-treated fiber has a shiny, metallic blue color. The average tensile strength and modulus values of these production yarns exceed 400 ksi/40 Msi while values as high as 614 ksi/49 Msi (Table I) have been obtained for lab-scale produced fibers.

PBZ polymers in general have outstanding thermal, oxidative, and hydrolytic stability [2]. Trans-PBZT and cis-PBO, in particular, are the most important and true rigid-rod PBZ polymers [3,4]. Therefore, they are ideal as reinforcing components in molecular composites.

---

* PBZ is the generic terminology used to refer to the class of rigid-rod heterocyclic polymers, which have been under development with support of the Air Force Materials Laboratory.

The specific mechanical properties (Fig. 1) of various high performance fibers and metals are compared in this chart. PBZT, because of its unique properties, occupies an area to itself.

MOLECULAR AND MICRO-COMPOSITES

Dr. T. Helminiak (U. S. Air Force Wright Research & Development Center) pioneered the concept of molecular composites (MC's) as early as 1978. A patent [4] was issued to him and his colleages wherein the matrix is not a thermoplastic. Their patent reads "Rod-like aromatic heterocyclic polymers are used as a reinforcement in coil-like heterocyclic polymer matrices to provide composites at the molecular level that are analogous to chopped fiber composites." In the strictest sense, in a true molecular composite the reinforcing component would be dispersed on a molecular scale without aggregation. However, theoretical and experimental considerations have shown that true molecular dispersion is attainable only at a few percent of rod content [5,6]. In practical applications, where the rod content would more likely be more than a few percent (e.g., for normal composite application, rod content is usually 60 volume %), aggregation is unavoidable. The scale of aggregation can range from a state where it is not visible even at very high TEM magnification to a state where there are clearly two phases. If the dispersion of the rigid-rod molecules is not on a molecular level but rather on a sub-micron scale, we call such composites micro-composites (MC's). Therefore, realistically, this discussion will be on micro-composites rather than molecular composites.

Why MC's? Potential advantages of MC's over conventional "string-and-glue" composites are better economics and potential superior performance. Better economics, because with MC's, the pre-pregging step is not necessary since the matrix is already built-in. Superior performance, because there is no macroscopic interface between the reinforcing and matrix components in MC's. The interface is on a sub-micron level and, therefore, the very high interfacial area can reduce stress concentration. The chart compares the relative sizes of the reinforcing component for conventional and micro-composites with two degrees of dispersion.

The general objective of our current research is to develop thermoplastic molecular composites based on PBZT into an industrially viable technology by developing process techniques to produce and fabricate bulk material forms. The program elements are essentially the same for the thermoplastic polyamide and "new" thermoplastic matrix system with one exception, i.e., research on basic processing technology and design/fabrication of equipment applicable for both polyamide and new systems. This presentation addresses primarily the polyamide system.

Thermoplastic Polyamide System

Six thermoplastic polyamide resins (Table II) were chosen and evaluated for the effects of crystallinity versus amorphous character and glass transition temperature. Four criteria (Table III) were used in screening the matrix candidates: Stability in strong acid solvents, physical and chemical compatibility, MC fiber properties and uni-directional bar properties.

Good compatibility between PBZT and the matrix resin (Table IV) was found to be important in achieving good properties. Compatibility was determined from calculated solubility parameters [7] and interfacial bond adhesion [8]. As-spun fibers were heat-treated to develop full property potential and properties were found to improve with increasing compatibility.

The solutions from which MC fibers are spun from can be isotropic or anisotropic depending on the solution concentration [5] (Fig. 2). When the solution is isotropic, viscosity increases with concentration in the normal man-

TABLE I.
HETEROCYCLIC RIGID-ROD POLYMERS

* WHY PBZ? - OUTSTANDING THERMAL, OXIDATIVE, &
  HYDROLYTIC STABILITY

* MOST IMPORTANT HETEROCYCLIC RIGID-ROD POLYMERS

  POLY P PHENYLENE BENZOBISTHIAZOLE (PBZT)
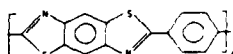
  POLY P PHENYLENE BENZOBISOXAZOLE (PBO)
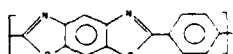
* HIGH MW PBZ POLYMER/PROCESS (J WOLFE OF SRI
  INTERNATIONAL) DEVELOPED UNDER AIR FORCE ORDERED
  POLYMER PROGRAM

* DU PONT DEVELOPED THE PROCESS TECHNOLOGY
  FOLLOWED BY FIRST SCALE-UP "PRODUCTIONS" OF 1,000
  DENIER/290-FILAMENT YARN FOR THE AIR FORCE

  * OTHER EARLY CONTRIBUTORS CELANESE, U OF
    MASS, CARNEGIE MELLON INSTITUTE
  * TEN/SE/MOD = 18-30 GPD/13.7 1%/135-2,400
    GPD

FIG. 1 SPECIFIC MECHANICAL PROPERTIES OF
REINFORCING FIBER COMPOSITES AND METALS
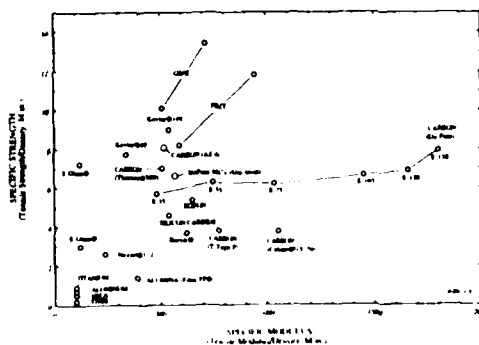
TABLE II. THERMOPLASTIC
POLYAMIDE (TPA) MATRIX RESINS

RESIN	TYPE	DRY Tg	Tm	INH-VIS*	DENSITY
TPA A	Amorphous	130°C		1.33	1.19
TPA B	Amorphous	132		1.87	1.19
TPA C	Amorphous	160		1.18	1.15
TPA D	Amorphous	195			1.07
TPA E	Crystalline	90	265	1.10	1.14
TPA F	Crystalline	145	285	1.70	1.4

* Inherent viscosity measured in methane sulfonic acid (MSA) solvent at 0.5 g/dl

TABLE III. MATRIX SELECTION CRITERIA

* STABLE IN STRONG ACID SOLVENTS

* PHYSICAL/CHEMICAL COMPATIBILITY

  MC FIBER QUALITY (SURFACE VOIDS, PHASE SEPARATION)

  SOLUBILITY PARAMETER

  INTERFACIAL BOND STRENGTH BETWEEN PBZT AND MATRIX

* MC FIBER PROPERTIES

  TENSILE PROPERTIES

  ORIENTATION

  DENSITY

* UNI-DIRECTIONAL BAR PROPERTIES

  FLEX STRENGTH/MODULUS

  SHORT BEAM SHEAR STRENGTH

TABLE IV. PBZT/MATRIX COMPATIBILITY
AND MC PROPERTIES
(PBZT TPA,60-40v)

MATRIX	TPA-B	TPA-C	TPA-D
SOLUBILITY PARAMETER (PBZT=28.3)	21.4	18.3	14.9
INTERFACIAL BOND ADHESION (PSI)	1,260	1,260	470

TENSILE PROPERTIES OF HEAT TREATED MC FIBERS

T M (ksi/Msi)	112/28.8	230-23.8	212/19.4
gpd	19.4/1,600	12.4/1.36	12.4/1.33
DENSITY	1.408	1.384	1.318
OA	**	8°	9.8°

CONCLUSION:

* GOOD COMPATIBILITY BETWEEN PBZT AND MATRIX RESIN
  IS IMPORTANT IN ACHIEVING BEST PROPERTIES
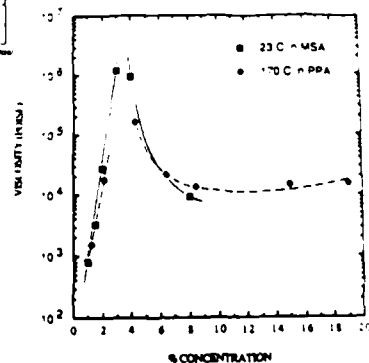
CONCLUSIONS:
- CRITICAL CONCENTRATION (Ccr) IS AT ~3.5% AND INDEPENDENT
  OF SOLVENT TYPE
- Ccr FOR QUATERNARY/ADDED SOLVENT SOLUTIONS IS ALSO
  BETWEEN 3% AND 4% TOTAL POLYMER CONCENTRATION

FIG. 2 PBZT SOLUTION VISCOSITY
IN PPA AND MSA SOLVENTS

ner. Since PBZT is a liquid crystalline material, the increase in solution viscosity will reverse when it reaches the critical concentration of about 3.5% and the solution becomes biphasic. The viscosity drops as sharply as the increase in the isotropic phase and then levels off at higher concentraiton.

State-of-the-art MC fibers (Table V) with tensile properties as good as uni-axial conventional carbon/epoxy composites were obtained from below critical concentration using a Du Pont patented process technology [9]. Further improvement in properties was achieved from higher concentration anisotropic solutions also using the same Du Pont technology. The high measured strength/modulus of 332 ksi/29 Msi (18.4/1,600 gpd) for the MC back calculated to 553 ksi/48 Msi (27.0/2,320 gpd) for neat PBZT indicates that rule-of-mixture has been achieved and, therefore, that we have a technologically sound process. Because of many technical problems in making MC's in prior art ternary technology [10, 11], Du Pont developed a proprietary mixed solvent/quaternary process which not only eliminated these problems but also gained several process advantages, such as flexibility in accepting different matrix resins. Comparison between this novel process versus prior art is shown in Table VI. The quaternary process for MC fiber properties made from below the critical concentration is between 1.5 to 2.5x higher than that from ternary. Above the critical concentration, the quaternary process is 48 to 55x higher than ternary.

Consolidated Products

Except in applications such as ropes or soft armors, most high tech applications require the high performance fibers to be converted into composites, which are typically articles composed of the fibers glued together with a matrix resin at a typical 60/40 volume ratio of reinforcing to resin materials. An "H" mold was used to make direct-wound uni-directional composite bars. Since MC fibers already have built-in thermoplastic matrix, composites were made without a pre-pregg..ng step, by simply applying heat and pressure to effect consolidation. Uni-directional MC composite bars have comparable flex, compressive and short-beam-shear properties as conventional PBZT/epoxy composites [2] and are just as deficient as PBZT in compressive strength as compared to carbon fibers [12]. As shown in Table VII, MC fiber precursors spun from below critical concentration appears to yield somewhat higher compressive strength, but the compressive strength is still only 1/5th that of carbon fiber-based composites. MC film precursor offers no advantage in compressive strength versus fiber precursor.

The tensile and compressive strength of PBZT, although representing a significant increase over other low modulus commercially available organic fibers [13], is in the range of other organic, high modulus fibers like Kevlar®. Nevertheless, the compressive strength of 30-41 ksi is considered low for primary structural applications. The high tensile and compressive moduli of PBZT, however, are as high as pan-based carbon fibers [14]. In addition, the fact that PBZT is not an electrical conductor offers an advantage over carbon fibers in applications where high stiffness, non-conductive and corrosion resistance are important(Table VIII).

An advantage of using thermoplastic matrix is reprocessability of composites. Uni-directional MC bars were found to recover 100% of their flex and SBSS properties when they were reconsolidated by remolding the failed bars after test failure. However, a test of recovery of tensile strength after test failure might be a more sensitive measure of repairability.

A correlation between fiber modulus and x-ray orientation angle was developed for PBZT [2] and its MC's. Since the polyamide matrices in the MC's do not contribute to the orientation significantly, the orientation angle values are the reflections of the PBZT molecular orientation. And since orientation angle is not a function of PBZT content while modulus is a function of PBZT content,

TABLE V. STATE-OF-THE-ART*
MC FIBER CONTAINING
COMPATIBLE TPA MATRIX
(PBZT/FX-3369, 60/40v)

	STRENGTH KSI (GPD)	MODULUS MSI (GPD)	O.A.
BELOW C critical	200 (11.0)	18 (971)	12*
ABOVE C critical	332 (18.4)	29 (1,600)	7*
	BACK CALCULATED TO NEAT PBZT		
	553 (27.0)	48 (2,320)	
UNI-AXIAL CONVENTIONAL CARBON/EPOXY COMPOSITE	210	21	

* USING A DU PONT PROPRIETARY TECHNOLOGY. U S PATENT 4,810,735

CONCLUSIONS:

* THE BACK-CALCULATED VALUES TO NEAT PBZT INDICATE THAT RULE-OF-MIXTURE HAD BEEN ACHIEVED

* EXCEEDED UNI-AXIAL CONVENTIONAL CARBON/EPOXY COMPOSITE PROPERTIES
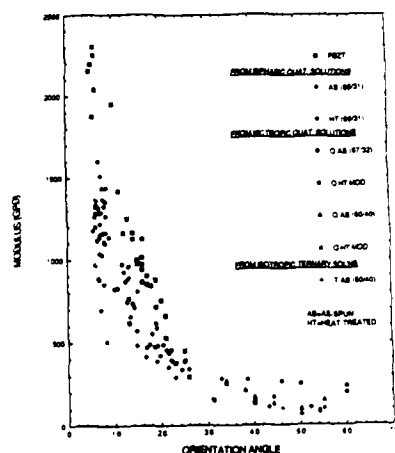
FIG. 3. MODULUS - ORIENTATION
ANGLE RELATIONSHIP OF PBZT & MC'S

TABLE VI. TERNARY vs QUATERNARY
MC FIBER TENSILE PROPERTIES

	TERNARY		QUATERNARY
PBZ CONTENT, WT %	30-70[11]	60[10]	69
BELOW C critical			
STRENGTH, KSI	80-105	127	200	162[a]
MODULUS, MSI	8.5	12	18	15-20[a]
ABOVE C critical			
STRENGTH, KSI	60		332	55[a]
MODULUS, MSI	0.6		29	48[a]
RATIO OF PROPERTIES ABOVE TO BELOW C critical			
STRENGTH	0.08		1.66	
MODULUS	0.07		1.65	

10 & 11 See list of references at the end of text
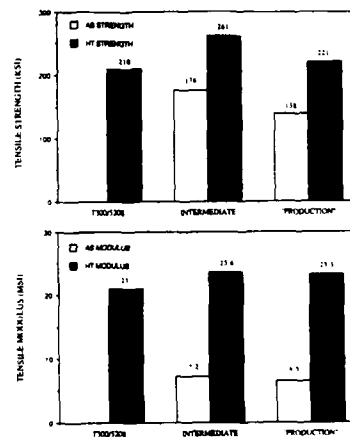
FIG. 4. PBZT/FX-3369 MC FIBER TENSILE
PROPERTIES vs T300/EPOXY UNI-COMPOSITE

TABLE VII. UNI-DIRECTIONAL MC BAR PROPERTIES
(PBZT/FX 3369, 60/40v)

	FLEX STRENGTH (KSI)	MODULUS (MSI)	COMPRESSIVE STRENGTH (KSI)	MODULUS (MSI)	SHORT-BEAM-SHEAR STRENGTH (KSI)
BELOW C critical					
FIBER	67	5.3	13-17	14-21	3.8-4.6
FILM			33		
ABOVE C critical	77	18	12	2.6	6.6
CONVENTIONAL COMPOSITES					
PBZT/EPOXY	61(68)	17	2.5(41)	18(21)	5.8(7.4)
CARBON/1.2	200	17	151	17	15

CONCLUSIONS:

* ACHIEVED COMPARABLE PROPERTIES AS CONVENTIONAL PBZT/EPOXY COMPOSITES BUT MC'S HIST AS DEPENDENT AS PBZT IN COMPRESSIVE STRENGTH AS COMPARED TO CARBON FIBERS PBZT STIFFNESS ASCENDED AS CARBON
* MC FROM ROTRIC AL CONCENTRATION GIVES SOMEWHAT HIGHER COMPRESSIVE STRENGTH BUT NOT SIGNIFICANT COMPARED TO CARBON
* IMPROPER FILM PROCEDURE OFFERS NO ADVANTAGE IN COMPRESSIVE STRENGTH VS FIBER PROCEDURE

TABLE VIII. ULTIMATE COMPRESSIVE PROPERTIES OF
UNI-DIRECTION COMPOSITES
REINFORCED WITH VARIOUS FIBERS
(FIBER/EPON® 826, 60/40v)

FIBER	STRENGTH (KSI)	STRAIN (%)	MODULUS (MSI)
T 68 DACRON®	14		
T 728 NYLON	15		
c PBO	18		10.0
ORLON® ACRYLIC	22	10.8	0.8
POP PI	20	6.0	0.9
PPD-PI	25	6.5	1.3
PBZT	30-41		21.1
T 430 NOMEX® ARAMID	34	5.2	1.7
KEVLAR® 49	40	2.2	11.0
PBI CELANESE	18	5.2	1.2
HS GRAPHITE (AS-4)	200	1.1	18.0
HM GRAPHITE (P 100)**	48		63.0
MC (PBZT/FX 3369)	32-37		26.0

Some data obtained by M Kaur, Du Pont
* Du Pont registered trademark
** S Kumar, SAMPE Quarterly, p 3 Jan 1989

the modulus vs. orientation angle relationship for MC's naturally falls below the relationship for neat PBZT (Fig. 3).

Status of Process Development

Spinning and heat-treatment processes were successfully scaled-up from laboratory, intermediate and finally to "production" scales. Numerous 60-lb "production" spin batches were made to complete a total of 25 lbs of 1,000 nominal denier/290-filament MC yarn. Therefore, the prognosis of the developed processes for commercial viability appears very good. MC fiber tensile properties from "production" runs are as good as intermediate-scale fibers after heat-treatment (Fig. 4).

MC Data Base Development

The "production" MC yarn will be used to produce consolidated plates with variety of orientation for testings in collaboration with Boeing Advanced Systems in order to develop the first comprehensive MC data base. A wide variety of mechanical, electrical and optical tests will be performed.

SUMMARY

A promising thermoplastic polyamide matrix candidate has been identified. Excellent spinning and heat-treatment processes were scaled-up from laboratory to "production" scale. Commercial viability appears very good. Consolidated MC fibers have exciting properies and are repairable with 100% recovery in properties. Consolidated uni-directional bars have comparable flex, compressive and short-beam-shear properties as conventional PBZT/epoxy composites and with the same deficiency in compressive strength. Modulus, however, is comparable to pan-based carbon/epoxy in tension/flex/compression.

REFERENCES

1. W.C. Uy, Air Force Report AFWAL-TR-82-4154, Part I, 1982.
2. J.F. Mammone and W.C. Uy, Air Force Report AFWAL-TR-82-4154, Part II, 1982.
3. J.F. Wolfe and B.H. Loo, U.S. Patent No. 4,225,700 (30 January 1980).
4. T.E. Helminiak, C.L. Benner, F.E. Arnold and G.E. Husman, U.S. Patent No. 4,207,407 (10 June 1980).
5. P.J. Flory, Macromolecules 11, 1138 No. 6 (1978).
6. W.F. Hwang, D.R. Wiff and C. Verschoore, Polymer Engineering and Science, 23 No. 14, 789 (1983).
7. P.A. Small, J. Applied Chem., 3, 71 (1953).
8. B. Miller, M.A. Tallent, K.P. Hewitt, K.L. Adams and G.A. Desio, Textile Research Institute Report No. 6 (1 July 1985).
9. W.C. Uy, U.S. Patent No. 4,810,735 (7 March 1989).
10. W.F. Hwang, T.E. Helminiak and D.R. Wiff, U.S. Patent No. 4,631,318 (23 December 1986).
11. W.F. Hwang, 6th Industry/Government Review of Thermoplastic Matrix Composites, Arlington, VA, 1989 (unpublished).
12. I.Y. Chang and J.K. Lees, J. of Thermoplastic Composite Materials, 1, 277 (1988).
13. M. Katz, E.I. du Pont de Nemours & Co. (unpublished).
14. S. Kumar, SAMPE Quaterly, 3 (1989).

MORPHOLOGY AND FORMATION OF FIBRILLAR STRUCTURE IN PBO FIBER

C.C. CHAU, J.H. BLACKSON, H.E. KLASSEN AND W.-F. HWANG
The Dow Chemical Company, Midland, MI 48674

ABSTRACT

Electron microscopy studies showed that the porous structure of PBO fiber may contain fractal geometries; i.e., the void spaces are self-similar with variations in magnification. At the fiber surface, a dense skin which consists of fibrils was observed. In the matrix, the fibril size is about 5 to 50 nm with the voids distributed randomly among the fibrils. The fractal dimension of voids in PBO fiber as determined by microscopy and image analysis was found to be 2.44. The fibrillated fiber showed a continuous fibril size distribution with no evidence of fibril size hierarchy. These observations suggest a nucleation and growth mechanism for the formation of the fibrillar structure in PBO fiber.

INTRODUCTION

The structure of high performance fibers is an interesting subject and has been studied for many years. Published data indicates that organic fibers are highly oriented in the fiber direction [1]. Studies on Kevlar aromatic polyamide fibers showed that rod shaped crystallites are oriented [2-4] along the fiber axis with layered stackings [5-7] held together by H-bonds, and with weak van der Waals' attractions in the lateral direction. Observations on PBT [8] have shown that these fibers could contain fibrils, with a fibril size 10 nm or smaller, oriented along the fiber axis. The fibrillar nature seems to allow the fiber to be fibrillated easily by both tensile and compressive deformation [3, 9] or by a simple peel test [10].

Interest is further revolving around the possibility of fibrillar hierarchy. Although still not clear, fibrillar morphology has been recognized as one of the most important features of organic fibers since mechanical properties, such as high tensile strength and modulus, and weak compressive strength [11], are believed to be closely related to the fibrillar nature of the fiber. In a continuing effort to understand the fibrillar morphology and the mechanism of fiber formation, microtomed thin sections of PBO fibers were examined by transmission electron microscopy. Details of the fibrillar morphology were observed and analyzed quantitatively. Some considerations regarding the fibrillar formation mechanism are given.

EXPERIMENTAL

(1) Electron Microscopy: PBO fibers were prepared from dopes of a copolymer of poly(phenylene benzobisoxazole) (PBO) in polyphosphoric acid (PPA). The spun filaments were collected in water, dried, and subsequently heat treated at elevated temperatures under tension. Fibers with a diameter of about 15 um were embedded in epoxy resin. Flat silicon embedding molds were used with the fibers oriented parallel to the long dimension of the mold. After appropriate trimming of the epoxy embedded sample, ultramicrotomy was performed at room temperature with a Reichert Ultracut E microtome to produce sections ranging in thickness from 40~70 nm. New areas of a diamond knife were used continuously to avoid damage from the cutting edge. Sections were collected on carbon supported copper TEM grids. Complete intact sections without folds were found difficult to obtain. Thin sectioned samples were examined using a JEOL 100 CX ATEM at an accelerating voltage of 100 KV.

(2) Image Analysis: Image analysis was performed by using a Kontron SEM-IPS image analyzer. Segments of images from TEM photomicrographs were transferred to the image analyzer using a high resolution TV camera. The captured image was then enhanced by expanding the gray level to the full 256 gray levels. The processed image was compared with the original image to insure proper selection of the desired region of the image.

(3) <u>Fiber Peel Studies</u>: Strands of fiber were sandwiched between two pieces of Scotch tape. The tape was then peeled apart. The peeled tape with the attached fibers was examined in an ISI-DS130C scanning electron microscope.

RESULTS AND DISCUSSION

(1) The Morphology of Fiber after Fibrillation

Sawyer and Jaffe [10] have suggested that fibers of liquid crystalline polymers may possess a hierarchical nature, e.g., macrofibrils, fibrils and microfibrils. In the present investigation fibers were examined on a macro and micro level in an attempt to determine if such a hierarchy exists in PBO. Examination of the peeled PBO fibers showed separated segments of various sizes as shown in Fig-1. The fibrils form a reticulated network with the larger fibrils mostly oriented along the fiber direction. The possibility of tearing prohibits determination of the basic structural unit by a hand peel test. The number and size distribution of the fibrils is shown in Fig-2. The distribution is continuous with the most probable size occurring at 35 nm or lower. Fibrillar size smaller than 20 nm is not clear or measurable from the micrographs. No hierarchical distribution could be identified within the area examined.

Fig-1 Fibrillar network produced by hand peeling of a strand of fiber

(2) Skin-Core Structure and the Morphology of PBO Fiber

An ultramicrotomed thin section of a fiber prepared from a copolymer of PBO is shown in Fig-3(a). The fiber cross-section consists of two regions of distinctly different characteristics. A low contrast region is seen around the periphery; it is probable that this is a skin. However, examinations of fibers from various spinning runs indicate that the skin morphology is not prevalent in PBO fibers. The average thickness of the skin in this particular sample is about 0.8 um as shown in Fig-3(b). The skin seems to consist of densely packed fibrils.
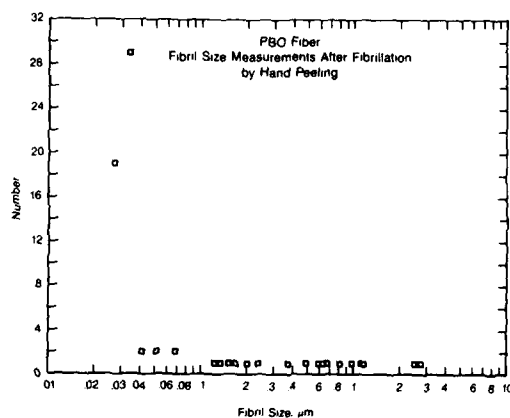
Fig-2 The number and size plot of fibrils in Fig-1(a) and (b) showing a continuous
distribution with no apparent size hierarchy
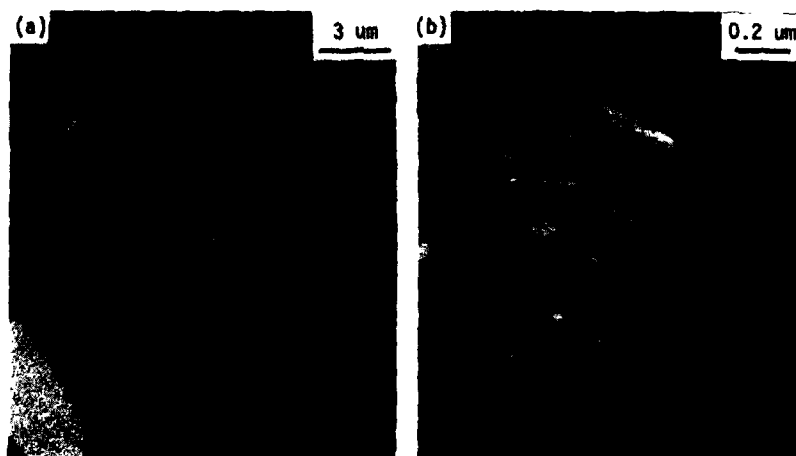
Fig-3 (a) The morphology of a microtomed thin section of a PBO copolymer fiber showing
skin-core structure (The dark stripes are folds of sample produced in microtoming)
(b) An enlarged view of a portion of skin in Fig-3(a) showing densely packed
fibrils in the skin

In the core, irregularly shaped fibrils are seen with boundaries separating them as shown in
Fig-4. The size of the individual fibril appears to range from about 5 to 50 nm and no size
hierarchy was observed. The size range is consistent with the order of 10 nm reported in PBT
[8]. Individual fibrils with abnormally large or small sizes are not observed. These fibrils are
presumably oriented along the fiber axis. Another feature evident in Fig-4, is the contrast

variation, which could indicate the presence of voids. A separate study by small angle x-ray diffraction concurred with such a possibility. These voids appear to be irregular in shape and are distributed randomly among the fibrils. The voids, although low in volume content, are well dispersed in the matrix with the size ranging from submicron to nanometer level. As is evident in Fig-3(b), some void area is created in this fragile material during microtomy.

100 nm

Fig-4 A detailed view of the cross-sectional morphology of fibrils in the core of a PBO fiber

Assuming that the relatively bright features are voids, the size and number of voids were measured from TEM micrographs using an image analyzer. The average void size was measured radially across the fiber at a magnification of 50 kx. The void size did not vary systematically with distance from the fiber center and the void spacing was variable. The void area percentage in the cross-section was measured at three different magnifications (10.8 kx, 87 kx, 216 kx) in order to detect voids of all sizes. The void area percentage was plotted as a function of the average void size for each area on a log-log scale as shown in Fig-5. While there is considerable scatter there is an inverse relationship between void area percentage and void size, i.e., most of the void volume is contributed by the smaller voids.

If the void space is considered to possess fractal [12] geometry within the studied magnification range, the fractal dimension may be determined from Fig-5. For a fractal object, the fractal dimension can be determined based on the number and size relationship: $n \sim r^{-D}$ ($0 \leq D \leq 3$), where n is the number of pores, r is the size of the pore, and D is the fractal dimension or Hausdorf dimension which relates number and size for a fractal object. For relating the area ratio of a species in a unit area to the size of the species, $r^2 n \sim r^{2-D}$ ($2 \leq D \leq 3$). The fractal dimension as calculated from the slope in Fig-5 is 2.44.

(3) Phase Separation and Fibril Formation

The fractal nature of voids implies a kinetic process of fibril formation resulting from phase separation. According to Flory's consideration [13], the phase diagram for a ternary system such as PBO, PPA and water, a nonsolvent, would consist of a narrow single phase region and a much broader two phase region where the homogeneous PBO/PPA solution is separated into a polymer-rich and a polymer-lean phase. It is therefore expected that voids will develop in fibers spun from a dry jet-wet spinning process in which the PBO/PPA dope is precipitated in water. Subsequent drying usually causes fiber to shrink. Complete densification, however, is not likely to occur.

Some mechanistic understanding can be obtained from the void characteristics. Since the average void size measurement across the fiber diameter shows no signs of spacial periodic variation, spinodal decomposition is not likely. Consider a polymer solution which is in contact with a precipitant, such as water, where precipitation takes place by heterogeneous nucleation, as time goes by the nuclei grow in size while new nuclei are developing. The process continues until the polymer composition is consumed. At that stage the polymer is precipitated in the form of a reticulated network. Examples showing such a precipitated polymer structure are those of asymmetric microporous membranes [14-16]. When the precipitation process occurs in a dope that is uniaxially oriented, the network is likely to develop in elongated fibrillar form. This consideration suggests that all fibrils are interconnected with voids between the fibrils. It is expected that the void density is proportional to fibril density. This relationship is assumed unchanged during drying and shrinkage. The relationship between number and size of fibrils can then be approximated by following a fractal growth model [17] proposed for rock formation.
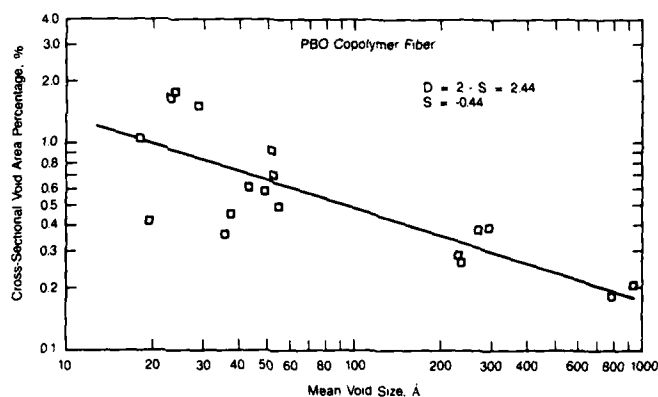
Fig-5 A log-log plot of cross-sectional void area percentage vs void size for a PBO fiber

The rate of nucleation can be expressed as $dN/dt = K_1 C^n$, and the rate of growth is $dR/dt = K_2 C^r$, where N is the number of nuclei, R is the size of fibril, C is the local polymer concentration, K_1 and K_2 are the respective rate constants, and n and r are the orders of nucleation and growth. For the coagulation of rigid rod polymers, the local polymer concentration, C, is assumed to be close to constant throughout in the shaped dope during precipitation. This is likely to be true due to the low mobility of rigid and oriented polymer chains.

Since the growth process depends upon local concentration to form an extended aggregate, the rate of growth can be reasonably assumed to be first order. The final fibril size should then be proportional to the rate of growth but inversely proportional to the rate of nucleation for a given polymer concentration. Namely, the fibril size and number can not be both maximized at any time t. Therefore, R is proportional to $(dR/dt)/(dN/dt)$, or $R \sim C^{1-n}$. The total fibril number N with a size R is expressed as $N \sim C^n$. The relationship between the fibril number and size can then be scaled as follows: $N(R) \sim R^{-(n/n-1)}$, where $0 \leq (n/n-1) \leq 3$. By definition this relationship shows that the number and size of fibrils are correlated by a fractal dimension:

n/n-1. Based on fibril and void size proportionality, the fractal dimension gives the order of nucleation, n=1.69. The kinetic equations governing the formation of fibrils may be expressed as $dN/dt = K_1 C^{1.69}$, $dR/dt = K_2 C$. These considerations suggest that the kinetics of fibril formation may be indicated from a fractal analysis of the porous structure developed within the fibrils.

SUMMARY AND CONCLUSIONS

(1) Electron microscopy showed that PBO copolymer fibers consisted only of fibrils with varying sizes in the range of 5 to 50 nm. No hierarchy in the fibrillar size was observed.

(2) In an isolated case, one PBO fiber was found to have a 0.8 um thick skin consisting of closely packed fibrils.

(3) It was assumed, based on TEM image contrast, that a small void content (0.1~1 vol%) existed within the PBO fiber. The small (2~100 nm) voids were randomly distributed throughout the fiber.

(4) The void appeared to contain fractal properties. The void density and size gave a fractal dimension of 2.44. Based on these observations, a nucleation and growth model is suggested for the formation of fibrillar structure with a variation in the order of nucleation.

ACKNOWLEDGEMENTS

REFERENCES

1. W.W. Adams and R.K. Eby, MRS Bulletin, Nov 16/Dec 31, 22 (1987)
2. L.S. Li, L.F. Allard and W.C. Bigelow, J. Macromol. Sci.-Phys., B22(2), 269 (1983)
3. R.J. Morgan, C.O. Pruneda and W.J. Steele, J. Polym. Sci., Polym. Phys., 21, 1757 (1983)
4. M. Panar, P. Avakian, R.C. Blume, K.H. Gardner, T.D. Gierke and H.H. Yang, J. Polym. Sci., Polym. Phys., 21, 1955 (1983)
5. M.G. Dobb, D.J. Johnson and B.P. Saville, J. Polym. Sci., Polym. Phys., 15, 2201 (1977)
6. S.C. Simmens and J.W.S. Hearle, J. Polym. Sci., Polym. Phys., 18, 871 (1980)
7. P.H. Young, Spectroscopy, 3, 9, 24 (1988)
8. Y. Cohen and E.L. Thomas, Polym. Eng. Sci., 25, 1093 (1985)
9. J.H. Greenwood, P.G. Rose, J. Mat. Sci., 9, 1809 (1974)
10. L.C. Sawyer and M. Jaffe, J. Mat. Sci., 21, 1897 (1986)
11. S. Kumar, IFJ/February, 4 (1989)
12. S.H. Liu, "Fractal and Their Applications in Condensed Matter Physics" in Solid State Phys (Academic Pre.), 39, 207 (1986)
13. P.J. Flory, "Principles of Polymer Chemistry", Chap. XIII, Cornell Univ. Pre., 1953.
14. J.G. Wijmans, J. Kant, M.H.V. Mulder and C.A. Smolders, Polymer, 26, 1539 (1985)
15. D.M. Koenhen, M.H.V. Mulder and C.A. Smolders, J. Appl. Polym. Sci., 21, 199 (1977)
16. H. Strathmann, K. Kock, P. Amar and R.W. Baker, Desalination, 16, 179 (1975)
17. A.J. Katz and A.H. Thompson, Phys. Rev. Lett., 54, 1325 (1985)

IN SITU COMPOSITES BASED ON THERMOTROPIC AND FLEXIBLE POLYMERS

GUIDO CREVECOEUR AND GABRIEL GROENINCKX
Catholic University of Leuven, Laboratory for Macromolecular Structural
Chemistry, Celestijnenlaan 200 F, B 3030 Leuven, Belgium

ABSTRACT

Blends of a thermotropic liquid crystalline polymer (TLCP) and a thermoplastic matrix were compounded. Upon subsequent injection moulding and spinning, the TLCP was deformed into fine fibrils in the matrix, giving in-situ reinforcement. Especially after spinning, the composite fibres contain fibrils with very high aspect ratio, and exhibit mechanical properties in accordance with simple composite models for modulus and strength.

INTRODUCTION

In-situ composites consisting of a thermotropic liquid crystalline polymer (TLCP) and a thermoplastic matrix material can be regarded as an intermediate between conventional (short) fibre reinforced composites and molecular composites. All three of these materials have in common that the aspect ratio of the reinforcing species is of great importance with respect to the final mechanical properties of the product. In short fibre composites the length of the fibres is limited by the processing method used, e.g. extrusion or injection moulding. A high aspect ratio can be obtained in molecular composites, where one or a few stiff single macromolecules are dispersed on a molecular level. Due to their intrinsic immiscibility with flexible polymers, the rigid macromolecules, typically being lyotropic liquid crystalline polymers, have to be dispersed in the thermoplastic matrix by casting from dilute solutions. Indeed, dispersion on a nanometer scale and outstanding mechanical properties can be obtained in such systems [1]. However, the solvent step provides an extra complication in industrial processing. Therefore, a reasonable alternative seems to be blending a TLCP with an engineering polymer in the melt, so that dispersion, elongation and orientation of the TLCP take place in one processing step [2-6]. An additional advantage is that, because the TLCP acts as a lubricant, the melt viscosity of the blend, contrary to those of short fibre reinforced composites, can be lowered as much as one or two orders of magnitude [7-10].

The present paper is concerned with blends of a commercial thermotropic polyester-amide, Vectra B 950, in a matrix consisting of a (miscible) mixture of polystyrene (PS) and poly-2,6-dimethyl-1,4-phenylene ether (PPE).

EXPERIMENTAL

Vectra B 950, which is believed to consist of 58 mole-% hydroxy naphthoic acid, 21 mole-% terephthalic acid and 21 mole-% 4 aminophenol, was purchased from Hoechst Celanese. Blends containing 70 weight-% PPE and 30 weight-% PS were kindly supplied by General Electric Plastics Europe. Vectra B 950 melts at 280°C, where it shows liquid crystalline behaviour. PPE and PS are known to be miscible over the entire composition range; the as received PPE/PS blend exhibits a single T_g at 177°C.

Blending was performed on a Berstorff corotating twin screw extruder at 320°C. Strands with a draw ratio (DR) of approximately 2.5 were taken directly from the extruder, and their morphology was examined. From the granulated strands, ASTM tensile bars were injection moulded at 320°C, and fibres were spun at approximately 310°C; the draw ratio was determined from the

haul-off speed and the throughput. Although fibres with different draw ratios were prepared, the discussion in the present paper will be confined to those having a draw ratio of approximately 30. The influence of draw ratio on the morphology and properties of the blends is described elsewhere [11].

Complex viscosity of the blends was examined on a Rheometrics RMS 500 mechanical spectrometer at 300°C, in plate-plate geometry, at a strain of 1 %, which is well in the linear region of Vectra. Dynamic modulus and loss angle in the solid state as functions of temperature, were measured on a Polymer Labs dynamic mechanical thermal analyser (DMTA) in bending mode. Cryogenic fracture surfaces were investigated using scanning electron microscopy (SEM). Furthermore, the PPE/PS matrix from the strands and composite fibres was dissolved in toluene, to yield the insoluble TLCP particles or fibrils which were examined under an optical microscope. The mechanical properties of the blends were determined on an Instron tensile tester, applying a strain rate of 1 mm.min^{-1} for the injection moulded parts and 50 %.min^{-1} for the fibres. The fibres with low TLCP content have a high strain to break, necking occurring over the entire sample; therefore the ultimate strength of these samples is corrected for the decrease in cross-sectional area, assuming incompressibility during necking. Molecular orientation of the TLCP in the fibres was measured using wide angle X-ray scattering (WAXS). Single fibres were placed in a Kiesig camera, and the orientation was characterized either by the peak width at half height ($w\frac{1}{2}$) or the Hermans orientation parameter P_2. Both parameters were obtained from an azimuthal scan over the strong equatorial 110 reflection of the TLCP. Background scattering resulting from the amorphous matrix was subtracted from the intensity profile prior to these calculations.

RESULTS AND DISCUSSION

The complex viscosity of the blends versus the TLCP content, for three different angular frequencies, is presented in fig. 1. A substantial decrease in viscosity is observed for the higher TLCP contents. The fact that the viscosity remains constant or even increases for the low contents, could indicate the presence of a yield stress in the TLCP. Due to this yield stress, the TLCP particles would act as rigid fillers at the low strain that was applied during the measurements. Complex viscosity behaviour with intermediate extremes has also been reported for blends of flexible polymers [12].

Storage modulus and loss tangent for a 50 % Vectra-50 % PPE/PS blend (compression moulded sample) versus temperature are shown in fig. 2. Three successive thermal transitions are observed: the Vectra β-transition at 70°C [13], the Vectra glass-transition at 140°C, and the PPE/PS T_g at 180°C. Fig. 2 clearly demonstrates the single T_g of the miscible PPE/PS matrix.

Fig. 3 contains scanning electron micrographs of an injection moulded tensile bar, an extruded strand and a fibre. It is readily seen that fibril formation is much more developed in the strand and the fibre than in the injection moulded part. Spinning and strand-extrusion involve extensional flows, whereas during injection moulding merely shear flow (a weaker flow due to its non-zero rotational component) takes place. When the PPE/PS matrix was dissolved in toluene, it appeared that the as spun fibres contained microfibrils with nearly infinite aspect ratio, in contrast with the only moderate aspect ratio of the fibrils in the injection moulded samples. Because of these high fibril aspect ratios, the best mechanical properties can be expected from the composite fibres. There is a tendency for the fibril diameter to increase with TLCP content from 0.2-0.6 μm for the 5 weight-% Vectra blend, to 0.4-2 μm for 25 % TLCP. The fibril thickness is determined by the particle size prior to elongation, which is the result of a dynamic equilibrium between dispersive mixing and coagulation in the twin screw extruder.
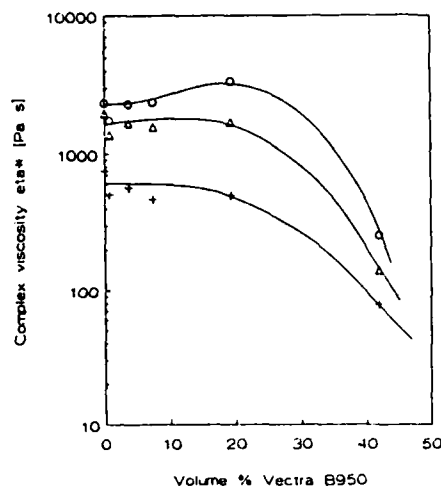
Figure 1. Complex viscosity versus volume fraction TLCP, for 101 (+), 1.6 (Δ) and 0.10 (o) rad.s⁻¹
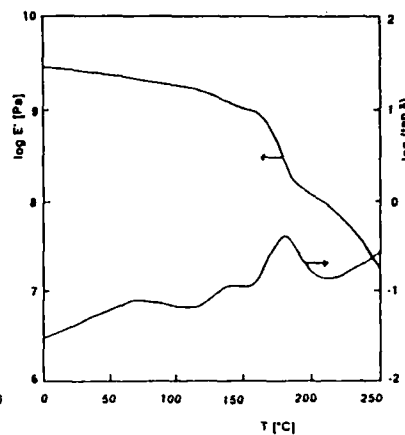
Figure 2. Storage modulus and loss tangent versus temperature, for 50 % Vectra-50% PPE/PS blend, freq.=10 Hz
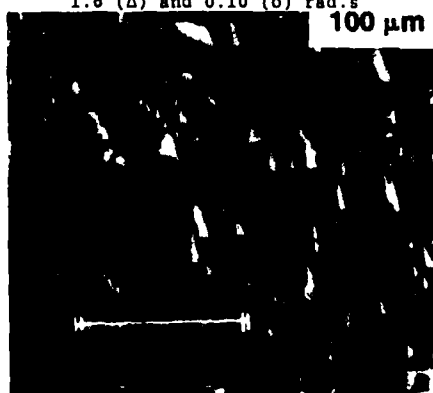
Figure 3. Scanning electron micrographs of cryogenic fracture surfaces. Injection moulded tensile bar, 10 % TLCP (a), strand, 25 % TLCP (b), and fibre, 10 % TLCP (c)
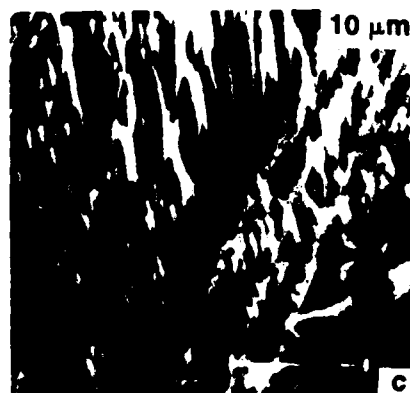
The tensile modulus of the injection moulded bars and the fibres, as a function of TLCP content is plotted in fig. 4a. The only moderate aspect ratio of the TLCP fibrils in the injection moulded samples gives rise to a modulus below the rule of mixtures [14]. Indeed, a curved plot is observed in fig. 4a. The tensile modulus of the fibres is seen to increase linearly with volume fraction TLCP. This is in full agreement with the morphological observation of microfibrils of nearly infinite aspect ratio that, according to composite theory [15], requires rule of mixtures for modulus:

$$E_c = V_f E_f + (1-V_f) E_m \tag{1}$$

where E_c, E_f and E_m are the modulus of the composite fibre, TLCP and matrix respectively, and V_f represents the volume fraction of TLCP. Moreover, the modulus of 74 GPa for the pure Vectra, suggests a satisfactory molecular orientation [16] for both the pure TLCP, and the TLCP dispersed in the composite fibres. Elongation to break for the fibres (plotted on a logarithmic scale in fig. 4b) falls from approximately 100 % for the pure PPE/PS to 1 % for the pure Vectra. Of course, this transition has great influence on the ultimate strength (fig. 4c). A minimum occurs at 20 volume-% TLCP, which can be understood qualitatively by indicating two limiting cases:

i) For high volume fractions of TLCP, the fracture behaviour will be dominated by the TLCP, i.e. the composite will break when the maximum strain of the TLCP is reached, and the strength can be described by the following equation [13]:

$$\sigma_c = V_f \sigma_f + (1-V_f) \sigma_f E_f / E_m \tag{2}$$

where σ_c and σ_f are strength at break of the composite and TLCP, respectively.

ii) For low TLCP contents, the TLCP cannot follow the plastic deformation of the matrix (possessing very high strain to break), and may therefore be regarded as voids. In this case the composite strength is given by:

$$\sigma_c = (1-V_f) \sigma_m \tag{3}$$

with σ_m the strength of the pure matrix material. Equations 2 and 3 are plotted in fig. 4c. The minimum in the experimental data is seen to coincide with the volume fraction at which equations 2 and 3 cross, but all experimental points are below the theoretical lines. However, during the derivation some assumptions are made that are only partially fulfilled. One of these is that for the higher volume fractions, the TLCP is assumed to exhibit linear deformation behaviour up to break, which it does not. Furthermore, for the lower LCP contents, the strength according to equation 3 is based on the strain to break for the pure matrix material, fig. 4b however, clearly demonstrates that the presence of the TLCP actually constrains the plastic deformation, thus also limiting the ultimate strength.

The Hermans orientation factor and peak width at half height versus volume fraction TLCP are shown in fig. 5. Molecular orientation of the TLCP as dispersed in the composite fibres is seen to improve with increasing TLCP content. Similar results have been observed for blends of polycarbonate and a thermotropic copolyester of poly(ethylene-terephthalate) and p-hydroxybenzoate [17]. A tentative explanation for this feature lies in the size of the TLCP droplets in the melt, just before entering the spinneret. Since the lower TLCP content blends contain smaller TLCP particles, these will have a higher resistance against deformation, due to interfacial tension [18,19]. Thus, a smaller deformation is imposed by the macroscopic flow, leading to a lower molecular orientation.

(a) (b)
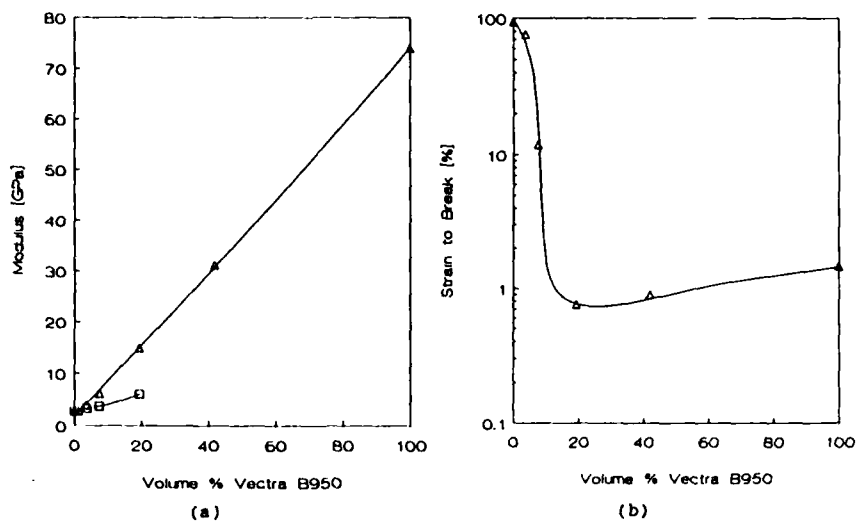
Figure 4. Young's modulus (a) and strain to break (b) versus volume fraction TLCP. □ injection moulded parts, Δ fibres
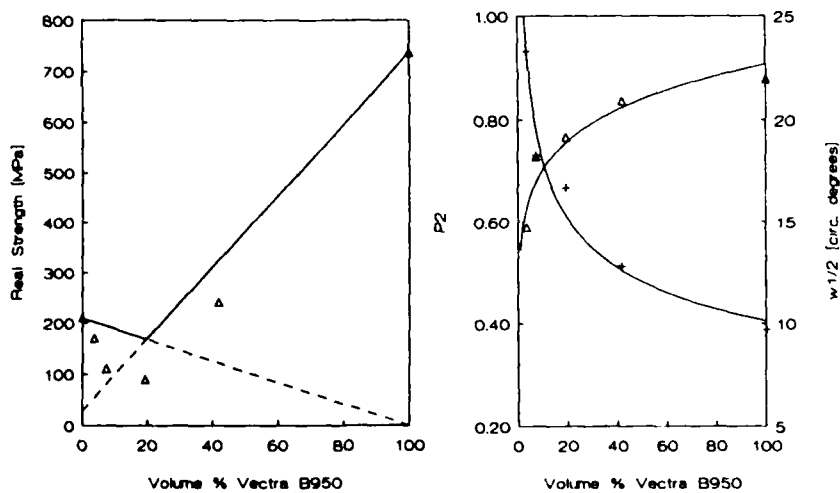
Figure 4c. Strength for composite fibres versus TLCP content

Figure 5. Hermans orientation factor (P_2), and peak width at half height ($w_{\frac{1}{2}}$) versus volume fraction Vectra

CONCLUDING REMARKS

Blends of a thermotropic liquid crystalline polymer and a matrix consisting of flexible polymers were injection moulded and spun into fibres. In both cases the formation of thin TLCP fibrils, oriented in the processing direction was observed. However, the average aspect ratio of these fibrils was found to be moderate in the injection moulded samples, but nearly infinite in the composite fibres. These observations clearly point out how much more effective elongational flow (spinning) is than shear flow (injection moulding) in inducing elongated structures. The mechanical properties of the composite fibres could be described by composite models for transversely isotropic geometry, i.e. rule of mixtures for modulus and an initial decrease, followed by an increase for strength versus TLCP content. Satisfactory molecular orientation of the dispersed TLCP fibrils in the composite fibres was achieved.

ACKNOWLEDGEMENT

REFERENCES

1. D.R. Wiff, T.E. Helminiak and W.F. Hwang, in High Modulus Polymers, edited by A.E. Zachariades (Marcel Dekker, New York, 1988), p. 225
2. G. Kiss, Polym. Eng. Sci. 27, 410 (1987)
3. R.A. Weiss, W. Huh and L. Nicolais, Polym. Eng. Sci. 27, 684 (1987)
4. P.D. Frayer, Polym. Comp. 8, 379 (1987)
5. A.I. Isayev and M. Modic, Polym. Comp. 8, 158 (1987)
6. W. Brostow, T.S. Dziemianowicz, J. Romanski and W. Werber, Polym. Eng. Sci. 28, 785 (1988)
7. K.G. Blizard and D.G. Baird, Polym. Eng. Sci. 27, 653 (1987)
8. B.L. Lee, Polym. Eng. Sci. 28, 1107 (1988)
9. A. Siegmann, A. Dagan and S. Kenig, Polym. 26, 1325 (1985)
10. M.R. Nobile, E. Amendola, L. Nicolais, D. Acierno and C. Carfagna, Polym. Eng. Sci. 29, 244 (1989)
11. G. Crevecoeur and G. Groeninckx, submitted Polym. Eng. Sci.
12. M.V. Tsebrenko, Intern. J. Polym. Mater. 10, 83 (1983)
13. T.S. Chung and P.E. McMahon, J. Appl. Polym. Sci. 31, 965 (1986)
14. J.C. Halpin and J.L. Kardos, Polym. Eng. Sci. 16, 344 (1986)
15. M.R. Piggott, Loadbearing Fibre Composites (Pergamon, Oxford, 1980), p. 62
16. T.S. Chung, J. Polym. Sci. B26, 1549 (1988)
17. S.H. Jung and S.C. Kim, Polym. J. 20, 73 (1988)
18. G.V. Vinogradov, N.P. Krasnikova, V.E. Dreval, E.V. Kotova, E.P. Plotnikova and Z. Pelzbauer, Intern. J. Polym. Mater. 9, 187 (1982)
19. P.H.M. Elemans, Ph. D. Thesis, Eindhoven University of Technology, 1989

MOLECULAR COMPOSITES OF RODLIKE/FLEXIBLE POLYIMIDES

S. R. ROJSTACZER, D.Y. YOON, W. VOLKSEN AND B.A. SMITH
IBM Research Division, Almaden Research Center, San Jose, CA 95120

ABSTRACT

Mixtures of a rodlike and a flexible polyimide were prepared by solution-blending of the respective poly(amic alkyl ester) and poly(amic acid), followed by solvent evaporation and thermal imidization. The size scale of the phase separation, as measured by light scattering, is primarily set during the demixing of the precursor polymers, with no significant coarsening observed due to the imidization performed at 400°C. The observed variation of the domain size with parameters such as composition, molecular weight and film thickness is discussed in terms of the miscibility of the precursor polymers as well as the thermal history to which these were exposed.

INTRODUCTION

Mixtures of rodlike and flexible polyimides have the potential to achieve the desired properties for applications in microelectronic packaging by combining the required thermal and mechanical properties characteristic to the rodlike component along with enhanced adhesion strength provided by the flexible polyimide. The use of such mixtures as thin film coatings, however, requires that any heterogeneity on composition has to be kept on a scale well below the micron level, raising the question of the feasibility of polyimide based molecular composites. Of particular interest in such systems is the effect of the imidization carried out at high temperatures on the morphology of the precursor blends.

Yokota et al. [1] studied mixtures of polyimides prepared by imidization of mixtures of different poly(amic acid) (PAA) precursors. Feger [2] and Ree et al. [3] showed, however, that mixtures of poly(amic acid)s can lead to the formation of copolymers rather than physical blends of homopolymers. The exchange reaction leading to the copolymer formation occurs due to the fact that the poly(amic acid) coexists with a small amount of anhydride and amine form through chain scission and recombination. The exchange reaction takes place either slowly at room temperature or during a slow curing procedure.

Recently, Ree et al. [4] showed that polyimide/polyimide blends can be formed from stable precursors mixtures if at least one of the poly(amic acid)s is replaced by its alkyl ester derivative. The poly(amic alkyl ester) (PAE) form provides a more stable polyimide precursor system than its PAA counterpart by eliminating the possibility for reequilibration reactions.

In the present paper, the polyimide blend system introduced by Ree et al. [4] is used to study the relationship between the miscibility of the precursor mixtures, the drying and curing conditions and the final morphology of the imidized mixtures.

EXPERIMENTAL

Fig.1 shows the chemical structure of 6F-BDAF and PMDA-PDA polymers synthesized for the present study. 6F-BDAF polyamic acids were prepared via classical solution polycondensation of sublimed hexafluoroisopropylidene diphthalic anhydride (6F) with distilled 2,2-bis(4-aminophenoxy-p-phenylene)hexafluoropropane (BDAF) in N-methylpyrrolidone (NMP). The degree of polymerization (DP) was controlled by the monomer stoichiometric imbalance using the diamine in excess. In this way, samples with estimated weight average molecular weight of 10,000 and 48,000 were obtained (DP=10 and DP=50, respectively). Meta-PMDA/PDA poly(amic alkyl ester) was prepared via low temperature solution polycondensation in NMP of the diacyl chloride with freshly sublimed p-phenylene diamine (PDA) [6]. Meta-diethyl dihydrogen pyromellitate was prepared similar to the procedure of Bell and Jewell [7] except that after most of the para-isomer had been selectively removed by slow concentration of the excess ethanol, the remaining ethanol was stripped and the residue twice crystallized from n-butyl acetate. This rendered the meta-isomer in greater than 90 % isomeric purity. The corresponding diacyl chloride was prepared by reaction of the diacid with an excess of oxalyl chloride in ethyl acetate at 60°C. The ethyl acetate was then stripped and the crystalline residue twice crystallized from hexane. The molecular weight of PMDA-PDA precursor measured by light scattering is 200,000.

Transparent common solutions of various PMDA-PDA/6F-BDAF ratios and a total polymer concentrations in the range 15-20% were prepared by mixing of the homopolymer solutions.

PMDA-PDA Polyamic Alkyl Ester

-2 EtOH

PMDA-PDA Polyimide

6F-BDAF Polyamic Acid

-2 H₂O

6F-BDAF Polyimide
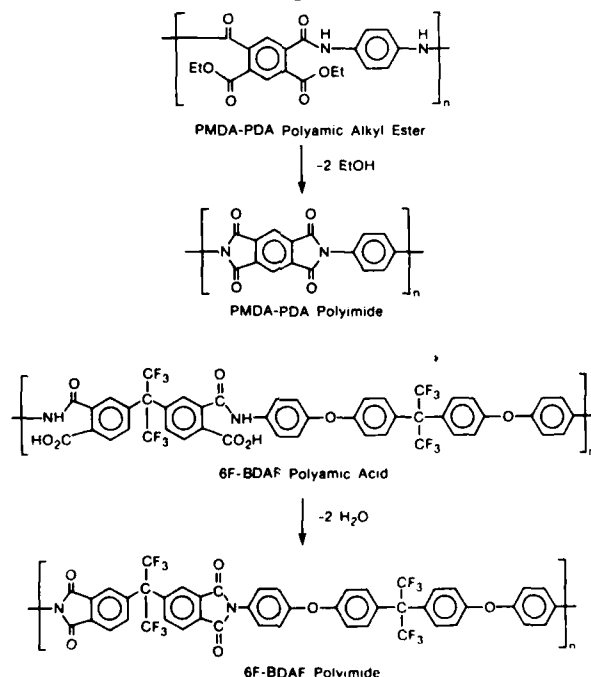
Fig.1. Chemical structure of PMDA-PDA and 6F-BDAF.

The ternary phase diagrams were determined by cloud point measurements performed during isothermal solvent evaporation at 75°C using a 2 mw red He-Ne laser and a photodiode detector positioned at 90° from the incident beam. The compositions corresponding to the binodal curve were calculated based on the weight loss of NMP at the cloud point.

Films of PMDA-PDA/6F-BDAF precursors were prepared either by doctorblading or by spinning, followed by a drying step performed either at 75°C for 90 min. or at 150° C for 15 min. The respective polyimide films were obtained by curing the dried precursor films at 400°C for one hour, using a heating rate of 5°C /min. Film thickness were measured by an Alpha-Step 200 (Tencor Instruments). The morphological observations were made on a Amplival Jena optical microscope operated in the phase contrast mode. The scattered light intensity from flat films was measured as a function of angle at a wavelength of 632.8 nm. The source was a polarized He-Ne laser with output power 1.8 mW, beam diameter 0.75 mm $(1/e^2)$, and beam divergence 1.1 milliradian. The light electric field was perpendicular to the plane of incidence and a film polarizer oriented parallel to the incident polarization was used in front of the PIN photodiode detector, to record the V_V intensity. The measured intensity was corrected for variation in scattering volume and reflectance at the sample surfaces to produce normalized scattering intensity values.

RESULTS AND DISCUSSION

Fig.2 shows the ternary phase diagram of the PMDA-PDA PAE / 6F-BDAF PAA / NMP system measured at 75°C, for two different molecular weights of 6F-BDAF. The compositions are in units of weight fraction, and the numbers on the right side of the ternary diagram are the overall polymer concentration corresponding to the compositions lying along the horizontal lines. Mixtures containing the low molecular weight 6F-BDAF in up to 15% of the solid contents did not show a detectable cloud point. Drying of these cosolutions for up to 40 min. yielded a transparent solid film.
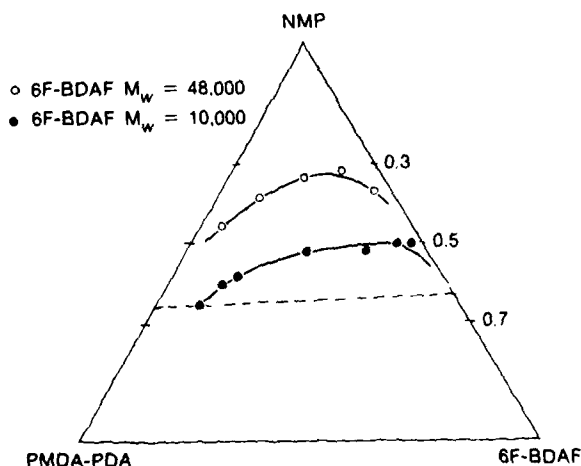
Fig.2. Ternary phase diagrams measured at 75°C (see text).

When dried at low temperatures, polyamic acids are known to be able to solidify while retaining a considerable amount of solvent. This gelation process is characterized by a large increase in the viscosity of the system and it affects some important properties such as planarization [6]. The gelation of polyamic acids in NMP has been attributed to the formation of PAA/NMP complexes stabilized by hydrogen bonding [7 - 9]. In order to investigate the possible effect of the gelation on the phase separation of the ternary mixtures, the drying of the homopolymer solutions was studied by isothermal thermogravimetric analysis. Fig.3 shows a plot of the polymer concentration as a function of annealing time at 75°C. The gelation is characterized by a substantial decrease in the rate of solvent evaporation. For the three solutions studied, the gelation takes place at polymer concentrations in the range of 62-65%.
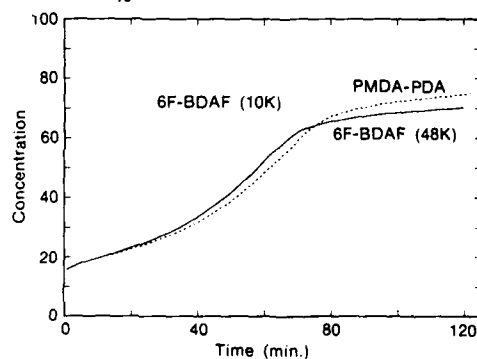
Fig.3. Polymer concentration during drying at 75°C.

The concentrations corresponding to the gelation point are represented by a dotted line in Fig.2. If the binodal curve of the low molecular weight 6F-BDAF mixtures is extrapolated to PMDA-PDA concentrations in excess of 85% of the solid contents, such a line would fall below the gelation line. Thus, the transparency of the mixtures in this composition range is believed to be a consequence of the large viscosity increase occurring at the gelation, which prevents phase separation, at least at long scales.

Fig.4a shows the optical micrograph recorded from a 50/50 PMDA-PDA/6F-BDAF (48K) blend dried at 75°C. The phase separated structure is characterized by spherical domains of diameter in the range of 1-3 μm. The light scattering curve measured from the same film is shown in Fig.4b. The scattering is represented as relative intensity versus the amplitude of the scattering vector q, defined as $q = \frac{4\pi}{\lambda} \sin \frac{\theta}{2}$. The peak in the scattering intensity indicates that the spatial concentration fluctuations have a characteristic wavelength. The domain size of the phase separated structures can be defined as $d = 2\pi/q_{max}$, q_{max} being the scattering vector corresponding to the maximum intensity. Fig.4b also shows that upon imidization, the scattering intensity increases by an order of magnitude while q_{max} remains unchanged ($d = 1.0\mu m$). In other words, the imidization appears to cause an increase in scattering contrast only, without significantly affecting the phase separated morphology. This behavior was observed in all the mixtures studied.
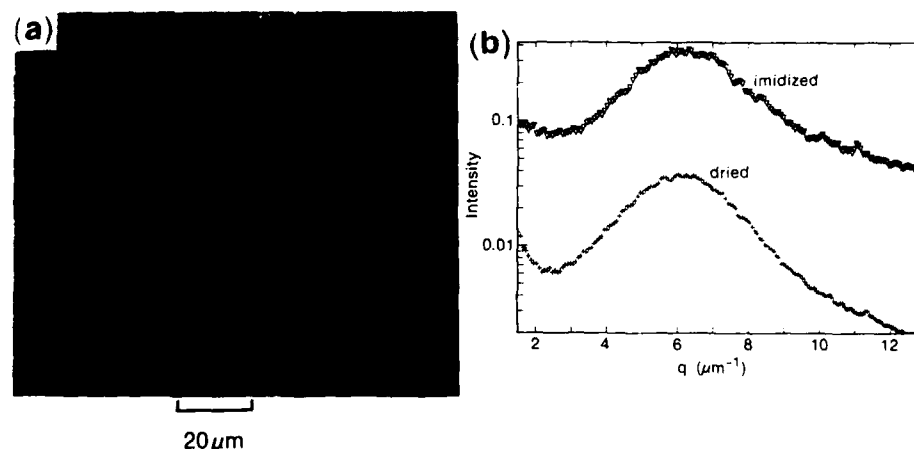
Fig.4. Phase-contrast micrograph from a 50/50 (48K) film dried
at 75 °C (a), and its light scattering curves (b).

Apart from a slight composition dependence, the domain size
measured from the mixtures containing the higher molecular weight
6F-BDAF was found to be insensitive to other parameters such as
drying conditions. This is in contrast to the behavior exhibited
by the blends containing the low molecular weight fluoro-polymer,
which showed that their phase separated morphology can be affected
by the rate of solvent evaporation. This is exemplified for the
most sensitive mixture, i.e., the 75/25 PMDA-PDA/6F-BDAF (10K) in
Fig.5, which shows the effect of film thickness and drying tem-
perature on the shape of the scattering curves. By changing the
thickness of the dried films from 70 to $15\mu m$, the domain size drops
from about 1.0 to $0.6\mu m$, while in the $8\mu m$ thick film, the disap-
pearance of the scattering peak accompanied by the decrease in the
scattering intensity indicates that if any phase separation oc-
curs, it is limited to scales below the wavelength of light. The
effect of thickness is believed to be related to the mass transfer
involved in the solvent evaporation.
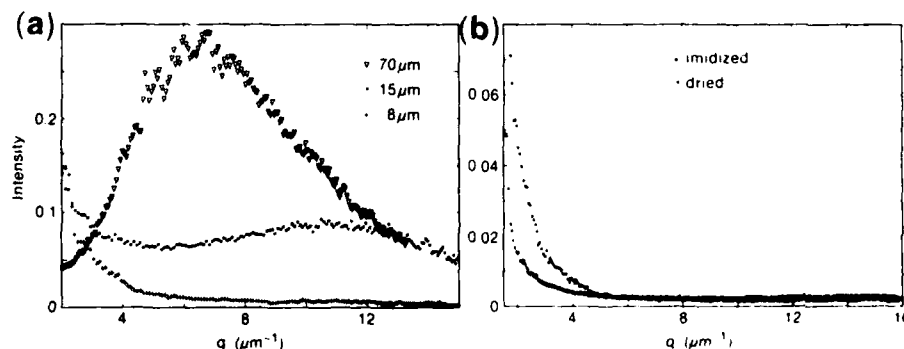
Fig.5. Scattering curves from 75/25 PMDA-PDA/6F-BDAF (10K) films:
(a) dried at 75 °C; (b) a $25\mu m$ film dried at 150°C.

Transparent, homogeneous films were also obtained by drying the 75/25 PMDA-PDA/6F-BDAF (10K) mixtures at 150°C into films of thickness of up to 25μm, which is the limiting thickness for obtaining films at 150°C without the formation of voids. It should be pointed out, however, that the phase diagram as well as the gelation are expected to be a function of temperature, and the effect of drying temperature can not be interpreted in terms of an increased solvent evaporation rate only.

The effect of molecular weight, film thickness, and composition on the domain size can be rationalized as a kinetic effect having to do with the difference in the polymer concentrations corresponding to the onset of phase separation and gelation. The fact that the morphology of the low molecular weight blends was found to be sensitive to the film thickness indicates that the time interval between the onset of the phase separation and the gelation is comparable to the time scale of the structure coarsening. This is in agreement with the observed trend that the sensitivity to such parameters was more pronounced in mixtures for which the binodal concentration is closer to the gelation point.

CONCLUSIONS

The morphology of the polyimide/polyimide mixtures studied was found to be set at the gelation point of the precursor cosolutions. The domain size of the phase separated morphology is affected by parameters such as film thickness and drying temperature, in particular in the more miscible mixtures. Transparent, fully imidized films of a rodlike polyimide containing up to 25% of a flexible component were obtained.

REFERENCES

1. R. Yokota, R.Horiuchi and M. Kochi, J. Polym. Sci.:Part C 26, 215 (1988).

2. C. Feger, in Polymeric Materials for Electronics Packaging and Interconnection, edited by J.H. Lupinski and R.S. Moore, ACS Symposium Series, 407, Washington 114 (1989).

3. M. Ree, D.Y. Yoon and W. Volksen, to be published.

4. M. Ree, D.Y. Yoon and W. Volksen, to be published.

5. V.L. Bell and R.A. Jewell, J. Polym. Sci.:Part A-1, 5, 3043 (1967).

6. S. Nishizaki and T. Moriwaki, J. Chem. Soc. Japan, 71, 1559 (1967).

7. D.R. Day, D. Ridley, J. Mario and S.D. Senturia, in Polyimides, Vol.2, edited by K.L. Mittal, Plenum Press, New York, 767 (1984).

8. P.D. Frayer, in Polyimides, Vol.1, edited by K.L. Mittal, Plenum Press, New York, 273 (1984).

9. M.J. Brekner and C. Feger, J. Polym. Sci.:Part C 25 , 2006 (1987).

10. M.J. Brekner and C. Feger, J. Polym. Sci.:Part C 25 , 2479 (1987).

EQUILIBRIUM AND NON-EQUILIBRIUM PHASES
AND PHASE DIAGRAMS IN BLENDS OF POLYMER
LIQUID CRYSTALS WITH ENGINEERING POLYMERS

WITOLD BROSTOW *, THEODORE S. DZIEMIANOWICZ *, MICHAEL HESS *, **
and ROBERT KOSFELD **
* Center for Materials Characterization and Department of Chemistry, University of North Texas, Denton, TX 76203-5371
* Himont U.S.A., Inc., 800 Greenbank Road, Wilmington, DE 19808
** FB6-Physikalische Chemie, Universität Duisburg, Postfach 10 16 29,
D-4100 Duisburg 1, Federal Republic of Germany

ABSTRACT

This work represents a continuation of earlier studies of blends of polymer liquid crystals (PLC) with ordinary engineering polymers (EP). We now focus on connections between mechanical and other properties and phase structures and phase diagrams. Pure PLC are already two-phase systems; in each case addition of an EP complicates the situation further. In particular, we are concerned with phases which we call quasi-liquids, at temperatures between the glass transition and the melting point. Quasi-liquids do not have the mobility usually associated with liquids - because of the presence of other constituents and also because of orientational effects produced by the mesogenic groups. In phase diagrams of PLC-containing systems one should also take into account non-equilibrium phases. We are trying to show how such diagrams make possible intelligent processing and a better control of properties of the PLC + EP materials.

INTRODUCTION

This paper represents a continuation of earlier work [1-4] aimed at mixing polymer liquid crystals (PLC) with ordinary engineering polymers (EP) in such a way that the valuable properties of PLC (reinforcement by mesogenic groups, stability at high temperatures, low isobaric expansivity, etc.) are preserved while costs are lower than that of pure PLC. However, in the present study we deal with variation of LC content in a series of PLC copolymers, while blends of one of these PLCs with an EP are dealt with in a companion paper [5].

While in earlier papers we used a variety of techniques and covered a wide range of properties, the present work is focused on phase structures and phase diagrams. Reasons for this are stated in the following Section.

PHASE STRUCTURES, PHASE DIAGRAMS AND INTELLIGENT PROCESSING

Properties of materials, polymeric or otherwise, are of course deter-
mined by chemical composition as well as by structures produced during pro-
cessing. For PLCs the situation is more difficult than for EPs; we know al-
ready from the first paper by Jackson and Kuhfuss [6] how easily acquire
PLCs orientation during processing; high anisotropy of properties ensues.
While in some cases the anisotropy is desirable, control of the resulting
properties is possible only if we have sufficient knowledge of morphologies
and phase structures, and also if we can locate each structure in the cor-
responding region in the phase diagram. While much interesting and useful
work on processing of PLCs and their blends has already been done, our par-
ticular approach consists in the determination of the appropriate phase
diagram first, and defining processing conditions only afterwards; we call
this approach intelligent processing. In the present paper we define some
peculiarities of phase diagrams of PLC-containing systems, and also we
present one phase diagram. A striking example of how knowledge of the
phase diagram makes intelligent processing possible is provided in the
companion paper [5].

It is customary to show in phase diagrams equilibrium phases only.
However, PLC-containing systems, apparently because of the presence of
rigid constituents, seem to show non-equilibrium phases with high longe-
vity. Hence, just as for inorganic glasses, we have to take these phases
seriously into account; sluggishness combined with easy orientation of
mesogens in PLCs affects processing and resulting properties to a high deg-
ree. Consequently, we postulate that non-equilibrium phases should be
included in phase diagrams of PLCs and PLC-containing systems.

In the course of our work we have dealt often with a phase which we
believe deserves a name: quasi-liquid. This is a the non-crystalline part of
a semi-crystalline polymer between its glass transition temperature and the
melting temperature. Except for elastomers when one then talks about the
leathery state (see for instance [7]), one calls such materials simply liquids.
However, in the case of PLCs in particular, that name is not appropriate;
not only the material does not exhibit the ordinary liquid mobility, but we
are more than one phase transition away from the isotropic liquid arising
from the same component. Further, the material is sluggish because of
the simultaneous presence of the crystalline component; while this is also
true for polymer "liquids" in ordinary semi-crystalline polymers, in PLCs
there is an additional contributions to sluggishness or to maintaining low
mobility because of rigidity of the mesogens. Finally, it is in the quasi-
liquid phase that the process of cold crystallization can occur.

CHOICE OF THE SYSTEM

A variety of structures of PLCs is possible, as classified by one of us [8,9]. The reason for the development of this classification is the fact that properties of a given PLC are defined first of all by the class to which it belongs. For this reason, in a number of cases it is not enough to talk about main-chain PLCs, since these can be longitudinal, orthogonal, stars, soft discs or rigid discs [8,9]. In the present work we have chosen a longitudinal PLC since at the present time these seem to be best known and understood. In particular, we have chosen the copolymers of poly(ethylene terephthalate) (PET) with p-hydroxybenzoic acid (PHB) studied already earlier by us [1-4] as well as by a number of other authors from different points of view [6, 10-18].

THE PHASE DIAGRAM

We have studied the phase diagram of PET/xPHB copolymers in function of the mole fraction x of the liquid crystalline (that is PHB) component. In the determination we have used a variety of techniques, including differential scanning calorimetry (DSC), wide-angle X-ray scattering (WAXS), thermomechanical analysis (TMA), as well as dynamic mechnical testing with a torsional pendulum. Some measurements on samples of the same composition were performed at several locations; hence this international collaboration. Because of the limited space, we do not provide here experimental details.

The resulting diagram is shown in Fig. 1. Non-equilibrium transition lines are included. We believe that in general they have to be included, since some non-equilibrium phases have fairly long lives; inorganic glasses come to mind in this context.

The regions in the diagram marked with Roman numbers contain the following phases:

I = PET crystals
   isotropic glass
II = PET crystals, PHB crystals
   isotropic glass, nematic glass
III = PET crystals, PHB crystals
   nematic glass
   quasi-liquid
IV = PET crystals
   quasi-liquid
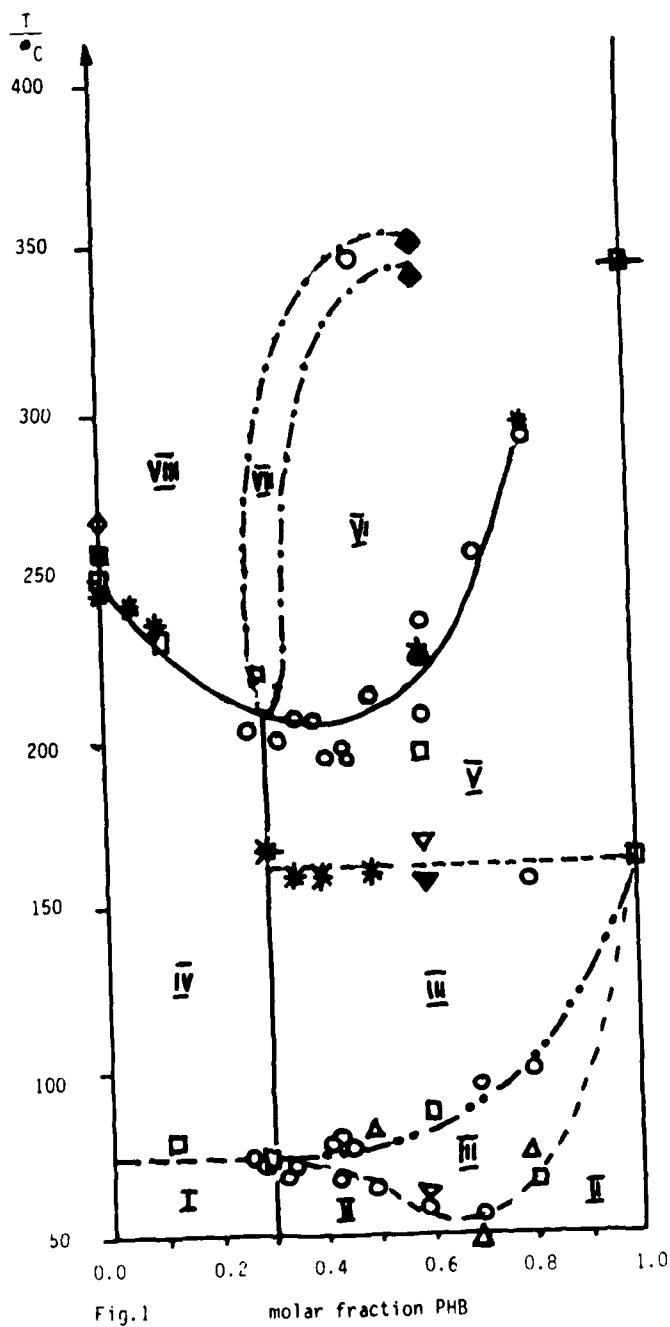
Fig.1   molar fraction PHB

V = PET crystals, PHB crystals
    quasi-liquid
VI = nematic
VII = nematic, liquid
VIII = liquid

The symbols in the diagram correspond to the following sources:

○ - This work, independently of the technique used and also inde-
pendently of the location where the experiments were performed.   Hence
some points come from more than one technique and/or more than one labo-
ratory
     ☐ - Meesiri et al. [12]
     ■ - Jeziorny [18]
     ◊ - Chou et al. [17]
     ◆ - Viney et al. [11]
     △ - Benson et al. [15]
     ▽ - Gedde et al. [14]
     ▼ - Hedmark [16]
     * - Jackson et al. [6]
     ☐ - Kricheldorf et al. [13]

An analysis of connections between the phases present and their posi-
tion in the diagram and properties will be presented in subsequent papers, in
part already in the companion paper [5].

References

1. R. Kosfeld, M. Hess and K. Friedrich,   Mater. Chem. & Phys. 18, 93
   (1987).
2. W. Brostow, T.S. Dziemianowicz, J. Romanski and W. Werber, Polymer
   Eng. & Sci. 28, 785 (1988).
3. K. Friedrich, M. Hess and R. Kosfeld, Makromol. Chem. Symp. 16, 251
   (1988).
4. F. Schubert, K. Friedrich, M. Hess and R. Kosfeld, Molec. Cryst. Liq.
   Cryst. 155, 477 (1988).
5. R. Kosfeld, F. Schubert, M. Hess and W. Brostow, the following paper in
   the same MRS Symp. Proceedings volume.
6. W.J. Jackson Jr. and H.F. Kuhfuss, J. Polymer Sci. Chem. 14, 2043
   (1976).
7. W. Brostow and R.D. Corneliussen, In Failure of Plastics, edited by W.
   Brostow and R.D. Corneliussen (Hanser Publishers, Munich - Vienna -
   New York, 1986), Chapter 1.

182

8. W. Brostow, Kunststoffe 78, 411 (1988).
9. W. Brostow, Polymer 31, in press (1990).
10. J. Menczel and B. Wunderlich, J. Polymer Sci. Phys. 18, 1433 (1980).
11. C. Viney and A. H. Windle, J. Mater. Sci. 17, 2661 (1982).
12. W. Meesiri, J. Menczel, U. Gaur and B. Wunderlich, J. Polymer Sci. Phys. 20, 719 (1982).
13. H. R. Kricheldorf, G. Schwarz, Makromol. Chem. 184, 475 (1983).
14. U. W. Gedde, D. Buerger and R. H. Boyd, Macromolecules 20, 988 (1987).
15. R. S. Benson and D. N. Lewis, Polymer Commun. 28, 289 (1987).
16. P. Hedmark, Ph.D. thesis, The Royal Institute of Technology, Stockholm, 1988.
17. Ch. Chou and S. B. Clough, Polymer Eng. & Sci. 28, 65 (1988).
18. A. Jeziorny, Polimery 34, 210 (1989).

STRUCTURE AND PROPERTIES OF BLENDS OF POLYCARBONATE
AND POLY(ETHYLENE-TEREPHTHALATE-CO-p-HYDROXYBENZOATE):
PHASE DIAGRAM AND MECHANICAL BEHAVIOR

ROBERT KOSFELD*, FRANK SCHUBERT*, MICHAEL HESS*, ** and WITOLD
BROSTOW**
* Department of Physical Chemistry, University of Duisburg,
  D-4100 Duisburg, Federal Republic of Germany
**Center for Materials Characterization and Department of Chemistry,
  University of North Texas, Denton TX 76203-5371

ABSTRACT

The investigation of the thermal behavior of polymer blends leads to
phase diagrams which involve important information about the system.
From these diagrams, equilibrium as well as non-equilibrium phases can
be deduced and ranges of miscibility or partial miscibility of the polymers
become obvious. Hence the diagrams are of a great value for processing of
advanced polymer blends, especially if a polyphasic polymers such as
a polymer liquid crystal is one of the constituents of the system.

INTRODUCTION

Polymer blending has become a promising method in the search
for polymeric materials with enhanced thermal and mechanical properties
(and sometimes also with lower prices). To achieve this, studies were
made on blends of ordinary engineering plastics (EP) with polymer liquid
crystals (PLC) in order to preserve high-temperature stability, reinforce-
ment by mesogenic groups, low thermal expansivities, etc. The large
number of polymers available and the different methods of mixing open
the way to numerous products. With a detailed knowledge of interrela-
tions between blending procedures, morphology of the resulting blend,
and mechanical as well as thermal behavior of the product, new mate-
rials can be tailored for sspecific applications

In earlier studies [1-4] the copolyester of poly(ethylene terephtha-
late and p-hydroxybenzoate (COP) was investigated in blends with poly-
(carbonate) (PC) and poly(ethylene terephthalate) (PET). Transesterifica-
tion, phase behavior in the ternary system with solvent and solid state
morphologies of the pure copolyester were studied. The thermal behavior
of different compositions of the copolyester is reported in [5].

MATERIALS

The liquid crystalline material used in this study is a COP containing 40 mole % PET and 60 mole % p-hydroxybenzoate (PHB). This material, with weight-average molecular mass M = 19,000, was first prepared by Jackson and Kuhfuss [6]. As discussed in [2], the polymer shows a two-phase morphology with island structure; see also [5] and papers cited therein. The EP was a poly(bisphenol-A-carbonate) with M = 31,000.

Most of the blends were prepared by dissolving certain amounts of the pure polymers in a chloroform + trifluoroacetic acid solvent system and subsequent combined precipitation of both polymers from this solution with acetone. The precipitate was dried under vacuum and then compression molded or extruded.

EPERIMENTAL TECHNIQUES

The blends were analysed with light- and electron- microscopes; calorimetric experiments were carried out with a Perkin-Elmer DSC-2 ; thermomechanical analysis was done using a Perkin-Elmer TMA; and the dynamic-mechanical analysis was performed with a torsion pendulum working at a constant frequency of 1 Hz made by Myrenne, Roetgen, FRG. WAX studies were executed with synchroton radiation at DESY in Hamburg.

RESULTS AND DISCUSSION

From light microscopy it became obvious that phase separation occured in the whole concentration range and that application of pressure resulted in a fine and very homogeneous distribution of the phases . The identification of the phases could be done as only the frozen-in nematic structures of the PLC are birefringent.

Calorimetry and dynamic mechanical analysis showed that there exists a very complex phase structure with several non-equilibrium phases. The localisation and the dimensions of these non-equilibrium phases is strongly infuenced by the degree of dispersion of the phases and by the thermal history of the sample. The non-equilibrium phases can be stabilized in a metastable state.

The most important part of the phase diagram with respect to the mechanical properties is shown in Fig. 1. A more detailed discussion of the whole diagram (broken vertical lines, the nature of various phases) will be the subject of future papers.
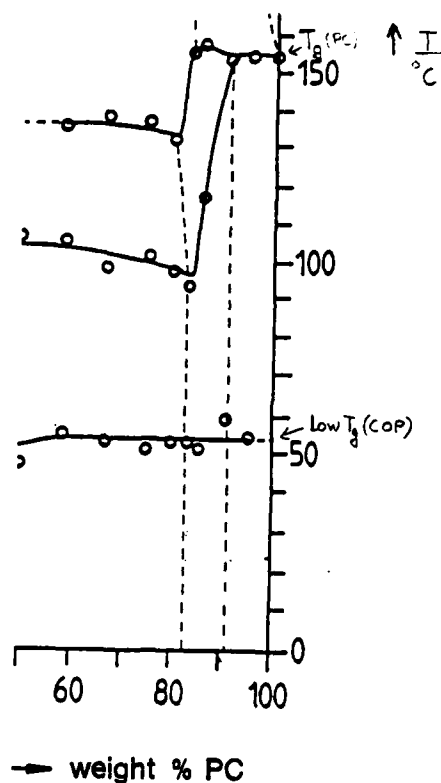
Fig. 1   A part of the phase diagram of COP containing 60 mole % PHB with
PC. Note the partial miscibility between 80 and 90 weight % PC.

The experiment also showed that the presence of COP assists - in fact ma-
kes possible - the nucleation of PC crystals; see Fig. 2.   In pure PC under
identical conditions the nucleation was not observed. COP did crystallize
too; the PHB-rich phases of COP could be identified as the regions where
the crystallization took place; see Figures 3 and 4.

Fig. 5 shows the influence of annealing on the dynamic-mechanical
behavior. The storage modulus is increased; the second glass transition
line, which can be attributed to PC, is less steep.

In Fig. 1 there is a region of partial miscibility between about 80
and 90 mole % PC. In this concentration range PC is capable of incorpora-
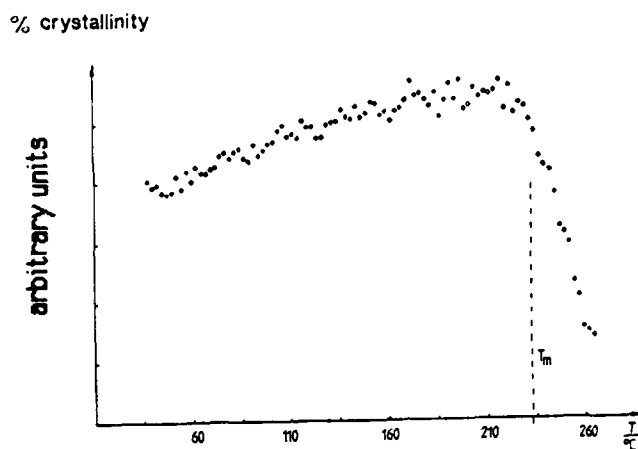
% crystallinity

Fig. 2   Change in crystallinity during a heating process which lasted 45 min.   WAXS experiment with synchrotron radiation.   80 weight % PC.
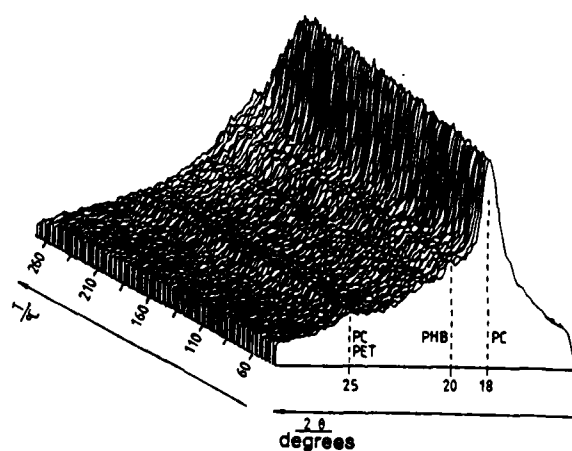
Fig. 3   Temperature-dependent WAXS.   80 weight % PC.
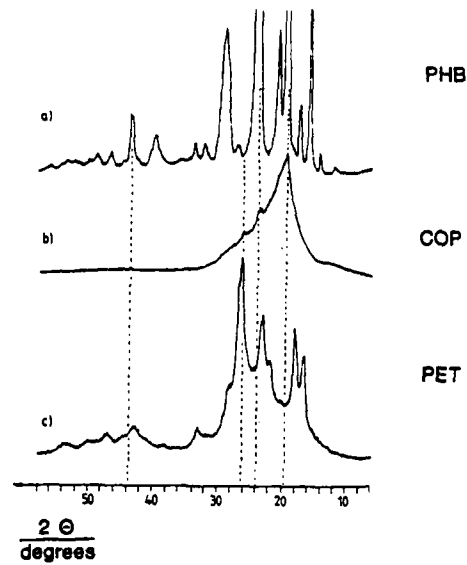
Fig. 4   WAXS powder diagram at 25°C.
a) Poly (PHB) with high crystallinity;
b) COP annealed for 18 hours at 4 MPa and 210-220°C;
c) PET annealed for 60 min at 4 MPa and 210-220°C.
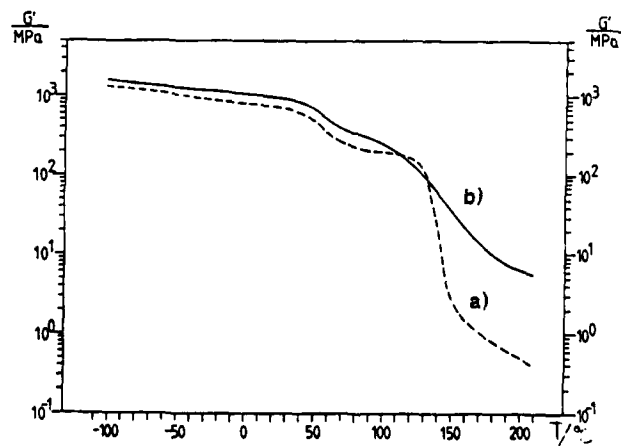
Fig. 5   Influence of sample preparation (crystallinity) on the storage modulus G'.
a) blend with 67 weight % PC annealed for 1 min.;
b) blend with 67 weight % PC annealed for 180 min.
Conditions: 4 MPa and 210-220°C.

188
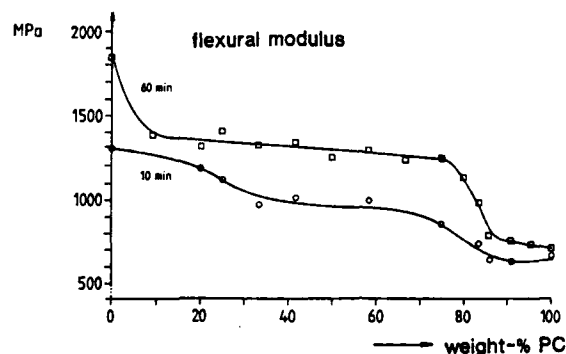
Fig. 6   Influence of crystallinity and composition on compression-molded
samples. Conditions: 4MPa and 210-220°C.

ting certain amounts of COP, as demonstrated by the decrease of the
glass-transition temperature of PC. By contrast, COP does not incorpo-
rate PC: there is no altering of the glass transition temperature of COP at
≈ 50°C.   As a consequence of the partial miscibility in this narrow con-
centration range, COP fibres which may be formed during an extrusion
process are glued together by a thin layer of PC.   This results in an inc-
rease of the flexural modulus which begins just in the concentration range
where partial miscibility is observed; see Fig. 6.   Further results related
to the flexural modulus, shear behavior and the relationship of properties
to the phase diagram of the pure COP [5] are in preparation.

ACKNOWLEGEMENT

REFERENCES

1. R. Kosfeld, M. Hess and K. Friedrich, Mater. Chem. & Phys. 18, 93
    (1987).
2. W. Brostow, T.S. Dziemianowicz, J. Romanski and W. Werber, Polymer
    Eng. & Sci. 28, 785 (1988).
3. K. Friedrich, M. Hess and R. Kosfeld, Makromol. Chem. Symp. 16, 251
    (1988).
4. F. Schubert, K.Friedrich, M. Hess and R. Kosfeld, Molec. Cryst. Liq.
   Cryst. 155, 477 (1988).
5. W. Brostow, T.S. Dziemianowicz, M. Hess and R. Kosfeld, preceding pa-
    per in the same MRS Proceedings volume.
6.   W.J. Jackson and H.F. Kuhfuss, J. Polymer Sci. Chem. 14, 2043 (1976).

CHARACTERIZATION OF POLYQUINOLINE BLENDS USING SMALL ANGLE SCATTERING

WEN-LI WU*, JOHN K. STILLE**, JOSEPH W. TSANG** AND ALEX J. PARKER**

*Polymers Division, Materials Science and Engineering Laboratory, NIST, Gaithersburg, MD 20899
**Colorado State University, Fort Collins, CO

ABSTRACT

To determine the compatibility between the rigid rod and the flexible chain polyquinolines, both small angle x-ray and neutron scattering measurements were conducted on blends containing deuterated flexible chains. The scattering intensities from both x-ray and neutron were reduced to their absolute scales in order to remove the scattering contribution from microvoids which tended to overshadow the signal of molecular origin. Quantitative information regarding the molecular dispersion in a 50/50 rigid rod and flexible chain blend was obtained. The result indicated that this material was partially segregated but not to the point of single component phases.

INTRODUCTION

Polyquinoline[1] is a candidate for molecular composites. In a molecular composite, rigid rod molecules are dispersed in a matrix of a flexible polymer, and thus individual molecular rods act as the reinforcing fibers. Molecular composites have the potential to combine the performance of a conventional composite with easy processing of thermoplastics while retaining excellent properties at high temperature. In an ultimate molecular composite, each molecular rod should be completely surrounded by flexible polymer molecules. There is, however, a strong tendency for the rigid rod molecules to aggregate and separate on a larger scale. To overcome this problem, a number of modifications to chemical compositions are being explored. There is still a need to develop test methods to characterize the degree of dispersion in these materials such that progress can be quantified. It has been demonstrated by the present authors that small angle scattering (SAS) is a viable technique for the structure determination of molecular composites in bulk[2]. The presence of microvoids has hampered the use of SAS for quantitative measurements of rigid rod polymers and their blends. To circumvent this difficulty, both small angle neutron and x-ray (SANS and SAXS) experiments were carried out on the same specimen. Because of the differences in the scattering contrast factors of the voids between x-ray and neutron scattering, the void contribution to the scattering intensity can be estimated and then removed.

This SAS scheme has been applied successfully to a polyquinoline multiblock copolymer composed of rigid rods and flexible blocks[2]. The result suggested that this copolymer was strongly associated but not yet segregated into phases of single components. The sample was prepared by a solution casting method, and it took a significant amount of time for the polymer to precipitate. In the present work the film samples were prepared by using the extrusion equipment at the Wright Patterson Air Force laboratory. The extrudate was rapidly coagulated in a nonsolvent bath. It is conceivable that the extent of mixing can be improved through this extrusion process. Both copolymer and blend samples were prepared. The SAS results for the copolymer, as will be shown later, support the notion that extrusion provides improved mixing compared to the solution

casting samples.

EXPERIMENTS

The multiblock copolymer used in this work has a number average molecular weight of 150,000, with each block having a value of about 17,000. This value corresponds to a degree of polymerization (DP) of 30 for each block. The blends were made of 50/50 rigid rod and flexible chain polyquinolines and their DPs were 660 and 330 respectively. The details for the chemical structure and the synthesis of this material can be found elsewhere[1]. The flexible chain component in both the block copolymer and the blends was partially deuterated to enhance the neutron scattering contrast. To prepare the SANS and SAXS samples a number of layers of the extruded films were stacked to randomize the molecular orientation within individual films.

A deuterated polyethylene (DPE) specimen was used to cross-calibrate the SANS and the SAXS instruments. Both the SANS and SAXS measurements were conducted at the NIST facilities. A silica gel specimen was used as the secondary absolute intensity standard for the SANS measurements.

RESULTS AND DISCUSSION

Based on the density values of the copolymer and the homopolymers, one has the following contrast factors for SAXS and SANS[2] intensity, I(q), expressed in their absolute scales.

$$I_{SAXS}(q) = 9.23 \ V(q) + 3.37 \times 10^{-2} S(q). \tag{1}$$

$$I_{SANS}(q) = 0.855V(q) + 9.46 \times 10^{-2} S(q). \tag{2}$$

V(q) and S(q) are the structure factor of the voids and the polymer respectively. Both quantities are expressed in terms of v which is the molar volume of the repeat unit of a rigid rod segment, and its value is $6.995 \times 10^{-22} cm^3$ corresponding to a bulk density of 1.32. The material studied in this work is composed of three components; they are microvoids, rigid and flexible chains with each component having a different scattering cross-section. Equations 1 and 2 are merely an approximation of a three-component scattering theory[3] for the case in which the volume fraction of the microvoid is rather small in comparison with the other two components. It is noteworthy that the volume fractions of the voids and the polymers are included in these factors V(q) and S(q).

The calculated results for V(q) and S(q) for the block copolymer are given in Figure 1. The height of the S(q) maximum is about 70, and it is substantially less than 400 as observed in the solution cast film[2]. Based on this finding we conclude that the extruded film has a more homogeneous molecular structure than the solution cast one. As was estimated in a previous publication[2], the peak height for the block copolymers with an ideal mixing is only 1.43. Apparently the extent of the molecular dispersion in the extruded film is still far from ideal; partial segregation between the rigid rod and the flexible chain polyquinoline still prevails.

The SAXS and the SANS results for the homopolymer blend lead to the results given in figure 2. The theoretical value of S(q) will be estimated for the ideal case in which all the chains are randomly dispersed regardless of their compositions or their rigidity. For this case one has the following expression for S(q)[4]:

$$\frac{1}{S(q)} = \frac{1}{S_{11}(q)} + \frac{1}{S_{22}(q)} - 2\chi \tag{3}$$

χ is the Flory-Huggins interaction parameter and $S_{11}(q)$ is the single chain correlation function for the flexible chain polymer. $S_{22}(q)$ is then the correlation function for the rigid rod. It is noteworthy that the factor involving the volume fraction is included in the functions $S11(q)$ and $S22(q)$.
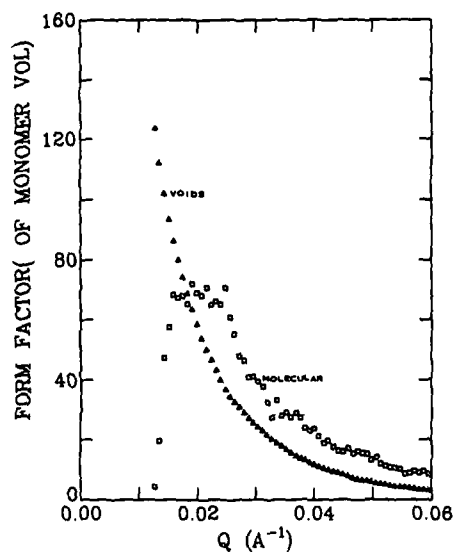
Figure 1: Form factors of the microvoids and the multiblock polyquinoline. The sample was prepared by a extrusion and followed by a rapid coagulation process.
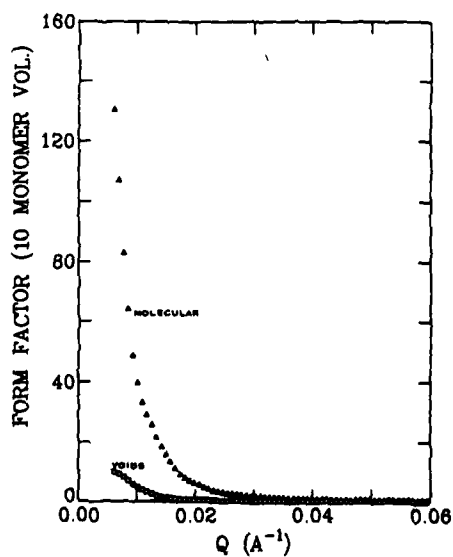
Figure 2: Form factors of the microvoids and the blend of high molecular weight polyqu olines.

Based on the DP values of 330 and 660 and the radii of gyration of 159 Å and 860 Å for polymer 1 and 2 respectively the calculated result of equation 3 is given in figure 3. The radius of gyration of the rigid rod is obtained from a light scattering measurement [1] and the value for the flexible one is estimated from a freely joint chain model; the monomer length in its fully extended state was chosen as the step length. The solid curve on figure 3 is for the case in which χ equals zero and the dashed line is for χ equal to 0.004 which is close to the critical value for phase separation. By comparing the experimental result (solid circles on the same figure) to the theoretical ones we conclude that the extent of segregation present in this blend is beyond that which can be described by a mean field theory such as equation 3.
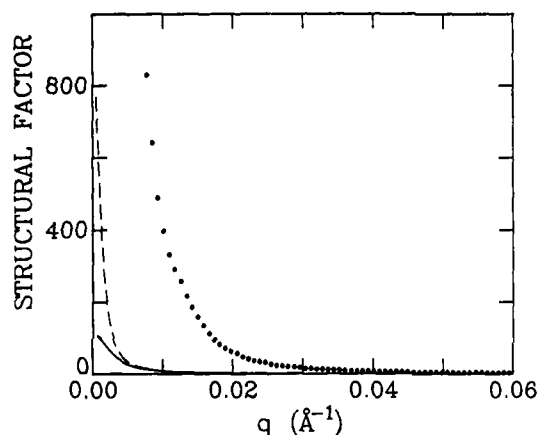
Figure 3: The theoretical form factor of the blend using equation 3; solid line for χ=0, dashed line for χ=.004. The experimental result of data points of figure 2 are also shown.

For a partially segregated blend, the form factor of the cluster can be approximated by a Debye type correlation function shown in equation 4 where ξ denotes the correlation length of the composition fluctuation.

$$\gamma(r) = \exp\left(-\frac{r}{\xi}\right) \tag{4}$$

The corresponding form factor in Fourier space is given as

$$S(q) = \frac{8\pi}{v}\,\phi(1-\phi)(\delta c)^2\,\frac{\xi^3}{(1+\xi^2 q^2)^2} \tag{5}$$

where δc stands for the amplitude of the composition fluctuation. The value of δc is unity for a completely segregated blend and zero for an ideal solution. The term ϕ denotes the volume fraction occupied by the rigid rod rich phase, hence $1-\phi$ is for the flexible chain rich phase.

The best fit between the experimental results and equation 5 is given in figure 4 via a Zimm type plot. The upward curvature of the experimental results in figure 4 explains why equation 2 fails to accommodate the experimental result. The best fit value of ξ is 115Å and the prefactor is 0.0015. By assuming the value of ϕ be 0.5, an ideal value for the case of a matched molecular weight between these two polyquinolines, the value of δc can be calculated according to the best fit value of the prefactor and gives a result of 0.4. This δc value suggests that the local compositional fluctuation of the rigid rod or the flexible chain is ∓20% from the mean value of 0.5. For a completely segregated blend the values of ϕ and δc are 0.5 and 1.0 respectively.

This results in a prefactor of 0.009 which is significantly greater than the best fit value of 0.0015. It is also noteworthy that the value of ξ is much less than 890Å ,the R_g of the rigid rod molecule. One possible explanation is that the rigid rod rich phase has the shape of a thin cylinder, and the value of ξ reflects the average lateral dimension of this cylindrical object.
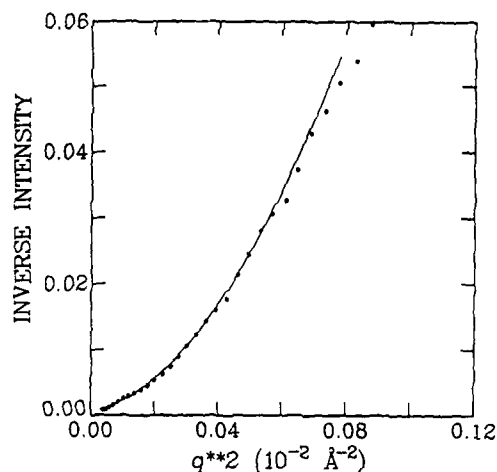
Figure 4: The data points for the observed form factor of the blend presented via a Zimm type plot. The best fit result using equation 5 is given as the solid line.

In figure 4 some deviation of equation 5 from the experimental data can be observed in the high q region, i.e. in the region of $\xi q \gg 1.0$. This is expected since equation 5 is merely an approximation of the scattering intensity for the low q region. In the high q region the intensity should decrease as q^{-1} or q^{-2} depending the local chain conformation in this partially segregated blend.

CONCLUSION

The high molecular weight polyquinoline blend studied in this work is partially segregated with a correlation length of 115Å which is much less than the R_g of the rigid rod molecules. Results for the block copolymer indicate that the extrusion process enhances the mixing of this material.

ACKNOWLEDGEMENT

REFERENCES

[1]   J. K. Stille, Macromolecules 14:870 (1981).   J. K. Stille, A. Parker, J. Tsang, G. C. Berry, M. Featherstone, D. R. Uhlmann, S. Subramoney, W. L. Wu, Contemporary Topics in Polymer Science, 6, (1989).
[2]   W. L. Wu, J. K. Stille, J. Tsang, and A. Parker, Proceedings of MRS meeting, Symposium J. (1988).
[3]   W.L.Wu, Polymer 23: 1907 (1982).
[4]   L. Leibler, Macromolecules 13: 1602 (1980).

Blends/IPN's

MISCIBILITY IN BLENDS OF POLYBENZIMIDAZOLE AND FLUORINE CONTAINING
POLYIMIDES

Hiroaki Yamaoka*, Norman E. Aubrey, William J. MacKnight** and Frank E. Karasz**
*Mitsubishi Monsanto Chemical Company, Yokkaichi Research & Development Dept.
1 Toho-Cho Yokkaichi-City, Mie, JAPAN
**Polymer Science & Engineering Dept., University of Massachusetts, Amherst, MA
01003

ABSTRACT

Blends of polybenzimidazole (PBI) with either of two fluorine-containing polyimides
were prepared by casting from solution and by precipitation. Dynamic mechanical
thermal analysis (DMTA) and differential scanning calorimetry (DSC) were used to study
miscibility in the two blend systems.
The blends of PBI with the first polyimide, the polysulfonimide PI-1, consisted of a
single phase when the blends contained less than 30 wt% PI-1; above 50 wt% PI-1,
phase separation occurred even at room temperature. The PBI blends containing the
second polyimide, PI-2, were immiscible.

INTRODUCTION

Miscible polymer blends consisting of high performance polymers, aromatic
polybenzimidazoles and polyimides, have been studied for several years [1-4].
Miscibility in these blend systems was confirmed by the presence of single, composition-
dependent T_g's lying between those of the constituent polymers, by well-defined
composition-dependent tan δ peaks associated with the glass transition and by the
formation of clear films.
In this contribution, the phase behavior in blends of polybenzimidazole (PBI) with two
fluorine containing polyimides, PI-1 and PI-2, is presented.

EXPERIMENTAL

Materials and blend preparation

Poly-2,2'-(m-phenylene)-5,5'-bibenzimidazole (PBI) (Hoechst-Celanese) was
used as the representative polybenzimidazole. The fluorine containing polyimides, PI-1
and PI-2, with the structures shown below were prepared by NASA-Langley.
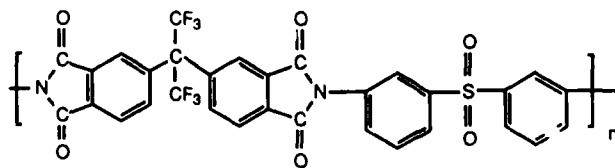
PI-1
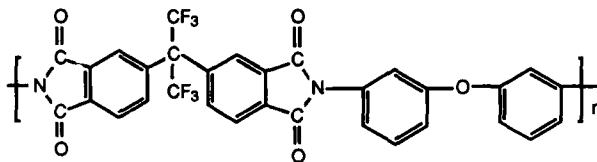
PI-2

Elemental analyses of PI-1 and PI-2 were performed by the University of Massachusetts Analytical Laboratories. $\overline{M}_w$ and $\overline{M}_n$ were obtained by size exclusion chromatography (SEC) using dimethylformamide as solvent at 60°C. Four columns of pore sizes 10^6, 10^5, 10^4 and 500 Å were used and were calibrated with poly(methyl methacrylate) standards. The results of elemental analysis and SEC are listed in Table I.

Table I
Elemental Analysis and SEC results for PI-1 and PI-2

Elemental Anaylses	$\overline{M}_w$	$\overline{M}_n$	$\overline{M}_w/\overline{M}_n$	T_g (°C)
PI-1				
Calc. C: 56.71% H: 2.13 N: 4.27 F: 17.37 S: 4.87	17.2	3.1	5.5	276
Found C: 54.88 H: 2.57 N: 4.08 F; 17.50 S: 4.96	x 10^5	x 10^5		
PI-2				
Calc. C: 61.18 H: 2.30 N: 4.61 F: 18.75	67.0	36.8	1.82	232
Found C: 61.22 H: 2.55 N: 4.65 F: 19.07	x 10^5	x 10^5		

Blends were prepared by mixing 3% (w/v) solutions of PBI and polyimides in N,N-dimethylacetamide (DMAc) in the desired proportions. The polyimides dissolved readily in DMAc under ambient conditions but even in a pressure vessel at 225°C, PBI left an insoluble residue which was removed by filtration. Films of PBI/PI-1 and PBI/PI-2 blends were prepared by casting 3% (w/v) solutions on glass plates. The solvent, DMAc, was evaporated under dry N_2 by heating to 80°C for 48 hours. The films were dried further under vacuum with a gradual increase in temperature, from 100 to 220°C in 20°C increments. Each temperature was held for two to three days; finally the films were held at 220°C for 7 days, until thermogravimetric analysis (TGA) showed less than 0.2% weight loss in a heating cycle from 100 to 350°C.

Precipitated blends were prepared by adding excess methanol to solutions containing PBI and the appropriate polyimide. A fine powder was obtained which was washed with water to remove residual DMAc and vacuum dried in the same way as the films. Residual solvent was also assessed by TGA. Differential scanning calorimetry (DSC) measurements were made on samples with residual solvent contents of less than 0.2 wt%; film and powder samples gave identical results.

Dynamic mechanical analysis and differential scanning calorimetry

Dynamic mechanical analysis (DMTA) experiments were carried out using a Polymer Laboratories DMTA equipped with a high temperature (500°C) head under dry

N_2. Films about 0.2 mm thick were used in the flexural mode, under constant strain, at 1 Hz. The scanning rate was 4°C/min in the temperature range from 150 to 450°C.

Differential scanning calorimetry (DSC) experiments were made under N_2 using film and powder samples with a Perkin-Elmer DSC-7 differential scanning calorimeter controlled by a 7500 PC. The heating rate was 20°C/min.

A Perkin-Elmer thermogravimetric analyzer was used to measure the residual solvent content of film and powder samples. The heating rate was 20°C/min and the experiments were performed under N_2.

RESULTS AND DISCUSSION

PBI/PI-1 blends

It is important to note that the blend samples were not heated above 220°C prior to determining T_g's. Thus the phase relationships observed in these systems can be regarded
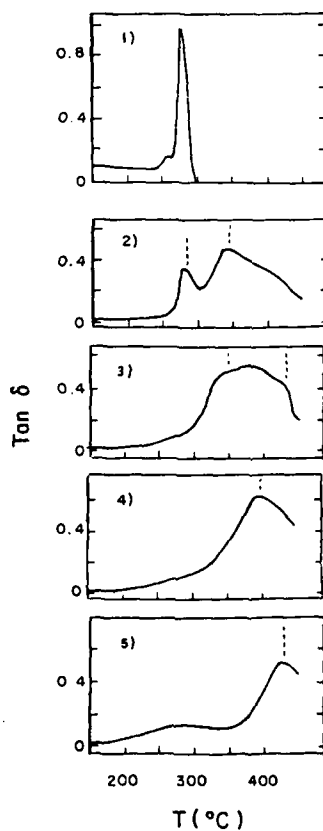
Fig. 1

Dynamic mechanical analysis of PBI/PI-1 Blends
1) PI-1, 2) PBI/PI-1:25/75 wt%, 3) PBI/PI-1: 50/50 wt%
4) PBI/PI-1: 75/25/wt %, 5)PBI

as stable to 220°C (or at least unchanging within the time scale of the experiment).

Figure 1 shows single, composition-dependent tan δ peaks indicating miscibility for the PBl/PI-1 blend up to a blend composition of about 30 wt% PI-1. The observed clarity and strength of the cast films is consistent with these results; the 85/15, 75/25 and 70/30 wt % PBl/PI-1 blends are clear and strong as expected of miscible, one-phase polymer systems.

When the PBl/PI-1 blend contained more than 50 wt% PI-1, two phases are observed for both film and powder samples. One phase, which appears to be a mixed phase has a T_g of about 345°C. According to the Fox equation [5] this T_g corresponds roughly to a blend composition of 50/50 wt% which appears to be the composition around which the limit of miscibility in the PBl/PI-1 bend system is reached. The second phase, with a T_g of 275°C corresponds to pure PI-1 (Fig. 1-(2)). At the blend compositions of 60/40 and 50/50 wt% a single, broad tan δ peak is observed (Fig. 1(3)). The broadening may be ascribed to phase separation which occurs as the sample is heated to temperatures above its T_g and may result in the presence of higher T_g mixtures whose damping behavior is then measured as the temperature is increased. The PBl/Ultem 1000 system [1,3] shows the same behavior except that these two polymers are miscible over the entire composition range.

The films cast from solutions of PBI and PI-1 have a physical appearance which is consistent with the phase behavior in these blends. The films become more opaque and' their strength decreases as the PI-1 concentration in the blend is increased beyond th. apparent miscibility limit of 50/50 wt%.

Phase behavior at high temperature

Figure 2 shows DMTA data for the PBl/PI-1 blends after heating to 450°C. A damping
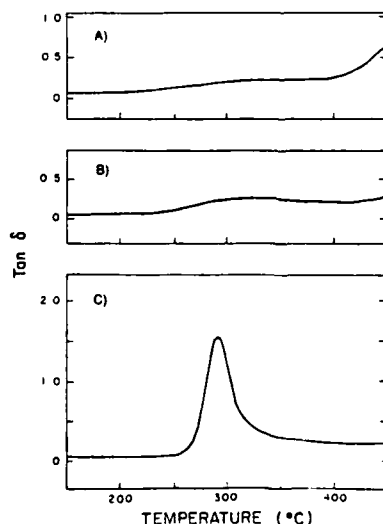
Fig. 2

Dynamic mechanical analysis of PBl/PI-1blends; samples heated to 450°C.
A) PBl/PI-1: 75/25 wt%, B) PBl/PI-1: 50/50 wt%, C) PBl/PI-1: 25/75/wt%

peak clearly associated with the polysulfonimide component is observed only for the PI-1-rich samples (Fig. 2C). The damping associated with a PBI-rich phase or pure PBI is apparently suppressed and shifted to higher temperatures as a result of crosslinking reactions known to occur in PBI at or above T_g [6,7]. To clarify the phase behavior for PBI-rich blends, DSC experiments were conducted on mixtures with blend compositions of 85/15, 75/25 and 70/30 wt% PBI/PI-1 before and after annealing at temperatures between 300 and 450°C. No indication of phase separation was observed although when the samples were annealed above 400°C, chemical changes apparently occurred. Thus the phase boundary for PBI/PI-1 blends at these compositions appears to be above 400°C, although the exact position of the boundary is obscured by the chemical changes which take place at high temperatures.

The PBI/PI-2 blends

Figure 3 shows DMTA measurements for the PBI/PI-2 blend system. In contrast to the results for the PI-1 containing blends, two separate transitions can be observed over the entire range of blend compositions. The T_g's of the two phases are slightly displaced from those of the pure components which indicates the presence of minor mixed phases. We were unable to obtain mixtures which clearly showed a single phase even at the extremes of the composition range. Similar small shifts were observed in the T_g peak corresponding to PI-2 which can be attributed to small amounts ($\leq$ 10 wt%) of PBI in this phase. This mixture appears to become phase separated after heating above 450°C.
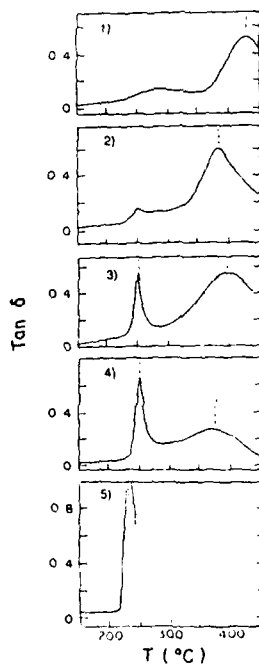
Fig. 3

Dynamic mechanical analysis of PBI/PI-2 blends
1) PBI, 2) PBI/PI-2: 75/25/wt%,3) PBI/PI-2: 50/50 wt%,
4) PBI/PI-2: 25/75/wt%, 5) PI-2

202

CONCLUSIONS

PI-1 exhibits partial miscibility in blends with PBI; the approximate phase behavior is shown schematically in Figure 4.

PBI/PI-2 blends are essentially immiscible except perhaps at blend compositions of 10 wt% or less of PBI.
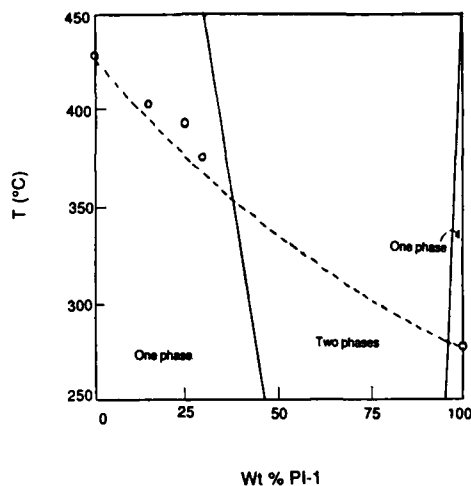
Fig. 4   Wt % PI-1

Schematic phase diagram for PBI/PI-1. The dotted line is the calculated T_g; the circles are the observed T_g.

REFERENCES

1. L. Leung, D. J. Williams, F. E. Karasz and W. J. MacKnight, Polym. Bull. 16,457 (1986).

2. S. Choe, W. J. MacKnight and F. E. Karasz, in Polyimides: Materials Chemistry and Characterization ed. C. Feger, M. M. Khojasteh and J. E. McGrath (Elsevier, Amsterdam 1989).

3. S. Choe, W. J. MacKnight and F. E. Karasz, in Multiphase Macromolecular Systems ed. B. M.
   Culbertson (Plenum, New York, 1989).

4. P. Musto, F. E. Karasz and W. J. MacKnight, Polymer 30, 1012 (1989).

5. T. G. Fox, Bull. Am. Phys. Soc. 1, 123 (1956).

6. H. Vogel and C. S. Marvel, J. Polym. Sci. 50, 511 (1961).

7. J. K. Gilham, Science 495, 1257 (1963).

SMALL ANGLE NEUTRON SCATTERING STUDIES OF BLENDS OF PROTONATED LINEAR POLYSTYRENE WITH CROSSLINKED DEUTERATED POLYSTYRENE

ROBERT M. BRIBER AND BARRY J. BAUER
National Institute of Standards and Technology, Polymers Division,
Gaithersburg, MD 20899, USA

ABSTRACT

Small angle neutron scattering (SANS) has been used to study the scattering function and thermodynamics of blends of linear protonated polystyrene (PSH) and crosslinked deuterated polystyrene (PSD). Two series of samples were synthesized. In both cases the samples were made by dissolving the linear PSH in deuterated (d_8) styrene monomer containing a small amount of divinyl benzene as a crosslinker which was then polymerized to form the PSD network around the linear PSH chains. The samples were all made at a concentration of 50/50 by weight PSD/PSH. A special effort was made to keep the samples single phase so that SANS could be used to study the thermodynamics of the system and compare with theory. This entailed working at relatively low crosslink densities (<1 mole % crosslink units). Series 1 is a set of samples with the same crosslink density varying the length of the linear chain. Series 2 is a set of samples containing the same length linear chain varying the crosslink density systematically. By extrapolating S(q) obtained from SANS to q=0 the zero angle scattering, S(0), was obtained. S(0) is inversely proportional to the second derivative of the free energy with respect to composition, $\partial^2(\Delta f/kT)/\partial\phi^2$. Assuming additivity of the free energies of mixing and elasticity, the portion of the zero angle scattering due to elasticity is calculated.

INTRODUCTION

Small angle neutron scattering has been used in recent years to study the thermodynamics of phase separation in linear polymer blends with much success [1-4]. In this work we wish to extend the use of neutron scattering to study the phase separation transition in systems where one of the components is crosslinked. The topic of linear polymer chains in networks has been studied in the past under the topic of semi-interpenetrating polymer networks (semi-IPN) but a careful review of this area shows that the systems studied are almost exclusively phase separated. Generally, the phase separation occurs during the polymerization and the systems exhibit a nonequilibrium, kinetically controlled two phase morphology [5-7]. The emphasis in the work presented here is on single phase systems and the thermodynamics which control the miscibility of the mixture.

THEORY

The classical theory for the free energy of a network swollen by a solvent due to Flory and Rehner [8] (and later revised by Flory [9]) can be extended to a network containing linear chains [10,11]. Assuming additivity of the free energies described by Gaussian rubber elasticity and a Flory-Huggins theory the free energy per unit volume of the system, Δf, can be written as

$$\frac{\Delta f}{kT} = \frac{3}{2N_c}(\phi_s^{2/3}\phi^{1/3} - \phi) + \frac{B\phi}{2N_c}\ln(\phi/\phi_s) + \frac{(1-\phi)\ln(1-\phi)}{N_b} + \chi\phi(1-\phi) \quad (1)$$

where ϕ is the volume fraction of the network, ϕ_s is the volume fraction

where the network is relaxed (the network reference state; usually taken as the composition where the network was formed), N_c is the average number of monomer units between crosslink points, N_b is the number of monomer units in the linear chain (b component) and χ is the Flory interaction parameter. The specific volumes of the different monomers have been left out for simplicity. The constant B has been generally taken as 2/f by Flory [9], where f is the functionality of the crosslink points in the network, but others have argued for different values [12-14]. The coexistence curve is obtained when the chemical potential of the linear b chains inside and outside the network are equal. The chemical potential of the b chains is given by $\mu_b = \partial(\Delta F/kT)/\partial n_b$ where ΔF is the total free energy of the system and n_b is the number of moles of the linear b chains [11].

$$\mu_b = \frac{\phi_s^{2/3}\phi^{1/3}}{N_c} - \frac{B\phi}{N_c} + \frac{\phi}{N_b} + \frac{\ln(1-\phi)}{N_b} + \chi\phi^2 \qquad (2)$$

Because the swollen network is in equilibrium with a phase of pure b chains, equation 2 can be used to calculate the coexistence curve directly (upon setting $\mu_b = 0$) without resorting to solving a set of simultaneous equations involving both μ_a and μ_b as is necessary in polymer blends. For the spinodal line extra care must be taken in calculating $\partial^2(\Delta f/kT)/\partial\phi^2$ in order to correctly account for the effect of fluctuations in composition on the already swollen network [15,16]. If this is done the equation for the spinodal (and the zero angle scattering) is given as

$$\frac{\partial^2(\Delta f/kT)}{\partial\phi^2} = \frac{B}{2N_c\phi} + \frac{\phi_s^{2/3}}{N_c\phi^{5/3}} + \frac{1}{N_b(1-\phi)} - 2\chi = \frac{k_n}{S(0)} \qquad (4)$$

where k_n is a contrast constant that depends on the type of radiation used for the scattering experiment. This equation also agrees with the criteria for when an elastic body becomes unstable to fluctuations given by

$$S(0)^{-1} \sim \frac{1}{\kappa + (4/3)G} \qquad (5)$$

where κ is the osmotic bulk modulus and G is the shear modulus [15-17]. Figure 1 shows a phase diagram calculated for network with $N_c=500$, $N_b=50$, $B=1/2$ and $\phi_s=0.5$. The ordinate is in arbitrary temperature units based on the observation that χ generally has the form A + B/T [1,2,18,19]. The addition of an elastic component to the free energy causes the phase diagram to be asymmetric. In addition, with the form of the free energy given in equation 1 there is no critical point with the phase transition being first order at all compositions.

$N_c = 500$ $N_b = 50$

single phase

two phase

Temperature

0.0 0.2 0.4 0.6 0.8 1.0

φ
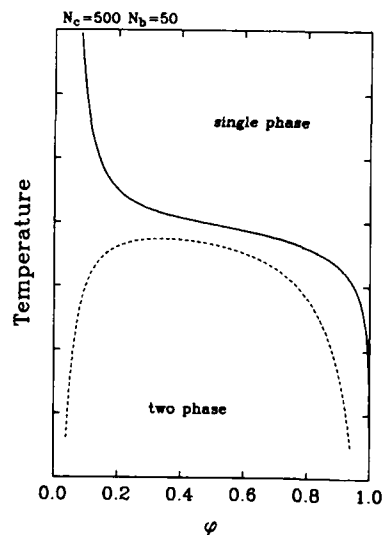
Figure 1: Phase diagram calculated for linear chains in a network.

The scattering from the blends studied in this work is expected to follow classical Ornstein-Zernike form with the total scattering given by

$$S(q) = \frac{S(0)}{1 + (\xi q)^2} \qquad (6)$$

where ξ is the correlation length of the concentration fluctuations in the system and q is the scattering vector ($q = (4\pi/\lambda)\sin\theta$). If the data follows equation 6 then a plot of $S(q)^{-1}$ versus q^2 should be linear with the correlation length being equal to the square root of the ratio of the slope to the intercept.

EXPERIMENTAL

Linear protonated polystyrene (PSH) was purchased from the Pressure Chemical company while the deuterated (d_8) styrene monomer and divinyl benzene was purchased from Aldrich [20]. The styrene was dried over calcium hydride and distilled. Azobis(isobutyronitrile) (AIBN) was used as the initiator. Samples were prepared by dissolving the PSH in the deuterated styrene monomer/divinyl benzene mixture. When the PSH was completely dissolved a few drops of a 10% AIBN solution in toluene was added to give 0.1 wt % initiator. The mixture was then sealed in a SANS cell and placed in a oven at 70°C overnight. The temperature was then increased to 130°C for an additional 12 hours. The samples were all made at a concentration of 50/50 by weight PSD/PSH. Series 1 is a set of samples with the same network ($N_c = 387$) varying the length of the linear chain ($N_b = 91$, 308, 422, 981, 1711 and 3413). Series 2 is a set of samples containing the same length linear chain ($N_b = 422$) varying the crosslink density systematically ($N_c = \infty$, 960, 475, 345, 260, 158). Table I gives the details of the two sets of samples. The crosslink densities were calculated based from the amounts of monomers charged to the reaction and a reported divinyl benzene activity of 57%.

The neutron scattering was done at the NIST SANS facility. The wavelength of the incident neutron beam was 9Å with a $\Delta\lambda/\lambda$ of 25% as determined by a rotating velocity selector. The scattering was performed

above T_g at 150°C. The data were collected by using a two-dimensional x-y detector and were corrected for scattering from the empty cell, incoherent background, and sample thickness and transmission. The scattering was placed on an absolute scale using a calibrated secondary standard. Data was then circularly averaged to obtain the S(q) versus q plots.

RESULTS AND DISCUSSION

The two series of samples provide a probe of different parts of the second derivative of the free energy as given in equation 4. If the assumption of additivity of free energies is valid, i.e.

$$\Delta f_{tot} = \Delta f_{mix} + \Delta f_{elas} \qquad (7)$$

then series 1, where the crosslink density is held constant, while the length of the linear chain is varied, allows examination of Δf_{mix}. *Series 2* on the other hand, keeps the length of the linear chain constant, while N_c varies, thereby probing Δf_{elas}.

Figure 2 presents the SANS data for the series 1 samples in both S(q) versus q and $S(q)^{-1}$ versus q^2 forms. As the length of the linear chain increases the scattering intensity also increases. In the $S(q)^{-1}$ versus q^2 plot the data forms a series of straight lines which move roughly parallel with progressively smaller intercepts as N_b increases. The sample with $N_b=3413$ was phase separated as indicated by the negative intercept in the $S(q)^{-1}$ versus q^2 plot. In analogy with linear polymer blends the slope of these lines is proportional to the square of the statistical segment length ℓ^2 [1,18]. The behavior of the samples in series 1 is qualitatively similar to that of a linear polymer blend as the temperature is changed.
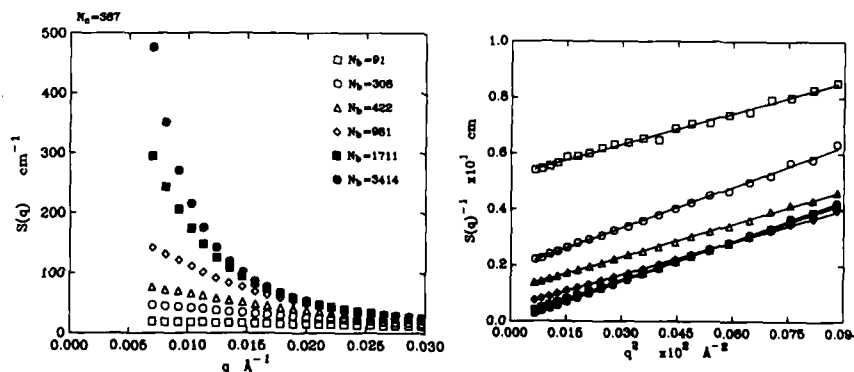
Figure 2: SANS data for the series 1 samples. S(q) versus q and $S(q)^{-1}$ versus q^2.

Figure 3 presents the SANS data for the series 2 samples. The *scattered intensity increases as* N_c *decreases.* The sample with the highest crosslink density ($N_c=158$) was phase separated. The phase separation of this sample can be attributed to the stretching of the network necessary to accommodate the linear chains at this crosslink density and its unfavorable contribution to the free energy of the system. The small χ between PSH and

PSD is not sufficient to explain the phase separation. Unlike the data for series 1 the S(q) versus q^2 plots show a systematic change in slope with increasing crosslink density.
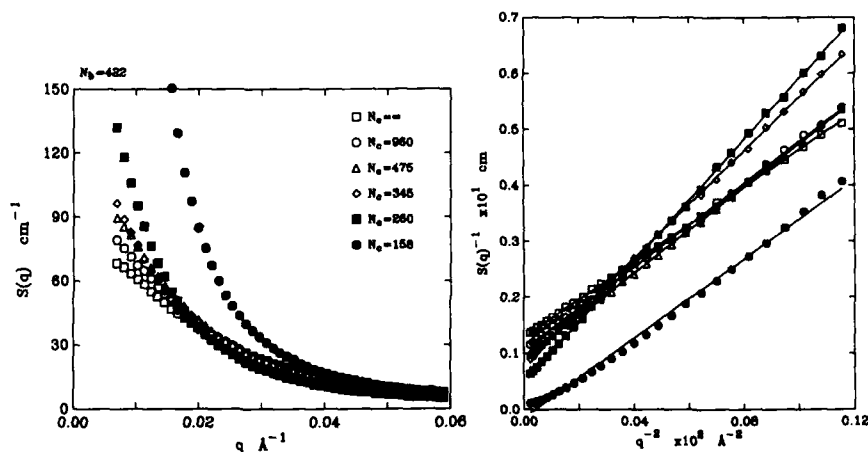
Figure 3: SANS data for the series 2 samples. S(q) versus q and $S(q)^{-1}$ versus q^2.

Rearranging equation 4 yields

$$\frac{k_m}{S(0)} = \frac{1}{N_b(1-\phi)} + \left[\frac{B}{2N_c\phi} + \frac{\phi_s^{2/3}}{N_c\phi^{5/3}} - 2\chi \right] \qquad (8)$$

indicating that a plot of $k_m/S(0)^{-1}$ versus $1/N_b(1-\phi)$ should give a straight line with a slope of 1 if the Flory-Huggins combinatorial entropy adequately accounts for the change in scattering brought about by the increase in the length of the N_b chains. Equation 8 also assumes that the χ parameter between the PSH chains and the PSD network is independent of the crosslink density. While recent studies h/ shown that χ can be a function N_c the effect should be small at the crosslink densities studied in this work [21]. Figure 4 is a plot of $S(0)^{-1}$ versus N_b^{-1}. The straight line is a linear least squares fit to the data and has a slope of 1.04±0.05. The x intercept yields the value of N_b where $S(0)^{-1}=0$ and the favorable free energy of mixing is just balanced by the elastic energy of the network and phase separation occurs. The value of N_b for phase separation from figure 4 is 12700. This is larger than what is found for the sample which phase separated ($N_b=3413$) but the extrapolation in figure 4 yields N_b^{-1} which will give relatively large errors in N_b. Assuming a value of $\chi=1.5 \times 10^{-4}$ for PSH/PSD [22] the elastic contribution to the second derivative of the free energy can be calculated from the intercept of the line in figure 4. The value of $\partial^2(\Delta f/kT)/\partial\phi^2_{elas}$ is 1.54×10^{-3}.
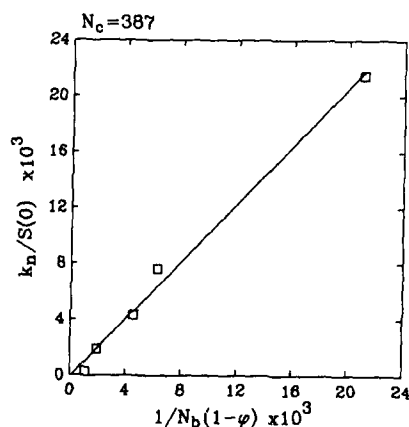
Figure 4: $k_n/S(0)^{-1}$ versus $1/N_b(1-\phi)$ for the series 1 samples.

For the series 2 samples equation 4 can be arranged

$$\frac{k_n}{S(0)} = \frac{1}{N_c}\left[\frac{B}{2\phi} + \frac{\phi_s^{2/3}}{\phi^{5/3}}\right] + \frac{1}{N_b(1-\phi)} - 2\chi \qquad (9)$$

and a plot of $k_n/S(0)^{-1}$ versus $1/N_c$ should give a straight line. Figure 5 shows such a plot. The line is a linear least squares fit to the data and the point where it crosses the x axis is the value of N_c where phase separation occurs $S(0)^{-1}=0$. The value of N_c obtained from the extrapolation is 160. This compares favorably with the value of $N_c=158$ where phase separation was observed to have occurred.
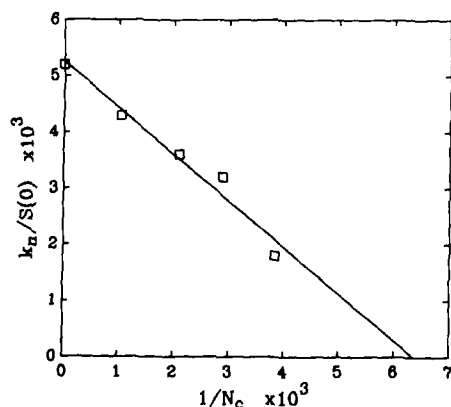
Figure 5: $k_n/S(0)^{-1}$ versus N_c^{-1} for the series 2 samples.

If the slope of the $S(q)^{-1}$ versus q^{-2} can be taken as proportional to the square of the statistical segment length, ℓ^2, as in linear polymer blends, then the systematic change in slope with increasing crosslink density for the series 2 samples indicates an corresponding increase in ℓ. The slope of the lines in figure 1 is proportional to an average of the statistical segment lengths for the two components in the mixture. The

implication is that either the PSH or the PSD chains (or both) are stretching as N_c decreases. The data cannot distinguish between the two possibilities, but one might speculate that the network chains are forced to stretch in order to accommodate the linear PSH chains. As N_c decreases this stretching increases until the free energy penalty caused by the deformation drives the system to phase separate. If one does not worry about the magnitude of ℓ^2 but examines instead the ratio of the slope of the $S(q)^{-1}$ versus q^2 plot at a given value of N_c to the slope for the uncrosslinked blend ($N_c=\infty$) an estimate of the amount of chain deformation, λ, can be made. The values of λ obtained for the series 2 samples in this manner are given in table I.

CONCLUSIONS

SANS has been used to study the thermodynamics of linear PSH chains in a crosslinked matrix of PSD. It was found that the addition of an elastic component to the free energy due the crosslinked PSD caused the system to phase separate at relatively low crosslink densities (<1 mole % crosslinking agent). This indicates the importance of accounting for the presence of a crosslinks on the compatibility of polymer blends, even in miscible systems. Classical Flory-Huggins free energy of mixing combined with Gaussian rubber elasticity has been used to calculate the zero angle scattering, $S(0)$ and compare with experiments. The combinatorial entropy of mixing term adequately describes the data for the samples where N_c is held fixed and the length of the linear chain, N_b, is varied. In the samples where N_b is fixed and N_c varied, a systematic increase in the average statistical segment length is observed, indicating that one or both of the components is being stretched as N_c decreases.

TABLE I
Series 1
$N_c=387$

N_b	$S(0)$ cm^{-1}	ξ Å^{-1}	$k_n/S(0)$ x10^4
91	19.2	26.3	215
308	54.0	51.1	76.2
422	95.6	62.6	43.0
981	220	93.6	18.7
1711	1494	263	2.7
3413[1]	****	****	****

[1]Sample with N_b=3413 was phase separated.

SERIES 2
$N_b=422$

N_c	$S(0)$cm^{-1}	ξÅ^{-1}	slope[1]	λ	$k_n/S(0)^2$	$\partial^2(\Delta f/kT)/\partial\phi^2$elas[3]
∞	79.0	51.9	3.37	---	5.2	----
960	65.9	60.0	3.71	1.05	4.3	4.4
475	113	66.3	3.82	1.06	3.6	-61
345	127	93.6	4.78	1.19	3.2	-101
260	227	111	5.41	1.27	1.8	-243
158[4]	***	***	***	***	***	***

[1]Slopes are from the $S(q)^{-2}$ versus q^2 plot. x 10^1
[2] x 10^3
[3] x 10^5
[4]The sample with N_c=158 was phase separated.

REFERENCES

1. Shibayama, M.; et al.; Macromolecules, 18, 2179 (1985)
2. Jelenic, J.; et al.; Makromol. Chem., 185, 129 (1984)
3. Briber, R.M. and Bauer, B.J.; Macromolecules, 21, 3296 (1988)
4. Bates, F.S.; et al.; Macromolecules, 19, 1938 (1986)
5. Sperling, L.H.; Interpenetrating Polymer Networks and Related Materials, Plenum, New York, 1981
6. Coleman, M.M.; et al.; Macromolecules, 20, 226 (1987)
7. Frisch, H.L.; et al.; Macromolecules, 13, 1016 (1980)
8. *Flory, P.J. and Rehner, J.; J. Chem. Phys.; 11, 455 (1943)*
9. Flory, P.J.; Principles of Polymer Chemistry, Cornell University Press, Ithaca, New York, 1953
10. Binder, K. and Frisch, H.L.; J. Chem. Phys., 81, 2126 (1984)
11. Bauer. B.J.; Briber, R.M.; Han, C.C.; Macromolecules, 22, 940 (1989)
12. James, H.; Guth, E.; J. Chem. Phys., 14, 669 (1947)
13. Hermans, J.J.; J. Polym. Sci., 52, 197 (1962)
14. Kuhn, W.; J. Polym. Sci., 1, 183 (1946)
15. Onuki, A.; Phys. Rev. A., 38, 2192 (1988)
16. Olvera de la Cruz, M.; Briber, R.M.; to be published
17. Landau, L.D. and Lifshitz, E.M.; Theory of Elasticity, Pergamom Press 1986
18. Han, C.C.; et al.; Polymer, 29, 2002 (1988)
19. Bates, F.S.; Macromolecules, 18, 525 (1985)
20. Certain equipment, instruments or materials are indentified in this paper in order to adequately specify the experimental details. Such identification does not imply recommendation by the National Institute of Standards and Technology nor does it imply the materials are necessarily the best available for the purpose.
21. McKenna, G.B.; et al.; Polymer Communications, 29, 272 (1988)
22. Bates, F.S.; et al.; Phys. Rev. Lett., 55, 2425 (1985)

"DYNAMICS OF PHASE SEGREGATION IN POLY-P-PHENYLENE TEREPHTHALAMIDE AND AMORPHOUS NYLON MOLECULAR COMPOSITES"

THEIN KYU, JAN CHANG YANG AND TSUEY ING CHEN
Institute of Polymer Engineering, University of Akron, Akron,
Ohio 44325

ABSTRACT

Time-resolved light scattering has been employed to elucidate the dynamics of phase segregation of poly-p-phenylene terephthalamide (PPTA)/ amorphous nylon (AN) molecular composites. Miscible PPTA/AN blends can be prepared from sulfuric acid solution by rapidly coagulating the solution in distilled water. The composites, however, undergo phase segregation upon thermal treatment and exhibit a miscibility window reminiscent of a lower critical solution temperature (LCST). Several temperature-jump experiments were undertaken from ambient to a two-phase temperature region of 240, 250 and 260°C. Time-evolution of scattering profiles are analyzed in accordance with non-linear and dynamical scaling theories.

INTRODUCTION

The field of molecular composites has gained considerable interest for its potential in structural applications, such as high modulus and high strength materials [1-8]. Conceptually, molecular composites are mixtures of two dissimilar polymers with vastly different configurations, in which the rigid component is dispersed in flexible matrix so that reinforcement takes place at a microscopic level. The maximum performance of the materials can be expected if reinforcement were to occur at a molecular level. It is difficult to meet such expectation due to the low entropy of mixing and high orientability of rigid component. The compatibility between vastly dissimilar polymers is always a central issue in multicomponent systems. The immense difference in the molecular topology, i.e. one being a rigid-rod and the other component being a flexible coil, makes the mixtures thermodynamically unstable [9]. However, such thermodynamic tendency for phase decomposition may be overcome by rapidly coagulating from a homogeneous ternary solution to give miscible systems [10].

These homogeneous mixtures processed from solution are generally in the form of thin films, fibers or precipitates, thus are of limited use. For structural applications, melt processing is required to consolidate into a desired shape. This consolidation step involves thermal cycle and flow which occasionally lead to thermally induced phase separation [10-13]. Hence, the understanding of phase behavior and its kinetics of phase decomposition during thermal consolidation is indispensable in order to gain control of the structure for improved materials properties [11].

The kinetics of thermally induced phase decomposition in poly-p-phenylene benzobisoxazole (PBZT)/nylon 66 was first studied jointly by the Air Force Materials Laboratory and us using time-resolved light scattering [11]. Phase segregation occurs above the onset of the melting temperature of nylon 66 and is dominated by the late stages of spinodal decomposition. The kinetic behavior is non-linear in character and follows power-law kinetics with exponents of -1/3 and 1, in close agreement with the prediction of Binder and Stauffer [14]. In the scaling analysis, the structure function exhibits universality with time, thereby confirming self-similarity of the system.

As a complementary study, we have examined the phase equilibrium of poly-p-phenylene terephthalate (PPTA)/ amorphous nylon (AN) [12,13]. The cross-hydrogen bonding was found to occur between amide groups of PPTA and

AN. However, it is not sufficient to prevent thermally induced phase separation. The mixture showed a phase behavior reminiscent of an LCST. In the present study, we focus our attention on the kinetic aspects of phase decomposition of PPTA/AN molecular composites. The advantage of the present system is that amorphous nylon shows no crystallinity, thereby simplifying the interpretation of dynamical results. Although PPTA is strictly not a rigid-rod, it has a tendency to self-associate as a result of hydrogen bonding and align with respect to each other due to its stiff extended molecular structure. The presence of such a complex PPTA structure may affect the dynamical behavior of phase decomposition. Temperature (T)-jump experiments were undertaken from ambient to a two-phase temperature region. Time-evolution of scattering curves are then analyzed according to non-linear theories [14-17] and dynamical scaling laws [18-21].

EXPERIMENTAL

Materials

Poly(p-phenylene terephthalamide) (PPTA, Mn ~ 20,000) was supplied by Du Pont Co. in the form of quarter-inch fiber (Kevlar 29). Amorphous nylon used in this study was Zytel 330 kindly supplied by Du Pont Co. Zytel 330 is a copolymer of (30/70) iso-/terephthalic acid and hexamethylene diamine with a molecular weight Mn ~ 14,000 and Mw ~ 50,000. The solvent used was 96% sulfuric acid from Fisher Co. The preparation method of molecular composites is thoroughly described in a previous paper [13].

Methods

Real time light scattering experiments were carried out using our static light scattering set-up described elsewhere [22]. The system consists of a 2 mW He-Ne laser with a wavelength of 632.8 nm. The scattered intensity was monitored using two-dimensional Vidicon detector (Model 1254 B, EG & G) in conjunction with a detector controller (Model 1216) and Optical Multichannel Analyzer (OMA III, Model 1460). Data analysis, such as background subtraction, smoothing, angle calibration, rescaling, etc., was undertaken on an off-line computer (IBM-PC). Temperature (T)-jump experiments were undertaken from ambient to 240, 250, and 260°C.

RESULTS AND DISCUSSION

In a previous paper [13], we have shown that PPTA/AN mixtures revealed an LCST with a minimum around 50/50 and at 225°C. When the 50/50 PPTA/AN was annealed at 240°C for 10 min, a scattering halo developed in the V_v (vertical polarizer with vertical analyzer) configuration. Interconnected domains were also discerned under a microscopic investigation, suggesting the possibility of spinodal decomposition (SD). If an alternative mechanism of nucleation-growth (NG) were to occur, the scattered intensity should monotonically decrease from q = 0 without revealing a maximum. This was not the case here. We carried out several T-jump experiments by rapidly transferring the specimen from ambient to two-phase temperatures. Figure 1 shows a typical time-evolution of scattering curves, following a T-jump to 250°C. The scattering maxima first occurs at relatively low scattering wavenumbers q, suggestive of large periodic fluctuations. Here, q is defined as $(4\pi/\lambda) \sin \theta/2$, where λ and θ are the wavelength of light and scattering angle measured in the medium, respectively. The scattering peak moves immediately to lower scattering angles with elapsed time associated with phase growth. There is no period at which the scattering peak is
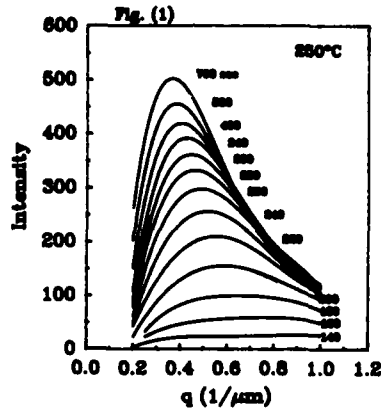
Fig. 1. Time-evolution of scattering curves for 50/50 PPTA/AN, following a T-jump from ambient to 250°C.

invariant, indicating the lack of a linear SD regime [23].

The non-linear growth may be best explained in terms of the dynamical scaling behavior in the late stages of SD [14-21]. This concept is implicit in the cluster diffusion-reaction theory of Binder and Stauffer [14] who proposed that the structure factor $S(q,t)$ for an isotropic system with dimensionality, d, obeys the scaling law

$$S(q,t) = \{q_m(t)\}^{-d} \tilde{s}[q/q_m(t)] \qquad (1)$$

where $\tilde{s}[q/q_m(t)]$ is a universal scaled function. The characteristic wavenumber $q_m(t)$, which is inversely proportional to the average cluster size $R(t)$, has a simple power law form,

$$q_m(t) \sim t^{-\varphi} \qquad (2)$$

where subscript $_m$ stands for peak maxima. The kinetic exponent φ has been predicted to have various values. The classical evaporation-condensation model of Lifshift and Slyozov [24] predicted that a droplet size grows according to the power law with exponent $\varphi = 1/3$, even though molecular details were not considered. Binder and Stauffer [14] postulated $\varphi = 1/(d+3)$ or $1/(d+2)$ in the intermediate regime (depending on temperature quenched depth into unstable region) and a value of 1/3 at late stages of decomposition. Furukawa [18] also predicted the same formulae, $\varphi = 1/(d+3)$ and $1/(d+2)$, for surface and bulk mobilities, respectively, in the asymptotic behavior of the kinetic equation. On the basis of non-linear statistical considerations, Langer, Bar-on and Miller [15] obtained $\varphi \sim 0.21$. The change of exponent from 0.2 to 0.28 was revealed in the simulation work of Marro et al. [16]. According to Siggia [17], hydrodynamic flow plays a crucial role in the coalescence of the growing domains in which the materials have to be squeezed out through interconnected channels. He estimated a value of 1/3 in the intermediate stage and 1 at late stages of SD. It appears that different mechanisms operate at different stages of decomposition, thus the power law is not expected to hold over the entire range of SD.

In Figure 2, are shown the plots of loq $q_m(t)$ versus log t for various T-jumps at 240, 250, and 260°C. The slopes were close to -1, in good agreement with the prediction of Siggia[17] for the coarsening driven by surface tension. As the T-jump temperatures were considerably high, the
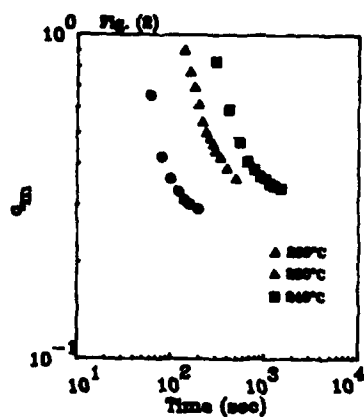
Fig. 2. Log-log plots of maximum wavenumber q_m versus phase separation time t for 50/50 PPTA/AN at various temperatures.
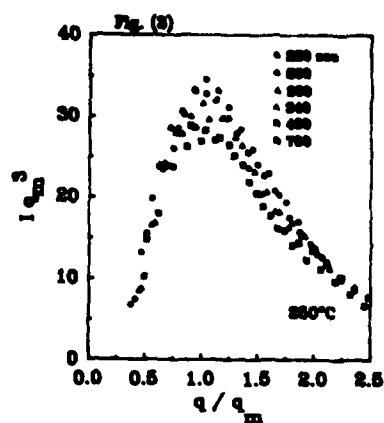
Fig. 3. Plots of $I.q_m^3$ versus q/q_m for 50/50 PPTA/AN at 250°C.
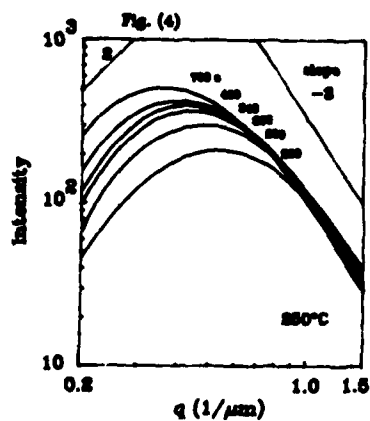
Fig. 4. Log-log plots of scattered intensity against scattering wavenumber for 50/50 PPTA/AN at 250°C.

liquid-liquid phase decomposition occurs very rapidly, thereby missing the early and intermediate stages of SD. At a later time, the slope changes to a smaller value due to the pinning effect. Wide-angle x-ray diffraction studies reveal the presence of small amount of disordered PPTA crystals in the blends. This mesophase structure may be anchored during rapid coagulation. If the amount of PPTA crystal were large, the diffusion process during phase growth may be reminiscent of a liquid-solid type. For such a case, Furukawa [21] predicted $\varphi = 1/2$, in which solid-liquid interphase mobility is dominant. Our experiment was not long enough in duration to discriminate the exact pinning mechanism.

In order to test with the scaling theory [18] we calculated the scaled structure function $s(q/q_m)$ for a three-dimensional case as follow;

$$s(q/q_m) = \{q_m(t)\}^3 \, S(q,t) \tag{3}$$

where the normalized structure factor $S(q,t)$ is defined as

$$S(q,t) \sim I(q,t)/\int I(q.t)q^2 dq \tag{4}$$

The denominator or the invariant function will be constant in the late stages of SD where the mean-square fluctuations of refractive indices reaches a limiting value. In such cases, normalization is not necessary. Figure 3 shows the plots of $I(q,t)q_m^3(t)$ against q/q_m for various times. The good superposition of the scattering curves suggests that the structure function is universal with time. The self-similarity behavior appears the same for all T-jumps studied here.

The shape of the scaled function is important, as it is associated with the correlation between clusters and their shapes. Furukawa [19] proposed that the shape of structure function can be scaled with $x = q\bar{R}$, i.e.,

$$\bar{s}(x) \sim x^2/[\gamma/2 + x^{2+\gamma}] \tag{5}$$

where γ is related to dimensionality d as follows;

$$\gamma = \begin{cases} d+1 & \text{for off-critical mixtures} \\ 2d & \text{for a critical mixture} \end{cases}$$

For three-dimensional growth, i.e., d=3, the asymptotic form of $\bar{s}(x)$ is x^2 at $q<q_m$ and x^{-4} at $q>q_m$ for off-critical mixtures. In the case of critical mixtures, an x^{-6} dependence has been suggested at $q>q_m$[21]. As can be seen in Figure 4, the slope of -3 was obtained at $q>q_m$, which is lower than that predicted for three-dimensional growth. We have to admit that our results cover only limited q range. Moreover, the initial fluctuation size is very large, i.e. q varies from about 1 to 0.3 μm^{-1} which corresponds to a periodic domain size of approximately 6 to 15 μm. Since the film thickness is about 10 μm, it is conceivable, although by no means conclusive, that the growth may be two-dimensional rather than three-dimensional, which would give a slope of -3 for off-critical mixtures. The slope at $q<q_m$ is close to the predicted value of 2. The effect of PPTA crystallization on the scattering profiles during phase growth should not be ruled out in explaining the behavior of asymptotic scaled structure function.

CONCLUSIONS

We have demonstrated that phase decomposition in PPTA/AN molecular composites appears to be dominated by late stages of SD. The surface mobility of PPTA mesophase appears to play a crucial role in the kinetics of

phase growth. The structure function exhibits universality with time, suggesting self-similarity. The asymptotic behavior of the scaled structure function suggests that the growth process may be two-dimensional because of thin specimens.

REFERENCES

1. Helminiak, T.E., Benner, C.L. and Arnold, F.E., Polym. Prep. ACS 16(2), 659 (1975).
2. Hwang, W.F., Wiff, D.R., Benner, C.L. and Helminiak, T.E., J. Macromol. Sci. Phys. B22, 231 (1983).
3. Hwang, W.F., Wiff, D.R., Verschoore, C., Polym. Eng. Sci. 23, 789 (1983); ibid. 23, 784 (1983).
4. Wiff, D.R., Timms, S., Helminiak, T.E. and Hwang, W.F., Polym. Eng. Sci. 27, 424 (1987).
5. Takayanagi, M. and Kajiyama, T., U.K. Patent No. 2,008,598 (1978).
6. Takayanagi, M., Ogata, T., Morikawa, M. and Kai, T., J. Macromol. Sci. Phys. B17, 591 (1980).
7. Takayanagi, M., Pure Appl. Chem. 55, 819 (1983).
8. Yamada, K., Uchida, M. and Takayanagi, M., J. Appl. Polym. Sci. 32, 5231 (1986).
9. Flory, P.J., Macromolecules 11, 1138 (1978).
10. Chuah, H.H., Kyu, T. and Helminiak, T.E., Polymer 28, 2129 (1987).
11. Chuah, H.H., Kyu, T. and Helminiak, T.E., Polymer 30, 1591 (1989).
12. Kyu, T., Chen, T.I., Park. H.S. and White, J.L., J. Appl. Polym. Sci. 37, 201 (1989).
13. Chen, T.I. and Kyu, T., Polym. Commun., submitted.
14. Binder, K. and Stauffer, D., Phys. Rev. Lett. 33, 1006 (1974).
15. Langer, J.S., Bar-on, M. and Miller, H.D., Phys. Rev. A, 11, 1417 (1975).
16. Marro, J., Lebowitz, J.L. and Kalos, M.H., Phys. Rev. Lett. 43, 282 (1979).
17. Siggia, E.D., Phys. Rev. A, 20, 595 (1979).
18. Furukawa, H., Phys. Rev. Lett. 43, 136 (1979); Phys. Rev. A, 23, 1535 (1981).
19. Furukawa, H., Physica A, 123, 497 (1984).
20. Binder, K., Phys. Rev. B, 15, 4425 (1977).
21. Furukawa, H., J. Appl. Cryst. 21, 805 (1988).
22. Kyu, T. and Saldanha, J.M., J. Polym. Sci. Polym. Lett. Ed. 26, 33 (1988).
23. Cahn, J.W. and Hilliard, J.E., J. Chem. Phys. 29, 258 (1958).
24. Lifshitz, I.M. and Slyozov, V.V., J. Phys. Chem. Solids 19, 35 (1961).
25. Hashimoto, T., Itakura, M. and Hasegawa, H., J. Chem. Phys. 85, 6118 (1986).

FACTORS INFLUENCING PROPERTIES OF SAN/PMMA BLENDS

R. SUBRAMANIAN, Y. S. HUANG, J. F. ROACH AND D. R. WIFF
GenCorp Research, 2990 Gilchrist Road, Akron, Ohio 44305

ABSTRACT

The versatility of polymeric blends is reflected in the range of usable end properties that can be achieved through alterations in the composition and/or effective control of the morphologies of the mixtures. Solvent cast and melt mixed blends of SAN and PMMA have been studied to understand the influence of PMMA tacticity and the acrylonitrile content of the SAN copolymer on their phase behavior. The results show a shifting of the cloud point curves and the miscibility windows for the blends of SAN with different stereo-regular PMMAs. This is interpreted as being due to specific interactions between the acrylonitrile and methacrylate groups. The 'goodness' of mixing in the melt mixed blends were determined by FTIR ATR spectroscopy. The effects of the processing conditions on the mixing characteristics and subsequent improvement in mechanical properties are discussed. The limits of mixing that can be achieved using standard mixing procedures and their role in affecting the end use properties such as the flexural strength will also be discussed.

INTRODUCTION

Miscibility in multicomponent polymeric systems is not always desirable; but gross phase separation invariably leads to inferior properties. As in block copolymers, controlled chemical structure and microphase heterogeneity in polyblends often lead to superior mechanical properties and improved processability [1-7]. Such intricate phase morphology can be obtained upon phase demixing (separation) of a homogeneous blend via a spinodal mechanism, which would result in phase domains approaching molecular dimensions ($\sim 10^2 A^\circ$) and the phase separated blend would behave like a self-assembled composite [8].

It has been known for quite sometime now that polymethylmethacrylate (PMMA) forms miscible blends with the copolymer, styrene acrylonitrile (SAN) over a limited range of acrylonitrile (AN) content [9]. This 'miscibility window' has been explained by Paul and Barlow [10] and others [11,12] as resulting from a dilution of the unfavorable interactions among the various segments, leading to a net negative contribution to the free energy of mixing, ΔG^M.

The SAN/PMMA system has been widely studied for phase behaviour by many researchers [9-12]. However, the investigations have been limited to blending SAN (with varying amounts of AN) with commercial, heterotactic PMMA (h-PMMA) and other higher order methacrylates [13]. The influence of PMMA tacticity on the phase behavior of this system has not been investigated. Isotactic, syndiotactic and heterotactic forms of PMMA exhibit large differences in T_g and other physical properties [14,15]. Thus, it is reasonable to expect these different PMMAs to behave differently when blended with SAN. Based on this consideration, a systematic study of the effects of PMMA tacticity on phase behavior, processing and mechanical properties of the blends was undertaken.

EXPERIMENTAL

a. **Materials**:

The polymers used in this study are described in Table 1. The SAN and h-PMMA materials were obtained from Dow Chemical Company (Tyril™) and Rohm and Haas Company (Plexiglass™) respectively. The isotactic PMMA (i-PMMA) was produced in-house by anionic techniques and the syndiotactic material (s-PMMA) was an experimental material obtained from Rohm and Haas.

Table I

POLYMERS USED IN THIS STUDY							
POLYMER DESIGNATION	% AN	T_g(°C)	$\overline{M}n$**x10³	Mw/Mn	% Tacticity*		
					i	h	s
SAN1	30	111·0	50.6	3·5	–		
SAN2	25	112·0	44	3·4	–		
SAN3	20	108·0	49.3	3·6	–		
SAN4	10.4	103·8	47.4	3·5	–		
h-PMMA	–	110·6	25.2	1·8	14	41	45
i-PMMA	–	59·0	41.0	6·0	83	13	4
s-PMMA	–	131·5	110.0	1·3	3	26	71

*Triad Analysis by ¹H NMR   **GPC Analysis Using PMMA Standards

b. **Sample Preparation for Light Scattering**:

The samples for determining the phase boundaries in the SAN/PMMA systems were prepared by solution casting from 1,2 dichloroethane (DCE) using procedures described in the literature [13]. Optical cloud points were determined using a standard laser light scattering apparatus. The morphologies in this system were identified using phase contrast optical microscopy.

c. **Melt Mixing**:

Laboratory scale mixing of the two polymers was performed to assess the effect of mixing on the end use properties of the binary blend. Blends of SAN (30% AN) with h-PMMA were prepared by four different techniques. To facilitate blending, the materials were first ground to a uniform particle size in a Condux grinder and dried overnight in a convection air oven at 100°C. Appropriate amounts of the samples were then melt mixed using the following:
   1. Haake Single Screw Extruder
   2. An in-house built Fiber/Film Processor with Static Mixer.
   3. Haake-Buhler Rheocord System 40
   4. Physical mixing using a blender, followed by compression molding.

d. **Mechanical Properties**:

Tensile stress-strain and 3-point flexural measurements were carried out on an Instron Model 1122 under a constant crosshead speed of 0.05"/min (1.27 mm/min). The flexural measurements were done as per specifications given in ASTM D790.

e. Estimation of 'Goodness of Mixing':

The extent of mixing between SAN and PMMA upon blending by the above methods was followed by optical phase contrast miscroscopy and comparison of FTIR spectra obtained from different sections of the samples. Generally speaking, a well mixed blend would show no streaks or islands when viewed under the microscope, and the FTIR of different sections of such a sample should be identical.

RESULTS AND DISCUSSION

a. Phase Behavior of SAN/PMMA Blends:

SAN1 (Table I) formed miscible blends with hetero and syndiotactic PMMA over the entire range of composition. The i-PMMA was immiscible with the SAN1 and so solution cast blends were prepared using SAN2. The dried films were all optically clear and exhibited a single T_g by DSC. The results are shown in Figure 1. The calculated lines were obtained using the Gordon-Taylor equation:

$$T_g = (W_A T_{gA} + K W_B T_{gB}) / (W_A + K W_B) \qquad (1)$$

where W_A and W_B are weight fraction of component A and B, and the value of K was taken as equal to 1 [16]. As can be seen from the figure, the experimental results fit quite satisfactorily to the theoretical line, for the SAN/i-PMMA and SAN/h-PMMA systems. More scatter is evident for the SAN/s-PMMA system.
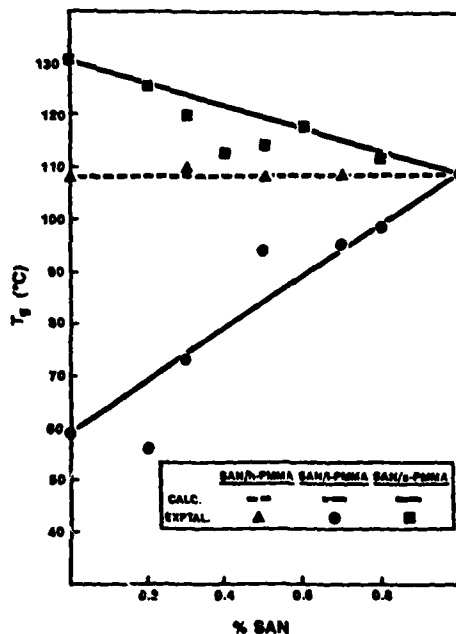
Figure 1. Glass transition temperatures of melt mixed blends obtained by DSC. The calculated lines were obtained using the Gordon-Taylor equation [16].

The phase boundaries in these SAN/PMMA systems were determined by locating the cloud points using the light scattering setup. The cloud points were measured by the detection of a sudden jump in the intensity of

220

the scattering profiles and the corresponding temperatures were plotted as a function of composition, thus generating the cloud point curves (CPC). The system forms a well modulated, two phase structure above the cloud point, similar to those discussed in the literature for other polymer pairs [17].

b. Effect of PMMA Tacticity:

All the three types of PMMA form miscible blends with SAN and exhibit LCST type behavior. Figure 2 is a plot of CPCs obtained at a heating rate of 2°C/min for the hetero, syndio and isotactic PMMA blended with SAN and shows clearly the effects of tacticity on the phase behavior. The hetero and syndiotactic blends behave similarly, whereas the isotactic blend shows a minimum in its CPC at higher SAN compositions.
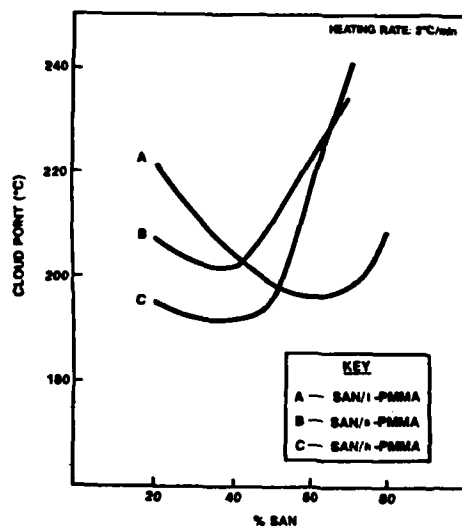
Figure 2. Cloud point curves of blends of SAN with isotactic, syndiotactic and heterotactic PMMAs. SAN1 was used to blend with s-PMMA and h-PMMA; SAN2 was used for blending with i-PMMA.

Blends of SAN1 through SAN4 with the three types of PMMA were also prepared and analyzed for their phase behaviour. The results, for 50/50 blends by weight of SAN/PMMA are given in Table II. It is clear that in

Table II

TACTICITY EFFECTS
Composition: 50/50

| % AN | CLOUD POINT (°C)* | | |
	SAN/h-PMMA	SAN/i-PMMA	SAN/s-PMMA
30	192	Immiscible	210
25	>300 or Decomposition	199	232
20	>300 or Decomposition	>300 or Decomposition	240
10.4	Immiscible	Immiscible	>300 or Decomposition

* Heating Rate 2°C/Min.

this system, the miscibility window is the largest for s-PMMA and is the smallest for i-PMMA. We have estimated the individual interaction parameters for the SAN/i-PMMA and SAN/h-PMMA systems from the phase boundary data using the procedures of Krammer and Kressler [18]. The results indicate enhanced interaction between the AN and methacrylate groups for the i-PMMA blends compared to the h-PMMA blends (X_{AN-MMA} = 0.085 and 0.07 respectively). The reduced width of the miscibility window for the SAN/i-PMMA could be related to this enhanced interaction.

c. Processing, Morphology and Mechanical Properties:

The pure components, h-PMMA, SAN (30% AN) and a 50/50 mixture of the two polymers were extruded using a Haake Single Screw Extruder with a slit die. The pure components gave optically clear (1cm x .1cm) strips. The blends, however, all appeared to be turbid at the surface. Cross sections of the extruded strips showed a clear inner core, with opacity increasing toward the outer regions. Figure 3 is a phase contrast optical photomicrograph of a microtomed cross-section of the extrudate and shows areas of incomplete mixing. To further confirm this state of incomplete mixing, FTIR spectra were obtained on various areas of these microtomed (15µm) samples. The spectra obtained from an area near the core appeared to be uniform. Analysis showed it to be essentially a 50/50 mixture of SAN and PMMA. The spectra obtained from an area near the skin that appears to be an inclusion showed PMMA to be the dominant component in this outer area. Outer areas show various combinations of SAN and PMMA, indicating incomplete mixing.
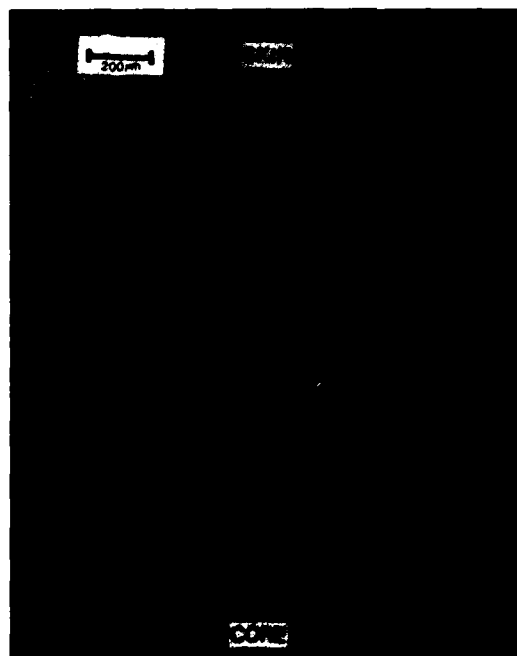
Figure 3. Optical phase contrast photomicrograph of a 15 µm thick cross-section of 50/50 SAN1/h-PMMA extrudate. The uniform dark areas are regions of good mixing.

To improve the mixing, two additional techniques were used. In the first attempt, about 30g of the two polymers were mixed in the Haake Buehler Rheocord System 40. The conditions that were varied included time of mixing, and mixing speed. The mixed samples were then molded at various temperatures and then subjected to flexural measurements (Table III). The flexural strength increased with molding temperature.

Table III

FLEXURAL STRENGTH vs. MOLDING TEMPERATURE

Sample: 50/50 SAN/h-PMMA

Mixing Conditions: Rheocord System 40; 180°C; 30 rpm; 6 Min.

MOLDING TEMPERATURE (°C)	FLEXURAL STRENGTH (MPa)
200	81.57
225	86.33
240	90.81
250	96.53
260	100.12

The polymers were also melt blended using the Fiber/Film Processor with static mixer and a coat-hanger die. The extruded films were all optically clear with no indication of phase separation. The samples were also analyzed for compositional homogeneity by FTIR and ^{1}H NMR. The results, shown in Table IV, indicate that good mixing was obtained using this technique. In the case of FTIR ATR the ratio of the absorbance of the C=O peak at 1150 cm^{-1} (due to PMMA) to that of the aromatic at 760 cm^{-1} (due to SAN) is a constant for various regions of the sample, indicating compositional homogeneity.

Table IV

COMPOSITIONAL ANALYSIS OF EXTRUDED SAMPLES – STATIC MIXER

SAMPLE SAN/PMMA	AREA	A1150/A750 (FTIR)	WT %* PMMA	WT %* SAN
(50/50)	1	1.62	49.2	50.8
(50/50)	2	1.62	53.2	46.8
(30/70)	1	0.52	28.6	71.4
(30/70)	2	0.67	30.0	70.0

* ^{1}HNMR

The samples were also directly compression molded in a vacuum press. The appropriately weighed mixtures were molded at 180°, reground and then remolded in a vacuum press at various temperatures. They were then analyzed for their flexural properties and compositional homogeneity. The results of the flexural measurements are shown in Figure 4. The solid line in the center of the figure is based on simple additivity rule for binary mixtures. The figure clearly shows an improvement in the properties when molded at 250°C. At this temperature, an interconnected

morphology is visible under the microscope. The samples molded at 200°C showed insufficient mixing as determined by FTIR. This is reflected in the data points falling quite close to the calculated line. The samples molded at 275°C, show both phase separation and the onset of sample degradation as evidenced by the appearance of slight brownish tinge in the sample.
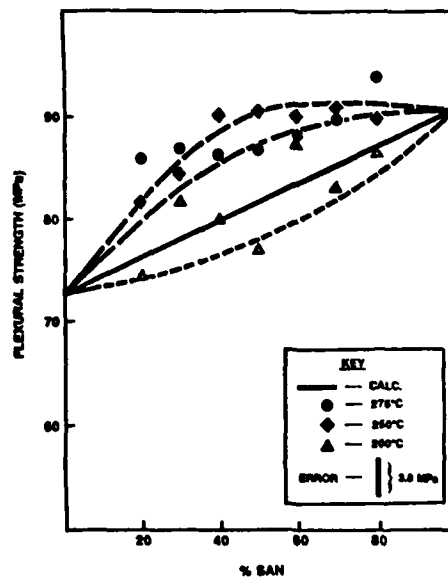
Figure 4. Flexural strengths (ASTM D790) of SANl/h-PMMA dry blended and compression molded at various points in the (T,ϕ) phase diagram. Measurements were performed at 23°C and 50% humidity.

Table V compares the flexural strength of blends obtained by the different techniques. The results indicate that the Rheocord 40 gave the best combination of good mixing and improved flexural strength. But the technique cannot be operated continuously like an extruder. It is, however, a very useful tool for exploratory mixing studies. The physical blending did not yield extremely well mixed samples. Nevertheless, the improvement in the mechanical properties shows that extremely intricate level of mixing may not be necessary for reinforcement, if the morphological contributions can be controlled [19].

Table V

PROCESSING TECHNIQUE vs. FLEXURAL STRENGTH

Sample: 50/50 SAN/h-PMMA
Processing/Molding Temp.: 250°C

PROCESSING TECHNIQUE	FLEXURAL STRENGTH (MPa)	MIXING CHARACTERISTICS
Extruder (Single Screw)	90.72	Average
Static Mixer	87.01	Good
Rheocord 40	96.53	Good
Compression Molding	90.12	Poor

224

CONCLUSIONS

The PMMA tacticity influences the phase behavior of blends with SAN by altering the windows of miscibility. The blends of SAN with s-PMMA has the widest miscibility window while the SAN/i-PMMA has the narrowest for the three isomers. The minimum in the CPC for the i-PMMA blends occurs at higher SAN compositions compared to the h-PMMA and s-PMMA blends.

FTIR ATR spectroscopy is a convenient way to determine the effectiveness of mixing in binary blends. Blending using the Rheocord System 40 followed by compression molding gives the best combination of adequate degree of mixing and improved flexural strength. However, the various techniques used for melt mixing left a complex history of shear, elongation, compression and spatial distribution on the multiphase melt of the polyblends. Hence the properties reported here could very well be a 'compromised' average.

ACKNOWLEDGMENT

REFERENCES

1. J. K. Gillham, L. C. Chan, A. J. Kinloch and S. J. Shaw, Intn'l. Conf. Toughening of Plastics II, 1, (1985).
2. L. A. Utracki, Intn'l. Polym. Processing, 2, 1 (1987).
3. J. W. Barlow and D. R. Paul, Ann. Rev. Mat. Sci., 11, 229 (1981).
4. S. Krause, J. Macromol. Sci. - Rev. Macromol. Chem. C7(2), 251 (1972).
5. O. Olabisi, L. M. Robeson and M. T. Shaw, "Polymer Polymer Miscibility," Academic Press, NY (1979).
6. I. C. Sanchez in "Polymer Compatibility and Incompatibility Principles and Practice," edited by K. Solc, MMI Press Symposium Series, Vol. 2, Harwood Publishers, NY (1982).
7. D. W. Fox and R. B. Allen, Encycl. Polym. Sci, and Engg., 3, 133 (1985).
8. J. D. Hoffmann and R. B. Miller in 'Advancing Materials Research,' edited by P. Psaras and H. D. Longford, Nat'l. Acad. Press, Washington, D.C. (1985).
9. M. Suess, J. Kressler and H. W. Krammer, Polymer 28, 957 (1987).
10. D. R. Paul and J. W. Barlow, Polymer 25, 487 (1984).
11. J. M. F. Cowie and D. Lath, Makromol. Chem. Macromol. Symp. 16, 103 (1988).
12. L. A. Utracki and B. D. Favis in Handbook of Polym. Sci. and Tech. Vol. 4, edited by N. P. Chemisinoff, Marcell-Dekker, NY (1989).
13. M. E. Fowler, J. W. Barlow and D. R. Paul, Polymer 28, 1177 (1987).
14. R. Subramanian, R. D. Allen, J. E. McGrath and T. C. Ward, Polymer Preprints 26(2), 238 (1985).
15. A. M. Walstrom, R. Subramanian, T. E. Long, J. E. McGrath and T. C. Ward, Polym. Preprints 27(2), 135 (1986).
16. K. Naito, G. E. Johnson, D. L. Atlana and T. K. Kweim, Macromol. 11, 1260 (1978).
17. T. Inoue, T. Ouigizawa, O. Yasuda and K. Miyasaka, ibid, 18, 57 (1985).
18. H. W. Krammer and J. Kressler, Makromol. Chem. Macromol Symp., 18, 63 (1988).
19. P. Van Ghelue, B. D. Favis and J. P. Challifoux, J. Mat. Sci. 23, 3910 (1988).

Dielectric Studies of Polyester/Polycarbonate Blends

James M. O'Reilly and Joseph S. Sedita, Eastman Kodak Company,
Corporate Research Laboratories, Rochester, NY 14650-2110

Abstract:

Dielectric and enthalpic relaxation times have been measured
as a function of composition and temperature. A fractional ex-
ponential (W-W) distribution of relaxation times fits both the
dielectric and enthalpic relaxation times with different valu-
es which are a function of composition. Free volume parameters
calculated using the WLF equation are not simple functions of
the composition. Concentration fluctuations are considered to
be important in these phenomena.

Introduction:

There is widespread interest in polymer blends which offer the
opportunity to obtain improved properties at lower cost. The
class of miscible and immiscible polyester/polycarbonate blends
have been extensively studied [1] and reviewed [2]. Copolyes-
ters of ethylene glycol (EG) and cyclohexanedimethanol(CHDM)
and terphthalic acid (T) and bisphenol A polycarbonate(PC)
blends were studied by Paul and co-workers [3-6]. These blends
were miscible under most conditions but because of high temp-
eratures, 250C and higher required for melt blending, trans-
esterification of the polymers may contribute to the miscibil-
ity. PET is not miscible with PC in the absence of transester-
ification. CHDMT is reported to be miscible with PC by Paul[7]
We will report dielectric and thermal properties of a20/80
mole% copolymer of EG/CHDM/T blended in an extruder withvari-
ous amounts of PC. The temperature dependence of the dielectric
and thermal relaxation times will be analyzed in termsof the
free volume models of relaxation.

Experimental:

Merlon M40 PC used in these studies has Mw=31,000 and Tg is
140C. The copolyester EG/CHDM 20/80 terphthalate is a commerc-
ial product of Eastman Chemicals and has Mw=39,000 and Tg is
85C. The blends were melt extruded at 285C and films were mol
ded in compression at 295C. DSC measurements were made using a
DSC II. Dielectric measurements were made using a DETA appara-
tus from Polymer Labs over a temperature range of -100 to 200
C and from 1 to 100 kHz. Only tanδ measurements are reported
here because they show all the interesting behavior and are
the most accurate.

Dielectric Results:

A beta relaxation process is observed in both the polyester
(Tmax =-10C) and polycarbonate homopolymers (Tmax = -50C). The
beta process of the blends appears to be an average of the two
pure component losses and little additional information is
discernible from these measurements. In the Tg region (alpha
relaxation) a single narrow peak is observed for each blend
and indicates that the blends are miscible (Fig. 1.) For the
pure polyester, an additional peak is observed at high tempera-
ture which is attributed to recrystallization of the polyester

and leads to an alpha' loss characteristic of semi-crystalline
polymers. The intensity of the loss peak is not a linear funct-
ion of the composition. This may be due to an anti-parallel
dipole-dipole interaction leading to a lower effective dipole
moment.
These data can be presented as Tmax (temperature of maximum
loss for different frequencies) as a function composition in
Fig. 2. It is apparent that the Tmax of dielectric loss is a
different function of composition than is the Tg determined
from DSC measurements. This result was initially surprising
because free volume considerations would suggest linear behav-
ior. Another representation of the frequency, temperature, and
composition dependence of the dielectric loss at Tg is shown
in Fig. 3. In this form it can be readily seen that the slopes
of the frequency vs temperature curves (i.e. activation energy
or WLF parameters vary systematically with composition. The
precision of the data is well represented in this curve. Repr-
oducibility of the temperature is better than one degree, the
composition is known to within a few percent and the error in
the frequency is negligible compared to the other variables.
These data can be fitted with a WLF/VTF equation to obtain the
parameters C1 and C2 for different compositions.

$$\log f(T) = \log f(Tg) \; \frac{-C1 \cdot (T-Tg)}{C2+(T-Tg)} = A - \frac{B}{T-To} \qquad (1)$$

The solid line in Fig. 3 is a non-linear regression fit of the
data and the calculated values of C1, C2, and log f(Tg) are
listed in Table I. Tg was taken as the onset temperature from
the DSC measurements at 20 deg/min.

Table I
Dielectric Relaxation Parameters

%PC	C1	C2	logfm(Tg)	fg	afx10[4]	β
0	10.7	39	.35	.040	10	.59
20	13.7	27	-1.6	.032	12	.54
50	13.3	54	.20	.032	6.0	.51
60	14.7	52	.32	.030	6.7	.43
80	13.3	63	1.34	.033	6.1	.61
100	11.3	48	2.4	.038	8.0	.50

Many polymers and other materials can be described by the
Williams-Watts distribution function for the alpha and beta
relaxation. We used the W-W function to fit the alpha relaxat-
ion of the blends as shown in Fig. 4. In order to cover a wide
reduced frequency range, the temperature data are converted to
reduced frequency using eq. 1 (8). Values of β calculated for
a frequency of 1kHz. are included in Table I. Data at higher
frequencies give slightly lower values of β which indicates
that the distribution broadens with temperature.

DSC Results:

The thermal behavior of these polymer blends reflects the lon-
ger relaxation times associated with conformational changes
and intermolecular energy changes at Tg. Tg changes with heat-
ing rate as shown in Fig. 5. and the activation energies, Ha,
calculated from the Arrhenius equation are listed in Table II.
The derived Ha show a maximum at high polycarbonate concentra-
tions but this maximum should not be given much emphasis beca-

Fig. 5. log fm vs temperature for different compositions, 0% PC, x 80% PC, + 40% PC, 60% PC, 80% PC, 100% PC.

Fig. 4. e"/e"max vs reduced frequency, inside curve 0% PC, middle curve 50% PC, outside curve 60% PC.

Fig. 1. tan vs. temperature for BG/CHDM/T / PC blends. ◊ 0% PC, x 50% PC, △ 50% PC, ○ 50% PC, + 100% PC.
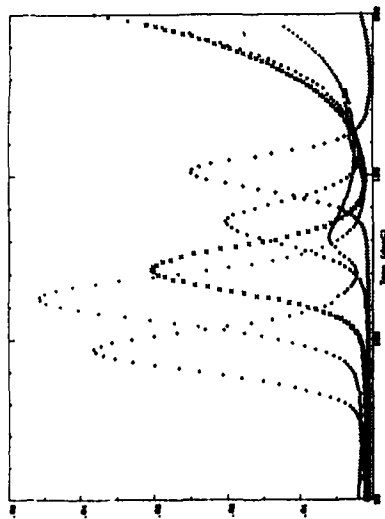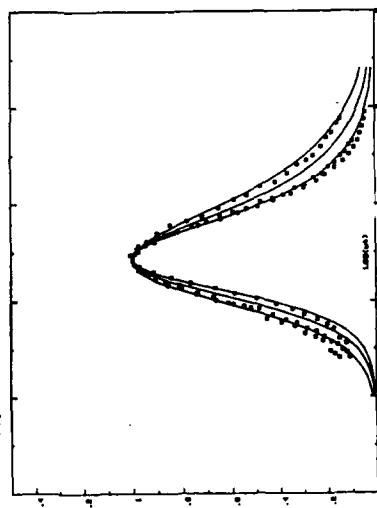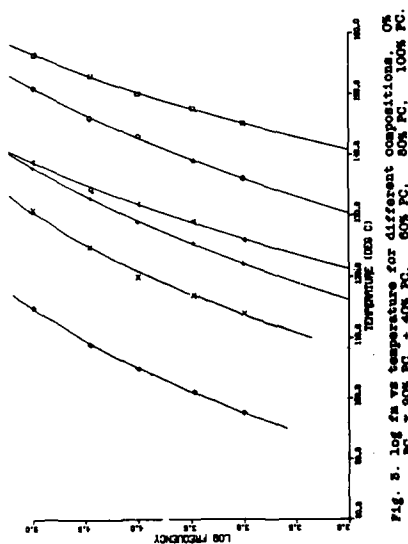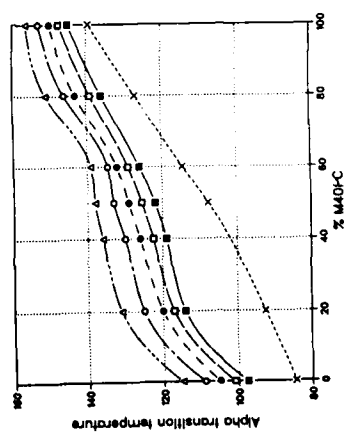
Fig. 3. Tmax and Tg vs composition, ■ 1Khz, ◻ 3khz, ● 100Kh, ○ 25.5Kh, △ 100khz, x 0.0C

use Ha of PC is low and the precision of the Ha is about ±20%.
The heating rate results for the 20% and 100% PC samples
appear to give low Ha's and the experiments were repeated for
the PC sample with similar results. Nevertheless Ha changes
with PC concentration. We have applied the widely used method
of enthalpy relaxation to these blends. Since the analysis is
fully described {9,10} only the essentials will be repeated
here. The parameters in addition to Ha, needed to characterize
the relaxation are the breadth of the distribution of relaxat-
ion times and the structure dependence of the relaxation times
which is proportional to {1-X}. A characteristic relaxation
time, to, is also necessary. The eq.2.

$$\ln \mathcal{T} = \ln \mathcal{T}o + \frac{XHa}{RT} + \frac{\{1-X\}Ha}{RTf} \qquad (2)$$

is used to analyze the data. Tf is the fictive temperature.
A characteristic of polymer blends is that the annealing peak
associated with aging is smaller or broaden with blending as
shown in Fig. 6. Only the short time aging behavior is report-
ed here because a shortcoming of this model is that the parme-
ters X and β change with long annealing times {11}. Values of
X and β derived from non-linear regression fits of the Cp cur-
ves of aged samples vary with composition and are listed in
TableII. An interesting feature of these data is the that the
distribution of relaxation times are narrower and more compos-
ition dependent for enthalpy relaxation than for dipolar rel-
axation (Fig. 7.). The changes in Ha with composition may
influence the calculated values of β . Nevertheless the dielec-
tric β's clearly show that Ha increases with PC concentration
and this effect directly or indirectly leads to the changes in
the enthalpic β's.

Table II
Enthalpic Relaxation Parameters

%PC	Ha kJ/mol	β	X
0	107	.68	.74
20	100	.71	.83
50	153	.45	.84
60	145	.51	.74
80	188	.41	.80
100	107	.74	1.04

Discussion:

The dielectric and enthalpic $\mathcal{T}$'s can be combined and analyzed
as shown in Fig.8. The dielectric $\mathcal{T}$'s are referenced to the Tg
at 20 deg./min and then the Tg's at other heating rates are
shifted relative to the 20 deg./min value. These data were then
re-analyzed using the WLF/VTF equation and the values were not
statistically different from the values in Table I except for
the 20 and 100% PC. In terms of the free volume models fg sho-
uld be a constant at Tg. In these blends it appears that fg
decreases and shows a shallow minimum with composition. We ex-
pected af to show a monotonic behavior with composition but it
fluctuates with composition. Because of the limited frequency
range and experimental uncertainties we do not want to specul-
ate about the fluctuations in af. However the changes in fg
are real and could be associated with negative volume changes
on mixing the blends {12}. Although the density changes on
mixing are usually less than 1% the changes in fg are larger
than this and reflect larger change in relaxation volume on
mixing. In addition the dielectric relaxation time at Tg

Fig. 7. Williams-Watts distribution function, beta vs composition for dielectric ■ and enthalpy □ relaxation.

Fig. 8. Log fm vs. temperature for dielectric and DSC heating rate data for compositions. ◇ 0%, X 20%, + 40%, △ 60% PC. ○ 60% PC, □ 100% PC.
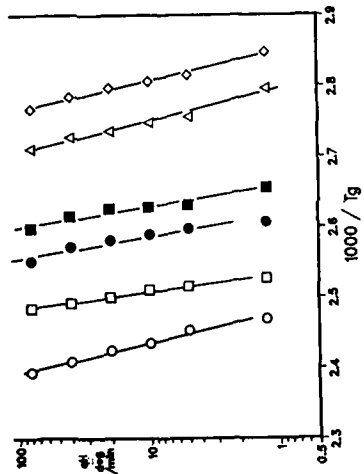
Fig. 5. Heating rate vs reciprocal Tg. ○ 0% PC, □ 20% PC, △ 60% PC, ● 60% PC, ■ 80% PC, ◇ 100% PC.
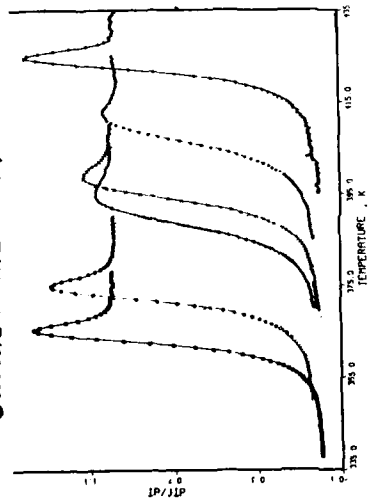
Fig. 6. Derivative of Cp curve, dif/dT vs. temperature. □ 0% PC ○ 20% PC, + 60% PC, x 60% PC, ◇ 80% PC, ▽ 100% PC.

varies with composition and this could be related to the chan-
ges in fg. Since the distribution parameters are different and
have different dependences on composition, it is clear that the
concentration fluctuations on a molecular level affect
properties in different ways.
We have learned from this study and related research that the
relaxational and time-dependent properties of polymer blends
are not simple monotonic functions of their compositions as
might be inferred from the glass transition behavior. These
phenomena are probably related to concentration fluctuations
in these blends which are intimately related to the thermo-
dynamic interactions between blend components.

References
1. O. Olabisi, L.M. Robeson, and M.T. Shaw, "Polymer-Polymer
   Miscibility" Academic Press, NY (1979).
2. R.S. Porter, J.M. Jonza, M. Kimura, C.R. Desper, and E.R.
   George, Polym. Sci. Eng. 29, 55, (1989).
3. C.A. Cruz, D.R. Paul, and J.W. Barlow, J Appl. Polym. Sci.
   23, 589, (1979).
4. C.A. Cruz, D.R.Paul, J.W. Barlow, ibid. 24, 2101 (1979)
5. R. S. Barnum, J.W. Barlow, D. R. Paul, 27, 4065 (1982)
6. E.A. Joseph, M.D. Lorenz, J. W. Barlow, and D.W. Paul,
   Polymer, 23, 112, (1982).
7. R.N. Mohn, D.R. Paul, J.W. Barlow and C.W. Cruz, J. Appl.
   Polym. Sci. 23, 575, (1979).
8. N.G. McCrum, B.E.Read, G.W. Williams, "Anelastic and
   Dielectric Effects in Polymers", Chap. 4, John Wiley, 1967
9. H. Sasabe and C.T. Moynihan, J. Polym. Sci. Polym. Phys.
   16, 1667, (1978)
10. I.M. Hodge and A.R. Berens, Macromolecules, 15, 762,
    (1982), and ibid. 16, 371, (1983), 16, 898, (1983).
11. J.T. Tribone, J.M. O'Reilly, and J. Greener,
    Macromolecules, 19, 1732 (1986).
12. M. Wolf and J.H. Wendorff, Polymer, 30, 1524, (1989)

Interpenetrating Polymer Networks and Related Topological Isomers

HARRY L. FRISCH
Department of Chemistry, State University of New York, Albany, NY 12222

ABSTRACT

We have studied the phase compatibility of simultaneous interpenetrating polymer networks poly (2,6-dimethyl-1,4-phenylene oxide) with a number of other polymer networks as a function of their solubility parameters. Even when the blends of the corresponding linear chain polymers are immiscible their interpenetrating polymer networks can be miscible in all proportions. We have also prepared the corresponding pseudo (or semi) interpenetrating polymer networks where one component is linear and in one system the polymeric catenanes. All these systems generally show microphase separation.

1. Introduction

Interpenetrating polymer networks (IPN's) are intimate mixtures of two or more crosslinked polymers, held together predominantly by permanent entanglements [1,2]. IPN's can be prepared sequentially, i.e. by swelling one formed crosslinked network by the monomers (or prepolymers) crosslinking agents and initiators (or catalysts) of the other network (s) and subsequently polymerizing in situ. They can also be prepared simultaneously i.e. by mixing all the monomers (or prepolymers), crosslinking agents of the different networks, initiators and catalysts and polymerizing all at the same time. We will restrict ourselves here to simultaneous IPN's. Besides their interest as macromolecular topological isomers these materials allow one to produce more controlled and/or enhanced phase miscibility [3]. IPN's are often the only way of producing miscible alloys of crosslinked polymers. Besides depending on kinetic factors such as whether the half-life of formation of permanent entanglements in the IPNs is shorter than the half-life for phase separation due to "uphill diffusion" the extent of incompatability is dependent on thermodynamic factors such as the free volume change or the magnitude of the positive enthalpy of mixing found in many systems. The latter can be crudely estimated by means of the solubility parameter [3] (δ) or parameters [3] (δ_d, δ_p, δ_h) associated with the corresponding linear polymers. To see the effect of the latter we will focus on the properties of a number of recently synthesized simultaneous IPN's [4-9] in which one network consists of crosslinked poly (2,6-dimethyl-1,4-phenylene oxide) (PPO) while the chemical nature of the other component will be varied.

Related to the IPN's are the pseudo (or semi) IPN's in which only one component polymer of the mixture is crosslinked and the other component is left as a linear polymer [1,2]. Finally if one polymer is available as a sufficiently large ring then such rings can be permanently trapped in a different crosslinked polymer network forming a macromolecular catenane [10-12]. We will briefly comment on these other macromolecular topological isomers of the PPO-IPN's.

2. PPO-IPN's

PPO can be conveniently crosslinked by first methyl brominating it using N-bromosuccinimide and then condensing the resulting bromine containing polymer with ethylene diamine. PPO was chosen because the linear polymer is compatible at all compositions with linear polystyrene (PS). It is not surprising therefore that the PPO-PS IPN's, in which the PS is crosslinked by a free-radical reaction, which does not interfere with brominated PPO condensation, using divinyl benzene and benzoyl peroxide, produces homogeneous single phase IPN's at all compositions [4]. There is a perfect match of solubility parameters (δ_d, δ_p, δ_h) of the linear polymers as can be seen from Table 1. Linear poly (methyl methacrylate) [5] (PMMA), linear poly (urethane acrylate) [6] (PUA),

Table I   Solubility Parameters and Glass Transition Temperatures of the Linear Polymers Corresponding to the Network Components of the IPN's.

Linear Polymer	Solubility Parameter (s)	Glass Transition Temperature (°C)
PPO	$\delta_d=8.6, \delta_p=3.0, \delta_h=2.0$	211
PMMA	$\delta_d=9.2, \delta_p=5.0, \delta_h=4.2$	105
PS	$\delta_d=8.6, \delta_p=3.0, \delta_h=2.0$	100
PUA	$\delta=9.1$	–
PB	$\delta=8.38$	−95
PDMS	$\delta=7.3$	−127

linear polybutadiene (PB) and linear poly (dimethyl siloxane) [7] (PDMS) are not miscible to any significant extent with linear PPO, as would be expected from the solubility parameters listed in Table 1. Simultaneous IPN's of PPO and PMMA, PUA, PB and PDMS can be produced employing free radical crosslinking which appears not to interfere with the PPO crosslinking mechanism. For experimental details we refer our readers to the original papers [4-9] which also describe how the pseudo-IPN's of some of these systems were prepared.

These IPN samples were studied by transmission electron microscopy. The glass transition temperatures (Tg) were obtained from differential scanning calorimetry and in some cases confirmed by rheovibron or other thermal-dynamical spectroscopy. Instron stress-strain measurements provided tensile stress and elongation to break data [4-9]. Measurements were made generally on both unextracted and solvent extracted samples. In a number of instances, on the homogeneous samples the average molecular weight between crosslinks (M_c) deduced from stoichiometry was confirmed by swelling studies. In general [4-9] these M_c values varied from about several thousand to a maximum of seventeen thousand [4].

Binder and Frisch [13] had already theoretically suggested that weakly interpenetrating simultaneous IPN's composed of immiscible linear chains could form single phase IPN's over essentially the whole composition range. Thus, the IPN's of PPO and PMMA, PPO and PUA and PPO and PB do this. Some particulars are given in Table 2. These generally transparent to slightly translucent materials show no microphase separation in their transmission electron micrographs and exhibit a single Tg intermediate in value to the Tg's of the pure component crosslinked networks [4-6,9].

When the solubility parameter difference (cf. Table 1) becomes
sufficiently large as with PPO and PDMS we found microphase separation at
almost all compositions [7,8]. These samples showed two inwardly
displaced Tg's and exhibited phase domains ranging from a few tenths of
nanometers to one to two hundreds of nanometers [8].

Table II Compatability of the PPO-IPN's and the weight percentage
of PPO at which the maximum value of the tensile strength to
break (ASTMD 638) is found

IPN	Linear Polymer Compatability	IPN Compatibility	Wt. % of PPO	Reference
PPO-PS	Miscible at all compositions	IPN's are single phase and exhibit a single Tg decreasing monotonically with wt % PPO	75	[4]
PPO-PMMA	Linear polymers are immiscible	"	60	[5]
PPO-PUA	"	"	80	[9]
PPO-PB	"	"	90	[6]
PPO-PDMS	"	IPN's exhibit two Tg's and exhibit phase separation; become most miscible around 90 wt. % PPO	90	[7,8]

Under certain conditions [7,8] around 10 weight percent PDMS single phase
IPN's could be found.

While the Tg's of these IPN's were always intermediate to the Tg's of
the pure crosslinked component networks and varied monotonically with
composition, the tensile stress to break (T.S., ASTM638) of all these full
IPN's showed a maximum at an intermediate composition, which is noted in
Table 2. The exact reasons for this have not yet been experimentally,
fully confirmed but the prevailing speculation [1,2,4] is that at those
compositions the IPN exhibits the maximum extent of permanent
entanglements which also need to be broken to provide ultimate failure of
the sample.

3. Other Topological Isomers Involving Crosslinked PPO.

The pseudo IPN's of cross-linked PPO and linear chains of the other
polymer are generally opaque to translucent solids except for the PS and
PUA. The pseudo IPN's of PPO and PMMA, PB and PDMS exhibit two glass
transition temperatures intermediate in value to the corresponding pure
polymers. The tensile strengths to break are usually monotone decreasing
functions with decreasing weight percentage of PPO.

A number of polymeric catenanes [10] of cyclic PDMS consisting of
rings from 33 to 122 siloxane units have been trapped in crosslinked PPO

234

[11,12]. As expected the larger the degree of polymerization of the cyclic PDMS the larger is the fraction of trapped (unextractable) cyclic in the PPO [14]. These solid materials exhibit a melting point close to that of the pure cyclic PDMS and a somewhat lower Tg than the pure crosslinked PPO. These polymeric catenanes reveal microphase separation with domain sizes of 10-50 μ [12]. The values of the tensile strength to break of these catenanes is smaller or of the same magnitude (within experimental error) as the pure crosslinked PPO.

4. Acknowledgement

5. References

1. D. Klempner and L.Berkowski, "Encyclopedia of Polymer Science and Engineering", (John Wiley and Sons, New York, 1989), Vol 8, p. 282.

2. K.C. Frisch, Jr. and D. Klempner, editors, "Recent Developments in Polyurethanes and Interpenetrating Polymer Networks", (Technomic Publishing Co., Inc., Lancaster, PA 1988).

3. O. Olabisi, L.M. Robeson and M.T. Shaw, "Polymer-Polymer Miscibility", (Academic Press, New York 1979).

4. H.L. Frisch, D. Klempner, H.K. Yoon and K.C. Frisch, Macromolecules, 13, 1016 (1980).

5. S. Singh, H.L. Frisch and H. Ghiradella, Macromolecules (in press).

6. H.L Frisch and Y.H. Hua, Macromolecules, 22, 91 (1989).

7. H.L. Frisch, K. Gebreyes and K.C. Frisch, J. Polym. Sci. (Chem. Ed.) 26, 2589 (1988); K. Gebreyes and H.F. Frisch, ibid. 26, 3391 (1988).

8. W. Huang and H.L. Frisch, Makromol. Chem. Suppl. 15, 137 (1989).

9. P. Mengnjoh and H.L. Frisch, Polymer Letters 27, 285 (1989); J. Polymer Sci. (Chem. Edit.) (in press).

10. D. Callahan, H.L. Frisch and D. Klempner, Polym. Eng. and Sci. 15, 70 (1975).

11. T.J. Fyvie, H.L. Frisch, J.A. Semlyen, S.J. Clarson and J.E. Mark, J. Polym. Sci. (Chem. Edit.) 25, 2503 (1987).

12. W. Huang, H.L. Frisch, Y. Hua and J.A. Semlyen, J. Polym. Sci. (Chem. Edit.) (in press).

13. K. Binder and H.L. Frisch, J. Chem. Phys., 81, 2126 (1984).

14. H.L. Frisch and E. Wasserman, J. Am. Chem. Soc., 83, 3789 (1961).

PART V

Ionomers/Structure

SMALL ANGLE X-RAY SCATTERING ON
POLY(ETHYLENE-METHACRYLIC ACID) LEAD AND
LEAD SULFIDE IONOMERS

BENJAMIN CHU*, DAN Q. WU
Department of Chemistry, State University of New York at Stony Brook, Long Island, NY 11794-3400
and WALTER MAHLER
Central Research & Development Department, Experimental Station, E.I. du Pont de Nemours & Co., Inc., Wilmington, DE 19880-0328
* author to whom all correspondence should be addressed.

ABSTRACT

The morphology of ionomers, e.g., poly(ethylene-methacrylic acid) (EMA) lead salts (EMA/Pb) and lead sulfide compounds (EMA/PbS), has been studied by using the techniques of small angle x-ray scattering (SAXS), anomalous SAXS (ASAXS), wide angle x-ray scattering (WAXS), and differential scanning calorimetry (DSC). EMA/Pb containing less than 5 wt% of lead exhibited two characteristic SAXS peaks which corresponded to the lamellar structure of the partially crystalline polymer matrix and the ionic structure of the lead aggregates that were present in the amorphous regions. The lead aggregates were not distributed uniformly and increased in packing density with increasing lead content. Both DSC and WAXS showed that the crystalline phase was present for all EMA/Pb samples and that the crystallinity decreased slightly with increasing lead content. ASAXS near the L_3 absorption edge of lead permitted the extraction of the scattered intensity of lead ions from the SAXS patterns of the superimposed crystalline and ionic structures. Correlation function analysis revealed that the ionic aggregates of the EMA/Pb containing 5 wt% of lead could be described by a liquid-like model with a short range order of 2-4 nm. EMA/PbS samples were made by a reaction of EMA/Pb ionomers with hydrogen sulfide. Instead of an ionic peak as shown by EMA/Pb samples, the SAXS patterns of EMA/PbS showed a broad diffraction peak located at the same q value as the lamellar peak of the EMA in acid form. The (lamellar) peak could be attributed to the interference between the PbS crystallites in the neighboring lamellae.

INTRODUCTION

Copolymer poly(ethylene-metharylic acid) (EMA, 85 wt% of ethylene) is partially crystalline because of the presence of a large amount of ethylene segments. EMA ionomers are usually the metal salts of EMA whose carboxylic acid groups have been partially or completely neutralized. Surlyn, (a trade mark of Du Pont) an EMA in sodium or zinc salt form, has been well-known for its superior properties as packaging and coating materials, thanks to the ionic crosslinks formed by the aggregation of metal ions. Although ethylene-carboxylate ionomers have been studied extensively on their structure-properties relations [1-12] and several models have been proposed to describe its morphology [4-5, 7, 10-11], controversies about which model to use still remain. This work aims at a better understanding of the morphology of EMA/Pb ionomers by carefully designed small angle x-ray scattering (SAXS) and anomalous SAXS (ASAXS) experiments and by utilizing the correlation function analysis, a straightforward and effective method of selecting a correct model and of determining the structural parameters from SAXS and ASAXS patterns covering a very broad q range.

Recently, Mahler treated EMA/Pb films with H2S to obtain a composite polymer material (EMA/PbS) possessing semiconductor properties [13]. In EMA/PbS samples, PbS crystallites are embodied in the semicrystalline polymer matrix. A morphological characterization of EMA/PbS is desirable because the size and the spatial arrangement of PbS particles are the key factors that control the semiconducting properties.

Anomalous small angle x-ray scattering is capable of varying the scattering power of a selected element [14-20]. Its application to the EMA/Pb and EMA/PbS samples allows us to remove any non-lead related scatterings including the reflection of the ethylene lamellae, possible impurities and voids and to study the structure and the spatial arrangement of lead ions or PbS particles in the polymer matrix. In this paper, the use of ASAXS technique in the EMA ionomer structural determination is exemplified by the EMA/Pb containing 5 wt% of lead.

EMA/Pb AND EMA/PbS IONOMERS

Poly(ethylene-methacrylic acid) (EMA) copolymer containing 15 wt% (or 5.4 mol%) of methacrylic acid had $M_w = 8.6 \times 10^4$ g/mol and $M_w/M_n \sim 7$. The EMA/Pb ionomer containing 20 wt% of

lead was obtained by neutralizing EMA with lead acetate. The neutralization was accomplished by milling EMA with lead acetate at 160°C. The ionomer sample containing 20 wt% of lead was then compression molded into films. The samples with 10, 5.0, 2.0, 1.0, and 0.2 wt% of lead were subsequently diluted from the 20 wt% sample by mixing with an appropriate additional amount of the lead-free EMA. Fairly homogeneous films could be obtained by reprocessing the sample several times. The ionomer films with a thickness ranging from 0.1 mm to 0.3 mm were essentially transparent. The samples were annealed at a 60°C vacuum oven for 24 hours before SAXS and ASAXS measurements.

EMA lead sulfide compounds (EMA/PbS) containing 20, 10, 5, 2, 1, 0.2 wt% of lead were made by exposure, respectively, of the corresponding EMA/Pb films to 1 atm H_2S at room temperatures for at least 2 hours. The change of color of the EMA/PbS films from light brown to black for 0.2 to 20 wt% of lead suggested the formation of PbS particles in the EMA polymer matrix.

Differential scanning calorimetry (DSC) measurements (using ~ 5 mg sample and 10 degree/min heating rate) of the EMA/Pb samples showed a slight decrease in heat of fusion and melting temperature with increasing lead content. Wide angle x-ray scattering (WAXS) showed the ethylene (110) and (200) reflections. Both DSC and WAXS suggest the presence of the ethylene crystalline phase, although the crystallinity decreases slightly with increasing lead content. WAXS of the EMA/PbS showed reflections of PbS crystallites that were enhanced (became sharper) with increasing lead content suggesting growth in the size of PbS particles in the semicrystalline polymer matrix.

Tables 1 and 2 list the DSC results, respectively, of the EMA/Pb and EMA/PbS samples.

Table 1. Physical Constants for EMA/Pb[a]

Pb content (wt%)	0	0.2	2	5	10	20
lamellar peak position (1/nm)	0.6	0.6	0.6	(0.6)[b]	-	-
ionic peak position (1/nm)	-	~3.6	3.5	3.5	2.9	2.5
ionic peak height	(4)[c]	~5	20	48	125	210
heat of fusion (J/g)	39		37	36	30	19
T_m (°C)	92		92	92	89	86

Table 2. Physical Constants for EMA/PbS[a]

Pb content (wt%)	0.2	1	2	5	10	20
lamellar peak position (1/nm)	0.6	~0.4	0.5	0.55	0.6	-
heat of fusion (J/g)	37	33		30	22	26
T_m (°C)	91	90		90	89	87

[a]Data of heat of fusion and melting temperature T_m were collected from the endotherms of second heating circle to ensure the same crystallization history for all samples.
[b]Appearance of lamellar peak was sensitive to sample annealing.
[c]Ionic peak was hard to observe. The scattered intensity value at $q \sim 3.6$ nm^{-1} was taken.

SMALL ANGLE X-RAY SCATTERING (SAXS)

All scattering experiments were conducted at the State University of New York (SUNY) X3A2 Beamline, National Synchrotron Light Source [21]. A small angle x-ray diffractometer (SAXD) equipped with a modified Kratky block collimator [22] and an x-ray photodiode array (PDA) detector [23] was capable of making SAXS as well as ASAXS measurements with a q ($=(4\pi/\lambda)\sin(\theta/2)$, with λ and θ being, respectively, x-ray wavelength and scattering angle) range of 0.03-13 nm^{-1}. A Si (111) double crystal monochramator with an energy resolution of ± 5 eV was used. A gold-coated quartz torroidal mirror (60 cm long, 60 mm radius) used in SAXS at $\lambda \sim 0.154$ nm was removed in ASAXS measurements near the L_3 absorption edge ($E_{edge} = 13040$ eV or $\lambda \sim 0.095$ nm) of lead, because it could not reflect and focus x-rays of wavelength shorter than 0.097 nm to the small angle x-ray diffractometer (SAXD) which was ~10 m away from the mirror. The x-ray beam had a cross-section of ~0.2 mmx~2.0 mm at the polymer sample. The distance between the sample and the detector was 220 mm. Desmearing was not needed for $q > 0.2$ nm^{-1}.

SAXS measurements were performed at room temperature. The SAXS patterns were corrected for detector sensitivity, parasitic scattering, detector dark counts, sample attenuation, incident x-ray intensity fluctuation, and normalized to 1 mm sample thickness and 1 sec experimental duration.

Figure 1 shows SAXS patterns for the EMA/Pb ionomers of, respectively, 20, 10, 5, 2, and 0 (in acid form) wt% of lead. A diffraction peak at $q \sim 0.6$ nm^{-1}, indicated by a double arrow, could be observed upto 2 wt% of lead (also in the sample with 5 wt% of lead after annealing the sample). The (lamellar) peak became less sharp and weaker with increasing Pb content and eventually disappeared. Another broad diffraction peak, located at $2.5 < q < 3.6$ nm^{-1}, marked by an arrow, shifted to a smaller q value and grew in peak height with increasing lead content.

The peak at $q \sim 0.6$ nm^{-1} is due to the lamellar structure of partially crystalline ethylene segments. Little dependence of the lamellar peak position on the lead content was observed suggesting that the lamellar structure was hardly affected by a small amount of lead aggregates (≤ 2 wt%) in agreement with the DSC results (Table 1). As DSC showed the presence of the ethylene crystalline phase even in the EMA/Pb with 20 wt% of lead, diminishing lamellar peak with increasing lead content suggests that the lead ions were distributed mainly in the amorphous region so that the electron density difference between the crystalline and the amorphous regions was reduced with more lead ions present in the amorphous region. The electron densities of the crystalline and the amorphous phases were about to be matched in the EMA/Pb containing 5 wt% of lead. Further increase in the lead content could certainly affect the formation of lamellar stacks because the aggregates of Pb groups could form crosslinks that would reduce the folding of ethylene segments and thereby the crystallinity. DSC also showed a decrease in the heat of fusion and the melting temperature especially in the sample containing 20 wt% of lead (Table 1). The disappearance of the lamellar reflection in the EMA/Pb samples of higher than 5 wt% of lead implied that (1) the lead ions were not distributed uniformly in the amorphous region, otherwise a lamellar reflection should have reappeared and peaked at the same q value as a consequence of "reversed-density" lamellae whose amorphous phase (containing ions) would have a higher electron density than that of the crystalline phase and/or (2) the scattering from the ionic aggregates oversnadowed that from the lamellae.

The peak at 2.5-3.6 nm^{-1} is clearly the ionic peak which originates from the lead ion aggregates. The magnitudes of the ionic peak as well as the small angle scattering (upturn) at $q < \sim 0.6$ nm^{-1}, another well-observed feature of ionomers [6], are increased with increasing lead content suggesting its contribution from the ions [25,26]. Table 1 lists the positions and the heights of the two characteristic peaks of the EMA/Pb samples.

Figure 2 shows SAXS patterns for the EMA/PbS samples containing, respectively, 20, 10, 5, 2, 1, and 0.2 wt% of lead. No appreciable ionic peak was observed. A broad diffraction peak at $q \sim 0.6$ nm^{-1} was observed for all the EMA/PbS samples. The peak position was located near the lamellar peak position of the ethylene crystalline matrix and could be related to the reflection of lamella-like structures due to the spatial distribution of PbS particles. The above interpretation could be supported by the following observations. At 0.2 wt% of lead, the number and the size of the PbS particles were so small that the reflection was due to inter-ethylene lamellae. At 1 wt% of lead, however, the reflection peak became less sharp with an ill-defined peak position. Since the electron density matching between crystalline and amorphous phases should occur near 5 wt% of lead as we have observed for the case of EMA/Pb with 5 wt% of lead, the ill-defined peak could only be attributed to the randomness in the concentration of the PbS particles in the periodic lamellar layers. This suggestion is supported by the EMA/PbS samples containing 2 or more wt% of lead. The increase in the reflection peak height and the shift of the peak from $q \sim 0.4$ nm^{-1} at 1 wt% to $q \sim 0.6$ nm^{-1} at 10 wt% illustrated that the PbS particles grew in size and at the same time arranged themselves in a more ordered manner. A similar lamellar peak growth pattern was observed in the polyethylene crystallization [27]. It is thus reasonable to conclude that in the EMA/PbS sample containing 1 or more wt% of lead, the PbS crystallites contribute to the lamellar reflection at $q \sim 0.6$ nm^{-1}. The reflection peak of the EMA/PbS samples was broader than that of the EMA and might be explained by the fact that the PbS particles with finite particle sizes would have a particle form factor superimposed to the lamellar reflection. The EMA/PbS with 20 wt% of lead showed very different behavior from the others. There, the PbS particles might no longer be confined within the ethylene lamellae. The peak positions of the EMA/PbS samples are listed in Table 2.

The most straightforward interpretation of the ionic peak as shown in Figure 1 was made by Longworth [4] who assumed that the ionic aggregates occupied the lattice points and attributed the ionic peak to Bragg reflection of those ionic aggregates. Thus the inter-aggregates distance could be estimated as $\sim 2\pi/q_{peak}$. MacKnight et al. attributed the ionic peak to core-shell shaped aggregates that had no inter-aggregate interference [7]. An alternative core-shell model was given by Hashimoto et al. [24]. Cooper et al., on the other hand, explained the ionic peak in terms of liquid-like inter-aggregates (spheres) interference [11]. The use of these morphological models, however, requires availability of the excess scattered intensity from the lead ions. Furthermore the model fitting of SAXS patterns measured in a limited q-range often prevents a critical comparison of the theoritical models with experimental data. These difficulties could be resolved by using ASAXS covering a very broad q
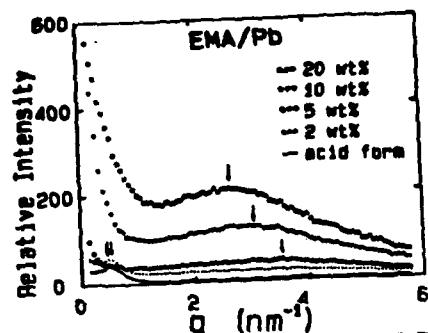
Figure 1. SAXS patterns of the EMA/Pb samples containing, respectively, 20, 10, 5, 2, and 0 (acid form) wt% of Pb. Double arrow indicates the reflection of the ethylene lamellae at $q \sim 0.6$ nm^{-1}. With increasing Pb content, the peak becomes less sharp and disappears for EMA/Pb with more than 5 wt% of lead. Arrow marks the ionic diffraction peak, $q \sim 2.5$-3.6 nm^{-1}, which is originated from the Pb ion aggregation. The Pb aggregates are not distributed uniformly in the amorphous region of the EMA polymer matrix.
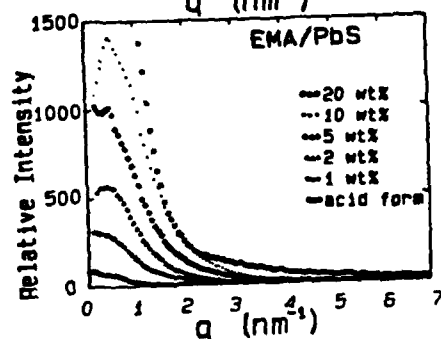
Figure 2. SAXS patterns of the EMA/PbS samples containing, respectively, 20, 10, 5, 2, 1, 0 (acid form) wt% of Pb. No appreciable ionic peak is observed. Instead, a strong and broad diffraction peak is seen at $q \sim 0.6$ nm^{-1}. For EMA/PbS with higher than 1 wt% of Pb, PbS particles, in crystalline form, are distributed in the amorphous region with certain ordering. The diffraction peak is due to interference of the PbS particles in neighboring lamellae. The PbS crystallites grows in size with increasing Pb content.
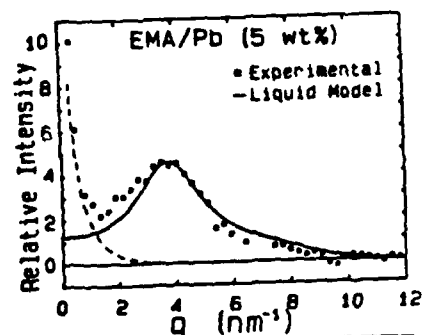
Figure 3. ASAXS difference scattering pattern (hollow squares) of the EMA/Pb sample containing 5 wt% of Pb, which was obtained by subtraction of the SAXS curve measured at 7 eV below the Pb $L3$ absorption edge (corrected for a fluorescence background) from that measured at 317 eV below the edge. Solid line represents fitting of the liquid-like model. Dashed line is the structure factor corresponding to a Debye-Bueche type inhomogeneity. The ASAXS pattern is well described by the two structures. The model parameters are shown in Figure 4.
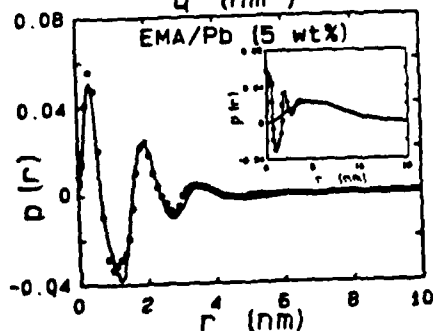
Figure 4. In the inset, the dotted line (○) is the correlation function $p(r) = r^2 \gamma(r)$ (Eq. 1) of the ASAXS difference scattering pattern (Figure 3). The broad hump can be fitted by a Debye-Bueche type equation for random inhomogeneity, $\gamma(r) = \exp(-r/a + r^2/b^2)$, with $a = 8.1$ nm and $b = 36$ nm (solid line). The squares, obtained by subtraction of two curves in the inset, represent a local structure that can be well described by the liquid-like model (solid line), with $R_{core} = 0.36$ nm, $R_{ca} = 0.72$ nm, and $V_p = 4$ nm^3.

range [19, 20, 28] and by applying correlation function analysis [29, 30] to the excess SAXS patterns due to lead ions only as suggested by Williams [31] and demonstrated by an example in the following section.

ANOMALOUS SMALL ANGLE X-RAY SCATTERING (ASAXS)

The ASAXS technique is one of the best methods for getting the pure scattering structure factor of metal ions. Correlation function analysis of the scattering profiles is the most effective and least-biased mean to demonstrate whether the ionic aggregates have inter-particle interferences [32]. We are here to present an example of using ASAXS to overcome the difficulties in determining an ionic structure in the presence of polymer lamellar structure.

SAXS measurements on the EMA/Pb sample were conducted at, respectively, $E = 13033$ eV (7 eV below the edge) and 12723 eV (317 eV below the edge). Each SAXS curve was accumulated for 200 sec. The energies were carefully chosen according to the anomalous scattering factors f' and f'' values of lead in the ionomer samples which had been *experimentally* determined [28]. The scattered intensity of lead ions could only be obtained by subtracting the SAXS pattern measured at 13033 eV from that at 12723 eV after fluorescence correction (matching SAXS patterns at $q > 10$ nm^{-1} where the form factor of lead ionic aggregates could be experimentally terminated). The experimental details will be described in our forthcoming paper [28].

Figure 3 shows the ASAXS difference scattering pattern for the EMA/Pb containing 5 wt% of lead (hollow squares). A lamellar peak at $q \sim 0.6$ nm^{-1} in the SAXS curves has been cancelled out by the subtraction. The ASAXS difference pattern, possessing two typical features of ionomers: an ionic peak and a small angle upturn, was due to lead ions only. One notes that the ionic peak terminates $q > 10$ nm^{-1}.

The electron density auto-correlation, $\gamma(r) = < \eta(r_1)\eta(r_2) >$, with η being the local electron density fluctuations and $r = |r_1 - r_2|$, is related to the scattered intensity $I(q)$ by [29, 30],

$$\gamma(r) = \int_0^\infty q^2 I(q) \frac{\sin qr}{qr} dq / \int_0^\infty q^2 I(q) dq \tag{1}$$

In the inset of Figure 4, the correlation function $p(r) = r^2 \gamma(r)$ of the smoothed ASAXS difference scattering pattern (Figure 3) shows a broad hump which can be fitted with an empirical equation (solid line): $\gamma(r) \sim exp(-r/a + r^2/b^2)$, with $a = 8.1$ nm and $b = 36$ nm. This equation is similar to well-known Debye-Bueche equation for random inhomogeneities [29], $\gamma(r) \sim exp(-r/a)$, with a defined as the correlation length. Fitting of the Debye-Bueche equation to the experimental correlation function yielded $a = 9.1$ nm, although the fitting was not as good as the empirical equation. The subtraction of the fitted (Debye-Bueche like) correlation function from the experimental overall correlation function yielded a difference curve as shown in Figure 4 (hollow squares). The damping oscillations seen in the difference correlation function are typical in the correlation function of a system with inter-particle interference. The difference correlation function could be well fitted to a liquid-like model [11] resulting in the following model parameters: radius of the ionic aggregates $R_{core} = 0.36 \pm 0.01$ nm, radius of closest approach $R_{ca} = 0.72 \pm 0.02$ nm, and volume per each ionic aggregate, $V_p = 4.0 \pm 0.4$ nm^3.

In Figure 3, the solid line and the dashed line are the structure factors corresponding to, respectively, the correlation function of the liquid-like structure, as shown in Figure 4 and the correlation function similar to Debye-Bueche's inhomogeneity, as shown in the inset of Figure 4. The ASAXS difference scattering pattern could be represented fairly well by the sum of the two types of structure factors.

Figures 3 and 4 reveal the following information about the lead ions. There are two structures in the EMA/Pb with 5wt% of lead: a Debye-Bueche type inhomogeneity with a correlation length of about 8-9 nm and a local structure that could be well described by the liquid-like model. The ionic peak can be attributed to the inter-aggregate interference while the small angle upturn is due to the inhomogeneous spatial distribution of the lead ions. The lead ion aggregates are quite small in size with a mean diameter of ~0.7 nm. The most probable inter-aggregate distance is ~2.0 nm (second peak in Figure 4) slightly greater than ~1.8 nm estimated from the Bragg spacing corresponding to the ionic peak position.

SUMMARY

By using the techniques of SAXS, ASAXS, WAXS, and DSC, the ionomer samples EMA/Pb and EMA/PbS could be well characterized. The lead aggregates and PbS crystalline particles were present in the amorphous region of EMA semicrystalline polymer matrix. The distribution of lead ions was not

uniform while certain ordering was observed for PbS particles. The presence of the crosslinks formed by the lead aggregates reduced the crystallinity of the polymer matrix. ASAXS was shown to be an effective method of extracting the scattered intensity of ions from complex scattering functions with backgrounds including the crystalline matrix, possible impurity, air bubbles, and voids. The ASAXS difference scattering pattern of the EMA/Pb sample containing 5 wt% of lead was analyzed by using the correlation function scheme. The structure and the spatial arrangement of the ionic aggregates could thereby be described. The liquid-like model could be used to depict the ionic peak with the local structure of the ionic aggregates represented by the correlation function, while the Debye-Bueche type long range inhomogeneity offered a good scheme to represent the small angle upturn.

ACKNOWLEDGEMENT

REFERENCES

[1]   R.W. Rees and D.J. Vaughan, *Polym. Prepr. Am. Chem. Soc. Div. Polym. Chem.*, 6, 287 (1965).
[2]   F.C. Wilson, R. Longworth and D.J. Vaughan, *Polym. Prepr., Amer. Chem. Soc. Div. Polym. Chem.*, 9, 505 (1968).
[3]   R. Longworth and D.J. Vaughan, *Nature (London)*, 218, 85 (1968); and *Polym. Prepr., Amer. Chem. Soc. Div. Polym. Chem.*, 9, 525 (1968).
[4]   R. Longworth, in *Ionic Polymer*, edited by L. Holliday (Halsted-Wiley, New York, 1975).
[5]   C.L. Max, D.F. Caulfield, and S.L. Cooper, *Macromolecules*, 6, 344 (1973).
[6]   T.R. Earnest, Jr. and W.J. MacKnight, *Macomolecules*, 10, 206 (1977) and *J. Polym. Sci., Polym. Phys. Ed.*, 16, 143 (1978)
[7]   W. J. MacKnight, W.P. Taggart, and R.S. Stein, *J. Polym. Sci., Polym. Symp.*, 45, 113 (1974).
[8]   J. Kao, R.S. Stein, W.J. MacKnight, W.P. Taggart, and G.S. Cargill, *Macromolecules*, 7, 95 (1974).
[9]   T.R. Earnest, Jr., Ph.D Thesis, University of Massachusetts, (1978)
[10] W.J. MacKnight and T.R. Earnest, *J. Polym. Sci: Macrom. Rev.*, 16, 41 (1981).
[11] D.J. Yarusso, S.L. Cooper, *Polymer*, 26, 371 (1985) and *Macromolecules*, 16, 1871 (1983).
[12] K. Tadano, E. Hirasawa, H. Yamamoto, and S. Yano, *Macomolecules*, 22, 226 (1989).
[13] W. Mahler, *J. Inorg. Chem.*, 27, 436 (1988).
[14] H. B. Stuhrmann, *Adv. Polym. Sci.*, 67, 123 (1985).
[15] J.C. Phillips and K.O. Hodgson, in *Synchrotron Radiation Research*, edited by H. Winick and S. Doniach, (Plenum, New York, 1980) and *Acta Cryst.*, A36, 856 (1980).
[16] R.C. Miake-Lye, S. Doniach, and K.O. Hodgson, *Biophys. J.*, 41, 287 (1983).
[17] P. Goudeau, A. Fontaine, A. Naudon, and C.E. Williams, *J. Appl. Cryst.*, 19, 19 (1986).
[18] J.P. Simon, O. Lyon, and D. de Fontaine, *J. Appl. Cryst.*, 18, 230 (1985).
[19] Y.S. Ding, S.R. Hubbard, K.O. Hodgson, R.A. Register, and S.L. Cooper, *Macromolecules*, 21, 1698 (1988).
[20] R.A. Register and S.L. Cooper, to be published in Macromolecules.
[21] B. Chu, J.C. Phillips, D.Q. Wu, in *Polymer Research at Synchrotron Radiation Sources*, edited by T.P. Russel and A.N. Goland, report no. BNL51847, Brookhaven National Laboratory, Upton, NY (1986) p.126 and J.C. Phillips, K.J. Baldwin, W.F. Lehnert, A.D. LeGrand, C.T. Prewitt, *Nucl. Instrum. and Methods in Phys. Res.*, A246, 182 (1986).
[22] B. Chu, D.Q. Wu, and C. Wu, *Rev. Sci. Instrum.*, 58(7), 1158 (1987).
[23] B. Chu, D.Q. Wu, and R. Howard, *Rev. Sci. Instrum.*, 60(10), 3224 (1989).
[24] M. Fujimura, T. Hashimoto, and H. Kawai, *Macromolecules*, 14, 1309 (1981) and 15, 136 (1982).
[25] B. Chu, D.Q. Wu, W.J. MacKnight, C. Wu, J.C. Phillips, A. LeGrand, C.W. Lantman, and R.D. Lundberg, *Macromolecules*, 21, 523 (1988).
[26] D.Q. Wu, J.C. Phillips, R.D. Lundberg, W.J. MacKnight, and B. Chu, *Macromolecules*, 22, 992 (1989).
[27] H. Song, R.S. Stein, D.Q. Wu, M. Ree, J.C. Phillips, A. LeGrand, B. Chu, *Macromolecules*, 21, 1180 (1988) and H. Song, D.Q. Wu, M. Satkowski, R.S. Stein, and B. Chu, *Macromolecule,*, in press.

[28]   D.Q. Wu, B. Chu, and W. Mahler, to be submitted to *Macromolecules*.

[29]   P. Debye and A.M. Bueche, *J. Appl. Phys.*, 20, 299 (1949) and H. Brumberger and P. Debye, *J. Phys. Chem.*, 61, 1623 (1957).

[30]   G. Porod, in *Small Angle X-ray Scattering*, edited by O. Glatter, O. Kratky, (Academic Press, London 1982)

[31]   C.E. Williams, *in Structure and Properties of Ionomers*, edited by M. Pineri and A. Eisenberg, (D. Reidel Publishing Co., Dordrecht 1987).

[32]   D.Q. Wu, B. Chu, R.D. Lundberg, and W.J. MacKnight, manuscript in preparation.

EXCIMER AND EXCITON FUSION OF BLENDS AND MOLECULARLY DOPED POLYMERS--A NEW MORPHOLOGICAL TOOL.

ZHONG-YOU SHI, CHING-SHAN LI and RAOUL KOPELMAN,
Department of Chemistry, The University of Michigan, Ann Arbor, MI 48109-1055.

ABSTRACT

Exciton-exciton and exciton-excimer triplet fusion kinetics is monitored in medium molecular weight P1VN/PMMA solvent cast films with concentrations from 0.005 to 100% (weight), at temperatures of 77 to 300 K, via time resolved fluorescence and phosphorescence (10 ns to 10 sec). The heterogeneity exponent (h) is 0.5 for isolated P1VN chains, zero (classical) for pure P1VN and "fractal-like" throughout certain concentration regimes. However, h is not monotonic with blend concentration but rather oscillates between zero and 0.5. Correlation is made with morphology changes (phase separation, filamentation). As expected, the triplet exciton kinetics is dominated by short-range hops (about 5 Å) and thus monitors the primary topology of the chains. At concentrations below 0.01%, the excitons are constrained to a truly one-dimensional topology. At higher concentrations there is a fractal-like topology. Similar studies were conducted on naphthalene-doped PMMA (1-20% weight). The lower concentration samples are neither segregated nor random solution phases.

INTRODUCTION

Can luminescence techniques establish themselves as important tools for polymer morphology? Industrial materials are becoming more complex, structurally, as they are being optimized for specific performance criteria. This complexity goes beyond the chemistry of copolymers and into the specific physical arrangement of composite materials containing monomers, homopolymers, and copolymers. This leads to heterogeneous mixtures containing microphase and interphase domains. There is a general belief that the microscopic structure of the material and its dynamic response are responsible for its desirable properties [1]. However, we know little about the morphology and dynamics at the 50 to 500 Å scale (typical polymer dimensions). Characterizing the structure and dynamics on this scale might lead to : (1) a better understanding of materials performance, (2) improved analytical methods for quality control, and 3) guidance for future synthesis of improved materials.

While spectroscopic methods have been around for a long time, the recent advances in laser technology and in the theory of photophysical processes have led to new approaches. Fluorescence and phosphorescence approaches, based largely on energy transfer (ET) and quenching, have been of much recent interest[1-7]. Here we focus on a relatively new approach of monitoring longer-range energy transport and energy fusion kinetics. This approach has been applied successfully to simple organic crystals, mixed crystals, crystallites embedded in porous membranes and glasses, and vapor-deposited organic films [8,9]. Most powerful has been the utilization of triplet excitation transport and fusion, via *delayed fluorescence* and *phosphorescence*. We apply this approach to the study of polymer blend micro-morphology.

TRIPLET EXCITON TRANSPORT

Triplet excitation transfer (TET) is characterized by an extremely short geometrical range, as short or shorter than electron transfer. The following table is adapted from Tazuke and Winnik [2]:

Interaction	Effective Range (Å)
Singlet ET (dipole)	10 to 100
TET (electron exchange)	4 to 15
Electron Transfer	4 to 25
Exciplex Formation	4 to 15
Excimer Formation	ca. 4
Chem. Bond Formation	ca. 2 to 4

For chromophores such as naphthalene, TET is limited, effectively, to 8 Å [8-10]. While excimer formation has a shorter range, its studies are usually contaminated by the much longer range of singlet ET, which leads to the formation of the excimer [3,4]. In addition, the much longer lifetime of the excited triplet state (e.g., 3 sec. in the naphthyl group, compared to 10^{-7} sec. for the excited singlet) makes it possible to study multistep energy transfer, i.e., exciton transport kinetics.
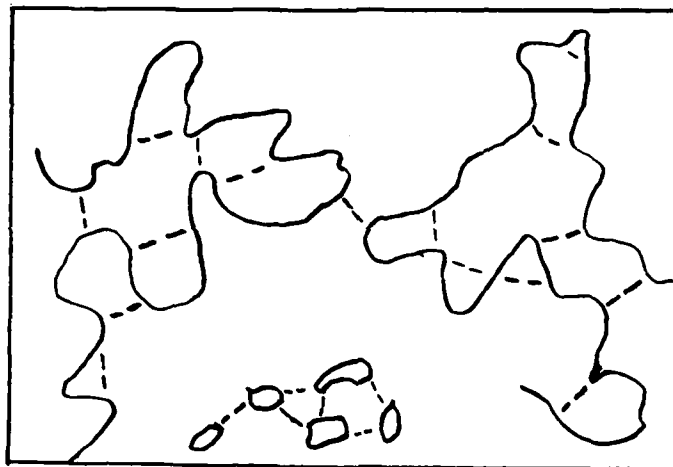
Fig. 1: Schematic description of naphthalene aggregates and polyvinylnaphthalene guest chains embedded in PMMA. The dashed lines are the "short-cuts" possible for singlet ET but not for triplet ET.

Long-range triplet exciton transport can be monitored by trapping at impurities or defects such as triplet excimers [8-10]. However, the most effective method seems to be that of triplet exciton fusion, which can take place anywhere, including at a trapping site. This fusion process is monitored not only by its effect on the triplet phosphorescence, but also by its creation of *delayed fluorescence*, with its highly increased quantum efficiency and its unmistakable time characteristics. In addition, fusion is a photophysical process which can characterize the geometry by which it is confined (see below), over a range of about 1000 Å or larger, but with a definition of about 5 Å (Fig. 1).

FRACTAL-LIKE TRANSPORT AND KINETICS

Recent insights into transport and reaction dynamics in restricted geometries and heterogeneous media have led to a "fractal" approach to diffusion controlled

kinetics [8]. Specifically, the rate coefficient for a bimolecular or pseudo-monomolecular reaction can be written as

$$k = k_1 t^{-h} \qquad 0 \le h < 1 \qquad (1)$$

where h is the "heterogeneity exponent," and k_1 is roughly the rate of a single hop. For classical processes (homogeneous, 3-dimensional media) h = 0 and k is the classical "rate constant." For a strictly one-dimensional topology h = 1/2. For most other situations (effective topology between one- and three-dimensional), $0 < h < 1/2$. Underlying this result is a non-Poissonian distribution of the reacting particles [8], due to the fact that diffusion in low dimensions is an inefficient stirring mechanism. (This is an expression of the non-recurrent nature of random walk in low dimensions.) The exponent h is thus sensitive to the local morphology. In addition, there are other short-time effects that are sensitive to the local morphology [8].

We note that eq.(1) is appropriate for both bimolecular reactions (such as A + A → Product) and pseudomonomolecular reactions (A + C → C + Product). In particular we deal here with: 1. Triplet homofusion:

$$T + T \to S \to h\nu \qquad (2)$$

where T is a triplet excitation, S a singlet excitation and hν a photon of fluorescence (or a phonon). 2. Triplet heterofusion:

$$T + T' \to T' + h\nu \qquad (3)$$

where T' is a defect (excimer) excitation. Both equations (2) and (3) are somewhat oversimplified [9] but are kinetically sound. In addition, there is the true monomolecular decay:

$$T \to h\nu' \qquad (4)$$

where hν' is a photon of phosphorescence (or a phonon). The homofusion process is thus described by

$$F = k_1' t^{-h} P^2 \qquad (5)$$

where F is delayed fluorescence and P phosphorescence, while the heterofusion process is given by

$$F = k_1'' t^{-h} P \qquad (6)$$

where h is the same and depends on the medium but not on the process. We note that proper time modulation of the laser pump and probing procedure will lead to either homofusion or heterofusion.

EXPERIMENTAL

Both P1VN (Mw = 100,000) and PMMA (Mw = 154,000) used in this study are purchased from Polyscience Inc. They are all further purified by multiple precipitation (3 times). For PMMA we use toluene as the solvent and methanol as the non-solvent, while for P1VN the solvent is dichloromethane and the non-solvent is methanol. The solvents used in the purifications are all spectral grade. It is believed that the purified polymers are free of monomers and low molecular weight impurities from the polymerization. The final precipitates are left in the air to dry for 1-2 days and then vacuum dried at about 70 °C (below their T_g s) for another 2 days ensuring that there is no solvent left in the polymer samples.

Film samples are cast by using the doctor blade technique. Different portions of polymers are carefully weighted. For the concentrations below 0.5%, we first dissolve 5.0 mg of P1VN in 50 ml toluene and then by taking out 0.5, 1.0, 2.5, and 5.0 ml of this solution, get corresponding weights of P1VN equal to 0.05, 0.1, 0.25, and 0.5 milligrams, respectively. These solutions are evaporated so that another solvent can be used. By adding different amounts of PMMA, we get 0.005%, 0.01%, 0.05%, 0.1%, (Wt/Wt) compositions. For each gram of solid polymer 4 ml dichloromethane is used as the solvent. The solutions are well stirred for several hours in order to get homogeneous mixtures. The substrates on which the films are cast are chosen to be aluminum plates. The casting surfaces are well washed and/or rinsed with water, soap, ethyl alcohol and dichloromethane. Films are cast in a nitrogen dry box. First, the well-stirred solutions are pored into the hollow of the blade which is on the surface of the substrate. By sliding the blade towards the other end a thin film is made through the groove of the blade. The newly cast films are left in the nitrogen dry box for several hours and then further dried in the vacuum oven at 70 °C for 2 days. The thickness of the finished film is about 20 μm. The sample preparation of naphthalene-doped PMMA was described before [11].

When experiments are performed at liquid nitrogen temperature (77K), the samples are immersed in a liquid nitrogen bath inside a quartz cryostat. Excitation light for this study is a Lambda Physics Excimer laser, with XeCl; it gives about a 10 nanosecond pulse at the wavelength of 308 nm and the line-width is several angstroms. Usually, the output power of the laser is much stronger than required; therefore, neutral density filters are used. For consistency, each set of experiments is performed at the same strength of excitation light.

For the kinetic studies the samples inside the cryostat are usually placed at 45° to the incident excitation and the emission signals are picked up by 2 UV grade lenses, which focus the light on the entrance slit of a SPEX 0.5 M double spectrometer. In order to pick up more signal and increase the signal-to-noise ratio, both the entrance and exit slits are open wide (about 1000 microns or more). For phosphorescence decay signals the monochromer is set at 5250 Å, while for the delayed fluorescence the signals are collected at around 3400 Å. These settings are based on the steady state emission spectra of P1VN/PMMA. At the exit slit a regular EMI PMT is attached. The samples with concentrations lower than 2%, due to the fact that the decay signals are weak and the films are relatively clear, are placed at 90° to the excitation light. The emission signals are collected at the back of the sample (similarly to the way in which absorption spectrum is taken). Both delayed fluorescence and phosphorescence decay emissions are first passed through a $CuSO_4$ solution (100g $CuSO_4 \cdot 5H_2O$/liter) to filter out the residual laser light. Then a 340 nm band pass filter is used before the PMT to collect the delayed fluorescence. For phosphorescence decay a 520 nm band pass filter is used. The current output from the PMT is fed into a Signal Averager (Princeton Applied Research Model 4202). The termination resistor is selected to be small enough to eliminate the intrinsic effect of the apparatus on the fast decay of the samples. A Wavetek Model 187 function generator provides the external trigger. For the early time decay data collections, the rising edge of an about 40 microseconds wide pulse is used to trigger the excimer laser, while the falling edge of the pulse is used to trigger the signal averager. The pulse-width is selected as a parameter to exclude the laser residual which is reflected into the spectrometer for the higher concentration samples. This setting together with the termination resistor and the resolution of the signal averager enable us to detect nothing while a blank stainless steel plate is used. Therefore, all the decay data reported here for the early time kinetics have a 40 microseconds offset. For the longer time kinetics studies the data are collected about 10 milliseconds after the laser fires.
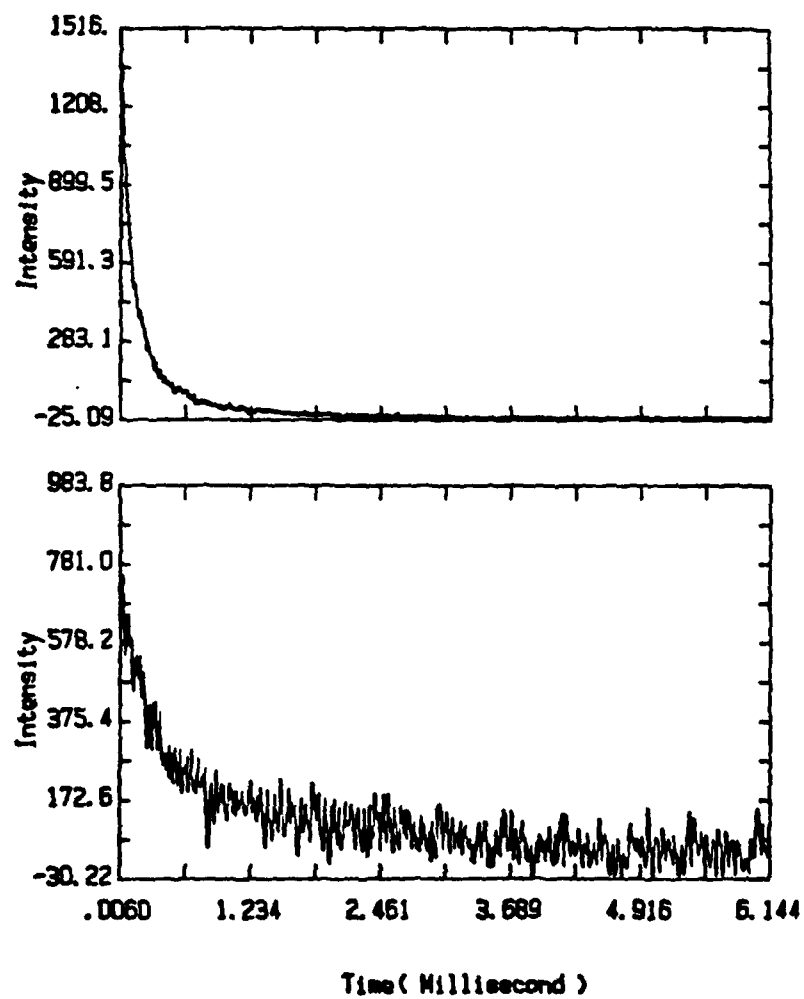
Fig. 2 Delayed fluorescence (top) and phosphoresence
decay for 50% blend

MICROSECOND LUMINESCENCE OF BLENDS

While the laser pulse is only 10 nanoseconds wide, the data collection begins after a delay of 40 microseconds. Cutting out shorter time responses eliminates: (1) prompt fluorescence; (2) artifacts due to phototube saturation; (3) early transient kinetic effects. The latter allows the formation of a stationary, kinetically ordered particle (free exciton) distribution [8]. Typical phosphorescence and delayed fluorescence decays in this microsecond (and early millisecond) regime are shown in Figure 2 for a 50% sample of P1VN/PMMA. We note that the decay of the delayed fluorescence is extremely abrupt, compared to the phosphorescence. A double-logarithmic representation of these data, $Ln(F/P^2)$ vs. $Ln(t)$, following eq.(5), is given in Figure 3. The curve has a definite negative slope ($h = 0.30 \pm 0.04$). Similar plots are shown for the sample of 100% (Fig. 4). We see that the last sample gives an essentially horizontal (classical) slope ($h = 0.01 \pm 0.01$).

MILLISECOND LUMINESCENCE OF BLENDS

In these experiments the data monitoring is started 10 ms after the exciting pulse (10 ns). The rationale is the assumption that by this time most energy "traps" (e.g., excimer forming sites) have been "filled" by the freely moving excitons, while the free exciton population has been depleted by both fusion and trapping (and to a lesser degree by natural decay). Double-logarithmic curves of $Ln(F/P)$ vs. $Ln(t)$, following eq.(6), for these millisecond (and early second) decays are given for samples of 0.01% (Fig. 5) and 50% (Fig. 6). We notice that the linear fits (on the Ln-Ln scale) are good but have definite negative slopes. These results, as well as the early-time (microsecond) decay time results, are plotted as a function of blend concentration (Fig. 7). For comparison, we have added to this plot the older (millisecond to second) results of Li and Kopelman [10], which were performed on some of the same blend samples, but with xenon lamp excitation (lower intensity), by first creating a steady-state excitation (illumination over about 10 sec) and then cutting off the excitation and monitoring over a time interval of 10 millisecond to 10 sec.

DISCUSSION OF BLEND MORPHOLOGY

The last figure (Fig. 7) shows a consistent trend of heterogeneity exponents (h) over four and a half decades of blend concentration. We first notice that we obtain the classical (h = 0) result for the non-blended material (100% P1VN). Whatever the exact morphology, it is obvious that here the exciton will be able to jump onto neighboring naphthyl groups in all directions (three-dimensional topology, on the average).

Going to the other extreme of highly diluted blends (0.005% and 0.01%), we may expect isolated P1VN chains. Provided that these are not highly folded (into "little balls" or micelle-like structures), the triplet-naphthyl excitons, whose jump-range is only about 5 Å, will usually find themselves moving in a one-dimensional topology (consisting of a chain of several hundred monomers). Remembering that for a one-dimensional topology our theory predicts h = 1/2, our very dilute blend data are fully consistent with a model of largely isolated, largely open P1VN chains.

Previous papers by Frank and collaborators [3,4] have shown that for P2VN/PMMA (and similar) blends, there appeared to be a phase-separation occurring at about 0.3% weight, for blends with orders of magnitude of guest and host molecular weights similar to those in our experiments (but note that we use P1VN, not P2VN). We thus expect some guest chain aggregation to start at about 0.1%. This is consistent with our decreasing h values (see Fig. 7). In addition, the monomer/excimer fluorescence ratios (R) and the optical scattering data for our P1VN/PMMA cast films [10] show a very similar concentration dependence to the
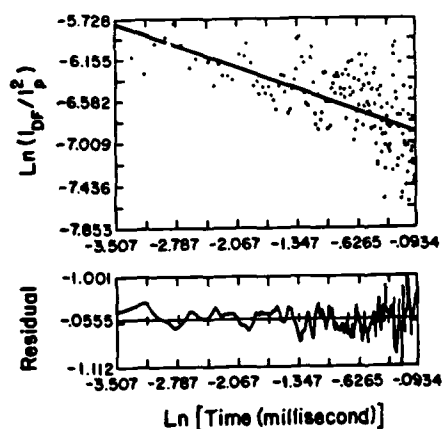
Fig. 3: 50% Blend (homofusion).
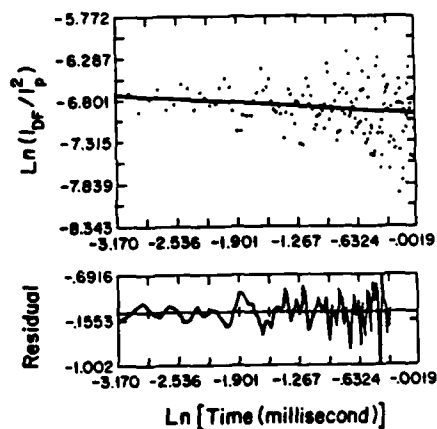
Fig. 4: 100% Blend (homofusion).
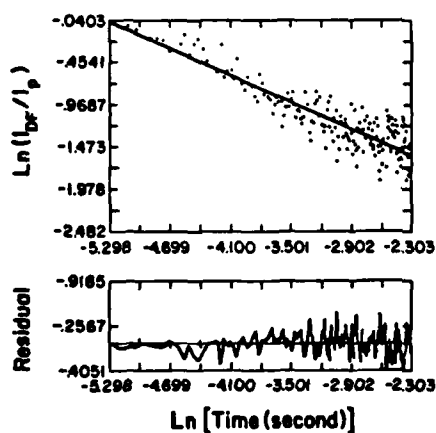
Fig. 5: 0.01% Blend (heterofusion).
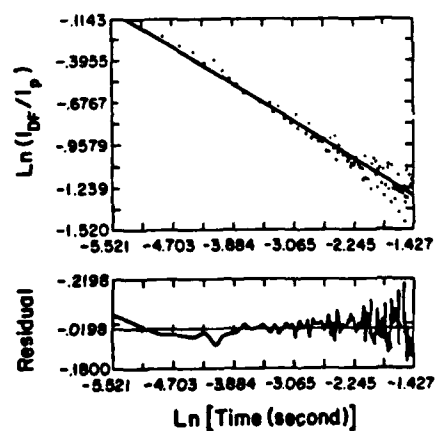
Fig. 6: 50% Blend (heterofusion).

Frank et al. [3,4] P2VN/PMMA cast films (with similar molecular weights). Based on the last two criteria one would assume that when the PVN guest concentration reaches about 10% weight, a fairly complete phase separation should occur. Furthermore, based on the fact that at 10% and higher no "monomer" fluorescence is observed (only excimer fluorescence), one would conclude that the PMMA rich phase contains little PVN.

Accepting the above picture, it is natural to expect the heterogeneity exponent h to decrease monotonically with increasing PVN concentration, and approach zero around about 10%. However, the opposite is observed (Fig. 7). A non-monotonic behavior is seen. This results in an h *increase*, reaching a maximum (close to 0.5) at about 10% PVN, then falling slowly and reaching h = 0 (the classical value) only at concentrations approaching 100% (but definitely not at 50%). We note that DSC measurements at 50% show a clear two-phase pattern only, after partial annealing of the films [10].

It has been recognized earlier [3] that kinetic restrictions during solvent casting could affect the attainment of equilibrium. In particular, the P2VN/PMMA blends appeared to be more miscible than predicted from equilibrium models (especially for higher molecular weights of PMMA). For simplicity, we assume here a "hairy" interface model, where the different phases are separated by a "fuzzy" interphase domain, i.e., PVN chain that penetrate significantly into the PMMA phases (and, possibly, vice versa). On the short-range scale typical of the triplet-transfer, these hairs have an effectively one-dimensional topology, while on the longer range singlet-transfer scale this is no longer true. The observed excimer/monomer ratios (R) appear to be affected by monomer-monomer *singlet* energy transfer. However, the triplet-triplet fusion is dominated by the short-range monomer-monomer *triplet* energy transfer. The triplet fusion kinetics are thus more sensitive to the topological details of the interface regions. A similar sensitivity of this method to domain interface topology has been demonstrated for vapor-deposited crystalline naphthalene films [9]. We also note that the fusion rate in the core regions (with h = 0) is faster than that at the interface regions (h > 0), so that the observed decays may be biased by the interfacial domains. Our heterogeneity exponent h is thus very sensitive to *local heterogeneities* and less sensitive to local homogeneities. On the other hand, a sample with *macroscopic heterogeneities* consisting of separated domains with sharp, rather than fuzzy, interfaces, would have resulted in local environments that are mostly homogeneous and thus would have given near-zero values for the heterogeneity exponent (h).

MOLECULAR DOPED POLYMERS (MDP)

The naphthalene doped PMMA films begin to scatter light at about 20% concentration (by weight). It is generally agreed [11] that at this concentration there are segregated, micron-sized, naphthalene crystallites. Under these conditions we expect to see classical behavior, i.e., h = 0. This is indeed observed: Figure 8 shows the naphthalene concentration dependence of the heterogeneity exponent h. Below 20% there is a monotonic increase as the concentration decreases. This excludes the total segregation model, for which h = 0. The naphthalene aggregates must be smaller than 1000 Å (at least in some directions) to give h > 0, based on an exciton mean free path of about 500 Å [8]. However, the aggregates also do not appear to be random (percolation) clusters. For such random clusters the percolation concentration would be on the order of 10% or higher, based on mixed crystal work [8]. At such a percolation concentration we expect h = 1/3, approximately. However, in the MDP samples, the value of h = 1/3 is reached only at about 1% naphthalene. Whatever form of aggregation that is responsible for this h = 0.3 value cannot be a random aggregation (under random aggregation we would have mostly monomers at 1%). We conclude that the dilute MDP has non-random guest aggregates, with sizes less than 1000 Å, at concentrations below 20%.
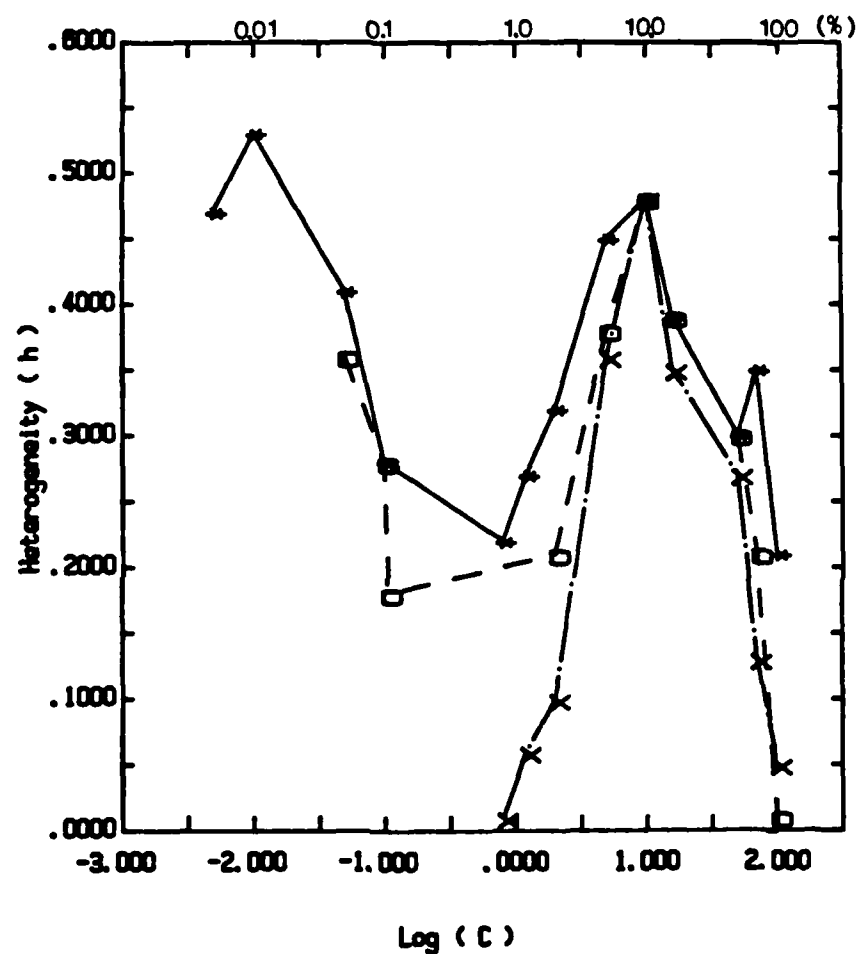
Fig. 7: Heterogeneity Exponent vs. Blend Concentration.

254
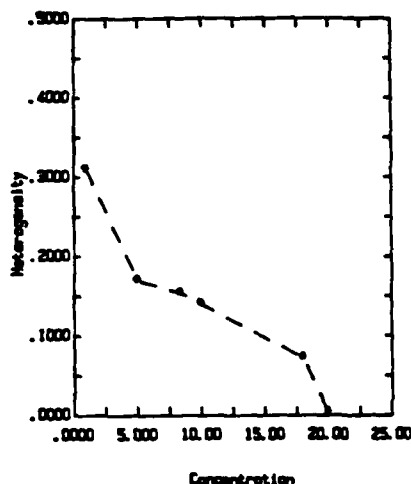
Fig. 8: Heterogeneity Exponent vs. MDP Concentration.

ACKNOWLEDGMENT

REFERENCES

1. M. A. Winnik, in Photophysical and Photochemical Tools in Polymer Science (NATO ASI Series C182), edited by M. A. Winnik (Reidel, Dordrecht, 1986), p. 611.

2. S. Tazuke and M. A. Winnik, in Photophysical and Photochemical Tools in Polymer Science (NATO ASI Series C182), edited by M. A. Winnik (Reidel, Dordrecht, 1986), p. 15.

3. C. W. Frank et al., in Photophysical and Photochemical Tools in Polymer Science (NATO ASI Series C182), edited by M. A. Winnik (Reidel, Dordrecht, 1986), p. 523.

4. C. W. Frank and Gelles, in Photophysical and Photochemical Tools in Polymer Science (NATO ASI Series C182), edited by M. A. Winnik (Reidel, Dordrecht, 1986), p. 561.

5. H. Morawetz, Science 240, 172 (1988).

6. K. A. Peterson et al., Macromolecules 20, 168 (1987).

7. N. Kim and S. E. Webber, Macromolecules 13, 1233 (1980).

8. R. Kopelman, Science 241, 1620 (1988).

9. L. A. Harmon and R. Kopelman, J. Phys. Chem. (in press).

10. C. S. Li and R. Kopelman, Macromolecules (in press).

11. E. I. Newhouse and R. Kopelman, Chem. Phys. Lett. 143, 106 (1988).

THE ORDERED BICONTINUOUS DOUBLE DIAMOND STRUCTURE IN BINARY BLENDS OF DIBLOCK COPOLYMER AND HOMOPOLYMER.

Karen I. Winey* and Edwin L. Thomas**
 * University of Massachusetts, Polymer Science and Engineering
Department, Amherst, MA 01003
 ** Massachusetts Institute of Technology, Materials Science and
Engineering Department, Cambridge, MA 02139

ABSTRACT

We report the observation of the ordered bicontinuous double diamond (OBDD) structure in binary blends of poly(styrene-isoprene) diblock copolymer and homopolystyrene. The overall polystyrene volume fraction range is 64 - 67 PSvol% for the OBDD structure in binary blends of a lamellar diblock (SI 27/22) and a homopolymer (14.0 hPS). This composition range is approximately within the polystyrene volume fraction range established for pure diblock copolymers in the strong segregation regime having the OBDD structure. Ordered lamellae are observed at approximately 65 PSvol% when the homopolystyrene molecular weight is greater than the molecular weight of the polystyrene block of the copolymer. This observation is discussed in terms of the decreased degree of mixing between the homopolymer and the corresponding block and the resultant effect on the interfacial curvature.

INTRODUCTION

Diblock copolymers contain two polymer chains which are covalently bonded to one another at one end. Immiscible polymer blends macrophase separate, whereas the connectivity within diblock copolymers limits the size of the phase separated domains and gives rise to periodic microphase separated morphologies. In the strong segregation limit the volume percent of the components in the diblock copolymer determines which morphology is observed: spheres on a body-centered cubic lattice, cylinders on a hexagonal lattice, the ordered bicontinuous double diamond (OBDD) morphology, or lamellae. The polymer chains are amorphous within these ordered domains.

The ordered bicontinuous double diamond microstructure is periodic in three dimensions and bicontinuous in that both the majority and minority components are continuous throughout the microstructure. The minority component is divided into two interpenetrating networks having diamond cubic symmetry. A color computer-generated image will assist the reader in visualizing this microstructure[1]. Both minority channels are separated from the majority component by a surface of approximately constant mean curvature. Similar bicontinuous structures have been proposed for surfactant-oil-water systems[2]. The OBDD microstructure has been observed previously in linear diblock copolymers and star diblock copolymers[3]. This paper will discuss a new method of producing the OBDD microstructure: binary blends of diblock copolymer and homopolymer.

EXPERIMENTAL

We limit our discussion to diblock copolymers which by themselves exhibit the lamellar morphology. The diblock copolymers used in this study were anionically synthesized by Dr. L. J. Fetters of Exxon. Poly(styrene-isoprene) and poly(styrene-butadiene) diblock copolymers are designated as SI and SB, respectively, followed by nominal block molecular weights given in kg/mol: SI 27/22 and SB 20/20. The polydispersities of the polystyrene block and the copolymer are less than 1.05. The homopolystyrenes from Pressure Chemical were characterized by Dr. Fetters and are designated as x hPS, where x is the molecular weight given in kg/mol. The homopolystyrene molecular weights range from 5.9 to 30.1 kg/mol and have a polydispersity of less than 1.08. The copolymer content of the blends examined ranges from 60 wt% to 80 wt% copolymer.

Our experimental procedure is more fully discussed in a previous paper[4]. Briefly, we prepared dilute solutions of the blend in toluene, a nonselective solvent. Bulk samples were made by allowing the solvent to evaporate slowly at room temperature to form 1 mm thick films. The samples are then annealed at 125°C for one week and quenched to room temperature in liquid nitrogen. This experimental procedure is designed to obtain near-equilibrium conditions characteristic of 125°C which is in the strong segregation limit for this system. Thin sections for transmission electron microscopy were cryomicrotomed at approximately -110°C and stained with aqueous OsO_4 vapors.

RESULTS AND DISCUSSION

Figure 1 exhibits an example of the ordered bicontinuous double diamond microstructure in the blend of 60.0 wt% SB 20/20 in 17.2 hPS. The micrograph exhibits the [111] projection of the OBDD as confirmed by computer simulations compared to digitized TEM data[5]. The [111] projection has been called the "wagon wheel" projection, since six spokes are seen to protrude from the axle, if one imagines the axle of a wheel perpendicular to the page; the spokes are light and the axle is dark at this composition. The added homopolystyrene selectively swells the polystyrene block of the copolymer to induce an order-order transition from lamellae to the ordered bicontinuous double diamond morphology. The homopolystyrene and the PS blocks are contained in the matrix region of the OBDD microstructure, while the PB blocks are in the channels.

There are four experimental parameters necessary to describe binary blends of homopolymer (A) and diblock copolymer (AB) at a fixed temperature. The AB diblock copolymer is fully described by two parameters, for instance, the molecular weight of the A block and the A composition of the copolymer. The copolymer content in the blend will be given as the weight percent of the copolymer. Finally, the homopolymer molecular weight must be specified to fully define these binary blends. We have explored the effect of the copolymer content in the blend and the homopolymer molecular weight.

Figure 2 shows a copolymer content series for the blend system of SI 27/22 and 14.0 hPS. At the lowest copolymer weight percent shown (64.0 wt%), polyisoprene cylinders are observed on a hexagonal lattice. The dark regions indicate the preferentially stained polyisoprene domains. The intermediate concentrations of 68.0 wt% and 70.0 wt% copolymer exhibit the OBDD structure with PI diamond channels, while a higher copolymer content (71.8 wt%)

Figure 1: Transmission electron micrograph of 60.0 wt% SB 20/20 in 17.2 hPS exhibits the ordered bicontinuous double diamond microstructure.
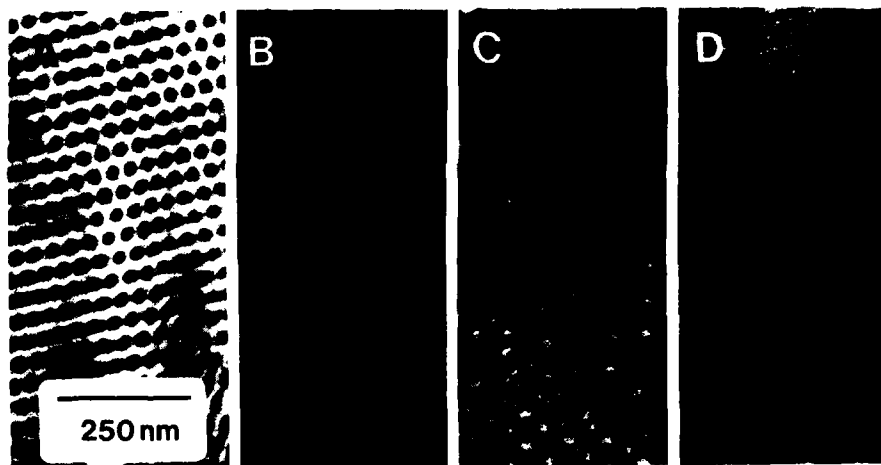
Figure 2: Copolymer content series of the blend system SI 27/22 and 14.0 hPS: a.) 64.0 wt% copolymer, cylinders on a hexagonal lattice; b.) 68.0 wt% copolymer, OBDD structure; c.) 70.0 wt% copolymer, OBDD; d.) 71.8 wt% copolymer, lamellae.

produces ordered lamellae. Thus, increasing the copolymer content of this blend system induces two transitions from cylinders to OBDD and from OBDD to lamellae.

For the purpose of comparison with pure linear diblock copolymers the copolymer content of the blend was converted to the overall polystyrene volume percent (Φ_{PS}). The value of Φ_{PS} increases as the copolymer content in the blends decreases. Figure 3 illustrates the morphology observed as function of Φ_{PS} for both the binary blend and the linear diblock copolymer. The squares indicate blends which have been prepared and their observed morphologies are indicated. The same sequence of morphologies are observed for both the diblock

Overall PS Volume Percent

Binary Blends
of SI 27/22
and 14.0 hPS

| Ordered Lamellae | OB DD | Hexagonal Cylinders |

Pure
SI 27/22

50.0 55.0 60.0 65.0 70.0 75.0

Linear
SI Diblocks

| Ordered Lamellae | OBDD | Hexagonal Cylinders |
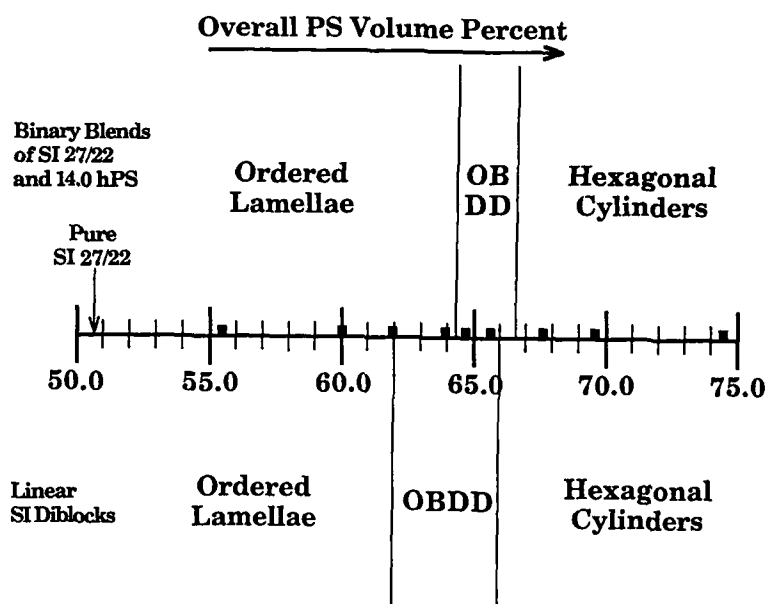
Figure 3: Observed morphologies as a function of overall polystyrene volume percent for linear SI diblock copolymers and binary blends [squares] of SI 27/22 and 14.0 hPS.

250 nm
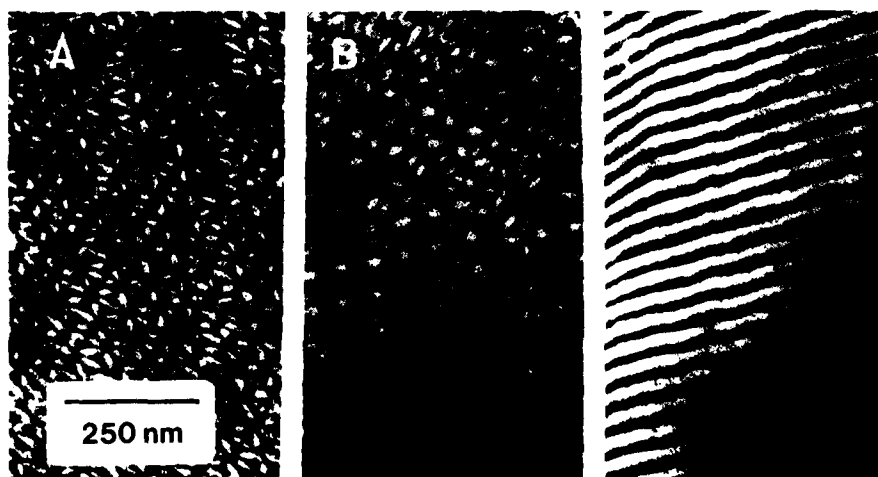
Figure 4: Homopolymer molecular weight series for 70.0 wt% SI 27/22 and various hPS: a.) 5.9 hPS, OBDD structure; b.) 14.0 hPS, OBDD structure; c.) 30.1 hPS, lamellae.

copolymer and the binary blend as Φ_{PS} increases: lamellae, the OBDD structure, and cylinders. The overall polystyrene volume percent windows for the OBDD microstructure are similar for the copolymer and the copolymer/homopolymer blend: approximately 62 - 66 vol% for the pure SI diblock copolymer[6] and approximately 64 - 67 vol% for the binary blend of SI 27/22 and 14.0 hPS. One might expect a biphasic region between the various ordered morphologies in the binary blend indicative of a first order phase transition. We have not observed such biphasic regions at this time.

Figure 4 shows a homopolymer molecular weight series in which the overall polystyrene volume percent is constant at $\approx$ 65 vol%. The binary blends of 70.0 wt% SI 27/22 and either 5.9 hPS or 14.0 hPS exhibit the OBDD microstructure. Increasing the homopolymer molecular weight to 30.1 hPS results in a lamellar morphology.

Leibler, Orland and Wheeler developed a diblock copolymer/homopolymer blend theory for the case of dilute, spherical micelles in a matrix of homopolymer[7]. Their free energy expression for a micelle includes the entropy of mixing in the corona region between the homopolymer and the corresponding block of the copolymer. This term is assumed to be inversely proportional to the degree of polymerization of the homopolymer. Kinning experimentally confirmed this trend for dilute, spherical micelles in blends of poly(styrene-butadiene) and homopolystyrene[4].

The degree of mixing within the corona influences the size of the corona and the mean curvature of the core/corona interface. We have previously reported a shape transition in a blend of 12.5 wt% SB 40/40 and hPS as a function of the homopolymer molecular weight. Blends made with 2.9 hPS and 7.4 hPS exhibit disordered spherical micelles, while a blend with 17.0 hPS exhibits disordered cylindrical micelles[8]. This shape change from spherical to cylindrical disordered micelles exhibits decreasing interfacial mean curvature as the degree of mixing in the swollen corona region decreases by increasing the homopolymer molecular weight. The experimental results discussed here are at considerably higher copolymer content, so that the corona-corona interaction induces long range order. At a low degree of mixing of the hPS into the PS block, the PS-PI interface in the SI/hPS blend maintains the flat, zero curvature lamellae of the pure copolymer, Figure 4c. A highly swollen PS block (via the addition of lower molecular weight homopolystyrene) causes the PS-PI interface to exhibit non-zero mean curvature, Figure 4a and 4b. The degree of mixing in the corona controls the interfacial curvature in such a way to obtain either lamellae or the OBDD microstructure at the same overall polystyrene composition.

Although not directly applicable to our present work, Wang and Safran have calculated the phase behavior of microemulsion systems of diblock copolymer (AB) separating A and B homopolymers[9]. Their model assumes no interaction between diblock interfaces (low copolymer content in the ternary blend) and no penetration of the homopolymers into the copolymer interface ("dry brush"). The transitions between cylinders, lamellae and bicontinuous structures were found by minimizing the curvature elastic free energy of the interface which is defined by the following coefficients: K as the bending elastic modulus, $\bar{K}$ as the saddle-splay elastic modulus, and c_0 as the spontaneous curvature. $\bar{K}$ was found to be always negative indicating that saddle shaped deformation is energetically unfavorable. In the Wang and Safran model, the OBDD structure, which exhibits saddle deformation, transforms to lamellae or cylinders, which do not exhibit saddle deformation as the magnitude of $\bar{K}$ increases. The OBDD structure in our experimental binary blends became lamellae as the homopolymer molecular weight or the copolymer content increases and became cylinders as the copolymer content decreases.

260

CONCLUSIONS

The ordered bicontinuous double diamond microstructure can be prepared in blends of diblock copolymer and homopolymer. The homopolystyrene selectively swells the polystyrene block of the SI copolymer to induce a transition from lamellae to the OBDD morphology. The overall polystyrene composition in OBDD blends is approximately 64 - 67 PSvol% in the case of SI 27/22 and 14.0 hPS; this composition is comparable to that of the OBDD structure in pure SI diblock copolymers. Finally, the ordered lamellae morphology is observed rather than the OBDD structure when the homopolymer molecular weight is too large which can be discussed in terms of preferred interfacial curvature.

ACKNOWLEDGEMENTS

REFERENCES

1. E. L. Thomas, D. M. Anderson, C. S. Henkee and D. Hoffman, Nature 334 (6184), 598 (1988).

2. S. M. Gruner, et al., Biochemistry 27 (8), 2853 (1988).

3. D. B. Alward, D. J. Kinning, E. L. Thomas and L. J. Fetters, Macromolecules 19 (1), 215 (1986); E. L. Thomas, D. B. Alward, D. J. Kinning, D. C. Martin, D. L. Handlin and L. J. Fetters, ibid., 19 (8), 2197 (1986); H. Hasegawa, H. Tanaka, K. Yamasaki and T. Hashimoto, ibid., 20 (7), 1651 (1987).

4. D. J. Kinning, E. L. Thomas and L. J. Fetters, J. Chem. Phys. 90 (10), 5806 (1989).

5. D. M. Anderson and E. L. Thomas, Macromolecules 21 (11), 3230 (1988).

6. D. A. Gobran, PhD thesis, University of Massachusetts, forthcoming.

7. L. Leibler, H. Orland and J. C. Wheeler, J. Chem. Phys. 79 (7), 3550 (1983).

8. D. J. Kinning, K. I. Winey and E. L. Thomas, Macromolecules 21 (12), 3502 (1988).

9. Z.-G. Wang and S. A. Safran, J. de Physique, in press; Europhys. Lett., in press.

STUDIES ON THE EXCESS FREE ENERGY AND THE EARLY STATE OF SPINODAL DECOMPOSITION OF THE BLEND d–PS/PVME AND THE ISOTOPIC BLEND d–PS/PS WITH SMALL ANGLE NEUTRON SCATTERING

D. SCHWAHN, T. SPRINGER, K. HAHN*, AND J. STREIB*
Institut für Festkörperforschung der Kernforschungsanlage Jülich GmbH,
Postfach 1913, D–5170 Jülich, Federal Republic of Germany
*BASF Aktiengesellschaft, D–6700 Ludwigshafen, Federal Republic of Germany

INTRODUCTION

The article deals with the phase diagram and spinodal decomposition of two polymers blends, namely d–PS/PVME and d(deutero)–PS/PS, investigated by small angle neutron scattering (SANS). The result of the static experiments is the excess free energy and the phase diagram. This is used as a basis for studies of non–equilibrium phenomena as spinodal decomposition. In polymer blends the Cahn–Hilliard–Cook theory of the early state of spinodal decomposition can be tested easily, because the blends have rather low relaxation rates; and they are meanfield systems [2,6] which makes interpretation simple, except in a very narrow temperature region near the critical point [6]. The kinetics in the isotopic blend d–PS/PS are so slow that the early states of spinodal decomposition can be studied within minutes. The presented SANS results have been performed at the KWS I small angle instrument at the FRJ–2 reactor in the KFA Jülich.

DETERMINATION OF THE EXCESS FREE ENERGY WITH CRITICAL SCATTERING

The excess free energy of a mixture can be determined from composition fluctuations in the mixed state which is studied by SANS. The static structure factor S(Q) for critical fluctuations of a blend in the Zimm approximation is given by [1,2]

$$\frac{1}{S(Q)} = \frac{\partial^2 g}{\partial \phi^2} + \frac{1}{3\phi(1-\phi)} \frac{R_g^2}{V_w} Q^2 . \tag{1}$$

Q is the scattering vector for the neutron, g the Gibbs free energy of mixing in units of kT, ϕ the concentration of one component, R_g is the radius of gyration, and V_w the weight average of the molecular volume, assuming the same volume for both components. The second derivative of g with respect to the composition ϕ is calculated from the Flory–Huggins model of polymer blend [1,2], namely

$$\frac{\partial^2 g}{\partial \phi^2} = \frac{1}{\phi(1-\phi)Vw} - 2\Gamma . \tag{2}$$

Γ is the generalized Flory–Huggins parameter (see eq. (4)) which describes the difference of the segmental interaction energy (or enthalpy). It depends only on the segmental properties of the molecular chains. Γ will be obtained from the scattering experiment.

In Fig. 1 results of critical scattering at different temperatures for a d–PS/PS mixture with $\phi = 0.48$ and $V_w = 0.91 \cdot 10^6 \, cm^3/mol$ are plotted vs. Q^2 (Zimm representation). The fitted straight lines show that the experimental data follow the Zimm approximation eq. (1) below $Q = 5 \cdot 10^{-3} \, Å^{-1}$. The extrapolated value of $S(Q \to 0)$ gives $\partial^2 g/\partial \phi^2$ and Γ by eq. (2). Similar experiments were performed for other compositions (see Ref. [3]).
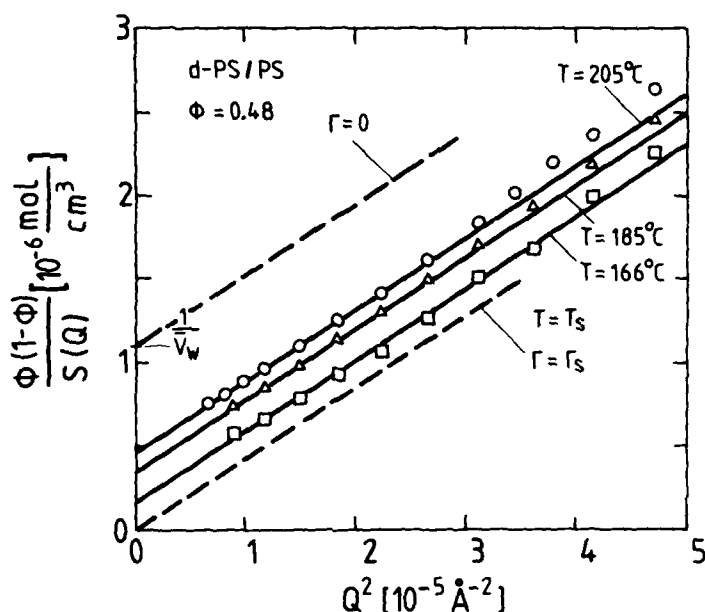
Fig. 1   Critical scattering of the d−PS/PS mixture at T = 166 ⁰C, 185 ⁰C and 205 ⁰C. The two dashed lines indicate the scattering curves at the spinodal, and at the compensation temperature, respectively.

The experiments show that Γ can be written as

$$\Gamma = \frac{\Gamma_h}{T} - \Gamma\sigma \tag{3}$$

with an enthalpic (Γ_h) and an entropic ($\Gamma\sigma$) term, which both depend on ϕ [3]. Because the SANS experiments determine $\partial^2 g/\partial\phi^2$, $\Gamma(\phi)$ is related to the usual Flory−Huggins parameter by

$$\Gamma = \chi - (1 - 2\ \phi)\ \frac{\partial\chi}{\partial\phi} - \frac{1}{2}\ \phi(1 - \phi)\ \frac{\partial^2\chi}{\partial\phi^2}, \tag{4}$$

and χ can only be calculated from Γ if the ϕ dependence of χ is known [3].

In Fig. 2 the generalized Flory−Huggins parameter Γ of d−PS/PS ($\phi = 0.5$) and d−PS/PVME ($\phi = 0.2$) is plotted as a function of the inverse temperature, using SANS results [3,6,7] (see also Ref. [4,5]). The spinodal temperature is defined by $\partial^2 g/\partial\phi^2 = 0$ (eq. (2)). Especially, the evaluated T_c of two molecular volumes are shown in Fig. 2. The slope of Γ, which is given by the enthalpy term Γ_h in Γ, is positive for d−PS/PS and negative for d−PS/PVME and accounts for an upper or for a lower critical solution temperature, respectively. The absolute value of Γ_h for d−PS/PVME is two orders of magnitude larger than for the isotopic mixture. The spinodal lines for the investigated d−PS/PVME and d−PS/PS mixtures are presented in Fig. 3 and 5, respectively.
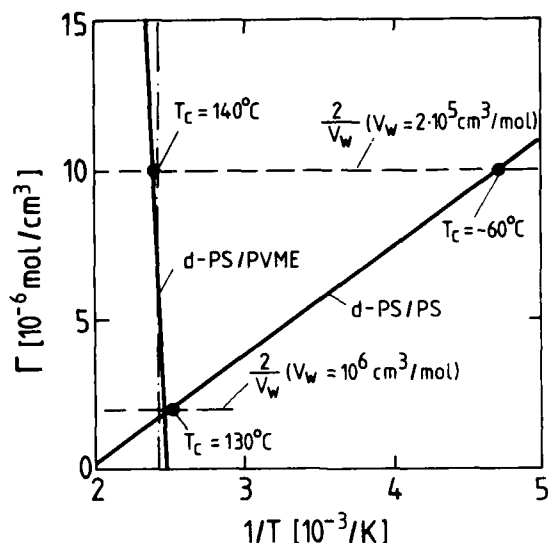
Fig. 2   Excess free energy of mixing (Flory–Huggins parameter) as a function of
the inverse temperature for deutero–PS/PS ($\phi = 0.5$) and d–PS/PVME
($\phi = 0.2$). The enthalpy contribution (see eq. (3)) is given by the slope of Γ.
Positive or negative values are responsible for the case of an upper or a
lower critical solution temperature, respectively (see Fig. 3 and 5), as
obtained from eq. (2) for $\partial^2 g / \partial \phi^2 = 0$.

EARLY STATE OF SPINODAL DECOMPOSITION

A blend is rapidly quenched from an equilibrium state at T_0 with the structure
factor $S_{T_0}(Q)$ to a final state kept at a temperature T with $S_T(Q)$. If T is in the
miscibility gap this state is unstable and the corresponding $S(Q)$ is the virtual
structure factor [2]. The Cahn–Hilliard–Cook (C–H–C) [9,10] theory extended by
Binder [2] for polymers leads to the time dependent structure factor

$$S_T(Q,t) = S_T(Q) + [S_{T_0}(Q) - S_T(Q)] \exp[-2\tau^{-1} t] . \tag{5}$$

The relaxation rate τ^{-1} is calculated with a nonlocal Onsager coefficient because of the
large size of the molecules, namely for $Q < 1/R_g$

$$\tau^{-1}(Q) \simeq 6 \, \tau_R^{-1} \, R_g^2 \, Q^2 \, \{1 - \frac{\Gamma}{\Gamma S} (1 + \frac{R_g^2}{3} Q^2)^{-1}\} \tag{6}$$

where τ_R is the characteristic time of molecular diffusion. The relaxation rate can be
connected with the collective diffusion constant

$$D_{coll} = 1/\tau \, Q^2 \text{ for } Q \to 0 . \tag{7}$$

SPINODAL DECOMPOSITION IN d–PS/PVME

The spinodal of a d–PS/PVME mixture with the molecular volumes of V_w(d–PS) = 227000 cm³/mol and V_w(PVME) = 53000 cm³/mol is plotted in Fig. 3. The spinodal has been calculated from Γ in Fig. 2 by means of eq. (2), using $\partial^2 g/\partial \phi^2 = 0$. The spinodal temperature of the investigated specimen $(\phi = 0.2)$ is 150 °C. The system was heated from the mixed (homogeneous) state at 149 °C up to 152 °C, about 2 K above T_c. The SANS measurement was immediately started when the temperature was reached; and took 30 sec. From then on the measurements were performed consecutively in periods of 30 sec.
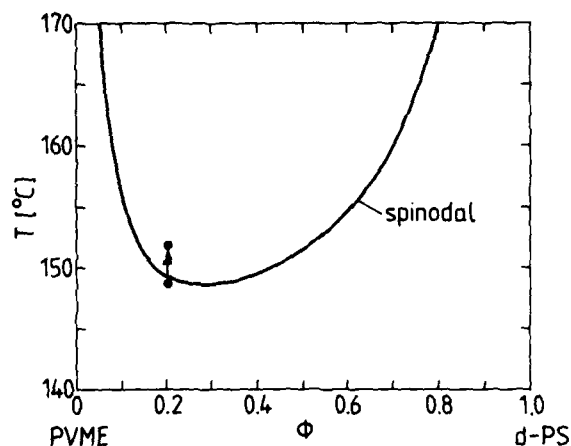
Fig. 3   Spinodal of d–PS/PVME mixture. V_w(d–PS) = 227000 cm³/mol and V_w(PVME) = 53000 cm³/mol).
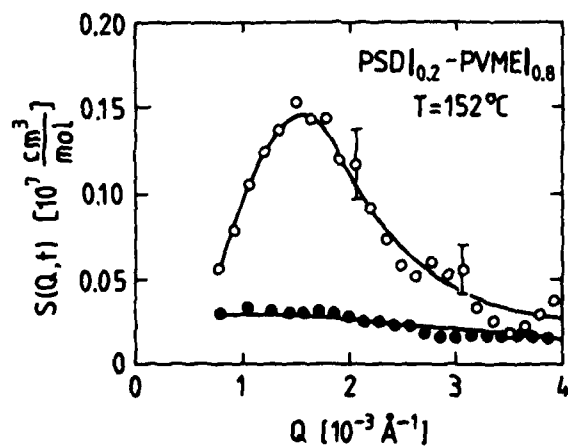
Fig. 4   Static structure factor at 149 °C (–•–) and structure factor –o– measured at 152 °C during the first 30 sec. of the decomposition process.

Fig. 4 shows the structure factors in the homogeneous region at $T = 149\ ^\circ C$ and after heating the blend into the region of the miscibility gap at $152\ ^\circ C$ (see arrow in Fig. 2). The peak at $Q_m = 1.6 \cdot 10^{-3}\ \text{Å}^{-1}$ is expected to correspond to the maximum growth rate i.e. the maximum of $(-\tau)^{-1}$ in eq. (8). Using the equilibrium data, the calculated value of

$$Q_m = [1.5/R_g^2\ (\Gamma/\Gamma s - 1)]^{1/2} \tag{8}$$

agrees roughly with the measured one. At later times a shift of the peak position to smaller Q is observed due to coarsening which is not described by eq. (5). Peak positions as small as $5 \cdot 10^{-5}\ \text{Å}^{-1}$ have been observed with the neutron double crystal diffractometer [7,8]. This is the first measurement of the early state of decomposition in this system. More experiments on this system are in preparation.

SPINODAL DECOMPOSITION IN d–PS/PS

The spinodal and the binodal of an isotopic d–PS/PS mixture (with $V_w = 0.91 \cdot 10^6\ \text{cm}^3/\text{mol}$) were calculated with Γ from the SANS experiments by eq. (2) in Fig. 5. We have investigated a $\phi = 0.48$ mixture with a $TS = (135 \pm 5)\ ^\circ C$ Fig. 6 shows the SANS results of demixing. It started from the homogeneous equilibrium state at $160\ ^\circ C$ and stopped after 3 weeks at $125\ ^\circ C$. All SANS measurements were performed at room temperature after a rapid quench below $TG = 100\ ^\circ C$. The data could be analyzed with eq. (5) and the solid lines in Fig. 6 shows the best fit. We find a collective diffusion constant of $D_{coll} = -1.4 \cdot 10^{-18}\ \text{cm}^2/\text{s}$. This system is in an earlier state of decomposition as it was found in d–PS/PVME. In this region the observed peak at $1.4 \cdot 10^{-3}\ \text{Å}^{-1}$ approaches the value expected from eq. (8) namely $Q_m = 7.6 \cdot 10^{-4}\ \text{Å}^{-1}$. Before coarsening occurs there is a change of the relaxation behaviour due to the presence of the glass transition [12]. The relaxation rate given by diffusion (eq. (6)) couples to additional and slow structural changes. This effect was observed in this system in a relaxation experiment where the initial and final temperatures were both in the homogeneous region. Only in the limit of small Q and small annealing time the system could be described in terms of C–H–C theory [3].
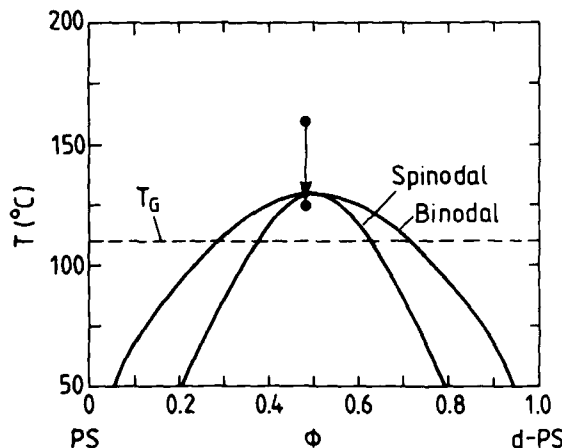
Fig. 5   Phase diagram of d–PS/PS with an average $V_w = 0.91 \cdot 10^6\ \text{cm}^3/\text{mol}$.
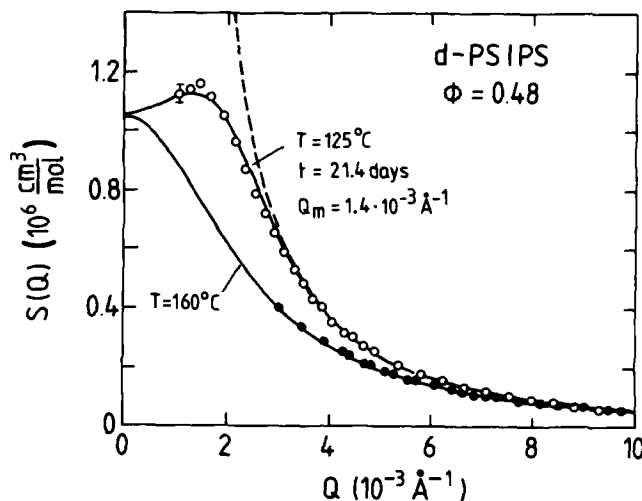
Fig. 6   Static structure factor at 160 °C and S(Q,t) after 3 week at 125 °C. The
dashed line is the virtual structure factor at 125 °C.

CONCLUSIONS

1) By means of SANS experiments we have determined the excess free energy
(Flory–Huggins parameter) of the d–PS/PVME and d–PS/PS and calculated the
phase diagrams with this quantity.

2) Kinetic experiments were carried out by quenching from the homogeneous to
the unstable state. In d–PS/PVME the peak position consistent with C–H theory was
observed. The subsequent coarsening with a shift of the peak position from 10^{-3} to
about $5 \cdot 10^{-5}$ Å^{-1} is found in Ref. [7,8]. For d–PS/PS the very early stage could be
measured which occur before the appearance of the unstable peak at Q_m.

REFERENCES

[1]   P.G. de Gennes, *Scaling Concepts in Polymer Physics* (Cornell Univ. Press,
        Ithaca 1979)
[2]   K. Binder, J. Chem. Phys. **79**, 6387 (1983)
[3]   D. Schwahn, K. Hahn, J. Streib, and T. Springer, submitted to publication
[4]   F.S. Bates and G.D. Wignall, Macromolecules **19**, 932 (1986)
[5]   P.F. Green and B.L. Dayle, Phys. Rev. Lett. **57**, 2407 (1986)
[6]   D. Schwahn, K. Mortensen, T. Springer, H. Yee–Madeira, and R. Thomas,
        J. Chem. Phys. **87**, 6978 (1987)
[7]   H. Yee–Madeira, JÜL–Report Nr. 2268 (1989)
[8]   D. Schwahn and H. Yee–Madeira, Colloid & Polymer Sci. **265**, 867 (1987)
[9]   J.W. Cahn, Acta Metall. **9**, 795 (1961)
[10]   H.E. Cook, Acta Metall. **18**, 297 (1970)
[11]   G.R. Strobl, Macromolecules **18**, 558 (1985)
[12]   J. Jäckle and M. Pieroth, Z. Phys. B **72**, 25 (1988)

MECHANICAL PROPERTIES AND STRUCTURE OF MELAMINE
FORMALDEHYDE/POLY(VINYL ALCOHOL) MOLECULAR COMPOSITES

KECHENG GONG AND XINGHUA ZHANG
Dept. of Polymer Science & Tech., South China Univ. of Tech.,
Guangzhou, P.R. China

ABSTRACT

The mechanical properties and structure of melamine formal-
dehyde (MF)/poly(vinyl alcohol) (PVA) composites were studied in
this paper. When PVA content was less than a certain value(about
20 weight %), both flexible strength and impact resistance were
improved obviously. While the impact resistance improvement re-
mained the previous trend the flexible strength didn't increase
so rapidly as before when the PVA content was more than 20%.
The morphology and reactivity of the prepolymer powder and
the morphology of the finished specimens were investigated by
means of microscope, infrared spectrum and transmission electron
microscope(TEM). The results indicated that molecular composite
structure was formed in this two-component system. The well-dis-
tributed PVA in this system was beneficial to the formation of
the molecular composite structure. That could explain the effects
of PVA on the mechanical properties and showed that the molecular
composite structure are favourable for making full use of the
macromolecular potentiality.

INTRODUCTION

Since melamine was synthesized in 1834 by Liebig [1] its
reactions with other chemicals have been studied. Melamine for-
maldehyde resin [2] extended the application of melamine. Like
urea formaldehyde (UF) and phenolic formaldehyde (PF) resin, MF
resin can be used as moulding and laminating materials, adhesive
and coating. In order to improve its toughness and to lower its
cost, a lot of modified, reinforced or filled products are deve-
loped for practical uses [3]. MF resin and its related products
are often used in paper and textile industry [4]. Particularly,
the aqueous solution of MF and PVA is mainly used in papermaking
[5]. The mechanical properties and structure of MF/PVA as mould-
ing material were studied in this paper. The results showed that
the molecular composite structure benefited the improvement of
the mechanical properties.

EXPERIMENTAL

Preparation of prepolymers

When one mol 37% formaldehyde solution with pH 8.0-8.5 was
heated to 60°C, 1/3 mol melamine was added into the solution.
As melamine solved completely, the temperature was elevated to
and kept at 85°C. As soon as one milliliter of this solution be-
came turbid when it was mixed with three milliliters of water at
room temperature, 5% aqueous solution of PVA was mixed with it.
The liquid mixture was stirred at 85°C for a period of time un-
til it became a homogeneous mixture. After that, the liquid was
put in a vacuum oven to eliminate water at 60°C for 72 hours.

Then the solid obtained from the oven was grinded into prepolymer powder (<100-mesh).

Measurement of Mechanical Properties

At 165°C, the powder was moulded into specimens with dimension of 150x15x10 mm³ under about 1500 kg/cm² pressure for 12 minutes. The flexible strength was measured at speed of 15mm/min according to GB1042-79 (National Standard of P. R. China). And the impact resistance of the samples without notches was measured according to GB1043-79.

Investigation of Structure

The homogeneous solution of MF and PVA was coated on an object carrier. After being dried, the sample on the carrier was observed under a microscope.

The prepolymer powder, after necessary preparation, was tested with infrared spectrum.

In addition, TEM was used to investigate the morphology of the moulded samples.

RESULTS AND DISCUSSION

Mechanical Properties

Both flexible strength and impact resistance of the composite were improved by the addition of PVA. The flexible strength and impact resistance were plotted in figure 1 against the PVA content (weight %). When PVA content was less than about 20%, as shown in Fig.1, the flexible strength of the material increased rapidly as the content increased. When PVA content was more than 20%, the flexible strength increased slightly. Not quite the same, the impact resistance straight increased all the way to 40% PVA. As we know, in most polymer blend and copolymer systems, the improvement of the impact resistance is achieved with the loss of
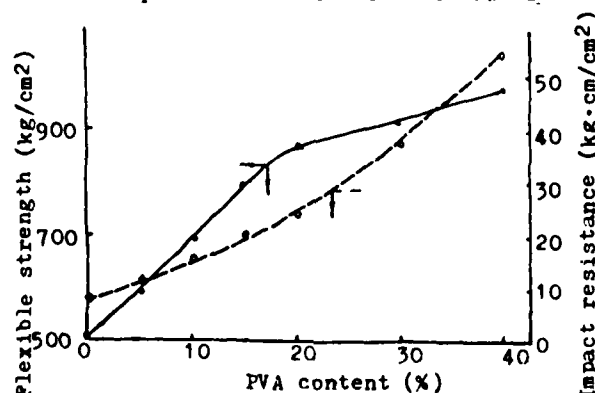
Figure 1 Relation of flexible strength and impact resistance to PVA content (w%) in the composites

the flexible and tensile strength. The effect of IVA in considerably wide content range on impact resistance and flexible strength depended on the structure of the composite.

Structure Analysis

The reactions, in which melamine is involved, have been studied for more than one hundred years. Until recent years some papers on the reactions of melamine and formaldehyde were still published[6]. Under the experimental condition of this paper,the reaction of melamine and formaldehyde was as follows

$$NH_2\text{-}\bigcirc\text{-}NH_2 + CH_2O \longrightarrow NH_2\text{-}\bigcirc\text{-}NHCH_2OH$$

where $NH_2\text{-}\bigcirc\text{-}NH_2$ = Melamine =
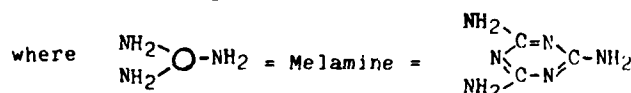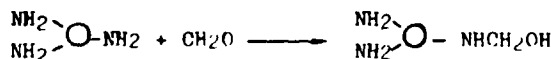
Although trihydroxymethylate could be gotten, the reaction product (MF prepolymer) was a mixture of several substitution derivates. Etherification along with some other reactions occurred when MF prepolymer was heated.The product of these reactions was a piece of crosslinded solid that was unmeltable and unsolvable.

Fig.2 showed the infrared spectrums of MF and MF/PVA(90/10) at different temperatures. The temperature elevated 10 degrees in one minute. Fig.3 was the differential spectrums at room temperature and at 180°C. Fig.4 showed the peak area of about 3500cm^{-1} in Fig.2. The area was indicated by the ratios of the peak area at different temperatures to that at room temperature.

Wavenumbers (cm^{-1}x10^{-2})

(a)   (b)
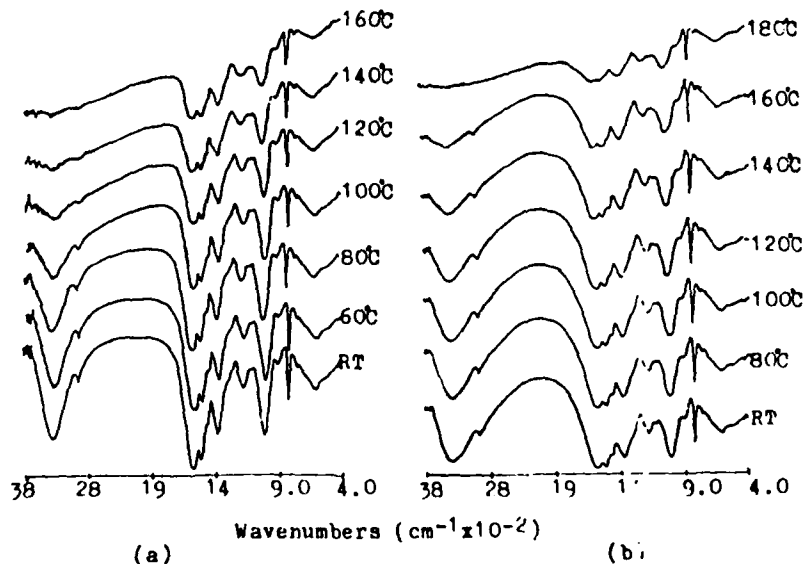
Fig.2 IR spectrums at different temperatures
Temperature elevated 10 C/min
(a) MF/PVA=100/0; (b) MF/PVA=90/10
*RT=room temperature

OH groups joined the reactions in this system when the prepolymer was heated. Fig.2 indicated that the 3500cm^{-1} peak (the IR absorption of O-H expansion vibration) reduced as temperature elevated. In Fig.3, it was found that the 990cm^{-1} peak (C-OH expansion vibration) became smaller for higher temperature. In addition, whether PVA was put in or not, OH groups(Fig.4) reacted to a quite high level(>90%).

Ether bonds formed in processing. This was proved by the increment of 1050cm^{-1}peak(C-O-C asymmetric expansion vibration) in Fig.3. Furthermore, we could know that the increment of 1050cm^{-1}peak in (b)(10% PVA) was obviously larger than that in (a)(0% PVA).

Fig.3 Differential spectrums between IR spectrums at 180 C and at room temperature (a) MF/PVA=100/0; (b) MF/PVA=90/10.

That was to say, when PVA was put in the system, more ether bonds formed.

The PVA phase was well distributed in this system. We could see that in Fig.5. It was significant that PVA phase distributed as a continuous network phase even only 10% PVA was put in (a). This may be caused by the effect of PVA like a surfactant. When PVA was more than 20%(b), MF phase took spherical shape. If PVA content was 40% (c) or more, the MF phase spheres were kept apart absolutely by the PVA phase.

The general reactivity of OH groups was decreased by PVA. The OH groups on the PVA molecular chain has lower reactivity than that in MF prepolymer. For the prepolymer containing low PVA content (e.g. 10%), in addition to that reason, the distribution of PVA phase played a important part. Because PVA phase was continuous, so MF phase was divided into fine drops. As a result, the general OH reactivity was reduced. The result was proved by the IR spectrums (Fig.4). In Fig.4, the 3500cm^{-1} peak area of the two samples decreased with the elevated temperature as the result

Fig.4 Variation of A/A* with temperature

A=3500 cm^{-1} peak (IR) area at a certain temperature
A*= A at room temperature (RT)

-------- MF/PVA=100/0

———— MF/PVA=90/10
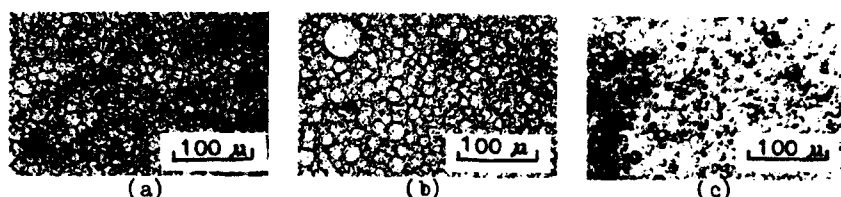
Fig.5 Microscope photographs of different MF/PVA ratios
MF/PVA: (a) 90/10; (b) 80/20; (c) 60/40.

of the reactions. For 0% PVA sample, the area changed most rapid-
ly at about 90°C, and for 10% PVA one, at about 120°C.

Molecular composite structure was formed in this composite
system. From our previous experimental result, we knew that PVA
phase was well-distributed even only 10% PVA was put in and the
OH groups reacted to a relatively high extent. So the crosslink-
age of the material increased especially in low PVA content range.
The close linkage of the two phase formed molecular composites.
TEM photographs of two samples were exhibited in Fig.6. Sample (a)
was the mould specimen of this experiment and sample (b) was made
from the specimen that MF prepolymer powder mixed directly with
PVA powder. The PVA phase (white) in (a) was fine and regular
whereas that was coarse and irregular in (b). Obviously, this
related to the distribution of PVA phase. In the prepolymer of
(a), the PVA phase was dispersed as the shape showed in Fig.5(b).
After the processing under certain pressure and temperature, the
two phase linked closely and the PVA phase was fine. On the other
hand, in sample (b), after the same processing, the two kinds of
powder combined together but not so closely as (a). Inevitably,
the mechanical properties of the composite were affected by their
molecular composite structure. Both flexible strength and impact
resistance were improved in comparison with the case of polymer
blends and copolymers.

For the samples containing more than 20% PVA, the MF phase
acted as a reinforcer in PVA. Because the PVA content was high
and the MF phase was in the shape of separated spheres, the mol-
ecular composite structure was not so significant as in the low
PVA content samples. Nevertheless, the impact resistance and
flexible strength were still improved.

Fig.6 TEM photographs of the MF/PVA(80/20) composites
The composites were made from
(a) solution mixture and (b) powder mixture.

SUMMARY

Because molecular composite structure was formed in MF/PVA composites, the flexible strength and impact resistance was improved significantly when PVA content was less than 20 weight %. As PVA content increased further until 40%, the impact resistance increased continuously while the flexible strength didn't increase so quickly as PVA content lower than 20%. In addition, the addition of PVA can change the morphology and reactivity of prepolymers and the morphology of the finished polymers.

REFERENCE

1. C. Goldschmidt, Chem. Ztg., 21, 460 (1897).

2. D. Braun, et al, Osterr. Chemie-Zeitschrift, Juli/August, 188-196 (1985).

3. R.J. Schupp, Modern Plastics Encyclopia, 1986-1987, 17-18.

4. G.X. Song, Suliao Keji, 1, 20-24 (1988).

5. Robert L. Adelman, Wilmington, Del., U.S. Patent No.4,461,858 (24 July 1984).

6. Anil Kumar, Polymer, 28 (1), 155 (1987).

Synthesis-Electro-Optical
Properties

MORPHOLOGICAL CONSEQUENCES OF
CATALYTIC HYDROGENATION OF POLYMERS IN THE BULK

LAURA R. GILLIOM, DALE W. SCHAEFER AND JAMES E. MARK*
Sandia National Laboratories, Albuquerque, NM 87185

ABSTRACT

When suitable catalysts are molecularly dispersed in polymers, the polymers can be modified without added solvent. This paper describes studies on the morphology of samples of trans-1,4-polybutadiene and syn-1,2-polybutadiene which have been partially deuterated in the bulk. The development of a peak in the SANS data for the 1,2-polybutadiene suggests the formation of small domains upon deuteration. Possible explanations for this observation, including chemical and physical heterogeneity, are evaluated. Results of SAXS and thermal measurements are also considered.

INTRODUCTION

We have previously shown that olefinic polymers can be hydrogenated in the bulk with transition metal catalysts [1]. The absence of added solvent is in contrast to more conventional solvent-based methods for polymer modification [2]. Both the molecularly dispersed (dissolved) catalyst and the flexible polymer chain provide the mobility required for high conversions to hydrogenated polymer. The reaction exotherm must be completely adsorbed by the polymer. Given the unique reaction conditions, it is appropriate to investigate the morphology of the product polymer at intermediate levels of hydrogenation.

Small-angle x-ray (SAXS) and small-angle neutron (SANS) scattering provide structural information on the 5-500Å length scale. Differential scanning calorimetry (DSC) probes physical transitions in materials. We have used these techniques to assess physical state and chemical heterogeneities resulting from the bulk modification. Typically, polymers were only partially deuterated. Since the huge difference in coherent scattering lengths of H and D enhances contrast between deuterated and undeuterated polymer regions, SANS is sensitive to chemical heterogeneity produced by localized deuteration. SAXS, on the other hand, is relatively insensitive to deuteration because of the small difference in x-ray scattering length of H and D. SAXS is, however, sensitive to density variations (e.g., crystallinity) on the 5-500Å length scale. This paper describes our studies using these techniques on trans-1,4-polybutadiene and syn-1,2-polybutadiene.

EXPERIMENTAL

Sample Preparation: Materials: Syn-1,2-polybutadiene (1,2-PB) was purchased from Polysciences. NMR analysis suggests approximately 10% 1,4-addition and 90% 1,2-addition. Purchased material was described as 28% crystalline. Trans-1,4-polybutadiene (1,4-PB), a gift of Gencorp, was 88% trans. Both polymers were purified by precipitation from toluene solution prior to use. Crabtree catalyst [Ir(COD)(py)(tcyp)]PF$_6$ (COD—1,5-cyclooctadiene; py—pyridine; tcyp—tricyclohexylphosphine) was prepared according to literature procedures [3]. Sample Preparation: To polymer (1.5g) dissolved in 25 mL benzene was added 15 mg catalyst. The

solution was poured into an open aluminum mold and was frozen in an acetone slurry. After demolding, solvent was removed from the solid mixture under vacuum at a rate sufficient to prevent melting. Deuterations: Deuterations were performed in a pressure reaction vessel (V=180mL) consisting of a glass sample container, pressure gauge and gas inlet port. Foam samples were initially pressurized to 40psig deuterium pressure. Samples of partially deuterated 1,2-PB were removed at 25, 66, and 85% conversion as determined by pressure drop and confirmed by sample weight gain. Samples of 1,4-PB were removed at 35 and 70% conversion.

Measurements: SAXS profiles were measured using the 10m SAXS facility at Oak Ridge National Laboratory. SANS data were taken at Los Alamos National Laboratory using the LQD camera. Observed slopes have error limits of ±0.4. Thermal measurements were obtained on a Perkin-Elmer DSC-7 system. Surface area measurements were based on nitrogen desorption (BET) with a Quantachrom Monosorb instrument.

RESULTS

Materials

Polymer samples were fabricated and used as foams in order to maximize the accessibility of hydrogen throughout the material. The foams were solution cast as described in the Experimental Section. Scanning electron micrographs of the foams showed a directional, columnar morphology with spacing between columns of tens of microns. Since no indications of catalyst crystallites were observed by scanning or transmission electron microscopy, the catalyst is believed to be fully solvated in the polymer. BET studies of the surface area of foams of 1,4-PB indicate a surface area between 7 and 11 m^2/g. Deuterations of the olefinic bonds in the foam samples were performed directly under mild conditions.

Small-Angle X-Ray Scattering (SAXS)

Figure 1 shows the SAXS data for the undeuterated and partially deuterated PB's. These curves represent the scattering cross section $I(Q)$ as a function of the scattering magnitude of the wave vector Q. The data have been radially averaged. The abscissa is related to the scattering angle θ as $Q = (4\pi/\lambda) \sin(\theta/2)$. Within the errors introduced by sample irreproducibility, the curves overlap. Therefore the data sets have been shifted to demonstrate that the shape of the curves is unchanged on deuteration. This result is consistent with the insensitivity of x-rays to low-Z elements.

Although there is some tailing off of the 66% 1,2-PB data at large Q, all of the curves in Fig. 1 are power-law with exponents near -4. Slopes of -4 are consistent with Porod's law and are the signature of sharp interfaces between phases. In this case, the interface in question is the polymer/air interface of the underlying foam structure. In fact, the specific interfacial area, σ, can be calculated from Porod's constant K_P, obtained from the magnitude of $I(Q)$ in the Q^{-4} regime [4],

$$K_P = Q^4 I(Q) \tag{1}$$

and

$$\sigma = K_P/2\pi\rho_0(\Delta\rho)^2 \tag{2}$$
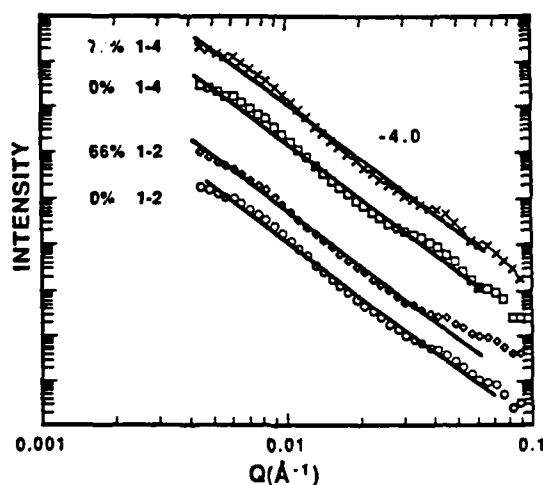
Figure 1. SAXS data for unreacted and partially hydrogenated syn-1,2-polybutadiene (1-2) and trans-1,4-polybutadiene

where ρ_0 is the foam density and $\Delta\rho$ is the scattering contrast in scattering length between the phases ($\Delta\rho = 9.9 \times 10^{-10}$ cm^{-2}). Using (2) we find $\sigma = 3$ m^2/g for the 1,2-PB foams and 8 m^2/g for the 1,4-PB foams. These results for the 1,4-PB agree well with the BET measured surface areas.

Small-Angle Neutron-Scattering (SANS)

Figures 2 and 3 show the development of SANS for 1,4-PB and 1,2-PB samples, respectively, as a function of deuteration. The data for the unreacted samples show power-law profiles at small Q flattening out at large Q. Using Eq. (2) we find that $\sigma = 6.7$ m^2/g for 1,?-PB and 15.4 m^2/g for 1,4-PB. These values of foam surface area are approximately twice that found by SAXS. It should be emphasized that the errors in these measurements are approximately 50% because of nonuniform sample thickness and sample inhomogeneities with respect to foam density.

Upon deuteration, only minor changes are observed for 1,4-PB samples. The slopes in the low-Q region become steeper indicating a non-distinct interface. Assuming a sigmoidal contrast profile, the interfacial thickness is calculated [5] to be 100+/-10Å. Presumably, the pore boundaries are preferentially deuterated leading to the observed interfacial contrast gradient. The measured foam surface area of partially deuterated samples is 4 m^2/g, somewhat smaller than that found for 0% deuteration. While this difference may be due to sample-to-sample inhomogeneity, some annealing of the porosity may be caused by the reaction exotherm.
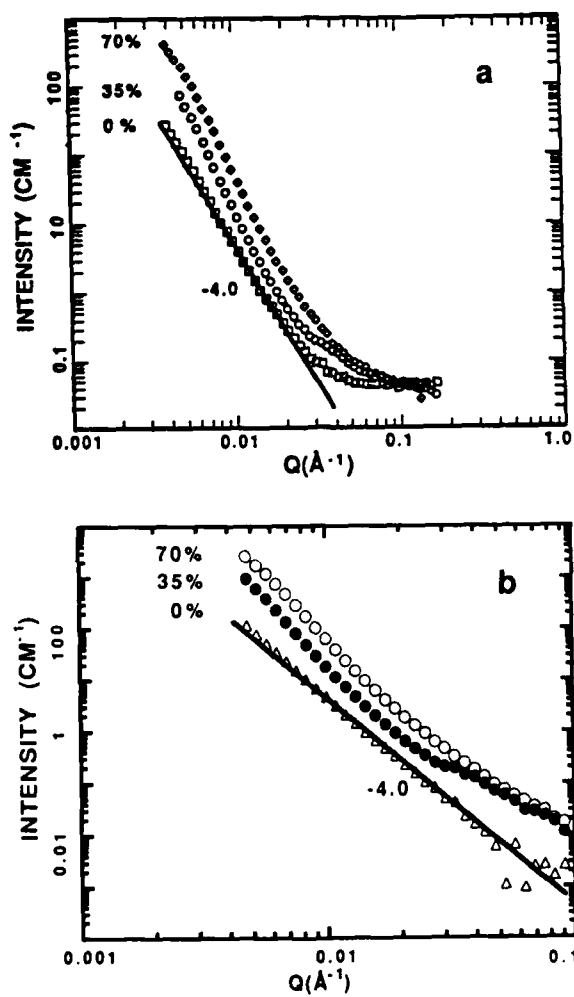
Figure 2. SANS data for unreacted and partially deuterated
trans-1,4-polybutadiene: (a) raw data; (b) corrected data
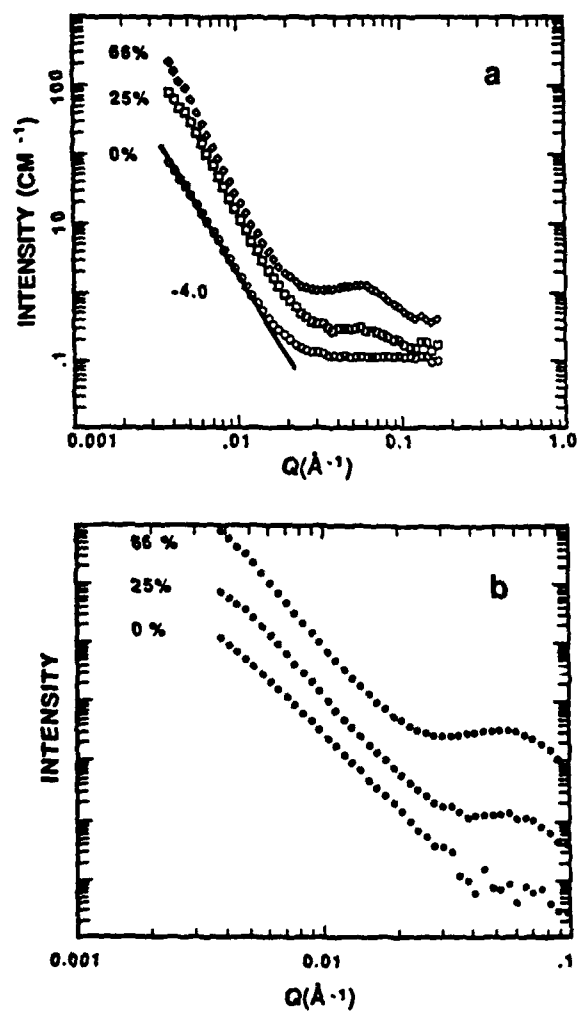
Figure 3. SANS data for unreacted and partially deuterated
syn-1,2-polybutadiene: (a) raw data; (b) corrected data.

Deuteration also leads to enhanced scattering in the high Q region. To more clearly reveal this change, the 0% and 35% data in Fig. 2a are replotted in Fig. 2b. Assuming the background is due to incoherent scattering, the data were first adjusted to match at high Q before background subtraction. This procedure scales the data to the same number of scatterers in the beam, compensating for unknown scale factors due to sample inhomogeneity. The featureless profile in Fig. 2a is at most indicative of a weakly phase separated system.

SANS results indicate a qualitatively different structure for the domains in the 1,2-PB system. A peak is now observed near $Q = .06\text{Å}^{-1}$ in the scaled, background-subtracted data shown in Fig. 3b. This peak is consistent with the formation of phase-separated domains upon deuteration. Limiting slopes of roughly -4 on the high-Q side of the peak indicate a distinct phase boundary. Since the contrast factor $\Delta\rho$ in equation (2) is uncertain here, the interfacial surface area was calculated [4] from Kp defined in equation (1) and an invariant, q,

$$\sigma = K_p \pi \phi (1-\phi)/\rho_o q \qquad (3)$$

$$q = \int Q^2 I(Q) dQ \qquad (4)$$

where ϕ is equal to the fraction of deuterated double bonds. This value of ϕ rests on the assumption that contrast arises solely from deuterated domains and not from density fluctuations (see Discussion). To avoid contributions from the pore interface, I(Q) is assumed to be flat below $Q = .05\ \text{Å}^{-1}$. Resulting surface areas are 402, 933, and 1094 m^2/g for 25%, 66% and 85% deuteration. The mean chord, or characteristic lengths, associated with these surface areas are 25Å, 28Å, and 31Å, respectively. The large increase in surface area with essentially no change in characteristic length implies that domain growth proceeds by development of new domains with minimal growth beyond 30Å. Similar behavior is reported for silica/siloxane systems [6]. The presence of a peak in I(Q) near $.06\text{Å}^{-1}$ implies that the domains are correlated in space. Although such a peak is usually associated with spinodal decomposition, a peak is possible if phase separation takes place by nucleation-and-growth. From Bragg's law, a domain spacing of 100Å is found. This value is somewhat larger than twice the characteristic lengths associated with the domains calculated from σ.

The low-Q data for 1,2-PB are consistent with foam pore surface areas of about 4 m^2/g. The surface area appears unchanged upon deuteration. An indication of preferential deuteration at pore boundaries was observed similar to that seen for 1,2-PB.

Thermal Measurements

Because of their stereoregularity, both the 1,2-PB and the 1,4-PB samples used in this study are semi-crystalline. Since the deuteration should not affect the polymer stereochemistry [7], the product saturated polymers were also expected to be crystalline. The glass transition temperatures and melt data of the unreacted and partially reacted polymers provide information on the polymer morphology.

Table I summarizes the thermal data obtained for the 1,2-PB samples. A single glass transition was observed at all levels of deuteration. The glass transition onset temperature descended gradually with deuteration. The melting temperature also decreased at higher levels of deuteration from that of the unreacted 1,2-PB. The reduced heat of fusion seen at 66 and 85% deuteration -- as well as the high conversion -- implies reaction of double bonds originally in crystalline domains. No melting transition

ascribable to the product syn-1-butene (the hydrogenation product of 1,2-PB) was observed in the range 25-175°C. Doi reports a melt temperature for syn-1-butene of 45°C [8]. That region was featureless in our scans.

Table I. Results of DSC Analysis of Partially Deuterated syn-1,2-Polybutadiene

%D$_2$	T$_g$(°C)	T$_m$(°C)	ΔH$_m$(J/g)
0	0	106	15.6
25	-14	105	15.1
66	-26	95	7.2
85	-30	90	4.1

Two endotherms, one at 42°C and one at 68°C, are present in the DSC plot for unreacted 1,4-PB, consistent with previous studies[9,10]. Upon deuteration, a substantial new endotherm appears due to the hydrogenated polybutadiene product which is similar to LDPE [11]. The product at 70% deuteration melts at 99°C. The original 42°C endotherm is still present although considerably reduced in size. The 68°C peak may be covered by the tail of the product melt. Unreacted 1,4-PB had a T$_g$ at -75°C. As expected for linear polyethylene, no glass transition was observed at high deuteration.

DISCUSSION

The most striking result of those described above is the difference in the SANS plots obtained for partially deuterated 1,2-PB and 1,4-PB. Specifically, the presence of a peak in the 1,2-PB data is unusual. This peak is similar to that observed for block copolymers and, thus, suggests domain formation. Four possible explanations for the origin of this peak have been considered:

Chemical Heterogeneity- The most interesting explanation is the possibility of a catalyst-localized reaction. Initially the catalyst is dissolved in the polymer matrix. If preferential reaction occurred on double bonds near the catalyst molecule and catalyst mobility were limited, regions of deuterated polymer in a matrix of unreacted polymer would appear. Such chemical heterogeneity could give rise to the observed SANS data, although the peak should disappear as the reaction goes to completion.

The data presented above imply the formation of domains of radius on the order of 30Å. The large increase in the surface area between domains with no change in characteristic length implies that deuteration proceeds by nucleation of new domains with minimal growth beyond 30Å. The DSC results on 1,2-PB do not show two distinct glass transitions as is expected for phase separated materials. It should be emphasized, however, that the domains under consideration are very small. It is not clear that such tiny domains would show a distinct glass transition.

282

Crystal-Excluding Reaction- If the amorphous regions of the polymer are deuterated preferentially as compared to the crystalline regions, the contrast between those regions may be enhanced in SANS. Although crystallites are deuterated during the course of the reaction, the DSC data for 1,2-PB suggest that reaction of amorphous regions occurs preferentially. Specifically, there is minimal change in the heat of fusion on going from 0% to 25% conversion. The size of the observed peak in SANS, however, increases substantially on going to 66% conversion. At this conversion level, crystallites must have reacted suggesting the domains are not the result of preferential deuteration of the amorphous phase. Furthermore, crystallites in these polymers would be expected to be microns in size. Structure on this length scale would not be detected by SANS.

Crystalline Product Formation- As mentioned above, the reaction product, syn-1-butene, may be semi-crystalline. If reaction occurs randomly throughout the material but only highly deuterated regions crystallize, the observed domains could be attributable to the contrast between highly deuterated crystalline domains and less deuterated amorphous regions. Further, SANS is known to be sensitive to density fluctuations. The peak may not be related to differences in deuteration but only to the density difference between the developing crystalline and amorphous regions. If this is the case, the size of the peak should increase with conversion as observed. In contrast, if the peak is related only to differences in deuteration, it should disappear at 100% reaction. No DSC peak attributable to the melting of product crystallites was observed; however, whether the melt transition of tiny crystallites could be observed is not clear. The SAXS data for the 66% 1,2-PB sample shows tailing in the high Q (low size) regime, possibly indicating the presence of tiny polydisperse crystallites.

Deuteration-induced phase separation- The observed peak in SANS might signify phase separation via spinodal-decomposition. In general, however, the peak would be expected to move to smaller Q as phase-separation progressed. The surface area would also be expected to decrease as coarsening progressed. Finally, the fully deuterated material would not be phase-separated and the peak should decrease beyond 50% deuteration. The restrictions imposed by the polymeric nature of the system could, of course, lead to unusual kinetic behavior. If a rubbery system became glassy, for example, miscibility at high deuteration would be kinetically impeded.

Miscellaneous- The peak in the SANS data may be due to catalyst crystallites, some feature of the foam fabrication, or of some other experimental variable. The fact that 1,4-PB had no such peak limits our concern about such miscellaneous factors.

CONCLUSION

Unfortunately none of the above interpretations is completely satisfactory. Models which attribute domain formation to preferential deuteration do not account for the persistence of the peak in the SANS data at high deuteration levels (where contrast should decrease). On the other hand, models that attribute the SANS peak to reaction-induced density differences (e. g. formation of lamellar crystals) fail to account for the absence of a similar peak in the SAXS profile. Further data on

fully deuterated and solution-reacted samples will be required to settle the issue. Irrespective of its origin, the presence of such a peak suggests interesting morphological consequences of catalytic hydrogenation of polymers in the bulk.

ACKNOWLEDGEMENTS

REFERENCES AND NOTES

*Permanent address: Department of Chemistry and The Polymer Research Center, The University of Cincinnati, Cincinnati, OH 45221

1. L. R. Gilliom, Macromolecules 22, 662 (1989).

2. See, for example, E. Marecnal "Chemical Modification of Synthetic Polymers" in Compreh. Polymer Sci., vol. 6, edited by G. Allen and J. Berington (Permagon Press, Oxford, 1989), p. 1.

3. R. H. Crabtree, S. M. Morehouse, J. M. Quirk, Inorg. Synth. 24, 173 (1986).

4. A. J. Hurd, D. W. Schaefer and A. M. Glines, J. Appl. Cryst 21, 864 (1988).

5. J. T. Koberstein, B. Mora and R. S. Stein, J. Appl. Cryst. 13, 34 (1980).

6. D. W. Schaefer, J. E. Mark, D. McCarthy;, Li. Jian C. -C. Sun and B., Farago, in Polymer Based Molecular Composistes, edited by D. W. Schaefer and J. E. Mark (Mat. Res. Soc. Symp. Proc., XX, Pittsburgh, PA 1990) pp. XX-XX.

7. NMR analysis of the hydrogenation products in both cases indicated that no change in stereochemistry had occurred. The analysis of the spectra for 1,2-PB, however, was hindered by the fact that the starting material contained approximately 10% 1,4-connectivity.

8. Y. Doi, A Yano, K. Soga, and D. R. Burfield, Macromolecules, 19, 2409 (1986).

9. M. Berger and D. J. Buckley J. Polym. Sci., A, 1, 2945 (1963).

10. P. Wang and A. E. Woodward, Macromolecules, 20, 2718 (1987).

11. A similar endotherm was observed in the solution hydrogenation of cis-1,4-polybutadiene. J. M. G. Cowie and 1. J. McEwen, Ibid., 10, 1124 (1977).

SYNTHETIC CONTROL OF MOLECULAR STRUCTURE IN ORGANIC AEROGELS

RICHARD W. PEKALA
Lawrence Livermore National Laboratory, Livermore, CA 94550

ABSTRACT

Organic aerogels have been formed from the aqueous, sol-gel polymerization of resorcinol with formaldehyde. These materials are transparent and have continuous porosity with cell/pore sizes of less than 1000 Å. Their microstructure is composed of interconnected colloidal-like particles with diameters of 30-200 Å. The particle size, cell size, surface area, and density of the aerogels are predominantly controlled by the catalyst concentration used in gel preparation.

INTRODUCTION

The sol-gel processing of metal alkoxides (e.g. tetramethoxy silane, aluminum sec-butylate) is a convenient method for tailoring the properties of inorganic materials at the molecular level. Sol-gel research has principally focused on the manipulation of silicate precursors to form polymeric or colloidal structures in solution. The hypercritical drying of crosslinked silica gels leads to the formation of a special class of open-celled foams referred to as aerogels. Aerogels have an ultrafine cell/pore size (< 1000 Å) and a solid matrix composed of interconnected colloidal-like particles or lightly crosslinked polymer chains. These particles or chains have characteristic diameters of less than 100 Å. The above microstructure is responsible for the unusual optical, thermal, and acoustic properties of these materials [1,2].

Our research has focused on <u>organic</u> syntheses which proceed through a sol-gel transition and can be controlled to give aerogels with specific properties. Organic aerogels have been synthesized from the base catalyzed, aqueous reaction of resorcinol with formaldehyde. In this reaction, resorcinol (1,3 dihydroxy benzene) is a trifunctional monomer capable of adding formaldehyde in the 2,4, and/or 6 ring positions. These intermediate products condense into polymeric "clusters" with diameters ranging from 30-200 Å. The resorcinol-formaldehyde (RF) "clusters" contain surface functional groups ($-CH_2OH$) which lead to further crosslinking and eventual gel formation.

RF gels are dark red in color and transparent, indicative of their ultrafine pore size. If the solvent in the pores of the gel is exchanged with a monomer such as methyl methacrylate, it is possible to form transparent molecular composites by polymerizing the monomer with a free-radical initiator or UV light. The final molecular composite consists of two continuous phases with poly(methyl

methacrylate) being the dominant phase (80-95% by volume).

In order to obtain organic aerogels, the RF gels are hypercritically dried from carbon dioxide. The resultant aerogels are dark red in color and transmit light. Because RF aerogels consist of a highly crosslinked aromatic polymer, they can be pyrolyzed in an inert atmosphere to form vitreous carbon aerogels. In a sense, both RF and carbon aerogels are molecular composites with air being the dominant phase.

The particle size, cell size, density, surface area, and modulus of organic aerogels largely depend upon the catalyst concentration (i.e. Na_2CO_3) used in the sol-gel polymerization. In this paper, the chemical manipulation of the aerogel microstructure will be discussed in detail. Characterization methods include TEM, BET nitrogen adsorption, and small angle scattering.

GEL PREPARATION AND DRYING

Resorcinol (99% purity), formaldehyde (37.5%; methanol stabilized), and sodium carbonate were used as received from commercial suppliers. All solutions were prepared from water which had been deionized and distilled. A typical gel formulation contained 0.29M resorcinol, 0.58M formaldehyde, and 1-6 mM sodium carbonate for a total of 5% solids. The molar ratio of [formaldehyde]/[resorcinol] was held constant at a value of 2.0 for all formulations.

RF solutions were poured into glass vials, sealed, and cured for 7 days at 85-95 °C. Depending upon the % solids and the catalyst level, gel times varied from several hours to days. After curing, the RF gels were removed from their glass containers and placed in a dilute acid solution (pH~2) at 50 °C to promote further crosslinking. Gel modulii showed a noticeable increase after the acid treatment.

In preparation for hypercritical drying, the gels were exchanged into an organic solvent (e.g. acetone). The solvent-filled gels were then placed in a jacketed pressure vessel (Polaron®, Watford, England) which was subsequently filled with carbon dioxide. After several days of exchanging the RF gels with fresh carbon dioxide, the vessel was taken above the critical point (T_c= 31 °C; P_c= 1100 psi). All samples were maintained at a temperature of 45 °C for a minimum of 4 hours before the pressure was slowly released over a period of 16 hours. At atmospheric pressure, the aerogels were removed from the vessel and characterized.

RESULTS AND DISCUSSION

In a manner similar to silica aerogels, the structure and properties of organic aerogels depend upon the amount of catalyst used in the sol-gel polymerization.

Because the pH of the RF solution decreases as the polymerization proceeds, all formulations are referenced by the [Resorcinol]/[Catalyst] ratio in the mixture. R/C ratios of 50-300 provide an acceptable range in which transparent gels are formed.

Resorcinol reacts with formaldehyde under alkaline conditions to form mixtures of addition and condensation products which react further to form a crosslinked network. The major reactions include: (1) the formation of hydroxymethyl derivatives of resorcinol, (2) the condensation of the hydroxymethyl derivatives to form methylene and methylene ether bridged compounds, and (3) the disproportionation of the methylene ether bridges to form methylene bridges plus formaldehyde as a byproduct. These reactions have been studied extensively by NMR [3,4].

In our current model of the RF polymerization, the base catalyst abstracts a proton from one of the hydroxyl groups on resorcinol to form the corresponding anion. Because the resorcinol anion is much more reactive than free resorcinol in solution, it quickly adds formaldehyde in an electrophilic aromatic substitution reaction at the 2,4 and/or 6 ring positions. Electrostatic repulsion retards interaction between the charged, substituted resorcinol molecules; however, additional monomers (formaldehyde and resorcinol) are able to add to this cluster. The functionality of the cluster increases as resorcinol is covalently attached; therefore, the probability of additional monomers reacting with the cluster increases. Titration, chromatography, and NMR data show that resorcinol is the first monomer to be completely consumed. As a consequence, only formaldehye is available to react at the outer surface of the RF clusters forming numerous hydroxymethyl groups. The above process is best described as reaction limited monomer-cluster growth.

The R/C ratio in a particular formulation is the primary factor which controls the number of clusters formed in solution and the size to which they grow. In the late stages of polymerization, cluster-cluster growth is ultimately responsible for gel formation through the condensation of surface hydroxymethyl groups. In terms of growth processes, the RF reaction is similar to the base catalyzed polymerization of TMOS [5-7].

The R/C ratio affects both the density and surface area of the aerogels. Table 1 shows the final density of both RF and carbon aerogels made from solutions containing 5% solids but varying R/C ratios. In all cases, some shrinkage occurs during hypercritical drying and the final densities exceed the target densities. The greatest amount of densification occurs for gels prepared under high catalyst conditions --- i.e. low R/C ratios. The relationship between the final aerogel density and the R/C ratio is not linear. In fact, the final densities plateau at a value ~15% higher than the theoretical value for R/C $\geq$ 150.

TABLE I

[Res]/[Cat]	Target Density	RF Density	Carbon Density
50	0.05 g/cc	0.088 g/cc	0.205 g/cc
100	0.05	0.067	0.123
150	0.05	0.057	0.098
200	0.05	0.057	0.085
300	0.05	0.064	0.084
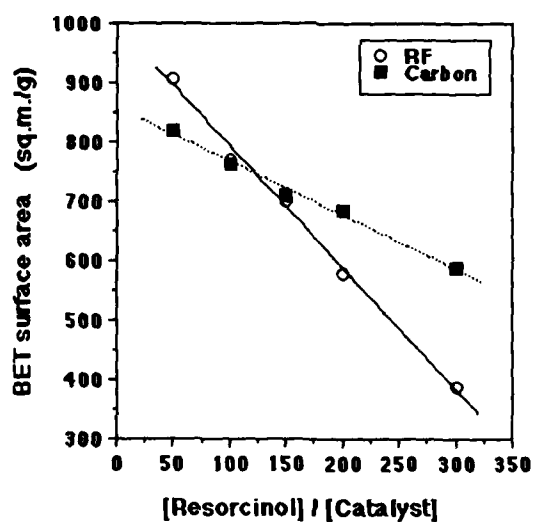
Figure 1. Aerogel surface areas as a function of the R/C ratio.

If the RF aerogels are pyrolyzed at 1050 °C in argon, the final carbon densities are still a function of the initial R/C ratio. The % mass loss is ~50% for all samples, yet aerogels synthesized under high catalyst conditions experience much greater volumetric shrinkage (~75%) during pyrolysis leading to higher final densities.

The BET surface areas of the above RF and carbon aerogels are shown in Figure 1. The observed trend shows that surface areas increase as the amount of catalyst increases in a formulation. A slightly stronger dependence of surface area upon the R/C ratio is observed for the RF aerogels as compared to the carbon aerogels.

The effects of the R/C ratio upon both density and surface area suggest differences in the RF gel structure which translate to the final dried aerogel. Figure 2 shows the microstructure of two RF aerogels synthesized at the extremes of our catalyst conditions. Each aerogel is composed of interconnected colloidal-like particles which were referred to as "clusters" in solution. At R/C=300, the particles have diameters of 160-200 Å and are connected in a "string of pearls" fashion. At R/C=50, the particles have diameters of 30-50 Å. These particles are fused together in such a manner that it is sometimes difficult to visualize individual particles or beads. This high degree of interconnection between the RF particles is reflected in mechanical property data which show that R/C=50 aerogels are 10X stiffer than R/C=300 aerogels at equivalent densities [8].

(a)   **(b)**

⊢⎯⊣

500Å
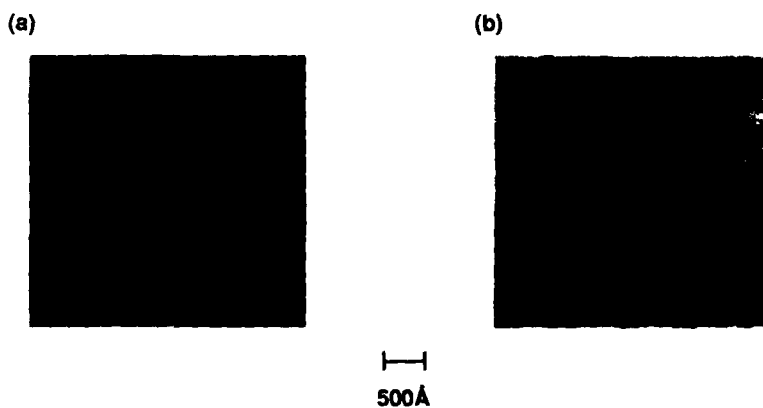
Figure 2. Transmission electron micrographs of RF aerogels prepared at 5% solids with different [resorcinol]/[catalyst] ratios: (a) 50 (b) 300.
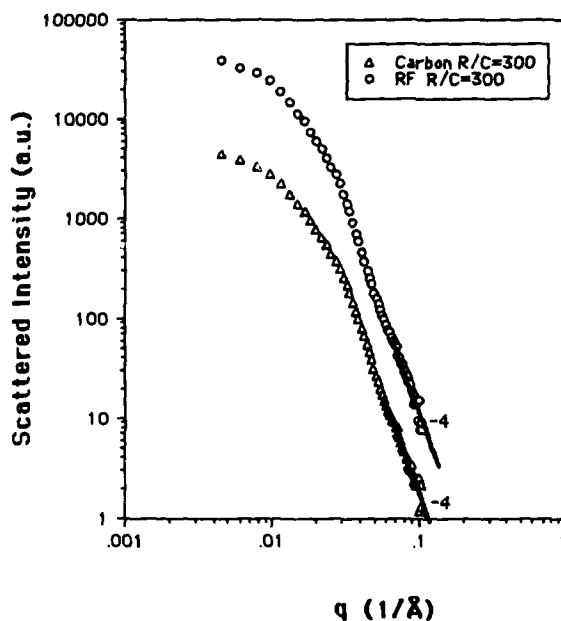
Figure 3. SAXS curves for selected RF and carbon aerogels.
Densities equal 0.065 and 0.085 g/cc, respectively.

Disordered materials such as aerogels often display "dilation symmetry" which means that they are geometrically self-similar over a given range of size scales. Small angle scattering can be used to evaluate the fractal dimensions (D,D_s) of a material [9-11]. In this method, fractals show a power law dependence of the scattering intensity $I(q)$ on the scattering vector, q. The latter quantity is defined such that $q = 4\pi/\lambda \sin(\theta/2)$ where λ is the wavelength and θ is the scattering angle. For fractals, the following relationships hold:

Mass Fractal $\qquad I(q) \sim q^{-D} \qquad 1 < D < 3 \qquad$ (1)

Surface Fractal $\qquad I(q) \sim q^{-(6-D_s)} \qquad 3 < 6-D_s < 4 \qquad$ (2)

Figure 3 shows the SAXS curves for RF and carbon aerogels synthesized at R/C=300. At large q, both curves roll over to a slope of -4 which indicates that these materials have smooth surfaces on a microscopic scale. At intermediate q values, $I(q)$ does not

show a power law dependence for either curve. The above data indicate that these materials are n̲o̲t̲ surface or mass fractals. The same finding applies to aerogels synthesized at other catalyst conditions. Only the correlation range, which relates to the median pore size, changes as a function of the R/C ratio. This data and other SAXS results will appear in a future publication.

SUMMARY

Organic aerogels with tailored physical properties (e.g. surface area, compressive modulus) can be formed from the sol-gel polymerization of resorcinol with formaldehyde. In this reaction , the [Resorcinol]/[Catalyst] ratio is responsible for the final aerogel microstructure. Although TEM reveals the microstructure of organic aerogels to be similar to silica aerogels, SAXS data show that these materials differ in that organic aerogels are n̲o̲t̲ mass or surface fractals.

ACKNOWLEDGMENTS

REFERENCES

[1] M. Gronauer, A. Kadur, and J. Fricke, in Aerogels, edited by J. Fricke (Springer-Verlag, New York, 1986) pp. 167-173; O. Nilsson, A. Fransson, and O. Sandberg, ibid., pp. 121-126.

[2] J. Fricke, Sci. Am. 258(5), 92 (1988).

[3] D.D. Werstler, Polymer 27, 757 (1986).

[4] A. Sebenik, U. Osredkur, and I. Vizovisek, Polymer 22, 804 (1981).

[5] C.J. Brinker and G.W. Scherer, J. Non-Crystalline Solids 70, 301 (1985).

[6] D.W. Schaefer, Science 243, 1023 (1989).

[7] D.W. Schaefer, MRS Bulletin 13(2), 22 (1988).

[8] J.D. LeMay, presented at the First Pacific Polymer Conference, Maui, Hawaii, December 1989 (unpublished).

[9] A. Craievich, M.A. Aegerter, D.I. dos Santos, T. Woignier, and J. Zarzycki, J. Non-Crystalline Solids 86, 394 (1986).

[10] R. Vacher, T. Woignier, J. Pelous, and E. Courtens, Phys. Rev. B 37(11), 6500 (1988).

[11] D.W. Schaefer and K.D. Keefer, Phys. Rev. Lett. 56(20), 2199 (1986).

SYNTHETIC PROCEDURES FOR PREPARING CROSS-LINKABLE ACRYLIC
COMB-LIKE COPOLYMERS VIA MACROMONOMERS

GANG-FUNG CHEN* AND FRANK N. JONES
Polymers & Coatings Dept., North Dakota State University, Fargo, ND
58102. *Present address: Ashland Chemical Company, Columbus, Ohio

ABSTRACT

A versatile procedure was developed for synthesis of acrylic comb-like
copolymers in three steps: (1) Hydroxyl terminated oligomers were
synthesized from methyl methacrylate, butyl acrylate and glycidyl acrylate
by free-radical initiated addition polymerization using a functional chain
transfer agent, 2-mercaptoethanol, and very low initiator levels. (2) The
oligomers were converted to macromonomers by reaction with isocyanatoethyl
methacrylate. (3) The macromonomers were polymerized by free-radical
initiation. Conditions during the first stage must be carefully selected to
minimize formation of difunctional material which could cause gelation in
the third stage. A variety of structures can be made such as comb-like
copolymers with homopolymer tines or comb-like homopolymers with copolymer
tines. Functional groups can be introduced by copolymerizing glycidyl
acrylate into the macromonomer. Assignment of comb-like structures is not
rigorously proven but is strongly supported by the synthetic route and by
DSC, FT-IR and chromatographic data.

INTRODUCTION

Comb-like polymers are distinguished from graft polymers by the close
and regular spacing of their side chains and from star polymers by the
attachment of the side chains to a polymeric chain rather than to a central
core. They share with star polymers the potentially useful property of
having much lower solution and bulk viscosities than linear polymers of
similar molecular weight. Comb-like copolymers are generally synthesized by
polymerization of macromonomers -- oligomers or polymers that contain a
single polymerizable group on one end. Macromonomers have been synthesized
by a variety of techniques [1] involving anionic [2], cationic [3], and
group transfer [4,5] polymerization.

Until recently there have been few reports of synthesis of
macromonomers by routes involving free-radical chain polymerization. If
such a process could be developed it would open an economical route to a
very wide variety of comb-like polymers including, possibly, structures that
have reactive sites for subsequent modification or cross-linking. A major
obstacle to development of such a process is the difficulty of attaching a
polymerizable group to one end of the great majority of macromonomer
molecules while suppressing the formation of molecules having two or more
reactive groups. A macromonomer contaminated with with polyfunctional
material can be expected to gel when polymerization is attempted.

In 1986 Albrecht and Wunderlich showed that these difficulties can be
overcome in the case of poly(methyl methacrylate) [6]. They synthesized
PMMA macromonomers with $\overline{M}_w$'s of 6500 to 23,000 by free-radical
polymerization of MMA in the presence of a functional chain transfer agent,
2-mercaptoethanol (2-ME), followed by fractionation and reaction of the
mono-hydroxy functional products with isocyanatoethyl methacrylate (ICEM).
Polymerization of these macromonomers yielded comb-like polymers with $\overline{M}_w$'s
on the order of 10^6 as determined by light scattering. The necessity of
fractionation may limit the utility of this method to relatively high T_g
materials. Thus it would be desirable to find a procedure that does not
involve fractionation.

Here we report the development of such a procedure -- one which appears to be relatively general with respect to monomer selection and product T_g. It will be shown that comb-like copolymers of methyl methacrylate (MMA),[8] butyl acrylate (BA) and glycidyl methacrylate (GMA) can be synthesized by a three-step procedure that can be idealized as follows:

```
  I•  +  M  +  HOXSH  --> IMMMMMMMMMMH + HOXSMMMMMMMMMMH + termination
1mol  1000mol  100mol      1mol           98mol              products
```

```
HOXSMMMMMMMMMMH + CH2=C(Me)COOYN=C=O --> CH2=C(Me)COOYNHCOOXSMMMMMMMMMMH
                         ICEM                         macromonomer
```

```
CH2=C(Me)COOYNHCOOXSMMMMMMMMMMH + I• --> comb-like copolymer
```

$$[I• = initiator, \ M = mixed \ monomers, \ X \ and \ Y = -CH_2CH_2-]$$
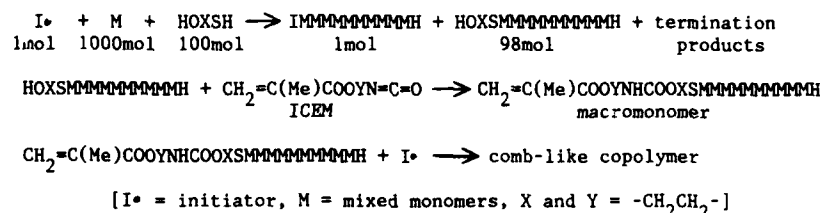
The first step, macromonomer synthesis, was performed under these conditions:

(1) Solution polymerization in toluene at 108 - 110 $^\circ$C or in methyl isobutyl ketone at 80 to 90 $^\circ$C.

(2) Monomer starved conditions.

(3) Low levels of initiator and high levels of chain transfer agent -- for example a 1000/100/1 or a 1000/50/1 mol ratio of monomer/2-ME/initiator, and

(4) Postheating the product to 140 to 175 $^\circ$C in most cases.

These conditions were chosen to minimize termination by combination (expected to lead to difunctional materials) and to virtually eliminate unreacted initiator before addition of ICEM. Deviation from these conditions generally gave materials that gelled during attempted polymerization of the macromonomer.

By adhering to these conditions a variety of structures including homopolymeric backbones with copolymeric tines and copolymeric backbones with homo- and copolymeric tines were synthesized.

EXPERIMENTAL DETAILS

Details can be found in the Ph.D. dissertation of G-F. Chen [7]. The synthetic procedures described here are representative.

Materials. Reactants were generally 97 to 99 % grades obtained or purchased from commercial sources and were used without further purification. Isocyanatoethyl methacrylate (ICEM) was obtained from Dow Chemical Company, which no longer supplies this material; other sources are said to exist. "Aromatic 100" is a mixed alkyl benzene solvent, bp 155 - 177 $^\circ$C, supplied by Exxon Chemical Company.

Synthesis of Hydroxyl Terminated Homo- and Co-polymers of Methyl Methacrylate (MMA) and Butyl Acrylate (BA). Solutions of 2-mercaptoethanol (2-ME) and 2,2'-azobis(isobutyronitrile) (AIBN) in the monomer(s) having a monomer/2-ME/AIBN mol ratio of 1000/100/1 or 1000/50/1 were added continuously during 2.5 h to a 3-necked reaction flask containing refluxing toluene in a N_2 atmosphere. The weight of toluene approximately equalled the weight of reactants. Stirring and refluxing were continued throughout the addition and for 4 h therafter. A sample was withdrawn to gravimetrically estimate conversion of monomer to non-volatile material;

conversion varied somewhat but typically ran 60 to 80 %. The resulting solution was gradually heated to 160 - 170 $^{\circ}$C and stirred under a nitrogen purge to volatilize solvent and unreacted monomers and to decompose residual initiator. The FT-IR specta had substantial peaks at about 3500 cm^{-1} (OH stretching) and were otherwise consistent with the assigned structures. Hydroxyl number determinations by the pyromellitic dianhydride/dimethyl-formamide method [8] showed in most cases that all or almost all of the 2-ME could be accounted for in the non-volatile material; in a few cases small amounts (< 10 %) of unreacted 2-ME was found in the volatile solvent/monomer distillate. After removal of volatiles the residues were dissolved in sufficient xylene to make 30 wt-% solutions.

In other experiments methyl isobutyl ketone was substituted for toluene in the above procedure and the reaction was carried out at 80 to 90 $^{\circ}$C. Conversions of up to 90 % were attained by this procedure.

Synthesis of MMA and BA Homo- and Copolymer Macromonomers. To the above solutions were added isocyanatoethyl methacrylate (ICEM) and dibutyl tin dilaurate (DBTDL); the amount of ICEM was a 10 mol % excess over the amount of 2-ME used in the above synthesis, and the concentration of DBTDL was 4.7 x 10^{-4} wt %. The total concentrations of reactants in xylene was about 30 wt %. The solutions were heated at 55 $^{\circ}$C with stirring overnight. Disappearance of the FT-IR peak at 3500 cm^{-1} (OH) and appearance of peaks at 3350 (NH) and 1640 cm^{-1} (urethane C=O) indicated complete reaction.

Synthesis of Comb-like Homo- and Copolymers. AIBN (2.5 mol/L) was added to the above solutions, and the solutions were heated with stirring under N$_2$ to 60 $^{\circ}$C. The solutions became very viscous within 5 to 10 min, and heating was continued briefly and the solutions were cooled. The solutions often gelled when lower AIBN concentrations or higher temperatures were used. GPC retention times of the comb-like polymers were relatively short, typically 22 to 24 minutes; in comparison, retention times of the hydroxyl terminated polymers from which they were made had retention times in the range 31 to 35 min. The comb-like copolymers contained small to modest fractions of long elution time material, presumably unreacted macromonomer or an unreactive fraction present in the macromonomer. Typical GPC traces are shown in Figure 1.

Synthesis of Hydroxyl Terminated Copolymers of BA with Glycidyl Acrylate (GA) and Conversion to Macromonomers. BA/GA mixtures (83/17 and 67/33 w/w) were polymerized by procedures essentially the same as those described above using MIBK as solvent. Reaction temperatures were 80 to 90 $^{\circ}$C, and no postheating step was used to remove solvent and unreacted monomers. Conversions were 84 to 88 %. These hydroxyl terminated copolymers were reacted with ICEM essentially as described above to yield macromonomers.

Synthesis of Comb-like Copolymers with Mixed Tines. Mixtures of homo- and copolymer macromonomers prepared as described above were polymerized with AIBN under conditions similar to those described above. In some instances it was necessary to heat the reaction mixture to about 90 $^{\circ}$C to complete polymerization, as indicated by GPC.

Test procedures. Differential scanning calorimetry (DSC) was effected with a du Pont Model 990 Thermal Analyzer using samples that had been heated under N$_2$ for 2 h to remove volatiles. Heating rate was 10 $^{\circ}$C/min. T$_g$ was taken as the onset of the endothermic deflection. Gel permeation chromatography (GPC) using Waters 100A, 500A, 1000A and 10000A columns in series; the solvent was tetrahydrofuran, and a Waters Model R401 refractive index detector was used.

RESULTS AND DISCUSSION

The synthetic conditions for hydroxyl terminated polymers were devised after a good deal of trial and error; they seem reproducible except that monomer conversions vary. This variation is attributable to the unusually low levels (0.07 wt %) of AIBN; 0.5 to 1.0 wt % is commonly used. Five such materials made with 1000/100/1 monomer/2-ME/AIBN ratios had $\overline{M}_n$ of 800 to 1000 and $\overline{M}_w/\overline{M}_n$ of 1.6 to 2.2 as measured by GPC; conversions were 68 to 100 %. Five similar materials prepared with 1000/50/1 ratios had $\overline{M}_n$ of 1400 to 2100 and $\overline{M}_w/\overline{M}_n$ of 1.5 to 2.4 at conversions of 60 to 99 %.

Conversion of the hydroxyl terminated polymers to macromonomers by reaction with ICEM and polymerization of the macromonomers is relatively straightforward providing hydroxyl terminated precursors are prepared as described. Substantial deviation from the recommended procedure generally afforded precursors that caused gelation during the third stage. The recommended procedures yield macromonomers that do not gel, although they become very viscous in 30 wt % solution. Some difunctional macromonomer is presumably present and causes bridging of comb-like structures, but its level is apparently low enough that gelation can be avoided.

GPC traces of a hydroxyl terminated poly(MMA/BA) (70/30 w/w) polymer and of the comb-like copolymer made from it are shown in Figure 1. In this case the monomer/2-ME/AIBN ratio was 1000/100/1. Retention times are marked on the Figure, and molecular weights of polystyrene calibration standards are also indicated. While it is likely that the hydroxyl terminated precursor has a molecular weight close to the indicated level, it is seems unlikely that the molecular weight of the comb-like copolymer can even be estimated in this way, as discussed below.

Figure 1. GPC Trace of an Hydroxyl Terminated poly(MMA/BA) Copolymer [A] and of A Comb-like Copolymer made from it [B]

Upper line: Retention time, min.
Lower line: Molecular weight of polystyrene standards
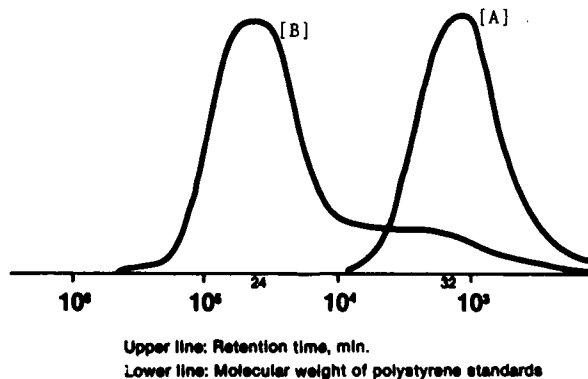
With the objective of making comb-like copolymers bearing functional groups as potential cross-linking sites we investigated copolymerization of glycidyl acrylate into the hydroxyl terminated precursors. Somewhat milder reaction conditions, described in the EXPERIMENTAL SECTION, were used in order to minimize the potential for side reactions. One side reaction of concern is the possibility of reaction of the thiol group of 2-ME with the oxirane ring of the glycidyl acrylate, an occurance that would increase

functionality of the hydroxyl terminated precursor and probably lead to gelation in step three. It proved possible to prepare hydroxyl terminated precursors of composition BA/GA in ratios 83/17 and 67/33. Successful conversion of these materials to comb-like copolymers, indicated that the chain transfer reaction is much faster than the oxirane addition reaction and consumes virtually all of the 2-ME.

Availability of different macromonomers opens possibilities for synthesis of a wide variety of structures involving copolymerization in the first stage or the third stage, or both. For example, copolymerization in the first stage and homopolymerization in the third will yield a relatively uniform comb-like copolymer. On the other hand, if two dissimilar macromonomers from the first stage are blended and then polymerized in the third stage, a comb-like copolymer with homopolymer tines can be expected. Evidence for the formation of such materials was provided by differential scanning calorimetry (DSC) studies (Table 1). Comb-like MMA/BA copolymers made from single copolymeric precursors displayed a single T_g, while comb-like copolymers of similar overall composition made from mixtures of homopolymeric precursors ("comb-like copolymers with homopolymer tines") displayed two T_g's, one presumably related to the T_g of the BA precursor and the other to the T_g of the MMA precursor. However, only the lower T_g's could be detected in the comb-like copolymers with a homopolymeric MMA tine and copolymeric BA/GA tines.

Table 1. T_g of Selected Hydroxyl Terminated Precursors and of Comb-Like Copolymers

Description	Composition (wt ratio)	T_g ($^\circ$C)
P-MMA precursor	OH terminated PMMA, M_n ca. 1000	40
P-BA precursor	OH terminated PBA, M_n ca. 1000	-60
BA/GA precursor A	OH terminated BA/GA 83/17 copolymer	-40
BA/GA precursor B	OH terminated BA/GA 67/33 copolymer	-35
Comb-like	MMA/BA-30/70, copolymer tines	-15
Comb-like	MMA/BA-50/50, copolymer tines	8
Comb-like	MMA/BA-70/30, copolymer tines	24
Comb-like	MMA/BA-30/70, homopolymer tines	-44, 39
Comb-like	MMA/BA-50/50, homopolymer tines	-43, 29
Comb-like	MMA/BA-70/30, homopolymer tines	-49, 39
Comb-like	MMA homopol., BA/GA 83/17 copolymer	-22
Comb-like	MMA homopol., BA/GA 67/33 copolymer	-17
Control	MMA/BA/HEMA-40/40/20 random copolymer	26

Gel permeation chromatography calibrated with linear polystyrene standards indicated molecular weights on the order of 10^5 for the comb-like copolymers, but little meaning is assigned to the absolute values. It is well known [6,9] that the hydrodynamic volume of highly branched polymers is much lower than that of similar polymers of the same molecular weight. Thus correlation of GPC retention times of comb-like polymers with those of linear standards can be expected to understate the molecular weight of the comb-like materials. For example, Albrecht and Wunderlich measured molecular weight of their comb-like PMMM as 10^6 by light scattering but only 4.5×10^4 by GPC, and Masson reported similar differences.

Retention times were shorter for polymers made at lower (60 vs. 90 $^\circ$C)

298

stage-three polymerization temperatures, indicating that, on a relative basis, lower temperatures favor higher molecular weight comb-like copolymers. A recent kinetic study of free-radical copolymerization of macromonomers showed that the reactivity of a growing chain with a macromonomer end toward a second macromonomer decreases as molecular weight increases.[10] This observation is attributed to a kinetic excluded volume effect. In the context of the present study, this result is consistent with the assignment of comb-like structures for the third-step products but suggests that further study of how reaction conditions affect molecular weight are warranted.

CONCLUSIONS

Here we have demonstrated an apparently versatile procedure for synthesis of short chain acrylic macromonomers by a free-radical initiated chain transfer process. These materials can be converted to an almost limitless variety of comb-like polymers and copolymers. Reactive functional groups can be incorporated by copolymerization of glycidyl acrylate. Assignment of comb-like structures is not rigorously proven but is strongly supported by the synthetic route and by DSC, FT-IR and chromatographic data.

REFERENCES

[1] P. R. Rempp and E. Franta, Adv. Polym. Sci, 58, 1 (1984).

[2] G. O. Schultz and R. Milkovich, J. Appl. Polym. Sci., 27, 4773 (1982).

[3] B. Ivan, J. P. Kennedy and V. Chang, J. Polym. Sci. (Chem. Ed.), 18, 1523, 1539, 3177 (1980).

[4] F. P. Boettcher, J. Macromol. Sci.-Chem, A22(5-7), 665 (1985).

[5] D. Y. Sogah and O. W. Webster, J. Polym. Sci., Polym Lett. Ed., 21, 927 (1983).

[6] K. Albrecht and W. Wunderlich, Angew. Makromol. Chemie, 145/146, 89, (1986).

[7] G-F. Chen, Ph.D. Dissertation, North Dakota State University, Fargo, ND 58105, pp 185 - 289.

[8] B. M. H. Kingston, J. J. Garey and W. B. Hellwig, Analy. Chem., 41(1), 86, (1969).

[9] Z. Grubisic, P. Rempp and H. Benoit, J. Polym. Sci., Polym. Lett. Ed., 5, 753, (1967).

[10] Y. Nabeshima and T. Tsuruta, Makromol. Chem., 190, 1635, (1989).

SYNTHESIS AND CHARACTERIZATION OF SEGMENTED COPOLYMERS OF A METHYLATED POLYAMIDE AND A THERMOTROPIC LIQUID CRYSTALLINE POLYESTER

Gregory T. Pawlikowski, R. A. Weiss and S. J. Huang
Box U-136, Institute of Materials Science, University of Connecticut, Storrs, CT 06269

ABSTRACT

A block copolymer consisting of liquid crystalline polyester segments and methylated polyamide segments has been synthesized. Solution polycondensation of acid chloride end-capped poly(terephthaloyl phenylhydroquinone) (LCP portion) with an amine terminated poly(N,N'-dimethylethylene sebacamide) was utilized to prepare the block copolymer. Characterization by differential scanning calorimetry, infrared spectroscopy, thermogravimetric analysis, optical microscopy and elemental analysis has been performed to verify the existence of the block copolymer that may have potential as a molecular composite material or self-reinforcing thermoplastic.

INTRODUCTION

Much of the high strength/high modulus composites currently available stem from the use of macrophase reinforced materials such as fiber reinforced composites and self reinforced thermoplastics where the reinforcement fiber phase is on the order of microns in diameter. Although these composite systems have attained widespread use as high strength materials, their strengths have been limited due to fiber imperfections, the tendency of the fibers to fibrillate and poor interfacial adhesion between the fiber reinforcement and matrix phase.[1] It is believed that reinforcement on a much finer scale (10 - 30 nm or less) would result in more efficient reinforcement and create stronger materials.[2] These types of materials have been termed molecular composites.

Molecular composites have been found to possess very high strength and stiffness. Hwang and coworkers[3] prepared molecular composites by solution blending poly(p-phenylenebenzobisthiazole) (PPBT) and poly(2,5(6')-benzimidazole) (ABPBI) (30/70). Spun fibers of this blend were found to have a Young's modulus of 117.0 GPa and a tensile strength of 1270 MPa. Molecular composites also require much less reinforcement loading for equivalent strength. Takayanagi[2] used solution blending techniques to prepare molecular composites of poly(p-phenyleneterephthalamide) (PPTA) with nylon 6 and nylon 66. He reported that this material, which contained only a few percent rigid-rod molecules, displayed the same mechanical properties as fiber reinforced plastics which employ 40 percent fiber reinforcement.

The majority of work on molecular composites is being done on solution blended systems. While these systems have been successful in achieving high strength molecular composites, the technique has limited processing potential and requires large amounts of harsh solvents. It would be more desirable to have a truly melt processible molecular composite capable of 'in situ' fiber formation of the reinforcement phase during processing. One possible route for obtaining such a material may be through the use of block copolymers of the reinforcing rigid-rod phase with the flexible-coil matrix phase. This chemical attachment could act to anchor the reinforcement phase to the matrix, creating a strong interfacial bond between the two phases. Also,

chemically linking the two incompatible polymers would provide the driving force for intermixing, resulting in better dispersion.[4]

The work presented here involves the solution polymerization of a block copolymer of a rigid-rod segment and a flexible-coil segment. The rigid-rod polymer used was a liquid crystalline polyester (LCP) (III) of phenyl-hydroquinone (PHQ) (I) and terephthaloyl chloride (TPC) (II) and the flexible-coil polymer was poly(N,N'-dimethylethylene sebacamide) (VI) prepared from sebacoyl chloride (IV) and N,N'-dimethylethylenediamine (V). This work represents the initial effort in our attempt to create a melt processible molecular composite material where the reinforcing phase forms an 'in situ' fiberous network during processing with diameters in the range of 10 - 30 nm or less.

EXPERIMENTAL

An oven dried, 200 ml round bottom, three necked flask was equipped with a gas inlet valve, a mechanical stirrer and a stopper. A 0.06 wt % PHQ/tetrachloroethane (TCE) solution was slowly added to a 0.04 wt % TPC/TCE solution containing 10 % molar excess TPC and 150% pyridine (acid acceptor) over a period of about 1 to 1.5 hours. The reaction mixture was left to stir for about 24 hours. One half of the LCP solution was precipitated in about 400 ml acetone. The precipitate was then washed with acetone and dried. The remaining half of the reaction mixture was immediately used to prepare the block copolymer with half of the N-methylated polyamide reaction mixture as described below.
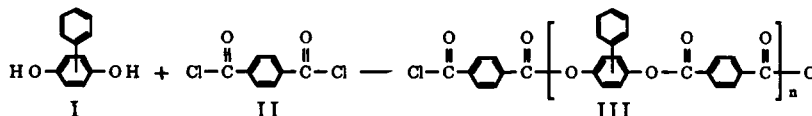
An oven dried, 200 ml round bottom, three necked flask was equipped with a gas inlet valve, a mechanical stirrer and a stopper. A 0.04 wt % N,N'-dimethylethylenediamine/TCE solution containing 150% pyridine was cooled down to approximately -15 °C. To the resulting cooled solution, 10% molar excess sebacoyl chloride was quickly added while rapidly stirring. The stirring was continued for approximately 24 hours while the reaction mixture was allowed to gradually warm to room temperature. Half of the polyamide solution was worked up for analysis. The remaining half was immediately used to prepare the block copolymer with half of the LCP reaction mixture from the reaction described previously.
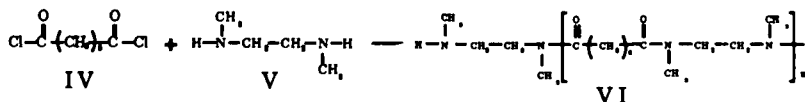
Preparation of the block copolymer was achieved through a nucleophilic acyl substitution reaction between the acid chloride terminated liquid crystalline polyester and the amine terminated polyamide oligomers. The half of the polyamide reaction mixture remaining in the reaction flask was stirred while the remaining liquid crystalline polyester portion was quantitatively transferred to the polyamide reaction flask. After 24 hours, the copolymer product was worked up for analysis by precipitating in approximately 500 ml

acetone. The precipitate was filtered, washed with acetone and dried in a vacuum oven.

$$III + VI \longrightarrow$$

VII
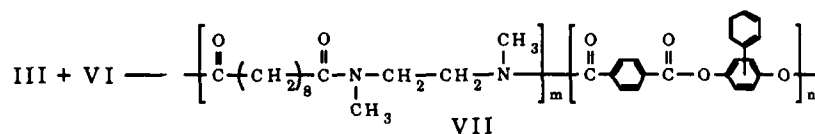
RESULTS AND DISCUSSION

Infrared spectroscopy

Infrared spectra were obtained on a Nicolet 60 SX FT-IR spectrometer. The most significant absorption of the N-methylated polyamide homopolymer was due to the N–C=O carbonyl stretch of the amide group at 1643 cm-1 (Fig. 1). Also significant in this spectrum is the absence of an absorption at 1715 cm-1 which would correspond to carboxylic acid endgroups. In contrast to the spectrum of the N-methylated polyamide, the spectrum of thᵣ 'P showed a strong absorption band at 1734 cm-1 due to the O–C=O carboᵢ stretching of the ester group (Fig. 1). A small but important absorption occurred at 1793 cm-1. This was due to the Cl–C=O acid chloride carbonyl stretch of the acid chloride endgroups.
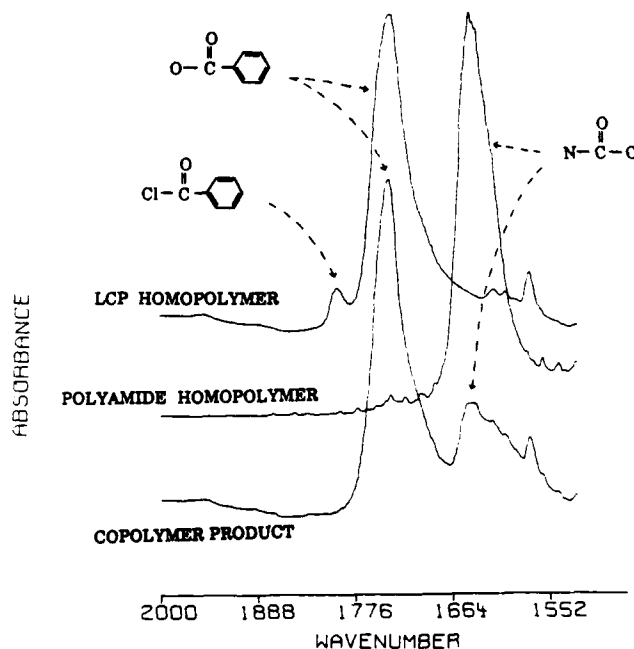
Fig. 1 Carbonyl stretch region of FT-IR spectra
for homopolymers and block copolymer.

In addition to other characteristic absorption bands from each of the homopolymers, the spectrum of the block copolymer shows absorptions due to the carbonyl stretch of both the LC polyester, at 1734 cm^{-1}, and the N-methylated polyamide, at 1643 cm^{-1} (Fig. 1). The absence of the 1793 cm^{-1} absorption due to the acid chloride carbonyl stretch of the LC polyester endgroups indicates that copolymerization of the two oligomers has occurred. In addition, the inability to extract the polyamide from the product clearly demonstrates that it is indeed a copolymer. Because of the extremely high solubility of the polyamide in many common solvents, any oligomer not chemically joined to the LCP block would have been washed away during precipitation of the copolymer product or during Soxhlet extraction of the copolymer product. In fact, Soxhlet extraction in methanol, a very good solvent for the polyamide, resulted in no significant weight loss. These two points combined with the FT-IR spectra provide strong evidence that the two segments were indeed chemically bonded.

Differential scanning calorimetry

Differential scanning calorimetry was performed on a Perkin-Elmer Series 7000 Thermal Analyzer equipped with a DSC cell. The rate at which the experiments were carried out was 20 °C/min. The DSC thermograms of the second heating and cooling for the homopolymers and the block copolymer is shown in Fig 2. The thermograms of the N-methylated polyamide homopolymer showed no first order transitions, indicating that this is an amorphous material with a glass transition temperature of approximately -10 °C. This is expected because of the disruption of hydrogen bonding due to the N-methyl groups.

The DSC thermograms of the LCP homopolymer showed a small glass transition at a temperature of 135 °C. On heating, the thermograms showed an endotherm due to the crystal to nematic transition and an exotherm on cooling corresponding to the reverse nematic to crystal transition. The thermogram of the second heating of the block copolymer indicated a glass transition temperature of 120 °C. At higher temperatures, the thermogram showed only a small, broad crystal to nematic endotherm if any at approximately 300 °C. On cooling, The thermogram of the block copolymer did not show any clear transitions, but the absence of a recrystallization exotherm is noted. At this time it is not fully understood why a recrystallization exotherm is not seen upon cooling.

Optical microscopy

Dark field microscopy was performed on a Nikon optical microscope equipped with cross polars, a hot stage and a Lintam TH600 temperature controller. As in the DSC experiments, the samples were heated and cooled at a rate of 20 °C/min. The microscopy of the liquid crystalline polyester homopolymer showed a birefringent material that remained solid to a temperature of about 330 °C at which point it started to melt. The molten liquid remained highly birefringent with a texture similar to nematic liquid crystalline polymers. Furthermore, this birefringence can be enhanced upon shearing the LCP between two glass coverslides.

The microscopy of the block copolymer was much more complex than the LCP homopolymer. At approximately 270 °C there existed an isotropic liquid phase surrounding a solid anisotropic phase. When the temperature

reached 330 °C, the anisotropic phase began to fragment and disperse into the isotropic phase. As the temperature was held isothermally at 340 °C, the LCP phase slowly dissolved into the isotropic phase to create a one phase, slightly birefringent system. Shearing the block copolymer at this temperature did not enhance the birefringence. Upon cooling, however, the birefringence of the LCP was able to be shear induced starting at about 300 °C. In the absence of shear, small highly birefringent specks of the LCP phase began to precipitate out of the one phase 'solution' at approximately 285 °C.
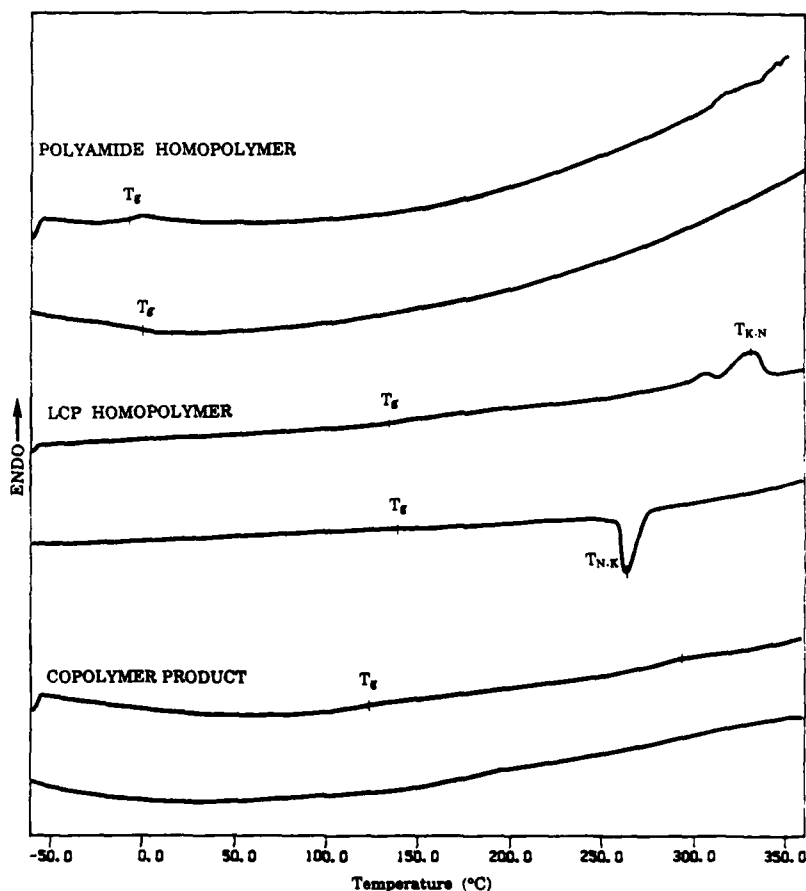
Fig. 2 DSC thermograms of 2nd heat and cool
for homopolymers and block copolymer.

Elemental analysis

The elemental analysis results of the LCP homopolymer showed that it contained the following percentages of each element: 72.47 % carbon; 3.66 % hydrogen; 19.54 % oxygen and 4.25 % chlorine. These percentages correspond most closely with the number of repeat units being five or n = 5. This indicates that the LCP homopolymer has an M_n of approximately 1780 g/mol. The percentages of the elements contained in the N-methylated polyamide homopolymer were found to be as follows: 50.67 % carbon, 10.00 % hydrogen, 18.20 % oxygen and 10.69 % nitrogen. Because this polymer does not contain unique endgroup elements, the results for this segment are not conclusive. However, these percentages best correspond to an N-methylated polyamide with ten repeat units or m = 10, which corresponds to an M_n of about 2630 g/mol.

CONCLUSION

It has been demonstrated that a solution polycondensation reaction between sebacoyl chloride and ten percent excess of N,N'-dimethylethylene diamine has been employed to prepare a low molecular weight, telechelic poly(N,N'-dimethylethylene sebacamide) with reactive amine endgroups. In a similar reaction, a low molecular weight, telechelic liquid crystalline polyester with reactive acid chloride ends was prepared from phenylhydroquinone and terephthaloyl chloride. Due to a stoichiometric imbalance in the copolymerization reaction, an ABA type block copolymer composed of flexible polyamide blocks (B) and rigid LCP blocks (A) has successfully been prepared through a solution polycondensation reaction between the reactive endgroups of the telechelic homopolymers. The existence of the block copolymer was verified by a combination of infrared spectroscopy, differential scanning calorimetry, optical microscopy, elemental analysis and solvent extraction. In each of these techniques, the results of the block copolymer were quite different from those of a physical blend of the two homopolymers.

REFERENCES

1. B. C. Auman and V. Percec, Polymer, **29**, 938 (1988).
2. M. Takayanagi, Pure Appl. Chem., **55**(5), 819 (1983).
3. W-F. Hwang, D. R. Wiff, C. Verschoore, G. E. Price, T. E. Helminiak and W. W. Adams, Polym. Eng. Sci., 23(14), 784 (1983).
4. M. Takayanagi, T. Ogata, M. Morikawa and T. Kai, J. Macromol. Sci.-Phys., B17(4), 591 (1980).

305

AGGREGATION STRUCTURE AND ELECTRO-OPTICAL PROPERTIES OF
(LIQUID CRYSTALLINE POLYMER)/(LOW MOLECULAR WEIGHT
LIQUID CRYSTAL) COMPOSITE SYSTEM

TISATO KAJIYAMA, HIROTSUGU KIKUCHI, AKIRA MIYAMOTO, SATORU MORITOMI AND
JENN-CHIU HWANG
Department of Applied Chemistry, Faculty of Engineering, Kyushu University,
Hakozaki, Higashi-ku, Fukuoka 812, Japan

ABSTRACT

A series of thin films composed of liquid crystalline polymer (LCP)
and low molecular weight liquid crystal (LMWLC) was prepared by a solvent-
casting method or by a bar-coating method. LCPs were of mesogenic side
chain type with strong or weak polar terminal groups in the side chain
portion. A mixture of smectic LCP (LCP with side chain of strong polar
end) and nematic LMWLC formed a smectic phase in a LCP weight fraction
range above 50 %. Also, a mixture of nematic LCP (LCP with side chain of
weak polar end) and nematic LMWLC with strong polar group induced a new
smectic phase in a LCP molar fraction range of 20~80 %. Reversible and
bistable electro-optical effects based on light scattering were recognized
for a smectic phase of a binary composite composed of LCP and LMWLC. A
light scattering state caused by many fragmented smectic lamellae appeared
in the case of application of an a.c. electric field below a threshold
frequency ($\sim$1 Hz). Furthermore, application of a 100 V_{p-p} a.c. field of
1 kHz made the transmission light intensity increased to 94 % within a few
seconds. The optical heterogeneity in a smectic layer composed of the side
chain group of LCP was caused by the difference of two forces based on both
dielectric anisotropy of the side chain and electrohydrodynamic motion of
the main chain. Since application of a low frequency electric field causes
an ionic current throughout the mixture film, it is reasonable to consider
that an induced turbulent flow of main chains by an ionic current collapsed
a fairly well organized large smectic layer into many small fragments,
resulting in an increase in light scattering. The response speed of LCP
upon application of an electric field increased remarkably by mixing LMWLC.
In the case of a smectic mesophase, turbid and transparent states remained
unchanged as it was, even though after removing an electric field.
Such a bistable and reversible light switching driven by two different
frequencies of electric field could be newly realized by both
characteristics of turbulent effect of a well organized large smectic layer
of LCP and rapid response of LMWLC. We believe that the LCP/LMWLC mixture
system is promising as a novel type of "light valve" exhibiting memory
effect (bistable light switching).

Key Words: polymer/(liquid crystal) composite, self-supported liquid
            crystalline film, light-intensity control, bistable light
            switching, memory light valve, large area display

INTRODUCTION

Recently, functional characteristics of low molecular weight liquid
crystals (LMWLCs) have been studied in many fields because of their unique
orientation behavior and hydrodynamic properties. Orientation of nematic
LMWLCs is easily controlled by applying electric or magnetic fields. The

molecular axes of LMWLCs with positive dielectric anisotropy orient along the direction of an applied electric field.

The authors have reported on preparation methods of polymer/LMWLC composite films as novel permselective membranes [1-7]. Polymer/LMWLC composite films, in which LMWLC is embedded in a three dimensional network of polymer matrix, exhibit a distinct jump in permeability since an abrupt change in thermal molecular motion occurs at the crystal-liquid crystal phase transition temperature, T_{KN}. The characteristic orientation and the hydrodynamic properties of nematic LMWLC materials can be applied for the control of permeation of molecules or ions[8-15]. The authors have also demonstrated that K^+ permeation through a crown-ether-containing composite film is largely governed by the dispersion state (homogeneous or phase-separated) of the immobilized crown ether[16-18].

Thermotropic liquid crystalline polymers with mesogenic side chain groups have both characteristics of polymer and liquid crystal. Recently, electro-optical properties of thermotropic LCP have been studied extensively. Since LCP in a mesomorphic state are more viscous than LMWLC, the magnitude of response time of LCP to an external stimulation such as electric or magnetic fields is much greater than that of LMWLC. Reversible and bistable electro-optical effect based on light scattering was recognized for a smectic phase of a binary composite composed of LCP and LMWLC[19-21]. Also, various types of polymer/LMWLC composite system have been reported as large-area and flexible light-intensity controllable films (light valve)[22-27].

In this study, large-area and flexible self-supported LC films in a smectic liquid crystalline state were prepared from a mixture of side chain type LCP and LMWLC. Aggregation state, phase transition behaviors and reversible and bistable electro-optical effect of the mixture system have been investigated.

EXPERIMENTAL

The chemical structures of the side chain type LCP and LMWLC are given in Figure 1. LCP with side chain of strong polar end was PCPHS of which the main chain of poly(methylsiloxane) and the side chain of mesogenic group were linked by a flexible aliphatic spacer (m=6). PCPHS was used in a smectic liquid crystalline state. Also, LCP with side chain of weak polar end was PMPPS of which liquid crystalline state was nematic. LMWLCs used were CPHOB and 50CB. CPHOB have a chemical structure similar to that of the side mesogenic group of PCPHS.

The phase transition behaviors and the aggregation state of the LCP/LMWLC composites were investigated on the basis of differential scanning calorimetry (DSC), polarizing optical microscopy (POM) and X-ray diffraction study.

In order to investigate electro-optical effect, the LCP/LMWLC composites were sandwiched between the two ITO-coated glass plates which were transparent electrodes. The distance between the two electrodes were maintained by the PET spacer of 4 μm thick with a hole of about 0.16 cm^2. Under an a.c. electric field, a change of the transmission light intensity through the cell was detected by means of a photodiode and was recorded with digital storage oscilloscope. The incident light source was He-Ne laser.

1. liquid crystalline polymer

(a) m=3 poly(4-cyanophenyl 4'-propyloxy
benzoate methyl siloxane) (PCPPS)

S-361-I (Tg=293K)

m=6 poly(4-cyanophenyl 4'-hexyloxy
benzoate methyl siloxane) (PCPHS)

K-297-S-421-I (Tg=260K)

$$\left(\begin{array}{c} CH_3 \\ | \\ -Si-O \\ | \\ (CH_2)_{\overline{m}}O-\bigcirc-\underset{\underset{O}{\|}}{C}-O-\bigcirc-CN \end{array}\right)_n$$
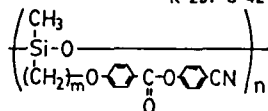
(b) poly(4-methoxyphenyl 4'-propyloxy
benzoate methyl siloxane) (PMPPS)

N-334-I (Tg=288K)

$$\left(\begin{array}{c} CH_3 \\ | \\ -Si-O \\ | \\ (CH_2)_3-O-\bigcirc-\underset{\underset{O}{\|}}{C}-O-\bigcirc-OCH_3 \end{array}\right)_n$$
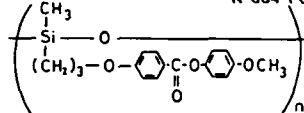
Figure 1 Chemical structures
of liquid crystalline polymers
and low molecular weight
liquid crystals.

2. liquid crystal

(a) 4-cyanophenyl 4'-hexyloxy benzoate
(CPHOB)

$$CH_3(CH_2)_{\overline{5}}O-\bigcirc-\underset{\underset{O}{\|}}{C}-O-\bigcirc-CN$$ K-339-N-354-I

(b) 4-cyano 4'-pentyloxy biphenyl (5OCB)

$$C_5H_{11}-O-\bigcirc-\bigcirc-CN$$ K-321-N-341-I

RESULTS AND DISCUSSION

1. The composite system composed of PCPHS/CPHOB

Figure 2 shows the phase diagram of the PCPHS/CPHOB composite which
was obtained on the basis of DSC, POM and X-ray studies. The glass
transition temperature, Tg of PCPHS decreased with an increase of CPHOB
ratio. This decrease in Tg might be caused by plasticizing effect of
CPHOB. Endothermic peaks attributed to both the crystal-mesophase
transition, T_{KM} of the side chain of PCPHS and that of CPHOB were observed
in temperature ranges of around 295-305 K and 315-335 K, respectively.
This result suggests that the composite forms the phase-separated structure
below T_{KM} of CPHOB, $T_{KM}(M)$, that is, the PCPHS and the CPHOB rich phases.
Since only one endothermic peak attributed to the mesophase-isotropic
transition, T_{MI} was observed, the composite forms homogeneously mixed
mesomorphic phase (molecular dispersion state) above $T_{KM}(M)$. Therefore,
CPHOB is miscible over a whole concentration range of PCPHS in both
isotropic and mesomorphic states. These conclusions were also confirmed by
POM observation. In order to investigate the aggregation state of the
PCPHS/CPHOB composite, the X-ray diffraction studies were carried out at a
temperature range above $T_{KM}(M)$ and below T_{MI} (denoted by "(B) Mesophase" in
Figure 2). The sharp low angle X-ray diffraction with a d-spacing of about
3.06 nm corresponding to a smectic layer spacing, was observed in a weight
fraction range of CPHOB below 40 wt%. In the case above 60 wt% of CPHOB,
this sharp X-ray diffraction disappeared and the diffuse diffraction was
observed because the mesomorphic state of the composite was nematic. In the
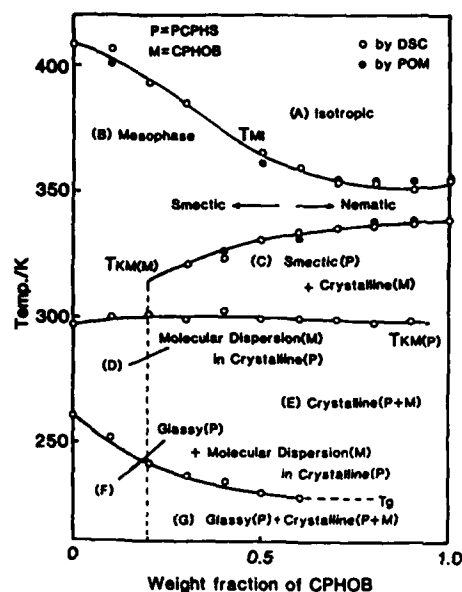
Figure 2 The phase diagram of the PCPHS/CPHOB composite system.
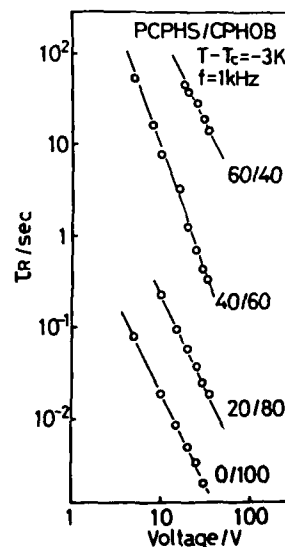
Figure 3 applied voltage dependence of τ_R for the PCPHS/CPHOB composites Tc is the pahse transition temperature between mesomorphic and istropic states.

cases of PCPHS and the PCPHS/CPHOB=(80/20) composite, the weak second order diffraction corresponding to a smectic layer was also observed. The second order diffraction intensity of the (80/20) composite became stronger than that of PCPHS. These results indicate that mixing CPHOB of about 20 wt% to PCPHS makes the regularity of smectic layer increased. Then, a smectic phase certainly existed in a mesophase region below the CPHOB fraction of 40 wt% and in the case above the CPHOB fraction of 60 wt%, the mesophase of the composite was nematic.

We investigated an electro-optical effect of the PCPHS/CPHOB mixture system based on birefringence. The composite film was sandwiched between the two ITO-coated glass plates of which the surfaces had been rubbed in one direction to obtain a homogeneous alignment of the mesogenic group. An application of a.c. electric field of 1 kHz to the mixture film resulted in a decrease of transmission light intensity under the crossed polarizers due to reorientation of the mesogenic group from a homogeneous alignment to a homeotropic one. The response time, τ_R, was defined as the time period for which transmission light intensity dropped to 50 % after applying an electric field. Figure 3 shows $\log \tau_R$-$\log V$ plots for various PCPHS/CPHOB mixture systems with different mixing ratios. τ_R increased remarkably by mixing CPHOB. The response time was inversely proportional to the 2nd power of the magnitude of electric field. This response characteristic indicates that driving force for reorientation of the mesogenic group of crystalline

PCPHS/CPHOB Mixture Systems

(1) 80/20 (Smectic)   Memory Effect

$$64\% \underset{\underset{7.5min}{\xleftarrow{200V\ 1kHz}}}{\overset{\overset{200V\ 0.1Hz}{\xrightarrow{10sec}}}{}} 6\%$$

(2) 60/40 (Smectic)   Memory Effect

$$94\% \underset{\underset{3sec}{\xleftarrow{100V\ 1kHz}}}{\overset{\overset{100V\ 1Hz}{\xrightarrow{1sec}}}{}} 5\%$$

(3) 50/50   No Memory Effect

$$94\% \underset{\xrightarrow{1kHz}}{\overset{D.C.}{\xrightarrow{\hspace{1cm}}}} 43\%$$

Off   Off

30V 1kHz   30V D.C.
600ms   87%   700ms
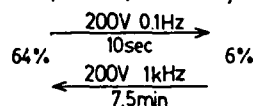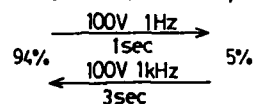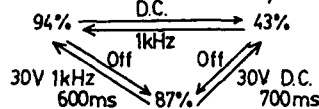
(4) 40/60 (Nematic)   No Memory Effect

$$95\% \underset{\xrightarrow{1kHz}}{\overset{D.C.}{\xrightarrow{\hspace{1cm}}}} 40\%$$

Off   Off

30V 1kHz   30V D.C.
100ms   84%   50ms
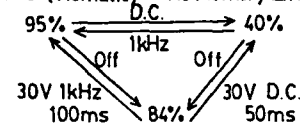
Figure 4 Change of turbid-transparent states and rise-response times for the smectic and nematic PCPHS/CPHOB composites under various conditions of an a.c. and d.c. electric fields.

molecules is attributable to the dielectric anisotropy of a LC molecule.

The electro-optical effect based on light scattering was also studied under various conditions of an a.c. electric field. The samples were sandwiched between the two non-treated ITO-coated glass plates. Transmission light intensity of He-Ne laser through the mixture film of PCPHS/CPHOB without any optical polarizers was measured by photodiode. The distance between the mixture film and the photodiode was 305 mm. In this measurement, the rise-response time was conventionally defined as the time period being necessary for a change from 10 % to 90 % of transmission light intensity. The as-cast PCPHS/CPHOB (60/40) mixture system of 4 μm thick in a smectic state transmitted 86 % of an incident light of He-Ne laser. As shown in Figure 4, the transmittance of incident light strikingly decreased to 5 % after applying an a.c. 100 V of 1 Hz due to a remarkable increase of light scattering. Furthermore, application of an a.c. 100 V of 1 kHz made the transmittance increased to 94 % within a few seconds. The degree of light intensity difference (contrast) between light scattering (turbid) and non-scattering (transparent) states could be changed reversibly by imposing an electric field with different frequencies. Even if an electric field was removed, each turbid and transparent state remained unchanged as it was, indicating bistable light switching. In the case of the PCPHS/CPHOB (40/60) mixture film in a nematic state, the response speed became much faster than that for the PCPHS/CPHOB (60/40) mixture film in a smectic state. However, both the transparent and turbid states could not be maintained without continuous application of an electric field. That is, there was no memory effect in the case of the PCPHS/CPHOB mixture film in a nematic state. The proposed molecular aggregation states are schematically illustrated in Figure 5 for the turbid and transparent cases. Since an application of a low frequency electric field induces an

310

Reversible & Bistable Light Switching
by (Liq. Cryst. Polym.)/(Low Mol. Wt. Liq. Cryst.) Comp. Systems

As-cast ⟶ Low Freq. ⟷ High Freq.
(ionic current) (no ionic current)

(1) Random (2) Turbulent Flow (3) Homeotropic
T= 86 ‰ 5 ‰ 94 ‰
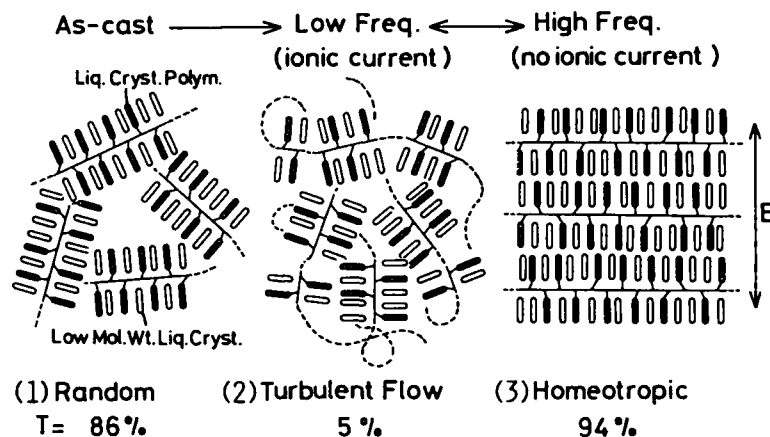
Figure 5 Schematic illustration of turbid and transparent
states for the PCPHS/CPHOB composite system under different
frequencies of an a.c. electric field.

ionic current throughout the mixture film, it is reasonable to consider
that an induced turbulent flow by an ionic current collapsed a fairly well
organized large smectic layer into many small fragments. This induces an
increase in light scattering and also, a decrease of transmittance up to 5
% (from (1) to (2) in Figure 5). Since a high frequency electric field
does not induce an ionic current, a large scale homeotropic alignment of
smectic layer is easily formed by dielectric characteristics of the
mesogenic group of the composite, increasing the transmittance up to 94 %
owing to a remarkable reduction of spatial distortion of smectic directors
and/or optical boundaries (mismatch of refractive indices) (from (2) to
(3)). Such a bistable and reversible light switching driven by two
different frequencies could be newly realized by both characteristics of
turbulent effect of LCP main chain and rapid response of LMWLC. We believe
that the LCP/LMWLC mixture system is useful as a novel type of "light
valve" exhibiting memory effect (bistable light switching).

2. The composite system of PMPPS/50CB
    PMPPS is nematic liquid crystalline polymer with side chain of weak
polar end. It has been reported that a binary mixture of nematic LMWLCs
with both strong and weak polar ends gives an induced smectic phase. In
this study, it has been investigated that this rule can be applicable to a
binary mixture of side chain type liquid crystalline polymer (LCP) with
side chain of weak polar end and LMWLC with strong polar group, which
individually exhibit a nematic phase. LCP was polysiloxane which attached
a terminal weak polar mesogenic unit of side chain (PMPPS) and LMWLC was
50CB. The chemical structures of PMPPS and 50CB are shown in Figure 1.
The characteristic X-ray diffraction patterns of nematic PMPPS and 50CB
were broad and obscure as shown in Figure 6. The PMPPS/50CB (50/50 in

311
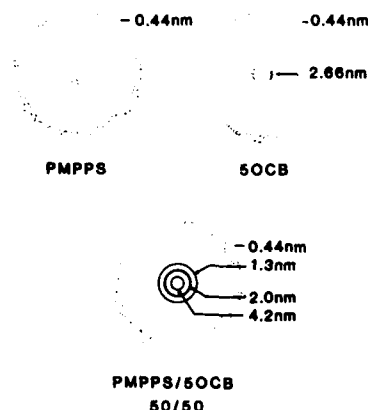
Figure 6 Schematic representation
of x-ray diffraction patterns of
PMPPS (nematic), 5OCB (nematic)
and the PMPPS/5OCB (50/50 mol %)
(induced smectic) composite.
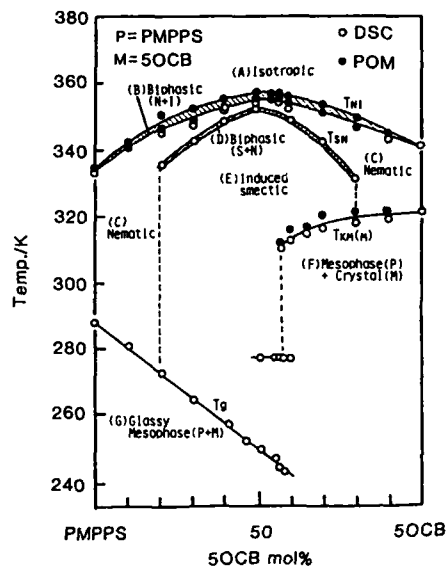
Figure 7 The phase diagram of the
PMPPS/5OCB composite.

mol%) composite exhibits sharp Debye rings which indicate an induced
smectic phase. A d-spacing of 4.2 nm may correspond to a repeating
distance of a mesogenic side group composed of PMPPS and 5OCB. The sharp
X-ray diffraction rings resulting from a smectic layer were observed for
the PMPPS/5OCB composite systems of which the fraction ranges 80/20~20/80
(mol%). Therefore, PMPPS is fairly miscible with 5OCB and the binary
mixture exhibits an induced smectic phase over a wide range of component
fraction.

The phase diagram of PMPPS/5OCB of Figure 7 was obtained on the basis
of DSC and POM studies. Tg of LCP decreased from 288 K to 244 K by
addition of 5OCB. A decrease of Tg may be caused by a plasticizing effect
of 5OCB. The narrow biphasic nematic-isotropic region of about 3 K wide,
where the nematic and isotropic phases coexist, could be recognized by POM
observation. An induced smectic phase appears in a range of 80/20-20/80 of
PMPPS/5OCB.

The electro-optical effect of the PMPPS/5OCB mixture based on light
scattering was also investigated under various conditions of an a.c.
electric field. Figure 8 shows the electro-optical effects of PMPPS, 5OCB
and the PMPPS/5OCB (50/50) composite. In the cases of electro-optical
measurements of PMPPS and 5OCB, there have been observed no distinguishable
optical change and a little change of transmittance of about 8 % upon on-
and off- electric fields, respectively. On the other hand, the PMPPS/5OCB

312
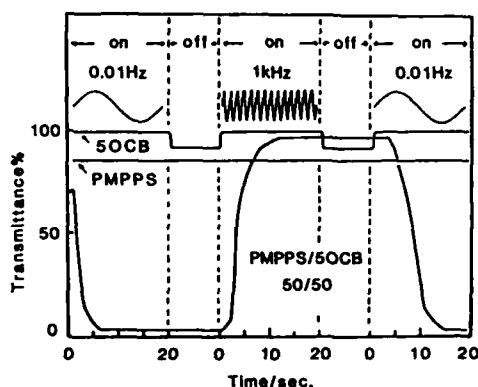
Figure 8 Electro-optical effect of PMPPS, 5OCB and the PMPPS/5OCB (50/50) composite under low and high frequencies of an a.c. electric field. The applied voltage was 200 V_{p-p} and the cell thickness was 16 μm.

(50/50) composite exhibited a bistable and reversible light switching driven by two different frequencies of an a.c. electric field in a similar fashion to the PCPHS/CPHOB composite system. In a low frequency range of about 0.01 Hz, an application of an electric field above the threshold voltage induced strong *light scattering state due to a remarkable* increase of optical heterogeneity being attributable to many collapsed fragments of smectic layer. This might be caused by a strong turbulent flow of main chain by ionic materials. Also, in a high frequency range above 10 Hz, the transmittance increased up to 98 % since a well organized homeotropic alignment was formed by dielectric characteristics of the composite. The reversible turbid- transparent change upon an application of electric field of low and high frequencies, respectively, can be explained schematically by Figure 5. Both transparent and turbid (light scattering) states could be stored stably, eventhough an electric field was turned off. Both rise and decay response times were in a range of several seconds.

The above results indicate that the rule of an induced smectic phase to a binary LMWLC mixture is also maintained to the PMPPS/5OCB mixture system and an induced smectic phase of the PMPPS/LMWLC composite system makes us expect that its electro-optical effect is promissing as a novel type of memory display (bistable light switching).

REFERENCES

1 T. Kajiyama, Y. Nagata, E. Maemura and M. Takayanagi, Chem. Lett., 1979, 679(1979).
2 T. Kajiyama, Y. Nagata, S. Washizu and M. Takayanagi, J. Membrane Sci., 11, 39(1982).
3 S. Washizu, T. Kajiyama and M. Takayanagi, J. Chem. Soc. Jpn., Chem. Ind. Chem., 1983, 838(1983).
4 S. Washizu, I. Terada, T. Kajiyama and M. Takayanagi, Polym. J. 16, 307(1984).
5 T. Kajiyama, S. Washizu and M. Takayanagi, J. Appl. Polym. Sci., 29, 3955(1984).

6 T. Kajiyama, S. Washizu, A. Kumano, I. Terada, M. Takayanagi and
   S. Shinkai, J. Appl. Polym. Sci., Appl. Polym. Symp., 41, 327(1985).
7 H. Kikuchi, A. Kumano, T. Kajiyama, M. Takayanagi and S. Shinkai, J.
   Chem. Soc. Jpn., Chem. Ind. Chem., 1987, 423(1987).
8 Y. Ohmori and T. Kajiyama, J. Chem. Soc. Jpn., Chem. Ind. Chem., 1985,
   1897(1985).
9 T. Kajiyama, S. Washizu and Y. Ohmori, J. Membrane Sci., 24, 73(1985).
10 A. Kumano, O. Niwa, T. Kajiyama, M. Takayanagi, K. Kono and S. Shinkai,
   Chem. Lett., 1983, 1327(1983).
11 H. Kikuchi, M. Katayose, A. Takahara, S. Shinkai and T. Kajiyama,
   Kobunshi Ronbunshu, 43, 669(1986).
12 T. Kajiyama, H. Kikuchi and S. Shinkai, J. Membrane, Sci., 36,
   243(1988).
13 T. Kajiyama, H. Kikuchi, M. Katayose and S. Shinkai., New Polym. Mater.,
   1, 99(1988).
14 T. Kajiyama, J. Macromol. Sci.-Chem., A25. 583(1988).
15 H. Kikuchi, J. Hattori, Y. Mori and T. Kajiyama, Kagaku Kogaku
   Ronbunshu, 15, 617(1989).
16 S. Shinkai, K. Torigoe, O. Manabe and T. Kajiyama, J. Chem. Soc., Chem.
   Commun., 1986, 933(1986).
17 S. Shinkai, S. Nakamura, K. Ohara, S. Tachiki, O. Manabe and
   T. Kajiyama, Macromolecules, 20, 21(1987).
18 S. Shinkai, K. Torigoe, O. Manabe and T. Kajiyama, J. Am. Chem. Soc.,
   109, 4458(1987).
19 S. Moritomi, A. Miyamoto, H. Kikuchi and T. Kajiyama, ..ept. Progr.
   Polym. Phys. Jpn., 31, 191(1988).
20 T. Kajiyama, H. Kikuchi, A. Miyamoto and Y. Morimura, "Frontiers of
   Macromolecular Science", IUPAC 505(1989).
21 T. Kajiyama, H. Kikuchi, A. Miyamoto, S. Moritomi and J.C. Hwang, Chem.
   Lett., 1989, 817(1989).
22 H.G. Craighead, J. Cheng and S. Hackwood, Appl. Phys. Lett., 40,
   22(1982).
23 J.L. Fergason, SID Int. Symp. Dig. Tech., 16, 68(1985).
24 P.S. Drazic, J. Appl. Phys., 60, 2142(1986).
25 J.W. Doane, N.A. Vaz, B.-G. Wu and S. Zumer, Appl. Phys. Lett., 48,
   27(1986).
26 H. Kikuchi, A. Miyamoto, A. Takahara, T. Furukawa and T. Kajiyama,
   Prepr. 2nd SPSJ Int. Polym. Conf. 33(1986).
27 T. Kajiyama, A. Miyamoto, H. Kikuchi and Y. Morimura, Chem. Lett., 1989,
   813(1989).

Interfaces/Mechanical Properties

DIBLOCK COPOLYMERS AT SURFACES*

Peter F. Green

Thomas M. Christensen#

Sanda National Laboratories

Albuquerque N.M. 87185-5800

Thomas P. Russell

Spiros H. Anastasiadis

IBM Research Division

Almaden Research Center

650 Harry Road

San Jose, California 95120-6099

Abstract

The surface properties of symmetric microphase separated diblock copolymers of polystyrene (PS) and polymethylmethacrylate (PMMA) were investigated using X-ray photoelectron spectroscopy (XPS), the specular reflectivity of neutrons and se·ondary ion mass spectrometry (SIMS). PS, the lower surface energy component, exhibited a preferential affinity for the free surface. For copolymers that are far from the bulk microphase separation transition (MST), the surface consists of a layer of pure PS. When the system is close to the MST the surface is a mixture of PS and PMMA. The PS surface excess can be described by a $N^{-1/2}$ dependence, where N is the number of segments that comprise the copolymer chain. It is shown that the surface undergoes an ordering transition at a temperature T_s that is above that of the bulk MST. The ordering of the bulk lamellar morphology is induced by an ordering at the surface. This is analogous to the ferromagnetic order observed in systems such as Gd at temperatures above the bulk Curie temperature. The results here are discussed in light of previous work on copolymer surfaces and in light of mean field theory.

Current Address: Dept. of Physics, Univ. of Colorado, Colorado Springs, Colorado 80933

Introduction

Diblock copolymers are technologically an important class of materials. They behave like surfactants, analogous to the way in which soap molecules behave at oil water interfaces. Because of this they are used to promote adhesion between the phases of immiscible polymers and, hence to improve the mechanical properties of these systems. Due to their unique surface properties block copolymers are used in a variety of biomedical and microelectronic applications.

The inherent incompatibility between the components of a block copolymer chain necessarily induces microphase separation at temperatures below the bulk microphase separation transition (MST). Unlike A-B polymer-polymer mixtures the phases are unable to grow very large because of the connectivity of the components. The resulting spatially periodic phases that form exhibit varying symmetries (cubic, cylindrical, double diamond and lamellar) that lower the free energy of the system [1-3]. The symmetry of a given copolymer system is dictated by the relative length of each constituent.The total number of segments, N, that comprise each chain, determine the size of the phases. The bulk properties of diblock copolymers are well understood. However, the surface properties of these materials are less well understood.

It is well documented in multicomponent systems that the lowest surface energy component preferentially segregates to a free surface in order to minimize the total free energy of the system [4]. Block copolymers are no exception. Indeed, the surface segregation of polymeric molecules is expected to be more severe than that which occurs in small molecule systems since the combinatorial entropy of mixing in these systems is very small (~1/N).

Much of the early work on copolymer surfaces was performed using contact angle [5] and surface tension measurements [6]. The data obtained using these techniques, though useful, provided limited information. For example, information concerning concentration profiles in the near surface region of the copolymers could not be obtained. More recent techniques include X-ray photoelectron spectroscopy (XPS) [7-11], ion scattering spectroscopy (ISS), transmission electron microscopy (TEM) [12,13], neutron reflectivity [14,15] and secondary ion mass spectrometry (SIMS) [16]. These techniques provide an additional means by which polymer surfaces may be better understood.

The experiments on copolymer systems, using TEM, XPS, contact angle and surface tension measurements, showed that the lower surface energy component of the copolymer chain exhibits a preferential affinity for the free surface. In some systems, such as the polystyrene/polydimethyl siloxane (PS/PDMS) [10] system, XPS studies showed that the lower surface energy component, PDMS in this case, completely covered the surface. In other systems, such as the PS/polyethylene oxide (PEO) [8] system, both phases were observed to coexist at the surface. The extent of the segregation in these and all other systems studied previously can not be correlated with the surface energy differences between the components as one might anticipate. There have been a number of reasons presented to explain this behavior.The morphology of the system could play a crucial role. In the case of the PS/PEO system, PEO crystallizes upon evaporation of the solvent used to cast the films and the crystallization kinetics, evidently, affects the mobility of the PS chains thereby prohibiting the PS chains from migrating to the surface. While this may be true of systems where one component crystallizes, there are other cases, such as the bisphenol-A-polycarbonate (BAPC)/PDMS system [7], in which both components are observed at the surface. Gaines [17] suggested that the criterion for liquid spreading should explain the descrepancy of whether the surface is covered by one component or both. We will show later that this criterion is inadequate for a description of copolymer surfaces.

Here the general question of what controls the surface composition of diblock copolymers is addressed. Why in some cases do both components appear at the surface while in others only one component is observed? It is also shown that in this diblock system the interactions between the molecules in the near surface region are modified such that they are weaker than in the bulk. The near surface region is shown to order at a temperature above the bulk MST. This phenomenon has been observed in rare earth metals that exhibit ferromagnetic order [18,19].

Experimental

A series of symmetric diblock copolymers of PS and polymethylmethacrylate (PMMA), each comprised of N segments, where N ranged from 275 to 5600, were studied. Further details about the polymers may be found elsewhere [21]. These copolymers were chosen since they all exhibit a lamellar morphology below the bulk MST and the glass transition temperatures of PS and PMMA are similar. The condition for microphase separation, which varies depending on the bulk morphology, is, for a lamellar phase, $\chi N=10.5$, where χ is the Flory-Huggins interaction parameter [20].

The bulk properties of these systems were well characterized using small angle X-ray scattering (SAXS) [21,22], secondary ion mass spectrometry (SIMS) [16] and neutron reflectivity [14,15]. The surface and near surface properties of these systems were characterized using XPS [23,24] and neutron reflectivity [14,15].

XPS

The XPS measurements have been described in detail elsewhere [23,24], therefore the description will be brief. High resolution XPS spectra were obtained using a Kratos XSAM800 spectrometer (fixed retardation ratio mode) and a hemispherical analyzer with a high resolution band pass energy of 10eV. A non-monochromatized 300 watt MgKα source was used.

Samples were prepared using three different procedures. Films ~5μm thick were prepared using solvent casting techniques. In some cases the mutual solvent , toluene, was allowed to evaporate rapidly in air while in other cases the solvent was allowed to evaporate slowly. Slow evaporation of the solvent was accomplished by placing films in an environment where the vapor pressure of toluene was high. Another series of films were prepared by first allowing the solvent to evaporate and then annealing them at 170^{0}C for many hours so that they reached equilibrium.

Spectra were recorded at normal angles to the sample surface and at 70^0, 45^0 and 20^0 with respect to the surface normal. The spectra of pure PS and of pure PMMA served as a basis for the analysis of the PS-PMMA copolymers. The spectra obtained were in good quantitative agreement with those found in the literature [25].

Following X-ray satellite subtraction and the subtraction of the background, the spectra were fitted using Gaussian line shapes with a FWHM of 1.5eV. Figure 1a shows the O1s doublet peaks of pure PMMA. The solid line drawn through the data is a convolution of two peaks, one at energy 533.8 eV and the other at 535.4 eV, representing the C=O and C-O-C bonding environments, respectively. Figure 1b shows a typical O1s doublet peak of a PS-PMMA copolymer. The relative fractions of both components at the surface were determined using two independent procedures which yielded results that were in excellent agreement. The first procedure was to divide the area of the O1s profile of the copolymer with that of pure PMMA; this yielded the surface fraction of PMMA. The second procedure involved recognizing that the contribution of PS to the C1s profile is twice that of PMMA and that the fraction of PS plus the fraction of PMMA is unity.

Neutron Reflectivity

The technique of neutron reflectivity is briefly described below since its use in the area of polymers is new. A more detailed description may be found in the literature [14, 15, 26, 27]. Consider the diagram shown in Figure 2 where neutrons impinge on a sample surface at glancing angles, θ. Neutrons are reflected at the corresponding angle θ.The neutron momentum normal to the sample surface is

$$k_{0,z} = \frac{2\pi}{\lambda} \sin \theta \qquad (1)$$

where λ is the wavelength of the neutrons. If the neutrons penetrate a medium characterized by
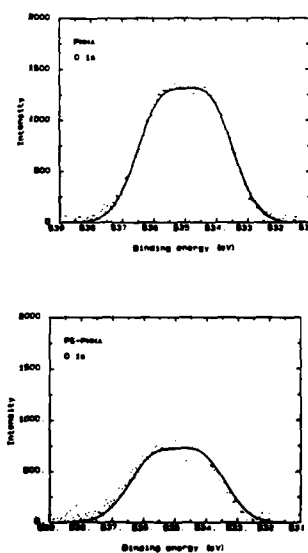
Figure 1: a) Normal angle (90⁰) XPS O1s profile of PMMA. This solid line is a convolution of two symmetric peaks representing the C-O-C and C=O bonding environments.The dots represent the data.
b) Typical normal angle O1s profile of a PS-PMMA copolymer.
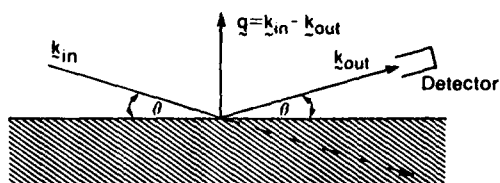
Figure 2: Schematic of the Neutron Reflectivity experiment.

a scattering length density of $(b/V)_j$ then the neutron momentum in the medium is

$$k_{j,z} = \left[k_{0,z}^2 - 4\pi \left(\frac{b}{V} \right)_j \right]^{1/2} \tag{2}$$

We may now consider the case where the scattering length density in the film varies as a function of depth in the film. Here the film is divided into j layers, each of thickness d_j and of scattering length density $(b/V)_j$; the substrate is designated as the $j+1$ th layer. d_j should be sufficiently thin in order to closely approximate the varying scattering length density of the real system. If the reflectance, or, equivalently, the reflection amplitude, from an interface is $r'_{j,j+1}$, where $r'_{j,j+1} = (k_{j,z} - k_{j+1,z})/(k_{j,z} + k_{j+1,z})$, then the reflection coefficient of the j th layer is

$$r_{j-1,j} = \frac{r'_{j-1,j} + r'_{j,j+1} \exp(2 \, i \, d_j \, k_j)}{1 + r'_{j-1,j} \, r'_{j,j+1} \exp(2 \, i \, d_j k_j)} \tag{3}$$

This recursion relation can be used to calculate the reflection coefficient of the $j-1$ th layer by replacing $j-1$ with $j-2$ and j with $j-1$. The recursion is continued until the reflection coefficient, $r_{0,1}$, at the free surface is obtained. The reflectivity is

$$R(k_0) = r_{0,1} \, r_{0,1}^* \tag{4}$$

One obtains from this experiment the reflectivity, R, as a function of the neutron momentum, k_0, which can be compared to the experimentally determined profile.

The reflectivity measurements were performed at the National Institute of Standards and Technology. The neutrons were of wavelength $\lambda=2.35$Å with $\Delta\lambda/\lambda=0.02$. The reflectivity profiles were obtained by varying θ in order to change the neutron momentum. More details of the experiment may be found elsewhere [14,15].

Results and Discussion
Bulk properties of the Copolymers
All the copolymers studied here exhibit a lamellar morphology in the bulk. This has been verified using SAXS [22], SIMS [16] and neutron reflectivity [14,15]. When films of these copolymers are cast from toluene, a mutual solvent, the lamellae are randomly oriented, as shown by ion beam analysis measurements [16,21,22]. The degree of orientation of the lamellae improves if the solvent evaporation rate is very slow. Under equilibrium conditions the lamellae are aligned parallel to the sample/substrate and air(vacuum)/sample interfaces, as shown by SIMS and reflectivity. The kinetics of the alignment process has been studied using SIMS and neutron reflectivity.The alignment process begins at the interfaces and then propagates through the bulk. The kinetics of the alignment process is a strong function of N, the rate decreases as N increases.

It is also clear from these measurements that for a copolymer with an interlamellar spacing of L and volume fractions of PS and PMMA of 0.5, the thickness of the layers adjacent to the interfaces is L/4, see Fig. 3. The width of the interfaces between the phases is E=50Å and is independent of N. Fig. 4 shows a typical reflectivity profile of a microphase separated copolymer. The inset in the figure shows the scattering length density profile used to calculate the reflectivity profile, represented by the line in the figure. The SAXS and reflectivity measurements show that L increases with N^α, as shown in Fig. 5. The solid line drawn through the data has a slope of 2/3 and the broken line 1/2. The value of α, obtained from the slope, should, in principle, indicate the degree of segregation in these systems, $\alpha=1/2$ for a
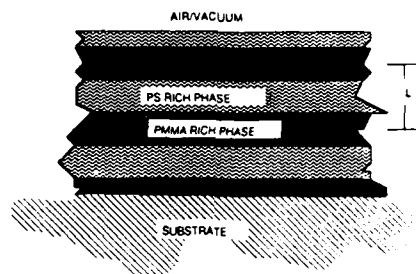
Figure 3:   Schematic of the PS-PMMA copolymer microstructure at equilibrium.
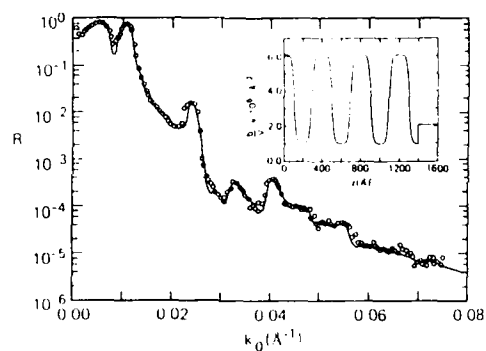
Figure 4:   Typical reflectivity profile of a microphase separated diblock copolymer The inset represents the scattering length density profile used to obtain the solid line drawn through the data.
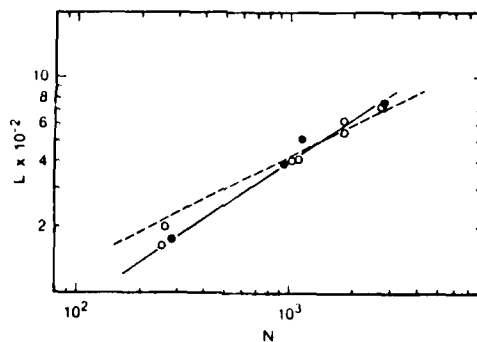
Figure 5:   The interlamellar spacing as a function of N.

weakly segregated system and $\alpha=2/3$ for a highly segregated system. However the limited range of N precludes a precise determination of this exponent.

A very important question, related to the subsequent discussion on surfaces, concerns the proximity to criticality (MST) of some of these systems. An indication of this can be obtained by looking at the ratio 2E/L, the volume fraction of the sample occupied by the interface, as a function of N (Figure 4). For the N=275 chain the ratio is 0.6 and for the longest chain 0.1. Based on measurements of the scattering length densities, the shorter copolymer chain systems were found to be phase mixed. This is strong evidence that these shorter chain systems are weakly segregated, ie. close to the MST. The much longer chains are in the strong segregation limit. In principle one could determine the degree of segregation by an analysis based on the value of α. The analysis of the 2E/L ratio and the fact that the components are phase mixed is a much more accurate indicator of the proximity of the system to the MST than the determination of the exponent α.

Surface Ordering in Diblock Copolymers (Theory)

Recently Fredrickson [27] developed a theory that addresses surface ordering in diblock copolymer systems near the weak segregation limit (2E/L is large). The system is considered to exhibit a lamellar morphology below the bulk below the MST. An expansion of the free energy is made in terms of an order parameter $\psi(r)$, which is the local deviation of the average density of the A component from its bulk value. The perturbing effect of the surface on the bulk is expressed in terms of a "bare" surface energy term, expressed in terms of a surface free energy density

$$f_s(\psi) = [-H\,\psi(r) + a\,\psi^2(r)/2]N^{-1}$$
(5)

H and a are phenomenological parameters that describe the effects of the surface potential on the bulk thermodynamic potential. Both H and a are defined such that they are proportional to N [27]. H is a field that may be related to a chemical potential, or surface energy difference, that favors one component at the surface; it is assumed to be small. In the PS/PMMA system the surface energy difference is less than 1 dyne/cm [29]. The parameter a describes the way in which the surface potential modifies the interactions between the molecules in the near surface region.

It is often justified to neglect the effect of surfaces on the bulk properties of materials since the number of atoms at a surface is considerably lower than that in the bulk. Near critical points, however, where the correlation length, or, equivalently, the concentration fluctuations, become very large, decoupling of the surface and bulk properties may not be justified. An example of this occurs when $a>0$. Here the local interaction parameter, in the vicinity of the surface, $\chi_{local}<\chi_{bulk}$, where χ_{bulk} is the interaction parameter in the bulk. In this case the surface orders at a temperature, T_s, above T_b, that of the bulk ($\chi\sim1/T$). The ordering at the surface can then induce ordering in the bulk. On the other hand the interactions at the surface may be sufficiently enhanced that $a<0$ or $a=0$. For $a<0$, $\chi_{local}>\chi_{bulk}$ ($T_b>T_s$) and the bulk may induce ordering at the surface. For $a=0$, the surface and bulk order spontaneously.

There are analogies between polymer surfaces and Ising ferromagnets [28]. In surface critical behavior of some systems that exhibit magnetic order it is customary to refer to a surface extrapolation length, λ [18]. In the case of polymer surfaces $\lambda=B/a$, where $B^{1/2}\sim N^{1/2}$ is a measure of the range of interactions between the molecules in the system. Physically, λ represents the depth of the region beneath the surface where effects due to the surface potential are important. λ should be on the order of a statistical segment length.

The manner in which the N dependence of the surface excess, ψ_1, of the more surface active species, was calculated from Fredrickson's work was discussed previously [23,24]. It was shown that

$$\psi_1 \approx \Lambda - \beta \, N^{-1/2} \tag{6}$$

The coefficients $\Lambda = H\lambda/B = H/a$ and $\beta = 2.7\Lambda^2\lambda$. It is clear that the slope of a ψ_1 versus $N^{-1/2}$ plot should show how the interactions in the vicinity of the surface are modified.

Surface Composition (Experiment)

The surface composition of the copolymer films was found to be controlled by the rate at which the solvent evaporated during the preparation of the films, as shown in Figure 6.

The triangles represent the PS surface fraction, ϕ_1, of the films produced by the rapid solvent evaporation process and the circles represent that of the samples produced using the slow solvent evaporation process. The average surface fraction of PS obtained for the samples produced using the slow solvent evaporation process is higher than that obtained for the other solvent cast films. As mentioned earlier, the systems produced using a rapid solvent evaporation process are characterized by randomly oriented microdomains [21,22] where some are oriented perpendicular to the free surface. The systems produced by very slow extraction of solvents, or annealed for long periods of time, are characterized by highly oriented lamellar microdomains which are parallel to the free surface where a PS rich layer is preferentially located. This explains why the average surface fraction of PS is higher for the films produced using the slow solvent extraction process. The data in this figure also shows a trend where ϕ_1 increases with N. This is strong evidence that as the degree of incompatibility increases the driving force for surface segregation increases. Evidently the reduction of the surface free energy that results from the surface segregation of the lower surface energy component to the free surface more than offsets the concomitant increase in the bulk free energy (decrease in combinatorial entropy). The total free energy of the system is therefore minimized.

Represented in Figure 7, by the triangles, is the surface excess of PS, ψ_1 ($\psi_1 = \phi_s - \phi_b$, where ϕ_s is the surface composition and ϕ_b is the bulk composition) versus $N^{-1/2}$ plot for the samples produced by the slow solvent evaporation process (near equilibrium structures). The data scales well with a $N^{-1/2}$ dependence. In the theory, this N dependence arises from the fact that $B^{1/2}$, which is a measure of the interactions between the molecules varies as $N^{1/2}$. This dependence applies in the range of N where the theory should not apply which suggests that the $N^{-1/2}$ is not associated with criticality. An estimate of the slope may be obtained if the constant term in equation 6 is set equal to 0.5, a value which the surface excess should approach for very large N. Based on the slope it is clear that λ, or equivalently a, is not only positive but ~ 3. This suggests that the local χ parameter in the vicinity of the surface is lower than that in the bulk ($\chi_{local} < \chi_{bulk}$). Furthermore, the surface potential modifies the interactions between the molecules at a depth of 3 segment lengths beneath the surface which is entirely reasonable.

The circles in Figure 7 represent the ψ_1 versus $N^{-1/2}$ dependence of films annealed at 170^{0}C for long periods of time under high vacuum conditions [31]. At very large N, where the system is in the strong segregation limit, the surface is composed only of PS, the lower surface energy component. For smaller values of N where the systems are weakly segregated the surface is composed of both PS and PMMA [30]. The difference in the relative values of the surface excess for the annealed and solvent cast films could be associated with the way in which the solvent alters the relative thermodynamic interactions between PS and PMMA.

Since $\lambda = 3$, then a>0 which suggests that $T_s > T_b$ ($\chi \sim 1/T$). Neutron reflectivity measurements on the shortest copolymer chain show that at a temperature above the bulk MST the surface begins to order, Figure 8, while the bulk is disordered. The existence of oscillations near the interfaces is evidence of surface ordering. In the bulk the oscillations are absent indicating the absence of order. As the temperature approaches the bulk MST, order begins to
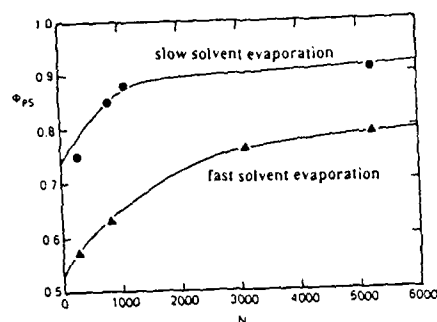
Figure 6: The surface fraction of PS, Φ_{ps}, as a function of N.
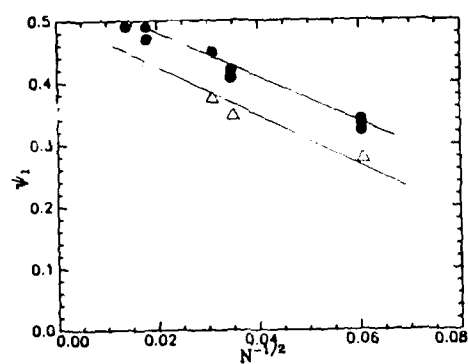
Figure 7: Surface excess of PS, ψ_1, as a function of $N^{-1/2}$. The circles represent data from samples that were annealed until they reached equilibrium and the triangles that of samples that were produced using the slow solvent evaporation process.
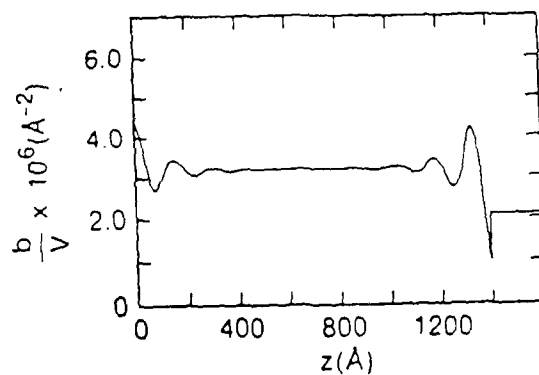
Figure 8: Scattering length density profile of a PS-PMMA copolymer above the bulk MST

propagate through the bulk. This is clear experimental evidence that near a critical point the surface orders and induces ordering in the bulk. This phenomenon has been observed in ferromagnetic systems where the spins in the bulk and in the surface order at different temperatures [19].

The application of the criterion for liquid spreading to the understanding of copolymer surfaces is too simplistic. It suggests that a liquid, A, will not completely wet another liquid, B, if the surface energy difference between them is smaller than the interfacial energy between the liquids. For long chains, certainly in the range of the chain lengths used here, the surface and the interfacial energies are independent of N. This criterion could not be correct since both complete and incomplete coverage is observed in this system. Furthermore, the main condition for applicability of this criterion is that the forces between the A and B components should be primarily van der Walls forces (no chemical bonds). In the case of copolymers, A and B are covalently bonded!

Conclusion

It has been shown that in copolymer systems the lower surface energy component exhibits a preferential affinity for the free surface whether the systems are prepared using mutual solvents or are annealed at sufficiently long times to produce equilibrium structures. In the case of the solvent cast films the surface composition is controlled, in part, by the rate at which the solvent evaporates from the film. The surface excess of PS increases as the degree of incompatibility between the segments of the copolymer increase for both solvent cast and annealed films. For the annealed systems at equilibrium, at very large N (strong segregation limit), the PS component completely covers the surface. At smaller N (weak segregation limit) both PS and PMMA are found at the surface. For the solvent cast films that were near equilibrium complete dominance of PS was not observed and this could be related to the fact that the solvent altered the thermodynamic interaction between the PS and PMMA segments.

It was also demonstrated that the critical points of the surface and the bulk are different. The surface orders at a temperature, T_s, above that of the bulk. As the temperature approaches T_b the correlation length becomes very large, consequently, the bulk microstructure orders.This is analogous to the ferromagnetic order observed in systems such as Gd[19] at temperatures above the bulk Curie temperature.

References

[1] I. Goodman, Ed., Developments in Block copolymers (Applied Science, New York, 1982).

[2] L. Leibler, Macromolecules 13, 1602 (1980).

[3] T. Ohta, K, Kawasaki, Macromolecules 19, 2621 (1986). A.N. Semenov, Sov. Phys. JETP, 61, 733 (1985).

[4] J. M. Blakley, in Chemistry and Physics of Solid Surfaces, Vol 2, edited by R. Vanselow (CRC Press, Boca Raton, FL, 1979).

[5] M.J. Owen and T.C. Kendrick, Macromolecules, 3, 458 (1970).

[6] A.K. Rostogi and L.E. St. Pierre, J. Colloid and Inf. Sce. 31, 168 (1969).

[7] R.L. Schmitt, J.A. Gardella Jr., J.H. Magill, L. Salvati, Jr., and R.L. Chin, Macromolecules 18, 2675 (1985)

[8] H.R. Thomas and J.J. O'Malley, Macromolecules 12, 323 (1979).

[9] N.M. Patel, D.W. Dwight, J.L. Hendrick, D.C. Webster and J.E. McGarth, Macromolecules, 21, 2689 (1988).

[11] J.E. McGarth, D.W. Dwight. J.S. Riffle, T.F. Davidson, D.C. Webber and R. Vishwanathan, Polym. Prepr. Am Chem. Soc. Div. Polym. Chem 20(2), 528 (1979)

[12] C.S. Henkee, E.L. Thomas and L.J. Fetters, J. Materials Sci. 23, 1685 (1988).

[13] H. Hasegawa, T. Hashimoto, Macromolecules 18, 589 (1985).

[14] S.H. Anastasiadis, T.P. Russell, S.K. Satija and C.K. Majkzrak, Physical Review Letters 62, 1852 (1989).

[15] S.H. Anastasiadis, T.P. Russell, S.K. Satija and C.K. Majkzrak, J. Chem. Phys.

(submitted).

[16] G. Coulon, T.P. Russell, V.R. Deline and P.F. Green, Macromolecules, 22, 2581 (1989).

[17] G.L. Gaines, Macromolecules, 14, 208 (1981)

[18] K. Binder, In Phase Transitions and Critical Phenomena, C. Domb, J.L. Lebowitz, Eds.; Academic Press, New York, Vol. 8 (1983).

[19] C. Rau and M. Robert, Physical Review Letters, 58, 2714 (1987).

[20] P.G. deGennes, Scaling Concepts in Polymer Physics (Cornell University Press, Ithaca, New York, 1979).

[21] P.F. Green, T.P. Russell, R. Jerome and M. Granville, Macromolecules, 21, 3266 (1988).

[22] P.F. Green, T.P. Russell, R. Jerome and M. Granville, Macromolecules, 22, 908 (1989).

[23] P.F. Green, T.M. Christensen, T.P. Russell and R. Jerome, Macromolecules, 22, 2189 (1989).

[24] P.F. Green, T.M. Christensen, T.P. Russell and R. Jerome, J. Chem. Phys. (in press).

[25] D.T. Clark, J. Peeling and J.M. O'Malley, J. Polym. Sci., Polym. Chem. Ed. 14, 543 (1976). D.T. Clark and H.R. Thomas, J. Polym. Sce. 16, 791 (1978)

[26] J. Als-Nielson, In Structure and Dynamics of Surfaces II, edited by M. Schommers and P. von Blanckenhagen (springer-Verlag, Berlin, 1987).

[27] G.H. Fredrickson, Macromolecules 20, 2535 (1987).

[28] S. Wu, Polymer Interfaces and Adhesion (Marcel Dekker, New York, New York, 1982) p. 73.

[29] The angle resolved measurements of these samples made by the slow solvent evaporation process showed variations only for the shortest copolymer system, the PMMA fraction varied from 0.25 to 0.18 in going from 90^0 to 20^0.

[30] The angle resolved measurements showed variations only for the shortest copolymer system, the PMMA fraction varied from 0.22 to 0.17 in going from 90^0 to 20^0.

[31] Many of the films, particularly the high N systems, that were not annealed long enough yielded values of ψ_1 that were closer to 0.5. After longer anneals they reached their equilibrium values.As N increased the time required to reach equilibrium increased appreciaby.

ON THE SCALE OF DIFFUSION LENGTHS OBSERVABLE BY NEUTRON REFLECTION: APPLICATION TO POLYMERS.

A. Karim, A. Mansour and G.P. Felcher Argonne National Laboratory, Argonne, IL 60439, T.P. Russell, IBM Research Division, Almaden Research Center, San Jose, CA 95120.

ABSTRACT

A systematic approach has been applied to neutron reflectivity data to study interdiffusion across an interface. It is shown that with this technique it is possible to probe interface broadening from ~10Å to upward of 200 Å, the upper limit being already within the range of observation of other techniques such as Rutherford backscattering spectrometry (RBS), forward recoil spectrometry (FRES) and secondary ions mass spectroscopy (SIMS). As example is analyzed the interdiffusion of a bilayered polymer system: a deuterated polystyrene (d-PS) layer on protonated polystyrene (h-PS).

Introduction

Neutron reflectivity[1] has emerged as a useful technique to probe interface broadening caused by diffusion across an interface on the nanometer scale. The technique relies on the contrast of the neutrons scattering length densities of the layers facing the interface. The quantity obtained in such experiments is the reflectivity (R) of the sample: this is a function of the component of the neutron momentum perpendicular to the surface, k_z. $R(k_z)$ is an optical transform of the scattering length density, as measured as a function of the depth z from the surface. In this paper, we define the range of interface widths measurable by neutron reflectivity, by taking the reflectivity curves at subsequent times of the diffusion process.

Limits of resolution

Consider a homogeneous layer of thickness z_2 on an infinitely thick lower layer; the indices 1, 2 and 3 indicate the vacuum above, homogeneous material and lower layer respectively. Then the reflectivity R is given by [2,3]

$$R = \frac{r_{12}^2 + \rho_{23}^2 + 2r_{12}\rho_{23}\cos 2k_2z_2}{1 + r_{12}^2\rho_{23}^2 + 2r_{12}\rho_{23}\cos 2k_2z_2} \tag{1}$$

The reflectance at the i,i+1 boundary is:

$$r_{i,i+1} = \frac{k_i - k_{i+1}}{k_i + k_{i+1}} \tag{2}$$

where $k_i = [k^2 - (b/v)_i]^{1/2}$ and $(b/v)_i$ = scattering length density of the ith layer, while $k = 2\pi Sin\theta/\lambda$. If symmetric interdiffusion[4,5] occurs between layers 2 and 3,

$$\rho_{23} = r_{23} \exp -2k_2 k_3 \sigma^2 \tag{3}$$

In conventional diffusion, the diffusion coefficient D is a function of the width $\sigma^2(t)$ and of time, namely[6]

$$D = \frac{\sigma^2(t)}{4t} \tag{4}$$

In this paper we would like to examine how to obtain σ^2 systematically from the experimental data in order to obtain the measurable range of diffusion coefficients.

The z_2 averaged expression for the reflectivity [eq(1)], is :

$$<R> = \frac{r_{12}^2 + \rho_{23}^2 - 2r_{12}^2 \rho_{23}^2}{1 - r_{12}^2 \rho_{23}^2} \tag{5}$$

which for large values of k can be approximated by the expression:

$$<R> \sim r_{12}^2 + \rho_{23}^2$$

$$\sim [\pi^2/k_1^4] [(b/v)_2^2 + ((b/v)_3 - (b/v)_2)^2 \exp - 4k_1^2 \sigma^2] \tag{6}$$

Thus Rk^4 vs k tends, for large values of k, to an asymptotic value. This value is different for an infinitely sharp 2,3 interface compared to when some interdiffusion has occurred across such a boundary; the decay to the new asymptote reaches a value $1/e$ for $k_1 = (1/4\sigma^2)^{1/2}$.

It is easy to see that the determination of σ becomes progressively ill defined for large σ. This is because the $1/e$ point occur for smaller values of k_1. Even if the more correct eq. (5) is used. rather than its asymptotic form, the relation between the experimental resolution, Δk, the precision by which σ can be determined:

$$dk/k = - d\sigma/\sigma \tag{7}$$

shows that extremely stringent requirements are progressively important on the angular resolution and the wavelength definition of the incident beam. Practically speaking, this method of analysis is convenient for values of σ less than 150Å. However it is possible to monitor diffusion over significantly longer distances by using derivatives of the reflectivity. In the normalized difference analysis, the infinitesimal changes in R with σ^2 is given by $R^{-1}(dR/d\sigma^2)$. Rather than giving the rather cumbersome - but easily derivable - complete expression, it is worthwhile to point out that the z-averaged expression of $R^{-1}(dR/d\sigma^2)$ is simply zero. On this flat base line, the envelope between the maxima and the minima of the reflectivity becomes:

$$\Delta(\frac{\partial R}{\partial \sigma^2}/R)= 4r_{12}\rho_{23}k_2k_3 [\frac{1}{r_{12}^2-\rho_{23}^2} - \frac{1}{1-r_{12}^2\rho_{23}^2}]$$ (8)

the exponential term which gives the broadening of the interface is now contained in the linear expression of ρ_{23} at the numerator of eq.(8); which means that the range over which σ can be measured is extended by a factor of $1/\sqrt{2}$.

In practical terms the difference between the reflectivities at times t', t" can be taken. It is easy to see that the relation holds:

$$\frac{R(t")-R(t')}{R(t")+R(t')} = 2D (\frac{\partial R}{\partial \sigma^2}/R) (t"- t')$$ (9)

where D is the diffusion coefficient as measured in the t"-t' interval.

Interdiffusion of polymers

We would like to apply directly this method of analysis to the study of the interdiffusion between two polymers. Neutron reflection can readily observe diffusion even over short time, when eq.(9) is not applicable. It is worthwhile then to compare the value of D obtained after relatively long annealing time with neutron reflectivity with that obtained by other techniques which have intrinsically less spatial resolution. Unfortunately, it has not been possible yet to apply directly eq.(9) on two accounts: the instrumental resolution has to be obtained more accurately than hitherto has been done, and the interval of annealing time t"-t' must be shorter than that presently employed. However we would like to compare the normalized difference plot with those calculated on the basis of a model, in which only the interface thickness has been changed.

Specific samples were prepared for the purpose, in the form of polymer bilayers on a flat round of silicon of 2" diameter. The lower layer of h-PS(Mw=233,000; thickness >3000Å) was spin coated on a silicon substrate from its solution in toluene and annealed for 48 hours at 160C. A layer of d-PS (Mw=203,000;thickness~600Å) was then separately spin coated on a glass slide and subsequently floated off on to a pool of water. The floating d-PS film was then picked up from beneath by the silicon substrate with the coated h-PS to form a bilayer. The bilayer was then placed under vacuum for 12 hours at room temperature to remove any water molecules that may have been trapped between the layers.

The neutron reflectivity experiments were perfc. med at the Intense Pulsed Neutron Source at Argonne National Laboratory. The experiment basically consisted of reflecting neutrons pulses between wavelengths 2-16 Å from the sample surface at very small angles of incidence (typically 1 degree) and measuring the number of reflected neutrons as a function of wavelength. The number of reflected neutrons normalized by the incident neutrons gives the reflectivity R, as a function of the neutron momentum k.

In Figure 1, experimental results are presented for the sample "as cast", and then annealed 22 and 53 minutes at 135C. Figure 1 shows also fits for the thickness of the layers d-PS/h-PS on Si, as well as the thickness of the interfaces. The fit to Figure 1(A) indicates a top layer d-PS of thickness 590Å on a "thick" lower layer. The thickness of the lower layer is certainly

Fig.1   R(k)k^4 as a function of k for a bilayered sample
of d-PS Mw=233,000) on top of h-PS
(Mw=203,000) before heating [1(A)] and after
heating for 22 minutes [1(B)] and 53 minutes
[1(C)]. The solid points are the experimental
data whereas the solid lines were calculated
using a bilayered model with a symmetric
interface between the upper and lower layer.
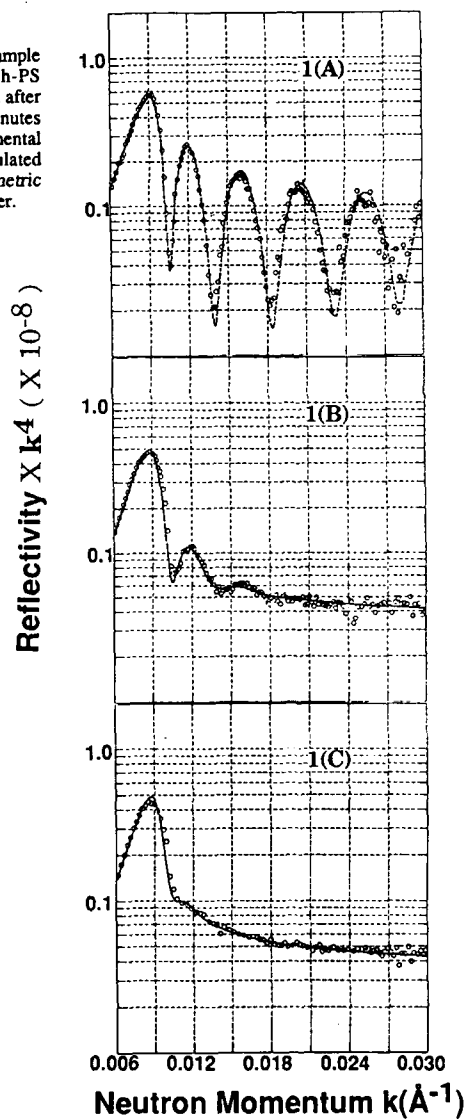
larger than 3000Å, which is the maximum distance which can be resolved for a beam of angular resolution of the order of 0.02°. The interface between the two polystyrene layers has initially a thickness σ= 10Å . The fit 1(B) shows that the interface has broadened to 135Å, as a result of diffusion after the first annealing; after the second annealing the broadening is 200Å. The reflectivity in Figure 1(C) is almost featureless. In order to observe clearly how well the broadening is determined we replot in Figure (2) the experimental and calculated normalized difference of 1(C) with its previous frame 1(B). The hollow circles indicate the experimental difference points whereas the lines are normalized difference curves for three different values of σ (=175, 200 and 250 Å) for fits to 1(C) with χ (= 4.6, 4.4, 5.2) respectively. Of the three σ values, σ=200Å has the minimum χ (the fit using this value of σ is shown in Figure 1(C)). The offset to the normalized difference from zero at large k in Figure2 is caused by a small error in normalization of reflectivity for 1(B). We also see that if the offset is neglected, the integral of the normalized fluctuations is nearly zero, in accordance with equation (8) - that the total area under the normalized difference curve be zero.

From the value of σ=200Å, is obtained a diffusion coefficient (cfr eq.(4)) D=3.43 x 10^{-16} cm^2/s at T=135°C. This value is already in reasonable agreement with that obtained for the same molecular weight at the same temperature from FRES measurements[7]: D=4.35x10^{-16}
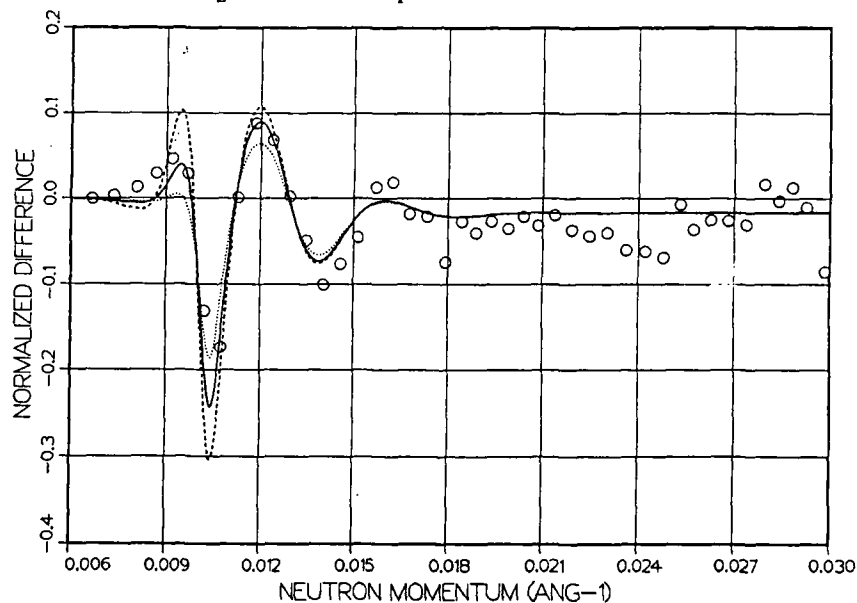
Fig. 2 Normalized difference curves as a function of k.
The open circles are the experimental data obtained from the measurements 1(B) and 1(C). The calculated reflectivity difference curves with 1(B) are shown by the solid line (σ=200Å), the dashed line(σ=250Å) and the dotted line (σ=175Å) for fits to 1(C).

cm^2/s and it is to be hoped that further improvements in the sophistication of the two techniques will yield results in yet better agreement and/or be able to focus on the causes of the discrepancy.

ACKNOWLEDGEMENT

REFERENCES

[1]   S.A. Werner, and A.G. Klein, in Neutron Scattering, edited by D.L. Price, and K. Skold (Academic Press, Ney York, 1989).

[2]   M. Born and E. Wolf, Principles of Optics (Pergamon, Oxford, 1975).

[3]   O.S. Heavens, Optical Principles of Thin Solid Films (Dover Publ., New York, 1965).

[4]   T.P. Russell, A. Karim, A. Mansour and G.P. Felcher,Macromolecules, 1890 (21) 1988.

[5]   M.L. Fernandez, J.S. Higgins, J. Penfold, R.C. Ward, C. Shackleton, and D.J. Walsh, Polymer, 1923 (29)1988.

[6]   J . Crank, The Mathematics of Diffusion, Oxford 1983.

[7]   P.F. Green, C.J. Palmstrom, J.W. Mayer and E.J. Kramer,Macromolecules, 501 (18) 1985.

NEUTRON REFLECTION STUDY OF SURFACE ENRICHMENT IN AN ISOTOPIC POLYMER BLEND

R.A.L. JONES*, L.J. NORTON**, E.J. KRAMER**,R.J. COMPOSTO[†], R.S. STEIN[†],T.P. RUSSELL[††], G.P. FELCHER[‡], A. MANSOUR[‡] and A. KARIM[‡]

*Present address: Cavendish Laboratory, Cambridge University, Madingley Road, Cambridge, CB3 0HZ, UK

**Materials Science and Engineering, Cornell University, Ithaca, NY 14850

[†]Department of Polymer Science and Engineering, University of Massachusetts, Amherst, MA 01003

[††]IBM Almaden Research Center, San Jose, CA 95120

[‡]Materials Science Division, Argonne National Laboratory, Argonne, IL 60439-4814

We have measured neutron reflectivities from the surface of films of deuterated polystyrene (d-PS) and protonated polystyrene (PS) blends before and after annealing, and used the results to determine the concentration versus depth profile of the films. After annealing, the surface is enriched in d-PS, with a surface excess proportional to the bulk concentration of d-PS, in agreement with previous measurements using forward recoil spectrometry[1]. The decay of the enhanced concentration into the bulk occurs over a length approximately equal to the bulk correlation length (~200 A), in close agreement with that predicted by current mean-field theory[2]. However, the agreement between the experimental reflectivity curves and the fitted curves is not completely adequate. Figure 1, a plot of k^4R against k, demonstrates this point for a 15% d-PS sample. The dashed line is the best fit assuming the mean field profile. The inset shows the corresponding concentration profile and a trial profile, solid line, which fits the data much better. The small deviation between the theoretical and trial profiles may be due to the assumption of the theory that surface interactions leading to enrichment is short ranged.

336

Figure 1

Figure 1
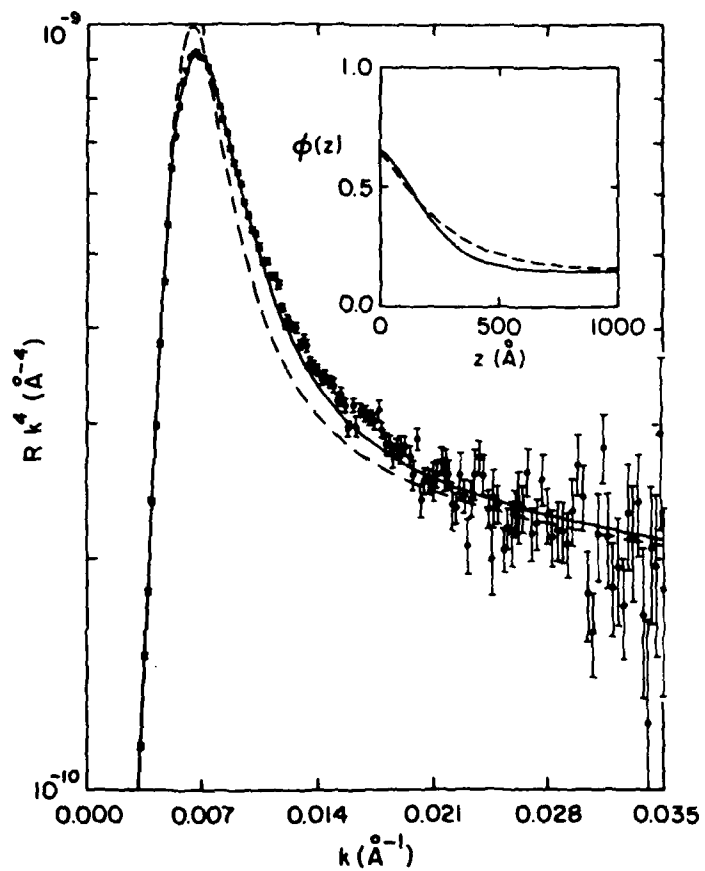
1. R.A.L. Jones, E.J. Kramer, M.H. Rafailovich, J. Sokolov, S.A. Schwarz, Phys. Rev. Let. $\underline{62}$, 280 (1989).

2. I. Schmidt and K. Binder, J. Physique $\underline{46}$, 1631 (1985).

3. R.A.L. Jones, L.J. Norton, E.J. Kramer, R.J. Composto, R.S. Stein, T.P. Russell, A. Mansour, A. Karim, G.P. Felcher, M.H. Rafailovich, J. Sokolov, X. Zhao, S.A. Schwarz, submitted for puplication.

X-RAY REFLECTIVITY AND FLUORESCENCE MEASUREMENTS FROM POLYSTYRENE-CO-BROMOSTYRENE/POLYSTYRENE INTERFACES

J. SOKOLOV[1], M. RAFAILOVICH[1], X. ZHAO[1], W.B. YUN[2], R.A.L. JONES[3],
E.J. KRAMER[3], R.J. COMPOSTO[4], R.S. STEIN[4], A.BOMMANNAVAR[5],M. ENGBRETSON[6]
1) QUEENS COLLEGE, FLUSHING, NY
2) ARGONNE NATIONAL LABORATORY, ARGONNE,IL
3) CORNELL UNIVERSITY, ITHACA, NY
4) UNIVERSITY OF MASSACHUSETTS AT AMHERST, AMHERST, MA
5) BROOKLYN COLLEGE, BROOKLYN, NY
6) OAK RIDGE NATIONAL LABORATORY, OAK RIDGE, TENN

ABSTRACT

X-ray fluorescence using synchrotron radiation at glancing angles of
incidence was used to measure interface widths for the highly immiscible
polymer blend system polystyrene/polybromostyrene (PS/PBr$_x$S, with
bromination level x = 0.8 bromine atoms per monomer). The interfacial
widths are for bilayers annealed for 4 hours and 24 hours at 141±1C are
found to be 100±20Å and 110±20Å respectively.

Introduction

The characterization of interface in polymer blend systems gives
valuable information on mechanical and thermodynamic properties of blends
and can be used to discriminate between the various proposed theories of
polymer phase behavior.[1] When dealing with highly immiscible blends, such
as PS/PBrS (for high levels of bromination), the interfaces between phases
may be of the order of 100Å or less and measurements of interfacial
profiles require high spatial resolution. We report here the results of a
study using the techniques of x-ray fluorescence under conditions of near
total external reflection (NTEF).[2] In the NTEF technique, the angular
dependence of the x-ray-excited fluorescence of a labeled species is
measured for angles of incidence near the critical angle θ_c for total
reflection - for polymers θ_c 1-2mrad (see Table 1). Below θ_c, only
evanescent waves penetrate the medium and the fluorescence is sensitive to
the surface region. In the case of 15keV x-rays incident on polymers the
sampling depth is typically 50-100Å. As the incident angle is increased to
$\theta > \theta_c$ deeper layers are probed, the total depth sensed being a function of
θ and the extinction length (Table 1) for x-rays in the scattering medium.
The total fluorescence signal from the labeled species, in this case
bromine, is given by,[2]

$$I_{Br}(\theta) = K\int\Phi_{Br}(z) \quad I_x(z, \theta) \exp(-\mu_{Br}z)dz \qquad (1)$$

where θ is the x-ray incidence angle, z is the depth into the sample, $\Phi_{Br}(z)$
is the concentration of Br atoms of z, $I_x(z, \theta)$ is the x-ray intensity at
depth z, μ_{Br} is the linear absorption coefficient for the characteristic Br
x-rays in the polymer [as $(1/\mu_{Br}) > 100\mu m$ and the bilayers studied were of
thickness $< 0.5\mu m$, μ_{Br} was taken as zero] and K is a constant taking account
of the atomic fluorescence cross-section and geometric factors such as
detector acceptance angle, efficiency, etc. Calculations of the electric

field intensity $I_x(z, \theta)$ were done using the standard matrix propagation method[3], in which the scattering medium is divided up into layers parallel to the surface of constant (within each layer) refraction index $n = Re(n) + iIm(n)$. The plane wave solutions of Maxwell's equations for each layer are joined so as to satisfy the boundary conditions of continuous tangential E and B fields. For the present calculations, 200-400 layers were used to determine the scattering properties of the ~0.5μm thick polymer samples. Typical computation times were approximately 100s on an IBM 3090 for an angular scan spectrum of 120 values of θ.

TABLE I

	Critical Angle (mrad)	1/e Extinction Length (μm)
PS	1.45	13,110.
PBr$_{0.8}$S		1.65 160.
Si(substrate)	2.07	418.

Experimental

Polystyrene (mw = 670K, polydispersity index = 1.15) was solution-brominated following the procedures outlined by Kambour and Bendler[4] to obtain PBr$_x$S with x = 0.8, which is known to be highly immiscible with PS of mw = 670K.[5] The degree of bromination was determined independently by mass microanalysis. PS/PBrS bilayers were deposited on 2 inch diameter polished silicon wafers in two steps: a) a 4000-5000Å thick PBrS film was spin-cast from a toluene solution onto the Si wafer and b) a 1200-2000Å PS layer, floated on water, was placed on top of the PBrS layer. Samples were annealed under vacuum for up to 24 hours at 141℃. X-ray reflectivity and fluorescence measurements were made at beamline X18B of the Brookhaven National Synchrotron Light Source. A monochromated x-ray beam of energy 15keV, selected to be above the Br Kα absorption edge of 13.474KeV, impinged on the polymer sample at angles θ varying from 0.5 to 5.0 mrad. The bilayer samples were mounted vertically with the beam collimated to ~0.9mm in the vertical direction and in the horizontal direction set large enough to ensure complete coverage of the 0.9mm x 2 inch 'footprint' for all angles of incidence. The reflectivity (mainly used to calibrate the scattering angle and to measure sample thickness) was determined using argon-filled gas detectors for both the incident and reflected beams while the Br fluorescence was measured with a solid-state germanium detector. Each angular spectrum of 120 data points took 20 minutes, or 10s/pt. No detectable radiation damage was observed for these runs.

Analysis

Figures 1-3 show a comparison of calculated and experimental fluorescence spectra for PS/PBrS bilayers annealed for 4 and 24 hours at 141±1℃. The interface was modeled with a hyperbolic tangent profile of

variable with w:

$$\Phi_{Br}(z) = (\Phi_\infty/2)\tanh((z-t)/w) + (\Phi_\infty/2) \quad z \langle d \qquad (2)$$

$$= 0 \qquad\qquad z \rangle d$$

where t is the thickness of the PS layer and d is the combined thickness of the PS and PBrS layers. The interface width w was allowed to vary from 10Å to 200Å while t and d were varied ±300Å about their nominal values. The best values for the PS layer thickness t was found to be 1200±50Å for both samples; the PBrS layer thickness (d-t) was 4800±150Å for the 4 hour anneal sample and 4400±150Å for the 24 hour anneal sample. Figure 1 shows calculations for the 24 hour sample for widths w of 70, 110, 150 and 200Å. The main spectral feature which is sensitive to w is the shoulder at about 1.75mrad (this feature tends to be reduced for samples with thicker PS layers-bilayers with t ~ 1900Å exhibited only one peak and proved difficult to analyze accurately). The optimum agreement between theoretical and experimental spectra was found for

w = 100±20Å [4 hour, 141Č anneal]

and 110±20Å [24 hour, 141Č anneal]

Overall agreement is quite satisfactory.

Conclusion

The technique of x-ray near-total external fluorescence (NTEF) has been demonstrated to be capable of studying interface formation on the small length scales of highly immiscible polymer blend systems. The PS/PBrS system is also suitable (by using deuterated PS or PBrS) for experiments using neutron reflectivity[6], the only other currently available technique used for high resolution polymer interface studies. Measurements of the same samples will allow direct comparisons between the two techniques, enhancing the reliability of both methods.
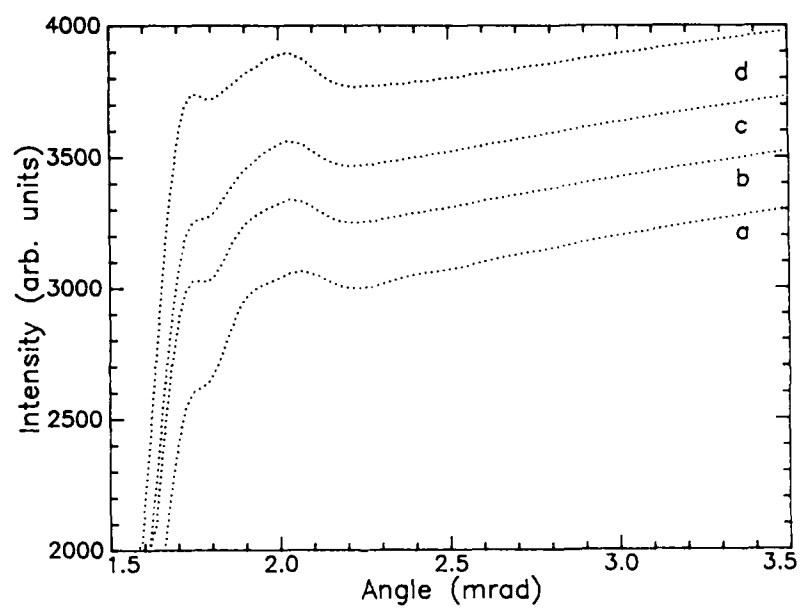
Fig. 1 Calculated fluorescence spectra of PS/PBrS interface of width w
equal to a) 70Å, b) 110Å, c) 150Å and d) 200Å. The PS layer is 1200Å thick
and the PBrS layer 4400Å for all spectra. The zero of each spectrum has
been shifted in multiples of 100 intensity units.
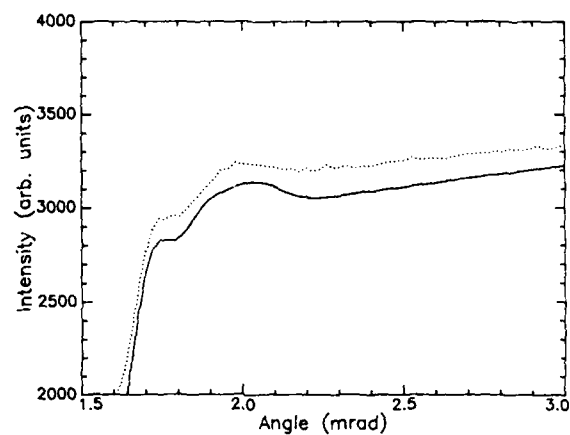
Fig. 2 Experimental (dotted) and calculated (solid line) spectra for the 24 hour, 141°C anneal sample. PS and PBrS layer thicknesses as in Fig. 1. Interfacial width w = 110Å. The zero of intensity has been shifted 100 units.
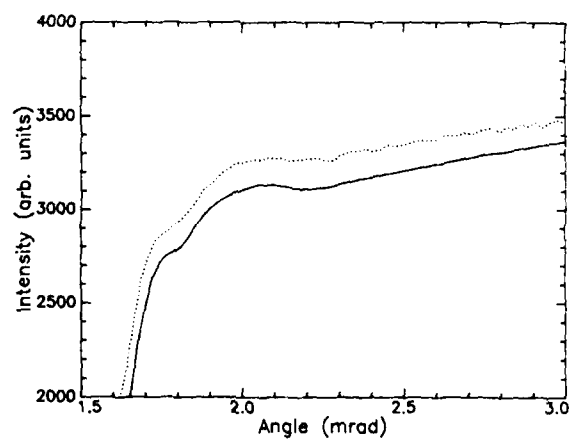
Fig. 3 Experimental (dotted) and calculated (solid line) spectra for the 4 hour, 141°C anneal sample. PS layer 1200Å, PBrS layer 4800Å and interfacial width w = 100Å. The zero of intensity has been shifted 100 units.

342

References

1. P.G. deGennes, J. Chem. Phys. 72, 4756 (1980), P. Pincus, J. Chem. Phys. 75, 1896 (1981), E. Helfand, in Polymer Compatibility and Incompatibility, ed. K. Solc, MMI Press, Harwood Academic Publishers, Chur (1982) p. 143, I. Schmidt and K. Binder, J. Physique 46, 1631 (1985).

2. J.M. Bloch, M. Sansone, F. Rondelez, D.G. Peiffer, P. Pincus, M.W. Kim and P.M. Eisenberger, Phys. Rev. Lett. 54, 1039 (1985), M.J. Bedzyk, G.M. Bommarito and J.S. Schildkraut, Phys. Rev. Lett. 62, 1376 (1989).

3. M. Born and E. Wolf, Principles of Optics (Pergamon, NY 1983).

4. R.P. Kambour and J.T. Bendler, Macromolecules 19, 2679 (1986).

5. G.R. Stobl, J.T. Bendler, R.P. Kambour and A.R. Schultz, Macromolecules, 19 2683 (1926) and Ref. 4.

6. M.L. Fernandez, J.S. Higgins, J. Penfold, R.C. Ward, C. Shackleton and D.J. Walsh, Polymer 29,, 1923 (1988), S.H. Anastasiadis, T.P. Russell, S.K. Satija and C.F. Majkrzak, Phys. Rev. Lett. 62, 1852 (1989).

INTERFACIAL SEGREGATION EFFECTS IN MIXTURES

OF HOMOPOLYMERS WITH COPOLYMERS

VIJAY S. WAKHARKAR, THOMAS P. RUSSELL and VAUGHN R. DELINE
IBM Research Division, Almaden Research Center, San Jose, CA 95120.

ABSTRACT

Secondary Ion Mass Spectroscopy (SIMS) has been used to study the surface and interfacial segregation of diblock copolymers in mixtures of the copolymer in the homopolymer. Symmetric, diblock copolymers of polystyrene (PS) and poly(methyl methacrylate) (PMMA), in either the PS or the PMMA homopolymers were investigated. In mixtures of the copolymer with the PS homopolymer, systematic surface enrichment of the copolymer as well as segregation of the copolymer to the polymer/Si interface or in the case of bilayered films to the polymer/polymer interface occurs with annealing treatments. These segregation effects persist over a large range of homopolymer molecular weights with changes in the kinetics of the segregation process being predominant.

INTRODUCTION

The structure and composition of the polymeric surface/interface and of the near-surface region controls some of the important properties and therefore the applications of such polymers. Hence an in-depth understanding of the surface and interfacial behavior of copolymers is essential towards optimizing the use of these polymers in various applications. Presently, various analytical techniques such as X-ray Photoelectron Spectroscopy (XPS) (1,2), Forward Recoil Spectrometry (FRES) (3) and Electron Microscopy (4,5) are being used to probe the structure of polymeric surface/interface and near surface i.e. interphase regions. Secondary Ion Mass Spectrometry (SIMS) has been applied previously in polymeric materials to study the interface induced orientation effects of diblock copolymers in thin films (6,7) and in diffusion studies (8). In this article we report on the use of SIMS to investigate the segregation effects at polymer interfaces. We have applied depth profiling in polymeric films to study surface segregation; segregation effects at polymer/substrate interfaces or in the case of multilayered films, segregation effects at polymer/polymer interfaces. SIMS has been used to obtain segregation profiles in real space as well as to study the kinetics of the segregation process.

EXPERIMENTAL

The polymers used in this study were purchased from Polymer Laboratories. 1, 3 and 10% mixtures of the copolymer in the PS homopolymer were prepared in toluene solutions. In the diblock copolymer used in this study, both the PS and the PMMA blocks were deuterated and is designated as PSD/PMMAD. The average molecular weight of the diblock copolymer was approximately 1.0×10^5. Films about 1600 Å thick were cast directly on cleaned silicon substrates. These films were then annealed in a vacuum oven at 170°C, which is above the glass transition temperature of either component. The annealing times ranged from a few minutes to tens of hours. A thin layer of Au ($\simeq$ 20-Å) was vapor evaporated on all the films in order to serve as marker for the air/polymer interface in the SIMS depth profiles. Subsequently, a PS layer of about 200-Å was spin coated on a glass substrate, floated on water, and then retrieved onto all the polymer films being analyzed via SIMS. This PS film prevents hydrogen contamination and acts as a buffer layer during the initial sputtering transition of the ion beam.

The SIMS depth profiles were obtained using a Cameca IMS-4F secondary ion microscope. A 3 KeV O^+_2 primary ion source provides a means of sputtering the specimen surface. The secondary ions sputtered from an 80 μm diameter area of the specimen are extracted, mass separated and analyzed using a mass spectrometer. The specific conditions for SIMS analysis are shown in table 1. It has been shown that these conditions provide high sensitivity and good depth resolution while depth profiling organic films (9). During the SIMS experiments the intensity of the secondary ion counts of $^1H^+$, $^2H^+$, $^{12}C^+$, and $^{197}Au^+$ are measured as a function of sputtering time for each film. The sputtering rate in homopolymers PS and PMMA was determined by using standard specimens of accurately known thickness. For the mixtures being used it was noted that the sputtering rate does not vary significantly from that of the respective homopolymers. However the sputtering rate was very dependent upon the experimental conditions and hence it is necessary to calibrate the sputtering rate during each experiment. Hence, knowing the sputtering rate, the intensity of the measured secondary ions versus sputtering time is readily converted into a depth profile.

Table I

Apparatus	Cameca IMS 4f
Primary Ions	O_2^+
Beam Current	200-300 nA
Raster	500 μ x 500 μ
Selected Area Aperture	80 μ diameter
Beam Size	~ 200 μ
Effective Depth Resolution	$\simeq$ 12 5 nm
Detected Secondary Ions	$^1H^+$, $^2H^+$, $^{12}C^+$, $^{197}Au^+$

The relative proportion of the protonated and deuterated polymers as a function of depth is indicated by monitoring the $^1H^+$ and $^2H^+$ signals. The $^{12}C^+$ signal is used as a matrix monitor ensuring that the sputtering rate is constant during the depth profiling. The monitoring of the $^{197}Au^+$ signal serves as an interface marker i.e. indicating the location of the original air/polymer interface prior to the placement of the PS buffer layer. It was noted that the measured sputtering rate of gold was approximately the same as that of PS under the conditions used. Hence the presence of gold serves only as an inert marker and does not perturb the sputtering rate.

RESULTS AND DISCUSSION

A typical SIMS depth profile for an as cast film of a mixture of 10% fully deuterated diblock copolymer PSD/PMMAD in the PS homopolymer is shown in figure 1. The position of the original air/polymer interface is indicated by the vertical dashed line on the left hand side, corresponding to the peak in the Au signal, while the polymer/silicon interface is indicated by the vertical dashed line on the right hand side. The initial transient in the signal where the secondary ion counts of carbon (C), hydrogen (H), deuterium (D) counts vary markedly occurs in the buffer layer of PS. Note that a steady state sputtering is achieved by the time the ion beam has reached the polymer film under investigation. The C counts, which serve as a matrix monitor, remain relatively constant throughout the entire thickness of the film. In this example, since we have a mixture of a fully deuterated copolymer in a protonated homopolymer, an examination of the deuterium (D) signal indicates where the copolymer is residing. Thus in the as cast film the copolymer has preferentially segregated to the polymer/silicon interface as indicated by the relatively high deuterium signal at that interface. Also note that there is a small surface enrichment of the copolymer as compared to the bulk. The H signal, which was relatively constant throughout the entire film thickness, drops at the polymer/silicon interface due to the segregation of the fully deuterated copolymer to this interface.

The depth profile for an identical film that was annealed at 170° C in vacuum for twenty hours is shown in figure 2. The dramatic change in the deuterium (D) profile is evident. Note that the C signal remains invariant throughout the sputtering of the film as before. The relatively high deuterium signal at the air/polymer interface now clearly shows the surface enrichment of the copolymer that has occurred due to the annealing treatment. The segregation at the polymer/silicon interface is also enhanced. The segregation effects can be clearly seen in figure 3 which is a composite of the two superimposed deuterium (D) profiles. Thus at sufficiently long annealing times the concentration of the copolymer in the bulk film is quite low, the copolymer now being present either at the air/polymer interface or at the polymer/silicon interface.
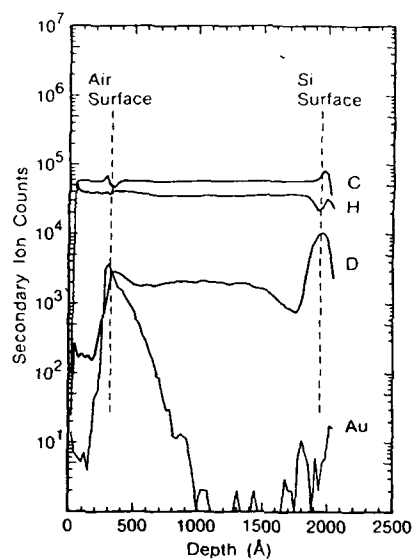
Figure 1. A SIMS *depth profile obtained from an* as cast film of a mixture of 10% PSD/PMMAD in PS (127 K).
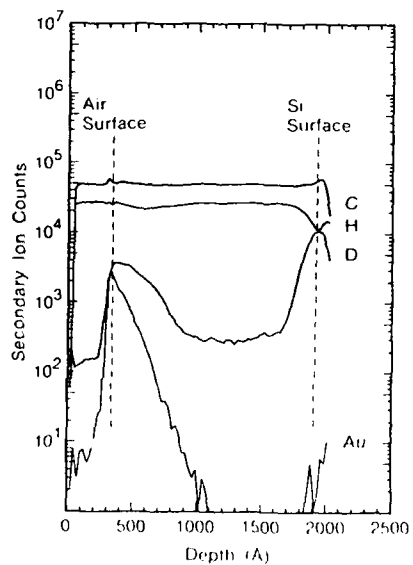
Figure 2 A SIMS depth profile obtained from an annealed film of a mixture of 10% PSD/PMMAD in PS (127 K) after annealing at 170° C for two hours

346
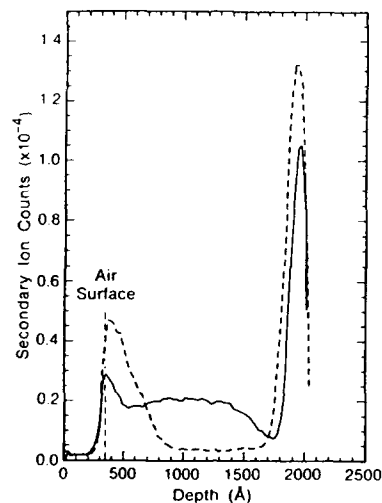
Figure 3. A composite of two superimposed Deuterium (D) profiles corresponding to a mixture of 10% PSD/PMMAD in PS (127 K). The solid line corresponds to an as cast film while the dotted line corresponds to a specimen annealed for 20 hours at 170°C.

The time dependence of the interfacial copolymer segregation was followed over a wide range of annealing times. Figure 4 shows the superimposed depth profiles at different annealing times for a 3% PSD/PMMAD copolymer dissolved in a PS homopolymer of 1.27×10^5 average molecular weight. The systematic surface enrichment of the copolymer due to the annealing treatment is clearly seen. At the polymer/silicon interface similar effects were observed. In this particular example it was noted that even a small annealing time, such as five minutes, was sufficient to observe detectable migration of the copolymer to the interfaces.
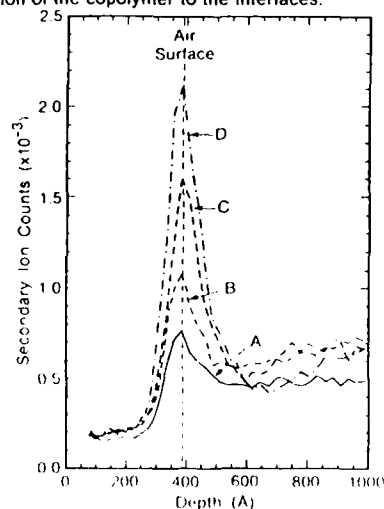
Figure 4 A composite of four superimposed Deuterium (D) profiles in the near surface region This corresponds to films of a mixture of 3% PSD/PMMAD in PS (127 k) and annealed at 170 C as indicated (A) As Cast (B) 5 min (C) 30 min (D) 120 min (from ref 10)
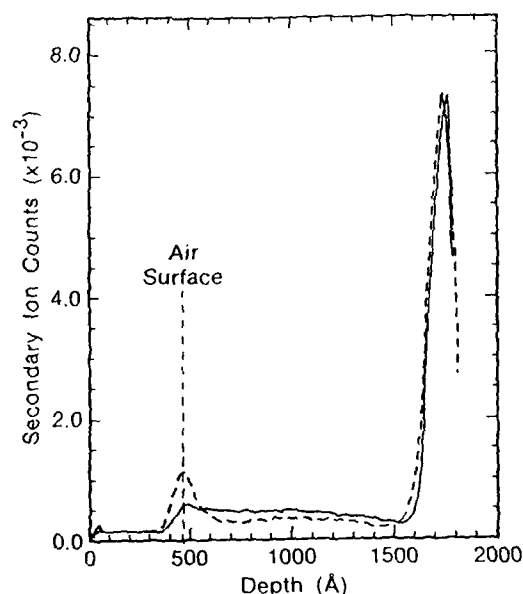
Figure 5. A composite of two superimposed Deuterium (D) profiles corresponding to a mixture of 3% PSD/PMMAD in PS (1150 K). The solid line corresponds to an as cast film while the dotted line corresponds to a specimen annealed for 20 hours at 170°C.

The molecular weight of the homopolymer PS in the mixture was varied from 1.75 x 10⁴ to 1.15 x 10⁶. Surface enrichment of the copolymer as well as its segregation to the polymer/silicon interface persists over the entire range of homopolymer molecular weight variation. Figure 5 shows a composite of two superimposed deuterium profiles corresponding to a mixture of 3% PSD/PMMAD in PS of average molecular weight of 1.15 x 10⁶. In this case it was necessary to anneal the specimen for several hours before any detectable migration of the copolymer to the interfaces was observed.

SIMS has also been used to examine polymer/polymer interfaces by depth profiling multilayered polymer films. For the bilayer films analyzed, the lower film corresponds to a mixture of 1% PSD/PMMAD in PMMA while the top layer corresponds to a mixture of 1% PSD/PMMAD in PS. The top layer was coated on a glass substrate, floated on water and then retrieved onto the first polymer layer. This bilayer film was then annealed and prepared for SIMS as described before. Figure 6 shows a typical depth profile for a bilayered film that was annealed for 48 hours. Thus in this case, in addition to the surface enrichment, segregation of the copolymer to the polymer/polymer interface also occurs.

CONCLUSIONS

SIMS has been used to investigate the interfacial segregation of diblock copolymers in mixtures of the copolymers with homopolymers. It was found that annealing treatments result in the systematic surface enrichment of the copolymer as well as its segregation to the polymer/silicon interface or in the case of bilayers to the polymer/polymer interface. The segregation effects were observed regardless of the molecular weight of the homopolymer and the bulk volume fraction of the copolymer in the mixture. The predominant effect of these changes was to influence the kinetics of the segregation process.

348
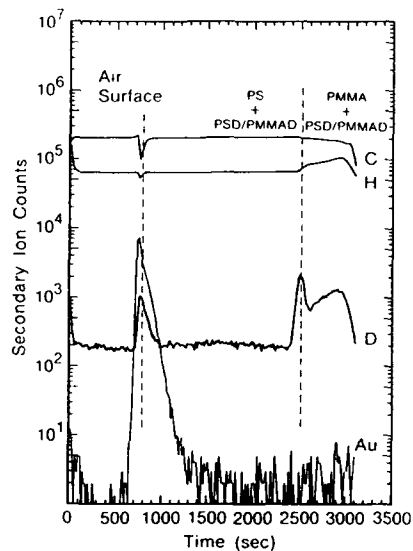
Figure 6. A SIMS depth profile obtained from a bilayer film that was annealed at 170°C for 48 hours.

REFERENCES.

1. P.J. Mills, P.F. Green, C.J. Palmstorm, J.W. Mayer and E.J. Kramer, *App. Phys. Lett.*, **45**, 9, (1984).
2. H.R. Thomas and J.J. O'Malley, *Macromolecules* **12**, 323, (1979).
3. P.F. Green, C.J. Palmstrom, J.W. Mayer and E.J. Kramer, *Macromolecules*, **18**, 501,(1985).
4. H. Hasegawa and T. Hashimoto, *Macromolecules*, **18**, 589, (1983).
5. C.S. Henkee, E.L.Thomas and L.J. Fetters, *J. Mater. Sci.*, **23**, 1685, (1983).
6. G. Coulon, T.P. Russell, V. R. Deline and P. F. Green, *Macromolecules* **22**. 2581, (1989).
7. T.P. Russell, V. R. Deline, V.S. Wakharkar and G. Coulon, *Materials Research Society Bulletin*, **Vol.XIV (No.10)**, 33,1989.
8. S.J. Whitlow and R.P. Wool, *Macromolecules*, **22**, 2648, (1989).
9. G.J. Scilla, *submitted to Anal. Chem.*.
10. V.S. Wakharkar, V. R. Deline and T.P. Russell, *Proceedings of the VII International SIMS Conference, September 3-8, Monterey, CA., (John Wiley & Sons Limited Publishers, 1989)*, **in press**

A NEW VARIABLE ANGLE FT-IR ELLIPSOMETER

J.L STEHLE * , O.T THOMAS * , J.P. PIEL * , P.EVRARD * ,
J.H.LECAT *, L.C HAMMOND **
* SOPRA, 26/68 Rue Pierre Joigneaux , 92270 BOIS-COLOMBES,
FRANCE
** ARIES/QEI, 5A1 Damonmill Square, Concord MA 01742, USA

ABSTRACT

Use of a Fourier-transform interferometer integrated with a variable incidence angle ellipsometer extends the spectral range and the capabilities of spectroscopic ellipsometry into the infrared. With a spectral range of 600 to 6600 cm-1, thick layers, such as epitaxial doped layers and polymers can be analysed.

A full description of this novel instrument will be given. Incidence angle can be varied automatically to enhance signal/noise and the ellipsometric data can be obtained together with vibrational absorption bands information to give a characteristic " fingerprint " of the layers.

Examples of spectra of HCN polymer on nickel, DMHS on aluminium and PMMA on silicon will be presented for various incidence angles and layer thickness.

I : INTRODUCTION

Since the year 1950, a great number of materials have been characterized by mean of an infrared ellipsometer (1) . As the rotation of the polarizer was manual, these measurements were tedious and time-consuming . The development by Stobie, Rao and Dignam of the first photometric infrared ellipsometer has been a great improvement (2). They show the great sensitivity of this technique by the measurement of formic acid chemisorbed on silver.

With the development of Fourier-transform spectrometers, a new generation of infrared ellipsometers is born, using a combination of a Michelson interferometer and a photometric ellipsometer. The first one was achieved by Roseler (3) in 1981. Today, it is an instrument in development at SOPRA. The first results and the possible applications will be shown.

II : THEORY

Ellipsometry is a non-destructive technique, determining the change of state of polarization of the light reflected on the surface of a sample. More precisely, the complex reflectance ratio r_p/r_s is measured, where r_p and r_s are the complex reflectances of p- and s- polarized light, respectively.

$$r_p/r_s = \tan\Psi\ e^{i\Delta}$$

The ellipsometric parameters $\tan\Psi$ and $\cos\Delta$ are a function of the refractive index and the thickness of each layer of the sample. In comparison with reflectometry, two parameters instead of one are obtained per wavelength, and this allows the determination of both real and imaginary parts of the materials, without using a Kramers-Kronig transformation. It means that there is no need to extrapolate the spectrum values outside the measuring range.

Different models are used to get a physical interpretation of the $\tan\Psi$ and $\cos\Delta$ spectrum. The most general one is a multilayer model, where thickness and composition of each layer are introduced as parameters in a regression program.

Beside this general approach, it is possible to use some data reductions concerning the particular case of one layer over a substrate. For a transparent layer, the real part of the index and the thickness can be calculated for each wavelength, knowing the substrate composition. If the thickness of the layer is known, a direct computation of both real and imaginary part of the index can be obtained.

Working in the infrared allows some simplification of the ellipsometric equations, because the thickness of the layer can often be considered as small, compared with the wavelength. Therefore, it is useful to introduce the following quantity (4) :

$$D = \ln(\ \tan\Psi\ /\overline{\tan\Psi}\ ) + i(\ \Delta - \overline{\Delta}\ )$$

where $\overline{\tan\Psi}$ and $\overline{\Delta}$ are the values of a bare substrate in the same conditions.
When the substrate is transparent in the infrared, the variations of the dielectric function can be directly seen on the spectrum of the real and imaginary part of the relative complex optical density D .

III : CHARACTERISTICS AND PERFORMANCES OF THE ELLIPSOMETER

The advantage of this technique, compared with reflectometry is that ellipsometry does not measure intensities but a polarization state of light. Thus, the precision of the measurement is not degraded by intensity fluctuations of the source, or electronic drifts. No reference spectrum is needed.

A Fourier transform has the following advantages on a monochromator :
    - it is a multiplex configuration, because all the wavelengths are simultaneously measured. Therefore, a spectrum is obtained faster and with a better signal to noise ratio than with a monochromator (Fellgett advantage (5)). A measuring time in the minute range is possible.
    - there is an energetic disadvantage of the monochromators compared to an interferometer (Jacquinot advantage (5)).

The Michelson interferometer of a Fourier transform spectrometer is followed by a photometric ellipsometer of rotating analyzer type (fig 1). Ge Brewster angle polarizers have been developed against grid polarizers to obtain a better degree of polarization over the whole spectral range. The spectral range goes from 6600 to 600 cm-1, and the resolution can be selected from to 2 to 32 cm-1.
    The sample reflects a collimated beam whose divergence can also be selected from 0.5 to 6 degrees by the software. As the sensitivity of the ellipsometric measurements is greatly dependent on the incidence angle, it can be automatically modified by the user, from 40 to 90 ,+/- 0.01 degrees.

At the end of the optical train, the liquid nitrogen cooled detector HgCdTe delivers an electrical signal. The processing of this signal contains two Fourier transforms, the first one to get the signal per wavelength, the second one to compute the ellipsometric parameters.
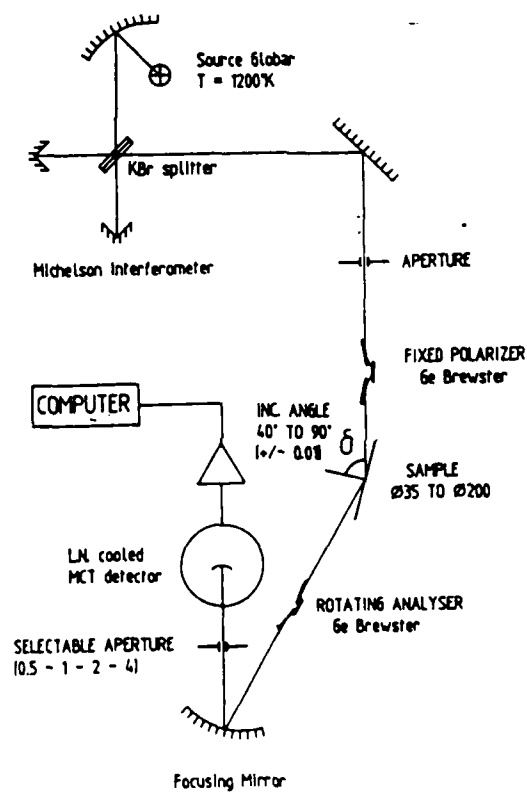
fig 1 : *Optical Schema of the Ellipsometer*

352
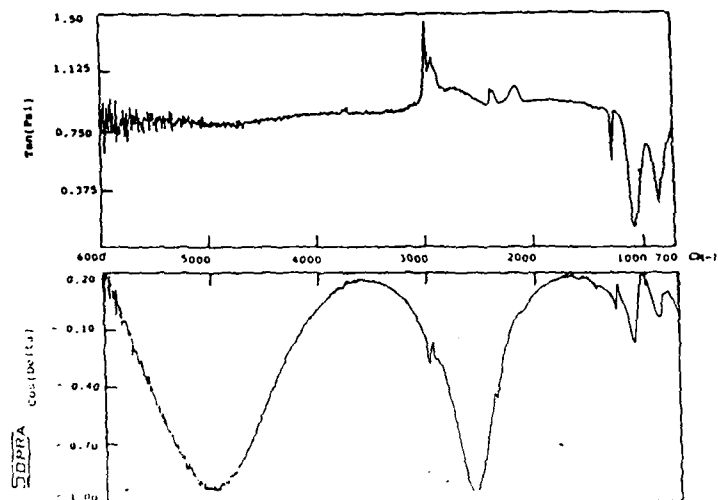
<u>fig 2</u> : tanΨ and cos Δ of HMDS(Hexamethyldisilane) on
Aluminium.
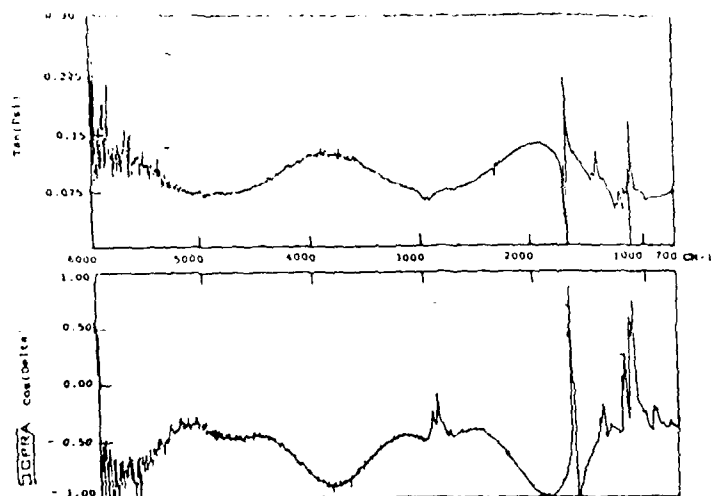
<u>fig 3</u> : tanΨ and cos Δ   spectrum of PMMA resist on
silicon
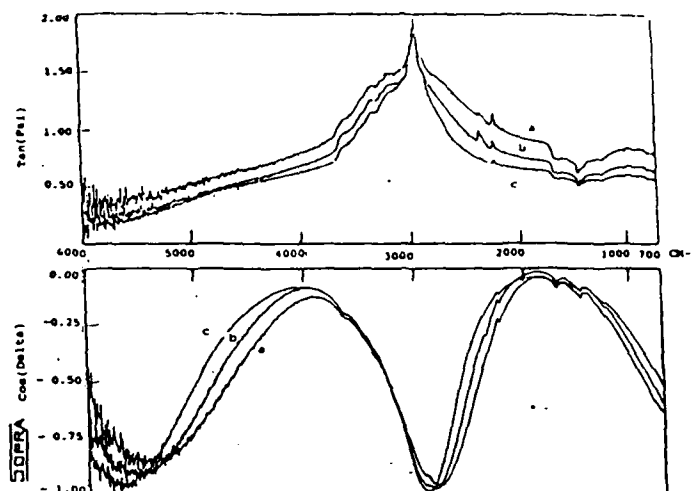
Fig 4 : tanΨ and cosΔ   spectrum of HCN polymer on Ni for
three incidence angles :   a : 65° ; b: 70°; c: 75°

V : APPLICATION TO SURFACES STUDIES

Dielectric function of bulk materials, such as metals, glasses, silicides, can have their n,k values directly calculated for each energy from the ellipsometric parameters tanΨ and cosΔ   . For instance, optical properties of Au have been studied by Jungk and Roseler using FTIR Ellipsometry (6).

Ellipsometric techniques have already proved their high sensivity in the visible spectral range for the study of film growth processes (7). Recently, experimental studies by R.BENFERHAT and B.DREVILLON using an infrared spectroscopic phase-modulated ellipsometer have showed that it was possible to get evidence of anisotropic orientation of one single monolayer of Langmuir-Blodgett films (8). The vibrational properties of hydrogenated amorphous silicon ultrathin films (less than 100 Å) have also been obtained by this technique (9).

Using a Fourier-Transform IR ellipsometer, the densification and the porosity in low temperature deposited oxide have been determined (10). The mean Si-O-Si bond angle was calculated from the peak IR values and related to the oxide density.

The Fourier Transform Ellipsometry can also offer a way of characterization of thick layered materials(Fig.2,3 and 4). Measurements of slightly doped Si Layers epitaxied on heavily doped Si substrates have been performed (11). With a 2 cm-1 spectral resolution, a 100 micron-thick layer can be studied. Thick porous silicon layers are also a possible application of this ellipsometer.

REFERENCES

(1) J.R BEATTIE
     Phil. Mag. 46 235 (1955)

(2) R.W STOBIE, B.RAO, and M.J. DIGNAM
     Applied Optics Vol 14, No 4, (1975) 999

(3) A.ROSELER
     Infrared Physics 21 349 (1981)

(4) M.J. DIGNAM, B.RAO, M. MOSKOVITS, and R.W. STOBIE
     Can. J. Chem. 49, 1115 (1971)

(5) A.E MARTIN
     Vol 9 in Vibrational Spectra and Structure
     Ed J.R Durig, Elsevier.

(6) G.JUNGK and A. ROSELER
     Phys.Stat.Sol (b) 137, 117, (1986)

(7) S.ANDRIEU, F. ARNAUD D'AVITAYA
     Surface Science 219 (1989) 277 - 293

(8) R.BENFEHRAT,B.DREVILLON and P.ROBIN
     MRS BOSTON Fall Meeting 1-6 Dec 1986.

(9) B.DREVILLON and R.BENFERHAT
     J.Appl.Phys. 63 (1988) 5088

(10) F.FERRIEU and R.A.B DEVINE
     To be published in J.Non-Crystalline Solids

(11) F.FERRIEU
     Rev. Sci. Instrum. 60 (1989) 3212

POLYMER MOLECULES AT INTERFACES:
STUDIES BY SMALL-ANGLE NEUTRON SCATTERING

W.C. Forsman and B.E. Latshaw*
*Department of Chemical Engineering, University of Pennsylvania, Philadelphia,
PA 19104.
D.T. Wu**
** Marshall Research & Development Laboratory, E.I. DuPont de Nemours & Company, 3500 Grays Ferry Avenue, Philadelphia, PA 19146

Introduction -- Our Experimental System

The behavior of polymer molecules at interfaces is an essential aspect of a wide variety of physical-chemical phenomena. For example, polymer molecules in the fiber-polymer interface play an important role in determining the mechanical properties of composites, and polymer molecules at the liquid-solid interface are critical in the stabilization of colloidal dispersions. In some cases polymer molecules are physically adsorbed at the interface and in other cases they are chemically bonded to the surface at one or more positions along the chain. To simplify the terminology, however, both cases will be referred to as polymer adsorption. The chains in the second case are said to be grafted to the surface. It is an example of this second case that we are concerned with in this paper, and in particular with polymer grafted to a finely divided substrate dispersed in a liquid.

Among the parameters of interest in this example of polymer adsorption are the number of polymer molecules adsorbed per unit surface area, and the polymer density profile -- that is, the density of polymer repeat units as a function of the distance from the adsorbing surface.

In principle, the length scales characterizing most density profiles makes them amenable to study by small-angle neutron scattering. Indeed, three laboratories have now demonstrated the feasibility of using small-angle neutron scattering for determining density profiles for polymers adsorbed at solid-solution interfaces of high surface-area substrates. Cosgrove and associates[1,2,3,4,5,6,7] have been studying the density profile of poly(ethylene oxide) adsorbed on the surface of polystyrene latex particles. Auvray, Cotton and their associates[8,9] have been examining acrylic polymers adsorbed on the inner surface of porous silica.

We recently completed a set of preliminary experiments at Brookhaven National Laboratory[10]. Our system was poly(n-butyl methacrylate) chemically bonded at one end of each chain to the surface of nearly monodisperse, 2000 Å silica spheres. The grafting density was one polymer molecule per 900 Å^2. The polymer was prepared by group transfer polymerization, with a narrow molecular weight distribution and an average molecular weight of 53,000.

Scattering measurements were made on dispersions of bare particles and particles with grafted polymer. We did contrast variation experiments using mixtures of hydrogenous and deuterated isopropanol (IPA) for the dispersant phase. Since IPA is a solvent for the polymer (albeit, a poor solvent), we assume that if the poly(butyl methacrylate) were not grafted to the surface it would have leached off of the substrate. We saw no evidence of leaching during our neutron scattering experiments.

Scattered intensities (after correcting for background) were directly proportional to the particle concentration for 1, 5 and 10 volume % dispersions. We took this to mean that there is no contribution to the scattered intensity from interparticle interference over our range of experimental scattering angles. This is to be expected for particles as large as 2000 Å.

Analysis: Uncoated Particles

Scattering from homogeneous spheres of radius R is determined by their scattering function, $F_s(Q)$, which is written:

$$F_s = V_s \left[\frac{3}{(QR)^3} \right] [\sin(QR) - (QR)\cos(QR)] \tag{1}$$

where

$$V_s = \text{The volume of the sphere} \quad \text{and} \quad Q = \frac{4\pi}{\lambda}\sin(\theta/2) \tag{2}$$

In equation 2, λ is the wavelength of the radiation and θ is the angle between the incident and scattered beams.

For most experiments, the scattered intensity, $I(Q)$, as a function of Q and the intensity of the incident radiation, I_0, is written as

$$I(Q) = I_0 a_s^2 F_s^2(Q) \tag{3}$$

The quantity a_s is the contrast between the sphere and the solvent (or dispersant). The contrast of any scattering object is given by

$$a_i = \rho_i - \rho_{sol} \quad \text{where} \tag{4}$$

ρ_i = Scattering length density of component i, and

ρ_{sol} = Scattering length density of solvent.

For spheres with diameters as large as 2000 Å the scattering function is well within the large-Q asymptotic scattering regime over our entire range of experimental Q. Furthermore, the sinusoidal oscillations are beyond the experimental resolution of Q. Consequently, the instrument gives the scattered intensity averaged over the individual detector elements. For 2000 Å spheres, equation 3 must be replaced by

$$I(Q) = I_0 a_s^2 <F^2(Q)> \tag{5}$$

which can be written as

$$I(Q) = \frac{Constant}{Q^4} \tag{6}$$

This same form of $I(Q)$ would apply to polydisperse spheres as long as they were all of 10^3 Å length scale or larger.

Scattering by the "Bare" Particles

If the silica particles had been homogeneous, our experimental $I(Q)$ would have been described by Equation 6. That is not, however, what we measured. Our experiments demonstrated significant deviations from Equation 6 at both ends of our experimental range of Q.

Modeling of scattering from spheres leads to the conclusion that deviations from equation 6 are the result of non-uniform particle composition. There are two quite different aspects to this non-uniformity -- aspects we could call "course grain" and "fine grain". They can be described as follows: (1) The SiO_2 concentration is not a constant throughout the particle, but is a smooth function of the radius -- this is the "course grain" non-uniformity. At this level of detail, we can think of a particle as a core surrounded by a shell, with a transition from core to shell that takes place smoothly over radii from about 100 Å to about 200 Å. The SiO_2 concentration is relatively constant for all radii greater than 200 Å. This "course grain" non-uniformity contributes deviations from equation 6 at the small-Q end of our experimental range.

(2) We also found that there are random density fluctuations throughout the particles. The size scale of the fluctuations is about 9 Å -- i.e., the "fine grain" non-uniformity. This is exactly the same type of random, short-range density fluctuation one finds in other glassy materials. This "fine grain" non-uniformity contributes deviations from Equation 6 at the large-Q end of our experimental range.[11]

These structural features are consistent with what one would expect, considering how the silica particles are made in the laboratory.[12] The most important result from this analysis is, however, that neither the "fine grain" nor the "course grain" non-uniformities interfere with interpretation of the scattering data in terms of the density profile of the grafted polymer.

In addition to scattering from the structural features associated with the body of the silica spheres, we found a significant scattering from a thin shell surrounding the particles, which we assume to be surface hydroxyl groups and an associated solvation layer. The scattering function for this shell is written

$$F_{SH} = V_S \left[\frac{3}{(QR)^2} \right] [(\sin QR)(\sin QD) + (\cos QR)(1 - \cos QD)] \tag{7}$$

where D is the thickness of the shell.

We conclude that the following equation adequately accounts for the scattering of "bare" particles:

$$\frac{I(Q)}{I_0} = a_S^2 \langle F_S^2 \rangle + a_{SH}^2 \langle F_{SH}^2 \rangle + 2a_S a_{SH} \langle F_S F_{SH} \rangle \tag{8}$$

where $\langle F_S^2 \rangle$ now takes into account the non-homogeneities of the sphere.

The Polymer Density Profile: Theoretical Analysis

The scattering function for the grafted polymer layer can be written

$$F_r = V_S \left[\frac{3}{(RQ)^2} \right] [\sin(QR)I_c + \cos(RQ)I_s] \tag{9}$$

where

$$I_c = Q \int_0^\infty \phi(Z) \cos(QZ) dZ$$

and

$$I_s = Q \int_0^\infty \phi(Z) \sin(QZ) dZ$$

The function $\phi(Z)$ is the polymer density profile expressed as volume fraction of polymer, and is a function of the distance from the surface, Z. The two integrals will be called the cosine and sine transforms of the polymer density profile. Expressing the transforms as Taylor series gives

$$\tag{10}$$

$$I_c = Q \langle Z^0 \rangle - Q^3 \frac{\langle Z^2 \rangle}{2!} + \cdots$$

and

$$I_s = Q^2 \langle Z \rangle - Q^4 \frac{\langle Z^3 \rangle}{3!} + \cdots$$

The zeroth moment of the density profile, $<Z^0>$, is just the integral over $\phi(Z)$ from 0 to ∞, and gives the polymer coverage of the substrate. The product of $<Z^0>$ and the specific volume of the polymer gives the coverage in mass of polymer per unit area of the substrate. The ratio $<Z>/<Z^0>$ is the average thickness of the polymer layer. It is clear, therefore, that much can be learned about the adsorbed layer just from the limiting behavior of the transforms as Q approaches zero.

Scattering from Spheres with Grafted Polymer

When the spheres have a grafted polymer layer, the scattered intensity is written

$$(11)$$

$$\frac{I(Q)}{I_0} = a_s^2 <F_s^2> + a_r^2 <F_r^2> + a_{sH}^2 <F_{sH}^2> + 2a_s a_r <F_s F_r> + 2a_s a_{sH} <F_s F_{sH}> + 2a_r a_{sH} <F_r F_{sH}>$$

By taking the difference between equations 11 and 8, we obtain the terms associated with the polymer layer.

$$\frac{\Delta I(Q)}{I_0} = a_r^2 <F_r^2> + 2a_s a_r <F_r F_s> + 2a_r a_{sH} <F_r F_{sH}> \qquad (12)$$

By evaluating the terms in equation 12 we get

$$\frac{(QR)^4 \Delta I}{9V_s^2 I_0} = a_r^2 (I_c^2 + I_s^2) - 2a_r a_s I_s + 2a_r a_{sH}[(\sin DQ)I_c + (1 - \cos QD)I_s] \qquad (13)$$

Given D, for every experimental value of Q, there are two unknowns in equation 13, I_c and I_s. In principle, by doing scattering experiments in only two mixtures of hydrogeneous and deuterated dispersants, and thus having data at two different contrasts, one has enough information to solve for the two transforms at every value of Q. This procedure is, even in principle, valid only if the nature of the polymer adsorption is independent of isotopic substitution in the dispersant. In practice, if I_c and I_s are to be determined with any reasonable level of confidence, one should have scattering data with several mixtures of hydrogeneous and deuterated dispersants.

The Question of a Depletion Layer.

Consider polymer chains grafted to a surface by one end. Suppose that the net polymer-surface interaction is not favorable for adsorption -- indeed, that if the chains were not grafted to the surface they would not adsorb. Under these circumstances there is theoretical reason to believe that the polymer density profile would be one with a maximum some distance out from the substrate surface. We could define a region from $Z = 0$ to some value of Z less than the value for the maximum in the density profile as a depletion layer -- i.e. a layer within the domain of adsorbed polymer that is both close to the substrate surface and significantly depleted of polymer.

For example, consider the two hypothetical polymer density profiles given below and shown in figure 1.

$$\phi_1 = (constant)e^{-aZ} \qquad (14)$$

and

$$\phi_2 = (constant)Z^2 e^{-aZ}$$

Figure 1
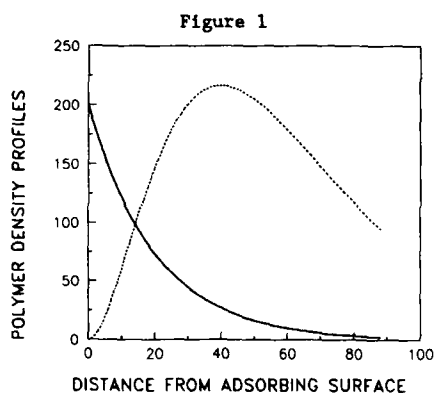
Polymer density profiles with and without a depletion
layer. The solid line represents $\phi_0(Z)$ and the dashed
line $\phi_2(Z)$. Units are arbitrary.

Profile $\phi_0(Z)$ shows no depletion layer. The density of polymer repeat
units drops off steadily with increasing Z. Profile $\phi_2(Z)$, on the other hand,
shows a depletion region. Definition of the depletion layer is rather arbi-
trary, but clearly there is little polymer between $Z = 0$ and $Z = 10$ (in
arbitrary units).
    Figures 2 and 3 show the sine and cosine transforms for the hypothetical
density profiles defined above.
Notice that, in the case of $\phi_2(Z)$, for increasing Q, both transforms go
through a maximum, cross the Q axis, demonstrate a minimum and then increase
towards zero. Behavior of the transforms for $\phi_0(Z)$, which shows no depletion
layer, is entirely different. They both demonstrate a maximum and then
decrease monotonically toward zero with increasing Q.
    At least for the family of hypothetical density profiles of the sort
given in equation 14, a depletion layer is characterized by profile transforms
that cross the Q axis and demonstrate both a maximum and a minimum. Further
analysis is under way. But in the interim, we suggest that these criteria may
serve to "fingerprint" the presence of a depletion layer.

Figure 2
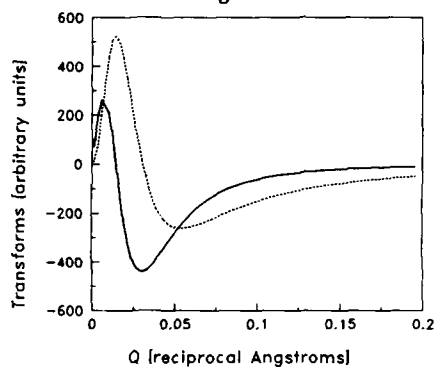
Sine and cosine transforms of $\phi_2(Z)$, the hypothetical
segment density profile that demonstrates a depletion
layer. Solid line; cosine transform. Dotted line;
sine transform.

Figure 3
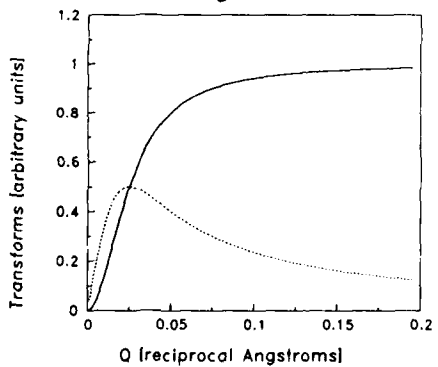
Sine and cosine transforms of $\phi_0(Z)$, the hypothetical
segment density profile that does not demonstrate a
depletion layer. Solid line; cosine transform.
Dotted line; sine transform.

Experimental Results: The Grafted Polymer Layer

We used equation 13 to determine I_C and I_S using scattering data taken from dispersions in 50, 60, 70 and 100% deuterated IPA. Preliminary calculations indicated that, as long as the scattering length density of the spheres is not too close to that of the dispersant (*i.e.*, not near the matching point), the first term on the right-hand side of equation 13 is negligible. This implies that scattering effects due to interference between the polymer layer and the hydroxyl shell, and the polymer layer and the body of the sphere are greater than the effect of scattering from the polymer layer itself. This is not unreasonable, since there is less mass of grafted polymer than mass of either sphere or hydroxyl layer.

Figure 4
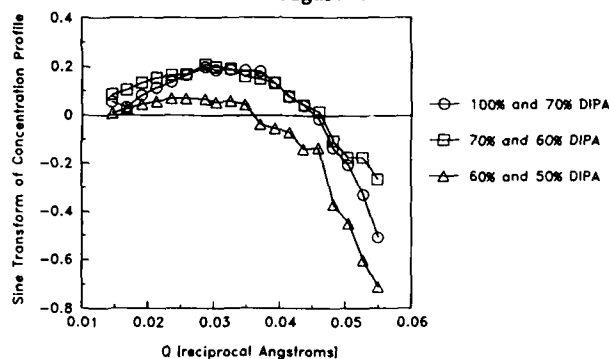
Experimental sine transform over a range of small Q.

Figure 5
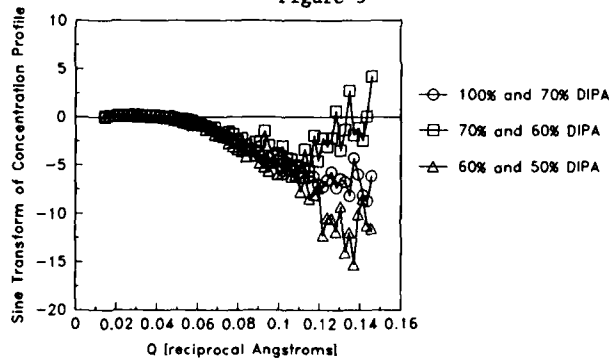
Experimental sine transform over an intermediate range of Q.

In the analysis shown here, we used combinations of 50 and 60%, 60 and 70%, and 70 and 100% deuterated IPA to determine three different $I_S(Q)$ functions. The average of these three were then used, along with experimental data to determine $I_C(Q)$ for each of the four dispersant mixtures.
The results are shown in figures 4, 5 and 6.

Figure 6

Experimental cosine transform over an intermediate range of Q.
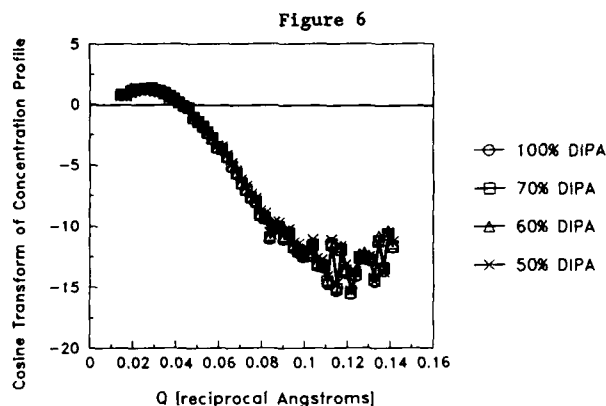
Agreement of the various transforms computed from the scattering results in the various dispersant mixtures was surprisingly good at low Q. However, the agreement between the $I_S(Q)$ for the three pairs of contrasts became quite unsatisfactory at higher Q. The poor agreement between $I_S(Q)$ determined from experiments using 50 and 60% DIPA and the other two sets (see figure 4) may be because these measurements were made too near the matching point of the spheres for the first term on the right hand side of equation 13 to be negligible.

Both transforms demonstrate a maximum and then become negative with increasing Q. The cosine transform then demonstrates a clear minimum. The behavior of $I_S(Q)$ with increasing Q is not so clear. Nonetheless, there is evidence of a minimum, especially if the 50-60% DIPA data (that which is suspect) is ignored.

We conclude that, to the extent we can rely on the criteria described above, the results indicate that the polymer density profile in our experimental system demonstrates a depletion layer. Additional scattering experiments and analysis are required before we can quantify the polymer density profile in detail.

References

1. K.G. Barnett, T. Cosgrove, B. Vincent, A.N. Burgess, E.L. Crowl y, T. King, J.D. Turner and Th.F. Tadros, *Polymer*, 22, 283 (1981).

2. Cosgrove, T.L. Crowley, B. Vincent, K.G. Barnett and Th.F. Tadros, *Faraday Symp. Chem. Soc.*, 16, 101 (1982).

3. T. Cosgrove, T.L. Crowley and B. Vincent, in Adsorption from Solution, edited by R.H. Ottewill, C.H. Rochester and A.L. Smith, (Academic Press, 1983).

4. T. Cosgrove, T.G. Heath, K. Ryan and T.L. Crowley, *Macromolecules*, 20, 2879 (1987).

5. T. Cosgrove, T.G Heath, K. Ryan and B. van Lent, *Polymer*, 28, 64 (1987).

6. T. Cosgrove, T.G. Heath, and K. Ryan, *Extended abstracts, American Institute of Chemical Engineers Annual Meeting*, paper 4D (1987).

7. T. Cosgrove, T.L Crowley, L.M Mallagh, K. Ryan and J.R.P. Webster, *Polymer Preprints*, 3, 370 (1989).

8. L. Auvray, and J.P. Cotton, *Macromolecules*, 20, 202 (1987).

9. L. Auvray, and J.P. Cotton, *Extended abstracts, American Institute of Chemical Engineers Annual Meeting*, paper 4E (1987).

10. W.C. Forsman and B. Latshaw, Paper presented at the annual meeting of the American Institute of Chemical Engineers, San Francisco, CA, November, 1989 (unpublished).

11. P. Debye and A.M. Bueche, *J. Appl. Phys.*, 20, 518 (1949).

12. W. Stober, A. Fink and E. Bohn, *J. Colloid Interface Sci.*, 26, 62 (1968).

MECHANICALLY INDUCED SILICA-SILOXANE MIXTURES.
STRUCTURE OF THE ADSORBED LAYER AND PROPERTIES OF THE NETWORK STRUCTURE

J.P. COHEN-ADDAD
Laboratoire de Spectrométrie Physique associé au CNRS, Université Joseph
Fourier, Grenoble I, B.P. 87 - 38402 St Martin d'Hères Cedex, France

ABSTRACT

Properties specific to silica-siloxane mixtures are analysed and discus-
sed. The effect of polymer adsorption is interpreted from the Gaussian statis-
tics of chains : the amount of adsorbed polymer Qr is proportional to the
square root of the chain molecular weight. The kinetics of adsorption is des-
cribed as a process of surface saturation. It is discussed as a function of
the silica concentration. The effect of swelling of the mixtures is interpre-
ted within the statistical framework proposed by Flory for ordinary gels.

I. INTRODUCTION

This description deals with typical properties observed from siloxane
polymers filled with silica particles. The addition of the particulate filler
to poly(dimethylsiloxane) (PDMS) chains was achieved from a mechanical mi-
xing . The contact of the polymer melt with the surface of silica gives
rise to a process of adsorption through the formation of hydrogen-bonds.
Each hydrogen-bond is supposed to link one silanol group of the surface to
one oxygen atom of the skeleton of a PDMS chain. Several hydrogen-bonds can
be formed between the silica surface and one end-methylated chain. This un-
dergoes an uniform adsorption. An end-adsorption occurs when siloxane chains
are hydroxyl terminated, in this case a double hydrogen bond is established
between one chain-end and one silanol group of the surface.

Investigations concerning properties of silica-siloxane systems are de-
veloped according to three main topics.

i) The first one deals with the interface formed by monomeric units bound
to the silica surface. This interface must be characterized from the number
r_c of contact points of one chain with the surface. It is also characterized
from the distribution of positions of these contact points upon the surface
of particles. The number r_c contributes to the determination of the free en-
thalpy of adsorption of one chain.

ii) The second topic concerns the interphase formed by loops and tails.
The interphase determines the transition between the solid state of silica
particles and the liquid state of the polymer defined from siloxane chains
which are more freely because they are not adsorbed. The interphase must be
characterized from the distribution of lengths of loops. Coated particles
which are not bridged to one another govern the flow process of mixtures cha-
racterized by low silica concentrations.

iii) An infinite cluster is formed when the concentration of particles
is high enough and the polymer chains have an appropriate length. This infi-
nite cluster results from a percolation process. It behaves like a permanent
gel when all free chains have been removed from the initial mixture. It must
be characterized from an effect of swelling induced by a good solvent or
from an effect of uniaxial stretching.

II. THE INTERFACE

Fumed silica was bought from Degussa. Aggregates are made from elementa-
ry beads. The average diameter of one bead is about 140 Å. Therefore, the
ideal specific area is 200 $m^2 g^{-1}$. However, the real specific area A_T measu-
red from particles is 150 $m^2 g^{-1}$ (B.E.T.). The discrepancy corresponds to the

reduction of surface used to build aggregates or agglomerates. The estimate of the average number of silanol groups participating in the adsorption process is $\sigma_e^{-1} = 1.8 \times 10^{-2}$ $\text{\AA}^{-2}$. Silica particles have a fractal character investigated from neutron scattering [1]. The fractal exponent is $D = 1.9$.

II.1 - Average number of contact points

The average number of contact points of one chain with the silica surface can be determined from either of two experimental ways.

The first one corresponds to the measurement of the residual amount of polymer Q_r^ℓ left bound to silica after removing all free chains [2]. This quantity is measured as a function of the polymer molecular weight $\overline{Mn}$, at constant silica concentration C_{si}. The weight Q_r^ℓ is defined per unit mass of silica ; it is found to obey a linear dependence upon the square root of $\overline{Mn}$:

$$Q_r^\ell = \chi_a \, \overline{Mn}^{1/2} \tag{1}$$

with $\chi_a = 4 \times 10^{-3}$ $(g/mole)^{-1/2}$. This law holds for chain molecular weights ranging from $\overline{Mn} = 1800$ to $\overline{Mn} = 3600 \times 10^2 g\,mole^{-1}$. A simple analysis of this result is given by assuming that the average number of contact points of one chain is :

$$< r_c > = \epsilon a \sqrt{N} \tag{2}$$

N is the number of skeletal bonds and ϵa accounts for the effect of chain stiffness. Then,

$$\chi_a = \frac{A_T \sqrt{Mm}}{\epsilon a \, \sigma_e \, A \, (1 + \mu_a)} \tag{3}$$

A is the Avogadro number and μ_a accounts for an effect of bridging between particles ; Mm is the average molar weight of one skeletal bond. Values of ϵa and μ_a are close to one.

The other experimental way used to determine $< r_c >$ is the magnetic relaxation of protons linked to PDMS chains. The time dependence of the relaxation function of the transverse magnetization exhibits two well defined parts. The first one varies rapidly with time ; it is associated with protons linked to adsorbed monomeric units. Its amplitude is m_B. The second one shows evolution with time. It corresponds to monomeric units forming loops and tails ; its amplitude is m_f. The ratio $\tau_B = m_B/m_B + m_f$ gives the fraction of monomeric units frozen by the adsorption process. For one chain :

$$\tau_B = (1 + \mu_a) \gamma_\nu \, \epsilon a \, \sqrt{N} \, / N \tag{4}$$

on average ; γ_ν accounts for frozen neighbours of monomeric units linked to the surface. Another expression of τ_B is :

$$\tau_B = \frac{A_T \, Mm \, \gamma_\nu}{\sigma_e \, Q_r^\ell \, A} \tag{5}$$

The experimental value of the slope of the straight line describing τ_B as a linear function of $1/Q_r^{\ell}$ is 0.09. The experimental value of the slope $(1+\mu_a)$ $\epsilon a \gamma_\nu$ in formula (4) is 3.3 . Considering that $A_T = 150 \text{ m}^2\text{g}^{-1}$ and $Mm = 37$ g mole^{-1} and $\mu_a = 4\times10^{-3}$ then the estimate of $\epsilon a (1+\mu_a)$ is 0.75 while $\gamma_\nu \simeq 5..$

It is considered that the condition of adsorption illustrated by formula (2) is firmly established from experimental results.

II.2 - Law of adsorption

The formation of the adsorbed layer results from a full immersion of all particles in the polymer melt. Consequently, aggregates and agglomerates are rapidly surrounded by polymer chains. This adsorption process is very contrasted to that observed from particles in suspension in a polymer solution   . It is characterized by two main features.

i) The whole surface of silica is instantaneously in contact with PDMS chains.

ii) PDMS chains compete with one another to be adsorbed on the surface. Chains in a molten polymer are known to obey a Gaussian statistics ; any chain formed from N skeletal bonds is swollen by a number of other chains equal to $\sqrt{N}$, on average. Any time one chain is in contact with the surface, $\sqrt{N}$ other chains are also in contact with the same area of the surface.

The condition of adsorption $<r_c> = \epsilon a \sqrt{N}$ has been recently given a simple interpretation by assuming that any adsorbed polymer chain pictures the random flight of a fictitious particle colliding a plane [3]. Considering an area A_T of the silica surface, the number of chains of N skeletal bonds forming r_c contact points is :

$$\nu_c(r_c,N) = \sqrt{\frac{2}{\pi}} \left(\frac{A_T}{\epsilon_a^c \sigma_e (1+\mu_a)}\right) \frac{\epsilon_c}{N^{3/2}} e^{-r_e^2/2N} \tag{6}$$

Formula (6) is the simplified expression of a more complicated distribution function [4]. Then, the total number of adsorbed chains is :

$$\nu_T = \int \nu_c(r_c,N) \, dr_c$$

or

$$\nu_T = \frac{\sqrt{2/\pi} \, A_T}{\epsilon_a^c \sigma_e (1+\mu_a) \sqrt{N}} \tag{7}$$

this leads to formula (3) and (4) with $\epsilon_a = \epsilon_a^c \sqrt{\pi/2}$.

II.3 - Clusters of contact points

The description of the adsorption process of one chain relies not only on the determination of the number r_c of contact points with the surface of particles but also upon the way these points are spread on silica. Positions $\vec{R}_j$ ($j = 1, 2, \ldots r_c$ of these contact points form a cluster. The radius of gyration of one cluster can be defined in the usual way :

$$(\vec{R}_G)^2 = \sum_{i,j} |\vec{R}_i - \vec{R}_j|^2 / 2r_c^2 \tag{8}$$

The average of $(\vec{R}_G)^2$ over all adsorbed chains leads to the mean square size of one cluster :

$$\epsilon_c^2 = \langle (\vec{R}_G^2) \rangle \tag{9}$$

A correlation function $g(\rho)$ can also be defined to characterize the cluster representing the binding site of one chain ; $g(\rho)$ is the probability that a contact point a distance ρ apart from another contact point belongs to the same chain. Although the detailed expression of $g(\rho)$ is not known, yet, it obeys simple properties : $g(o) = 1$ and

$$\sum_\rho g(\rho) = \sqrt{8/\pi} \; \epsilon_a^c \sqrt{N} \tag{10}$$

The simplest guess about the distribution of contact points of one chain is to assumed that it represents a two-dimensional random flight. Considering, for the sake of simplicity, that the mean number of bonds in each loop is $\sqrt{N}/\epsilon a$, then the mean square step of the random flight is $\sqrt{N} \, b^2/\epsilon a$; consequently the mean area associated with the two-dimensional random flight is :

$$\sigma_a = \Pi \; \epsilon_c^2 = \Pi \langle r_c \rangle \sqrt{N} \, b^2/6\epsilon a$$
$$= \Pi \, N \, b^2/6 \tag{11}$$

b is the average length of one skeletal bonds ; the quantity σ_a must be compared with the area actually covered by one chain :

$$\sigma_c = \langle r_c \rangle \sigma_e = \epsilon a \, \sigma_e \sqrt{N}$$

Thus,

$$\sigma_a/\sigma_c = \Pi \sqrt{N} \, b^2/6\epsilon a \, \sigma_e \tag{12}$$

This result shows that about $\sqrt{N}$ chains are adsorbed upon the area $N \, b^2$, of the silica surface.

III. THE INTERPHASE

Properties of the interphase are determined by the structure of loops and tails, i.e. by the distribution of lengths of corresponding chain segments.

III.1 - Average thickness

Neglecting the effect of bridging of particles, due to polymer chains, the average thickness $\bar{e}$ of the adsorbed layer is estimated from the specific area A_T and the amount of polymer Q_r bound to silica :

$$\bar{e} = Q_r/A_T \, \rho \tag{13}$$

it must vary as the square root of the chain molecular weight.

III.2 - Structure of loops

By neglecting tails, loops can be described within the framework used in Section II.2. Thus, a given configuration of one adsorbed chain is characterized by r_c contact points i.e. r_c loops ; the multiplicity of a loop formed from n_j skeletal bonds is β_j $(j = 1, 2, \ldots L_c)$. The total number of dif-

ferent kinds of loops is L_c. Then :

$$\sum_{j=1}^{L_c} \beta_j = r_c \quad \text{and} \quad \sum_j n_j \beta_j = N.$$

The statistical weight of this configuration is :

$$\Omega(N,n_j,\beta_j;r_c) = \left(\frac{2}{\pi}\right)^{r_c/2} r_c! \prod_{j=1}^{L_c} 1/(\beta_j!(n_j)^{3\beta_j/2}) \tag{14}$$

with

$$\sum_{j=1}^{L_c} \Omega(N,n_j,\beta_j;r_c) = \Pi (N;r_c) \tag{15}$$

and

$$\Pi (N;r_c) = \sqrt{2/\pi} \; (r_c/N^{3/2}) \exp(-r_c^2/2N)$$

The distribution function (14) leads to the description of specific properties of the adsorbed layer such as the total number of loops longer than a given number n_c, for example.

The adsorbed layer plays a crucial role in the determination of viscoelastic properties of silica-siloxane mixtures. The degree of stiffness of loops controls the elasticity response of these systems.

IV. GEL BEHAVIOUR

An infinite cluster is formed through a percolation effect when the concentration of silica particles is high enough and polymer chains are not too short. For example, strong gels obtained from silica concentrations are higher than .09, .17 and .29 (w/w) when chain molecular weights are 3600×10^3, 1500×10^3 and 70×10^3 g/mole^{-1} , respectively.

The random lattice formed from silica aggregates behaves like a permanent gel after removing all free chains. The gel is permanent as long as the constraint applied to the mixture is weaker than a given threshold determined from the number of contact points and the lengths of loops. One of the most characteristic property of these permanent gels is the swelling effect observed in the presence of a good solvent. The maximum swelling ratio Qm depends upon the texture of loops connecting silica particles. The swelling ratio Qm is defined by dividing the volume of swollen polymer in the mixture by the volume of dry polymer. The volume of silica is not taken into consideration to calculate Qm. As it is well known from the simplest descriptions of the swelling effects of ordinary polymeric gels, an estimate of Qm is obtained by considering that the effect of osmotic pressure is in equilibrium with the effect of elasticity of chain segments. The main difficulty encountered in describing the swelling process of silica-siloxane mixtures concerns the determination of the length of active chain segments involved in the cohesion of the gel. A simple way used to overcome this difficulty is to consider that the number of active segments is equal to the total number of hydrogen bonds $\mu_H^o = A_T/\sigma_e$ formed on the silica surface ; while the average length of a segment is given by $Q_m/\rho_p\mu_H^o$, ρ_p is the pure polymer density . Then, according to the theory proposed by Flory, the swelling effect is well described from :

$$Q_m^{5/3} - Q_m/2 = Q_r^{\ell}/v_s\rho_p\mu_H^o \tag{16}$$

where v_s is the molecular volume of solvent. This description has been found to be in agreement with experimental by varying both Qr and the number of links between the silica surface and PDMS chains. This number is varied by treating the silica surface to prevent silanol groups from forming hydrogen bonds .

V. KINETICS OF ADSORPTION

The amount of polymer adsorbed on the silica surface is a time dependent function $Qr(t)$ until an equilibrium is reached. At the end of the mechanical mixing most part of the surface is covered by PDMS chains. The surface is nearly saturated by this initial amount of polymer hereafter called $Qr(o)$. However, chain segments defining loops may be too stretched because of the presence of constraints exerted during the mechanical mixing. The structure of the binding site of any given chain is supposed to vary with time until an equilibrium between retractive forces and hydrogen-bonds is obtained. This corresponds to the completion of the surface saturation. The description of the adsorption process relies upon two hypothesis. It is considered as resulting from a conventional diffusion process occuring in the presence of an absorbing screen . Also, it is supposed to obey an excluded surface effect : the adsorption process occurs on free parts of the surface, only. Then,

$$Qr(t) = Q_r^\ell - (Q_r^\ell - Qr(o))\exp -\sqrt{t/\theta} , \qquad (17)$$

typical values of θ are $10^2 - 10^3$ hours ; they depend upon the temperature of adsorption. End-hydroxylated chains are more rapidly adsorbed than end-methylated one [5]. The increase of the concentration of silica has been found to increase the rate of adsorption of PDMS chains. This experimental result has been given a simple interpretation. Considering long polymer chains, the addition of silica particles induces an effect of bridging between particles. The limit value of the amount of adsorbed polymer is expressed as :

$$Q_r^\ell (\mu_a) = Q_r^m (1+\mu_a) \qquad (18)$$

where Q_r^m corresponds to the maximum amount of polymer adsorbed on the surface, without any bridging effect. The parameter μ_a depends upon the concentration of silica. Then, it can be shown that the time constant θ is also a function of μ_a. More precisely :

$$\theta(\mu_a) = \theta/(1+\mu_a)^2 \qquad (19)$$

θ is measured in the absence of bridges between particles. The value of the ratio

$$\sqrt{\theta(\mu_a)} / Q_r^\ell(\mu_a)$$

has been estimated for three concentrations of silica : 3., 2.5 and 3.2 for C_{si} = .09, .17 and .29 w/w, respectively. The increase of the rate of adsorption upon addition of silica results mainly from the effect of bridging induced by polymer chains. The activation energy of adsorption corresponds to about 18 Kcal mole^{-1}.

VI. CONCLUSION

The mixing of silica particles to siloxane chains does not correspond to a simple addition of hard objects to a fluid medium. The elementary process of adsorption, is well localized by the formation of one hydrogen bond ; the corresponding energy of adsorption is hardly higher than the thermal energy, at room temperature. This process induces a polymer-silica interaction well appropriate to the determination of a broad range of properties of the mixtures. The fractal character of particles is also involved in the specific behaviour of this finely divided matter.

REFERENCES

(1) Schaefer, D.W., MRS Bulletin (1986), XIII, 22.

(2) Cohen-Addad, J.P., Roby, C. and Sauviat, M., Polymer (1985), 26, 1231.

(3) Cohen-Addad, J.P., Polymer (1989), 30, 1820.

(4) Feller, W. "An Introduction to Probability Theory and its Applications"(1968)

(5) Cohen-Addad, J.P., Huchot, P., Jost, P., Pouchelon, A., Polym.(1989),30,143.

THE EFFECT OF MASKED ISOCYANATES ON THE MECHANICAL PROPERTIES OF MY720/DDS EPOXY RESIN

N. RUNGSIMUNTAKUL, S.V. LONIKAR, R. E. FORNES*, AND R.D. GILBERT
North Carolina State University, Fiber and Polymer Science Program, and
*Physics Department, P. O. Box 8202, Raleigh, NC 27695-8202

ABSTRACT

The mechanical properties of epoxy resins and epoxy resin/graphite fiber composites are adversely affected by moisture absorption. Incorporation of masked isocyanates that unmask to release isocyanates in situ at the cure temperatures (150-177°C) reduce the equilibrium absorption up to ~70%. Dynamic mechanical analyses and stress-strain properties of epoxy resins containing masked isocyanates were examined to determine their effect on mechanical properties. The ultimate Tg of the epoxy is reduced by incorporation of masked isocyanate, but the actual Tg is comparable to the "as cured" Tg of the epoxy. The dynamic moduli up to the Tg are relatively unaffected. In a number of cases, the initial modulus, elongation at break and peak stress are equal or better than the unmodified resins.

INTRODUCTION

In structural and aerospace applications, epoxy resins are used as the matrices in fiber reinforced composites that have high strengths and moduli and are light weight. The adverse effect of moisture on mechanical properties is one major drawback of epoxy resins. Upon curing, the epoxy-amine systems generate hydrophilic groups such as hydroxyl, secondary and tertiary amine groups and residual oxirane and primary amine groups (and in some cases sulfone) that can interact with water. Water is also absorbed into the unoccupied volume of the cured epoxy resins. The sorbed water plasticizes the resins, lowers the glass transition temperature (Tg), causes swelling, induces stresses, chemical bond cleavage and debonding of the fiber-matrix interface. Enhanced craze initiation and crack propagation reduce the serviceability of composites. Attempts to reduce moisture absorption of epoxy have been reported by several workers. (See Fisher et al.[1], Hu et al. [2] and references therein.)

Fisher et al. [1] showed that the polar functional groups in cured tetraglycidyl-4,4'-diaminodiphenyl methane (TGDDM) - diaminodiphenyl sulfone (DDS) (73/27 wt%) thin films reacted with α, α, α-trifluoro-m-tolyl isocyanate (MTFPI) in dimethylsulfoxide (DMSO) at 70°C, and reported a 54 % reduction in moisture absorption. Hu et al. [2] obtained 75 and 69 % reductions in equilibrium water absorption by reacting the hydroxyl, amine, and epoxide functional groups of cured TGDDM-DDS epoxy thin film (20-50 μm thick) with pentafluorobenzoyl chloride and 2, 4-difluorophenyl isocyanate in N, N'-dimethylacetamide, respectively. The reactants were allowed to diffuse into

the resin films which had been previously swollen with solvent. This technique is not feasible with the thicker films ≥150 μm) because the films crack due to successive swelling.

The objectives of this study were to study the effect of masked isocyanates, incorporated into TGDDM-DDS epoxy prior to curing, on reduction in moisture absorption and on the mechanical properties of the epoxy and its composite. Dynamic mechanical analysis and tensile tests were employed.

EXPERIMENTAL

MY720 Araldite® Epoxy (primarily TGDDM) was placed into a mixing jar at 105-110°C. The calculated amount of DDS (27 wt%) was added slowly into the mechanically stirred TGDDM. The mixture was stirred until all the DDS was apparently dissolved. The prepolymer was degassed at 110°C for 30 min, cooled in a desiccator, removed and stored in nitrogen filled bags in a refrigerator at 5°C.

The masked isocyanates were synthesized according to procedures reported by Lonikar et al. [3] from cyclohexyl isocyanate, hexamethylene diisocyanate or phenyl isocyanate masked with alcohols, phenols or fluorinated phenols (Table 1). They were incorporated into the epoxy by slowly adding to the heated prepolymer (105-118°C) and stirred until completely dissolved.

Thin, bubble-free films with uniform thickness were prepared by curing the prepolymer between the extra smooth Teflon® sheets. The sample thickness was controlled by using a Mylar® film as a spacer (0.02cm thick). The samples were degassed at 110° C for 30-45 min and cured at 150°C for 1 h and 177°C for 5 h under a nitrogen atmosphere.

The graphite/epoxy composite samples were prepared by hand-winding graphite fiber tows around a 9cm x 5cm x 0.1cm Teflon® window to keep the graphite in place. The prepolymer was applied on both side of the tows and cured in the same manner as the resins.

Water absorption of the cured epoxies specimens immersed for 6 months was measured gravimetrically at 25°C. The dynamic mechanical analyses (DMA) were made with a Rheovibron Viscoelastometer DDV-II-C (Toyo Baldwin Co., Japan) equipped with a Autovibron automatic system (Imass, U.S.A.), at a frequency of 11 Hz and a heating rate of 2.5°C/min over the temperature range of -120 to 300°C. The Tg was defined by the temperature at the maximum of the loss tangent spectrum (α-transition). The tensile tests were performed using a Instron tensile tester at a speed of 5 mm/min (ASTM D 882) and a gauge length of 2.54 cm.

RESULTS AND DISCUSSION

DSC and IR verified that the masked isocyanates reacted with the epoxy [3]. No unreacted epoxides remained in the system following the cure at 177°C. The

DMA and reductions in water absorption are listed in Table 2. In general, significant reductions of water absorption were obtained. The highest reduction, 70%, was obtained with masked isocyanate #9.

A typical DMA spectrum of the "control" epoxy is shown in Figure 1a where the storage modulus (E') and the loss tangent (tan δ) are plotted as a function of temperature. The DMA results agree well with those previously reported [4]. There are 3 transitions in the tan δ spectrum: a γ- transition around -60°C, attributed to the crank shaft rotational motion of the glycidyl portion of the epoxy after reaction with curing agent [4,5]; an α-transition at 180-200°C or the "as cured Tg" associated with vitrification before the epoxides fully react; and an α-transition around 285°C or the ultimate Tg (Tg∞) associated with the fully crosslinked system. The average elastic modulus E' at 25°C is 2.16 x 10^{10} dynes/cm^2 (for a Length/Area (L/A) = 901 cm^{-1}) and is 1.71 x 10^{10} dynes/cm^2 (for LA= 702 cm^{-1}). L/A affects the modulus value: the higher the L/A the higher the apparent modulus [4] . Approximately the same L/A was used in order to compare the moduli of the "control" and the modified epoxies.

In general, the DMA spectra of the epoxies containing masked isocyanates have 2 transition peaks: a γ-transition around -60°C and an α-transition approximately 38 to 130°C lower than the Tg∞ of the "control" epoxy. The α-transition peak of most of the modified epoxies is broader and has a higher magnitude than that of the "control" epoxy. The broadening of the transition region on the tan δ spectrum can be attributed to a broader molecular weight distribution and a plasticizing effect of the masked isocyanate [6]. (The magnitude of tan δ is related to the distance between crosslinks, M_c, as well as the presence of plasticizers.) The increase in magnitude of tan δ_{max} with increasing M_c (or lower crosslink density) reflects the increasing ability of polymer to absorb energy as the molecular constraints are reduced; the greater separation of crosslinks permits greater mobility of chain segments [7]. The incorporation of the masked isocyanates #2, #7, #8, and #9 caused a higher magnitude of the tan δ peak. Therefore, the epoxies containing these masked isocyanates probably have a lower degree of crosslinking than the "control" epoxy. The epoxies containing masked isocyanates #5 and #10 have a lower magnitude of tan δ and a much broader peak. This may be due to a broad molecular weight distribution between crosslinks or to heterogeneous crosslinked structures. Since both masked isocyanates have low unmasking temperatures, they probably unmasked and reacted with TGDDM or DDS before all the DDS reacted with TGDDM.

The DMA spectrum of the epoxy containing 26 mole % of masked isocyanate #7 is shown in Figure 1b. The Tg∞ is about 177°C, and the E' is 2.35 x 10^{10} dynes/cm^2 (L/A = 1066 cm^{-1}). Masked isocyanate #7 unmasks at about 180°C. At this temperature, most of the TGDDM probably has reacted with DDS. The masked isocyanate #7 therefore reacts with the OH and NH groups on the epoxy rather than reacting with the TGDDM. The result is a more uniform M_c than the epoxy containing masked isocyanate #5, and the tan δ peak at transition is narrower. The Tg∞ is lower than the "control" epoxy, possibly because of the plasticization of the polymer network and the flexibility of the crosslinks involving hexamethylene groups of the diisocyanate. However, the room

Table 1   Masked isocyanates Data

No.	Isocyanate	Masking Agent	Melting Temp.(°C)	Unmasking Temp.(°C)
1	α,α,α-Trifluoro-o-tolyl isocyanate	Pentafluorophenol	73	-
2	Phenyl isocyanate	Phenol	125	130
3	Phenyl isocyanate	FC-10**	88	130
4	Hexamethylene diisocyanate	FC-10**	105	185
5	Hexamethylene diisocyanate	n-Butanol	88	120
6	Hexamethylene diisocyanate	Pentafluorophenol	169	170
7	Hexamethylene diisocyanate	Phenol	136	180
8	Cyclohexyl isocyanate	Phenol	137	130
9	Cyclohexyl isocyanate	Pentafluoro-thiophenol	148	130
10	Cyclohexyl isocyanate	2,4-Difluoro-benzylalcohol	83	120
11	Phenyl isocyanate	ATBN	-	-
12	Phenyl isocyanate	DDS	173	175

*   Solution unmasking temperature
**   FC-10 = $C_{7.5}F_{16}SO_2N(C_2H_5)CH_2CH_2OH$

Table 2   Ultimate glass transition temperatures, loss tangents, elastic moduli and reduction in water absorption of the "control" epoxy and epoxies containing masked isocyanates, and the Tg∞ of the composites

Masked Isocyanate Number	Mole (%)	Wt (%)	Resin Tg∞ (°C)*	tan δ max	E' at 25°C (x 10^{-10} dynes/cm^2)	% Reduction in water absorption	Composite Tg∞ (°C)*
Control	-	-	285****	0.48	2.16 1.71***	-	286
2	20	28	183	1.11	1.51***	40	187
5	20	22	247**	0.32	2.30 1.78***	17	226
7	26	29	177	0.80	2.35 2.09***	39	186
	49	44	155	0.93	1.83***	55	
8	20	28	192	0.99	2.15	45	186
9	20	37	169	1.04	2.10	70	171
10	20	33	246**	0.39	1.83	30	199
11	-	9	228	0.77	1.53	0	242
12	-	35	243	0.65	1.50	11	246

*   Temperature at which tan δ is maximum
**   Broad tan δ peak
***   Short autovibron sample (L/A $\leq$ 718 cm^{-1})
**** The "as-cured" Tg is ~180°C

Table 3   Tensile properties of "control" epoxy and epoxies containing masked isocyanates

Masked Iso-cyanate Number	Wt%	Peak stress $(\times 10^{-8}$ dynes/cm$^2)$	Change in Stress (%)	Peak Strain (%)	Change in Strain (%)	Initial Modulus $(\times 10^{-10}$ dynes/cm$^2)$	Change in Modulus (%)
Control-		6.5	-	8.2	-	1.6	-
2	28	6.7	+3	8.5	+4	1.7	+6
5	22	6.5	0	8.2	0	1.6	0
7	29	8.1	+25	8.4	+2	1.6	0
8	28	4.0	-38	4.7	-43	1.5	-6
9	37	3.5	-46	4.6	-44	1.7	+6
10	33	6.2	-5	8.2	0	1.6	0
11	9	4.6	-29	7.8	-5	1.2	-25
12	35	6.2	-5	10.2	+24	1.2	-25
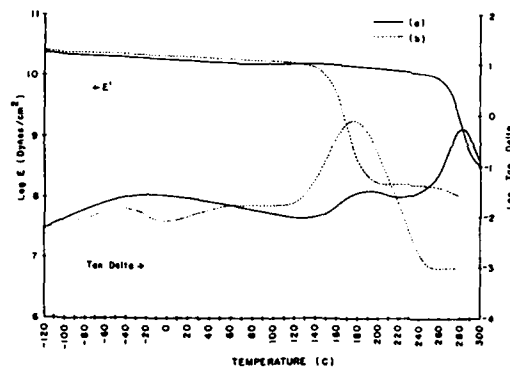
Figure 1   Dynamic mechanical spectra of (a) "control" epoxy (b) epoxy containing masked isocyanate #7
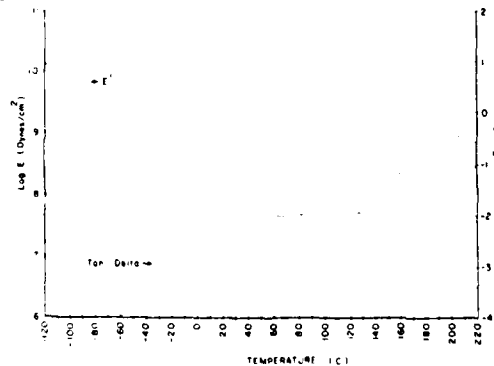
Figure 2   Dynamic mechanical spectra of a T300/epoxy composite containing masked isocyanate #7

temperature E's are higher than the "control" epoxy, possibly because of a reduction in the matrix free volume which would restrict the short-range motion of the matrix polymer chains [8-10].

The DMA spectra of T300/epoxy composites containing masked isocyanate #7 are shown in Figure 2. The $Tg\infty$, tan δ and E' of the composites are summarized in Table 2. The $Tg\infty$'s of most of the T300/epoxy containing masked isocyanates are about the same as the epoxy resins except for those containing masked isocyanates #5 and #10. The $Tg\infty$'s of the latter two are ~20°C lower than the Tg's of most the modified epoxies. The tan δ peaks of these two composites are narrower than those of the corresponding resins. The reason for this change is not clear.

The magnitudes of the tan δ peaks at the α-transition of all the composites are slightly lower than those of the corresponding resins. However, the magnitudes of the tan δ peaks of the composites containing masked isocyanates are higher than the "control" composite, which suggests that the former had a lower extent of cure.

The E' of all the composites found in this study are lower than those of the corresponding resins. This may be due to 1) low length/area ratio, 2) the composites were manually prepared and therefore they were non-uniform, and perhaps 3) poor adhesion of the epoxy to the fibers. Also, the E' of the modified composites should not be compared with the "control" composite because of difficulty in controlling the weight ratio of the graphite fiber to epoxy. However, from the DMA data of these hand-prepared composites, no major adverse effects are caused by the incorporation of the masked isocyanates on the interface between the fibers and the matrix.

The peak stresses, peak strains and initial moduli form tensile measurements of films of the modified epoxy resins are reported in Table 3. The typical stress-strain diagram of TGDDM-DDS epoxy reveals a yield point, which was also observed by Morgan [11]. The initial moduli of epoxy films containing masked isocyanates #2 and #9 were about 6% higher than the "control" epoxy. The initial modului obtained with the specimens having masked isocyanate #5, #7 and #10 incorporated were about the same as that of the "control" epoxy, but for the specimen containing masked isocyanate #8 was about 6% lower. The lowest moduli were obtained from epoxies containing 9 wt% of ATBN-PhNCO and 35% DDS-PhNCO (-25%). In general, the tensile moduli are in relative agreement with the DMA results.

Epoxies containing masked isocyanates #2 and #7 had higher peak stresses, peak strains and initial moduli than the "control" epoxy, and therefore higher toughness than the"control" epoxy. Epoxies containing masked isocyanates #5 and #10 had about the same peak stresses, peak strains and initial moduli as the "control" epoxy, or about the same toughness. Epoxies containing masked isocyanates #8, #9 and #11 had lower peak stresses and peak strains than the "control" epoxy. Epoxy containing #12 had a lower peak stress and initial modulus but higher peak strain than the "control" epoxy.

SUMMARY

The incorporation of a series of masked isocyanates into TGDDM-DDS epoxy results in specimens with properties: 1) with Tg's that are 38- 130°C lower than the Tg∞, but are about the same as the "as cured" Tg of the "control" epoxy, 2) with dynamic elastic moduli at room temperature up to the Tg and initial tensile moduli of the epoxies containing masked isocyanates that are generally about the same or higher than the "control" epoxy.

The DMA of T300 graphite fiber/epoxy composites (90°-orientation) made from epoxies containing masked isocyanates showed that the Tg's were about the same as the corresponding unfilled epoxies. There was no evidence of adverse effects of the masked isocyanates on the interfacial region.

REFERENCES

1. C.M. Fisher, R.D. Gilbert, R. E. Fornes, and J. D. Memory, J. Polym. Sci.: Polym. Chem. Ed., 23, 2931 (1985).
2. H.P. Hu, R. D. Gilbert, and R. E. Fornes, J. Polym. Sci., Part A, Polym. Chem. Ed., 25 (5), 1235 (1987).
3. S. V. Lonikar, N. Rungsimuntakul, R. D. Gilbert and R. E. Fornes, J. Polym. Sci., Polym. Chem. Ed., accepted for publication.
4. T. W. Wilson, R. E. Fornes, R. D. Gilbert, and J. D. Memory, J. Polym. Sci.: Part B: Polym. Phys., 26, 2029 (1988).
5. J. D. Keenan, Master Thesis, University of Washington, Seattle, 1979.
6. L. E. Nielsen, Mechanical Properties of Polymers and Composites, Vol. 2, Marcel Dekker Inc., New York, 1974.
7. T. Murayama and J. P. Bell, J. Polym. Sci., Part A-2, 8, 437 (1970).
8. N. Hata, R. Yamauchi and J. Kumanotani, J. Appl. Polym. Sci., 17, 2173 (1973).
9. N. Hata and J. Kumanotani, J. Appl. Polym. Sci., 21, 1257 (1977).
10. J. A. Sauer, J. Polym. Sci.,Part C: Polym. Symp., 32, 69 (1971).
11. R. J. Morgan, in "Advances in Polymer Science No. 72", K. Dusek, Ed., Springer-Verlag, New York, 1985, p.1.

A STUDY OF SHORT METAL FIBER REINFORCED COMPOSITE MATERIALS

W. C. Chung
Division of Technology, One Washington Square, San Jose State
University, San Jose, CA 95192-0061

ABSTRACT

Over the years, the conventional involvement of short
fiber reinforced composites in electrical applications has
been as electrical insulation. Contrary to this approach,
with the increasing need of better electromagnetic
interference (EMI), radio-frequency interference (RFI)
shielding and control of electrostatic charge distribution
(ESD) for computer, defense, space exploration and some
high-tech structural components, it is expected that the
development of conductive polymeric composite materials will
grow strongly and significantly.

An experimental investigation is designed to
systematically evaluate the mechanical properties and
electrical properties of metal fiber reinforced composites
subjected to various loading conditions. In this study,
chopped Inconel 601 (nickel base) metal fiber with a fixed
fiber aspect ratio (length/diameter ratio) is used to
reinforce commercially available thermoset polyester resin.
Mechanical testing of custom made samples, failure analyses
using visual inspection, light microscopy and SEM are
conducted to understand the fracture behaviors and possible
failure causes in such composites. The feasibility of using
metal fiber polymeric composites in structural/electrical
applications is discussed in this paper.

INTRODUCTION

Polymers have been well known for their electrical
insulating properties and great strides have been made in
electrical and electronic applications, mainly related to
electrical insulation. Consequently, research has been
directed to improve the dielectric strength of polymers so
that they can be used for better insulators. In the past few
years, with the advent of electrically conductive polymers,
their potential to perform as active roles in conducting
electricity has been discovered and realized (ref. 1). Recent
polymer researches have revealed that polymers can indeed
conduct electricity as well as metals. Now the electrically
conductive polymers can be used as antistatic coatings, fuel
cell catalysts, solar electrical cells, photoelectrodes in a
photogalvanic cell, protective coatings on electrodes in
photoelectro-chemical cells, and as light weight, inexpensive
batteries.

Due to the increasing need of light weight, low cost, moldable, and high specific strength for defense and high-tech applications, it is expected that the development of electrically conductive polymeric materials will grow rapidly. It is understood that conductive plastic housings and molded parts can be beneficial to the controls of electromagnetic interference (EMI), radio-frequency interference (RFI) shielding and electrostatic charge discharge (ESD) distribution. Advanced research studies have shown that there are three possible methods to make polymers conductive. The first approach is to apply a thin conductive coating onto the molded part. This approach, however, is costly and not efficient because of involving a two-step operation which increases the difficulties in obtaining a good adhesion as well as a uniform coating. The second approach is often held by synthesis or by doping (ref. 2-5). Synthesis is done by side reactions. One of the major side reactions involves the benzene ring. Other reactions lead to branched and cross-linked polymers. Doping involves oxidation and reduction reactions. This method, usually produces polymeric compounds such as polyacetylene and polyphenylene, although is proved to be effective and has been widely used, problems rise from conductive polymers themselves such as their processability, stability, mechanical and physical properties, etc. The last approach, proposed in this study, is to incorporate electrically conductive fillers in the polymeric resin matrix. Many conductive materials such as carbon, metals, metal-coated fillers in the form of powders, flakes, particles, particulates, and fibers can be randomly dispersed into a resin matrix and form a so-called "conductive composite." This approach so far appears to be a viable solution to the development of conductive polymers. Due to the lack of systematic research study in this area, material properties are hardly found in the application of such materials. Much research is urgently needed to fully understand the interrelationships among structure, property and processing prior to their commercial utilizations (ref. 1-6).

The conductive polymeric composite was first presented in 1966 by Garland (ref. 7). He used silver particles, approximately 50 to 200 microns in diameter, to reinforce a thermoset phenol-formaldehyde (Bakelite) resin matrix. His experimental data indicated that metal-filled polymers undergo a sharp transition from an insulator to a conductor at a critical volume concentration of metal fillers. In his study the electrical resistivity remained almost constant until the silver volume concentration of 38% is reached – then it droped drastically and the whole composite became an electrical conductor. Since Gurland's work, many other researchers have reported different sharp transition from insulators to conductors at different volume concentrations (ref. 8-15). Among their studies, Dearaujo and his co-investigator (ref. 10) had found that normally at least 40% volume fraction of metal fillers was needed in order to make a composite conductive.

Recently, because of short fiber reinforced composites can offer design flexibility, weight reduction, energy savings and high-volume production for structural applications, they are widely used in automotive, recreation, business machinery, electrical appliance, and military applications. Metal fiber reinforced composites become highly desirable to meet the aforementioned requirements not only for load-bearing capability but electrical conductivity as well, which normally metal particle reinforcement cannot achieve. However, not much work has been done in this area. Experimental data were found only limited to individual cases. Davenport (ref. 16) mentioned in his study that the metal fiber length (L) to diameter (D) ratio (known as aspect ratio) in a composite must have 100 or more in order to induce electrical conductivity. He demonstrated the electrical conductivity should be a function of L/D. In addition, the fiber packing density is a significant factor which is closely associated with the ratio of L/D (ref. 17). Bigg and stutz investigated a stainless steel fiber (8 microns in diameter, aspect ratio: 750) reinforced ABS system, and found that the composite had an electrical resistivity of 0.70 ohm-cm at the fiber volume concentration of 1% (ref. 18). They also claimed in their research that a highly conductive composite can be achieved with a low concentration of metal fibers by simply using high aspect ratio fibers. Their work, although seems very promising, yet needs to be proved. Most of the metal fiber reinforced composites were emphasizing on the electrical properties rather than the mechanical properties.

Nickel has long been considered as preferred metal because of its low electrical resistivity. In this study, Inconel 601 nickel based fiber with a dimeter of 8 microns and an aspect ratio of 125 was heavily used to reinforce a commercially available thermoset polyester resin. Composite samples were made in coupon shapes depending on the test requirements. Both mechanical and electrical measurements were further conducted to help understand the micromechanical behavior as well as electrical conductivity.

SPECIMEN PREPARATION AND TESTING

Chopped Inconel 601 metal fibers were donated by Bekaert Fiber Technologies. To prevent the sizing effect from the interfacial bonding between fiber and rein matrix, a thin water-soluble PVA (polyvinyl alcohol) coating originally attached to fibers was removed from Inconel fibers prior to the process. Fiber volume concentration, varied from 0% to 50%, was carefully controlled as material parameter to conduct this study. Metal fibers were completely mixed with appropriate amount of polyester resin and MEKP (Methyl Ehtyl Ketone Peroxide) curing agent in a chemical beaker based on a predetermined volume ratio. The mixure was then poured into an aluminum mold for cure. Traditional compression molding practice was employed in the curing process, pressure was around 17 psi (1.17 x 10³ Pa) and temperature was set at 356°F (180°C). Specimen dimensions were carefully prepared according to ASTM standard test methods.

RESULTS

Table 1. Tensile Test:

Fiber Ratio (v%)	Tensile Strength (MPa)	Young's modulus (Gpa)
0	55	23
5	50	23
10	41	23
15	42	25
20	44	23
25	51	26
30	47	25
35	43	29
40	38	29

Table 2. Impact & Flexure Tests:

Fiber Ratio (v%)	Impact Strength (J/m)	Flexural Strength (MPa)
0	17	65
5	17	68
10	18	66
15	18	68
20	21	70
25	19	71
30	22	71
35	25	71
40	23	72

Electrical Measurement:

Resistivity: 6.79 x 10-6 ohm-cm
Very high resistance at fiber ratios below 30%
Resistivity -- 1.0 ohm-cm at 45%

The tensile and flexure tests were performed in a screw-driven computer-asisted Satec testing machine. A testing speed of 0.1 in./min. (2.54 mm/min.) was used for tensile and flexure tests. The ASTM method D257 was also followed to measure the volume resistance of each sample. The test data were collected and discussed in the following sections.

RESULTS AND DISCUSSION

Tensile test data, as shown in Table 1, have demonstrated that fiber concentration can indeed increase the tensile strength of the composite. Young's modulus is also improved as well. It is interesting to note that the small fiber concentration at the ratio lower than 10 volume percent will not contribute to the increase of entire tensile strength. According to the study, fiber concentration at 25 % has the maximum UTS. It is found that fiber orientation along the pulling direction will have significant effect to tensile properties. Since the specimens are prepared through a casting process, the fiber orientation in all direction is assumed the equal. Impact test data (in Table 2) reveal that impact strength increases with the addition of metal fibers. However, there is a limitation set at 35%. Low fiber concentration impairs the impact strength of the composite. Optical microscopy indicates that because of the existing of metal fibers, small air bubbles are attached to fiber ends, which is believed to be responsible for the degraded impact strength. Three point (flexture) test data show that fiber fillers can improve the flexural strenth of the composite, as shown in Table 2. It is also noticed that metal fibers can dissipate some energy in a crack propagation. In other words, with the addition of metal fibers the crack pattern of a given composite shifted from a pure tension failure mode toward a more shear failure mode, which increases the flextural properties. Fiber pull-outs and fiber breakage are some evidence. In the electrical measurements, a critical fiber concentration is recorded. Electrical resistivity of 1.0 ohm-cm is measured at the fiber volume ratio of 45%, which is unexpected high. However, when fiber concentration falls below 30% the electrical resistance remains almost constant, that is the composite is an electrical insulator. In this study, metal fiber reinforced composites did undergo a sharp transition which is inconcert of Garland's work (ref. 7).

CONCLUSION

Because of excellent electrical conductors, metal fibers are suitable additives for inducing electrical conductivity in traditionally known insulators, polymer materials. Inconel metal fibers, although proved to be effective reinforcing elements, are considerably denser than expected.

It is found, during this study, that the explanation of the fracture behavior in a metal/polymer composite is often difficult to make, because it involves with many unseen factors such as stress concentration, orientation effect, viscoelastic behavior etc.. While significant progress has been made, much work still needs to be done. A systematic approch including experimental and theoretical techniques should be developed to help understand the micromechanisms and to elucide the interrelationships among structure, property and processing. Several factors such as fiber concentration, fiber aspect ratio, interface compatibility between fiber and marix can then be studied accordingly. The aforementioned suggestions, if applicable, may lead to a complete data bank setup which may eventually benefit all the designers, engineers, and scientists who are using conductive composites in their work.

ACKNOWLEDGEMENTS

REFERENCES

1. Kaner, R. B. and MacDiarmid, A. G., Plastics That Conduct Electricity, Sci. Amer., Feb. 1988, pp. 106.

2. Blythe, A. R., Electrical Properties of Polymers, Cambridge University Press, New York, 1979

3. Chidsey, C. and Murray, R. W., Electroactive Polymers and Macromolecular Electronics, Science, Jan. 3. 1986, pp. 25.

4. Davidson, T., Polymers in Electronics, American Chemical Society, Washington D. C., 1984.

5. Ferraro, T. R. and Williams, J. M., Introduction to synthetic Electrical Conductors. Academic Press, New York, 1987.

6. Skotheim, T. A., Handbook of Conducting Polymers, vol. 1 and 2. Marcel Dekker, New York, 1986.

7. Garland, J., Trans. Metall. Soc. AIME. 275, 1966, pp. 642.

8. Aharoni, S. M., Jour. Appl. Phys., 43, 1972, pp.2463.

9. Kusy, R. P. and Corneliussen, R. D., Polym. Eng. Sci., 15, 1975, pp. 107.

10. DeAraujo, F. T. and Rostenberg, H. M., Jour. Phys., Sec. D, Appl. Phys., 9, 1976, pp. 1025.

11. Nicodemo, L., et al., Polym. Eng. Sci., 18, 1978, pp. 293.

12. Shorokhova, V. I. and Kuzmin, L. L., Sov. Plast., 3, 1965, pp. 26.

13. Scheer, J. E. and Turner, D. J., Adv. Chem., 99, 1971.

14. Bigg, D. M., composites, 10, 1979, pp. 95.

15. Kwan, S. H., et al., Jour. Matl. Sci., 15, 1980, pp. 2978.

16. Davenport, D. E., Polym. Sci. Tech., 15, 1981, pp. 39.

17. Milewski, J. V., Ph.D. Thesis, Rutgers University, 1973.

18. Bigg, D. M. and Stutz, D. E., Polym. Comp., 4, 1983, pp.40.

19. Edwards, J. H. and Feast, W. J., Polymer, 327, 1984.

20. Reyonlds, J. R., Chemtech, July 1988.

21. Krieger, J., Chem. Eng. News, June 1987.

22. Cotts, D. B. and Reyes, Z., Elec. Conduc. Organ. Polym. dv. Appl., Noyes Data Corp., New Jersey, 1986.

Miscellaneous/Conventional Composites

DEFORMATION BEHAVIOR OF POLYMER GELS
IN ELECTRIC FIELD

Toshio Kurauchi, Tohru Shiga, Yoshiharu Hirose and Akane Okada
TOYOTA Central Research and Development Laboratories Inc.
41-1, Nagakute, Aichi, 480-11, JAPAN

ABSTRACT

The deformation of poly(acrylic acid)-co-(acrylamide) gels and poly(vinyl alcohol)-poly(acrylic acid) gels under an electric field was investigated. Bending of these ionic gels was induced by an electic field. Using this deformation, we constructed a prototype of a robot hand having soft fingers, and an artificial fish able to swim.

INTRODUCTION

A polymer gel is a crosslinked polymer network swollen in a liquid medium. Polymer gels, "solid-liquid coexistant materials", are candidate "biomimetic materials". Recently, their mechanical strength becomes very close to living muscle. In a soft structure of gels, a motion of polymer network and a diffusion of ions take place easily by an external stimulus. Therefore, polymer gels have various possibilities as advanced functional polymers.

A typical function of a gel containing ionic groups is to bend reversibly under the influence of an electric field[1], making it useful in some actuators driven by an electric field. In this paper, deformation of the gels under an electric field is presented.

DEFORMATION OF POLYMER GELS UNDER AN ELECTRIC FIELD

Acrylic acid-acrylamide copolymer gels (PAAm gels) swollen in aqueous electrolyte solution show three types of deformation under the influence of a d.c. electric field ; shrinking, swelling and bending, as shown in Fig.1.[2] The type of deformation depends on the fraction of sodium acrylate (AANa) in the PAAm gel, the shape of the PAAm gel and the position of the gel between the positive and the negative electrodes. A PAAm gel with a low fraction of AANa shrinks on the surface facing to the positive electrode (Fig.1(a)) and a gel with a high fraction of AANa swells on the positive electrode side (Fig. 1(b)). When a rectangular gel is placed parallel to the electrodes, bending of the gel takes place toward the positive electrode (Fig.1(c)) or toward the negative electrode (Fig.1(d)), according to the fraction of AANa. The critical fraction of AANa is about 25mol%. This bending behavior is similar to the buckling of a bimetallic strip submitted to a variation of temperature. Because we observed the bending deformation with gels having different ionic groups, such as SO_3Na and NR_4Cl, the phenomenon is considered to be a general property of ionic
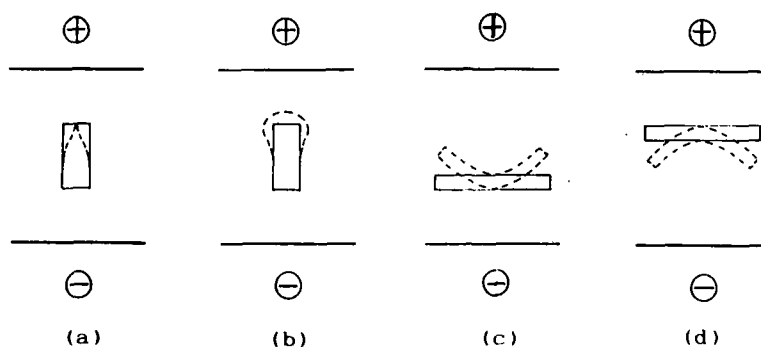
Fig.1 Deformations of PAAm gels under d.c. electric field.
(a) and (c):for small fraction of AAna
(b) and (d):for large fraction of AAna

gels. Of course the direction of the bending is inversed, when
the sign of the ionic groups is changed.

BENDING OF PAAm GELS WITH HIGH FRACTION OF AANa

In Fig.2, the weight gain of a PAAm gel (rectangular bar :
8×8×80mm) is plotted as a function of the strain in bending.
When the PAAm gel bends semicircular, the strain in bending is
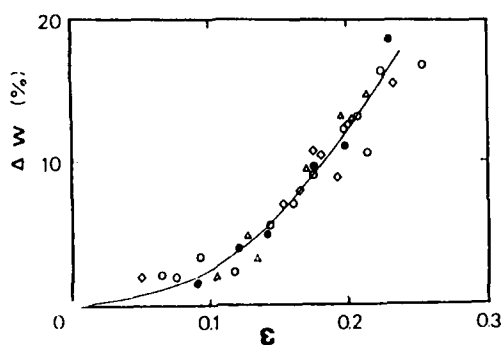
Fig.2 Weight gain of PAAm
gels plotted as a
function of strain
in bending.
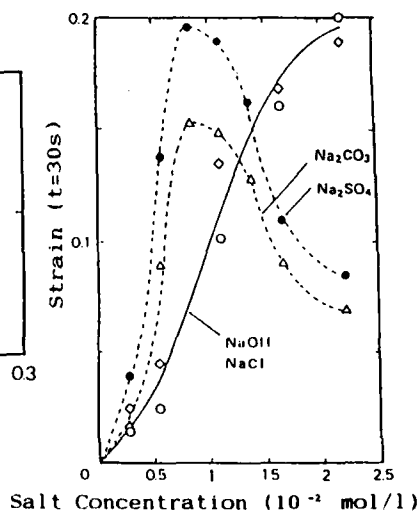
Fig.3 Bending speed plotted
as a function of salt
concentration.
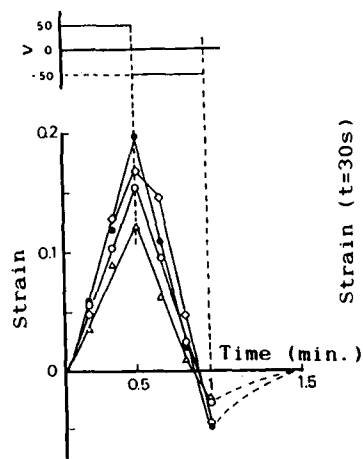
Fig.4 Time dependence of
the strain when the
polarity of the
applying voltage
is changed suddenly.
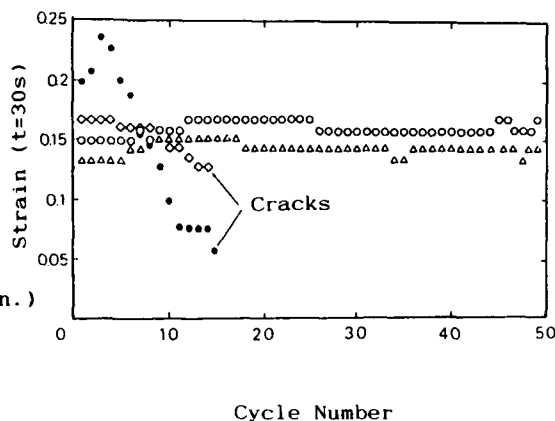
Fig.5 Fatigue-rupture.

In Figs.4 and 5, symbols
show (O):NaOH, (●):Na₂SO₄,
(◇):NaCl and (△):Na₂CO₃ .

0.225. At that time, a weight gain of 15% was observed, as
shown in Fig.2.

The bending speed of the PAAm gel depends on three factors.
The bending speed is proportional to the field strength and the
concentration of -COO⁻ in the gel. The speed is plotted as a
function of salt concentration outside the gel in Fig.3, where
the strain after 30 seconds from the beginning of d.c. supply
of 50V is taken as the vertical axis. There is a maximum in the
bending speed, and the salt concentration giving the maximum
depends on the valence of the ions.

By the change of polarity (+50V , -50V), the strain can be
recovered as shown in Fig.4. This suggests that it can be bent
repeatedly by an a.c.electric field.

The number of cycles to "fatigue-rupture" depends on the
kind of electrolytes in the solution. In basic electrolyte
solutions, such as NaOH and Na₂CO₃ , the bending speed of PAAm
gel is constant up to 50 cycles. In neutral salt solutions,
such as NaCl and Na₂SO₄ , the speed slows gradually, as shown in
Fig.5. Some cracks occur on the surface of the gel after 14 or
15 cycles.

BENDING MECHANISM

The volume of a gel is controlled by osmotic pressure¹¹. The
osmotic pressure ¥ is given as the sum of ¥₁ , ¥₂ and ¥₃ which
correspond to the osmotic pressure due to the solubility of the
solvent in the polymer chain, rubber elasticity and ion
concentration difference between the inside and the outside of
the gel, respectively¹¹.

$$\pi = - (\ln(1-v) + v + \chi v^2) RT / V_1$$
$$+ (v^{1/3} - v/2) RT \nu_e / V_0 + (\Sigma C_i - \Sigma C_f) RT$$

where v is the volume fraction of the polymer network, χ is the solubility parameter, V_0 is the volume of the polymer network under the dry condition, ν_e is the number of chains, V_1 is the molar volume of the solvent, C_i and C_f are the ion concentrations inside and outside of the gel, respectively, R is the gas constant and T is the temperature.

At equilibrium, the osmotic pressure π of the gel is equal to that of the surrounding aqueous solution, π_0. Then, π_1, π_2 and π_3 have the definite values, respectively. When a d.c. electric field is applied on the gel in the aqueous solution, the counter ion and the free ion can drift to the positive or the negative electrode, whereas the polyion can not move. Then, π_3 varies and the value of π deviates from π_0. The swelling or the shrinking of the gel occurs until the gel reaches its new equilibrium state. Since the ions drift at the different speeds, depending on their size and valencey, the osmotic pressure of the positive side is unequal to that of the negative side, and bending of the gel occurs.

PVA-PAA GEL

Although PAAm gels bend like a finger under an electric field, because they contain 99% water, their mechanical strength is so weak that they break easily. It is necessary to improve the mechanical properties of the polymer gels, to apply them as actuators.

A PVA-PAA (poly(vinyl alcohol)-poly(acric acid)) gel is prepared as follows ; poly(vinyl alcohol) saponified over 95% and poly(acric acid) were desolved in a mixed solvent of water and DMSO. The pregel solution was frozen and thawed repeatedly. The resultant gel, which turns white at this point, was

crystalline
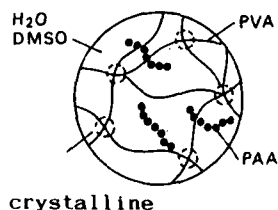
Fig.6 Conceptional
picture of
PVA-PAA gel.
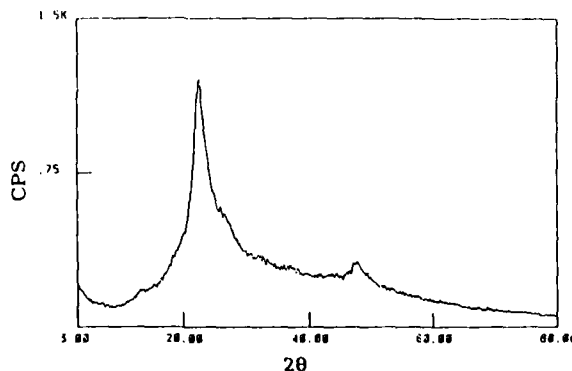
Fig.7 Diffracted X-ray from the dry
PVA-PAA gel.
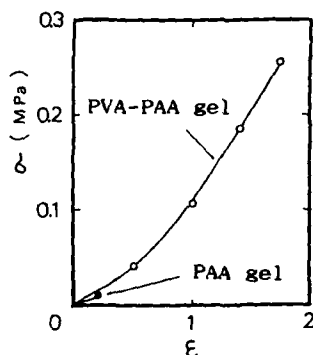
Fig.8 Tensile stress-
strain curves.
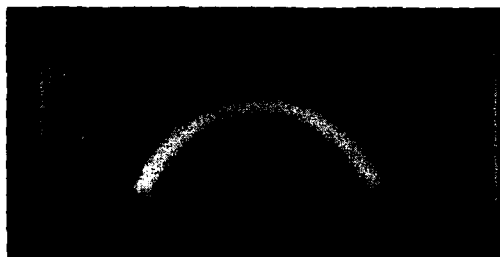
Fig.9 Bending of the
PVA-PAA gel.

immersed in a NaOH aqueous solution for a long time in order to
dissociate the carboxyl groups.

The PVA-PAA gel obtained contains 90% water. Polymers in
this PVA-PAA gel may form an interpenetrated polymer network,
as shown in Fig.6. The X-ray diffraction profile from a dry gel
is shown in Fig.7.

Fig.8 shows the stress - strain curve of the PVA-PAA gel in
a tensile test. The tensile strength and the elongation to the
rupture of the PVA-PAA gel are more than 50 times as large as
those of the PAAm gel, and are close to those of rubber
vulcanizates. The PVA-PAA gel appeared to possess high shear
strength and toughness.

The PVA-PAA gel bends toward the negative side under a d.c.
electric field, as shown in Fig.9. The bending speed of the
PVA-PAA gel is almost equal to that of the PAAm gel.

POLYMER GEL ACTUATOR

Fig.10 shows a robot hand with four gel fingers composed of
a PVA-PAA gel. The each gel is rectangular bar whose sizes are
60mm in length and 6×7mm in cross section. To bend the gel, a
pair of electrodes is located near the gel. The positive
electrode is fixed with a spacer apart from the gel. The
negative electrode is embeded on the surface of the other side
of the gel. The robot hand can pick up a fragile egg in safety
in a Na₂CO₃ solution by applying an electric field of 50V.

Fig.11 shows an artificial fish composed of a plastic plate
as a float and a PVA-PAA gel as a tail (30mm in length, 10mm in
width and 1mm in thickness). In Na₂CO₃ solution with electrodes
set on each side, the fish swims by waving the tail as the
polarity of the electric field (50V) is changed alternately.
The swimming speed is about 2cm/s.

We demonstrated that a body can be transfered by mechanical
deformation of polymeric material. This exhibits a new type of
functionality of a polymeric material.

394

Fig.10 Robot hand.
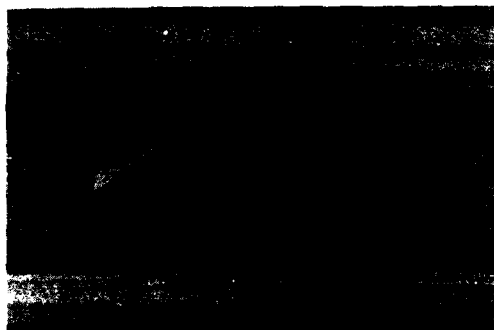
Fig.11 Artificial fish.

CONCLUSION

The mechanical response of the PAAm and the PVA-PAA gels upon the electric field was examined experimentally. The gels can be bent by appling a d.c. electric field across the gels. The deflection of the gel is considered to occur due to the drift of ions under the influence of the applied electric field. Using this deformation, we constructed a prototype of a robot hand having soft fingers, and an artificial fish having a soft tail, both driven by the electric field. The next subjects are to realize the more rapid response of the gel and to increase the modulus in order to increase a work to the external.

References

1. T. Shiga and T. Kurauchi, Japanese Polymer Preprints, 36, 2894 (1987).
2. T. Tanaka, Science 218, 467 (1982).
3. P.J. Flory, Principles of Polymer Chemistry, (Cornell Univ. Press, Ithaca, 1953).
4. I. Ohmine and T. Tanaka, J. Chem. Phys., 77, 5725 (1982).

BIAXIAL EXTRUSION OF POLYIMIDE LARC-TPI AND LARC-TPI BLENDS

R. ROSS HAGHIGHAT*, LUCY ELANDJIAN, AND RICHARD W. LUSIGNEA
*Foster Miller, Inc., 350 Second Avenue, Waltham, MA 02254

ABSTRACT

Biaxial films of polyimide LARC-TPI and LARC-TPI/liquid crystal polymer Xydar® were extruded directly from the melt for the first time via an innovative new extrusion technique. Three types of films, neat LARC-TPI, LARC-TPI/10 wt percent and 30 wt percent blends were processed as a part of this NASA funded program. This new process offers an alternative technique to costly post-processing stretching of both solution cast and sheet extruded films. The post-processing step is often required to enhance certain properties. Processability was greatly enhanced by incorporating Xydar. The coefficient of thermal expansion was reduced from 34 ppm/$^\circ$C for the neat LARC-TPI to 15 ppm/$^\circ$C for the 10 wt percent Xydar blend and ultimately down to 1 to 3 ppm/$^\circ$C for the 30 wt percent blend films in the direction of extrusion. The maximum improvement in stiffness was realized by incorporating 10 wt percent Xydar (2.8 GPa up to 4.9 GPa). Tensile strength, however, experienced a drop as a result of Xydar addition, probably caused by inefficient mixing of the two phases.

INTRODUCTION

Today's growing demand for high temperature, high performance, and low coefficient of thermal expansion (CTE) polymers requires the development of new polymeric systems and novel processing techniques [1]. One such polymeric system drawing much recent attention is the polyimide [2].

In our study, polyimide LARC-TPI (Figure 1) developed by NASA was processed both in the neat form and with additives into biaxial films by melt extrusion. To our knowledge, this marks the first time a polyimide has been melt extruded directly from the fully imidized powder into biaxial films. Our film processing made use of an innovative extrusion technique which imparts biaxial orientation in the films during processing, rendering post-processing orientation unneccessary. Post-processing stretching is an often required step for property enhancement. Through this innovative processing, films with a variety of orientations from near uniaxial to balanced biaxial can be extruded in a one-step process without the shortfalls of other competing film processing techniques.

Fiber reinforced polymer composites have been shown to considerably improve the engineering performance of various polymers and have found

LARC-TPI
Thermoplastic Polyimide
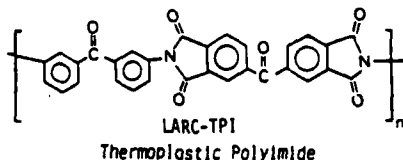
Figure 1. Chemical Composition of LARC-TPI

numerous applications in aircraft, automotive, and marine industries. The traditional inorganic filaments such as glass and graphite are consistently challenged by newly developed high modulus and high strength polymeric systems. Examples of such systems include polyaramide (Kevlar®), and more recently thermotropic liquid crystalline polymers (LCP). LCPs can be processed in the melt state and are capable of forming highly oriented crystalline structures when subjected to shear above their melting point [3]. Their rod-like molecular conformation and stiff backbone chains allow the LCPs to form fibrous chains. Examples of LCPs include Xydar and Vectra® manufactured by Ammoco and Hoechst Celanese, respectively.

Experimental

LARC-TPI is produced under a licensing agreement with NASA by Rogers Corporation of USA, and Mitsui Toatsu Chemical of Japan. Both manufacturers produce polyamic acid solutions for film casting and fully imidized powders for injection molding. Mitsui Toatsu also manufactures LARC-TPI 1500 extrusion grade polyimide which exhibits a modestly lower melt viscosity than the injection molding grade LARC-TPI 1000 and is thermally more stable. Mitsui LARC-TPI 1500 was the only grade of LARC-TPI successfully extruded into films both in the neat and the blend forms.

Thermotropic liquid crystal polymers (LCP), Xydar, and Vectra were considered as additives to LARC-TPI. Their presence is thought to (a) enhance processability of LARC-TPI by reducing the melt viscosity; (b) create a fibrous network which in itself gives rise to a self-reinforcing mechanism in the composite similar to fiber reinforced composites; (c) contribute to molecular order within the composite causing a rise in the stiffness and resulting in a decrease in the coefficient of thermal expansion (CTE) due to restricted movement of the molecular chains.

The LCP selection process included considering compatibility in the following areas: temperature, rheology, and particle size. Xydar was the most suitable candidate LCP available for use in this study. In all, the following types of films were successfully biaxially extruded:

* Neat LARC-TPI
* LARC-TPI/10 Xydar
* LARC-TPI/30 Xydar

The individual powders were seperately dried in an N_2-purged oven at $120^{\circ}C$ for 12 hours followed by dry mixing of the two components and redrying under the same conditions prior to extrusion.

Extrusion was carried out with a specially designed laboratory scale blown-film apparatus. Using this extruder, biaxially oriented polymeric films were formed by adjusting a series of easily controllable variables such as shear rate, feed rate and take-up speed. Orientation here refers to controlling the direction of the polymer chain molecules to tailor properties in the plane of the film. Visual inspection of the transparent films revealed preferred biaxial orientation. Angular orientation was verified by both optical microscopy and by manually measuring the molecular chain orientation with respect to the machine direction.

Results

Table 1 summarizes the studied properties of the extruded films. Comparing the tensile strength values of the near uniaxial and the ±24 deg films, the

effect of orientation becomes clear. The tensile strength of the near uniaxial film of neat LARC-TPI was 28 percent higher than the ±24 deg film (126 MPa compared to 98 MPa). This property improvement was more pronounced with increasing Xydar content (45 percent increase at 10 wt percent Xydar and 60 percent at 30 wt fraction). The stiffness also followed a similar trend. Figure 2 plots the stiffness versus wt fraction LCP. A higher than expected increase in stiffness was seen at 10 wt percent Xydar. Although we are currently studying the mechanism giving rise to this phenomenon, it is possible that 10 wt fraction is the loading level at which the Xydar fibril network is most efficiently oriented under shear.

Table 1. Properties of Extruded LARC-TPI and LARC-TPI/Xydar Blends

Film	Tensile Strength MPa		Stiffness GPa		CTE ppm/$^{\circ}$C
	MD*	TD**	MD	TD	MD
Neat LARC-TPI ±24 deg orient.	98	104	2.8	2.8	34
Neat LARC-TPI near uniaxial	126	–	2.6	–	28
LARC-TPI/10% Xydar ±24 deg orient.	80	52	2.1	2.3	16-18
LARC-TPI/10% Xydar near uniaxial	113	83	4.8	2.7	14
LARC-TPI/30% Xydar ±24 deg orient.	63	–	2.0	–	5-7
LARC-TPI/30% Xydar near uniaxial	108	–	3.3	–	1-3

*Machine direction
**Transverse direction
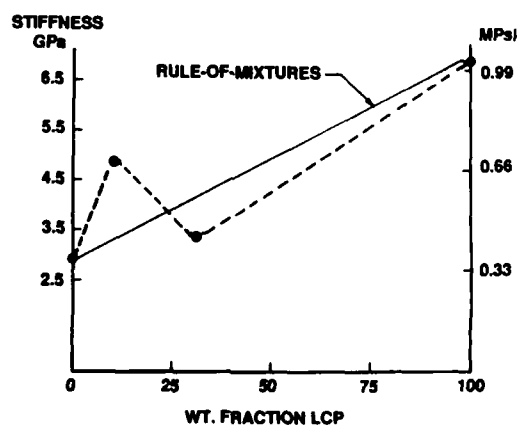
Figure 2. Stiffness versus Wt Percent LCP

Figure 3 is a plot of the CTE versus wt fraction LCP for the near uniaxial extruded films. Addition of even small amounts of Xydar dramatically decreased the CTE. At 10 wt percent, the CTE was reduced by greater than 55 percent. The results suggest that the Xydar addition alters the mechanism and probably substantially hinders molecular chain movement within the extruded films. Further work is underway in this area which will address these initial findings.

Figures 4 and 5 are photomicrographs of tensile failed films of the neat and the 30 percent Xydar, respectively. The morphologies, as suggested by the micrographs, are noticeably different. The failure mechanism, as suggested by the micrographs, was matrix failure followed by fiber failure. There is evidence of fiber pull-out to support this theory.

CONCLUSIONS

Through a novel process, we successfully extruded biaxial films of LARC-TPI polyimide and blends of LARC-TPI with the LCP Xydar. To our knowledge this is the first time a thermoplastic polyimide has been extruded directly from the melt into biaxial films. This simple one-step process presents an alternate means of producing high performance polyimide films in high volumes and cost-effectively. It eliminates the often neccessary post-processing film stretching to enhance certain properties. It also eliminates the often toxic devolatilization of solvents associated with casting operations.

We have shown that through LCP blending the tensile modulus can be increased. LCP incorporation also lowered the expansion coefficient (CTE) from 34 ppm/$^\circ$C in the neat film down to 1 to 3 ppm/$^\circ$C at 30 wt percent Xydar loading.
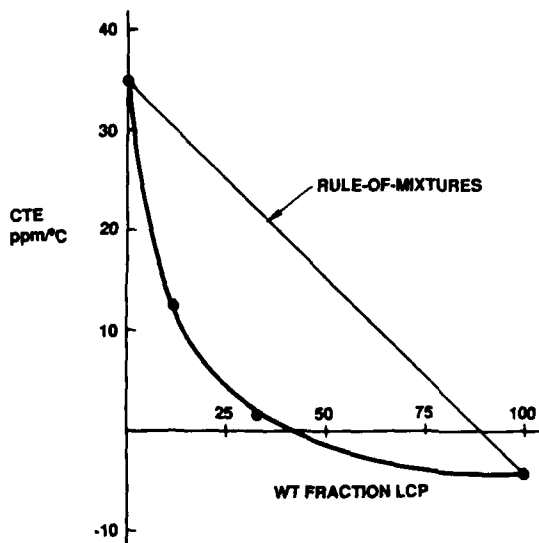
Figure 3. Coefficient of Thermal Expansion versus Wt Fraction LCP

Work is currently underway on parallel programs to further study polyimides. We seek to better understand their processing parameters and means of enhancing their properties.
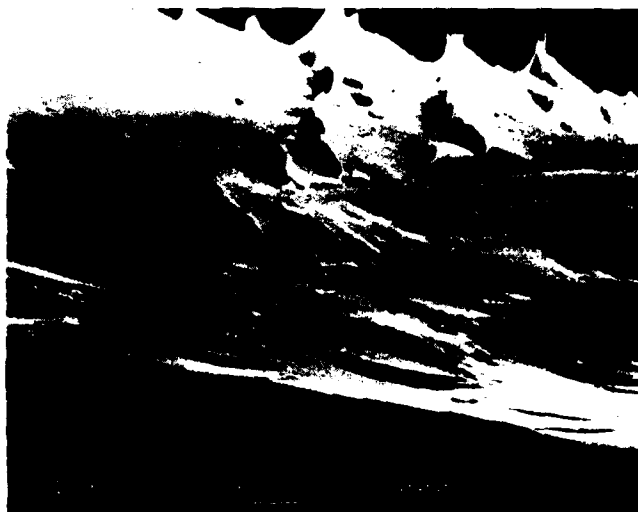
Figure 4. SEM Micrograph of Biaxially Extruded Neat LARC-TPI
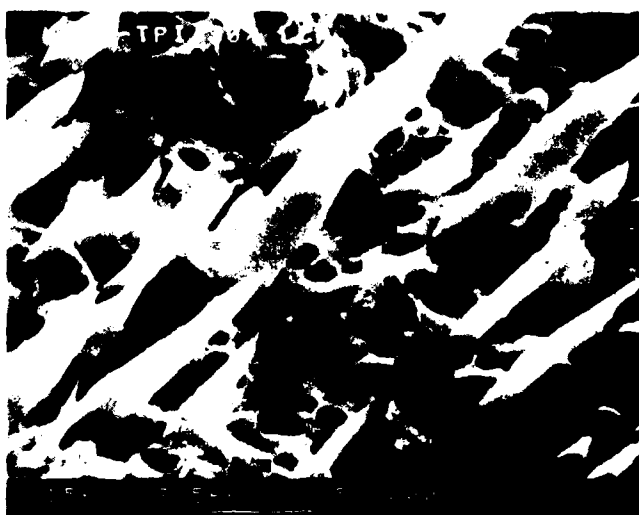
Figure 5. SEM Micrograph of Biaxially Extruded
LARC-TPI/30 percent Xydar Blend Film

400

REFERENCES

1. Walker, C.C., Proceedings Second International Conference on Polymides, pp. 429 (1985).

2. Sherman, D.C., et al., "Neat Resin and Composite Properties of Durimid High Temperature Thermoplastic Polyimides," Proceedings of the 33rd International SAMPE Symposium, March 1988.

3. "How Well Do Various Blends of LCP and Nylon 12 Work?", Plastics Engineering, pp. 39-41, October 1987.

ACKNOLWEDGEMENT

STRUCTURAL STUDIES OF SEMIFLEXIBLE FLUOROCARBON CHAINS CONTAINING AN AROMATIC CORE

A. SCHULTE, V. M. HALLMARK, R. TWIEG, K. SONG AND J. F. RABOLT
IBM Research Division, Almaden Research Center, San Jose, CA 95120-6099

ABSTRACT

The molecular structure of a series of perfluoroalkane oligomers having two $F(CF_2)_n$ chains attached to a phenyl group in the para position has been studied by Fourier Transform and conventional Raman spectroscopy at ambient and low temperatures. From comparison with model compounds bands attributable to both the substituted phenyl ring and the perfluoroalkane chains could be assigned. In particular, the low frequency region was investigated as a function of temperature and pressure in order to assess the impact of the rigid aromatic core on the bandshapes and frequencies.

1. INTRODUCTION

The use of fluorocarbon oligomers as model systems to study semiflexible polymers is well established [1,2,3] and has provided a significant insight into the role of backbone conformation on chain stiffness. In addition to perfluorocarbon oligomers a series of diblock [4,5] and triblock [6] semifluorinated alkanes have been synthesized and their crystal and conformational structure studied extensively. Of particular interest in the triblock series was the effect of a semiflexible hydrocarbon center block on the frequency and intensity of the low frequency Raman active longitudinal acoustic mode (LAM). Results indicate that at room temperature the center block participates, with the fluorocarbon end blocks, in the accordion-like motion characteristic of LAM. Above the melting point, on the other hand, the disordered hydrocarbon segment serves as a weak coupling spring perturbing the LAM frequency of each end block.

It is the purpose of the present study to replace the semiflexible hydrocarbon block with a rigid aromatic core and then assess its effect on both the intensity and frequency of LAM.

2. EXPERIMENTAL METHODS

The p-bisperfluoroalkylbenzenes were prepared by copper mediated condensation of the appropriate perfluoroalkyl iodide with p-diiodobenzene in dimethylsulfoxide. The purification of the crude products was accomplished by multiple recrystallization from acetic acid.

Differential scanning calorimetry (DSC) measurements were performed on a Du Pont 910 DSC with a 1090 controller. A scanning rate of 10 °C /min was used.

Scanning Raman measurements were recorded by using a Jobin Yvon HG 2S double monochromator configured for photon counting and interfaced to a Nicolet 1180 data system. Variable temperature studies were carried out in a vertical Harney Miller cell. The sample temperature was maintained constant to within ± 3 °C.

Raman experiments on samples under pressure were performed in the backscattering geometry using a Waspalloy diamond anvil cell with metal gaskets. The pressure was determined in situ from the peak position of a ruby fluorescence line with an error of ± 1 kBar.

Fourier transform Raman spectra were collected with a Bomem DA3.02 interferometer using a thermoelectrically cooled InGaAs detector [7]. The excitation source was a Spectron Model SL50 cw Nd:YAG laser.

3. RESULTS AND DISCUSSION

Thermal analysis. DSC curves of the semifluorinated phenyl triblocks (FnPhFn) show strong melting endotherms between 60 and 180 °C , as shown in Fig. 1.
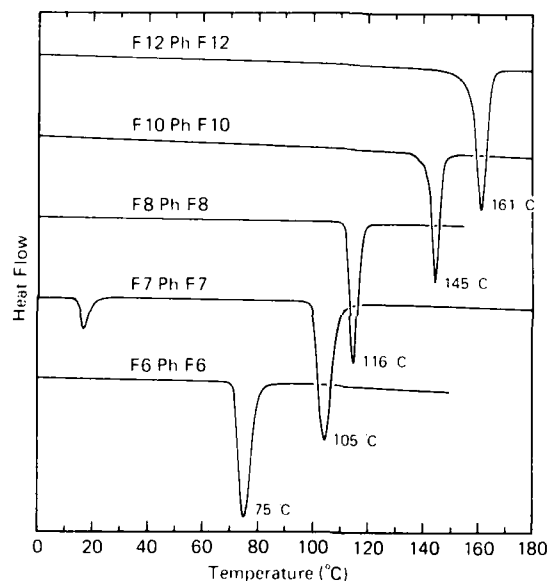
Fig. 1 DSC thermograms of some semifluorinated n alkanes scanned at a rate of 10 °C /min. Temperatures refer to the peak positions.

The melting temperature increases with the length of the fluorocarbon chains in a way similar to the perfluoro alkanes. However, the compound F7PhF7 exhibits an anomalously higher melting temperature and its DSC curve is typified by a weaker endotherm around 17 °C , characteristic of a solid-solid phase transition.

The heats of fusion increase continuously with the length of the fluoroalkane chain, from 31 $\frac{kJ}{mol}$ (F6PhF6) to 60 $\frac{kJ}{mol}$ (F12PhF12).

Raman measurements. In Figure 2, the Raman spectra of three semifluorinated phenyl triblocks are compared with those of perfluoro-n-alkanes having the same chain lengths.
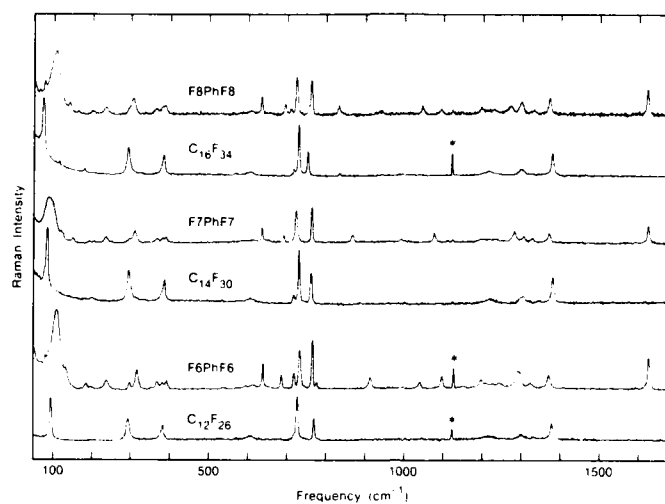
Fig. 2 Unpolarized Raman spectra (50 - 1700 cm^{-1}) of p-bisperfluoroalkylbenzenes and perfluoro-n-alkanes. The asterisk denotes a spurious emission line due to the room light.

Fig. 3 Raman spectra of p-bisperfluoroalkylbenzenes recorded with Fourier transform spectrometer. A resolution of 4 cm^{-1} was used with a laser power of 700 mW at 1.064 μm.
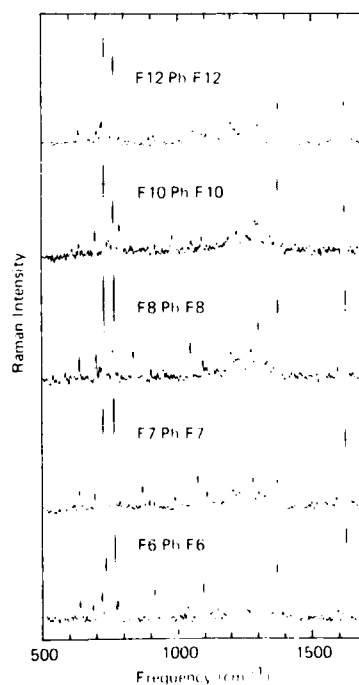
Most clearly, a new band due to the $C = C$ stretch of the phenyl ring occurs around 1625 cm^{-1}. In addition, there are bands due to the ring at 1095, 695 and 635 cm^{-1}, which are not present in the perfluoroalkanes and do not shift with the chain length. This conclusion is emphasized by the spectra in Fig. 3 measured with Fourier transform Raman spectroscopy. This technique uses excitation in the near infrared and allows the Raman spectrum to be obtained in the absence of fluorescence. In this way the Raman spectra of all the FnPhFn compounds synthesized, which displayed varying amounts of fluorescence could be measured. As above, bands attributable to the phenyl ring can be recognized. The sharp bands in the 700 - 750 cm^{-1} region and the smaller ones between 300 and 350 cm^{-1} are assigned to various $-CF_n$ modes. In the region from 800 to 1100 cm^{-1} a number of bands whose frequencies change with chain length can be seen. For instance, the band at 915 cm^{-1} shifts to 788 cm^{-1} when going from F6PhF6 to F10PhF10. These bands can be used to plot out portions of dispersion curves for the polymer [1].

The low frequency spectra (below 200 cm^{-1}) are in the case of the perfluoroalkanes dominated by an intense sharp band with a peak frequency varying inversely with chain length. It has been assigned to the Raman-active longitudinal acoustic mode (LAM-1). On the other hand, the low frequency spectra of the FnPhFn oligo. show an intense but rather broad band, without a systematic correlation with the ch. .ength. This band may be attributable to a lattice mode involving librations of the phenyl ring. Thus the insertion of the ring into the fluorocarbon chain seems to have perturbed the vibrational normal mode structure enough to remove or diminish the LAM mode intensity.

Previous studies [6] on triblock semifluorinated n-alkanes have shown that no decoupling of the chain vibration occurs at the juncture between helical and planar zigzag conformations. In addition, there was reasonable agreement between the observed LAM values and those calculated with the skeletal and point mass approximations [6,8]. Preliminary normal mode calculations were performed along these lines to investigate the effect of a rigid core on the LAM in phenyl triblocks with semifluorinated n-alkane chains. The results indicate that the geometrical change has a significant effect on the LAM frequency and intensity, though it may not decouple LAM vibrations over the entire chain.

Temperature and Pressure Studies. Decreasing the temperature produces only expected changes in vibrational linewidths in the frequency region above 150 cm^{-1} (Fig. 4). By far the largest change occurs in the very intense low frequency band for the compound F7PhF7. When lowering the temperature from 22 °C to -71 °C the peak position is shifted by about 30 cm^{-1} to higher wavenumbers. Also the width of the band becomes narrower, which is consistent with a restriction of the ring motion.

F7PhF7 is the only compound of the series exhibiting a rather substantial change in the Raman spectrum as well as a thermal transition below room temperature. Therefore it appears to be in a different phase at room temperature than its even chain length analogs, perhaps due to a different crystal structure or to different conformation of the fluorocarbon chains.

Naively one would expect that similar changes as upon cooling occur when applying pressure, since in both cases the packing increases. The Raman spectrum of F7PhF7 recorded at various pressure (Fig. 5) shows two major effects on the intense low frequency band. At a pressure near 4 kBar the band narrows and moves to lower frequency, suggesting a restriction of the ring libration. Above 9 kBar a new band at 625 cm^{-1} appears [9], which has been assigned to the planar zigzag form of fluorocarbon chains. This indicates that the fluorocarbon portion of the molecules have undergone
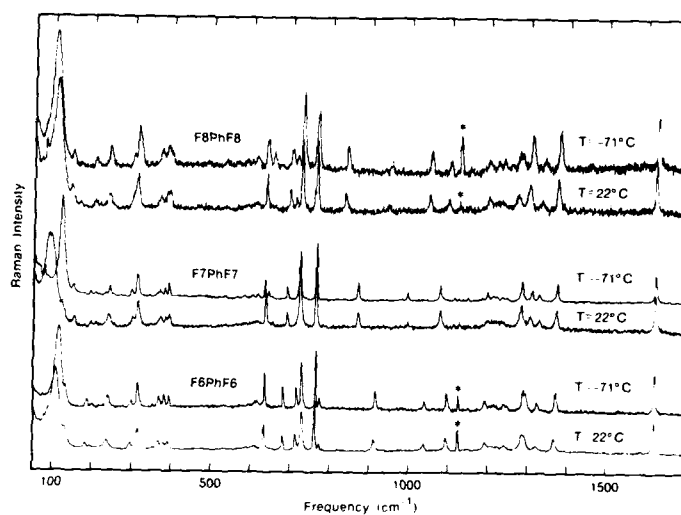
Fig. 4 Raman spectra (50 - 1700 cm^{-1}) of FnPhFn at ambient and low temperatures. The asterisk denotes a spurious emission line due to the room light.
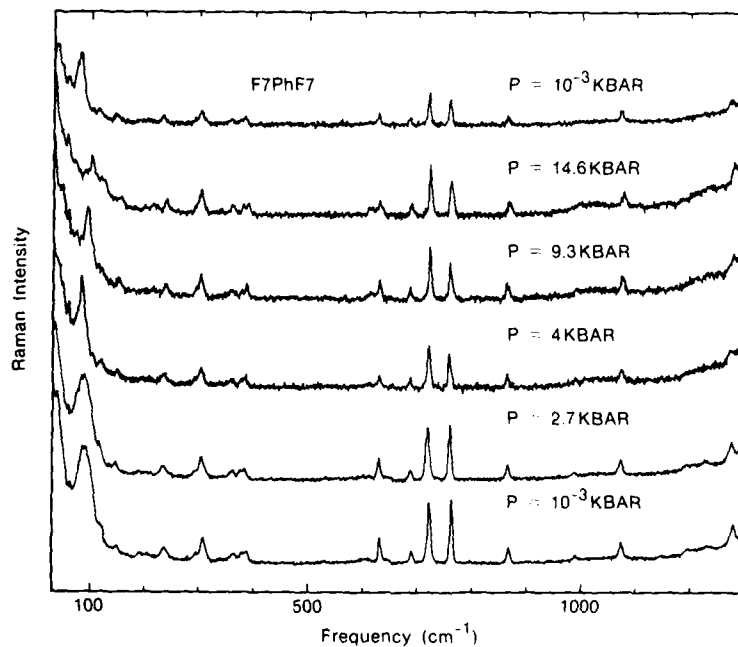
Fig. 5 Raman spectra (20 - 1300 cm^{-1}) of FnPhFn as a function of pressure. The upper spectrum was taken after releasing the pressure.

a conformational change. Correspondingly the low frequency band broadens again and shifts up in frequency, as the lattice mode changes in response to the new molecular packing of the fluorocarbon chains.

4. CONCLUSIONS

The molecular structure of a series of semifluorinated alkane chains containing a rigid core have been characterized by Raman spectroscopy in the visible and in the near infrared. Vibrational bands due to the phenyl ring and the alkane chains have been identified. The low frequency spectrum is dominated by a broad band, which we attribute to a lattice mode involving ring libration. This band undergoes large frequency and bandwidth changes as a function of temperature, particularly for the case of F7PhF7 which exhibits a solid-solid phase transition. Although preliminary normal mode calculations indicate that insertion of a ring into the fluorocarbon chain does not necessarily decouple LAM vibrations over the entire chain, significant perturbations in the LAM position and intensity are possible. This may account for the fact that no band attributable to LAM is observed for these compounds.

REFERENCES

1. J. F. Rabolt and B. Fanconi, Macromolecules **11**, 740 (1978).
2. G. Masetti, F. Cabassi, G. Morelli, G. Zerbi, Macromolecules **6**, 700 (1973).
3. M. J. Hannon, F. J. Boerio, J. L. Koenig, J. Chem. Phys. **50**, 2829 (1969).
4. R. Twieg and J. F. Rabolt, J. Polym. Sci., Polym. Phys. Ed. **21**, 901 (1983).
5. G. Minoni and G. Zerbi, J. Polym. Sci., Polym. Lett. Ed. **22**, 533 (1984).
6. R. Twieg and J. F. Rabolt, Macromolecules **21**, 1806 (1988).
7. C. G. Zimba, V. M. Hallmark, J. D. Swalen, J. F. Rabolt, Appl. Spectr. **41**, 721 (1987).
8. T. Shimanouchi, M. Tasumi, Indian J. Pure Appl. Phys. **9**, 958 (1971).
9. C. K. Wu and M. Nicol, Chem. Phys. Lett., **21**, 153 (1973).

THE EFFECT OF LOW POWER AMMONIA AND NITROGEN PLASMAS ON CARBON FIBRE SURFACES

**C.JONES AND *E.SAMMANN
National Centre for Composite Materials Research, University of Illinois, Urbana, Ill.61801;*Materials Research Laboratory, University of Illinois.(**Now at Liverpool University, England)

ABSTRACT

The effect of low power nitrogen and ammonia plasmas on carbon fibre surfaces has been studied using X-ray photoelectron spectroscopy(XPS) and scanning electron microscopy (SEM). A comparison is made between two polyacrylonitrile based fibres and a pitch based fibre. Grazing angle techniques have been exploited to probe only the first 12-15A of the fibre surface. Plasma treatments were carried out in an insitu plasma treatment cell which was attached to a PHI 5400 X-ray photoelectron spectrometer enabling the immediate effects of the plasma to be studied before the treated surface was exposed to air.

INTRODUCTION

The properties of composite materials are not only governed by the properties of the individual components but also by the interface between them. Successful reinforcement of composite materials is only achieved by obtaining sufficient stress transfer between fibre and matrix. This can be realised by physical and/or chemical adhesion between the two. However, for recent applications an extremely strong interface is not always desirable. It would be ideal to be able to design the interfacial properties to suit a particular application for example increase stiffness or promote toughness at the interface. One method of achieving this would be to chemically graft a monomer with a suitable backbone onto the fibre surface. It would also be necessary for this monomer to be fully compatible with the resin. An ideal example would be another epoxy with the desired backbone. Some of the most common curing agents for epoxy resins are amines. These allow curing of the resin at room temperature. It would therefore seem beneficial to introduce amines onto the fibre surface which would certainly have the potential to react with the epoxy coating at room temperature. The effect of ammonia plasmas on fibre reinforcement has been examined by several research groups[1-5], however, a thorough understanding of the chemical changes induced on fibre surfaces and whether or not they play a a role in fibre resin adhesion is yet to be determined.

A method of selectively introducing amines onto the surface would be a great advantage. Introducing the desired fibre surface chemistry without destroying the mechanical properties of the fibre itself would also prove very useful. Most of the plasma treatments used to date however, remove a substantial amount of material causing pits to form in the fibre surface [e.g.2,3]. This has led the authors to develop a low power plasma (<1W) treatment which only alters the chemistry of the immediate surface layers without causing severe etching of the fibre[6]. In this paper we report the selective introduction of C/N functionality onto three types of carbon fibre.

EXPERIMENTAL

The fibres used in this study included untreated and unsized T300 fibres (supplied by Amoco Performance Products) and HMU fibres (supplied by Hercules). Sized but untreated pitch based fibres from Amoco, thoroughly washed to remove any sizing, were also examined.

Plasma treatments were carried out in an *in situ* plasma chamber attached to a PHI 5400 X-ray photoelectron spectrometer. A half wavelength helical resonator was formed from a 100- turn coil wound directly on the outside of the tube and centred within a

shield made from 3" diameter brass tubing. A simple self-excited two transistor oscillator delivered radio energy to the centre of the helix at resonant frequency (approx. 15MHz). Low power levels (<1W) were sufficient to sustain a plasma within the tube. Continuous gas flow was maintained from a leak valve at one end of the tube to a butterfly valve at the other, which opened to a turbo molecular pump. The pressure within the cell was kept constant at 0.1Torr during plasma treatment. A more detailed description of the cell is given elsewhere[6]. This enabled the immediate effect of the plasma on the fibre surfaces to be studied before being exposed to air. The fibre samples were electrically isolated from the supporting rod, using a piece of mica sheet, allowing a controlled bias, with respect to the grounded supporting rod, to be applied to the fibres independent of the RF power exciting the plasma. Fibre surfaces were examined using X-ray photoelectron spectroscopy before and after treatment. The spectra were collected at grazing angles to enhance the signal from the immediate surface layers of the fibre[7]. The binding energies reported in this paper have been reference to the main graphitic peak in the carbon 1s spectrum which is given as 284.3eV and all intensity ratios have incorporated the relative sensitivities calculated for a hemispherical analyser (C1s 0.296, N1s 0.477, and O1s 0.711) [8]. The nitrogen 1s spectra were curve fitted using a Gaussian/ Lorentzian peaks shape in a non linear least squares curve fitting program [8].

Scanning electron micrographs were obtained with a Hitachi S800 microscope. With its field emission gun magnifications of 100-300 thousand could be achieved.

RESULTS AND DISCUSSION

Fig.1 shows the spectra obtained from fibres exposed to an ammonia plasma for 60 seconds. This is the first time that C/N functional groups have been observed with out the presences of oxygen containing groups. Widescan spectra (Fig.1a) taken at both bulk and surface sensitive angle indicate that the nitrogen containing functionality introduced is predominantly within the first 12-15Å of the fibre surface. The N:C ratio did not change with exposure time to the plasma and the difference between that obtained from surface and bulk sensitive data remained. This indicates that the reaction remains on the surface of the fibre and does not proceed deeper within the graphite layers as electrochemical reactions [7]. Significant etching of the fibre surface was not observed in the SEM micrographs suggesting that saturation of surface sites has taken place.

The nitrogen 1s spectrum reveals that the plasma introduces three type of nitrogen containing species onto the fibre surface. Signals at binding energies 398.9eV, 400.4eV and 402.8eV were observed. The two main signals are very similar to those produced on electrochemically treating the fibres in ammonium salt electrolyte [9]. However, in this case peak assignment to amide functionality is invalid since an oxygen 1s signal was not detected. The binding energy of $PhNH_2$ has previously been reported as 399.1eV [10]. The relaxation energy associated with the ejection of a photoelectron is far greater for a graphitic like lattice than that obtained from a benzene ring [11,12] and hence a shift of -0.2eV from that observed with $PhNH_2$ is not unlikely for amines groups on carbon fibre surfaces. -C=NH groups could also give rise to a signal around 398.8eV. The signal at 400.4eV arises from aliphatic amine functionality. The peak at highest binding energy is most probably due to a positively charged ammonium species similar to that observed by Chang and Navalov [13]. Cyano (-C≡N) were not detected. These groups are unlikely to remain on the fibre surface as they would be prone to electron assisted desorption.

All the chemically shifted shifted signal intensity seen in the surface sensitive carbon 1s spectrum (Fig.1c) is due to C/N functionality. The chemical shift for $-C-NH_2$ is expected to be around 1.3-1.5eV from the main peak. -C=NH would lead to a chemically shifted signal between 2.2 and 2.5eV from the main peak. There is certainly a large amount of signal intensity in both these region confirming the nitrogen 1s data.The signal intensity around 6eV from the main peak is due in part to a $\pi-\pi*$ shakeup satellite.

Nitrogen plasma treatments yielded very similar results to those obtained from
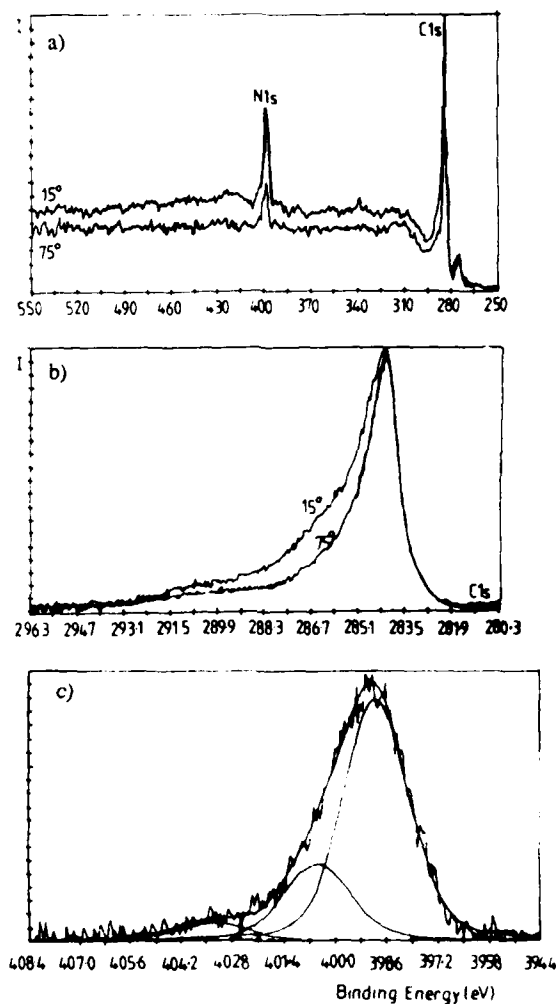
Figure 1. XPS Spectra From T300 Carbon Fibres Treated With An Ammonia Plasma For 5 Minutes a) Widescan, b) Carbon 1s, and c) Nitrogen 1s (curve fitted)

fibres exposed to an ammonia plasma. However, the nitrogen plasmas were unable to remove all the C/O from the fibre surface and the amount of nitrogen containing groups was slightly less than those obtained from ammonia plasma treatment. The nitrogen 1s spectrum obtained from these fibres consisted of three signal at identical binding energies as those described above but with a different relative ratio. The relative intensity of the signal at 398.9eV was less for fibres treated in a nitrogen plasma. The hydrogen contained within these functional groups is thought to arise from the external surface of the fibres in the form of C-H.
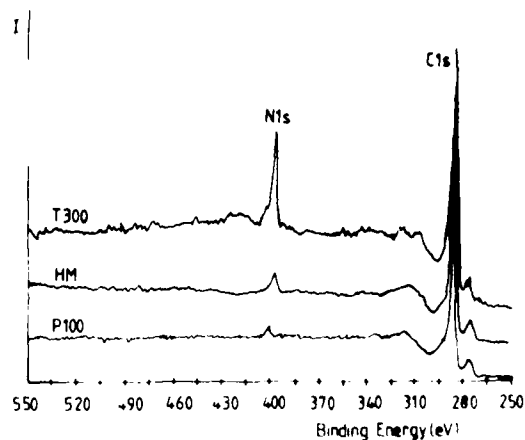
Figure 2. Widescan XPS Spectra of Three Different Types of Carbon Fibres Treated With An Ammonia Plasma

Fig.2 shows widescan spectra (taken at a take off angle of 15°-surface sensitive angle) from three different types of fibres after exposure to an ammonia plasma for 5 minutes. Each fibre has behaved differently to the plasma, the lower modulus PAN based fibre being the most reactive. The main structural elements of carbon fibre surfaces are graphitic plates or crystallites which are roughly aligned along the fibre axis. Their size and degree of alignment increase with increasing graphitization temperature during processing. The P100 fibres have a very similar structure to that of highly orientated pyrolytic graphite yet the crystallites on the PAN-based T300 surfaces (the fibres being graphitized at a much lower temperature) are much smaller and less aligned and hence the number of edge sites an defects is far greater in the latter case. (The HM fibres have a surface structure in between the two.)The lack of reactivity shown by the pitch based fibres compared to the T300 fibres tends to indicate that chemical change has only occurred on the edge sites (and defects) and not on the basal planes. As the percentage of edge sites increases, so does the amount of "nitrogen" incorporated onto the fibre surface during treatment.

This lack of reactivity of the higher modulus fibres is undesirable since the aim of the treatment was to introduce amine groups in sufficient concentration to promote chemical bonding between the fibre and resin. The method suggested by Stoller and Allred [1] was to pretreat the fibres in an argon plasma for approximately 10 seconds prior to ammonia plasma exposure. This resulted in a 30% increase in the amount of amine functionality incorporated onto polyaramid fibres. In our case, the number of nitrogen containing groups did increase on the higher modulus fibres with Ar pretreatments but only by a very small amount. This is due to the lack of sputtering taking place in these low power plasmas. Pretreatments in an air plasma were also performed in a hope that the oxygen functionality on the surface would be substituted by nitrogen containing groups. In these cases, most of the C/O groups were removed and only a very small number of nitrogen containing species incorporated.

A more successful method of increasing the number of amine groups introduced was to accelerate ions from the plasma to increase their impact energy on the fibre surfaces. This was done by biasing the fibre samples to a negative potential with respect to a ground electrode within the plasma. Fig.3 shows the widescan spectra of HMU
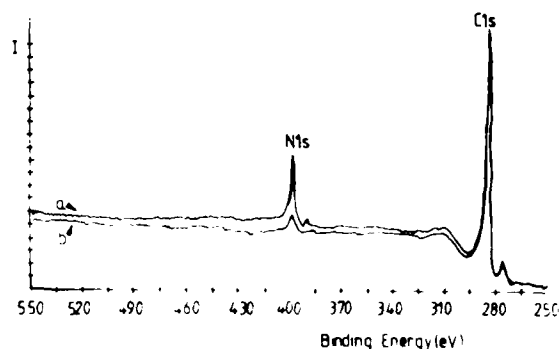
Figure 3. Widescan XPS Spectra Of HMU Fibres Treated In An Ammonia Plasma a)With
And b) Without Bias During Treatment.

fibres that have been exposed to an ammonia plasma with and without sample biasing.
The N:C ratio has increased from 0.07 to 0.18 on applying the sample bias and is
approaching that of lower modulus fibre (0.22). A increase in chemically shifted species is
also observed in the carbon 1s spectrum of these treated fibres. The nitrogen 1s spectra of
these treated fibres is very similar to the lower modulus fibres in that three species are
detected at 398.9eV, 400.3eV and 402.8eV. Their relative intensity ratios are very similar
to the unbiased lower modulus fibres for both nitrogen and ammonia plasma exposures. A
similar result was obtained for nitrogen plasma treatments. Examination of SEM
micrographs from these treated samples reveals that little damage has been done to the
fibre surface. Although there was an increase in the amount of nitrogen functionality
incorporated onto pitch fibres by biasing the fibres during treatment (N:C 0.01 to 0.05),
the overall number of nitrogen containing species remained very small compared to the
PAN based fibre and will be expected to have little effect on the interfacial shear strength
of the composites.
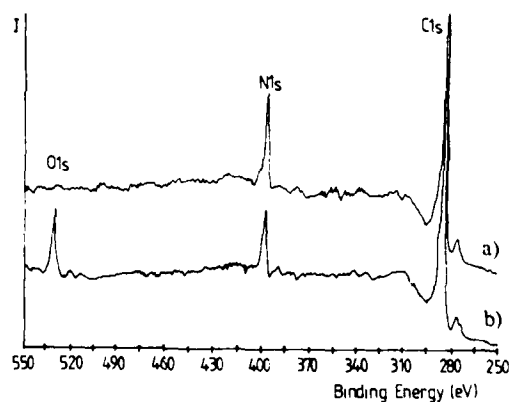
Figure 4. Widescan XPS Spectra Of T300 Carbon Fibres Treated In An Ammonia Plasma
a)Before, And b) After Exposure To Air.

Exposure To Air

Fig.4 shows the widescan spectra of fibres treated with an ammonia plasma before and after exposure to air. There is a significant pickup of oxygen upon air exposure. However, no change in the carbon 1s or nitrogen 1s spectra is detected e.g. evidence of -COH or -NO signal intensity, suggesting that oxidation has not taken place. It was concluded that this oxygen pickup was due to a strongly bound physisorbed layer. The oxygen 1s spectrum consisted of a single species with binding energy 532.4eV which is characteristic of a strongly bound -OH species and in this case most probably arises from moisture in the air. The amount of 'oxygen' pickup was directly related to the number of C/N functional groups introduced onto the fibre during surface treatment. This physisorbed layer would certainly inhibit the desired fibre/epoxy chemical bonding in composites. Both Loh [4] and Evans [14] tried to compare the effects of ammonia plasma on structurally different carbon surfaces. Unfortunately, in both cases their samples were exposed to air before chemical analysis was carried out.

4.CONCLUSIONS

Both ammonia and nitrogen plasma were successful in introducing amine functionality onto carbon fibre surfaces. The reactivity of a fibre to a plasma was shown to depend largely on the structure of its surface. Reactivity increased along the series P100-HM-T300. The number of nitrogen containing groups was dramatically increased by biasing the HM fibres to a negative voltage (10-30V). This increase occurred for both ammonia and nitrogen plasmas. Exposure of the treated fibres to air resulted in a strongly physisorbed layer onto the fibre surface most probably arising from moisture in the environment. This may inhibit any desired reaction between fibre and resin during composite processing. It is therefore suggested that treated fibres be immersed into resin or a suitable coating material prior to exposure to air.

REFERENCES

1. H.M.Stoller and R.E.Allred, *Proc. of 18th Internat. SAMPE Tech.Conf.*, 993 (1986).
2. J.B.Donnet, M.Brendle, T.L.Dhami and O.P.Bahl, *Carbon*, 24, No.6, 757 (1986)
3. Sun Mujin, Hu Baorong, Wu Yisheng, Tang Ying, Huang Weiqui and Da Youxian, *Composites Science and Technology*, 34, 353 (1989)
4. I.H.Loh, R.E.Cohen, and R.F.Baddour, *J.Mat.Sci.*, 22, No.8, 2937 (1987).
5.`` J.C.Goan, US Patent 3,776,820 Dec.4 1973 assigned to the Great Lakes Corporation.
6. C.Jones and E.Sammann, in press, Carbon (1989).
7. C.Jones, *Carbon*, 27, No.3, 487 (1989)
8. Perkin Elmer 5400 XPS Software (1989).
9. C.Kozlowski and P.M.A.Sherwood, *Carbon*, 24, No.3, 357, (1986)
10. R.Nordberg, H.Brecht, R.G.Aldridge, A.Fahlmann and J.R.Van Wazer, *Inorg.Chem.*, 9, 2469 (1970)
11. C.Kozlowski, Ph.D Thesis, Inorganic Chemistry, (1984) (Newcastle Upon Tyne, England)
12. D.W.Davis and D.A.Shirley, *J.Elec.Spec. and Rel.Phenom.*, 3, 137, (1974).
13. S.G.Chang and T.Novakov, *Amorphous Enviroment*, 9, 495, (1975).
14. J.F.Evans and T.Kuwana, *Analytical Chemistry*, 51, No.3, 358 (1979).

DETERMINATION OF PARTICLE SIZE OF A DISPERSED PHASE
BY SMALL-ANGLE X-RAY SCATTERING

FRANK C. WILSON
   Polymer Products Dept., DuPont Experimental Station, P O Box 80323,
Wilmington, DE 19880-0323

ABSTRACT

   A method for determining particle diameters up to ca 500 nm is described.
X-ray data are obtained with an ultra-high resolution Bonse-Hart
diffractometer and subsequently desmeared. The resultant data, viewed as the
invariant argument $h^2I(h)$, are interpreted as arising from a log-normal
distribution of independent spherical particles.   The distribution is
characterized by its median value and breadth.

INTRODUCTION

   Small-angle x-ray scattering has long been used to obtain estimates of
particle sizes.   Very little has been published recently in terms of the
methodology, but utilization of, and references to the technique are very
common.   Guinier and Fournet [1] and Hosemann and Bagchi [2] provide
comprehensi·· discussions of the technique as commonly cited today.   The
methods were developed before the easy availability of computers and rely on
the interpretation of plots of   the data, typically with tangent
extrapolations.   With   "conventional"   small-angle diffractometers, the
practical upper limit of particle-size determination is of the order of 100
nanometers, but the Bonse-Hart diffractometer [3,4] extends this range to
almost a micrometer.

   The impetus for this work was the need to develop a procedure for
measuring particle sizes in "rubber-toughened" polymers, where a dispersed
elastomeric phase is employed to enhance the impact resistance of a host
polymer.   The particle sizes are typically a few tenths of a micrometer
(requiring the Bonse-Hart instrument) and the method is totally dependent upon
the availability of a computer to synthesize the modeled curves. Although the
method was developed for polymer blends, it is not restricted to them and can
be employed for any two-phase system where the dispersed phase is present as
approximately spherical "particles".   The   only requirement is that a
reasonable electron-density difference exists between the two phases. As well
as polymer blends (solid-in-solid), we have characterized discrete particles,
voids, emulsions and dispersions (solid-in-gas, gas-in-solid, liquid-in-liquid
and solid-in-liquid). The sizes which can be accommodated range from about 10
to 500 or more nanometers, depending upon the breadth of the distribution.

DISCUSSION

   When observed at sufficiently high resolution, as is possible with a
Bonse-Hart small-angle x-ray diffractometer, the scattering from dispersed
particles smaller than about one micrometer in diameter conveys obvious
information about the size and distribution of size of such particles. Figure
1 shows the small-angle scattering from four polymer blends of nearly
equivalent composition (an elastomer dispersed in a semi-crystalline polymer)
but different processing history. The data are displayed as the small-angle
invariant, which is obtained by multiplying the desmeared small-angle
intensity by the square of the scattering angle (which is proportional to h).
It is apparent that the scattering from all four samples differs
significantly, and it would be useful to quantify the differences among the
samples with regards to some average size and size distribution.
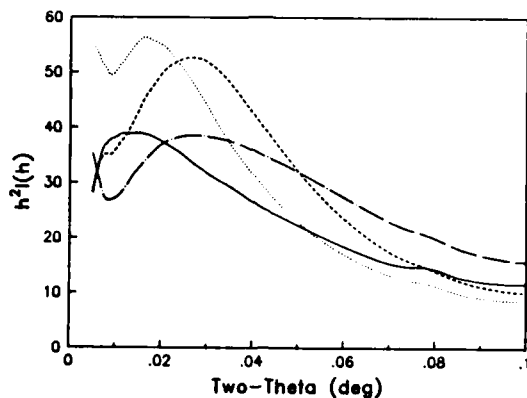
Figure 1 — Invariant Plots for Blends

The scattering observed from independently scattering spheres of radius "r" is given by the equation 1, the Rayleigh equation [5], where u = hr:

$$I(h) = \varphi^2(u) = \frac{9}{u^4}\left(\frac{\sin u}{u} - \cos u\right)^2 \tag{1}$$

The limit as "u" becomes large (since $\sin(u)/u$ approaches zero and $\cos^2 u$ approaches 1/2) is given by equation 2 [6]:

$$I(h) = \varphi^2(u) \longrightarrow \frac{9\cos^2 u}{u^4} \longrightarrow \frac{9}{2} \cdot \frac{1}{u^4} \tag{2}$$

which shows an inverse 4th power relationship with angle at higher angles. The validity of this relationship is demonstrated by Figure 2, which shows the scattering observed from polystyrene particle-size standards. The ordinate is the third power of "h" times the observed (smeared) intensity, since slit smearing changes an inverse 4th power relationship to an inverse 3rd power. As "u" approaches zero, the Rayleigh equation can be approximated by a Gaussian relationship, as in equation 3:

$$I(h) = \varphi^2(u) \simeq \exp\left(-\frac{u^2}{5}\right) \tag{3}$$

which is the well known Guinier approximation [7].
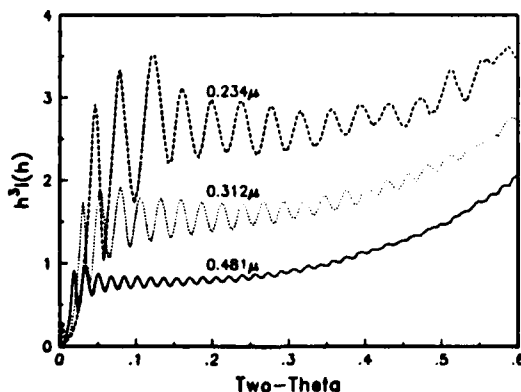
Figure 2 — Observed Data from PS Standards

Since the ripples in the scattering, which are implicit in the Rayleigh equation, are obliterated when there exists any significant particle-size distribution, the scattering from spheres of a given size can be modeled by a curve which is Gaussian at low angles and inverse 4th power at high angles. Since the Gaussian and inverse 4th power curves cross twice, a smooth interpolation can be used to join them. Figure 3 shows the Gaussian, inverse 4th power and interpolated curves displayed as the invariant argument, where they are most easily and usefully visualized. Since the modeled intensity is multiplied by a number proportional to the square of the angle, the Gaussian curve starts at zero and the inverse 4th power curve becomes an inverse square.
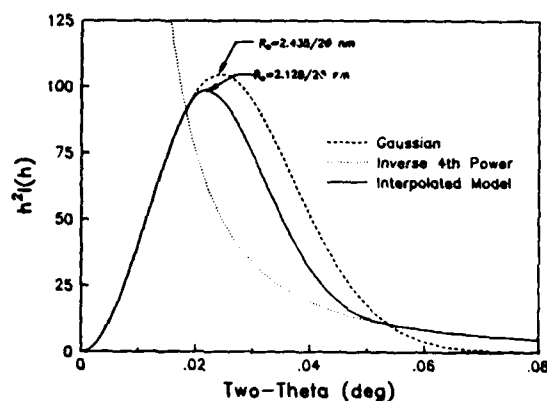
Figure 3 — Invariant Plots for Dia. = 250 nm

In Figure 4, this interpolated approximation is plotted with curves derived from the Rayleigh equation (1) and showing the scattering expected from a monodisperse population and from a narrow particle-size distribution. Beyond the first maximum, the approximation effectively bisects the ripples arising from the cos^2 term of equation 2 for both curves derived from the Rayleigh equation.
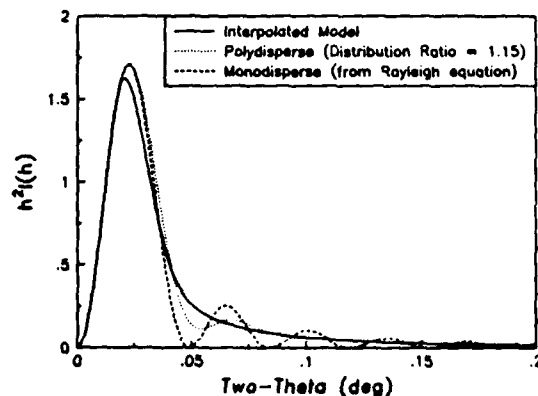
Figure 4 — Invariant Plots for Dia. = 250 nm

In order to predict the scattering from a finite distribution, the logarithm of the diameter of the particles is assumed to be normally distributed and this is approximated by summing the contributions of 23 fractions, equally spaced with regard to the logarithm of the relative size, between plus and minus 3-sigma. The logarithm at 1-sigma differs from that at the center of the distribution by an amount corresponding to the ratio of sizes which characterizes the breadth of the distribution. This "Distribution Ratio" and the size (diameter) at the center of the distribution serve to characterize the log-normal distribution fully. Since the area of the invariant curve is proportional to the amount of that fraction present regardless of the particle-size (hence the name "invariant"), the contributions can be summed directly. The center of the distribution is a median value, with half the mass of the dispersed phase consisting of larger particles and half the mass consisting of smaller particles. Figure 5 shows the expected scattering from distributions with a characteristic diameter of 250 nm and distribution ratios varying from one (monodisperse) to three. The contributions from the larger particles causes the invariant maximum to shift to lower angles while the contributions from the smaller particles raises the level at higher angles.
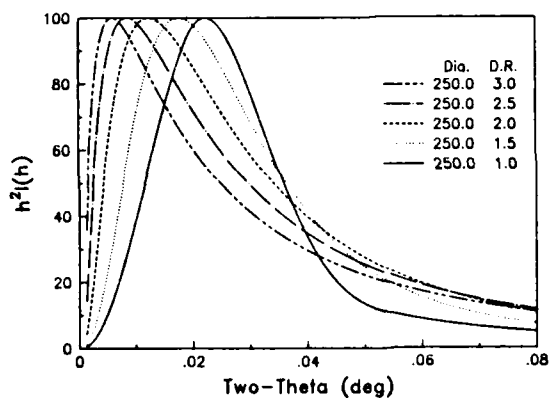
Figure 5 — Invariant Curves with Same Median

Figure 6 is similar to figure 5 except that each curve has its maximum where it occurs for a 250 nm monodisperse population. The method for determining median particle-size and distribution-breadth is implicit in this figure: The position of the maximum is inversely proportional to the diameter of a monodisperse particle size; the breadth of the peak (taken as the ratio of the position of the high-angle half-maximum to that of the maximum) enables the empirical calculation of the median diameter and distribution ratio. As the method has evolved in our laboratory, the characterization of a blend is accomplished by displaying the invariant curve on a graphics terminal and locating the position of the maximum with the graphics cursor. The computer is programmed to locate the position of the high-angle half-maximum, calculate the median diameter and distribution ratio, and then calculate and overlay the expected invariant curve for this distribution. At times, a slight movement of the estimated position of the maximum provides a more satisfactory visual match between the observed and calculated invariant curves, but the estimated median diameters and distribution ratios seldom change significantly.
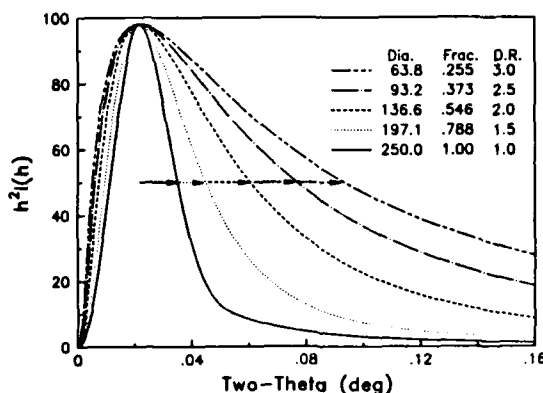
Figure 6 — Invariant Curves with Same Maximum

Figure 7 shows the match between observed and calculated invariant curves for two of the samples of Figure 1. The positions of the maxima are nearly the same, but the shapes (or widths at half-maximum) are obviously different. This difference in shape leads to significant differences in the estimated median diameter and distribution ratio as noted in the figure. Figure 8 shows a histogram of particle sizes that is generally furnished with the results from a sample. Although there is no real additional information beyond the mean diameter and distribution ratio, a visual presentation of the skewed distribution and enumeration of the mode and mean values has proved useful. The individual bars represent the mass of particles in a given 25 nm range. The mode is contained in the tallest bar and is always less than the median, and the mean is located at the horizontal center of gravity of the figure and is always greater than the median. The median is near the line between the bars with the fine shading and those that are cross-hatched. Comparison of results such as these with those from electron microscopy are in generally good agreement, usually within a factor of two. Considering the assumptions and averaging implicit in both techniques, this is satisfactory. Typically the electron diffraction results are smaller, indicating a favoring of the more common particles--nearer the mode. One should bear in mind that an electron microscopy result is usually based on observation of a few hundred particles and is commonly an "eyeball" estimate; for a typical irradiated volume of about 10 mm^3, the x-ray technique averages over about 10^{12} particles.
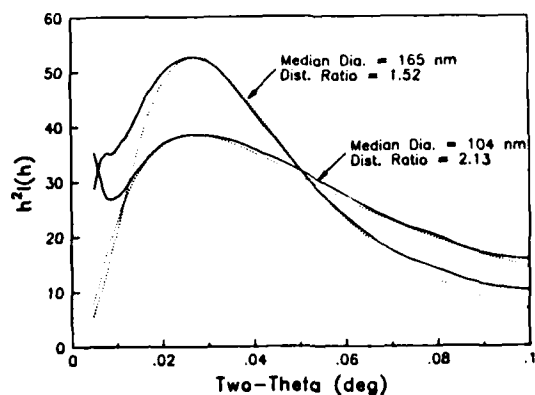
Figure 7 — Fitted Invariants for Blends
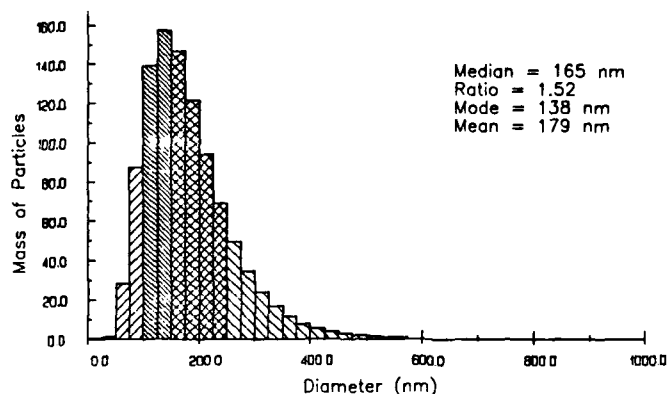
Figure 8 — Histogram of Particle Sizes

CONCLUSIONS

The method described here provides a useful characterization of polymer blends when the dispersed phase consists of particles which are nearly spherical. The assumption of a log-normal particle-size distribtion has not proved to be particularly restrictive. A surprisingly good fit between observed and calculated curves is obtained in a great majority of cases, and the kind of information generally desired is usually that of trends among generally similar samples. The x-ray data themselves commonly are sufficient to answer the question: "Are the observed differences in properties due to a difference in particle size (and/or distribution)?". *In essence, two items of* input, the position of the invariant maximum and the high-angle half-height, are used to determine two items of output, the median particle-size and the distribution ratio. Granted that a great variety of particle size distributions could lead to indistinguishable scattering curves, allowing for models other than the log-normal would offer so many degrees of freedom as to make results much less useful in general.

REFERENCES

1. A. Guinier and G. Fournet, Small-Angle Scattering of X-Rays, (John Wiley & Sons, Inc., N.Y., 1955), Chapter 4

2. R. Hosemann and S. N. Bagchi, Direct Analysis of Diffraction by Matter, (Interscience Publishers Inc., N.Y., 1962), Chapter XVII

3. Koffman, Advances in X-ray Analysis, XI, 334-338, 1967

4. O. Glatter and O. Kratky, Small Angle X-Ray Scattering, (Academic Press, London, New York, 1982), pps 69-72

5. Lord Rayleigh, Proc. Roy. Soc. (London), A90, 219 (1914)

6. A. Guinier and G. Fournet, op. cit., p 17

7. A. Guinier, Ann. phys., 12, 161-237 (1939)

SYNTHESIS AND CHARACTERIZATION OF A THERMOTROPIC POLYALKANOATE OF 4,4'-DIHYDROXY-α,α'-DIMETHYLBENZALAZINE

H. FRIUTWALA, A. L. CIMECIOGLU AND R. A. WEISS
Polymer Science Program, Institute of Materials Science, University of Connecticut, Storrs, CT 06269-3136

INTRODUCTION

Several research projects in our laboratory have used an LCP based on 4,4'-dihydroxy,a-a' dimethylbenzalazine, that was first synthesized by Roviello and Sirigu [1,2]. Copolymers with the following general structure,
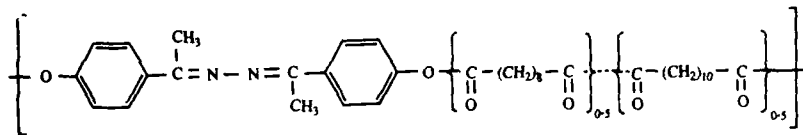
have been used in self-reinforcing polymer blends[3] and are currently being used in small angle neutron scattering studies of the molecular conformation of an LCP in a nematic field. In this latter study, it is imperative that the polymer be well characterized, especially with respect to molar mass and thermal stability. This paper describes the effect of molar mass and thermal history on the thermal stability and transitions of this particular LCP.

EXPERIMENTAL

Materials:

Hydrazine monohyrate (Eastman Kodak), 4-hydroxyacetophenone (Aldrich), pyridine (Anhydrous, Aldrich), triethylamine (Gold Label, Aldrich) and chloroform (HPLC, Aldrich) were used as supplied. N-methylpyrrolidone (NMP) (Aldrich) was dried by refluxing over calcium hydride, distilled and was stored over molecular sieves Type 3A. Sebacoyl chloride and dodecanedioyl dichloride (Aldrich) were purified by vacuum distillation and stored under nitrogen prior to use. All other solvents used were reagent grade and were employed without further purification.

Polymer Synthesis:

4,4'-dihydroxy-a,a'-dimethylbenzalazine was prepared according to the reported procedure, M. pt. 225-226 °C[4]

Solution polymerization was carried out in a three-neck round bottom flask (500 mL) equipped with an addition funnel, a reflux condenser and a mechanical stirring assembly under nitrogen atmosphere, according to the following general procedure. The diol (20-35 mmol) was dissolved in a solution of chloroform (70 mL) containing an excess of the acid acceptor (pyridine or triethylamine; 5-25 mL) and, in some cases, a small amount of NMP (5-10 mL). The latter helped to facilitate dissolution of the otherwise insoluble azine in chloroform. An equivalent or a slight excess (1 mole%) of a 50/50 molar mixture of the acid chlorides (sebacoyl/dodecanedioyl; 20-35 mmol) in chloroform (30 mL) was added to the solution over a period of 10 min-1.5 h. with vigorous stirring. The temperature was maintained between 0-60 °C. Following completion of the addition, the solution was stirred vigorously for a further 4 h.

After completion of the reaction, the mixture was diluted with chloroform (ca. 50 mL) to reduce its viscosity. The products were then recovered by precipitation into methanol (500-1000 mL). They were broken up and washed in a high speed blender, filtered, further washed with aliquots of methanol, methanol/water, and water and were finally dried in vacuo at 60-70 °C for at least 24 h. In all cases, the yields were near quantitative

Polymer Characterization

A number of analytical techniques were used to characterize these liquid crystalline polymers (LCP), including differential scanning calorimetry (DSC), thermal gravimetric analysis (TGA),and gel permeation chromatography (GPC).

DSC: A Perkin Elmer DSC-7 was used to measure the enthalpy changes and specific heat changes associated with the thermal transitions. The samples were heated at 20 ^{0}C and cooled at 10 ^{0}C in all experiments. The cell was continuously flushed with dry nitrogen.

TGA: A Perkin Elmer TGA-7 was used to study the thermal stability of the LCP.in a dry nitrogen. Both dynamic and isothermal experiments were made. Following the TGA experiments, GPC measurements were made on the same samples in order to assess the effect of thermal history on the molar mass of the polymer.

RESULTS AND DISCUSSION

Characterization of thermal transitions. The DSC thermograms of the LCP are shown in the Fig. 1. The polymer had a glass transition temperature (T_g) of 24 ^{0}C, and a nematic to isotropic transition (T_{N-I}) at 245 ^{0}C. The polymer showed two peaks, T_1 & T_2, in the temperature range of 140-160^{0}C and exhibits a nematic mesophase above 160^{0}C and up to T_{N-I}. The neutron scattering studies (Fig. 2) indicate the possibility of an additional mesophase just before the solid to nematic transition, which would give a peak in the DSC thermograms. As seen in Fig. 1 the cooling curve does not show two crystallization peaks. A detailed investigation of this somewhat surprising behaviour is currently underway in our laboratory.

The effect of the weight average molar mass on the thermal transitions is shown in Fig. 3. Below a molar mass about 50000 (polystyrene equivalent), T_1, T_2 and T_{N-I}, increases with increasing molar mass and the transition temperatures plateau at higher M_w's. There is relatively small change in T_g with changes in molar mass.

The effect of thermal history on the transitions is shown in Fig. 4. Prior to each run the sample was annealed at elevated temperature. The sample was then cooled back to its starting temperature and the subsequent heating scans are shown in Fig. 4. Annealing at elevated temperature raised T_g. This was a consequence of the reduced crystallinity of the polymer. There was no significant influence of annealing time on T_1 and T_2 when the sample was annealed at 220^{0}C. The peaks moved to lower temperatures as the sample was annealed for longer period at temperatures close to its and above the T_{N-I}. The transitions were broadened as the annealing time was increased. Thus, the order of the melt and the kinetics of ordering are affected by annealing, and this did not appear to be due to polymer degradation as indicated by only minor changes in molar mass as discussed below. This was also evident in the neutron scattering contour plots (Fig.3), during which sample was annealed for long periods of time at elevated temperatures.

Characterization of Thermal Stability. The LCP was stable up to 350 ^{0}C as shown by the TGA thermogram in Fig. 5 As with the DSC experiments, the LCP was exposed to various annealing temperatures for varying lengths of time. The details of these experiments are summarized in Table I. In most cases the mass loss was < 1%. After TGA analyses, the same samples were dissolved in chloroform for GPC analyses. These results are also given in Table I. Annealing at 220 ^{0}C actually appeared to increase the molar mass, which suggests that some additional polymerization or

FIG.1
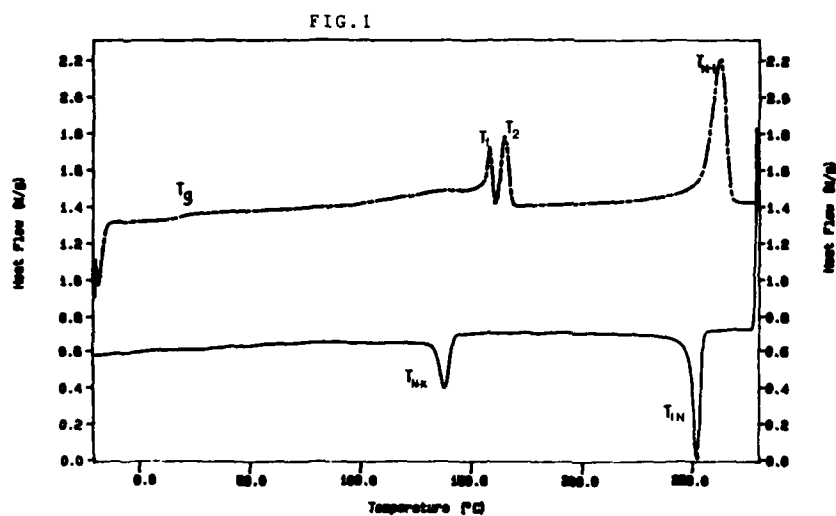
1. A typical DSC thermogram of the LCP under investigation.

FIG:2
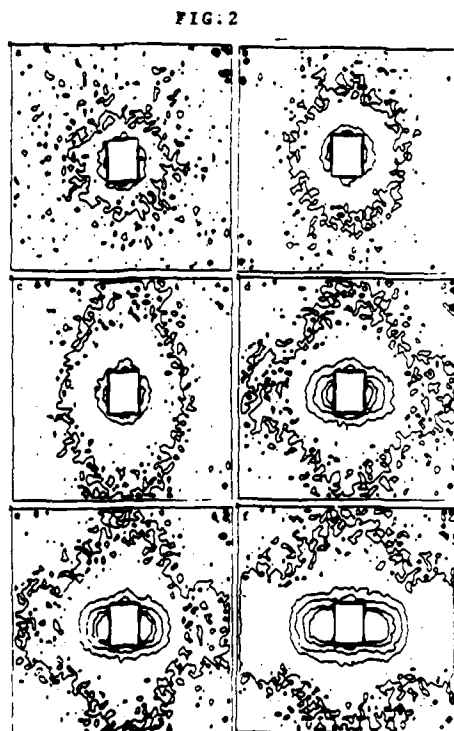
2. Neutron scattered intensity in the plane perpendicular to the incident beam at (a) 250°C, (b) 220°C, (c) 200°C, (d) 170°C, (e) 160°C and (f) 150°C. Magnetic field direction is on the horizontal axis.

equilibration of the molar mass took place. At 240 °C, which is in the broad clearing transition, and at 260 °C, which is in the isotropic region, the molar mass decreased with increasing annealing time. The molar masses reached with annealing for one hour at each temperature were similar and corresponded to about a 10% reduction in molar mass from the starting polymer (i.e., no high temperature annealing). In any event, the molar mass of the LCP after all the annealing histories given in Table I were above 50,000, and therefore, the changes in molar mass were most likely not responsible for the changes in crystallization and mesophase formation described earlier.

FIG. 3
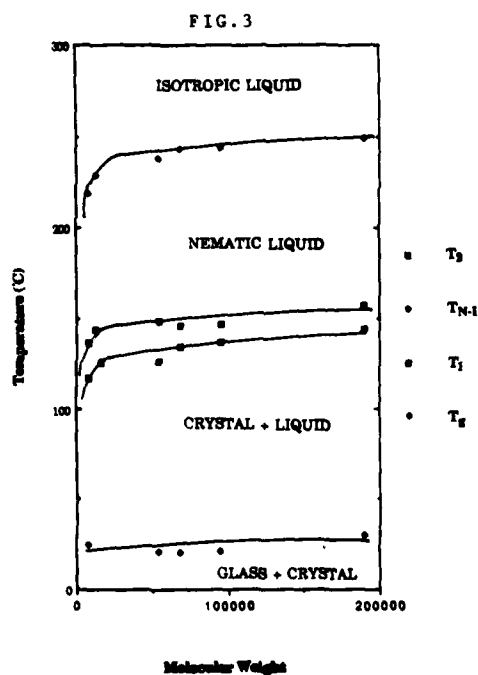
3. Effect of the molecular weight on the thermal transitions.

FIG. 4
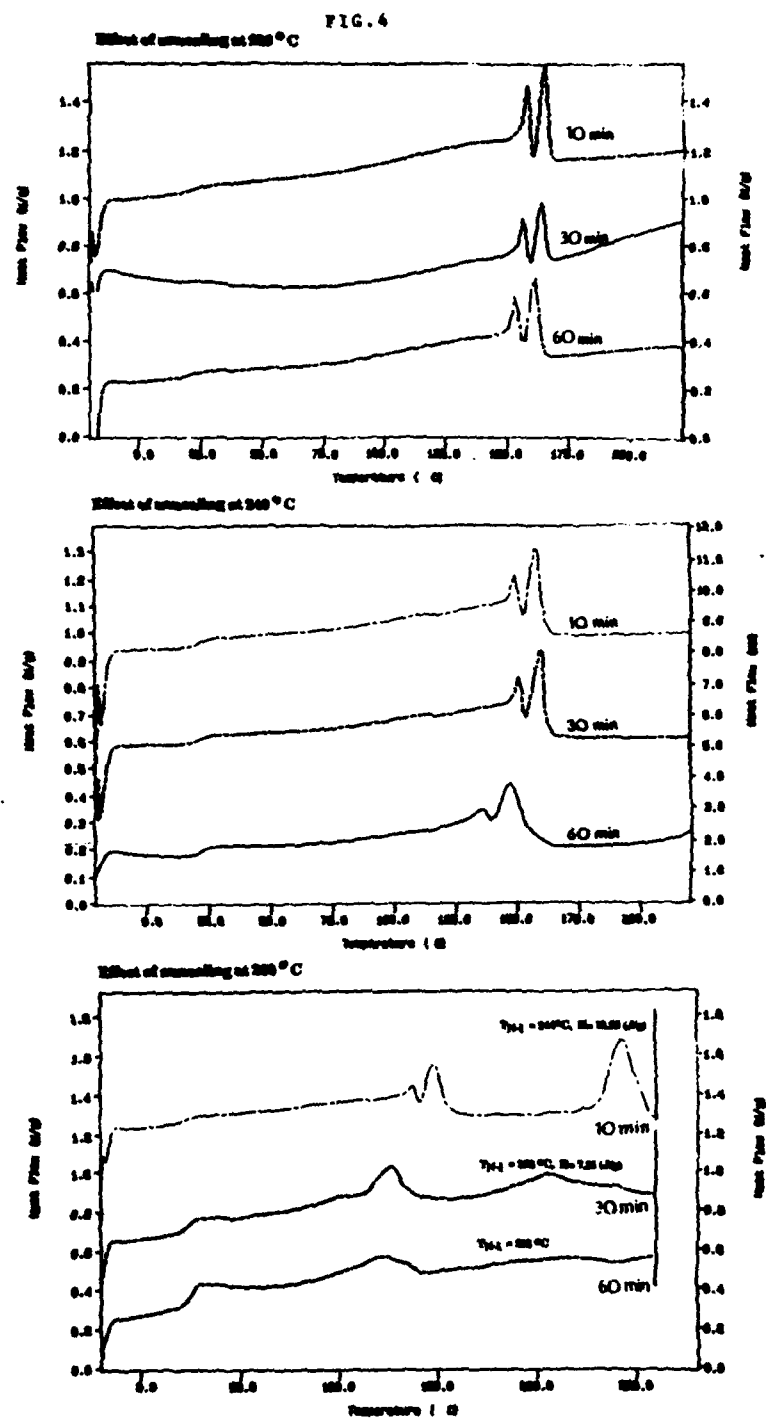
4. Effect of annealing on the thermal transitions.

FIG.5

PERKIN-ELMER
7 Series Thermal Analysis System
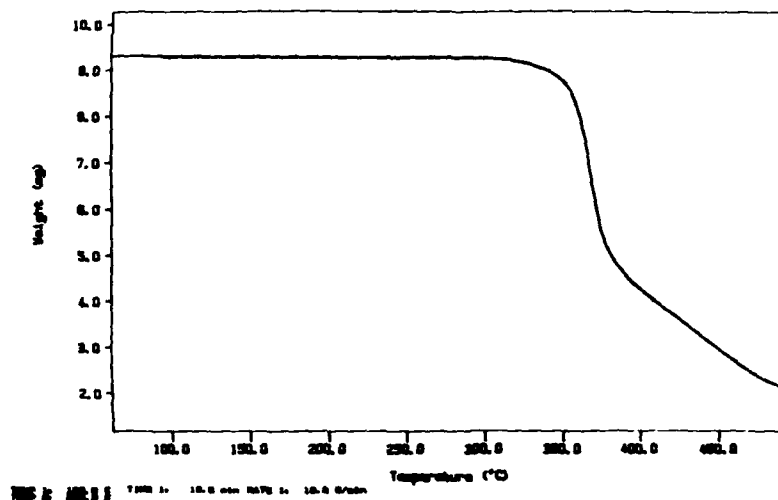
5. TGA curve of the polymer.

TABLE I

ANNEALING TEMP (C)	TIME (Min)	Mw	Mw/Mn
220	10	57900	3.2
220	30	77000	3.55
220	60	78700	3.69
240	10	75000	3.46
240	30	66000	3.36
240	60	57050	3.08
260	10	69500	3.57
260	30	64700	3.87
260	60	60400	3.79
Neat	-	77700	2.39

1. Effect of annealing temperature/time on molecular weight of the polymer.

CONCLUSION

The liquid crystalline polymer discussed in this report is relatively stable at high temperatures, and a small reduction in its weight and molecular mass was only observed after prolonged exposure to such temperatures. Neutron scattering results seem to indicate that there is a second mesophase prior to the nematic transition. The nature of this additional phase is not clearly identified as yet and is currently under investigation.

REFERENCES

1. Roviello A. and Sirigu R., J. Poly Sci., poly. lett. ed. 13 455 (1975)
2. Roviello A. and Sirigu R., Eur. Poly. J. 15 61 (1979)
3. Weiss R, Huh W.S., Nicolais L., Pol. Eng. Sci. 27 684 (1987)
4. Blout E.R,Eager V.W., and Golfstein R.M. J. Am. Chem. Soc. 68 1983 (1946)

Author Index

Subject Index

MATERIALS RESEARCH SOCIETY SYMPOSIUM PROCEEDINGS

MATERIALS RESEARCH SOCIETY SYMPOSIUM PROCEEDINGS

MATERIALS RESEARCH SOCIETY SYMPOSIUM PROCEEDINGS

MATERIALS RESEARCH SOCIETY SYMPOSIUM PROCEEDINGS

MATERIALS RESEARCH SOCIETY SYMPOSIUM PROCEEDINGS

Recent Materials Research Society Proceedings listed in the front.

MATERIALS RESEARCH SOCIETY CONFERENCE PROCEEDINGS